

**Method Development and Mechanistic Investigations of Nickel-Catalyzed C–N and
C–H Functionalizations**

by

Alexander William Rand

A dissertation submitted in partial fulfillment
of the requirements for the degree of
Doctor of Philosophy
(Chemistry)
in The University of Michigan
2020

Doctoral Committee:

Professor John Montgomery, Chair
Associate Professor Peter Scott
Professor Corey Stephenson
Associate Professor Nathaniel Szymczak

Alexander William Rand

alexrand@umich.edu

ORCID iD: [0000-0002-7099-5870](https://orcid.org/0000-0002-7099-5870)

Dedication

This dissertation is dedicated to my friends and family who have encouraged me to pursue my dreams and aspiration. To my parents, Mitch and Angela, for their unwavering support and encouragement throughout my entire education. And to my brothers, Jake and Ben, for bringing me never ending joy throughout the darkest and lightest of times.

Acknowledgements

Firstly, I would like to thank my advisor, John Montgomery, for granting me the opportunity to work under his mentorship throughout my time at Michigan. I am especially grateful for his willingness to let me explore my own intellectual interests from an early point in my graduate career. I would not have developed into the person I am now had it not been for his openness to new ideas, however crazy they may have sounded.

I would like to thank my colleagues in the Montgomery for all of their support. To my early mentors, Eric Wiensch and Alex Nett, who encouraged me to explore new ideas and be conduct meaningful experiments. To my lab mates, Wes Pein, Annabel Ansel, Kirk Shimkin, Cole Cruz, Yishu Xu, Mo Chen, Rosa Vasquez, Daniel Nasrallah, Jonathan Perkins, Sara Alektiar, Santi Cañelles and Takuya Yoshida for making the lab a fun and collaborative place to grow. I would especially like to thank Wes Pein, Annabel Ansel, Cole Cruz, and Nick Chiappini for their continuous support and for reading countless manuscripts.

I would also like to thank my peers in the department for doing everything in their power to help me succeed as a graduate student. My colleagues in the Sanford lab, Christo Sevov and Yichao Yan, for their overwhelming help with electrochemistry and idea generation. My colleagues in the Stephenson lab, Rory McAtee, Ted McClain, James Collins, and Gabe Magallanes, for their unwavering support in all things

photochemistry. My colleagues in the Szymczak lab, Jessi Wilson and John Kiernicki, for their advice and assistance in approaching organometallic problems.

Thank you to the members of the NSF Center for Selective C–H Functionalization for all of their help throughout my studies. I cannot imagine a more collaborative and engaging group of people. I am deeply inspired by you all.

To Dr. John F. C. Turner and Professor Jeffrey Cannon, for encouraging me to pursue research. I would not have made it to graduate school if not for your mentorship and guidance.

I am very thankful to have found a great group of friends outside of the lab who have made my time in Ann Arbor nothing but joyful. To Erin Lynch, Jacob Johnson, Sara Wong, Adam Banker, Katie Knoedler, Anton Maisnikov, Andrew Vitek, Sarah Walker, and Andrew Gerlach, who have made weekend trips to Kentucky an integral part of my life. To Samuel Wylie, Rachel Wilson, Nathan Reynolds, Greg Tucker, Andrew Bernard, and Tim Everhart for constant companionship and emotional support.

Finally, to my family for constant love and support in all aspects of my life.

“The mountains are calling and I must go, and I will work on while I can,
studying incessantly”

Table of Contents

Dedication	ii
Acknowledgements	iii
List of Tables	x
List of Equations	xiii
List of Figures.....	xiv
List of Abbreviations	xxiii
Abstract.....	xxviii
Chapter 1	1
1.1 Introduction.....	1
1.2 Catalytic C–N Functionalization	2
1.2.1 Amide Bond Activation	2
1.2.2 Katritzky Salts For C–N Bond Activation	3
1.2.3 Aniline Bond Activation	4
1.2.4 Aryl Trialkylammonium Salt Activation	6
1.2.4.1.....C–C Bond Forming Reactions	6
1.2.4.2.....C–Heteroatom Bond Forming Reactions.....	11
1.2.4.3.....C–H Bond Forming Reactions.....	18

1.2.4.4.....Summary of Aryl Trialkylammonium Salt Functionalizations	20
1.3.....Importance and Utility of Aryl Silanes in Synthesis.....	20
1.3.1 Aryl Silanes in Materials and Medicinal Chemistry.....	20
1.3.2 Traditional Synthesis of Aryl Silanes	21
1.3.2.1.....C–H Functionalization to Access Aryl Silanes.....	21
1.3.2.2.....C–O Activation to Access Aryl Silanes.....	23
1.4.....Results and Discussion.....	26
1.4.1 Developing a Nickel-Catalyzed Silylation of Aryl Trialkylammonium Salts ...	26
1.4.2 Substrate and Silane Scope of the Nickel-Catalyzed Silylation of Aryl Trialkylammonium Salts.....	36
1.4.3 Optimization of the Nickel-Catalyzed Reduction of Aryl Trialkylammonium Salts to Arenes	40
1.4.4 Substrate Scope of the Reduction of Aryl Trialkylammonium Salts to Arenes	43
1.4.5 Mechanistic Investigations into the Silylation and Reduction of Arenes	44
1.4.6 Synthetic Demonstrations	47
Chapter 2	52
2.1.....Introduction.....	52
2.2.....Distal C–H Functionalization Using Amines and their Derivatives.....	54
2.2.1 Hofmann-Löffler-Freytag-type Reactions for Distal C–H Functionalization ...	54
2.2.2 N–H Cleavage for Distal Functionalization of C–H bonds	57
2.3.....Proximal C–H Functionalization using Amines and their Derivatives.....	61
2.3.1 C–C(sp ³) and C–C(sp) Bond Formations	61
2.3.2 C–C(sp ²) Bond Formation	69

2.4..... Results and Discussion.....	77
2.4.1 Attempts at Intercepting PCET/HAT Intermediates.....	77
2.4.2 Optimization of Metallaphotoredox-Catalyzed Arylation.....	82
2.4.3 Reaction Scope of α -Arylation of <i>N</i> -Alkyl Benzamides.....	93
2.4.4 Limitations in the Functionalization of <i>N</i> -Alkyl Benzamides.....	96
2.4.5 Enantioselective α -Arylation of <i>N</i> -Alkyl Benzamides.....	99
2.4.6 Applications and Synthetic Demonstrations.....	111
2.4.7 Functionalization of Other Weak C–H Bonds.....	113
2.4.8 Summary of the α -Arylation of Benzamides, Tertiary Amides, and Aldehydes.....	117
Chapter 3.....	119
3.1..... Overview of PET and Photochemical Thermodynamics.....	119
3.2..... Initial Mechanistic Investigations.....	122
3.2.1 Mechanisms Involving a 1,5-HAT.....	124
3.2.2 Testing the Validity of Nitrogen-Centered Radical Formation.....	127
3.3..... Discussion of Mechanistic Hypotheses.....	131
3.3.1 Deprotonation of Benzamides for Direct Oxidation.....	131
3.3.2 Direct C–H PCET to Form an α -Amidyl Radical.....	134
3.3.3 α -Amidyl Radical Formation from a HAT Agent.....	141
3.3.3.1..... Phosphate and Sulfate Radicals for HAT.....	141
3.3.3.2..... Halide Radicals as HAT Agents for α -Amidyl Radical Formation....	145
Chapter 4.....	163
4.1..... General Supporting Information.....	163

4.2.....	Experimental Details for Chapter 1	165
4.2.1	General Procedures for Chapter 1	165
4.2.1.1.....	General Procedure for Nickel-Catalyzed Silylation of Aryl Trialkylammonium Salts:.....	165
4.2.1.2.....	Modified General Procedure using Air-Tolerant Nickel(0) Catalyst:	166
4.2.1.3.....	General Procedure for Nickel-Catalyzed Reduction of Aryl Trialkylammonium Salts:.....	166
4.2.1.4.....	General Procedures for Reductive Amination:	167
4.2.1.5.....	General Procedures for Suzuki-Miura Coupling:	167
4.2.1.6.....	General Procedures for Aryl Trialkylmmonium Salt Formation:	168
4.2.2	Starting Material Synthesis:	168
4.2.3	Calibration Curves:	181
4.2.4	Silylation Substrates:	189
4.2.5	Reduction Substrates:.....	214
4.2.6	Synthetic Demonstrations:	219
4.2.7	Large Scale Silylation:	231
4.3.....	Experimental Details for Chapter 2	232
4.3.1	Synthesis of Catalysts and Ligands:	232
4.3.2	General Procedures for PCET Reactions:.....	234
4.3.3	Synthesis of Phosphate Bases:	235
4.3.4	General Procedures for the Synthesis of BiOx Ligands:	236
4.3.5	Synthesis of Starting Materials:	238
4.3.6	General Procedures for the Synthesis of Benzamides:	240

4.3.7	Controls and Additive Screening:	255
4.3.8	UV-Vis Data:	258
4.3.9	General Procedures for the α -Arylation of Benzamides:	258
4.3.10	Enantioselective α -Arylation of Benzamides:	285
4.3.11	Absolute Stereochemistry of Benzamides	297
4.3.12	Synthetic demonstrations:	299
4.4Experimental Details for Chapter 3	305
4.4.1	Deuterium Studies:	308
4.4.2	Synthesis of New Compounds	310
4.4.3	Stern-Volmer Analysis.....	316
4.4.4	CV Data:	320
4.4.5	Catalyst Degradation Studies	324
4.5Spectra of New Compounds.....	329
Bibliography	463

List of Tables

Table 1-1 Initial ligand screen for the silylation of aryl trialkylammonium salts.	26
Table 1-2 Solvent effects on the silylation of aryl trialkylammonium salts.	27
Table 1-3 Assessment of ligands for the silylation of aryl trialkylammonium salts at 40 °C.....	29
Table 1-4 Screening of organic and inorganic bases for the silylation of aryl trialkylammonium salts.....	30
Table 1-5 Probing compatible silanes in the silylation of aryl trialkylammonium salts. Reactions were analyzed by GCMS.....	32
Table 1-6 Glorius-type screen of different additives and their effect on aryl silane yield.	33
Table 1-7 Substrate scope for the silylation of aryl trialkylammonium salts using triethyl silane. ^a Yields in parenthesis are isolated yields.	36
Table 1-8 Silane scope of for the silylation of aryl trialkylammonium salts.....	38
Table 1-9 Effect of solvent and temperature on the reduction of aryl trialkylammonium salts.	40
Table 1-10 Evaluation of different ligands and reaction times for the reduction of aryl trialkylammonium salts.....	41
Table 1-11 Evaluation of different reductants on the yield of arene.	42
Table 1-12 Substrate scope for the reduction of aryl trialkylammonium salts.	44

Table 1-13 Effects of TEMPO on a) the silylation and, b) the reduction of aryl trialkylammonium salts.....	46
Table 2-1 Base and solvent screen for distal arylation of tertiary C–H bonds.	79
Table 2-2 Base screen for distal arylation of secondary C–H bonds.....	80
Table 2-3 Determination of the aryl source for C-H arylation.	82
Table 2-4 Ligand screen for arylation of benzamide 2-91.....	83
Table 2-5 N-donor ligand screen with 2-91.....	84
Table 2-6 Modifications of arylation conditions for 2-91.	85
Table 2-7 Comparison of redox properties and yields of photocatalysts.....	86
Table 2-8 Head-to-head comparison of ligands under extended reaction times.....	87
Table 2-9 Evaluation of BiOx ligands for enantioselective α -arylation.	88
Table 2-10 Effects of catalyst loading, photocatalyst, and solvent on yield.....	89
Table 2-11 Aryl bromide scope for the arylation of <i>N</i> -alkyl benzamides.	93
Table 2-12 Benzamide scope for the arylation of <i>N</i> -alkyl benzamides.	95
Table 2-13 Incompatible nitrogen protecting groups and amides.	96
Table 2-14 Incompatible aryl bromides and inseparable products.	97
Table 2-15 Comparison of the properties of PC1 and PC6.	99
Table 2-16 Racemization of enantioenriched arylation product.....	100
Table 2-17 Change in enantioselectivity over time using different photocatalysts.....	101
Table 2-18 Effects of temperature on α -arylation enantioselectivity.	102
Table 2-19 Comparison of yield and enantioselectivity for cooled photoreactors.	103
Table 2-20 Reaction scope of enantioselective arylation of benzamides. ^a Yield determined by GCMS. ^b Reaction run for 24 h.	107

Table 2-21 Arylation of DMAc using metallaphotoredox catalysis.	114
Table 2-22 Examination of different bases in the arylation of benzaldehyde.	114
Table 2-23 Examination of different photocatalysts for the arylation of benzaldehyde.	115
Table 2-24 Ligand screen for the arylation of benzaldehyde with bromobenzene.	117
Table 3-1 Redox properties of nickel(II) complexes.	147
Table 3-2 Summary of Stern-Volmer analysis for alpha-arylation of benzamides.	151
Table 3-3 Studies by Doyle of restoring reactivity of aryl bromides and iodides by adding TBACl.	153
Table 3-4 Knowles' study on the effects of adding TBAF on yield to C–H PCET reaction that requires hydrogen bonding between the photocatalyst and base.	154
Table 3-5 Knowles' study on the effects of adding TBAF on the yield for a N–H PCET reaction that does not require hydrogen bonding to the iridium photocatalyst.	155
Table 3-6 Studies by Barriault on counterion effects on HAT using iridium photocatalysts. ^a Reaction run at room temp.	156
Table 3-7 Effects of adding tetrabutylammonium salts to the α -arylation of benzamides.	158
Table 3-8 Effects of reaction stoichiometry on yield when adding TBABr.	161
Table 4-1 GCMS analysis of competition experiments between 2-91 and 3-7.	315

List of Equations

Equation 1: Thermodynamics of electron transfer for a molecule in the ground state...	121
Equation 2: Thermodynamics of electron transfer for a molecule in the excited state...	121
Equation 3 Calculating excited-state reduction potentials using CV and $E_{0,0}$	122
Equation 4 Bond dissociation free energy.	128

List of Figures

Figure 1-1 Nickel-catalyzed esterification of amides.	2
Figure 1-2 Synthesis of Katritzky salts and reduction to give radicals.....	3
Figure 1-3 Sandmeyer reaction the functionalization of anilines.	4
Figure 1-4 Ruthenium-catalyzed ketone-directed cleavage of C–N bonds.	5
Figure 1-5 Kumada coupling of aryl trialkylammonium salts.....	6
Figure 1-6 Palladium-catalyzed Kumada coupling and chemoselectivity of aryl trialkylammonium salts.....	7
Figure 1-7 NHC-Ni catalyzed Suzuki-Miyaura coupling with aryl trialkylammonium salts.	8
Figure 1-8 Nickel-catalyzed Negishi coupling with aryl trialkylammonium salts.	9
Figure 1-9 Sonogashira coupling using aryl trialkylammonium salts.	10
Figure 1-10 Stoichiometric studies with using NHC-Ni-Ar complexes generated from trialkylammonium salts.....	11
Figure 1-11 Nickel-catalyzed borylation of aryl trialkylammonium salts.....	12
Figure 1-12 Nickel-catalyzed borylation of benzyl and aryl trialkylammonium salts.	13
Figure 1-13 Stannylation of aryl trialkylammonium salts under light irradiation.	14
Figure 1-14 Nickel-catalyzed phosphorylation of aryl trialkylammonium salts.....	15
Figure 1-15 Etherification of aryl trialkylammonium salts.	16
Figure 1-16 Nickel-catalyzed transamination of aryl trialkylammonium salts.	17

Figure 1-17 Methods for the reduction of aryl trialkylammonium salts to arenes.	18
Figure 1-18 Traditional methods for aryl silane synthesis.....	21
Figure 1-19 Iridium and rhodium catalyzed C–H silylation of unactivated arenes.....	22
Figure 1-20 Boron-catalyzed C–H silylation of arenes.	22
Figure 1-21 KO- <i>t</i> -Bu catalyzed C–H silylation.....	23
Figure 1-22 Nickel-catalyzed silylation of inert C–O bonds.....	24
Figure 1-23 Reduction of aryl trialkylammonium salts and limitations of this method...	40
Figure 1-24 Deuterium incorporation for the silylation and reduction of aryl trialkylammonium salts.....	45
Figure 1-25 Head-to-head comparison of triethyl silane with different silanes.	45
Figure 1-26 Synthetic demonstrations for the silylation of aryl trialkylammonium salts. a) using nitro-groups for SnAr and aryl silane precursors, b) rapid diversification of simple arenes in route to aryl silanes and, c) using anilines as directing groups.....	48
Figure 1-27 Synthetic demonstrations of silylation of aryl trialkylammonium salts. a) large-scale silylation of an aryl trialkylammonium salt and, b) comparison of in situ generated catalysts and air-stable pre-catalysts.	50
Figure 2-1 Mechanistic pathways for, a) α -functionalization of amines and, b) α - functionalization of amides.....	52
Figure 2-2 Inorganic and organic photocatalysts used in photoredox catalysis.	53
Figure 2-3 Explanation of selectivity for the Hofmann-Löffler-Freytag reaction.....	54
Figure 2-4 Use of N–F reagents for C–C bond formation.....	55
Figure 2-5 <i>In situ</i> HLF reactions for oxidation, amination, and arylation.....	56
Figure 2-6 Thermodynamic cycle for PCET.	57

Figure 2-7 General mechanism for oxidative PCET.....	58
Figure 2-8 Photocatalytic PCET for distal alkylation.....	58
Figure 2-9 Distal allylation of trifluoroacetamides using metallaphotoredox catalysis.	59
Figure 2-10 Distal alkylation of trifluoroacetamides using alkyl bromides.	60
Figure 2-11 α -amidyl radicals for cyclizations.	61
Figure 2-12 Alkylation of simple amides with styrenes.	62
Figure 2-13 Enantioselective alkylation pyridyl lactams.....	63
Figure 2-14 Alkoxythiocarbamate-directed alkylation of pyrrolidines.	63
Figure 2-15 Tetrabutylammonium decatungstate-catalyzed alkylation of amides.	64
Figure 2-16 Photocatalytic alkylation of carbamates with electron-deficient olefins.	65
Figure 2-17 Enantiospecific alkynylation of carbamates.....	66
Figure 2-18 Metallaphotoredox-catalyzed alkylation of amides and carbamates using alkyl bromides.....	67
Figure 2-19 Using electrostatic interactions for the alkylation of primary amines.	68
Figure 2-20 Alkylation of triflamides using electron-deficient olefins.	69
Figure 2-21 Friedel-Crafts-type arylation of amides using photoredox catalysis and persulfates.	70
Figure 2-22 Nickel-catalyzed and mechanistic hypothesis of the arylation of THF and amides.	71
Figure 2-23 Metallaphotoredox-catalyzed arylation of amides and weak C–H bonds.....	72
Figure 2-24 Palladium-catalyzed enantioselective arylation of thioamides with boronic esters.	73

Figure 2-25 Arylation of cyclic amides and saturated heterocycles, and mechanistic hypotheses.....	74
Figure 2-26 Metallaphotoredox-catalyzed arylation of carbamates and unactivated C–H bonds.....	75
Figure 2-27 Metallaphotoredox-catalyzed and preliminary enantioselective arylation of amides and weak C–H bonds.....	76
Figure 2-28 Proposed distal arylation enabled by metallaphotoredox processes.....	77
Figure 2-29 Identification of oxidative decomposition product.....	81
Figure 2-30 Isolation of trace arylation product.....	81
Figure 2-31 Comparison of 2-93 and 2-91 in the arylation of benzamides.....	84
Figure 2-32 Revised mechanistic hypothesis to explain regioselectivity.....	88
Figure 2-33 Optimized conditions for the arylation of benzamides.....	90
Figure 2-34 Inconsistent enantioselectivity using different photocatalysts.....	99
Figure 2-35 Different photoreactor setups used to maintain low temperatures during α -arylation reactions.....	104
Figure 2-36 Different photoreactor setups used to maintain low temperatures during α -arylation reactions.....	105
Figure 2-37 Aluminum photoreactor for enantioselective α -arylation.....	106
Figure 2-38 Relation between enantioselectivity and σ - for para-substituted benzamides.....	109
Figure 2-39 Relation between enantioselectivity and σ for para-substituted aryl bromides.....	110
Figure 2-40 Methods for removing <i>para</i> -methoxybenzoyl groups.....	111

Figure 2-41 Proximal and distal for the divergent/convergent functionalization of amides.	112
Figure 2-42 Serendipitous discovery of DMAc arylation.....	113
Figure 2-43 Evaluation of different electrophiles and aldehydes for cross-coupling.....	116
Figure 3-1 Orbital diagram for excited state Ru(bpy) ₃ ²⁺ photocatalyst.....	120
Figure 3-2 N–H PCET-mediated α-amidyl radical formation via, a) intermolecular HAT, and b) 1,5-HAT/chainwalking from an amidyl radical.....	122
Figure 3-3 Evidence against amidyl radical formation.....	124
Figure 3-4 Mechanistic evidence against a 1,5-HAT. a) α-arylation of substrate with shorter alkyl chains, and b) α-arylation of substrates containing a quaternary carbon center.....	125
Figure 3-5 Intermolecular competition between α-proteo and α-deutro benzamides.....	126
Figure 3-6 Thermodynamic cycle to determine the BDFE of a reaction.....	127
Figure 3-7 Comparison of K ₃ PO ₄ in EtOAc and Cs ₂ CO ₃ in DMF for the α-arylation of benzamides.....	129
Figure 3-8 Direct oxidation of a deprotonated benzamide to give α-amidyl radicals. ...	131
Figure 3-9 Effects of HAT reagents on protonated and deprotonated trifluoroacetamides and triflamides.	132
Figure 3-10 Inhibited reactivity of potassium benzamide salts in α-arylation.	133
Figure 3-11 C–H PCET of benzamides to give α-amidyl radicals.	134
Figure 3-12 Effects of substitution at the 3,3'-position of iridium photocatalysts.....	134
Figure 3-13 UV-Vis titration of Cs ₂ CO ₃ to a solution of PC1.....	135
Figure 3-14 Changes in UV-Vis when adding Cs ₂ CO ₃ to a solution of PC1.	136

Figure 3-15 a) hydrogen bond-enabled C-H PCET, and b) newly proposed photocatalyst modifications to inhibit hydrogen bonding.....	137
Figure 3-16 Synthesis of a novel bipyridyl ligand with blocked hydrogen bonding sites.	138
Figure 3-17 Synthesis of a photocatalyst with blocked hydrogen bonding sites.....	139
Figure 3-18 α -arylation using a photocatalyst with blocked hydrogen bonding sites. RSM = recovered starting material.	140
Figure 3-19 Phosphate radical formation to give α -amidyl radicals.....	141
Figure 3-20 Addition of persulfates as HAT agents for the α -arylation of benzamides.	142
Figure 3-21 Use of a soluble phosphate base for the α -arylation of benzamides.	143
Figure 3-22 Potential mechanism for halide radical formation from a Ni(III) species. .	145
Figure 3-23 Synthesis of BiOxNi(II) complexes.....	146
Figure 3-24 α -arylation of benzamides using a discrete <i>i</i> -PrBiOxNi(II)Cl ₂ complex.	147
Figure 3-25 α -arylation of benzamides using a discrete <i>i</i> -PrBiOxNi(II)ArBr complex.	148
Figure 3-26 α -arylation of benzamides using a discrete BiOxNi(II)ArBr complex. RSM = recovered starting material.....	149
Figure 3-27 Revised mechanistic hypothesis for α -arylation of benzamides.	150
Figure 3-28 Possible competing pathways for, a) N-arylation and b) C-arylation, when using BiOxNi(II)ArBr.....	152
Figure 3-29 Comparison of hydrogen bonding between the photocatalyst and phosphate base in, a) single-site PCET and, b) multi-site PCET.....	155
Figure 3-30 Effects on reaction color with and without TBABr.	159

Figure 4-1 Plot of 1-81a area versus (std area x [1-81a]) / [std] fitted to $y = mx + b$ where $m = 1.6459$ and $b = -2 \times 10^8$ with a R_2 of 0.9994.	182
Figure 4-2 Plot of 1-81c area versus (std area x [1-81c]) / [std] fitted to $y = mx + b$ where $m = 0.5795$ and $b = -1 \times 10^8$ with a R_2 of 0.99674.	183
Figure 4-3 Plot of 1-81b area versus (std area x [1-81b]) / [std] fitted to $y = mx + b$ where $m = 0.951$ and $b = 4 \times 10^7$ with a R_2 of 0.9998.....	184
Figure 4-4 Plot of 1-88b area versus (std area x [1-88b]) / [std] fitted to $y = mx + b$ where $m = 1.5018$ and $b = 0$ with a R_2 of 0.99963.	185
Figure 4-5 Plot of 1-86b area versus (std area x [1-86b]) / [std] fitted to $y = mx + b$ where $m = 2.2662$ and $b = 0$ with a R_2 of 0.97223.....	185
Figure 4-6 Plot of 1-87b area versus (std area x [1-87b]) / [std] fitted to $y = mx + b$ where $m = 2.1214$ and $b = 0$ with a R_2 of 0.99673.....	186
Figure 4-7 Plot of 1-97b area versus (std area x [1-97b]) / [std] fitted to $y = mx + b$ where $m = 0.9816$ and $b = -6.9783$ with a R_2 of 0.95217.....	187
Figure 4-8 Plot of 1-84b area versus (std area x [1-84b]) / [std] fitted to $y = mx + b$ where $m = 1.3793$ and $b = 0$ with a R_2 of 0.99639.	188
Figure 4-9 Plot of 1-85b area versus (std area x [1-85b]) / [std] fitted to $y = mx + b$ where $m = 2.2235$ and $b = 0$ with a R_2 of 0.98064.....	188
Figure 4-10 Plot of 1-98b area versus (std area x [1-98b]) / [std] fitted to $y = mx + b$ where $m = 29.763$ and $b = -2 \times 10^9$ with a R_2 of 0.96197.....	189
Figure 4-11 Evaluation of different aryl sources in the α -arylation of benzamides.	255
Figure 4-12 Controls for α -arylation of benzamides.	255
Figure 4-13 Evaluation of sub-stoichiometric additives.	255

Figure 4-14 Attempted trapping of carbocation or radical intermediates.....	256
Figure 4-15 Examination of different bases in the α -arylation of benzamides.....	256
Figure 4-16 Evaluation of different solvents in the α -arylation of benzamides.	257
Figure 4-17 UV-Vis of PC1 with and without 2-160.	258
Figure 4-18 UV-Vis of 2-160.	258
Figure 4-19 Synthesis of enantiopure 2-111.....	297
Figure 4-20 Competition experiment between 2-91 and 3-7.....	309
Figure 4-21 Quenching experiment with PC1 and varied PhBr in EtOAc.	316
Figure 4-22 Quenching experiment with PC1 and varied 2-91 in EtOAc.....	316
Figure 4-23 Quenching experiment with PC1 and varied <i>i</i> -PrBiOxNiCl ₂ in EtOAc.	317
Figure 4-24 Quenching experiment with PC1 and varied PhBr in DMF.	317
Figure 4-25 Quenching experiment with PC1 and varied benzamide in DMF.	318
Figure 4-26 Quenching experiment with PC1 and varied <i>i</i> -PrBiOxNiCl ₂ in DMF.....	318
Figure 4-27 Quenching experiment with PC1 and varied Cs ₂ CO ₃ in DMF.....	319
Figure 4-28 Quenching experiment with PC1 and benzamide, and varied Cs ₂ CO ₃ in DMF.....	319
Figure 4-29 CV of benzamide 2-91.....	321
Figure 4-30 CV of benzamide 2-96.....	321
Figure 4-31 CV of benzamide 2-160.....	322
Figure 4-32 CV of benzamide 2-91 and 2-160.....	322
Figure 4-33 CV of PC12.....	323
Figure 4-34 CV of 3-24.....	324
Figure 4-35 LCMS and analysis of PC1.....	326

Figure 4-36 LCMS analysis of Ir-dF before and after subjecting to reaction conditions.
..... 327

Figure 4-37 LCMS Q-TOF traces for three different photocatalyst at 0 hours (in green)
and 12 hours (in blue), overlaid. 328

List of Abbreviations

Me	methyl
Et	ethyl
<i>i</i> -Pr	isopropyl
<i>n</i> -Pr	propyl
<i>n</i> -Bu	butyl
<i>n</i> -Pent	pentyl
<i>n</i> -Hex	hexyl
hex	hexanes/hexyl
<i>t</i> -Bu	<i>tert</i> -butyl
<i>t</i> -Amyl	<i>tert</i> -amyl
Cy	cyclohexyl
Ph	phenyl
Py	pyridine
Boc	<i>tert</i> -butyloxycarbonyl
TFA	trifluoroacetic acid
COD	1,5-cyclooctadiene
TBS	<i>tert</i> -butyldimethylsilyl
TEMPO	(2,2,6,6-Tetramethylpiperidin-1-yl)oxyl
Pd/C	palladium on carbon

MS	molecular sieve
NHC	<i>N</i> -heterocyclic carbene
THF	tetrahydrofuran
Tol	toluene
NMP	<i>N</i> -methylpyrrolidone
DMF	dimethylformamide
DMAc	dimethylacetamide
glyme	dimethoxyethane
Et ₂ O	diethyl ether
DCM	dichloromethane
DMF	dimethylformamide
DME	dimethoxyethane
DMSO	dimethylsulfoxide
MeCN	acetonitrile
EE	2-ethoxyethanol
SIMes·HCl	1,3-dimesityl-4,5-dihydro-1 <i>H</i> -imidazol-3-ium chloride
IMes·HCl	1,3-dimesityl-1 <i>H</i> -imidazol-3-ium chloride
SIPr·HCl	1,3-bis(2,6-diisopropylphenyl)-4,5-dihydro-1 <i>H</i> -imidazol-3-ium chloride
IPr·HCl	1,3-bis(2,6-diisopropylphenyl)-1 <i>H</i> -imidazol-3-ium chloride
IPrCl·HCl	4,5-dichloro-1,3-bis(2,6-diisopropylphenyl)-1 <i>H</i> -imidazol-3-ium chloride
IAd·HCl	1,3-bis(1-adamantyl)imidazol-3-ium chloride
ICy·HCl	1,3-dicyclohexyl-1 <i>H</i> -imidazol-3-ium chloride
IPr* ^{OMe} ·HCl	1,3-bis(2,6-dibenzhydryl-4-methoxyphenyl)-1 <i>H</i> -imidazol-3-ium chloride

acac	acetylacetone
PMHS	poly(methylhydrosiloxane)
TMDSO	1,1,3,3-tetramethyldisiloxane
KHMDS	potassium bis(trimethylsilyl)amide
DMPB	4,4'-dimethoxybenzophenone
TBADT	tetrabutylammonium decatungstate
DTBP	di- <i>tert</i> -butylperoxide
1,4-BQ	1,4-benzoquinone
DMAP	4-dimethylaminopyridine
TBAF	tetrabutylammonium fluoride
TBACl	tetrabutylammonium chloride
TBAB	tetrabutylammonium bromide
TBAI	tetrabutylammonium iodide
TBHP	<i>tert</i> -butylhydrogenperoxide
<i>m</i> -CPBA	meta-chloroperoxybenzoic acid
LAH	lithium aluminum hydride
pin	pinacolato
bpy	2,2'-bipyridine
dtbbpy	4,4'-di- <i>tert</i> -butyl-2,2'-bipyridine
4,4'-diMebppy	4,4'-di-methyl-butyl-2,2'-bipyridine
4,4'-diOMebppy	4,4'-di-methoxy-butyl-2,2'-bipyridine
5,5'-diMebpy	5,5'-di-methyl-butyl-2,2'-bipyridine
5,5'-diCF ₃ bpy	5,5'-di-trifluoromethyl-butyl-2,2'-bipyridine

dtbbpy	4,4'-di- <i>tert</i> -butyl-2,2'-bipyridine
1,10-phen	1,10-phenanthroline
terpy	2,2':6',2'' terpyridine
bpp	2,6-di(pyrazol-1-yl)pyridine
PyBiOx	bis(oxazolinyl)pyridine
DPPE	1,2-bis(diphenylphosphino)ethane
DPPF	1,1'-bis(diphenylphosphino)ferrocene
rt	room temperature
°C	temperature in degrees Celsius
min	minute(s)
h	hours(s)
d	day(s)
ee	enantiomeric excess
er	enantiomeric ratio
dr	diastereomeric ratio
atm	atmospheric pressure
equiv	equivalent
CFL	compact fluorescent lamp
RSM	recovered starting material
GCMS	gas chromatography mass spectrometry
BDFE	bond dissociation free energy
HAT	hydrogen atom transfer
PCET	proton-coupled electron transfer

NMR	nuclear magnetic resonance
MLCT	metal-to-ligand charge-transfer
ET	electron transfer
ISC	intersystem crossing
OA	oxidative addition
RE	reductive elimination

Abstract

Due to the pervasiveness of carbon-nitrogen and carbon-hydrogen bonds in molecules possessing biological activity, the development of new technologies to manipulate these functional groups at any stage of a synthesis has been a long-standing interest of organic chemists. However, catalytic methods for functional group interconversion have been largely hampered due to their inherently high C–N and C–H bond strength, and the presence of multiple, similarly reactive sites within close proximity. The work described herein focuses on efforts to develop two distinct methodologies to functionalize typically inert C–N and C–H bonds using nickel catalysts, as well as mechanistic investigations into the latter process.

Anilines and their derivatives are synthetically valuable groups that can be transformed into a plethora of useful functionality. By utilizing solvent polarity and ligand size, *N*-heterocyclic carbene-nickel catalysts (NHC-Ni) were shown to convert aryl trialkylammonium salts into either aryl silanes or the parent arene. This method was shown to be chemoselective for aryl trialkylammonium salts over functionalities that are otherwise reactive under NHC-Ni conditions. Further, by varying the silane source, four different aryl silanes were found to be accessible.

Amide bond couplings are among the most prevalent reactions utilized in medicinal chemistry. Although this important motif can be used as a strong directing group in the C–H functionalization of arenes, decorating the C–H bonds of *N*-alkyl benzamides remains

an underexplored area. Thus, a new method was developed, using metallaphotoredox catalysis, to functionalize α -C–H bonds of *N*-alkyl benzamides to furnish α -aryl *N*-alkyl benzamides. This transformation was extended to variety of aryl bromides and benzamides, and an enantioselective variant was developed by employing a chiral bisoxazoline (BiOx) ligand. Furthermore, mechanistic studies were undertaken to better understand the rationale for α -functionalization over δ -functionalization.

Chapter 1

Catalytic Reduction of Aryl Trialkylammonium Salts to Aryl Silanes and Arenes

1.1 Introduction

Simple alkyl and aryl amines are readily available from commercial feedstocks. Typically, these chemicals are produced via “second functionalizations” from olefins and aromatic hydrocarbons on industrial scale.¹ In this process, alkyl amines are usually synthesized through the dehydration of alcohols derived from fermentation or olefin hydration. Anilines, on the other hand, are largely produced from the nitration of benzene and other aromatics, followed by metal-catalyzed reduction. The incorporation of nitrogen into hydrocarbon-based scaffolds is frequently viewed as the first step in the synthesis of more complex molecules, and often the aniline or amine functionality is retained in the target molecule. Further, protecting group strategies for these functional groups have been extensively developed to enable compatibility through dozens of steps, making them ideal handles for downstream derivatization. Regardless, because of their intrinsic value, stability, and requisite harsh conditions for installation (i.e. high temperatures and acidic conditions) these functional groups are less often thought of as ideal for functional group interconversion, and thus methods for their removal have been less explored.²⁻³

Methods to functionalize C–N bonds can be broken up, into five basic categories. These categories are as follows: amide bond activation, pyridinium salt functionalization through one- and two-electron pathways, direct aniline cleavage, diazonium salt

functionalization, and trialkylammonium salt functionalization. For the purpose of this thesis, a strong emphasis on C(sp²)-N activation will be discussed, with C(sp³)-N activation mentioned when necessary to explain the progress of the field.

1.2 Catalytic C–N Functionalization

1.2.1 Amide Bond Activation

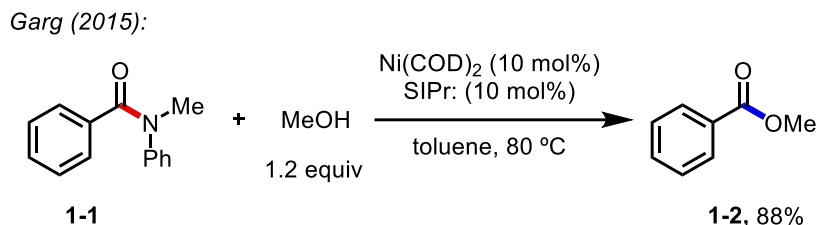


Figure 1-1 Nickel-catalyzed esterification of amides.

With their exceptional bond strength, amides have been a challenging, yet rewarding focal point of many C–N bond cleavage methods. Traditional methods for esterification and organometallic addition into amides require forcing conditions or specialized reagents, such as Weinreb amides, to avoid over addition. However, recent advances in transition metal catalysis have opened the door to mild approaches for new C–O, C–N, and C–C bond forming reaction from amides. Beginning in 2015, the Garg lab successfully showed that nickel(0) complexes could be used to cleave unactivated amides under exceedingly mild conditions (Figure 1-1).⁴ Since then, numerous reports from Garg,⁵ Szostak,⁶ and others, have extended this method to use amides in Suzuki-Miyaura,⁷⁻¹¹ Negishi,¹² Mizoroki-Heck,¹³⁻¹⁴ esterification,¹⁵ transamination,¹⁶⁻¹⁷ amination,¹⁸ and decarbonylation/ reduction.¹⁹⁻²³ The resilience of amides to C–N bond cleavage in many transformations has enabled a paradigm shift in how synthetic chemists make strategic disconnections.

1.2.2 Katritzky Salts For C–N Bond Activation

Since their discovery more than 40 years ago, pyridinium salts have been used as a convenient method to activate C–N bonds.²⁴⁻²⁵ Their ease of preparation and the ability to modulate their steric and electronic properties have led to the synthesis of countless derivatives to promote productive bond cleavage while inhibiting undesired pathways (Figure 1-2). Recently, with the resurgence of single-electron transformations, especially those mediated by photocatalysts and first-row transition metals, a surfeit of new methods

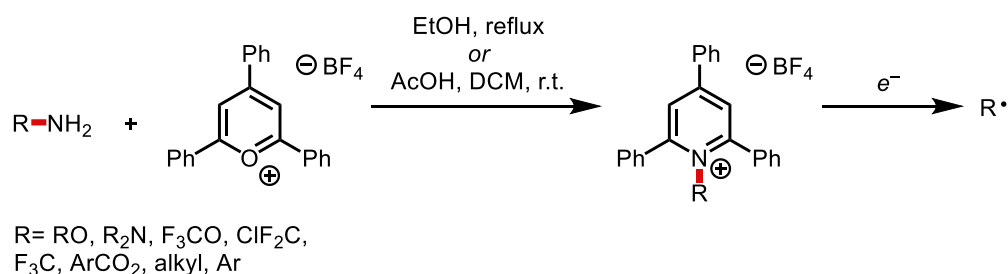


Figure 1-2 Synthesis of Katritzky salts and reduction to give radicals.

have emerged which use these powerful reagents to address unmet synthetic challenges.²⁶⁻
²⁷ Among these transformations include the activation of primary, secondary, tertiary, and aryl C–N bonds. These reagents have been used in Suzuki-Miyaura,²⁸⁻³² Negishi,³³ Mizoroki-Heck, Minisci,³⁴ borylations,³⁵ carbonylations,³⁶⁻³⁷ reductive couplings,³⁸⁻⁴² and transaminations.⁴³ Overall, the use of Katritzky salts for C–N bond functionalization have added numerous methods for constructing C(sp²)–C(sp²), C(sp²)–C(sp³), and C(sp²)–heteroatom bonds, paving the way for future opportunities in late-stage functionalization.

1.2.3 Aniline Bond Activation

Anilines and their derivatives, are commonly found in materials or medicines, ranging from dyes for clothing to active pharmaceuticals.⁴⁴⁻⁴⁶ Their strong donicity in electrophilic aromatic substitution (S_{EAr}) allows for predictable reactivity, and their available lone pair of electrons is useful in directing C–H functionalizations of arenes.⁴⁷⁻⁵² Similarly, they provide a platform to build the carbocyclic core for a number of heterocycles, such as indoles and triazoles, through reactions like the Larock indole synthesis or click chemistry.⁵³ While a versatile functional handle, methods to convert anilines to other groups remains under explored.

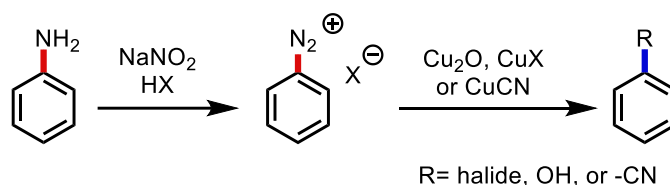


Figure 1-3 Sandmeyer reaction the functionalization of anilines.

With the discovery of the Sandmeyer reaction in 1884, the view of anilines changed from being a terminal functional group to a handle from which to build molecular complexity (Figure 1-3).⁵⁴ Aryl halides, phenols, and nitriles could all be accessed in a short synthetic sequence beginning from the same starting material.⁵⁵ With the advent of cross-couplings in the late twentieth century, interest was revived in the use of anilines for C–C bond formation through their conversion to diazonium salts.⁵⁶⁻⁵⁷ Despite these large advances in the field of aryl diazonium salt functionalization, the need for unsubstituted anilines greatly restricts the accessible starting materials. Additionally, the instability of diazonium salts, manifested in their propensity for explosions and run-away reactions caused by highly exothermic release of N_2 gas, often hinder their use beyond small laboratory settings or necessitate specialized flow setups.⁵⁸

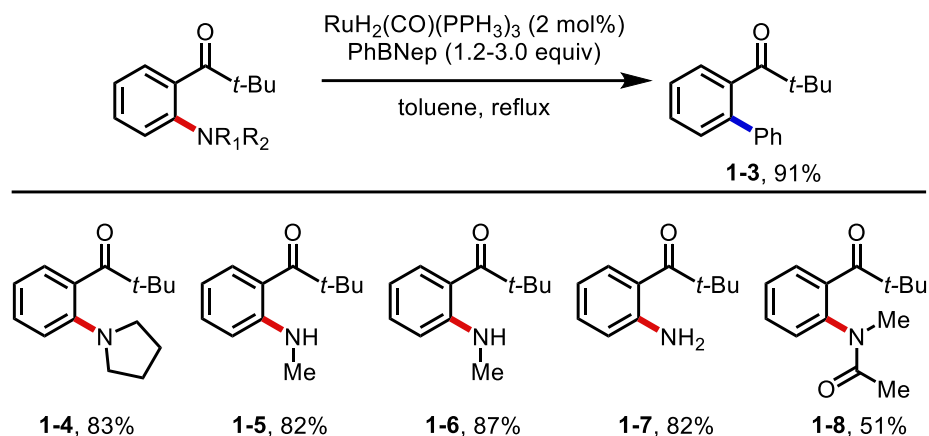


Figure 1-4 Ruthenium-catalyzed ketone-directed cleavage of C–N bonds.

Ideally, no pre-activation would be necessary to cleave $\text{C}(\text{sp}^2)\text{--N}$ bonds, and reactions would be run with low catalyst loadings of earth abundant metals and inexpensive ligands, to give only ammonia as a byproduct. This idea has been very challenging to implement due to several factors including the high strength of $\text{C}(\text{sp}^2)\text{--N}$ bonds, which is accentuated by their ability to delocalize electrons into π -systems. Further anilines and ammonia tend to bind strongly to metals, thus inhibiting catalysis. Despite these challenges, several groups have directly used anilines and dialkyl anilines (Figure 1-4), without pre-activation, to transform C–N bond to $\text{C}(\text{sp}^2)\text{--C}(\text{sp}^2)$ bonds,⁵⁹⁻⁶² $\text{C}(\text{sp}^2)\text{--C}(\text{sp}^3)$,⁵⁹ $\text{C}(\text{sp}^2)\text{--B}(\text{OR})_2$,⁶³ and $\text{C}(\text{sp}^2)\text{--H}$ bonds.⁶⁴⁻⁶⁵

Of these aforementioned methods, several drawbacks include high loadings of catalyst (10-20 mol%), the use of expensive precious metals (i.e. ruthenium), the need for directing groups to promote C–N bond activation, highly reactive organometallic reagents (i.e. Grignards) which limit functional group compatibility, and lastly, high temperatures or harsh UV light. While each of these methods have major drawbacks, they have all advanced our understanding of C–N functionalization and have highlighted the challenges associated with activating such a robust functional group. Building upon these impressive methods, current efforts aim to strive for more ideal reactions that use low loadings of non-

precious metals, are tolerant of sensitive functional groups, and do not generate excessive waste.

1.2.4 Aryl Trialkylammonium Salt Activation

1.2.4.1 C–C Bond Forming Reactions

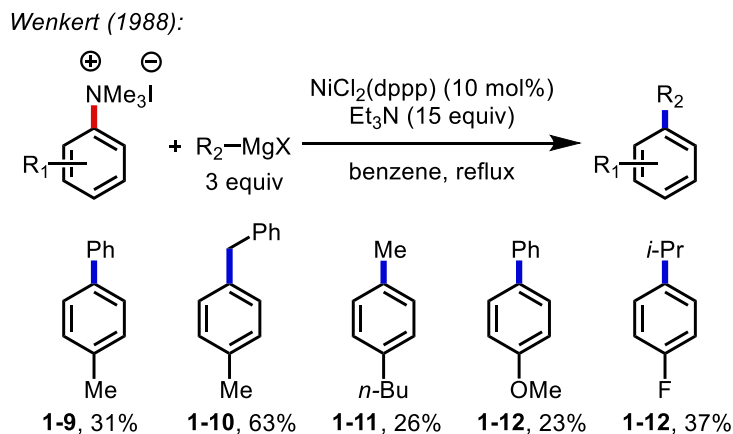


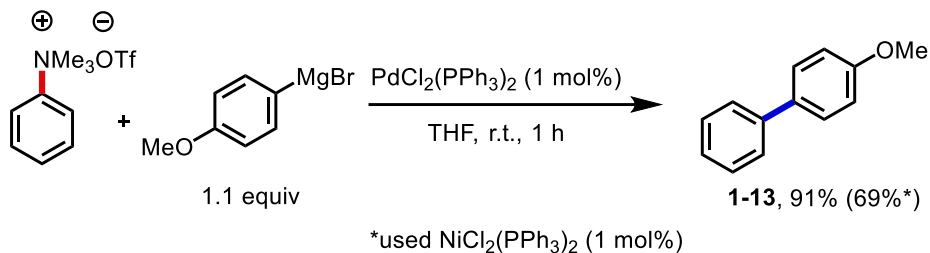
Figure 1-5 Kumada coupling of aryl trialkylammonium salts.

In a seminal report published in 1988,⁶⁶ Wenkert demonstrated the use of aryl trialkylammonium salts as suitable substrates in Kumada couplings using a phosphine-supported nickel catalyst (Figure 1-5). This major advancement C–N functionalization marked a significant change from previous methods of activating aniline derivatives, such as diazonium salts, in that alkylated anilines could be used in these reactions. As dealkylation methods to access unsubstituted anilines often require harsh conditions and give low yields of the desired product,⁶⁷ this strategy of exhaustive alkylation circumvents these issues. The byproducts of these reactions are simple tertiary alkylamines, such as trimethylamine, which are generally benign and easily removed upon work-up. Additionally, aryl trialkylammonium salts can be accessed under mild conditions, in high yields, and produce convenient, easy to handle solids that are bench-stable for extended periods of time.

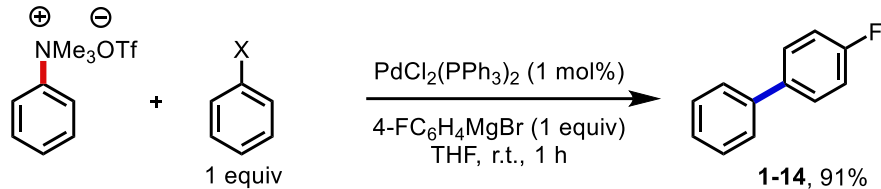
Building upon the work of Wenkert, several methods have emerged that use either iron or palladium to perform the Kumada couplings of aryl trialkylammonium salts with both alkyl and aryl Grignard reagents. An iron-catalyzed method described by Wang *et al*

Reeves (2010):

A)



B)



PhX	yield	recovered ammonium salt	recovered PhX
PhCl	94%	0%	97%
PhBr	94%	4%	92%
PhI	93%	53%	41%
PhOTf	91%	22%	80%

Figure 1-6 Palladium-catalyzed Kumada coupling and chemoselectivity of aryl trialkylammonium salts.

first highlighted the ability to use alkyl Grignards, in combination with an earth-abundant, ligand-free iron catalyst.⁶⁸ While several electron-deficient aryl trialkylammonium salts could be used, no examples of isolated π -systems bearing electron-neutral or -rich substituents are mentioned. This suggests that these systems either did not work or were low yielding, which was in line with the reactivity observed by Wenkert when using electron-rich aryl trialkylammonium salts.⁶⁶ Additionally, the lack of examples using aryl Grignards and the need for excess coupling partner (2 equivalents of Grignard) leaves room for further development of this methodology.

A complimentary method to the iron- or nickel-catalyzed Kumada cross-coupling of aryl trialkylammonium salts, developed by Reeves and co-workers,⁶⁹ allows for a greater scope of aryl Grignards and ammonium salts (Figure 1-6a). Using an air-stable palladium catalyst, PdCl₂(PPh₃)₂, these reactions can be conducted with only 1.1 equivalent of aryl Grignard at room temperature. A unique counterion effect was elucidated, which lead to greater reactivity of ammonium triflate salts compared to previous systems that employed iodide salts. Although this method focused on couplings using palladium salts, cross-couplings could also be achieved with low loadings of NiCl₂(dppp) (1 mol%) when non-coordinating counterions were used. In competition experiments, aryl Grignards were found to react preferentially with trialkylammonium salts over aryl chlorides and bromides, highlighting the chemoselectivity of this method (Figure 1-6b).

MacMillan (2003):

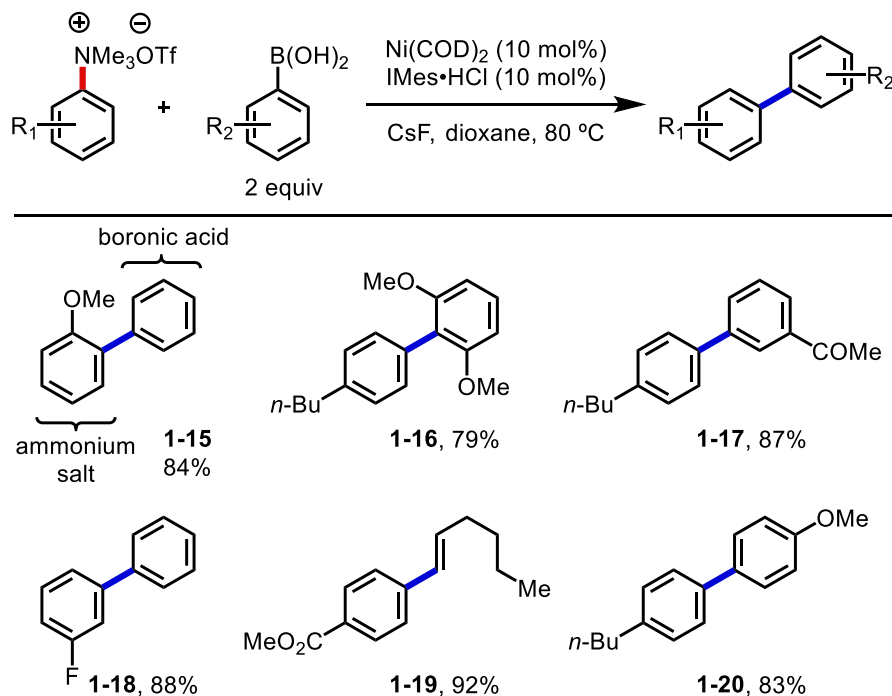


Figure 1-7 NHC-Ni catalyzed Suzuki-Miyaura coupling with aryl trialkylammonium salts.

Shortly after the first report of Kumada couplings with aryl trimethylammonium salts, the MacMillan group reported a nickel-catalyzed method to access biaryls and

styrenes using aryl boronic acids, esters, or alkyl boranes as the coupling partner (Figure 1-7).⁷⁰ This represents one of the first reports of ammonium salt functionalization using NHC-Ni(0) catalysts. Their method provides high yields of biaryls with exceptional electronic and steric variation, both on the aryl trimethylammonium salt and the aryl boron species. While the functional group tolerance in this report is limited, it is expected that the mild reaction conditions and lack of stoichiometric organometallic reagents would allow for this method to be extended to numerous other arenes.

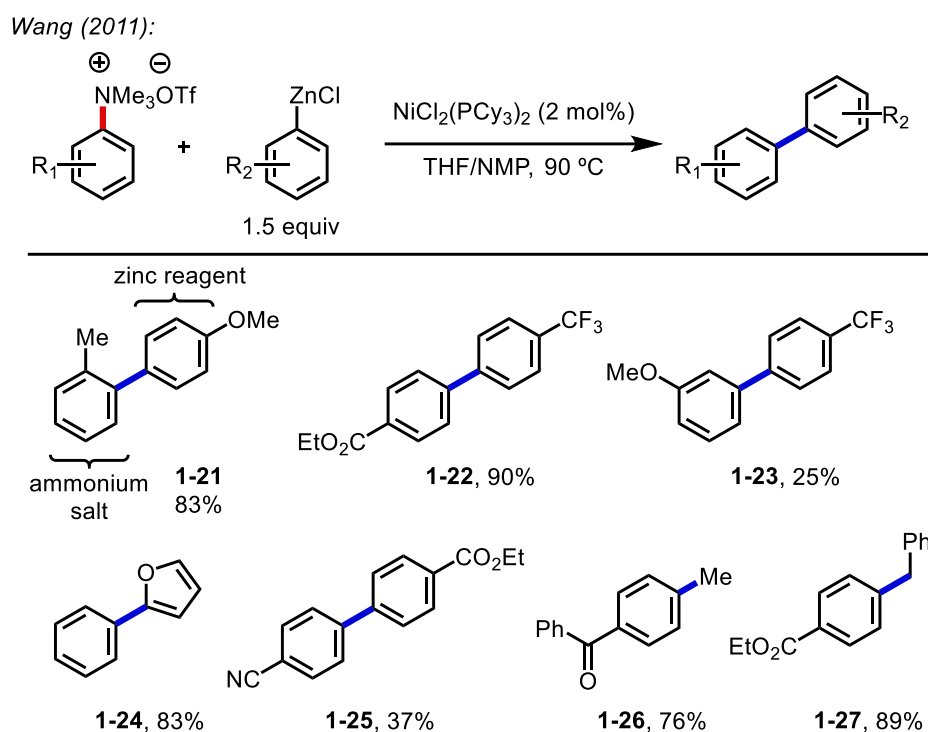


Figure 1-8 Nickel-catalyzed Negishi coupling with aryl trialkylammonium salts.

Organozinc reagents are widely available and often tolerate a number of functional groups compared to organolithium and organomagnesium reagents due to their lower nucleophilicity and basicity. Work by the Wang group has showcased the ability of nickel-phosphine catalysts to cross-couple alkyl- and aryl-zinc reagents with aryl trialkylammonium salts (Figure 1-8).⁷¹⁻⁷³ While functional group tolerance is greater than initial Kumada reports, (substrates bearing esters, nitriles, and ketones can be successfully

used in this procedure) this reaction is still limited in scope, especially for organozinc reagents bearing β -hydrogens, which were not mentioned presumably due to their propensity to undergo detrimental side-reactions such as β -hydrogen elimination. Overall, this method has advantages in the ability to convert ammonium salts into methyl or benzyl groups using low loadings of a nickel catalyst, something that had not be previously demonstrated in related systems of ammonium salt functionalization.

Cao (2019):

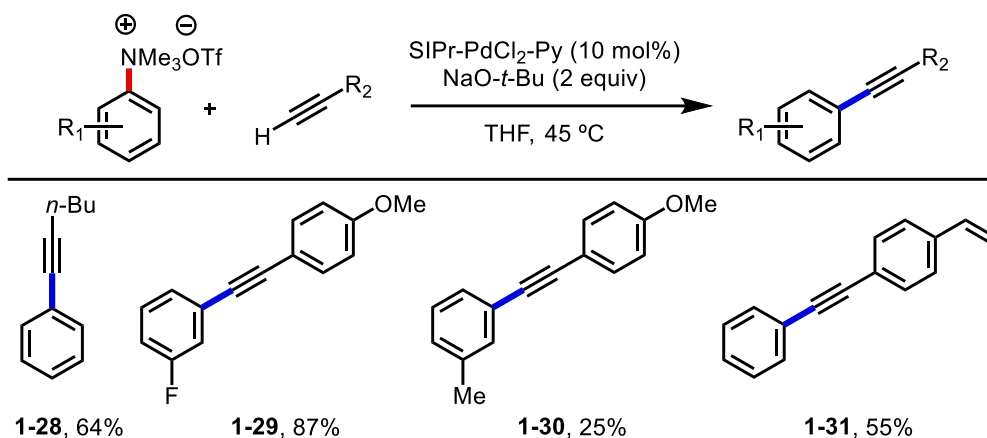


Figure 1-9 Sonogashira coupling using aryl trialkylammonium salts.

In a recent report by the Cao group,⁷⁴ aryl trialkylammonium salts were utilized as coupling partners in a palladium-catalyzed Sonogashira reactions (Figure 1-9). Their findings highlight the need for bulky NHC ligands and alkoxide bases in aryl trialkylammonium salt functionalization. This method allows for the synthesis of non-symmetrical alkyl and aryl alkynes under relatively mild conditions. Both electron-rich and electron-poor ammonium salts and alkynes were tolerated, though electron-poor systems often required extended reaction times and gave substantially lower yields. While the good chemoselectivity of this method was demonstrated with substrates bearing alkyl and aryl halides, as well as olefins capable of engaging in Heck-type reactions, the need for high loadings of palladium remains the largest detriment of this reaction.

Uchiyama (2016):

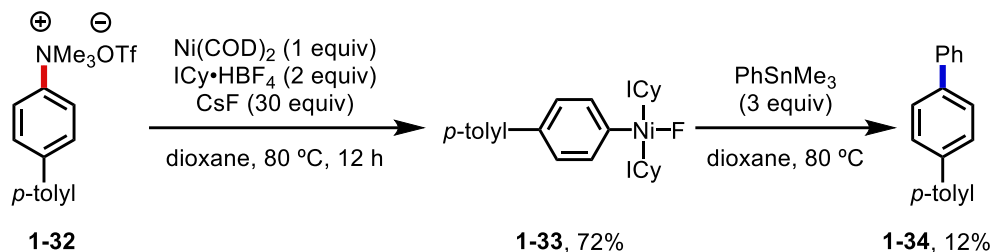


Figure 1-10 Stoichiometric studies with using NHC-Ni-Ar complexes generated from trialkylammonium salts.

Previously missing from the list of C–C bond forming reaction for ammonium salts, a Stille variant of this reaction was explored by Uchiyama (Figure 1-10).⁷⁵ As Stille reactions are typically tolerant of a number of sensitive functional groups, this reaction scope compares to that of the Suzuki and Negishi reactions for aryl trialkylammonium salts. However, additional insights were gained in stoichiometric studies through the isolation of a (NHC)₂Ni(II)ArF species. Despite using an excess of CsF in this reaction, it was determined that CsF was not necessary for oxidative addition to aryl trialkylammonium salts, and that the *trans*-(NHC)₂Ni(II)ArF complex was resilient to transmetalation with PhSnMe₃. Overall, this method shed crucial insights into the activation of ammonium salts using NHC-Ni complexes and the difficulties in transmetalation.

1.2.4.2 C–Heteroatom Bond Forming Reactions

With the advent of the Suzuki cross-coupling, the synthetic community has had a resurgence in methods to install boronic acids and esters. In a seminal report by the Itami lab,⁴⁸ both benzylic and aryl trialkylammonium salts were shown to be competent in the nickel-catalyzed borylation of ammonium salts using B₂Pin₂ (Figure 1-11). Tri-*n*-butyl phosphine with either Ni(COD)₂ or Ni(NO₃)₂•6H₂O provided the best yields for aryl ammonium and benzylic salts, respectively. This method tolerated substitution at the *ortho*-

, *meta*-, and *para*-position for the borylation of aryl ammonium salts, and tolerated several functional groups such as methyl ethers and benzophenones. Unfortunately, this method fails to give appreciable yields with isolated aromatics bearing strongly electron-withdrawing substituents such as trifluoromethyl groups or ketones. Despite its limitations, this method provides a convenient method to access aryl boronic esters and was influential in further developments in C–N borylation.

Itami (2015):

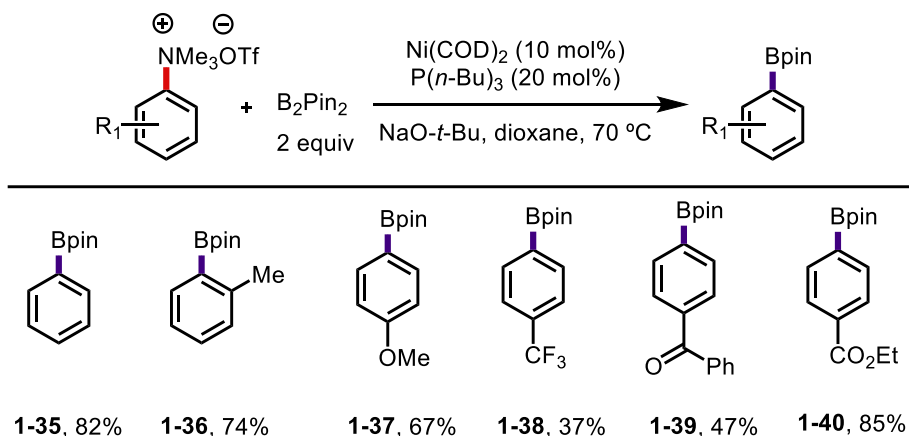


Figure 1-11 Nickel-catalyzed borylation of aryl trialkylammonium salts.

A powerful method developed in the Watson lab highlighted the utility of using benzylic ammonium salts to access enantioenriched benzylic boronates.⁷⁶ This method employs a nickel(0) or nickel(II) salt in conjunction with inexpensive PPh_3 as a ligand to enable the enantiospecific transformation of a number of secondary benzylic ammonium salts to pinacol boranes through an $\text{S}_{\text{N}}2$ type process. The advantages of this transformation lie in the simplicity of the catalyst system, the ability to conduct the reaction at room temperature, and the availability (or facile accessibility) of enantiopure benzylic amines for this reaction. Drawbacks acknowledged by the authors include the need for extended π -systems and the limitations of substitution pattern on the aromatic rings, though the

Shi (2016):

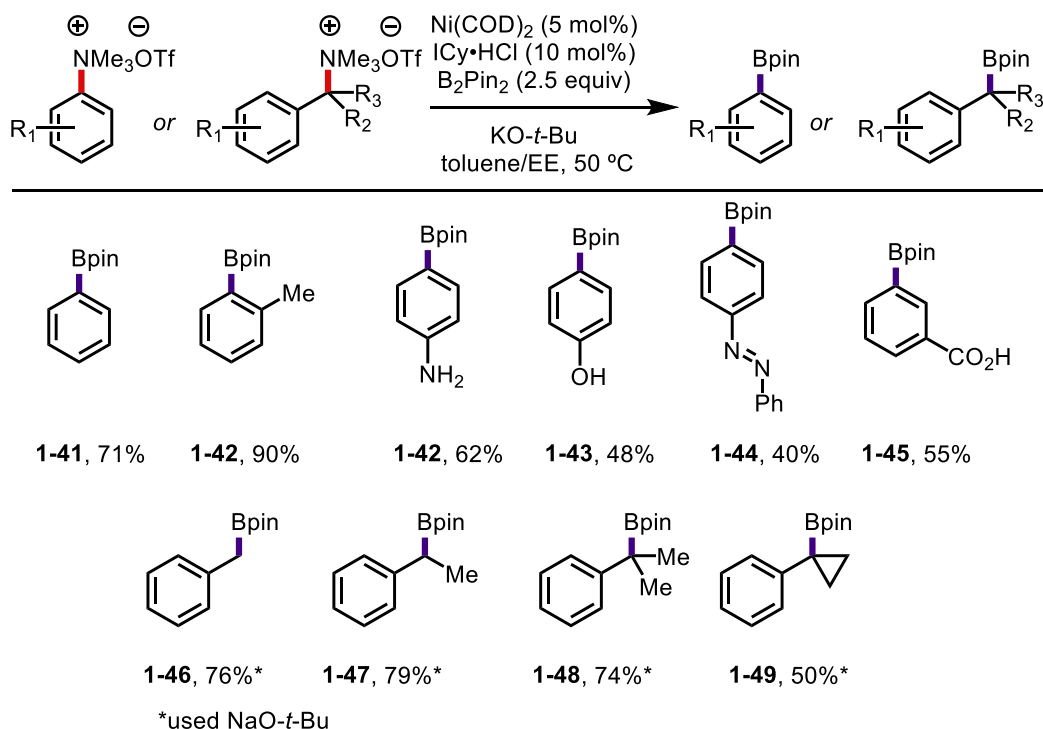


Figure 1-12 Nickel-catalyzed borylation of benzyl and aryl trialkylammonium salts.

former could be partially addressed by increasing the temperature and altering to the catalyst system.

Building upon the work of Itami and Watson, the Shi group improved upon ammonium salt borylation (Figure 1-12).⁴⁴ Key findings include the use of NHCs such as $\text{ICy}\cdot\text{HCl}$ as ligands and $\text{KO}-t\text{-Bu}$ as the base, which allowed them to lower the nickel loading from 10 mol% to 5 mol%, while still providing good yield of boronic esters. Their greater functional group tolerance is highlighted in the numerous examples of primary, secondary, and tertiary benzylic ammonium salts. Arguably, the greatest advancement of this method is the ability to efficiently convert aryl trialkylammonium salts containing isolated π -systems to aryl boronic esters. Numerous functional groups such as amides, free amines, carboxylic acids, phenols, and azobenzene were well tolerated, including

substrates with steric hindrance flanking the ammonium salt, giving high yields of sterically congested aryl boronic esters.

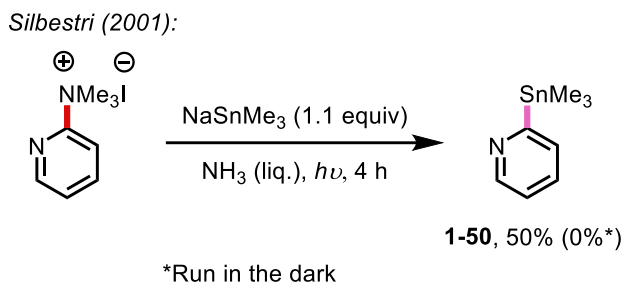


Figure 1-13 Stannylation of aryl trialkylammonium salts under light irradiation.

While traditional cross-couplings typically engage in two electron processes in elementary steps such as oxidation, transmetalation, and reductive elimination, there has been a revived interest in exploring odd-electron chemistry to enable new transformations. Prior to the report by Silbestri and coworkers,⁷⁷ mechanisms involving aryl trialkylammonium salts only evoked two electron processes. In their report, aryl trialkylammonium salts are converted to aryl stannanes using sodium trimethylstannide in liquid ammonium (Figure 1-13). Under these conditions the Silbestri group was able to show that light was beneficial to the reaction, with most substrates giving yields between 0 and 12% yield in the dark, while the analogous reactions run under irradiation using 250W UV lamps (350nm) gave yields in 50-100% range. The substrates reported to undergo this transformation were very simple arenes, most with functionality in the *para*-position, though one example of a pyridine was demonstrated, albeit in moderate yield. Based on the requirement for constant light irradiation and the observation that *p*-dinitrobenzene inhibited the reaction, the authors propose a chain process stemming from an $S_{\text{RN}}1$ (unimolecular radical nucleophilic substitution) reaction. Additionally, they were able to show that arenes bearing both ammonium salts and bromides reacted to give mixtures of distannylated and dehalogenated products. Despite the observed novel

reactivity of aryl trialkylammonium salts in this report, the requirement for cryogenic temperatures and liquid ammonia, as well as the limited substrate scope leave room for further advances in ammonium salt functionalization.

Wang (2019):

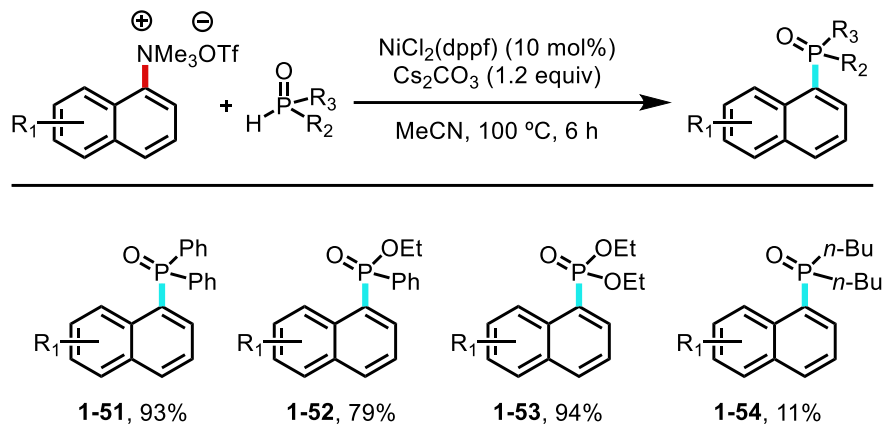


Figure 1-14 Nickel-catalyzed phosphorylation of aryl trialkylammonium salts.

Building upon the wealth of knowledge for nickel-catalyzed aryl trialkylammonium salt functionalization, the Wang lab developed an efficient method to construct C(sp²)-P bonds (Figure 1-14).⁷⁸ Using NiCl₂(dppf) as a catalyst, ammonium salts can serve as aryl electrophiles for the coupling with a number of diarylphosphine oxides, dialkoxyphosphine oxides, and arylalkoxyphosphine oxides. While the scope of this reaction was rather broad for the phosphonate coupling partner, the reaction was restricted to extended π-systems, though 2-pyridyl, benzyl, and allyl ammonium salts could be used, suggesting that a stabilized π-allyl is necessary for oxidative addition to take place, a not uncommon observation in pseudohalide functionalizations.

In a recent report by Uchiyama, etherification was achieved using aryl trialkylammonium salts and alkoxides or phenoxides under metal-free conditions (Figure 1-15).⁷⁹ This method efficiently couples a wide variety of simple, as well as, sterically encumbered alcohols bearing diverse functional groups. A number of aryl

trialkylammonium salts were compatible, though this method was limited to electron-neutral or electron-deficient systems, presumably due to the S_NAr -type nature of this reaction. Because of the efficiency and simplicity of this reaction (conducted at room temperature, using bases commonly found in synthetic labs, and the absence of transition metal catalyst), this method remains the state-of-the-art method for converting ammonium salts to ethers.

Uchiyama (2018):

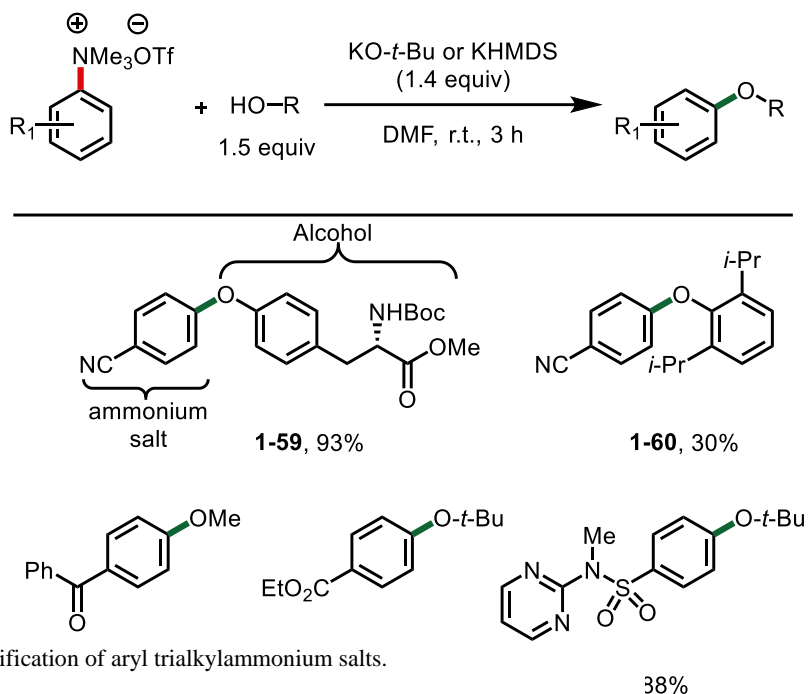


Figure 1-15 Etherification of aryl trialkylammonium salts.

Although there are numerous methods to for alkylating C–N bonds, changing the identity of the alkyl group on *N*-alkyl aniline is challenging. Owing to the lack of mild methods and low yields for $C(sp^3)$ –N dealkylation,⁶⁷ there are few ways to circumvent these issues using existing methods. One alternative to $C(sp^3)$ –N dealkylation is to cleave the $C(sp^2)$ –N bond and replace it with a different amino group. Drawing inspiration from aryl trialkylammonium salt functionalization to give C–C bonds, the Wang group approached this problem by exhaustively alkylating amines, followed by treatment with a

catalytic amount of nickel in the presence of the desired amino group (Figure 1-16).⁸⁰ Gratifyingly, using low loadings of Ni(COD)₂ with an NHC and alkoxide base, they were

Wang (2014):

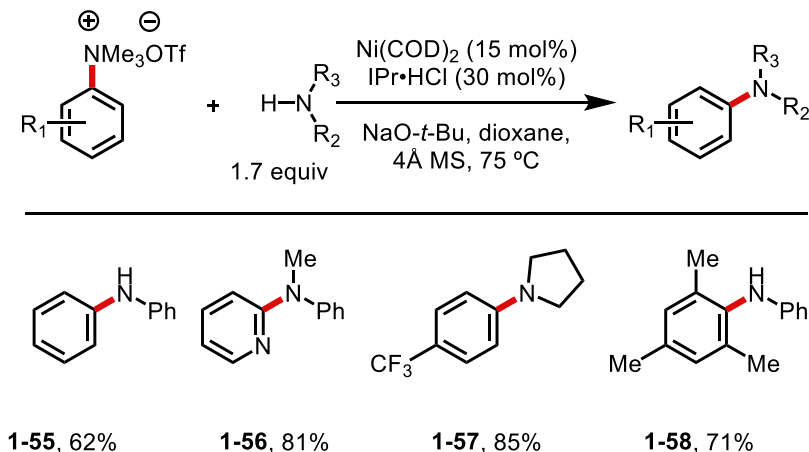
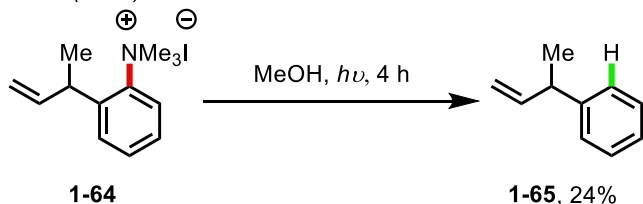


Figure 1-16 Nickel-catalyzed transamination of aryl trialkylammonium salts.

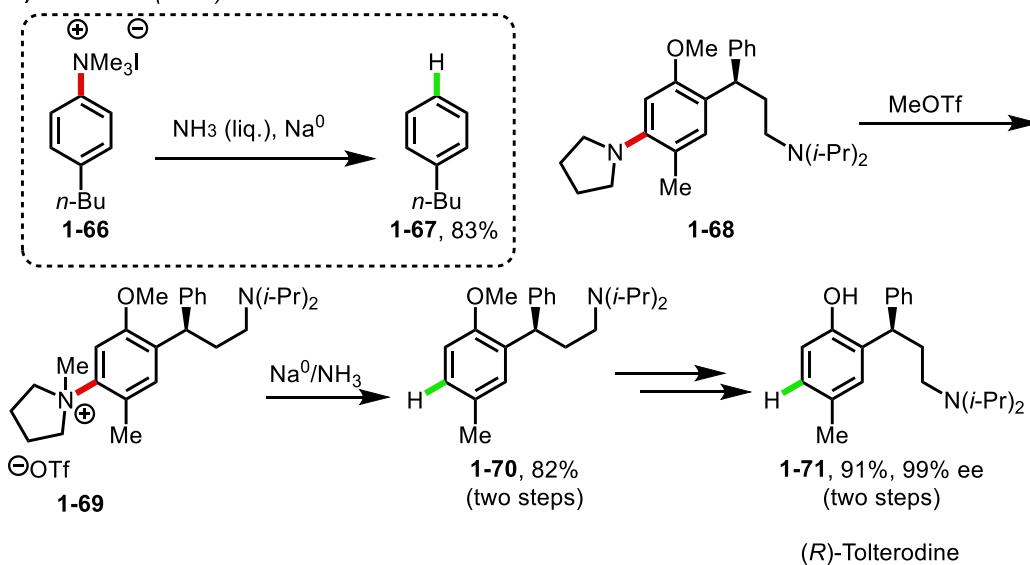
able to install primary, and secondary (both cyclic and acyclic) amines in high yields. This method is quite robust and allows for differing electronics around extended and isolated π -systems. Steric hindrance slightly effects the reaction, but to a lesser degree than other ammonium salt activation methods. The authors noted a strong counterion effect that they attribute to a base-nickel interaction, which stabilizes the active catalyst as well as facilitate the deprotonation of the incoming amine. This counterion effect is a common theme throughout ammonium salt literature.

1.2.4.3 C–H Bond Forming Reactions

A) Scholl (1986):



B) MacMillan (2009):



C) Wang (2016):

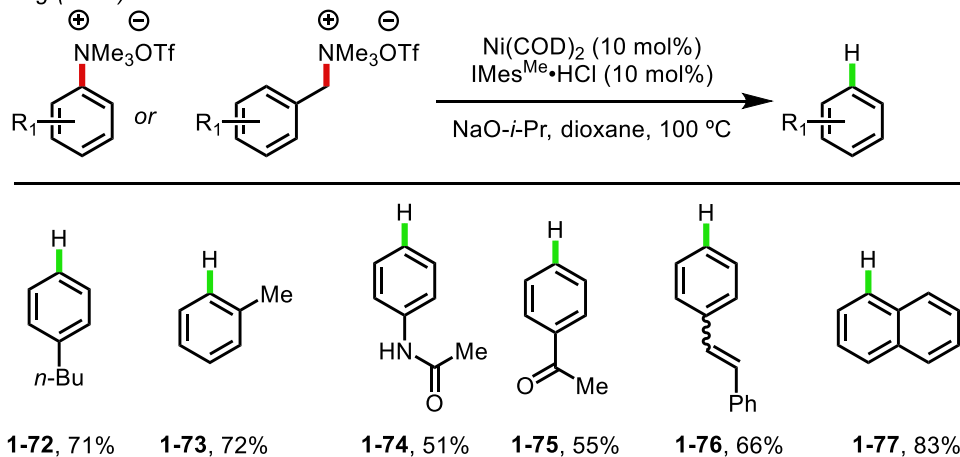


Figure 1-17 Methods for the reduction of aryl trialkylammonium salts to arenes.

Methods for the removal of dialkylamines to give reduced arenes are a useful, yet under explored area of C–N functionalization. Reported in 1986 by Scholl and coworkers,⁶⁴ photosolvolysis of aryl trialkylammonium salts using UV light leads to low yields of

deaminated arenes (Figure 1-17a). These reactions are thought to take place *via* a photo-*Emde* degradation upon excitation with high-energy light. This mechanism was probed using radical traps, wherein the 1,5-cyclization could be isolated when using *ortho*-allyl benzene derivatives. While mechanistically interesting, these reactions are often low yielding and have low functional group tolerance, making this non-ideal for a general ammonium salt reduction.

In a seminal report by the MacMillan lab,⁸¹ Birch reduction conditions (sodium in liquid ammonia), following quaternization with methyl iodide or methyl triflate, provided clean deamination of dialkylarylamines (Figure 1-17b). Whereas this method tolerates a number of different electron-rich aromatics and heterocycles for *ipso* reduction, dissolving metal conditions can be problematic for a number of functional groups and could potentially lead to over reduction of substrates. Still, the authors were able to demonstrate the power of dimethylanilines in directing Friedel-Crafts reactions through the enantioselective synthesis of (*R*)-tolterodine.

Complementary to the Birch reduction developed by MacMillan, Guan and co-workers developed a mild method to reduce benzyl and aryl trialkylammonium salts to toluenes and arenes (Figure 1-17c).⁸² This method leverages the mechanistic understanding gathered from similar ammonium salt activations to develop a Ni-NHC system, using NaO-*i*-Pr as a reducing agent, to furnish the desired arenes in high yield. This reaction is tolerant of a number of functional groups including esters, amides, ketones, and styrenes that might otherwise not be compatible under dissolving metal conditions. Both extended π -systems and isolated aromatics could be used in this reaction with no loss in fidelity. Despite the requisite high reaction temperatures (100 °C), this method is a convenient way to utilize

the directing ability of dialkylanilines prior to traceless removal under reduction conditions.

1.2.4.4 Summary of Aryl Trialkylammonium Salt Functionalizations

Since the initial report of coupling Grignard reagents with aryl trialkylammonium salts, the synthetic community has explored other catalytic transformations to access new C–C bonds through Kumada,^{66, 68-69} Suzuki-Miyaura,^{70, 83} Negishi,⁷¹⁻⁷³ Sonogashira,⁷⁴ and Stille cross-couplings.⁷⁵ Similarly, aryl trialkylammonium salts have been used to form new C–heteroatom bonds through borylation,^{44, 48, 76} stannylation,⁷⁷ phosphorylation,⁷⁸ etherification,⁷⁹ and transamination,⁸⁰ demonstrating the utility of ammonium salts in C–N functionalization. However, methods to reduce aryl trialkylammonium salts to the parent arenes are underdeveloped,^{64, 81-82} and furthermore, accessing other C–heteroatom bonds such as aryl silanes have not yet been realized.

1.3 Importance and Utility of Aryl Silanes in Synthesis

1.3.1 Aryl Silanes in Materials and Medicinal Chemistry

Due to their versatility in materials chemistry,⁸⁴ ability to serve as bioisosteres in medicinal chemistry, and usefulness as a nucleophilic coupling partner, aryl silanes are valuable functional groups. Their properties have been leveraged in semiconductors and polymers, spurring the development of new materials with highly tuned charge transfer and physical properties.⁸⁵⁻⁸⁶ In pharmaceuticals, trimethylsilyl arenes have been used as *tert*-butyl mimics to increased lipophilicity and metabolic stability.⁸⁷ Their stability is also evident by the ability to carry these functional groups through multistep syntheses, only to be activated under very specific conditions. Lastly, these groups have found use in cross-

couplings and functional group interconversion through reactions such as the Hiyama-Denmark coupling^{85, 88} and oxidations to phenols or aryl halides.⁸⁹ The properties of aryl silanes are often ideal in a synthetic setting where their low toxicity and predictable reactivity allow for convenient handling and functionalization.⁹⁰

1.3.2 Traditional Synthesis of Aryl Silanes

The versatility of aryl silanes has led to numerous methods for their preparation, largely deriving from silanes, disilanes,⁹¹⁻⁹² and electrophilic silanes such as silyl chlorides.⁹³ Of these methods, the most common way to access aryl silanes remains lithium-halogen exchange or Grignard formation from aryl halides, followed by quenching with an electrophilic silyl reagent such as a silyl chloride (Figure 1-18). This method has

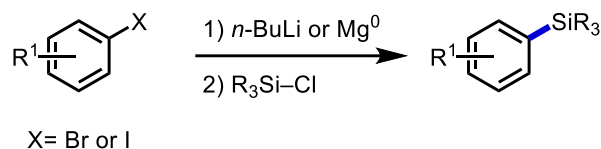


Figure 1-18 Traditional methods for aryl silane synthesis.

advantages in that aryl halides and silyl chlorides are abundant and these reactions are often high yielding. However, this method requires harsh conditions, including the use of highly nucleophilic and basic organometallic species as well as reactive electrophiles, placing substantial limitations on the reaction scope. Similarly, aryl halides cannot always be carried through multistep syntheses, requiring early installation of the silane group. Moreover, there are far fewer methods to install silanes from pseudohalides,⁹⁴ which are often much more abundant, have greater diversity of substitution patterns, and are usually less expensive.

1.3.2.1 C-H Functionalization to Access Aryl Silanes

Hartwig (2014 & 2017):

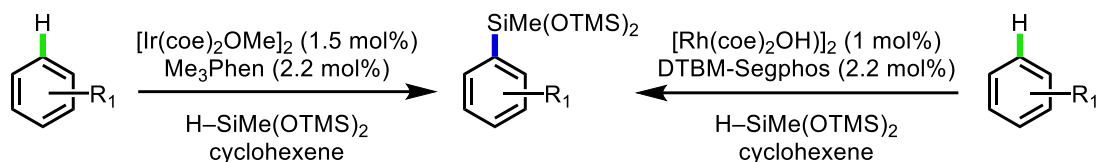


Figure 1-19 Iridium and rhodium catalyzed C–H silylation of unactivated arenes.

A common alternative to lithium-halogen exchange to form aryl silanes, C–H silylation has emerged as a powerful, yet mild method to forge C(sp²)–Si bonds.⁹⁵ The Hartwig group has established several methods using rhodium⁹⁶⁻⁹⁷ and iridium⁹⁸⁻¹⁰² to catalyze C(sp²)–H and C(sp³)–H silylation (Figure 1-19). These methods use commercially available silanes and produce only H₂ as a side-product in the reaction, exemplifying their mildness over lithium-halogen exchange. While arenes possessing C(sp²)–H bonds are much more abundant than aryl halides or pseudohalides, the requirement for a sacrificial hydrogen acceptor in many cases, as well as the limitations in regioselectivity, often requiring the use of directing groups,^{91, 103} are among the largest limitations of these methods. Additionally, the use of designer ligands and precious metals, such as palladium,⁹¹⁻⁹² platinum,¹⁰⁴ rhodium,¹⁰⁵ ruthenium,^{103, 106} and iridium,⁹⁸⁻¹⁰² pose a non-trivial problem in implementing these reactions on large scale. With these considerations in mind, further developments in orthogonal synthesis of aryl silanes are necessary.

To date, there have been a few methods to install aryl silanes under metal-free

Zhang (2016):

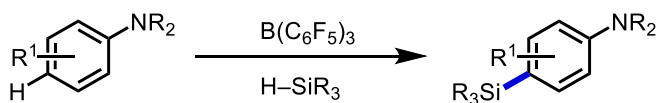


Figure 1-20 Boron-catalyzed C–H silylation of arenes.

conditions.¹⁰⁷ The one distinct approach uses a strong boron-based Lewis acid, in conjunction with electron-rich arenes to form aryl silanes (Figure 1-20).⁸⁹ The

regioselectivity is highly predictable due to the Friedel-Crafts-type nature of this reaction. Many silanes can be installed using this method, though the prerequisite for high temperatures and highly electron-rich arenes limit this reaction to very specific classes of arenes.

Grubbs & Stoltz (2015 & 2017):

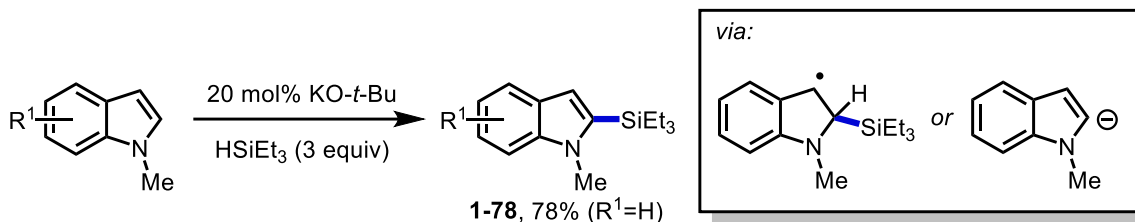


Figure 1-21 KO-*t*-Bu catalyzed C–H silylation.

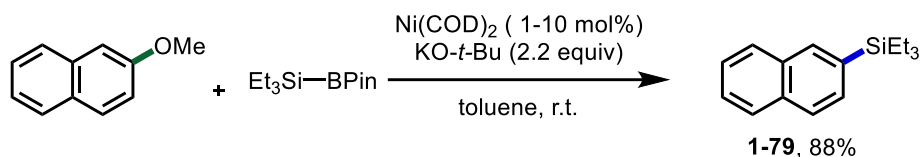
In a collaborative effort between the Stoltz and Grubbs group, important advances in metal-free C–H silylation were developed using KO-*t*-Bu as a catalyst (Figure 1-21).¹⁰⁸ Mechanistic evidence for this powerful method suggests it might follow a different paradigm, relying on 1 e[−] chemistry, whereas all other methods mentioned above engage in 2 e[−] pathways.¹⁰⁹⁻¹¹⁰ This method provides complementary reactivity to rhodium and iridium methods in accessing electron-rich and silylated heterocycles, and has inspired work by other groups in base-mediated methods for silylation of heterocycles.¹¹¹ Although this system efficiently forms C(sp²)–Si bonds from C(sp²)–H bonds, the requirement for specific substrate electronics leaves room for further developments for aryl silane formation.

1.3.2.2 C–O Activation to Access Aryl Silanes

Recently, work by the Martin lab has shown that other phenol derivatives, such as anisoles, can also be used to access aryl silanes (Figure 1-22).¹¹²⁻¹¹⁴ This method has substantial advantages over lithium-halogen exchange in that phenols are an order of

magnitude more abundant than aryl halides and that the reactive the organometallic species is formed in catalytic quantities, permitting a greater functional group tolerance. While some of these methods can be conducted under mild conditions, air- and moisture-sensitive reagents, such as silylboranes,^{94, 114} are required for some C–O activations, which in many cases require more steps to synthesize than the desired aryl silane, making these routes

Martin (2013):



Montgomery (2017):

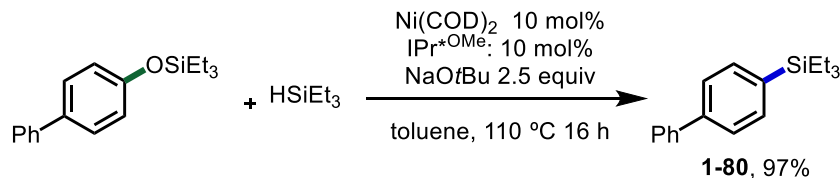


Figure 1-22 Nickel-catalyzed silylation of inert C–O bonds.

inefficient for synthetic chemists.

Related work by our lab has developed a protocol to convert silyl-protected phenols to aryl silanes (Figure 1-22).¹¹⁵ A wide variety of both extended π -systems and isolated aromatics could be effectively used in this chemistry. Orthogonal functional groups often cleaved in nickel C–O activation, such as methyl ethers, pivalates, and carbamates are unreactive under these conditions, allowing silyloxyarenes to be carried through multi-step synthesis unscathed.

Although both these strategies have advantages over other alternative methods in that less expensive metals, such as nickel, can be used, and that regioselectivity is less problematic since there is typically only one reactive site (opposed to multiple C–H bonds in C–H silylation reactions), they are not without their drawbacks. Typically, C–O

activation requires elevated temperature and a large excess of silane reagent. They also struggle to install more complex silanes beyond simple trialkyl silanes, which are less useful in further functionalizations, such as Hiyama-Denmark couplings, due to their low polarizability.^{85, 116}

Overall, there are many methods to install aryl silanes beginning from aryl halides, simple arenes, or phenol derivatives. Of these methods, transition metal catalyzed processes have overcome many of the requisite harsh reaction conditions required in the installation of aryl silanes, though there still remain unaddressed limitations for these methods. While there are a few methods that use abundant C–H or C–O bonds to install silanes, there has been limited research in using C–N bonds as potential coupling partners to form aryl silanes. Taking advantage of the stability and unique reactivity of aryl C–N bonds offers the prospect of developing new methods to access aryl silane, thus circumventing the challenges of existing methods in installing these motifs at the final-stages of a synthetic sequence.

1.4 Results and Discussion

1.4.1 Developing a Nickel-Catalyzed Silylation of Aryl Trialkylammonium Salts

Reaction scheme showing the nickel-catalyzed silylation of aryl trialkylammonium salt **1-80** (4-iodophenyltrimethylammonium iodide) with triethylsilane ($\text{Et}_3\text{Si-H}$, 5 equiv) to produce silylated product **1-81a** (4-(triethylsilyl)phenyl) and reduced product **1-81b** (4-phenylphenyl). Conditions: $\text{Ni}(\text{COD})_2$ (10 mol%), ligand (10 mol%), $\text{NaO-}t\text{-Bu}$ (2.5 equiv), toluene, 90 °C, 12 h.

entry	ligand	yield 1-81a ^a	yield 1-81b ^a	1-81a : 1-81b
1	IMes•HCl	6%	46%	1:7.7
2	SIMes•BF ₄	16%	43%	1:2.7
3	IPr•HCl	74%	20%	3.7:1
4	SIPr•HCl	56%	29%	1.9:1
5	IPr ^{Me} •HCl	65%	23%	2.8:1
6	IPr ^{*OMe} :	86%	14%	6.1:1
7	IPr ^{*OMe} •BF ₄	76%	17%	4.5:1

Table 1-1 Initial ligand screen for the silylation of aryl trialkylammonium salts. ^a Yields were determined by GCMS analysis using tridecane as an internal standard.

Drawing inspiration from work within our own lab on the silylation of silyloxyarenes, conditions for the development of this transformation mirrored those optimized results. At the onset of this study, different NHC ligands were targeted for the silylation of aryl trialkylammonium salts using trialkylsilanes. Initial screens commenced with **1-80**, $\text{Ni}(\text{COD})_2$, NHC ligands, HSiEt_3 , and $\text{NaO-}t\text{-Bu}$ in toluene at 90 °C for 12 hours (Table 1-1). Surprisingly, all the NHCs tested gave varying amounts of silylation (**1-81a**), with $\text{IPr}^{\text{*OMe}}$ performing the best (Table 1-1, entry 6)! Also interesting, most of the NHCs tested gave appreciable amounts of reduced product, with smaller ligands like IMes giving the best results (Table 1-1, entry 7); this is important to note because at the time catalytic

methods for the removal of ammonium salts and aniline derivatives required harsh conditions, cryogenic temperatures, and were not tolerant of a number of functional groups. Focusing on the silylation of aryl trialkylammonium salts first, further optimization was pursued in the hopes of suppressing undesired reduction and lowering the temperature. Although reactivity was observed at room temperature, reactions were ultimately conducted at slightly elevated temperatures (40 °C) for reproducibility.

Reaction scheme: 1-81 + Et₃Si-H (5 equiv) $\xrightarrow[\text{solvent, 40 } ^\circ\text{C, 6 h}]{\text{Ni(COD)}_2 \text{ (10 mol\%)} \text{ IPr}^*\text{OMe}\cdot\text{HCl (10 mol\%)} \text{ NaO-}t\text{-Bu (2.5 equiv)}$ 1-81a + 1-81b

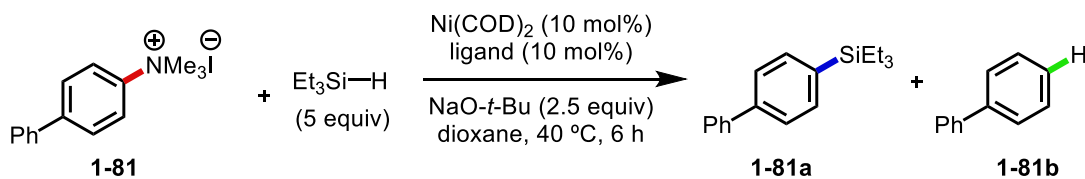
entry	ligand	time	yield 1-81a ^a	yield 1-81b ^a	1-81a:1-81b
1	Et ₂ O	6 h	5%	7%	1:1.3
2	DME	6 h	<1%	3%	–
3	THF	6 h	65%	35%	1.8:1
4	dioxane	6 h	89%	11%	7.7:1
5	toluene	6 h	4%	6%	1:1.4
6	CH ₃ CN	6 h	5%	71%	1:54.2
7	MeOH	6 h	<1%	<1%	–
8	DMF	6 h	<1%	80%	–
9 ^b	dioxane	6 h	77%	16%	4.9:1
10 ^c	dioxane	6 h	77%	18%	4.2:1
11 ^d	dioxane	6 h	7%	20%	1:2.9

Table 1-2 Solvent effects on the silylation of aryl trialkylammonium salts. ^a Yields were determined by GCMS analysis using tridecane as an internal standard. ^b 5 equiv sulfolane; ^c 1 equiv MeOH added. ^d 1 equiv H₂O added.

From here, variety of solvents were screened in this reaction (Table 1-2). It was observed that solvent identity played a crucial role in this reaction. Several acyclic ethereal solvents, such as Et₂O and DME (Table 1-2, entries 1 & 2), did not provide ample amounts of the desired silylated product, however, cyclic ethereal solvents like THF and dioxane performed well (Table 1-2, entries 3 & 4), giving full conversion. While THF gave a 1.8:1 ratio of silylated to reduced product, dioxane gave a more selective, 7.7:1 ratio. Other non-polar, aprotic solvents like MeCN or toluene did not provide substantial amounts of silylated product (Table 1-2, entries 5 & 6), nor did polar-protic or polar-aprotic solvents like MeOH or DMF (Table 1-2, entries 7 & 8). However, DMF did provide substantial amounts of the reduced product (**1-81b**), which will be discussed in a later section. Using this information regarding solvent control for chemoselective conversion of aryl trialkylammonium salts to silanes or arenes, a more extensive screening of ligands was undertaken.

Having identified dioxane at the best solvent for this reaction, a broader set of ligands were reexamined. Phosphine-type ligands such as PPh₃ and PCy₃ did not give appreciable amounts of either silylation or ammonium salt reduction (Table 1-3, entries 1 & 2). Small NHCs or those bearing alkyl substituents, such as IMes, SIMes, and ICy, also failed to convert the starting material to the aryl silane (Table 1-3, entries 3-5). Interestingly, bulkier NHCs, like IPr (Table 1-3, entry 6), gave some amount of aryl silane and furthermore, changing the electronics of the imidazolium ring had a noticeable effect (Table 1-3, entries 7-9). Thus far, bulky, more electron-rich NHCs, like IPr^{Me}, gave the best results. It was not surprising that when comparing these ligands to IPr^{*OMe}, a drastic increase in yield was observed (Table 1-3, entry 10). The high steric demand and increased

electron density of the NHC side-arms on IPr*^{OMe} seemed to bolster the yields for silylation, while minimizing the production of reduced arene. This trend holds well with



entry	ligand	yield 1-81a ^a	yield 1-81b ^a	1-81a : 1-81b
1	PPh ₃	<1%	5%	–
2	PCy ₃	<1%	<1%	–
3	<1%	6%	<1%	–
4	SIMes•HCl	5%	19%	1:3.8
5	ICy•HCl	<1%	1%	–
6	IPr•HCl	14%	7%	2:1
7	IPr•HCl	15%	7%	2:1
8	IPr ^{Me} •HCl	21%	5%	4.6:1
9	IPr ^{Cl} •HCl	12%	8%	1.5:1
10	IPr* ^{OMe} •HCl	89%	11%	7.7:1
11 ^b	IPr* ^{OMe} •HCl	54%	13%	4.3:1
12 ^c	IPr* ^{OMe} •HCl	77%	15%	5.2:1

Table 1-3 Assessment of ligands for the silylation of aryl trialkylammonium salts at 40 °C. ^a Yields were determined by GCMS analysis using tridecane as an internal standard. ^b Run at 25 °C. ^c Run using 5 mol% Ni(COD)₂ and 5 mol% IPr*^{OMe}•HCl for 19 h.

other nickel-catalyzed silylation methods explored within our lab.¹¹⁵ As mentioned earlier, it was found that lowering the temperature had a negative effect on yield (Table 1-3, entry 11 and lowering the catalyst loading gave a slight drop in the amount of silylated arene

produced (Table 1-3, entry 12). These most optimized conditions were carried forward as the identity of the base was next examined.

entry	ligand	yield 1-81a ^a	yield 1-81b ^a	1-81a : 1-81b
1	LiO- <i>t</i> -Bu	41%	5%	8:1
2	NaO- <i>t</i> -Bu	89%	11%	7.7:1
3	KO- <i>t</i> -Bu	48%	7%	6.5:1
4 ^b	NaO- <i>t</i> -Bu	72%	13%	5.6:1
5	none	<1%	<1%	–
6	NaOMe	24%	<1%	–
7	Cs ₂ CO ₃	<1%	<1%	–
8	Et ₃ N	14%	7%	6.8:1
9	pyridine	55%	12%	4.5:1

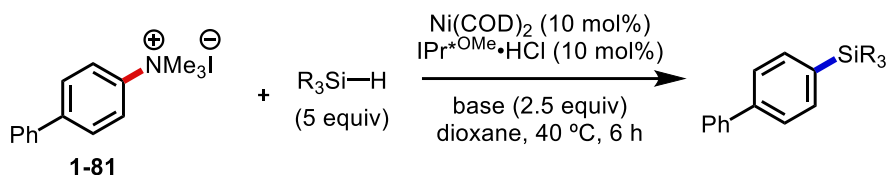
Table 1-4 Screening of organic and inorganic bases for the silylation of aryl trialkylammonium salts. ^a Yields were determined by GCMS analysis using tridecane as an internal standard. ^b Using 1 equiv of base.

Despite the initial success of NaO-*t*-Bu, the effects of counter ions on similar systems necessitated an evaluation of bases for this reaction. A strong counterion effect was observed in this system, with LiO-*t*-Bu and KO-*t*-Bu underperforming when compared to NaO-*t*-Bu (Table 1-4, entries 1-3). The amount of base used was also important as seen from the reduction in yield when using 1 equivalent or no reaction when omitting the base altogether (Table 1-4, entries 4 & 5). Lastly, other inorganic and organic bases were less effective than NaO-*t*-Bu in this chemistry (Table 1-4, entries 6-9).

As discussed in other methods of aryl trialkylammonium salt activation,^{79-80, 115} the identity of the counterion can play a crucial role in reaction efficiency – similar empirical results were also observed in this chemistry. Further, in this reaction, we hypothesize that the base serves several roles. Initially, the base is responsible for the deprotonation of the NHC salt to form a nickel-carbene complex. Therefore, the base used in this reaction must be strong enough to deprotonate an imidazolium salt, while non-nucleophilic enough to engage in other, off-cycle, coupling reactions, such as etherification or transamination, mentioned earlier in this chapter. Secondly, the base is responsible for sequestering any acid generated in the reaction. While the byproducts of this reaction are tertiary amines, which could in theory act as the base for this reaction, the high volatility of these species could result in their loss to the headspace of the reaction or atmosphere, necessitating additional exogenous base. Thirdly, mechanistic studies and the observation of important counterion effects in these types of reactions, the base could be engaging with the catalyst to promote some energetically demanding step in the catalytic cycle.

Earlier reports suggest on C–O activation of aryl ethers suggest that nickel-ate species are responsible for high reactivity in related transformations.¹¹⁷⁻¹¹⁹ Specifically, the addition of an alkoxide base to a low-valent nickel species likely results in an anionic complex, allowing for more facile oxidative addition. Therefore, the identity of the counterion of the base could play a crucial role in the stability and energetics of nickel-ate complex formation. Similarly, this negatively charged nickel-ate complex could engage with the cationic substrate through electrostatic interaction, leading to productive catalysis. Using more polar solvents, however, which can stabilize charged species, could potentially discourage these electrostatic interactions between the substrate and catalysts. Contrarily,

less polar solvents may favor the formation of cage-species to minimize the solvation of charged species, which both favors nickel-ate complex formation and catalyst-substrate

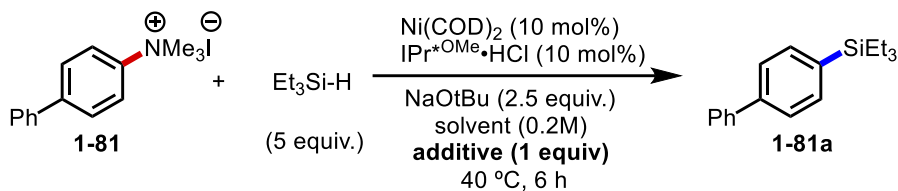


entry	silane	yield ^a
1	Et ₃ SiH	86%
2	PhMe ₂ SiH	60%
3	BnMe ₂ SiH	85%
4	allylMe ₂ SiH	<1%
5	Et ₂ SiH ₂	<1%
6	PhMeSiH ₂	<1%
7	(EtO)Me ₂ SiH	<1%
8	(EtO) ₃ SiH	<1%
9	(TMSO) ₃ SiH	<1%
10	Me(TMSO) ₂ SiH	15%
11 ^b	(TMS) ₃ SiH	<1%
12 ^c	Me ₃ Si-SiMe ₃	<1%

Table 1-5 Probing compatible silanes in the silylation of aryl trialkylammonium salts. Reactions were analyzed by GCMS. ^a All yields are isolated yields.

interaction. While detailed study of the solvent/base effects observed are outside the scope of this research, empirical data suggests that, of the solvents and bases examined, dioxane/NaO-*t*-Bu gave the best yields of aryl silane. These results are supported by other

literature reports, as discussed above. Regardless, due to the limited knowledge of the



entry	additive	yield 1-81a ^a
1	2-hexene	68%
2	1-octene	<1%
3	ethylbut-2-ylonate	<1%
4	methyl acetamide	4%
5	benzotrile	<1%
6	benzaldehyde	34%
7	acetophenone	63%
8	1-bromodecane	<1%
9	1-chloro-2-methylbenzene	<1%
10	4-bromobenzotrifluoride	<1%
11	triethylamine	48%
12	morpholine	50%
13	octylamine	5%
14	1-methyl indole	74%
15	benzofurane	9%

Table 1-6 Glorius-type screen of different additives and their effect on aryl silane yield. ^a Yields were determined by GCMS analysis using tridecane as an internal standard.

active catalytic species in transformations such as the ones described

within this chapter, it is important to consider all of these factors in designing similar

transformations.

Lastly, in order to access synthetically useful aryl silanes, an array of different silanes were tested in this reaction (Table 1-5). Complementary to existing methods of C–H and C–O silylation, several different silanes could be successfully incorporated. Of these silanes tested, simple alkyl and aryl silanes performed best (Table 1-5, entries 1-3), as well as the synthetically useful Me(TMSO)₂SiH (Table 1-5, entry 10), albeit in low yields. During this screen, it was found that silanes bearing allyl or alkoxy groups were incompatible in this reaction (Table 1-5, entries 4 & 7-9). Unfortunately, silanes with multiple hydrides or silicon-silicon bonds could also not be used in this transformation (Table 1-5, entries 5 & 6).

After identifying the optimum conditions and compatible silane coupling partners for this transformation, a brief Glorius-type screen was conducted to evaluate the preliminary functional group tolerance.¹²⁰ To do so, a series of small molecules containing different functional groups (1 equivalent of each additive) were added at the start of a productive reaction. Each reaction was then analyzed for yield of aryl silane. From these experiments, it was found that internal alkenes gave only small decreases in yield, while terminal alkenes and alkynes inhibited product formation (Table 1-6, entries 1-3). Some electrophiles, such as ketones, and aldehydes to a lesser extent, gave small decreases in yield (Table 1-6, entries 6 & 7). Acetamides and benzonitriles were detrimental to product formation (Table 1-6, entries 4 & 5). All aryl and alkyl halides tested in this reaction proved incompatible, and thus gave no yield of the desired product (Table 1-6, entries 8-10), which is contrary to that observed with aryl trialkylammonium salts in Kumada reactions.⁶⁹ Tertiary and secondary amines could be tolerated in this reaction, while adding primary

amines resulted in very low yields (Table 1-6, entries 11 & 12). Lastly, several nitrogen-containing heterocycles, like indole were tolerated to some degree, though benzofuran was not (Table 1-6, entries 14 & 15).

1.4.2 Substrate and Silane Scope of the Nickel-Catalyzed Silylation of Aryl Trialkylammonium Salts

Trialkylammonium Salts

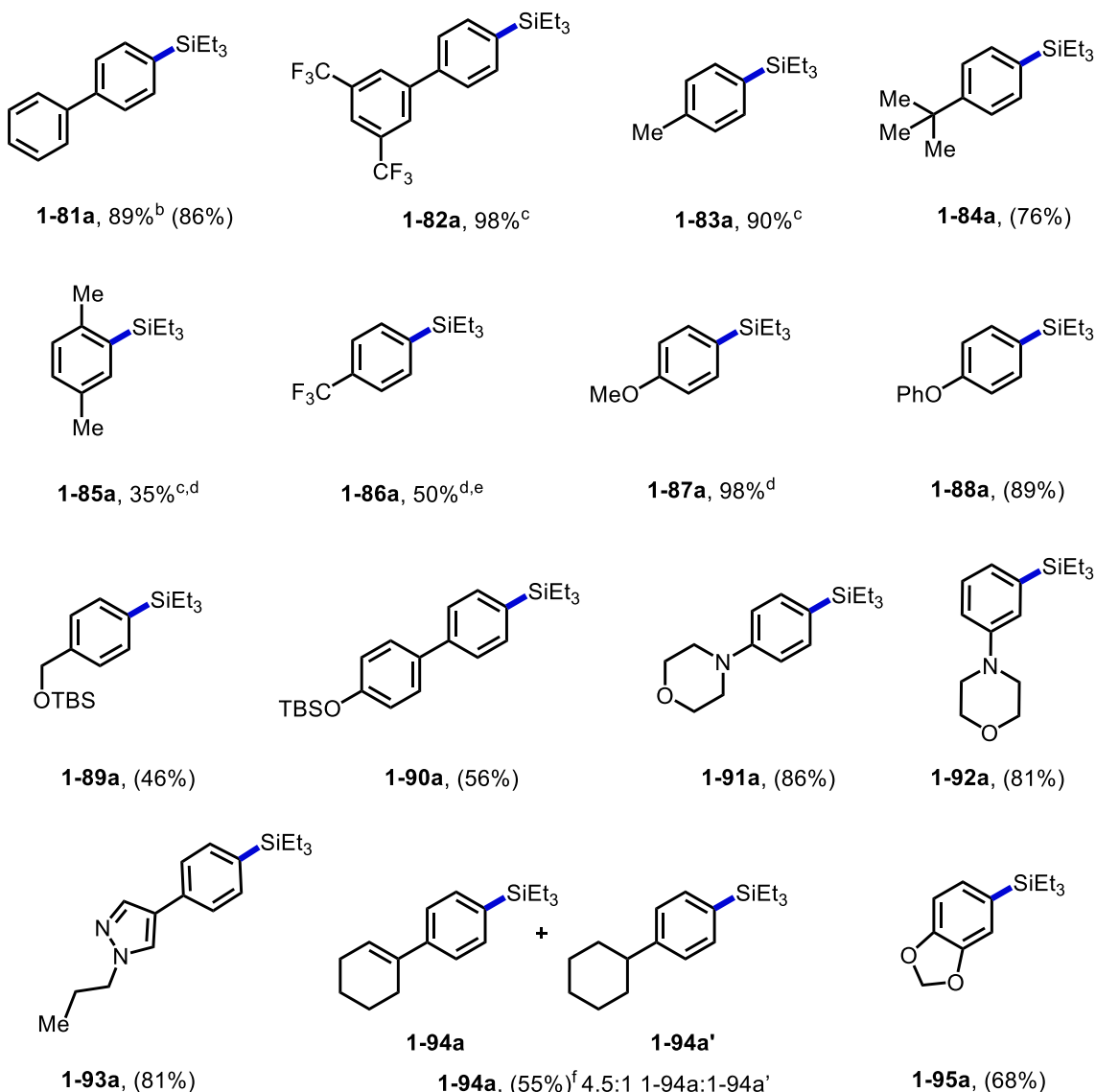
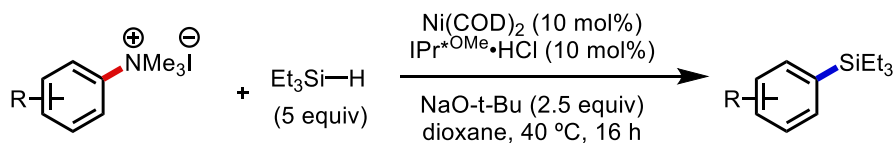


Table 1-7 Substrate scope for the silylation of aryl trialkylammonium salts using triethyl silane. ^a Yields in parenthesis are isolated yields. ^b Yield was determined by GCMS analysis using tridecane as an internal standard. ^c 3 equiv of silane used. ^d Yield determined by NMR using CH₂Br₂ as an internal standard. ^e 2 equiv of silane used. ^f Reaction run under a stream of nitrogen.

Having established optimized conditions for the silylation of aryl trialkylammonium salts, and briefly exploring the tolerance of several small molecules, the substrate scope of this reaction was explored using triethyl silane (Table 1-7). As observed in the optimization, biphenyls such as **1-81a** and **1-82a** were well tolerated, as were isolated π -systems such as **1-83a** and **1-84a**, though ortho substitution was detrimental to yields (**1-85a**). While electron-deficient aromatics (**1-86a**) provided modest yields, electron-rich systems, such as anisoles (**1-87a**), phenyl ethers (**1-88a**), and silyl protected alcohols (**1-89a**) and phenols (**1-90a**), gave modest to excellent yields. These examples also exemplify the chemoselectivity for ammonium salt activation over other C–O electrophiles that have been shown to react under similar conditions.^{114-115, 121} Gratifyingly, saturated and unsaturated heterocycles were well tolerated in this reaction (**1-91a**, **1-92a**, and **1-93a**). Lastly, sensitive functionality, such as olefins (**1-94a**) and acetals (**1-95a**) gave the desired products in good yields. Notably though, over the course of the reaction with **1-94a**, it was observed that a near equal ratio of hydrogenation of the alkene was observed. As these reactions were run in a sealed tube, we hypothesized that H₂ gas was being generated under the reaction conditions, leading to nickel-catalyzed hydrogenation of the olefin. To avoid these deleterious side-reactions, **1-94a** was run with a N₂ inlet rather than in a sealed tube, to sweep the headspace. Gratifyingly, this increased the ratio of non-hydrogenated to hydrogenated product to 4.5:1. Overall, a number of useful functional groups and sterically and electronically differentiated aryl trialkylammonium salts were tolerated, demonstrating the utility of accessing aryl trialkyl silanes from aniline derivatives.

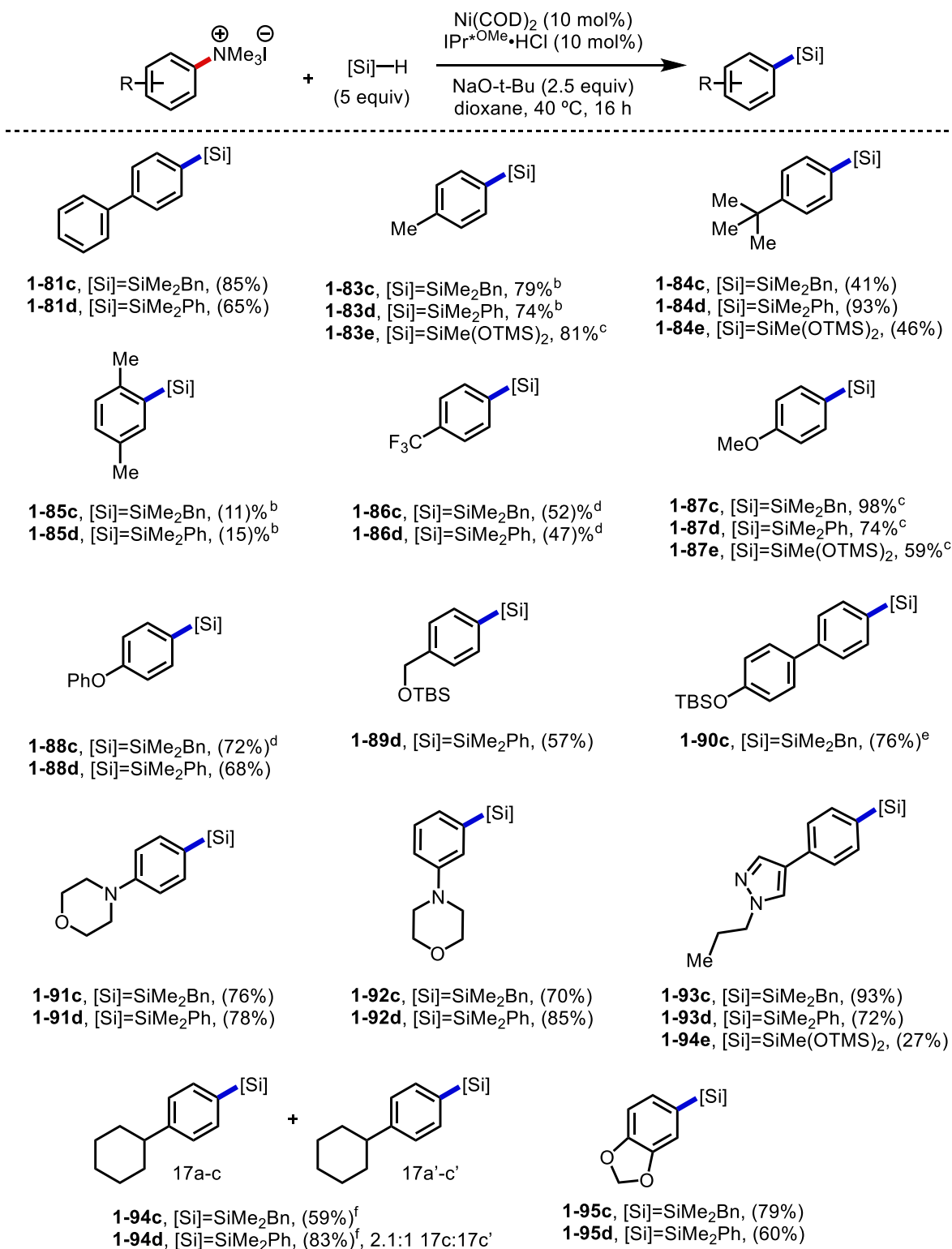


Table 1-8 Silane scope of for the silylation of aryl trialkylammonium salts. ^a Yields in parenthesis are isolated yields. ^b 3 equiv of silane used. ^c Yield determined by NMR using CH₂Br₂ as an internal standard. ^d 2 equiv of silane used. ^e Run on a 0.52 mmol scale. ^f Reaction run under a stream of nitrogen.

Having assessed the substrate scope of silylation aryl trialkylammonium salts using

triethyl silane, other silanes were tested (Table 1-8). BnMe_2SiH followed a similar trend to that of Et_3SiH , providing good to excellent yields in most cases. As expected, this silane performed poorly with electron-deficient arenes and gave very low yields for substrates containing ortho-substitution. However, unlike the reaction using triethyl silane, the integrity of the alkene was preserved when **1-94** and BnMe_2SiH were subjected to the reaction conditions. PhMe_2SiH had similar reactivity to Et_3SiH , suffering from the same pitfalls in ortho-selectivity, though a 2.1:1 ratio of non-hydrogenated to hydrogenated product was observed when subjecting **1-94** to the reaction conditions.

Lastly, although $\text{Me}(\text{TMSO})_2\text{SiH}$ provided low yields of silyated product, the value of these products in down-stream functionalization prompted an examination of the substrate scope (Table 1-8). Some isolated aromatics provided modest to good yields, and some heterocycles were tolerated. However, unlike the PhMe_2SiH and BnMe_2SiH , $\text{Me}(\text{TMSO})_2\text{SiH}$ did not provide the desired product, or provided very low yields, for a number substrates. This low reactivity could be due to the different electronics of the silane (related alkoxy silanes also were not compatible in this system) or the large steric profile of the silane (TMS_3SiH , which is very bulky, did not work in this reaction). Nonetheless, this silane could be used in several substrates, bringing access to useful aryl silanes from aryl trialkylammonium salts.

1.4.3 Optimization of the Nickel-Catalyzed Reduction of Aryl Trialkylammonium

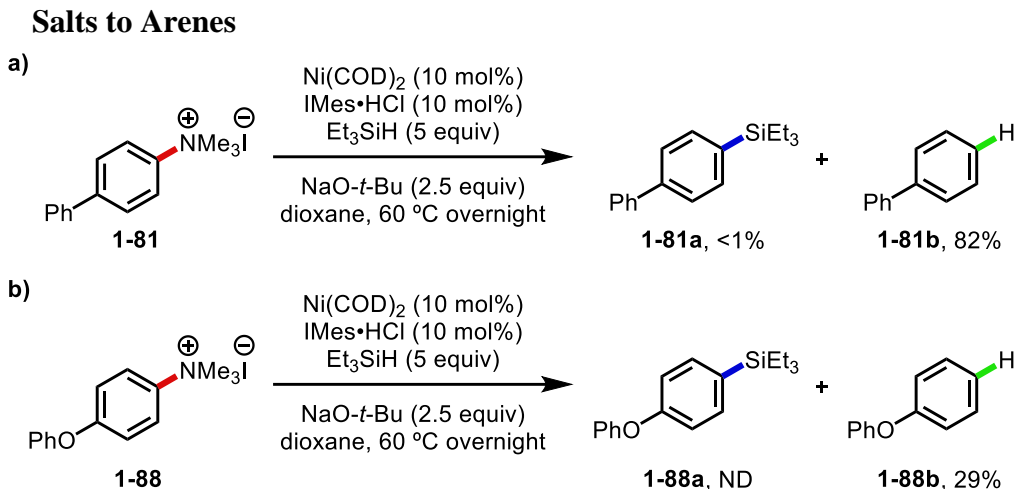
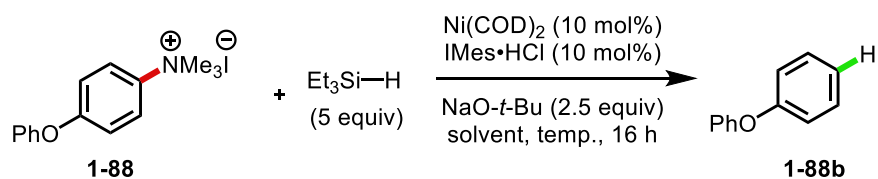


Figure 1-23 Reduction of aryl trialkylammonium salts and limitations of this method.

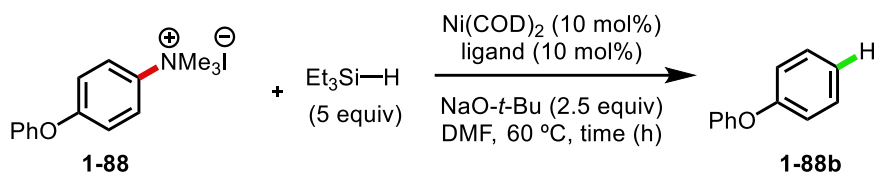
During the exploration of the silylation of aryl trialkylammonium salts, it was discovered that the identity of the NHC and solvent had a drastic effect on the ratio of silylation and reduction to the parent arene. Having developed a robust method to convert



entry	solvent	temperature	yield 1-88b ^a
1	dioxane	60 °C	29%
2	THF	60 °C	27%
3	DMF	60 °C	56%
4	DMF	21 °C	60%
5	DMF	40 °C	51%
6	DMF	80 °C	58%

Table 1-9 Effect of solvent and temperature on the reduction of aryl trialkylammonium salts.

aniline derivatives into four different silanes, the removal of this group was next

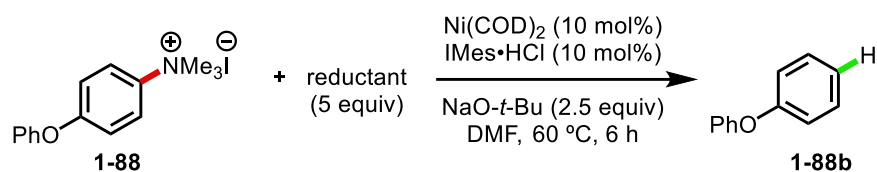


entry	ligand	time	yield 1-88b ^a
1	IPr*OMe•HCl	12 h	49%
2	IAd•HCl	12 h	46%
3	SIMes•HCl	12 h	47%
4	IMes•HCl	24h	56%
5	none	12 h	15%
6 ^b	IMes•HCl	1 h	57%
7 ^b	IMes•HCl	2h	60%
8 ^b	IMes•HCl	5 h	56%
9 ^b	IMes•HCl	8 h	57%

Table 1-10 Evaluation of different ligands and reaction times for the reduction of aryl trialkylammonium salts.

explored. As there were limited examples of mild, catalytic reductions of ammonium salts known at the time of this study, optimization commenced using the same model substrate used silylation. Upon brief examination of this reaction, it was found that using IMes as the ligand and warming the reaction to 60 °C overnight provided 82% of the desired biphenyl product (**1-81b**), with trace amounts of silylated product (**1-81a**). However, when the scope of this reaction was evaluated, this method proved highly substrate specific (Figure 1-23), giving low yields in all cases that did not contain a *para*-substituted aryl or alkyl group. Because the reaction seemed over optimized for one specific class of aryl trialkylammonium salts, a new model substrate, one containing a more challenging electron-rich aryl core (**1-88**), was used.

Using **1-88** as a model substrate, the identity of the solvent was reexamined (Table 1-9). Other ethereal solvents, such as THF did not provide increase in yield (Table 1-9, entry 2), however, when using DMF a large increase in yield was observed at 60 °C (Table 1-9, entry 3). There was no large effect on yield when raising the temperature to 80 °C, and the reaction could be conducted at ambient temperature (21 °C) with negligible results (Table 1-9, entries 4-6).



entry	reductant	yield 1-88b ^a
1	Me(TMSO) ₂ SiH	18%
2	<i>i</i> -Pr ₃ SiH	24%
3	Ph ₃ SiH	48%
4	Et ₃ SiH	56%
5	Et ₂ SiH ₂	54%
6	Ti(<i>i</i> -PrO) ₄	42%

Table 1-11 Evaluation of different reductants on the yield of arene.

In evaluating the ligand for this reaction, it was found that IMes still performed the best, though this reaction was rather promiscuous, giving modest yields with a number of NHCs (Table 1-10, entries 1-4), and even some yield when ligand was omitted (Table 1-10, entry 5). These reactions were also determined to be rapid, giving no significant change in conversion by GCMS after 2 hours (Table 1-10, entry 7). This much faster reaction rate, when compared to the silylation reaction, may be explained by the greater solubility of the reaction components in DMF, as opposed to dioxane.

To examine the source of hydride in this reaction, several common silanes and metal alkoxides were evaluated. A general trend between the size of the reductant and the yield was observed, as the very large Me(TMSO)₂SiH provided the lowest yield (Table 1-11, entry 1), followed by *i*-Pr₃SiH, and Ph₃SiH (Table 1-11, entries 2 & 3). Small silanes, such as Et₂SiH₂ and Et₃SiH performed comparably (Table 1-11, entries 4 & 5), and Ti(*i*-PrO)₄ gave modest yield of the product (Table 1-11, entry 6). Given the cost and its overall availability in most synthetic labs, further exploration of this reaction was conducted with Et₃SiH.

1.4.4 Substrate Scope of the Reduction of Aryl Trialkylammonium Salts to Arenes

Having identified the optimum conditions for reduction of aryl trialkylammonium salts, an evaluation of the substrate scope was undertaken (Table 1-12). Given the boost in yield for challenging substrate **1-88**, these new conditions were tested on the model substrate for silylation. Gratifyingly, the reduced arene (**1-81b**) was formed in 98% yield, which was better than the previously optimized conditions. Other extended π -systems, such as biphenyls **1-96b** and naphthalenes **1-97b** could be used in this reaction. Substrates containing orthogonal functional groups previously shown to be reactive using nickel-NHCs, like silyloxyarenes (**1-90b**), silyl ethers (**1-89b**), and phenyl ethers (**1-88b**) were well-tolerated in this reaction.^{114-115, 121} Contrary to the method developed for silylation of aryl trialkylammonium salts, while electron-deficient systems gave synthetically useful yields (**1-86b**), electron-rich aromatics (**1-87b**) gave synthetically low yields. While *para*-substituted aromatics (**1-84b**) gave good yields, substrates with *ortho* substitution showed poor reactivity (**1-85b**). Lastly, several trialkylammonium salts containing saturated and

unsaturated heterocycles could be used in this method, including pyridines (**1-98b**), pyrazoles (**1-93b**), and morpholines (**1-91b**).

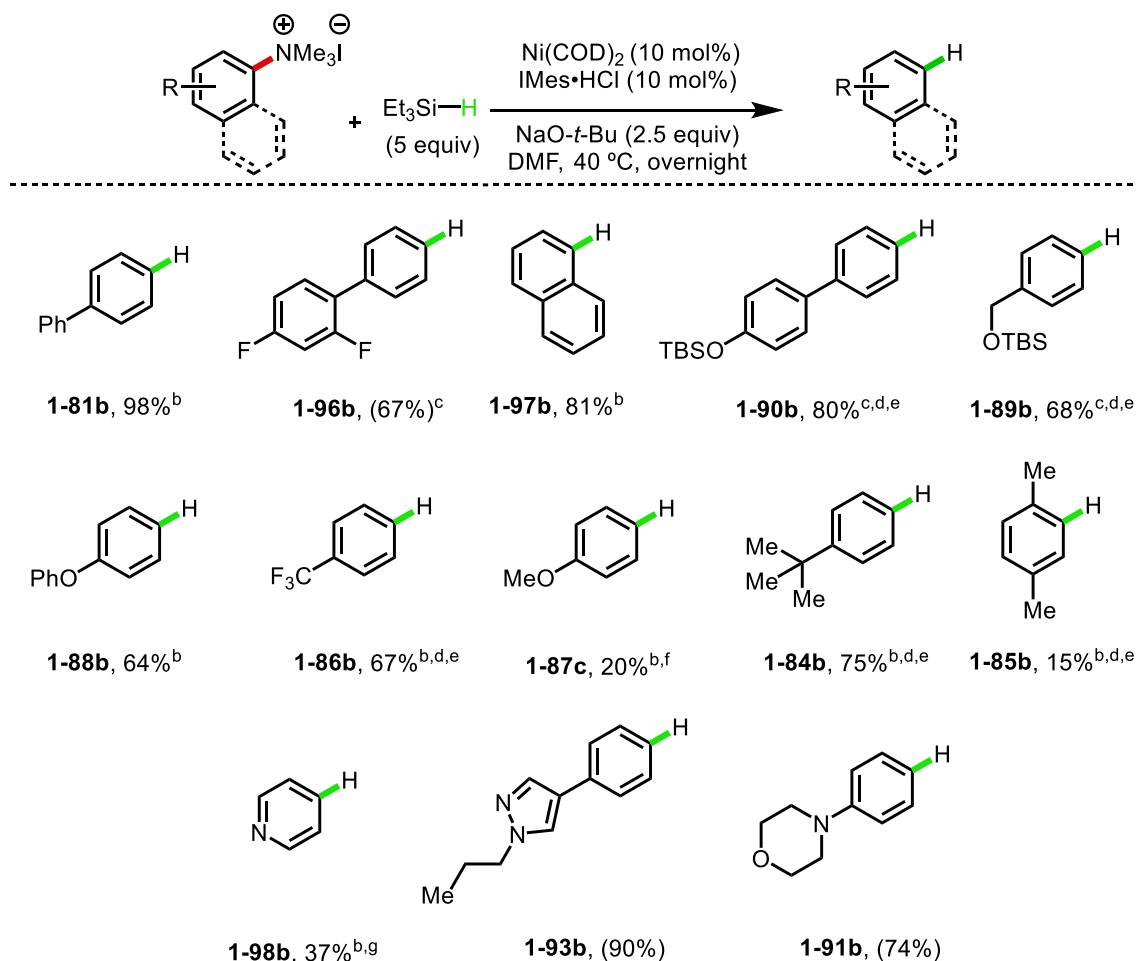


Table 1-12 Substrate scope for the reduction of aryl trialkylammonium salts. ^a Yields in parenthesis are isolated yields. ^b Yield determined by GCMS using tridecane as an internal standard. ^c Run at 20 °C. ^d Yield determined by NMR using CH_2Br_2 as an internal standard. ^e Run at 60 °C. ^f 40 °C in dioxane. ^g Run at 90 °C in dioxane.

1.4.5 Mechanistic Investigations into the Silylation and Reduction of Arenes

Having demonstrated the utility of aryl trialkylammonium salts to divergently synthesize either aryl silanes or reduced arenes, the mechanism of these reactions were briefly investigated. First, the source of the hydride for the reduction of aryl trialkylammonium salts was examined (Figure 1-24). Using triethylsilyl deuteride, the model reaction was conducted for both the reduction and silylation. It was found that under the silylation conditions, no deuterium was incorporated into the product. However, for the

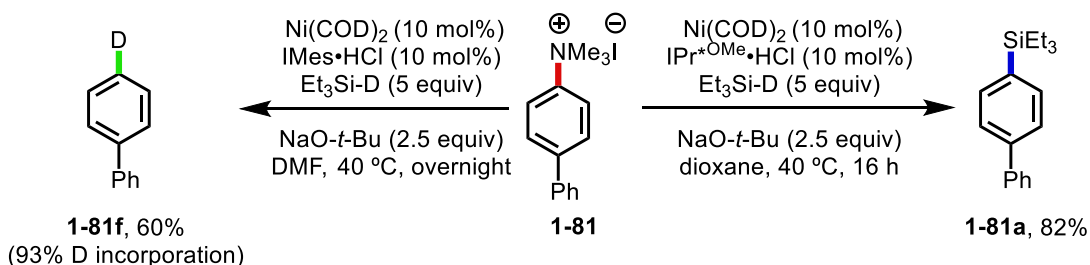


Figure 1-24 Deuterium incorporation for the silylation and reduction of aryl trialkylammonium salts.

reduction, 93% deuterium incorporation was observed (**1-81f**). This suggests the silane serves as the hydride source in these reactions, rather than the trimethylamine that is generated through the cleavage of the C–N bond of the ammonium salt.

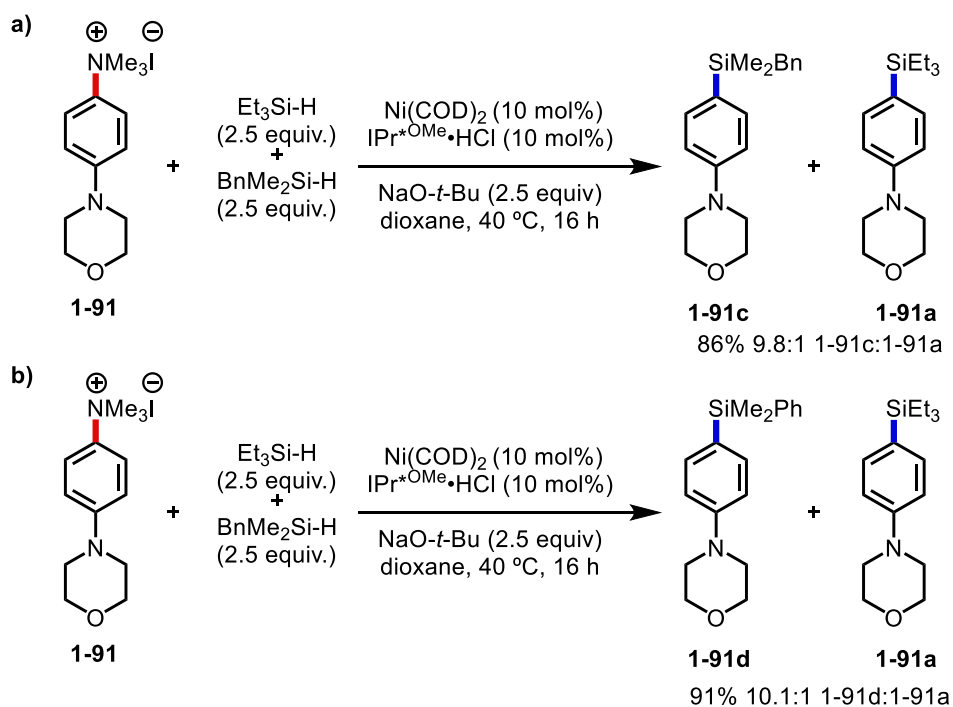


Figure 1-25 Head-to-head comparison of triethyl silane with different silanes.

Next, the observation that different silanes provided different yields prompted study into their rates of reactivity (Figure 1-25). To assess if some silanes reacted faster than others, head-to-head comparisons were performed by using equal amounts of two different silanes in the same reaction flask. When comparing BnMe₂SiH to Et₃SiH, it was

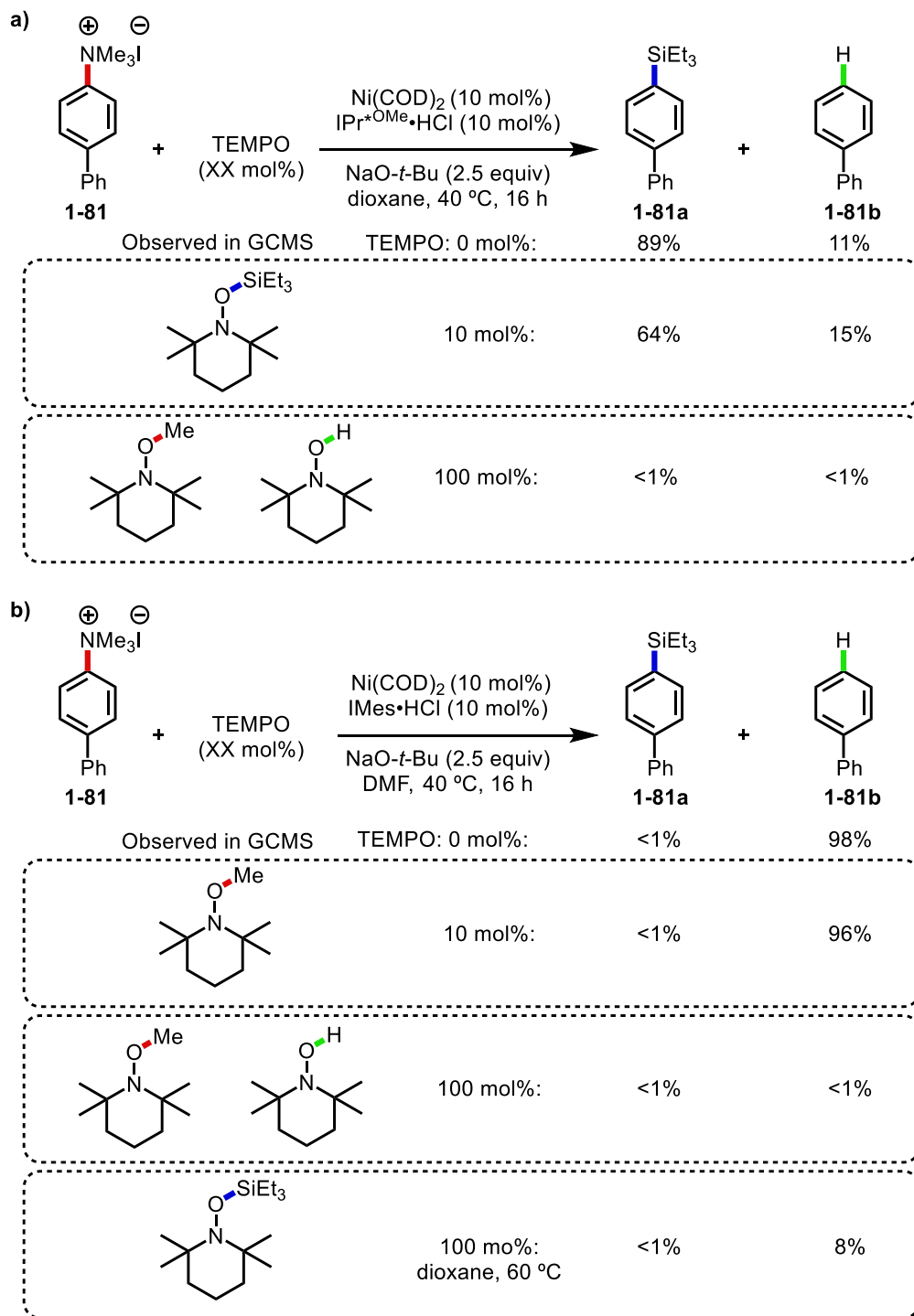


Table 1-13 Effects of TEMPO on **a)** the silylation and, **b)** the reduction of aryl trialkylammonium salts.

found that BnMe_2SiH reacted significantly faster than Et_3SiH , giving an over yield of 86% and 9.8:1 ratio of products (Figure 1-25a). Similarly, comparing PhMe_2SiH to Et_3SiH , near identical results were observed, with a 91% overall yield and 10.1:1 ratio of products

(Figure 1-25b). As this differing aptitude for reactivity was surprising, future studies should be conducted to determine why lower yields were often observed for either BnMe_2SiH or PhMe_2SiH compared to Et_3SiH .

Following investigations into the reactivity of different silanes, studies into the potential of a radical-type mechanism were probed (Table 1-13). To trap any free-radicals, reactions were run with either 10 mol% or 100 mol% of TEMPO. When comparing the model reaction to that with 10 mol% TEMPO, a slight decrease in yield was observed for the silylated product (Table 1-13a). However, when adding 100% TEMPO, the reaction was completely inhibited. TEMPO adducts with a triethylsilyl group were observed by GCMS for the reaction using 10 mol%, and both methyl and proton adducts were observed for the reaction run with 100 mol%. While further inquiry into the exact mechanism of this reaction is warranted, these results support the possibility of a radical mechanism.

For the reduction reaction, the yield was unaffected by the inclusion of 10 mol% TEMPO (Figure 1-13b). However, the reaction was completely inhibited when 100 mol% TEMPO was added. Similarly, methyl TEMPO adducts were observed by GCMS for the reaction with 10 mol%, and methyl and proton adducts were observed for the reaction with 100 mol%. Interestingly, no silyl adducts were observed for either reduction reaction. While the exact nature of each mechanism is unknown, this data supports the possibility of radical intermediates being formed at some point in the catalytic cycle, for both reactions.

1.4.6 Synthetic Demonstrations

The utility of these two methods rely on the robustness and availability of anilines and their derivatives. Anilines are strong *ortho*- and *para*-directing groups for electrophilic aromatic substitution ($\text{S}_{\text{E}}\text{Ar}$) reactions, and therefore can be viewed as a traceless directing

group if they are removed or converted into a valued added product, such as an aryl silane. Additionally, as anilines are often accessed from nitroarenes, which also are very useful as *meta*-directors or nucleophilic aromatic substitution (S_NAr), these too can be viewed as traceless handles for the installation of functionality on aryl silanes.

To highlight the ability of nitroarenes to serve as aryl silane precursors, a synthetic sequence was undertaken that utilized this group to install other functionality that might

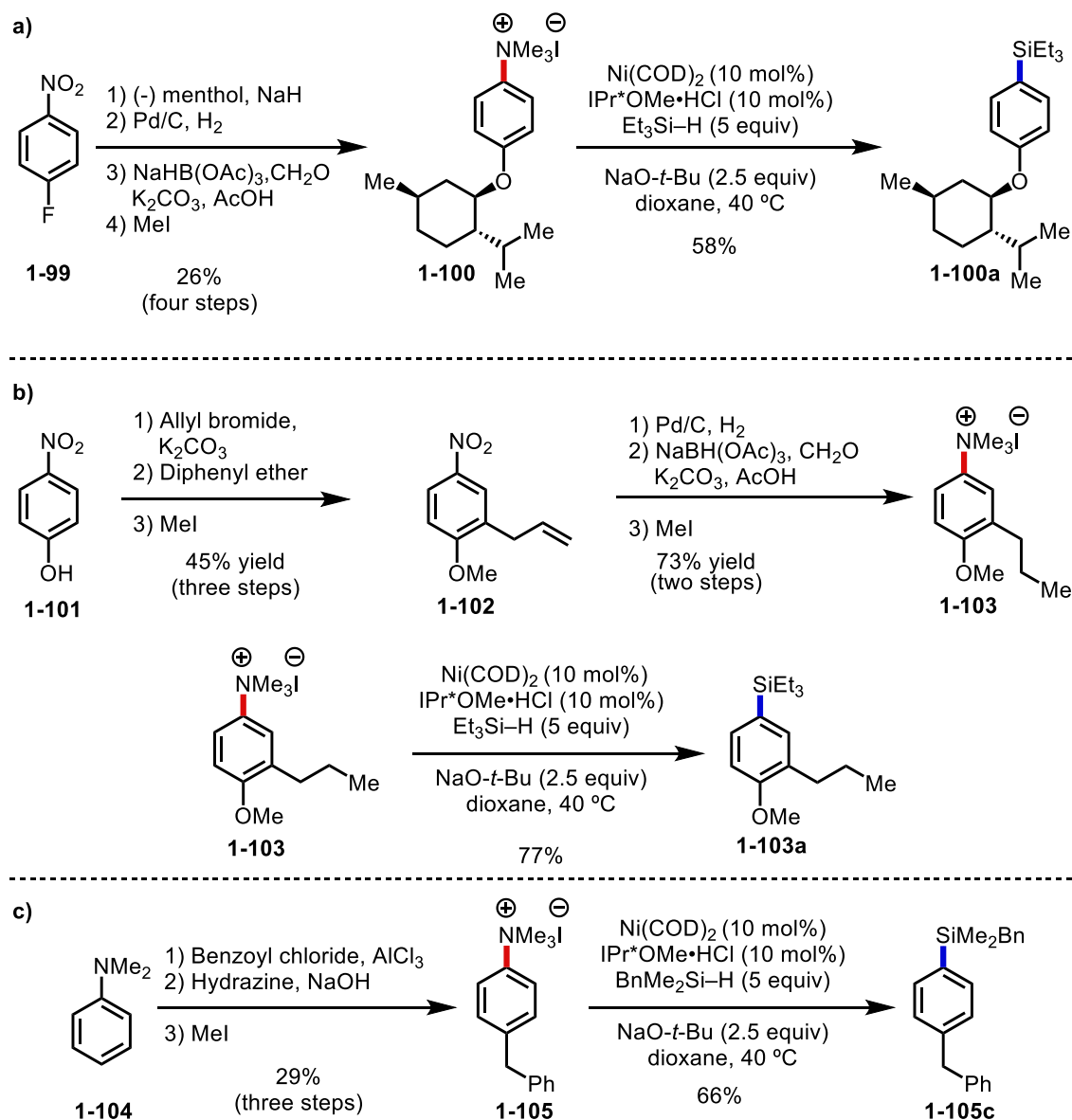


Figure 1-26 Synthetic demonstrations for the silylation of aryl trialkylammonium salts. **a)** using nitro-groups for S_NAr and aryl silane precursors, **b)** rapid diversification of simple arenes in route to aryl silanes and, **c)** using anilines as directing groups.

not be possible with other silylation methods (Figure 1-26a). First, through an (S_NAr) of 4-fluoronitrobenzene (**1-99**) with menthol, an aryl ether was synthesized. Following this, reduction of the nitro group with Pd/C and H_2 gave the parent aniline. From here, a two-step alkylation of the aniline provided the requisite aryl trialkylammonium salt (**1-100**) for silylation in 26% yield over four steps. Silylation of this enantiopure aryl ether then gave the desired product in 58% yield.

The usefulness of the nitroarenes was also shown through the rapid installation of diverse functionality (Figure 1-26b). Beginning with 4-nitrophenol (**1-101**), alkylation with allyl bromide, then a Claisen rearrangement and alkylation, gave methyl ether **1-102** in 45% yield over three steps, requiring no silica gel chromatography. Next, the nitro group and olefin were reduced using Pd/C and H_2 , then exhaustive alkylation of the aniline provided the ammonium salt (**1-103**) in 73% yield over two steps, without silica gel chromatography. Finally, this aryl ammonium salt was converted to the aryl silane (**1-103a**) using the method developed herein in 77%. This synthetic sequence gives access to a highly decorated aryl silanes in a succinct sequence starting from a commercially available nitroarenes.

Lastly, the directing abilities of anilines were demonstrated through the Friedel-Crafts acylation of **1-104** (Figure 1-26c). This compound could then be reduced under Wolff-Kishner conditions and finally, alkylated to give the benzyl-substituted aryl trialkylammonium salt **1-105** in 29% over three steps. Using this compound and $BnMe_2SiH$, the silyl arene (**1-105c**) was accessed in 66% yield. As anilines can be readily accessed from many commodity chemicals, and are robust enough to survive harsh

synthetic sequences, they can now serve as useful precursors for silyl groups late in synthetic sequences.

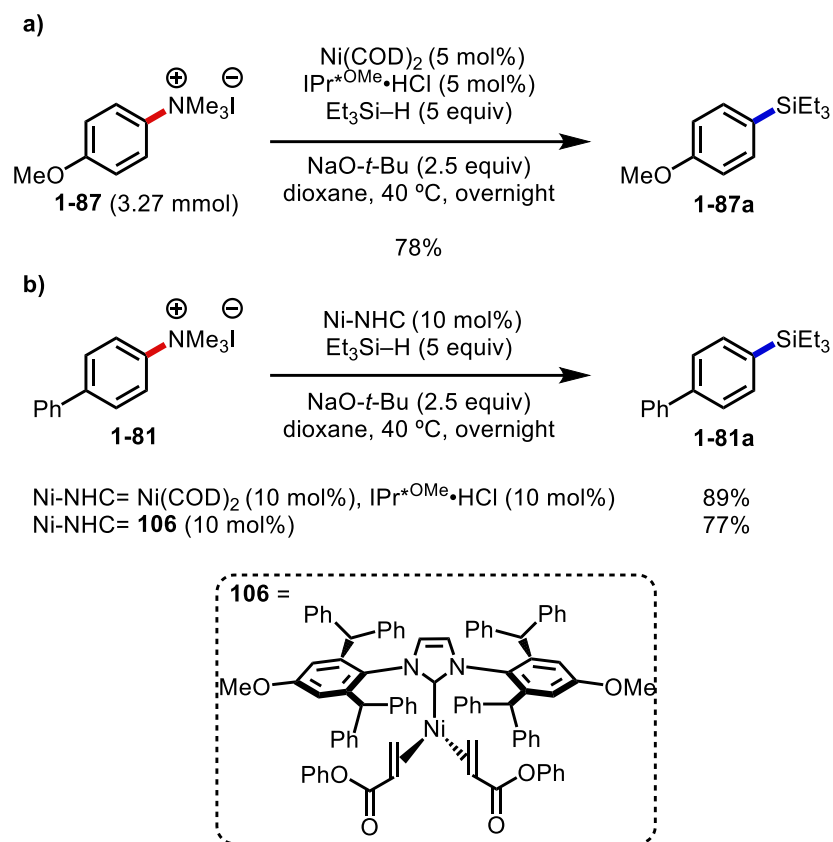


Figure 1-27 Synthetic demonstrations of silylation of aryl trialkylammonium salts. **a)** large-scale silylation of an aryl trialkylammonium salt and, **b)** comparison of in situ generated catalysts and air-stable pre-catalysts.

In a final effort to highlight the utility and of this method, a large scale reaction was run, using only 5 mol% Ni(COD)_2 and 5 mol% $\text{IPr}^*\text{OMe}\cdot\text{HCl}$, which afforded 77% isolated yield of the desired product (Figure 1-27a). This reaction could also be run using a commercial air-stable pre-catalyst (**1-106**) developed within our lab. When comparing the optimized conditions to that of the pre-catalyst, a synthetically useful yield is attained, allowing facile access into these types of transformations (Figure 1-27b).

Overall, their relative abundance, ease of access, and robust nature make anilines and their derivatives highly valuable in synthesis. We thus aimed to take advantage of these characteristics and developed an efficient method to access aryl silanes from aryl

trialkylammonium salts. Four different silanes were shown to be competent in this reaction, providing access to a variety of aryl silanes in modest to excellent yield. Orthogonal to this transformation, the reduced arenes could also be accessed by changing the identity of the NHC ligand and solvent. Both of these methods could be conducted under exceptionally mild conditions and have a broad substrate scope. Furthermore, several experiments were conducted to better elucidate the mechanism of these reactions. Lastly, the synthetic utility of the silylation of aryl trialkylammonium salts, as a strategy for late-stage functionalization, was demonstrated. Specifically, nitroarenes and anilines were employed to give site-selective installation of various functional groups. These functional groups were subsequently transformed into aryl silanes, with overall good yields on several decorated aromatics. Ultimately, the utility of the silylation and reduction to the parent arene offer a novel and synthetically useful strategy to access new chemical space, beginning from commercially accessible starting materials via sustainable transition metal catalysis.

Chapter 2

Enantioselective α -Arylation of *N*-Alkyl Benzamides Using Synergistic Metallaphotoredox

2.1 Introduction

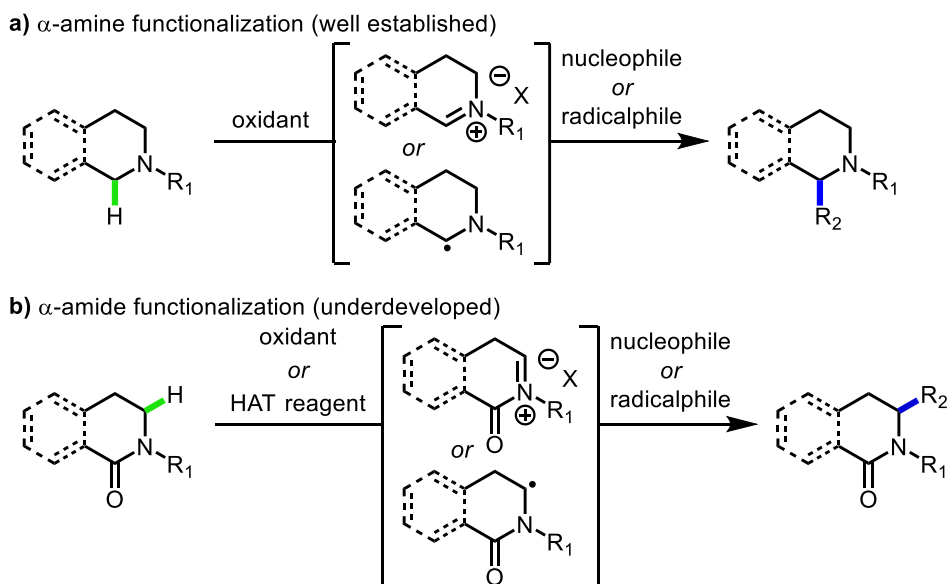
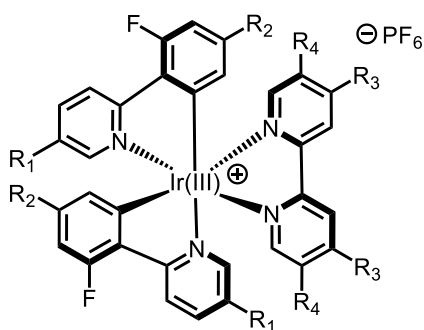


Figure 2-1 Mechanistic pathways for, **a)** α -functionalization of amines and, **b)** α -functionalization of amides.

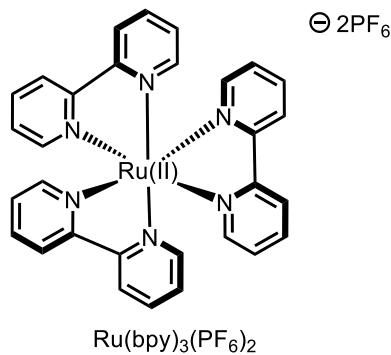
Aliphatic amines are present in a large number of natural products, pharmaceuticals, and agrochemicals, and are therefore an important motif throughout chemistry. Recently, a nascent area of interest has been developing for new methods for the last-stage diversification of alkyl amines and their derivatives. Of these methods, C–H functionalization through photoredox catalysis has emerged as a versatile strategy to form new C–C, C–O, and C–heteroatom bonds at the α -carbon of aliphatic amines under

exceedingly mild conditions. Until more recently, photoredox was largely limited to the functionalization of tertiary amines, which possess relatively low oxidation potentials. Through this manifold, tertiary amines can be oxidized to give α -amino radicals or iminium species, which can then be trapped (Figure 2-1). Although a great deal of effort has gone into understanding the fundamental processes that govern photoredox-catalyzed tertiary amine functionalization, far less is known about amide functionalization.

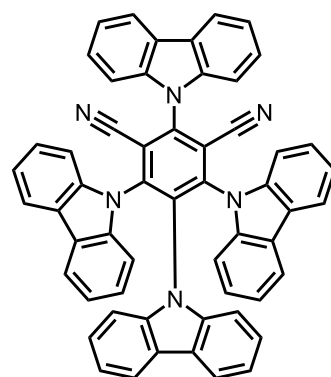
Inorganic photocatalysts:



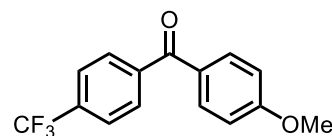
- PC1** $R_1 = \text{CF}_3, R_2 = \text{F}, R_3 = \text{F}, R_4 = t\text{-Bu}, R_5 = \text{H}$
PC2 $R_1 = \text{CF}_3, R_2 = \text{F}, R_3 = \text{F}, R_4 = \text{H}, R_5 = \text{CF}_3$
PC5 $R_1 = \text{Me}, R_2 = \text{F}, R_3 = \text{F}, R_4 = t\text{-Bu}, R_5 = \text{H}$
PC6 $R_1 = \text{CF}_3, R_2 = \text{CF}_3, R_3 = \text{F}, R_4 = t\text{-Bu}, R_5 = \text{H}$
PC7 $R_1 = \text{F}, R_2 = \text{F}, R_3 = \text{F}, R_4 = t\text{-Bu}, R_5 = \text{H}$
PC8 $R_1 = \text{CF}_3, R_2 = \text{F}, R_3 = \text{F}, R_4 = \text{H}, R_5 = \text{H}$
PC9 $R_1 = \text{CF}_3, R_2 = \text{CF}_3, R_3 = \text{CF}_3, R_4 = t\text{-Bu}, R_5 = \text{H}$



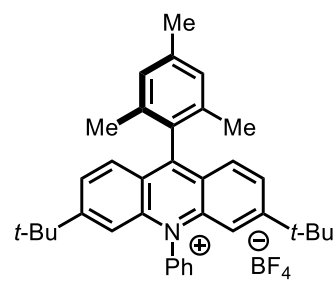
Organic photocatalysts:



4CzIPN



PC4



PC3

Figure 2-2 Inorganic and organic photocatalysts used in photoredox catalysis.

As this field has developed, the scope of amine derivatives that can be activated has increased. This is largely due to the concomitant development of organo-photoredox catalysts with higher oxidation potentials, and the ability to engage multiple catalytic

processes in the same reaction flask, such as metallaphotoredox catalysis (Figure 2-2). Due to their prevalence in medicinal chemistry and biologically relevant molecules, functionalization of amides has been a topic of increased interest. Amides, which are less prone to single-electron oxidation, are more challenging to engage in photoredox processes. To combat this poor reactivity, several novel strategies have been developed to address these limitations, including hydrogen atom transfer (HAT), proton-coupled electron transfer (PCET), oxidation of inorganic bases, energy transfer, and direct oxidation. For the purpose of this thesis, these methods will be discussed briefly, in addition to alternative strategies for distal-, and proximal-functionalization of amides and amine derivatives.

2.2 Distal C–H Functionalization Using Amines and their Derivatives

2.2.1 Hofmann-Löffler-Freytag-type Reactions for Distal C–H Functionalization

Hofmann-Löffler-Freytag (1881):

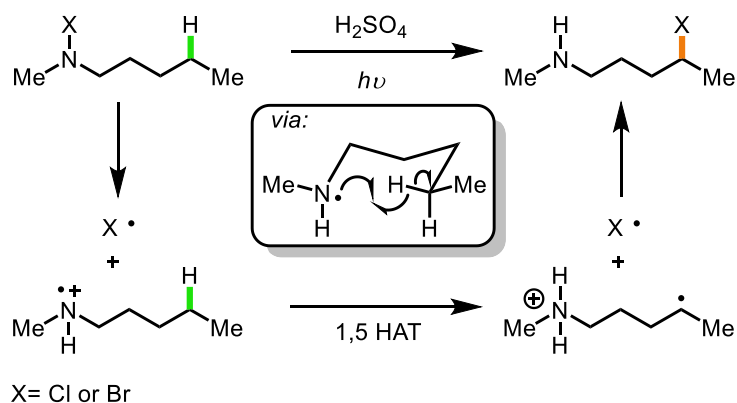


Figure 2-3 Explanation of selectivity for the Hofmann-Löffler-Freytag reaction.

As early as the 1880s, the conversion of distal C–H bonds to more useful functional group handles have been an area of burgeoning interest.¹²² With the advent of the Hofmann-Löffler-Freytag (HLF) reaction, amines became a tool for installing halogens

along an alkyl chain (Figure 2-3). Unlike traditional halogenation using Cl_2 or Br_2 and light, which create statistical mixtures of products, the HLF reaction can predictably and efficiently install chlorine or bromine at the δ -position of aliphatic secondary amines. Despite this powerful advancement in site-selective C–H halogenation, the HLF reaction still requires the installation of highly reactive N–Cl or N–Br bonds, which derive from caustic, and oxidizing reagents that have inherent substrate constraints.

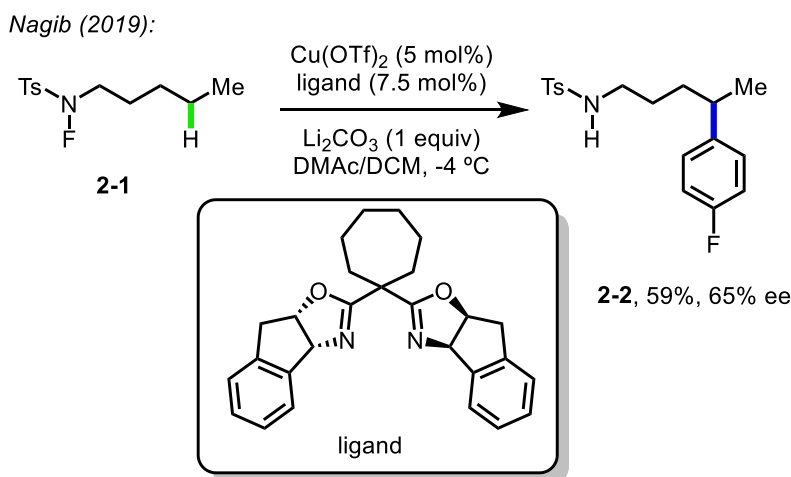


Figure 2-4 Use of N–F reagents for C–C bond formation.

Mechanistically, the HLF reaction has provided a platform for further developments in distal C–H functionalization. It is currently understood that homolysis of the N–X bond by light forms an X-centered radical and N-centered radical, the latter of which can abstract a C–H from the δ -position. Due to the highly organized, chair-like transition state, this reaction typically undergoes a 1,5-HAT, providing regioselective C–X bond formation. Although, there are many methods that take advantage of conformational bias to perform 1,5-HATs, or use clever strategies to perform 1,N-HATs ($N=2, 3, 4, 6, \text{ or } 7$),¹²³⁻¹²⁶ the need for further transformations to access C–C or C–heteroatoms has prompted exploration of streamlined approaches to distal functionalization.

The HFL is a powerful method that has enabled the installation of functional groups on unactivated aliphatic chains. Its simplicity and site-selectivity have been a guiding principle for others who expanded these transformations beyond simple amines.¹²⁶⁻¹³⁰ Most importantly, the HFL has established HAT from an N-centered radical as a feasible method for C–H functionalization.¹³¹⁻¹³⁵ This innovation has inspired the study of other nitrogen-centered radicals, thus set the stage for novel transformations including the direct formation of C–C bonds from unactivated C–H bonds.

The Nagib group was able to show the utility of merging the HFL reaction with downstream cascade reaction sequences,¹³⁶ in order to install arenes at distal C–H bonds (Figure 2-4).¹³⁷⁻¹³⁸ As the traditional HFL reactions struggle to incorporate fluorine, this reaction serves as a powerful, yet mild method to overcome these limitations. Using a copper catalyst, Nagib and co-workers were able to take advantage of a chiral ligand for

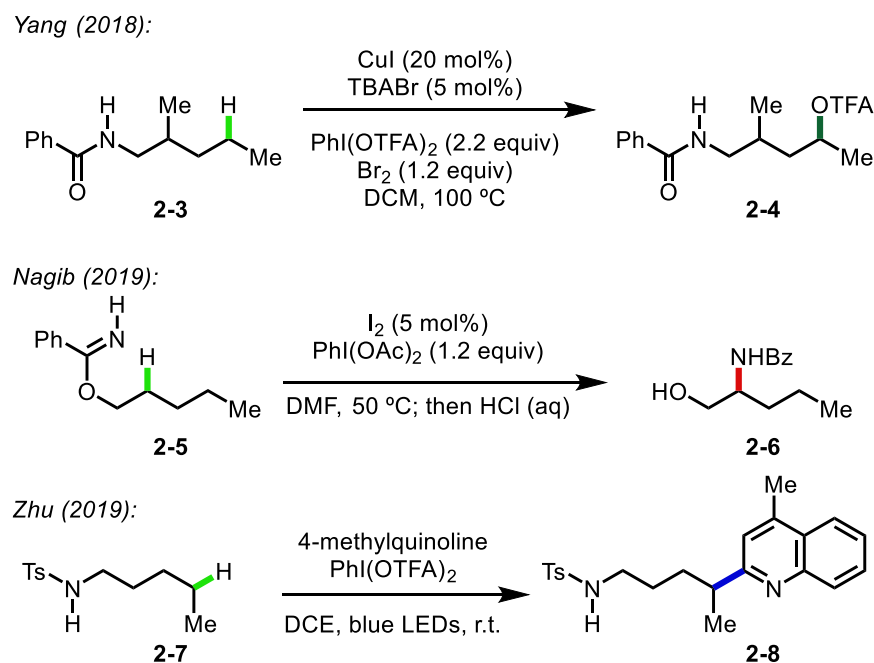


Figure 2-5 *In situ* HFL reactions for oxidation, amination, and arylation.

the enantioselective distal arylation of aliphatic amines, which cannot be easily accessed using other methods.

Similar strategies have been developed that utilize *in situ* generated N-centered radicals from iodine or bromine and hypervalent iodine reagents.¹³⁹⁻¹⁴¹ These *in situ* protocols have allowed for the installation of other functional groups including oxygenation,¹⁴² amination, and arylation (Figure 2-5).¹⁴³⁻¹⁴⁵ As only a catalytic amount of reactive radical is generated at one time, site-selectivity is mediated through intramolecular C–H functionalization, allowing for high levels of regiocontrol. Additionally, the use of stable and readily accessible amines, imines, and amides provides a practical advantage over the synthesis of reactive N–X species in the HLF reaction. Lastly, unique transformations, such as distal arylations, can be performed in a single step, a feat not previously demonstrated through traditional HLF reactions.

2.2.2 N–H Cleavage for Distal Functionalization of C–H bonds

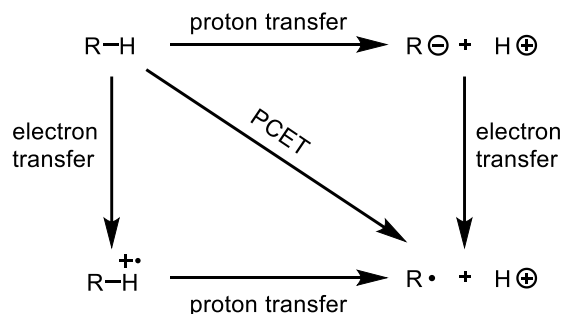


Figure 2-6 Thermodynamic cycle for PCET.

Initially defined by Mayer and co-workers,¹⁴⁶⁻¹⁴⁷ proton-coupled electron transfer (PCET) involves the simultaneous transfer of a proton and electron to two different orbitals

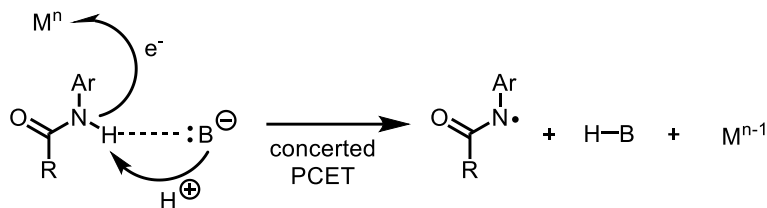
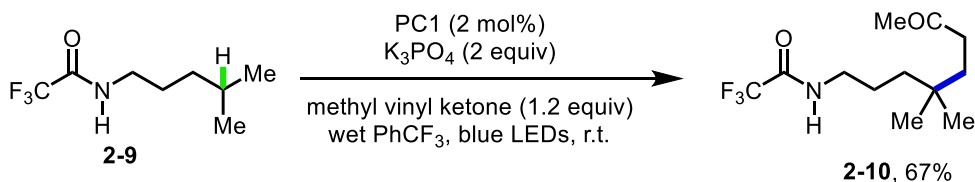


Figure 2-7 General mechanism for oxidative PCET.

of a given substrate(s) (Figure 2-6). The concerted nature of this transformation allows for significantly lower barriers of activation for the formation of nitrogen-centered radicals than the two-step process of deprotonation then oxidation, or oxidation then deprotonation.¹⁴⁸⁻¹⁴⁹ It is important to note that this phenomenon has been reported under

Rovis (2016):



Knowles (2016):

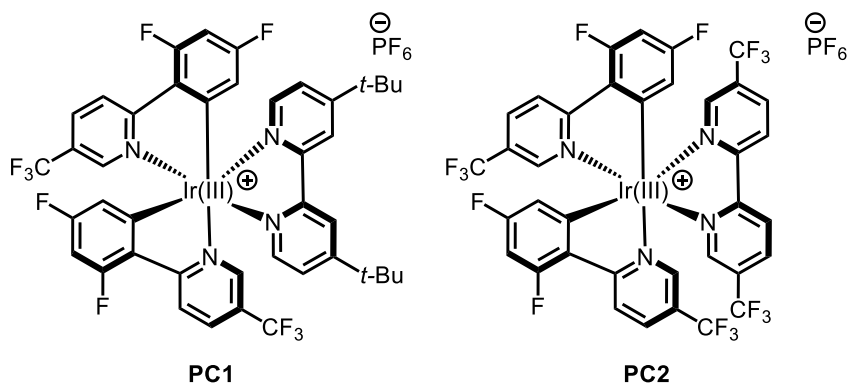
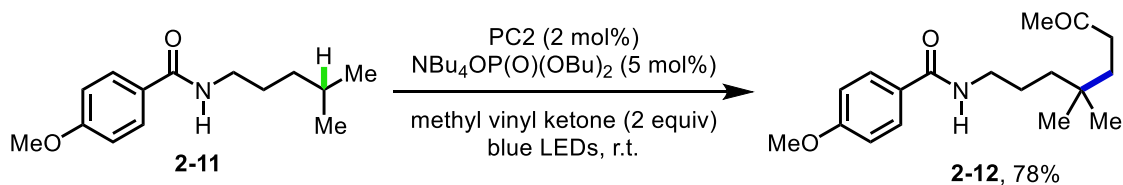


Figure 2-8 Photocatalytic PCET for distal alkylation.

basic, oxidizing conditions and acidic, reducing conditions.¹⁵⁰ Generally, this

transformation proceeds via concerted deprotonation by a basic moiety (B) and electron transfer by a transition metal (Mⁿ) (Figure 2-7). The exceptionally mild conditions (ie utilizing weaker oxidants/reductants and bases/acids) make this method amenable to sensitive substrates.

Applications of this theory have more recently been applied by Rovis and Knowles to catalytic systems¹⁵⁰⁻¹⁵³ for the distal functionalization of amides (Figure 2-8).¹⁵⁴⁻¹⁵⁵ In these simultaneously published reports, the combination of an iridium photocatalyst and a weak phosphate base allowed of the formation of an amidyl radical under very mild conditions. These radicals are then transferred through a favorable 1,5-HAT, which can be captured with Michael acceptors through a Giese-type reaction. Although these methods provide new avenues to forge C–C bonds, their transformation is limited to C(sp³)–C(sp³) bond formations, leaving room for further development of this area.

Tambar (2019):

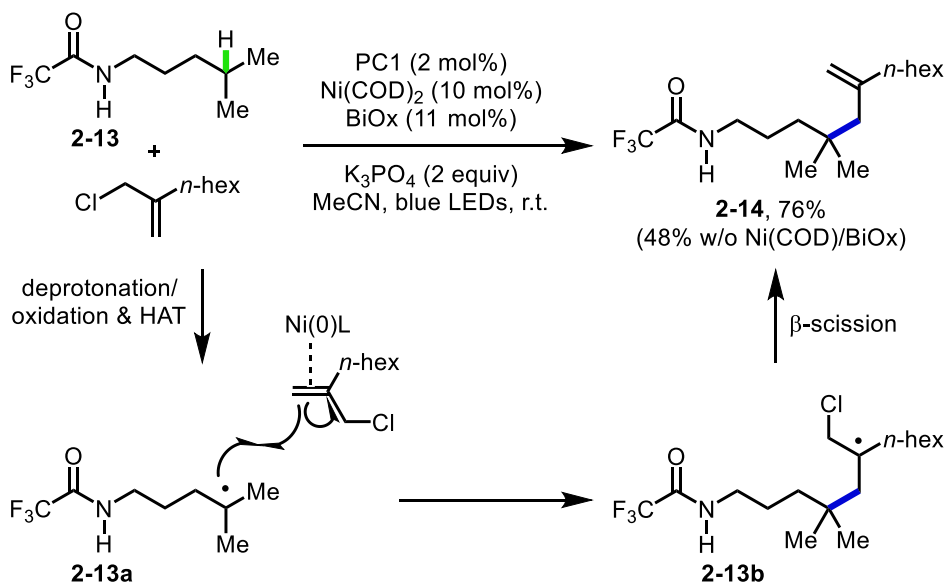


Figure 2-9 Distal allylation of trifluoroacetamides using metallaphotoredox catalysis.

These transformations described by Rovis and Knowles revived interest in generating amidyl radicals for distal C–H activation,¹⁵⁶ which provide reactive

intermediates for other functionalization, such as allylations¹⁵⁷ and alkylation,¹⁵⁸ or in some cases other substrates classes beyond amides.^{124, 159} The first of these, explored by the Tambar group, used trifluoroacetamides for the distal allylation of C–H bonds (Figure 2-9). In this system, an alkyl radical formed through the deprotonation and oxidation of an amide, followed by a 1,5 HAT can be captured by nickel-bound allyl chlorides. In their mechanism they propose a π -complex between the nickel and allyl chloride rather than oxidative addition by the metal. Interestingly though, moderated yields were observed when omitting nickel from the reaction, suggesting more complicated interactions are at play.

Rovis (2019):

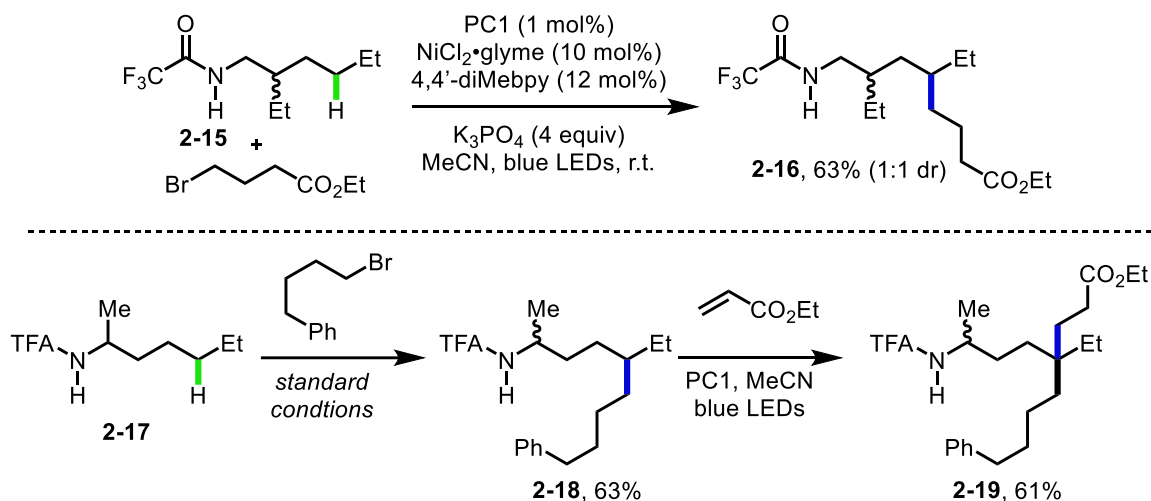


Figure 2-10 Distal alkylation of trifluoroacetamides using alkyl bromides.

In a recent report by the Rovis lab, a similar principle of intercepting reactive intermediates formed from amidyl radicals was implemented for the distal alkylation of trifluoroacetamides (Figure 2-10).¹⁵⁸ In this procedure, Ni-bpy complexes were used to capture fleeting radicals which were generated from a 1,5-HAT from an amidyl radical. Further, they were able to showcase the site-selectivity of an orthogonal reaction developed in their lab, the δ -alkylation of trifluoroacetimides with electron deficient olefins, using

previously optimized conditions, to give all-carbon quaternary centers. In contrast to the Tambar report, the Rovis group was able to expand the scope of electrophiles for C–H alkylation to unactivated alkyl bromides. Regardless, this work demonstrated another instance of selective, distal C–H functionalization using nitrogen-centered radicals and HAT.

Despite great advances in this field, methods to install new C(sp³)–C(sp²) bonds distal from amides has yet to be realized. The ability to intercept reactive intermediates within a catalytic cycle provides new opportunities for reaction development with underexplored substrate classes. As one can imagine engaging multiple catalysts in the same reaction, similar to work done by the Tambar lab,¹⁵⁷ PCET could potentially be leveraged for a number of unique transformations that cannot be accomplished solely by HLF-type reactions. Overall, catalytic methods using PCET or HAT to provide distal functionalization are a powerful tool that is currently under-utilized in the synthetic community and is a large topic of on-going research.

2.3 Proximal C–H Functionalization using Amines and their Derivatives

2.3.1 C–C(sp³) and C–C(sp) Bond Formations

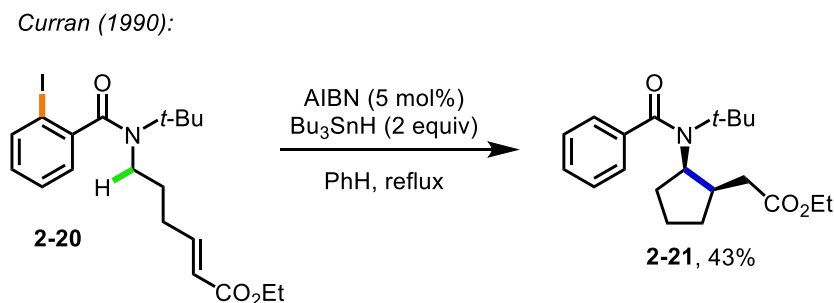


Figure 2-11 α -amidyl radicals for cyclizations.

Methods to form new C–C(sp³) bonds have made a recent resurgence in active research. The same challenges that plague method development for functionalizing strong

C–H bonds, namely high oxidation potentials and high BDE, require new strategies to overcome. Fortunately, a number of metal-mediated and photocatalyzed processes have been leveraged to achieve α -amide alkylation. Thus, this section will focus on oxidative methods to functionalize α -C–H bonds of amides, either using stoichiometric oxidants such as peroxides or by employing catalytic transition metals or photocatalysts. Through these strategies, new methods to for alkylation and allylation have been developed, however, many limitations remain, leaving ample room for improvement.

Beginning in 1990, the Curran group performed annulations of *N*-alkyl and aryl benzamides (Figure 2-11).¹⁶⁰ Using AIBN and Bu₃SnH, halides could be abstracted from arenes using tin-centered radicals. Owing to their instability, these aryl radicals rapidly underwent a 1,5-HAT to give α -amidyl radicals, which were trapped intramolecularly using styrenes, arenes, and unsaturated esters. Despite the limited methods at the time for α -amidyl radical formation, this method was able to leverage novel reactivity to provide valuable carbocycles and serves as a stepping-stone for future amide functionalization.

Mao (2014):

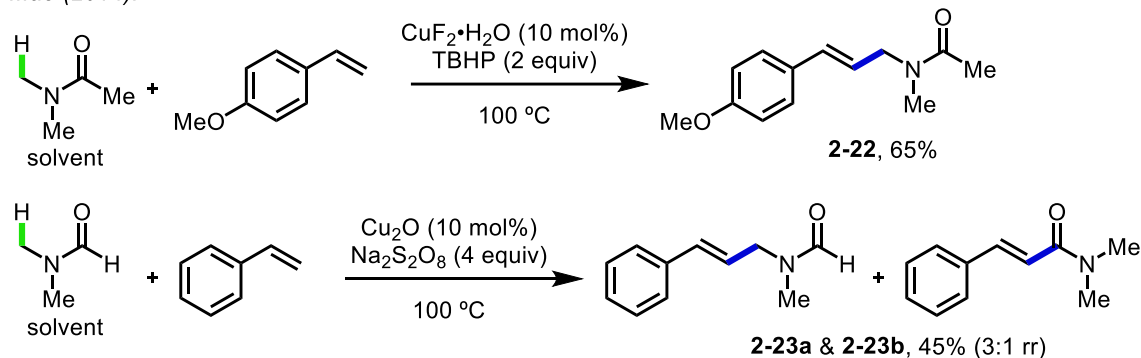


Figure 2-12 Alkylation of simple amides with styrenes.

Since Curran's report, other metal-mediated and metal-catalyzed methods have been developed to alkylate amides. Specifically, the Mao and Li groups were able to alkylate simple amides using a copper/ *tert*-butyl hydrogen peroxide (TBHP) system.¹⁶¹⁻¹⁶²

In the method developed by Mao, α -amidyl radicals from DMAc and NMP were accessed through a HAT process, which could then be trapped using styrene or unsaturated carboxylic acids to give alkyl and alkenyl amides (Figure 2-12). Unfortunately, this method suffers from several drawbacks including high reaction temperatures, high loadings of metal salt, modest yields, and the use of solvent quantities of amide. Additionally, regioselectivity was low for substrates that possessed other weak C–H bonds such as DMF.

Shibata (2015):

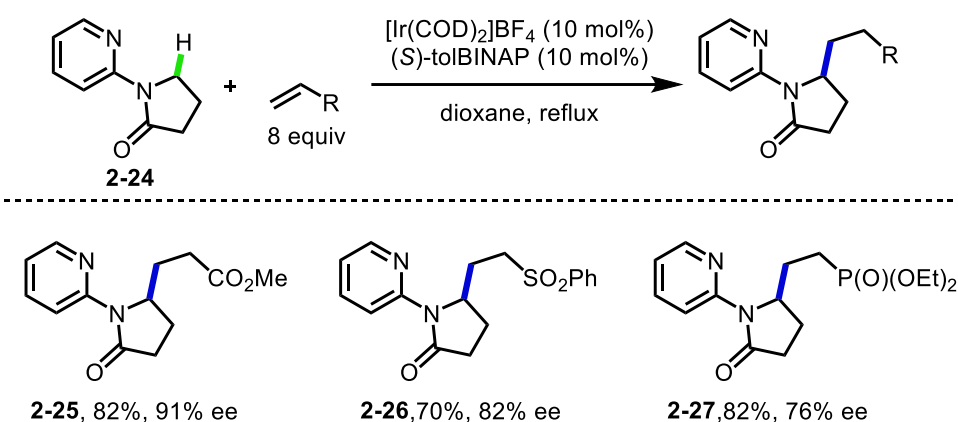


Figure 2-13 Enantioselective alkylation pyridyl lactams.

Using a well-defined iridium catalyst, the Shibata group was able to enantioselectively alkylate lactams with styrenes (Figure 2-13).¹⁶³ These reactions gave

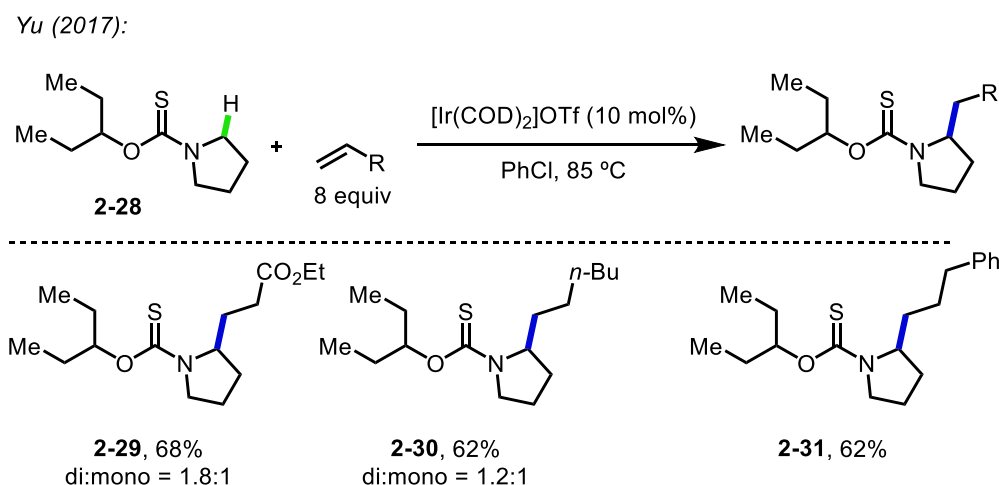


Figure 2-14 Alkoxythiocarbamate-directed alkylation of pyrrolidines.

good yields and good to excellent enantioselectivity using a commercially available chiral phosphine ligand. While the identity of the directing group and the structure of the lactam were not modified, the olefin could be changed to unsaturated esters, phosphonates, and sulfones. Lastly, these products were transformed into enantio-enriched γ -amino acids, which are valuable building blocks in organic synthesis.

Complementary to the report by Shibata, the Yu group was able to alkylate alkoxythiocarbamates using an iridium catalyst (Figure 2-14). Advantages to this system include the extended substrate scope and the ability to incorporate both activated and unactivated alkenes in this reaction. Unfortunately, this reaction requires high loadings of precious metal catalyst, and, unlike the Shibata report, also suffers from over alkylation and poor diastereoselectivity. Overall, this represents an alternative to existing methods of alkylation of amides, which use alkyl bromides or activated olefins.

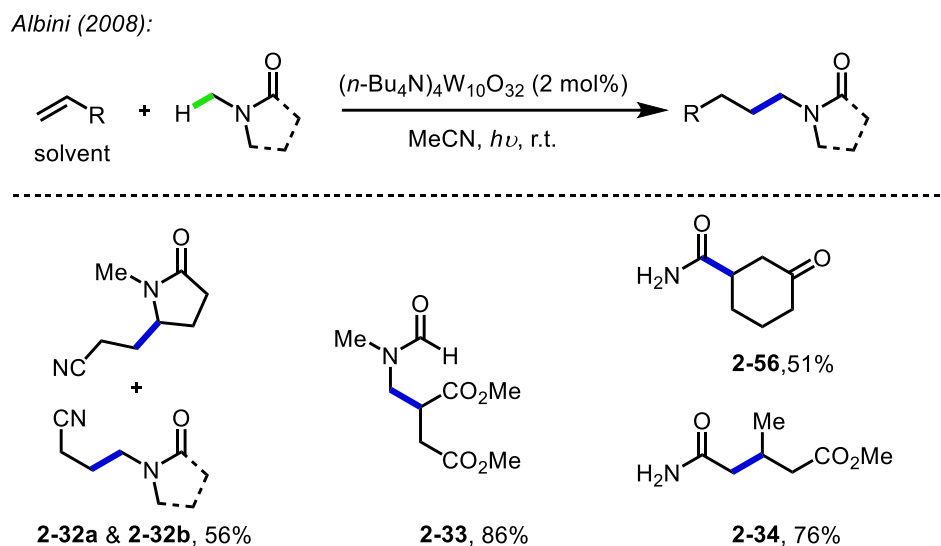


Figure 2-15 Tetrabutylammonium decatungstate-catalyzed alkylation of amides.

One of the first reports of photocatalytic amide α -alkylations was disclosed by the Albini group using a tetrabutylammonium decatungstate photocatalyst (TBADT) (Figure 2-15).¹⁶⁴ In their reaction, a photo-excited TBADT abstracts a weak α -C–H bond of simple

amides, which then forms a radical that is subsequently trapped by an electron-deficient olefin. While this method uses amides as the limiting reagent, a major advancement in this field, the electron-deficient olefin is used in solvent-quantities in order to attain higher yields. Similarly, the use of a strongly oxidizing photocatalyst prohibits the incorporation of some functionality in this report, though this represents a large advance in catalytic, proximal functionalization of amides.

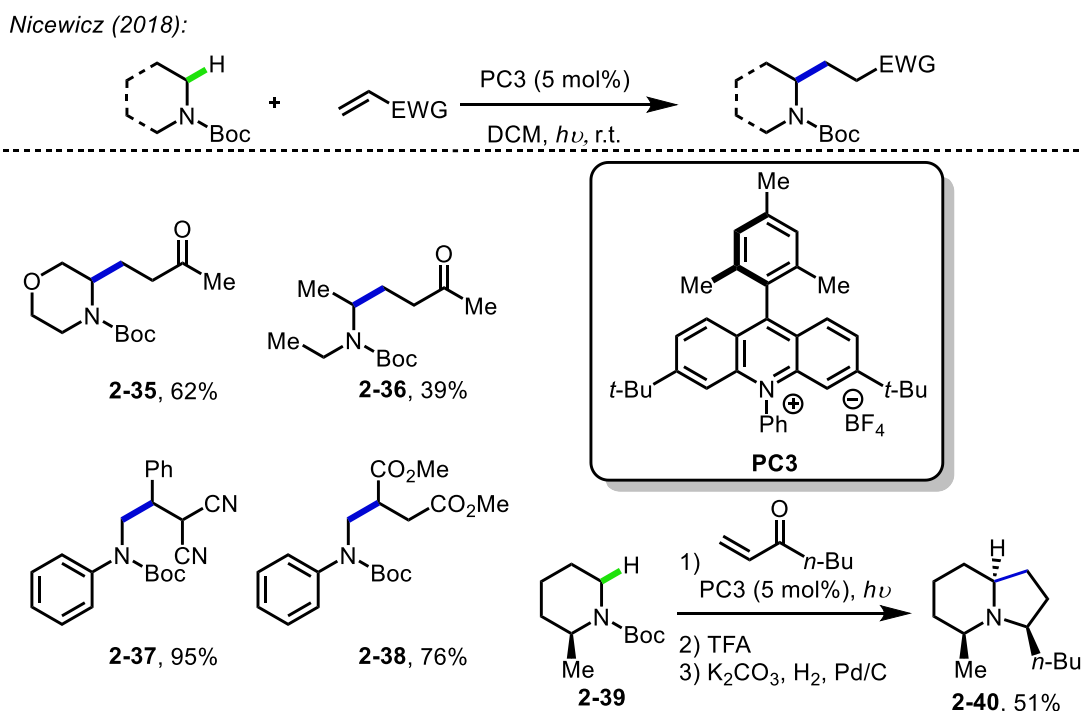


Figure 2-16 Photocatalytic alkylation of carbamates with electron-deficient olefins.

Building upon this seminal report of photocatalytic α -alkylation of amides, the Nicewicz group was able to show that strongly oxidizing acridinium photocatalysts were capable of directly oxidizing tertiary carbamates (Figure 2-16).¹⁶⁵ These conditions were amenable to numerous cyclic and acyclic Boc-protected amines, as well as several electron-deficient olefins including unsaturated ketones, esters, and sulfones. When applied to an enantio-enriched substrate this reaction was shown to be highly diastereoselective, paving

the way for the enantioselective synthesis of (+) monomorine (**2-40**) in 51% yield over three steps.

Unlike previously mentioned transition metal-catalyzed methods, the formation of enantioenriched amides and carbamates via photocatalysis is challenging due to the radical nature of the coupling partners. To address this, the Inoue group leveraged chiral sulfoximines, in conjunction with benzophenone as an HAT mediator, to form new C(sp³)-C(sp) bonds from α -C-H bonds of amine derivatives (Figure 2-17).¹⁶⁶ Key to this transformation was the development of an appropriate chiral auxiliary (**2-42**), which transferred stereochemical information through a concerted, chair-like transition state. While they were able to demonstrate this reaction on a number of protected amines,

Inoue (2015):

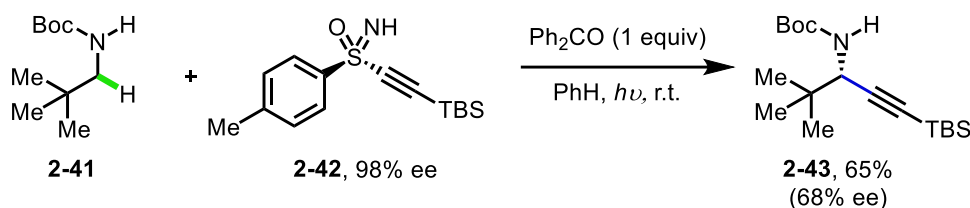


Figure 2-17 Enantiospecific alkylation of carbamates.

including amides, benzamides, and carbamates, the enantiospecificity was low in many cases, highlighting the difficulty in enantioselective C-H functionalization, especially in odd-electron systems.

Using a metallaphotoredox system, the MacMillan lab reported the α -alkylation of amide and carbamate C-H bonds (Figure 2-18).¹⁶⁷ The key to site-selectivity in their system was a polarity-match/ mismatch, which allowed for abstraction of stronger C-H bonds in the presence of weaker ones. Due to the electronics of the resultant quinuclidine radical cation, more hydridic C-H bonds are preferentially functionalized, as evident in the alkylation of amides containing benzyl and ether groups. They were able to use a large

variety of primary and secondary alkyl bromides, or tosylates in cases where the alkyl bromide was too volatile, to form new C(sp³)-C(sp³) bonds. Lastly, the authors demonstrated the high regioselectivity of this process by derivatizing the α-carbamate C-

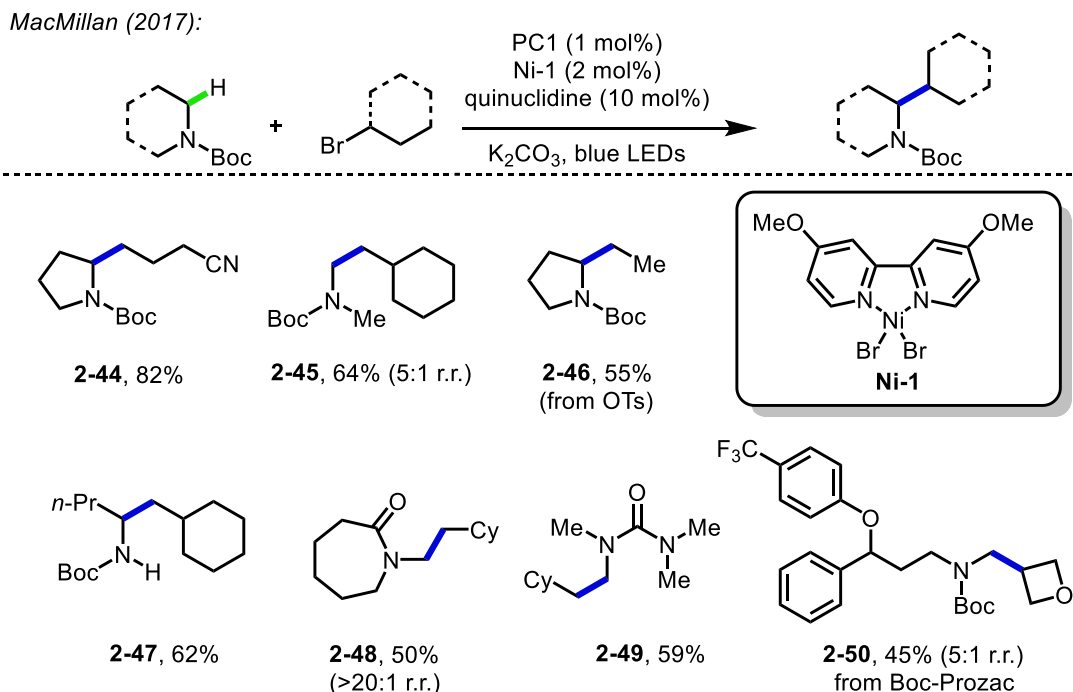


Figure 2-18 Metallaphotoredox-catalyzed alkylation of amides and carbamates using alkyl bromides.

H bonds of Boc-protected Prozac (**2-50**), which contains numerous C(sp³)-H bonds, including a benzylic ether, which has a lower BDE than those adjacent to the Boc-protected amine. As one of the first general metallaphotoredox methods, this work highlights the power of merging two catalytic cycles to develop new bond disconnections under mild reaction conditions.

Most recently, a method for the photocatalytic proximal alkylation of primary amines to give lactams was developed in a collaboration between the Schoenebeck and Rovis labs (Figure 2-19).¹⁶⁸ The use of CO₂, which traps the basic amine as a carbamate, allows for an electrostatic interaction between the negatively charged substrate (**2-51a**) and positively charged HAT reagent. This interaction is thought to direct the HAT to the α-C-

H bonds, to form a radical that can then be trapped by an electron-deficient olefin. This method represents a monumental achievement for the functionalization of non-tertiary amines, which have been challenging for photoredox due to their higher oxidation potentials, ability to be over oxidized, and their basicity.

Schoenebeck & Rovis (2018):

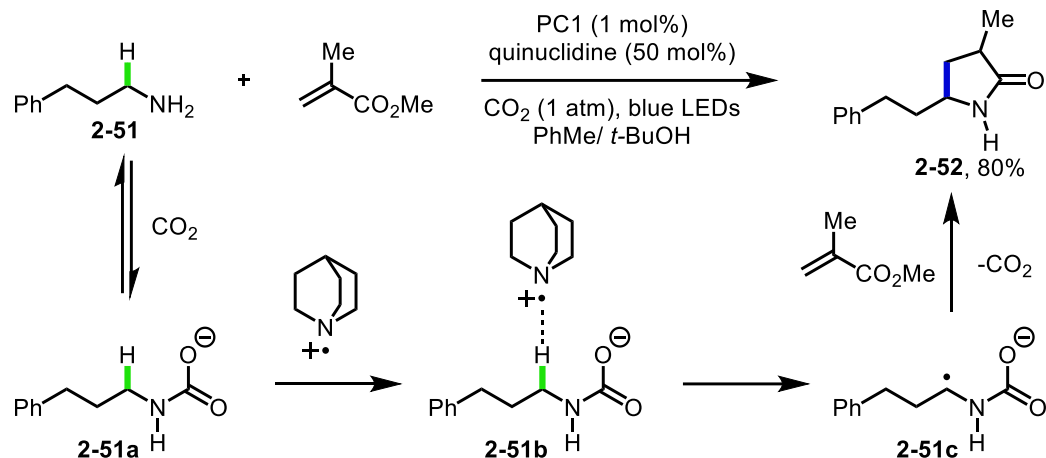


Figure 2-19 Using electrostatic interactions for the alkylation of primary amines.

Building upon the work of MacMillan, the Rovis group were able to achieve similar results for the alkylation of triflamides using electron-deficient olefins (Figure 2-20).¹⁶⁹ Although not explicitly mentioned in the Rovis report, it is thought that this reaction goes through a pairing of electrostatics, such as the one reported by Schoenebeck and Rovis.¹⁶⁸ In particular, experimental evidence supports the HAT of α -C–H bonds occurs between a deprotonated triflamide and the radical-cation of a quinuclidine species. Regardless of the mechanism, this provides an orthogonal method to the report by MacMillan to alkylate amine derivatives. This reaction is quite general, providing the desired product from triflamides containing secondary and tertiary α -C–H bonds, as well as using a number of electron-deficient olefins such as unsaturated esters or nitriles, malonates, and styrenes.

Furthermore, the site-selectivity was better elucidated when comparing the regioselectivity of their earlier report using trifluoroacetates (**2-58**), which provide distal functionalization.

Rovis (2019):

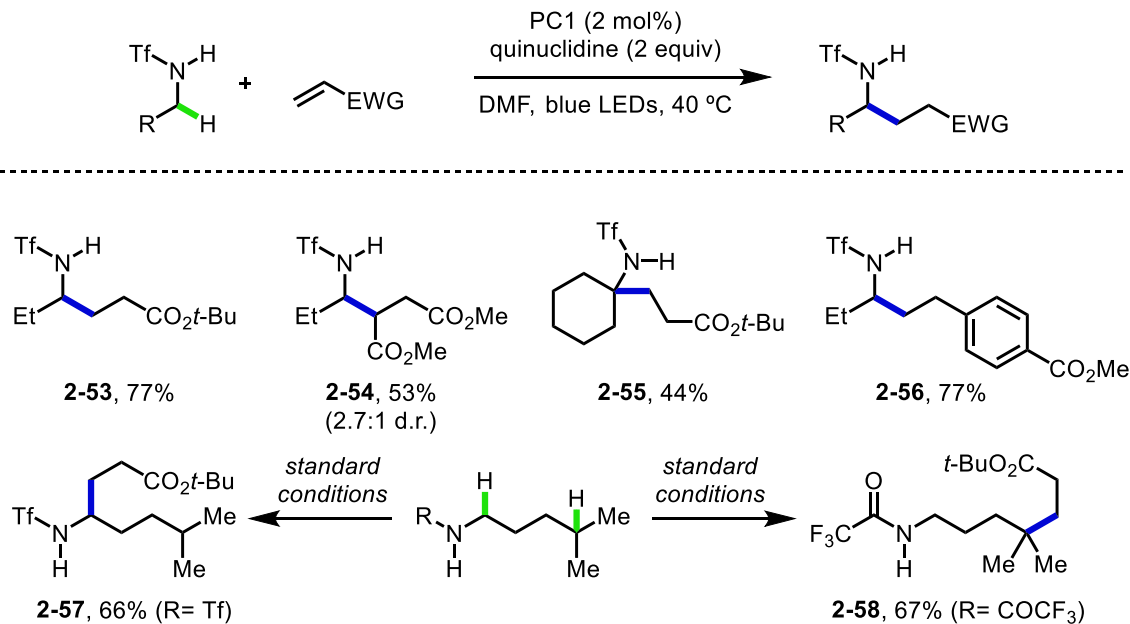


Figure 2-20 Alkylation of triflamides using electron-deficient olefins.

Many of these recent reports leverage novel photoredox or metallaphotoredox systems to circumvent the problems mentioned above and have opened new avenues of chemical research. Although these methods have elucidated several potential mechanisms for α -C–H alkylation, a general explanation for site-selectivity and chemoselectivity is still underdeveloped and poorly understood, leaving opportunities for detailed mechanistic investigations.

2.3.2 C–C(sp²) Bond Formation

Not unlike alkylation and heteroatom bond formation, there has been a great deal of interest in directly forming new C–C(sp²) bonds from α -amide C–H bonds. Two distinct approaches, namely one-electron and two-electron processes, have been developed to circumvent issues of activating and functionalizing amides. Within these approaches there

are several distinct mechanisms stemming from transition metal-catalysis, reagent-controlled oxidation, photoredox, and metallaphotoredox catalysis. Important to the developments described herein, an emphasis on mechanism and currently limitations will be discussed when appropriate. While there are many recent methods to install C–C(sp²) bonds proximal to amine derivatives, these methods are often uniquely substrate dependent and require new systems or further optimization to extend them to related substrate classes. Furthermore, very little exploration of enantioselective arylation has been described for proximal C–H arylation of amines and their derivatives.

Stephenson (2012):

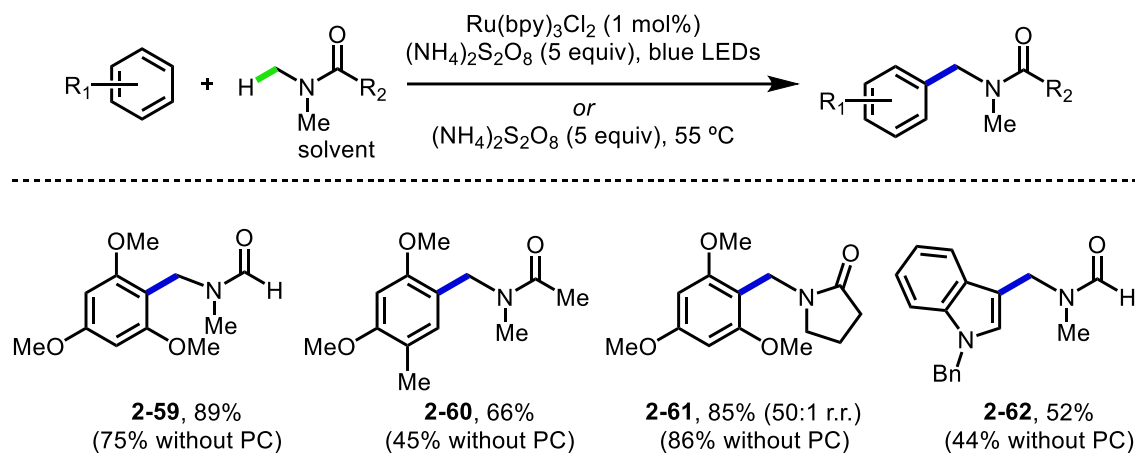


Figure 2-21 Friedel-Crafts-type arylation of amides using photoredox catalysis and persulfates.

Among the earliest methods of α -arylation of amides, the Stephenson group demonstrated the ability to two unique systems for the functionalization of simple amides (Figure 2-21). Using persulfate salts with or without a ruthenium photocatalyst allowed for the formation of an *N*-acyliminium species, which could be trapped by an electron-rich arene through a Friedel-Crafts-type reaction. Experimentally, they determined that the photocatalytic method provided better yields for most substrates, but that the product can be generated under thermolysis alone. These results indicated that persulfate could

potentially serve multiple roles in this reaction. Due to the constraints of Friedel-Crafts-type reactions, only very electron-rich substrates delivered appreciable yields of the desired products. Among the other limitations of this method are the need for solvent-quantities of amide, which prohibit the use of more complex substrates due to cost and efficiency. While it is believed that this reaction undergoes initial SET oxidation of the amide, followed by a facile second SET and loss of a proton to deliver *N*-acyliminium intermediates, this transformation can also be understood as a two-electron process due to the nature of the Friedel-Crafts-type reactivity.

Lei (2013):

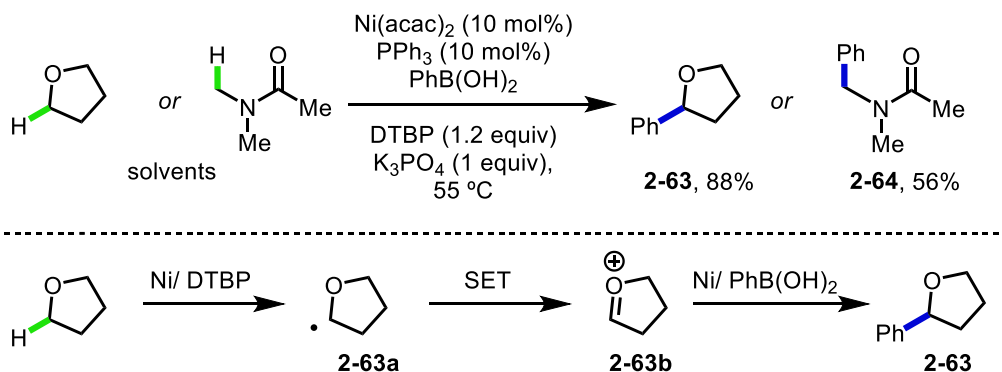


Figure 2-22 Nickel-catalyzed and mechanistic hypothesis of the arylation of THF and amides.

Shortly after the report by Stephenson, the Lei group was able to leverage DTBP and a nickel catalyst for the arylation of THF and simple amides (Figure 2-22). Similar to the mechanism reported by Stephenson *et al*, they propose an initial HAT followed by SET of the substrate by nickel and DTBP (**2-63a**). This process generates oxocarbeniums or *N*-acyliminium ions (**2-63b**), which can then be trapped by nucleophilic aryl species. This method is once again limited to simple systems as solvent quantities of the ether and amides are necessary for appreciable yields. While this reaction works with several functional groups on the boronic acid, the high temperatures and strongly oxidizing conditions prohibit the use of other sensitive functionality.

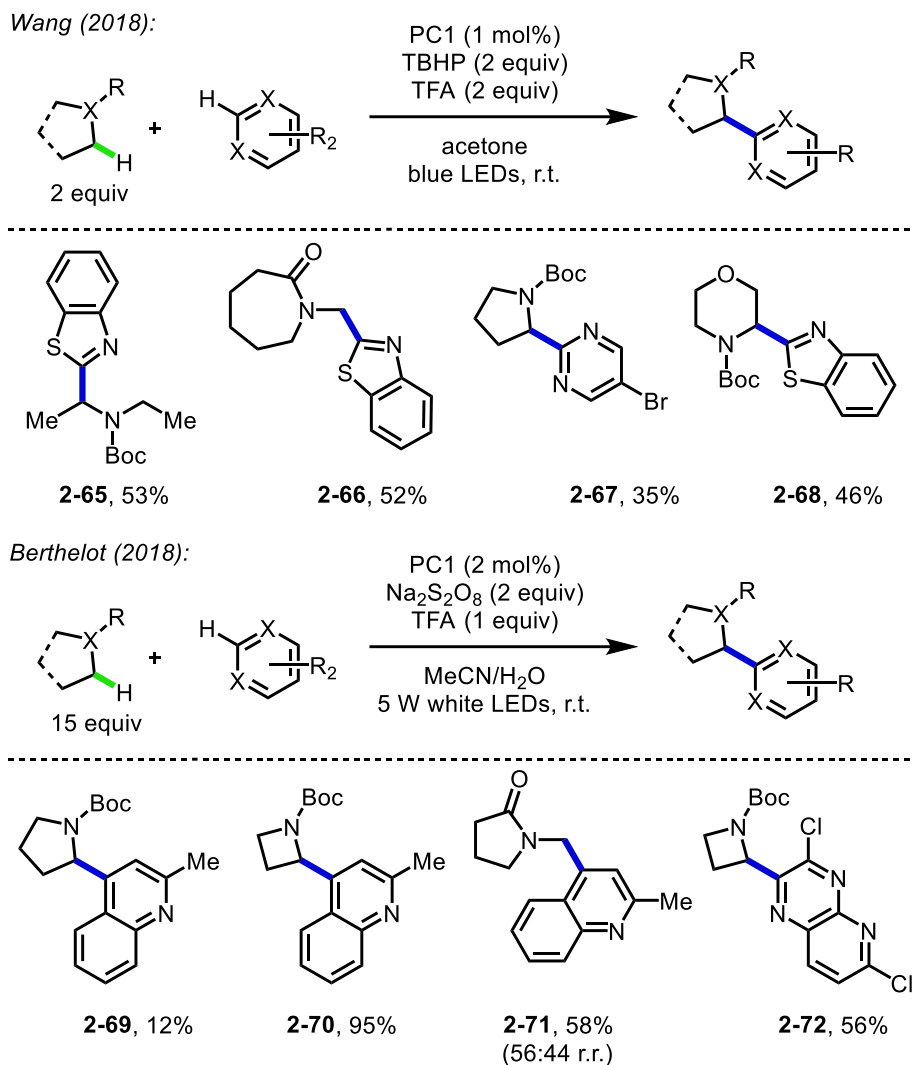


Figure 2-23 Metallaphotoredox-catalyzed arylation of amides and weak C–H bonds.

Work done by the Wang and Berthelot groups have implemented photoredox strategies, combined with stoichiometric oxidants for the α -arylation of amide C–H bonds (Figure 2-23).¹⁷⁰⁻¹⁷¹ Both of these methods provide heteroarylation of C–H bonds through a Minisci processes using a number of simple and complex amides, as well as a diverse group of arens. A major advancement in this field, the Wang group was able to avoid some of the pitfalls of other methods by employing near stoichiometric quantities of each coupling partners. Specifically, these methods provide a complement to those developed

by the Stephenson group as abundant arenes and a slight excess of amide are used to provide α -arylated amides in good yields.

Yu (2016):

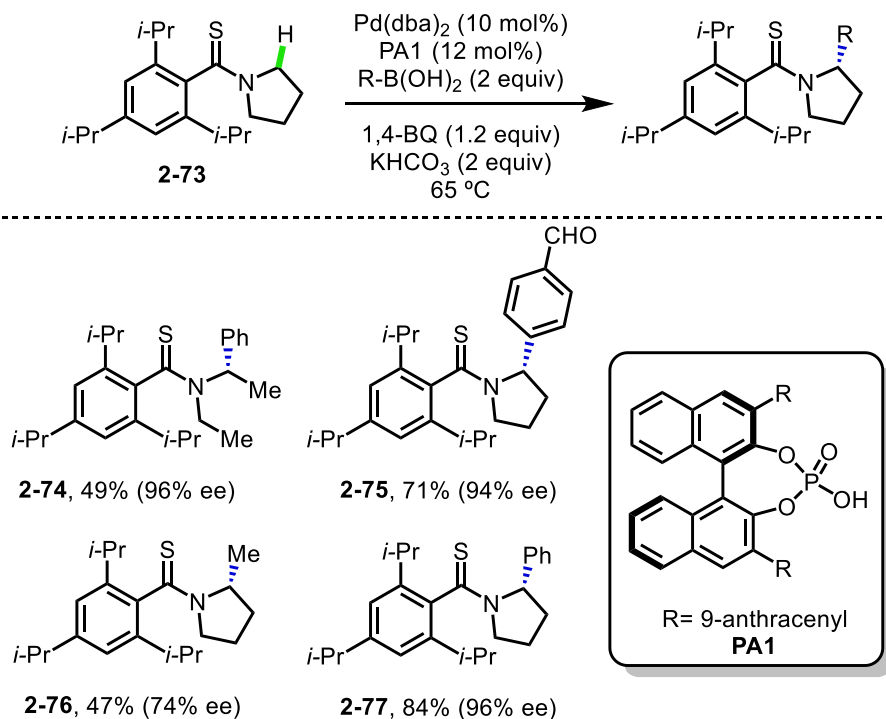


Figure 2-24 Palladium-catalyzed enantioselective arylation of thioamides with boronic esters.

Among the methods developed for α -C–H arylation of amides through a two-electron manifold, the Yu lab explored the ability of thioamides to direct enantioselective arylations using a palladium catalyst (Figure 2-24).¹⁷² Key advances in this method are the use of a phosphoric acid (**PA1**) to transfer chirality to the products and the use of near-stoichiometric amounts of coupling partners, which include abundant aryl boronic acids and both cyclic and acyclic thioamides. As this report details one of the first enantioselective methods to access α -aryl amides from C–H bonds, this serves as a benchmark for future developments in this area.

In an effort to develop a mild method to directly arylate C–H bonds of THF and simple amides, the Molander group used an iridium/nickel metallaphotoredox system (Figure 2-25).¹⁷³ Though this study still used solvent quantities of THF or amides, they were able to utilize a number of electron-rich and -poor aryl bromides, including several heteroaromatics. Mechanistically, they investigated nickel's role in the formation of α -THF and α -amide radicals. Specifically, they examined the possibility of oxidation of nickel(II)ArBr (**2-79**) by iridium, energy transfer to nickel by iridium, and direct excitation

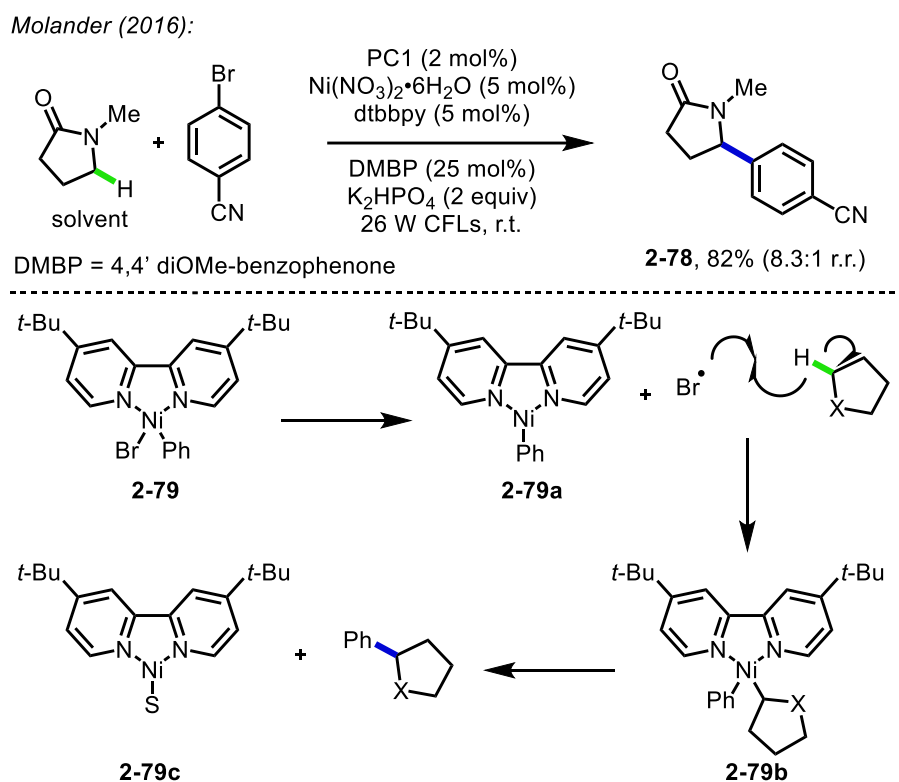


Figure 2-25 Arylation of cyclic amides and saturated heterocycles, and mechanistic hypotheses.

of nickel by light. Through their mechanistic studies they concluded that C–H functionalization is initiated by a bromine radical, though they were unable to determine if it occurred through the latter two pathways.

To address the limitations in their initial report, the MacMillan group uncovered a method to selectively arylate α -C–H bond of amides (Figure 2-26).^{167, 174} Key to their

findings were the exclusion of quinuclidine, as well as the use of a less electron-rich bipyridyl ligand for nickel (**Ni-2**). They were able to demonstrate this transformation on many substrates with varying C–H bond strength, ranging from cyclohexane to Boc-protected amines, with an impressive scope of aryl bromides including those bearing

MacMillan (2018):

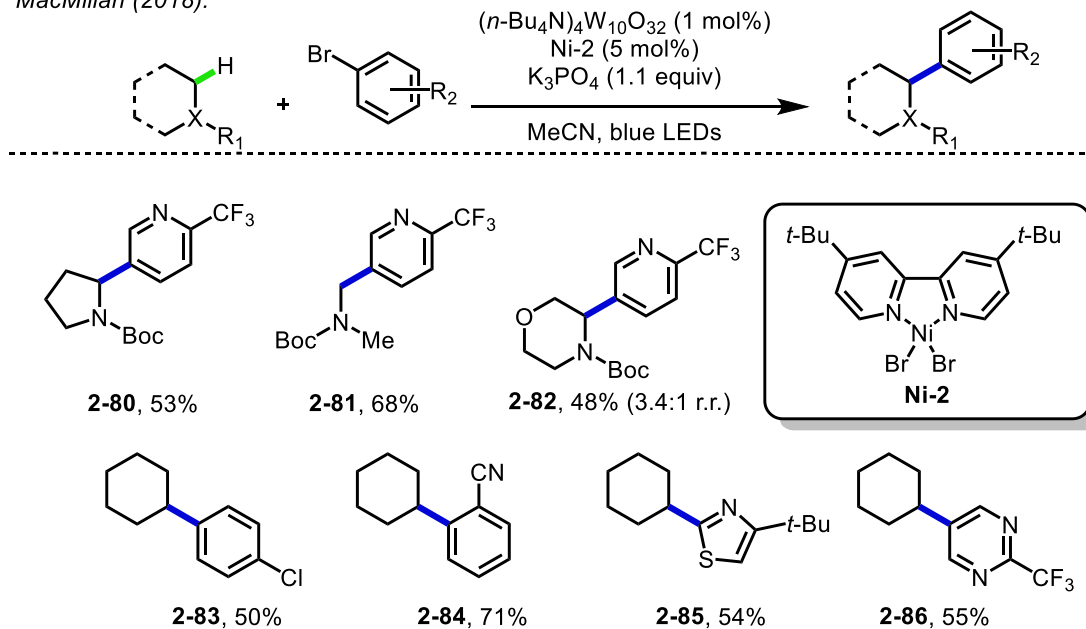


Figure 2-26 Metallaphotoredox-catalyzed arylation of carbamates and unactivated C–H bonds.

sensitive functional groups or containing heteroaromatics. This method represents an effective way to install arene moieties at unactivated C–H bonds, though insights to the mechanism, which could provide a better understanding for future developments, were not discussed.

Complementary to the metallaphotoredox systems developed by the MacMillan lab, the Martin group implemented a similar strategy to arylate THF and simple amides, using aryl bromides and solvent quantities of substrate (Figure 2-27).¹⁷⁵ This report was also extended to alkylations and contains a deeper discussion on the potential mechanisms for metallaphotoredox reactions. From their investigations, the authors de-convolute the interplay between the photocatalyst (**PC4**) and the nickel catalyst, and suggest that the

triplet ketone is responsible for both HAT from the organic substrate and SET with the nickel catalyst, enabling C(sp³)-C(sp²) bond formation.

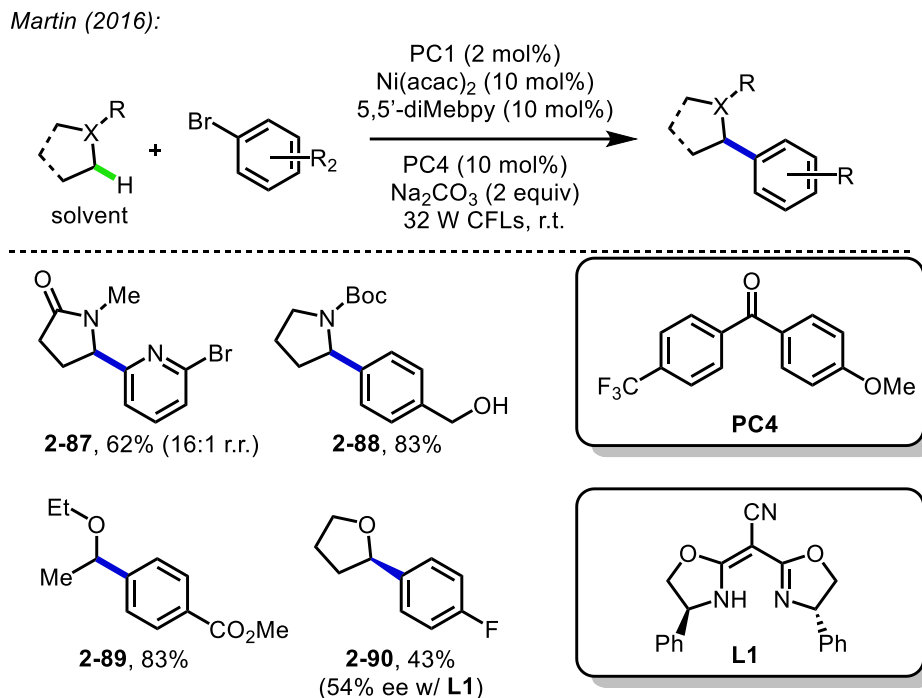


Figure 2-27 Metallaphotoredox-catalyzed and preliminary enantioselective arylation of amides and weak C-H bonds.

The limited methods for α -functionalization of amides and their derivatives with arenes has resulted in tremendous growth of new transformations in the last few years. Although existing methods have extended the use of arenes, aryl boronic acids, and aryl halides as coupling partners, limited substrate scope and often the need for solvent-quantities of amide are among the largest challenges to be addressed. While there has been some success in developing enantioselective α -arylation of amides and THFs, these systems typically require high loadings of expensive metals, strong directing groups, and in most cases provide little or no enantioselectivity. Furthermore, mechanistic studies conducted in several of these experiments have elucidated potential mechanisms, though changing variables such as photocatalyst, coupling partner, and ligand class have been shown to drastically change the reaction profile. As a result, there is an unmet need for the

development of more unified processes for enantioselective arylation, and studies to better understanding of the principles that control reactivity and selectivity in amide C–H functionalization.

2.4 Results and Discussion

2.4.1 Attempts at Intercepting PCET/HAT Intermediates

Inspired by the recent work of Rovis and Knowles, and with our lab's expertise in nickel catalysis and ligand design, it seemed logical to target the distal C–H functionalization of amides using metallaphotoredox. Nickel has been shown to engage

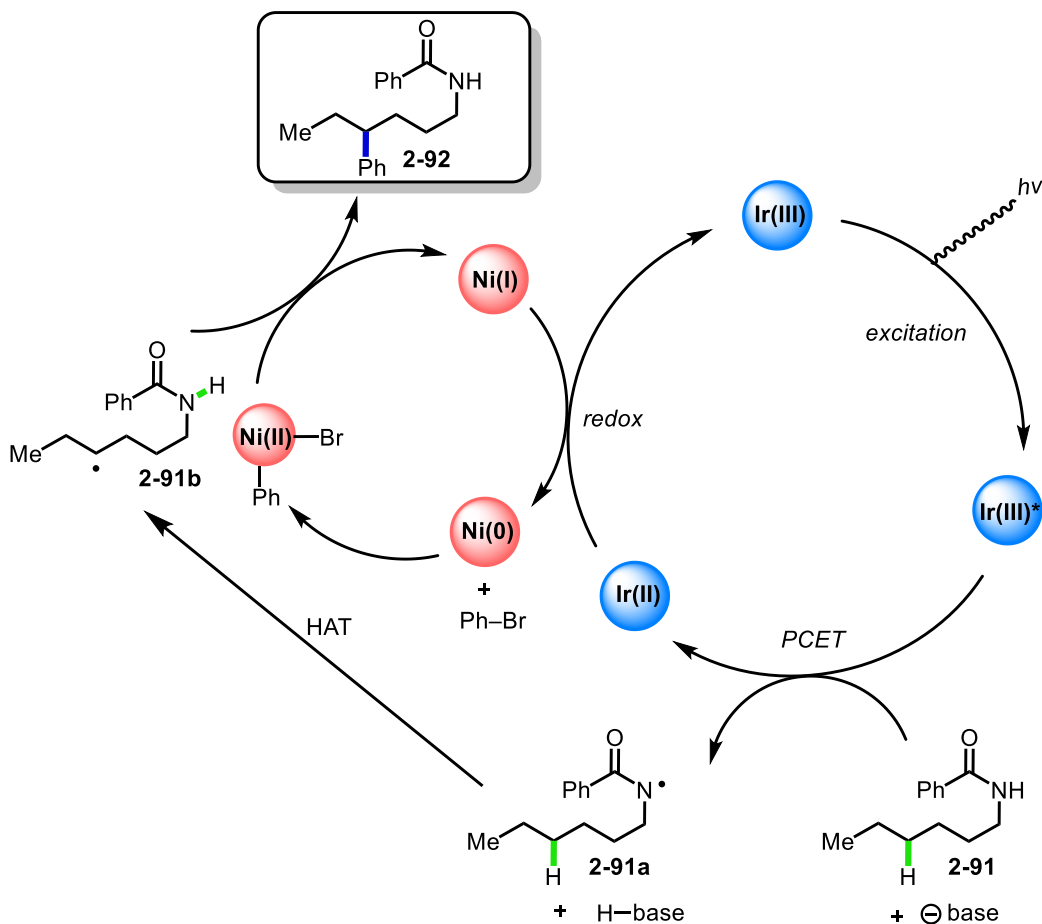


Figure 2-28 Proposed distal arylation enabled by metallaphotoredox processes.

synergistically with several organic and inorganic photocatalysts, and with its privileged reactivity in activating a wide range of electrophiles (from aryl and alkyl halides to aryl trialkylammonium salts), this catalyst system seemed like an ideal starting point for our investigations. We envisioned a strategy in which nickel and a photocatalyst would act in tandem to functionalize distal, unactivated C–H bonds. While many groups have looked at distal functionalization, there are very few reports of site-selective arylation of unactivated C–H bonds using metallaphotoredox, leaving ample room for methods development in this area.

With this idea in mind, a potential catalytic cycle was devised that would potentially allow us to leverage intermediates described by Rovis and Knowles (Figure 2-28). In this system, an iridium(III) photocatalyst would be excited by visible light, which could then interact with a phosphate base and a *N*-alkyl benzamide in order to perform a PCET. This would form an amidyl radical (**2-91a**), which would then site-selectively undergo a 1,5-HAT to form a carbon-centered radical **2-91a**. From here, we thought we could capture this carbon-centered radical with an electron deficient metal, deriving from the oxidative addition of nickel to an electrophile. Initially, we chose aryl bromides and chlorides due to their ease of oxidative addition to nickel and precedent from other metallaphotoredox reactions. Upon capturing the nascent carbon-centered radical, the nickel(III) species would then be poised for reductive elimination delivering **2-92** and a nickel(I) species. The catalytic cycle could then be completed by interaction of the two metals through the oxidation of iridium(II) to iridium(III) and reduction nickel(I) to nickel(0).

At the onset, we envisioned several challenges in developing the distal arylation of *N*-alkyl benzamides. First, we were unsure which electrophile would be best suited for this

transformation, therefore equal quantities of chlorobenzene and bromobenzene were used during initial screenings. Second, the identity of the ideal base/photocatalyst system was largely unknown. As Rovis and Knowles used different iridium polypyridyl (ppy)

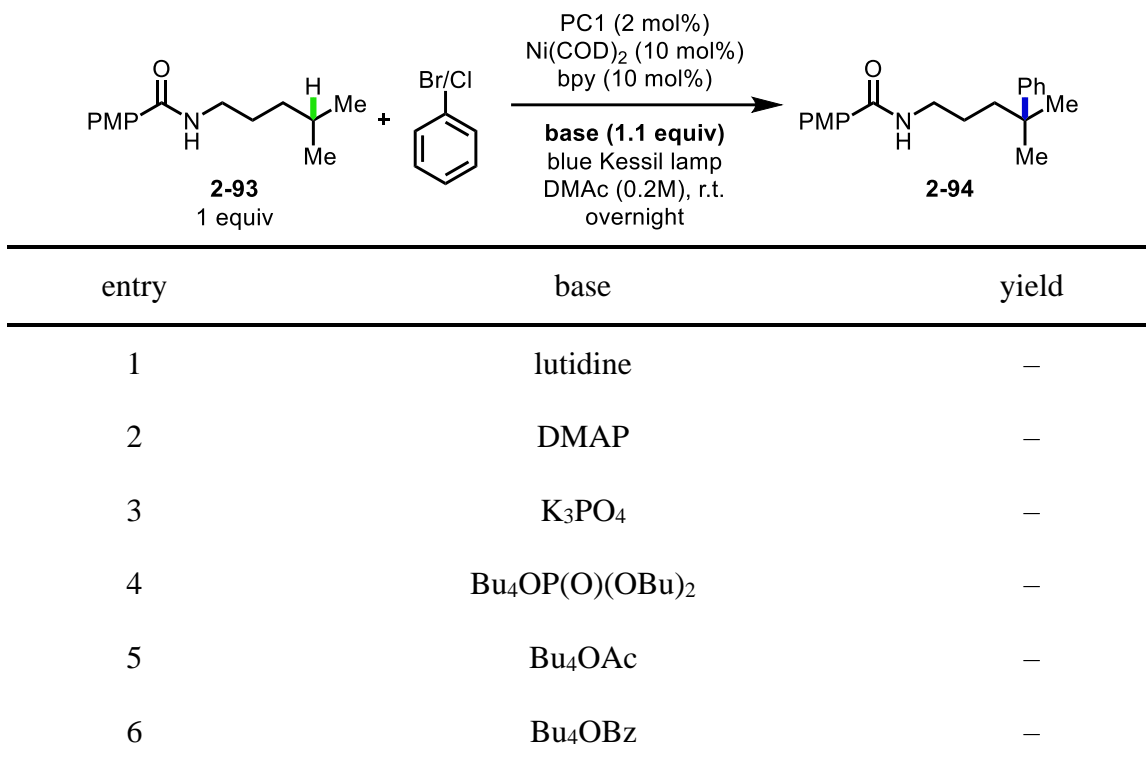
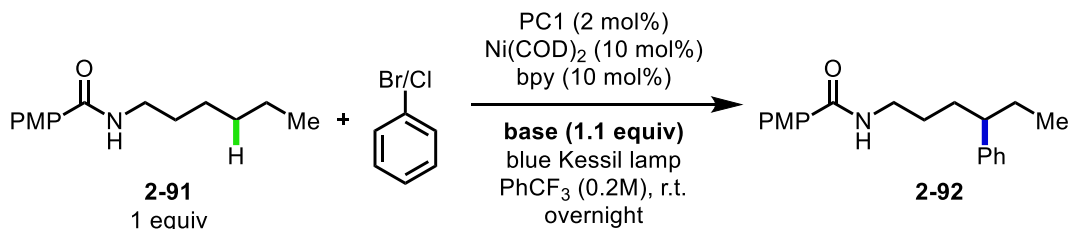


Table 2-1 Base and solvent screen for distal arylation of tertiary C–H bonds.

complexes and phosphate bases, we decided to try both systems, as well as a blend of the two (i.e. bases from one, photocatalysts from the other). Additionally, other bases shown to be competent in PCET chemistry, such as benzoates, DMAP, and lutidine were also examined.¹⁵⁰ Third, the difference in substrates for the Rovis and Knowles reports led us to explore both *N*-alkyl benzamides and trifluoroacetamides for this chemistry. Lastly, bpy, which has been shown to be competent in several related metallaphotoredox systems, was used in conjunction with Ni(COD)₂ to activate the aryl halide. As the number of variables in this reaction were numerous, and extensive screening would inevitably be necessary, the Knowles substrate was chosen as a good place for initial reaction exploration.



entry	base	yield
1	lutidine	—
2	DMAP	—
3	K ₃ PO ₄	—
4	Bu ₄ OP(O)(OBu) ₂	—
5	Bu ₄ OAc	—
6	Bu ₄ OBz	—

Table 2-2 Base screen for distal arylation of secondary C–H bonds.

Aware of recent work pertaining to metallaphotoredox and PCET, early attempts to access distal arylated products commenced with *N*-alkyl benzamide (**2-93**). It was thought that the stability of the formed tertiary radical would allow ample opportunity for capture by nickel. Thus, we commenced screening base combinations using **PC1**, Ni(COD)₂, bpy, and both PhBr and PhCl in DMAc under irradiation overnight by a blue Kessil lamp. Unfortunately, analysis by TLC and GCMS showed only unreacted starting material (Table 2-1). While substrates that formed tertiary radicals worked well for Rovis and Knowles, we hypothesized that the highly congested carbon-radical could preclude combination with a nickel species due to steric clash. Thus, switching to a substrate that

would form a secondary radical (**2-91**), we screened the same set of conditions only to find similar results (Table 2-2).

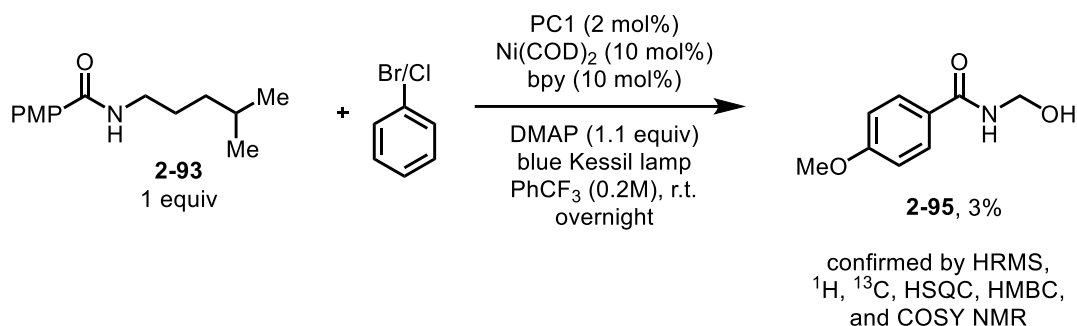


Figure 2-29 Identification of oxidative decomposition product.

Unsure of what variable could be responsible for the lack of reactivity, the identity of the solvent was next examined. To our delight, when using PhCF₃ instead of DMF and DMAP as a base, trace amounts of a new product was observed by TLC (Figure 2-29). The trace product was successfully isolated, though its ¹H NMR indicated this was not the desired product nor the starting material. After analysis by HRMS, HSQC, HMBC, ¹³C, and ¹H NMR, this product was identified as an oxidative decomposition product **2-95**. While this was not the desired product, it did show that some reaction was occurring in under these conditions, spurring a broader screen of conditions to promote distal functionalization.

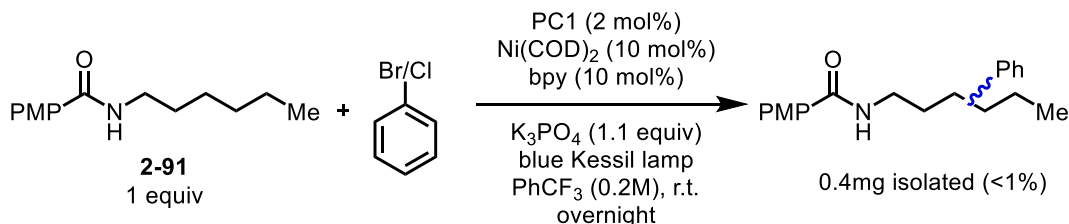
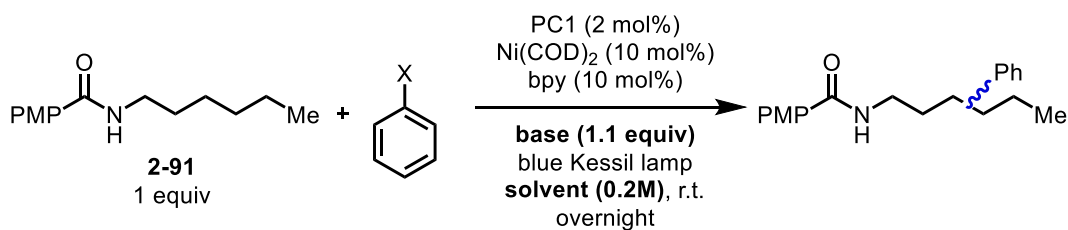


Figure 2-30 Isolation of trace arylation product.

Although substrate decomposition was observed when using PhCF₃ as a solvent, we were pleased to see at least some reactivity, therefore screening was continued using this solvent. We next turned our attention to interrogation the importance of the base in this reaction. Guided by Rovis and Knowles, screens were expanded to include K₃PO₄ and

NBu₄OP(O)(OBu)₂. From these screens, what was initially perplexing was that oxidative decomposition was only observed in the substrate that would form a tertiary distal radical. To confirm that no decomposition occurred in the substrate that would give a distal secondary radical, a battery of bases were re-evaluated. Although no signs of decomposition product were identified, a new spot was observed by TLC for the reaction using K₃PO₄ (Figure 2-30). Upon isolation of 0.4 mg (<1%) of the new spot, analysis by GCMS was conducted. Gratifyingly, the peak in the GCMS had an identical mass to the desired product! Due to the low amount of product, more screens were performed in the hopes of both identifying a better system and enabling isolation of enough product to confirm its structural identity.

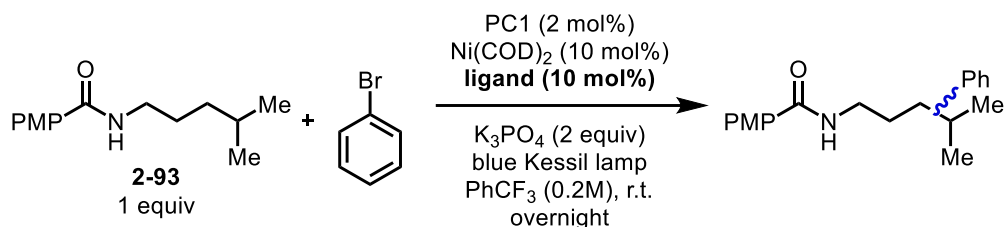
2.4.2 Optimization of Metallaphotoredox-Catalyzed Arylation



entry	aryl halide	base	solvent	yield
1	PhBr	K ₃ PO ₄	PhCF ₃	trace
2	PhBr	K ₃ PO ₄	DMAc	6%
3	PhCl	K ₃ PO ₄	PhCF ₃	—
4	PhCl	K ₃ PO ₄	DMAc	—
5	PhBr	Bu ₄ OP(O)(OBu) ₂	PhCF ₃	trace
6	PhBr	Bu ₄ OP(O)(OBu) ₂	DMAc	trace

Table 2-3 Determination of the aryl source for C-H arylation.

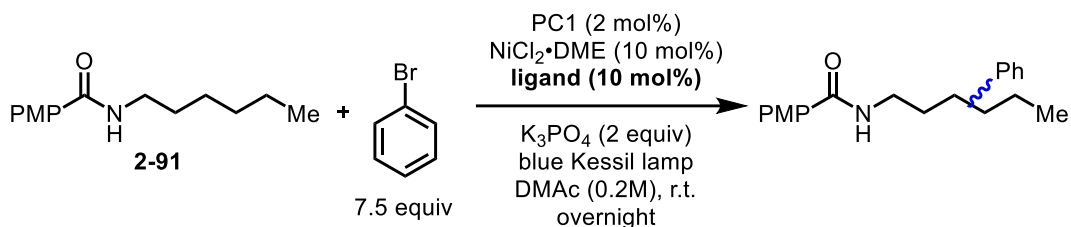
In order to determine the exact source of the aryl group, systematic screens were performed with both PhCl and PhBr using DMAc or PhCF₃ as the solvent and K₃PO₄ or



entry	ligand	yield	entry	ligand	yield
1	terpy	–	9	IMes:	–
2	1,10-phen	4%	10	IPr*OMe:	–
3	Bathocuproine	–	11	PCy ₃ (20 mol%)	–
4	Neocuproine	–	12	PPh ₃ (20 mol%)	–
5	dtbbpy	6%	13	DPPE	–
6	4,4'-diOMebpy	4%	14	DPPF	–
7	4,4'-diMebpy	2%	15	dtbbpy (with PhI)	–
8	bpy	–			

Table 2-4 Ligand screen for arylation of benzamide **2-91**.

NBu₄OP(O)(OBu)₂ as the base (Table 2-3). From these experiments, it was determined that the aryl group was coming solely from PhBr, rather than PhCl (Table 2-3, entries 2 & 4). Additionally, while reactions containing NBu₄OP(O)(OBu)₂ returned only starting material and trace product (Table 2-3, entries 5 & 6), the combination of K₃PO₄ in DMAc delivered observable, isolable product formation (3.9 mg, 6% isolated yield). The mass and spectra were identical to the previously isolated functionalized amide.



entry	ligand	yield (GCFID)
1	1,10-phen	8% (isolated)
2	4,4'-diOMebpy	5%
3	2,2-bis((4S)-(-)-4-isopropylloxazoline)propane	6%
4	BnBiOx	11% (10% isolated)
5	(+)-2,2'-isopropylidenebis[(4R)-4-benzyl-2-oxazoline]	6%
6	bis(pyrazole)pyridine	3%
7	(R)-Ph-quinox	1%
8	(S)-2-(4,5-dihydro-4-isopropyl-2-oxazolyl)quinoline	3%

Table 2-5 N-donor ligand screen with **2-91**.

Having identified a base/solvent combination that delivered the desired product, efforts were directed at screening different ligands for nickel (Table 2-4). Due to the success of bpy in this reaction, other bpy-like and phenanthroline-like ligands were examined. Although the benzamide arylation product was formed with *N*-alkyl benzamide (**2-93**),

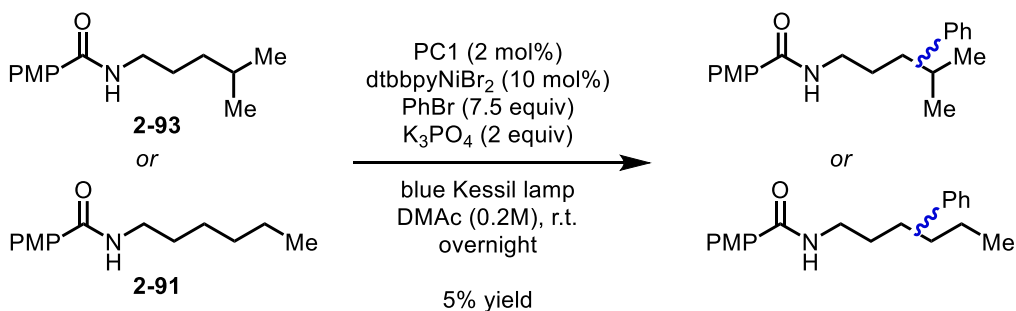
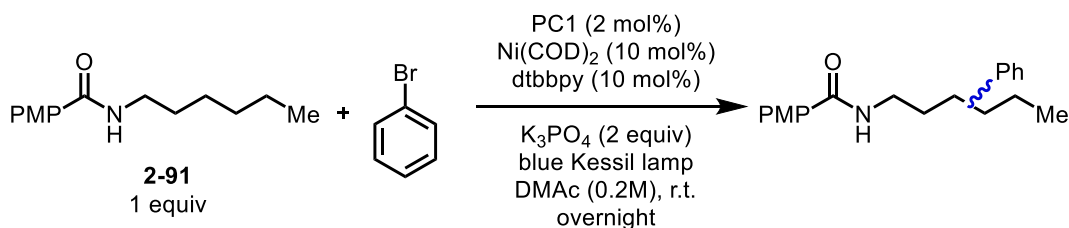


Figure 2-31 Comparison of **2-93** and **2-91** in the arylation of benzamides.

experiments were also conducted in parallel with *N*-alkyl benzamide (**2-91**) (Figure 2-31). Of the ligands examined, several provided small amounts of benzamide arylation, ranging from 1.4 mg (2%) with 4,4'-diMe bpy (Table 2-4, entry 7) to 3.4mg (6%) with dtbbpy (Table 2-4, entry 5). Other ligands, such as NHCs, phosphines ligands, or bpy were unsuccessful in this reaction. Also, it was noted that using PhI as the aryl source did not provide any of the desired product (Table 2-4, entry 15), therefore, further optimization was conducted PhBr as the electrophile using the Ni(COD)₂/dtbbpy system.



entry	conditions	yield (GCFID)
1	as written	6%
2	add 10 μ L H ₂ O	—
3	dtbbpyNiBr ₂ instead of Ni(COD) ₂ /dtbbpy	5% (5% isolated)
4	4-bromobenzotrifluoride instead of PhBr	trace

Table 2-6 Modifications of arylation conditions for **2-91**.

As this point in the optimization, small modifications were made to the reaction conditions, such as the addition of H₂O (Table 2-6, entry 2) or using more activated aryl bromides (Table 2-6, entry 4), but these proved inconsequential, or in some cases, detrimental. One notable observation was that the use of a discrete Ni(II) complex, dtbbpyNiBr₂ (Table 2-6, entry 3), gave comparable yields to the *in situ* generated dtbbpyNi(0) complex. We believe that this result might indicate that a nickel(0) complex is not necessary for aryl halide activation through oxidative addition, as proposed in our

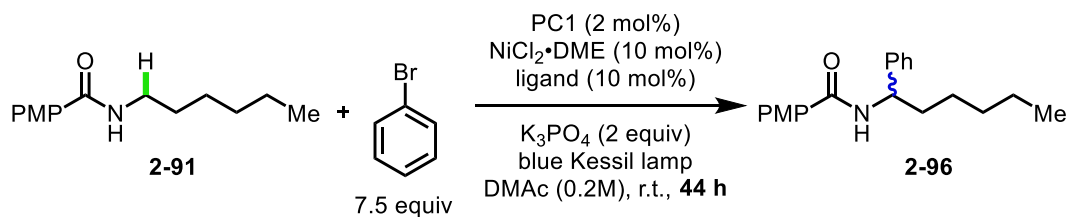
initial mechanistic hypothesis. Whether this Ni(II) salt was being reduced *in situ*, or playing a different role in the mechanism will be discussed in more detail in Chapter 3. Due to overall stability and operational simplicity, further screenings were conducted using Ni(II) salts over air-sensitive Ni(0) pre-catalysts.

entry	photocatalyst	oxidation potential	reduction potential	yield
1	PC2	1.68	-0.43	2%
2	[Ir(dF(CF ₃)ppy) ₂ (4,4'-dCF ₃ bpy)](PF ₆)	1.65	-0.51	6%
3	[Ir(dF(CF ₃)ppy) ₂ (5,5'-dFbpy)](PF ₆)	1.61	-0.9	8%
4	PC1	1.37	-1.21	15%
5	4CzIPN	1.35	-1.04	2%
6	PC8	1.32	-1.00	13%
7	Eosin Y	0.83	-1.11	0%
8	Ru(bpy) ₃ (PF ₆) ₂	0.77	-0.81	0%
9	[Ir(ppy) ₂ (dtbbpy)](PF ₆)	0.66	-0.96	0%

Table 2-7 Comparison of redox properties and yields of photocatalysts.

With a better grasp on the base and nickel pre-catalysts necessary for this reaction, as well as subsequent ligands screenings, the identity of the photocatalyst was next examined (Table 2-7). A number of common iridium-based, as well as ruthenium and organic, photocatalysts were synthesized and tested. Using NiCl₂·DME, BnBiOx, and

K_3PO_4 in DMAc under irradiation with a blue Kessil lamp, a series of photocatalysts with different redox potentials were examined. While the Knowles report relied on a highly oxidizing photocatalyst, use of several catalysts competent in their work (Table 2-7, entries



entry	ligand	yield (GCFID)
1	1,10-phen	7%
2	BnBiOx	19% (15% isolated)

Table 2-8 Head-to-head comparison of ligands under extended reaction times.

1-3) were ineffective for this chemistry. In fact, it appears as though a sharp drop off in yield happens when a the photocatalyst is either strongly or weakly oxidizing, with **PC1** and **PC8** providing the best results (15% and 13% respectively) (Table 2-7, entries 4 & 6). It is also important to note that the strongly oxidizing organic photocatalyst, 4CzIPN, which has an oxidation potential between **PC1** and **PC8** only gave trace amount of the product (Table 2-7, entry 5). This unusual observation will be discussed further in Chapter 3, as it relates to mechanism of this transformation.

Having determined the optimum photocatalyst, a number of commercially available N-donor ligands were examined. 1,10-phenanthroline gave 8% and BnBiOx gave 10% isolated yield (Table 2-8). Although these are within error, further optimization continued with BnBiOx after the determining that longer reaction times gave better yields when compared to 1,10-phenanthroline. Additionally, as BnBiOx is derived from amino acids,

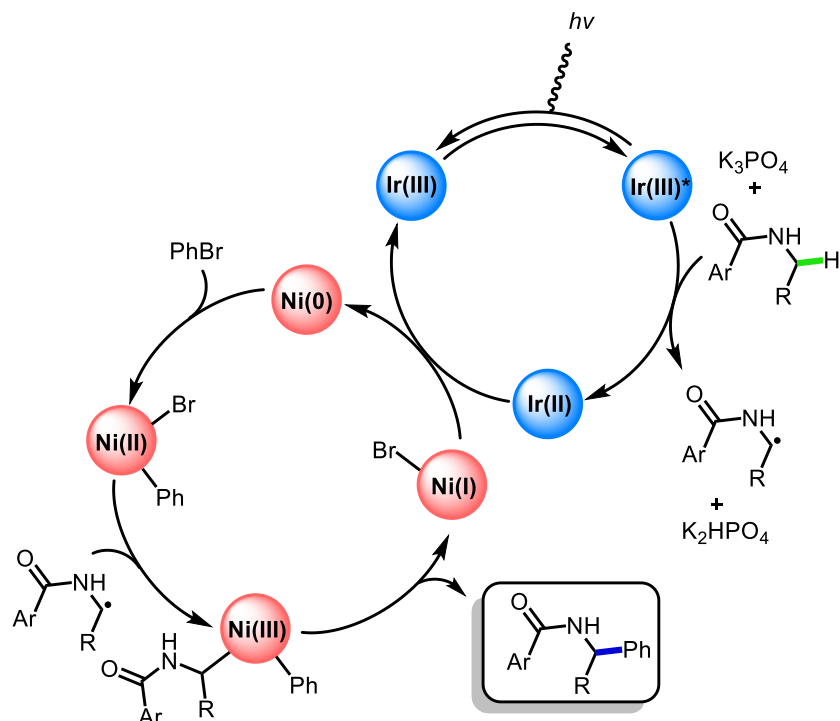
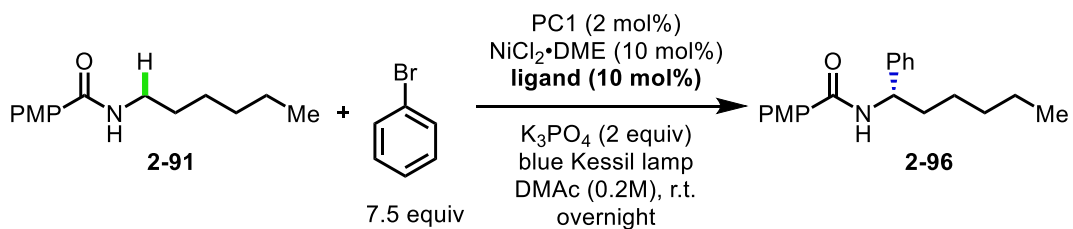


Figure 2-32 Revised mechanistic hypothesis to explain regioselectivity

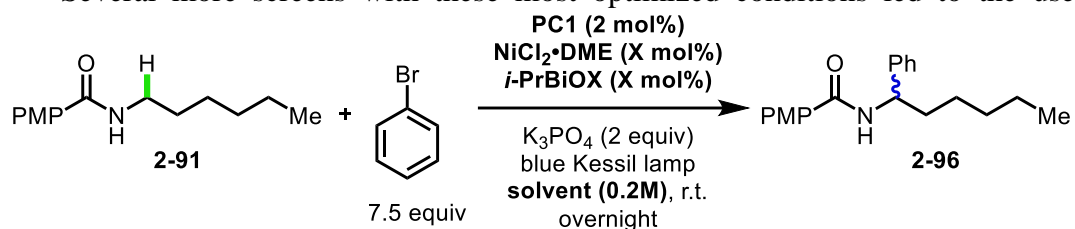
not only is the scaffold modular due to the abundance of 1,3-aminoalcohols, but also it was hypothesized that the chirality of the ligand could potentially be transferred to the product.



entry	ligand	yield
1	BiOx	19%
2	BnBiOx	22%, 32% ee
3	MeBiOx	13%, 44% ee
4	<i>i</i> -PrBiOx	13%, 79% ee

Table 2-9 Evaluation of BiOx ligands for enantioselective α -arylation.

Several more screens with these most optimized conditions led to the use of



entry	nickel/ligand loading	photocatalyst	solvent	yield (GCFID)
1	5 mol%/ 5 mol%	PC1	EtOAc	46%
2	5 mol%/ 10 mol%	PC1	EtOAc	38%
3	10 mol%/ 10 mol%	PC1	EtOAc	24%
4	10 mol%/ 20 mol%	PC1	EtOAc	29%
5	20 mol%/ 20 mol%	PC1	EtOAc	5%
6	30 mol%/ 30 mol%	PC1	EtOAc	trace
7	5 mol%/ 5 mol%	PC1 (1 mol%)	EtOAc	23%
8	<i>i</i> -PrBiOxNiCl ₂ (5 mol%)	PC1	EtOAc/DMAc (9:1)	45%
9	5 mol%/ 5 mol%	PC1	EtOAc/DMAc (9:1)	52%
10	5 mol%/ 5 mol%	PC2	EtOAc/DMAc (9:1)	23%
11	5 mol%/ 5 mol%	PC5	EtOAc/DMAc (9:1)	45%
12	5 mol%/ 5 mol%	PC6	EtOAc/DMAc (9:1)	56%
13	5 mol%/ 5 mol%	PC7	EtOAc/DMAc (9:1)	45%
14	5 mol%/ 5 mol%	PC8	EtOAc/DMAc (9:1)	28%

Table 2-10 Effects of catalyst loading, photocatalyst, and solvent on yield.

NiCl₂·DME, BnBiOx, **PC1**, and K₃PO₄ in DMAc under irradiation by blue Kessil lamps overnight at room temperature, which provided the product in 19% yield by GCFID

analysis (Table 2-8). At this point, full characterization of the product was performed. Surprisingly, when analyzed by both the 1D and 2D NMR, it was determined that the distal arylated product was not being formed under our reaction conditions. Instead, α -arylation was exclusively observed. While perplexed by this discovery, a brief search in the literature revealed that there are very few methods to directly functionalize α -C–H bonds; of these methods there are even fewer that formed C(sp³)–C(sp²) bonds, such as the ones formed in this reaction. Viewing this as an opportunity to develop a new method for α -amide C–H functionalization, efforts proceeded to increase yields to synthetically useful numbers.

As mentioned earlier, BnBiOx, a chiral N-donor ligand, was found to provide the desired product in 19% yield. We hypothesized that an enantiopure ligand could transfer chirality from nickel to the product. SFC (supercritical fluid chromatography) analysis of the product was performed to determine if enantioinduction was transferred from the ligand. When analyzing the product by SFC, we were delighted to find that BnBiOx gave 32% ee (Table 2-9, entry 2)! Efforts were made to synthesize and test other BiOx ligands in this reaction. We observed that *i*-PrBiOx could provide the product in 79% ee when run overnight at room temperature (Table 2-9, entry 4) (see optimization of ee in section 2.4.5). While the ee for this reaction was good, further efforts focused on increasing the yield for the racemic reaction before proceeding with optimization of ee in this system.

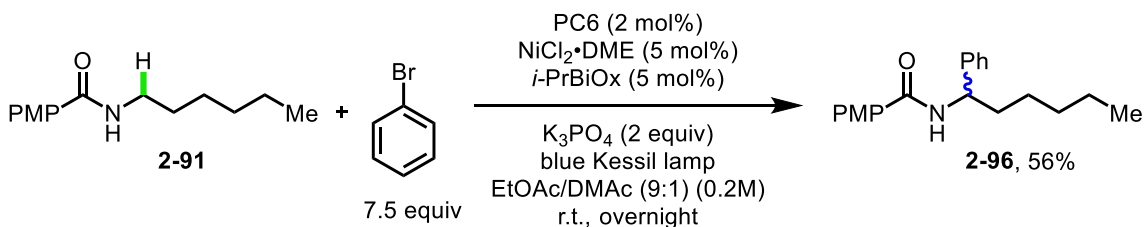


Figure 2-33 Optimized conditions for the arylation of benzamides.

Upon further investigation, it was found that the loading of nickel and iridium had drastic effect on the yield of this reaction. When attempts were made to add a second loading of catalyst(s), there were negligible effects on the yield. Though, when reducing the catalyst loading of nickel to 5 mol%, drastic increases in yield were observed (Table 2-10). In many metallaphotoredox reactions the catalyst loading of iridium photocatalyst is much lower than nickel, sometimes on the order of 0.1 mol%. When trying to reduce the catalyst loading of iridium, precipitous drops in yield were observed. Additionally, throughout these experiments, small amounts of solvent arylation were observed through GCMS analysis, prompting the switch to a more inert solvent. Ethyl acetate was found to give comparable results in this reaction, and in some cases, a mixture of EtOAc/DMAc gave superior results. From these experiments, it was determined that the optimum catalyst loading was 5 mol% of nickel and ligand and 2 mol% of iridium, which gave 56% of the desired product (Figure 2-33).

During this optimization, another observation was made relating to the base used in this reaction. Tribasic potassium phosphate was found to provide the highest yields in this reaction, though other phosphate bases, such as dibasic or monobasic potassium phosphate, gave significantly lower yield. Although not entirely clear at this point what the role of the base was throughout the reaction, the same trends held for other weak inorganic bases. As K_3PO_4 is insoluble in EtOAc, attempts were made to use other common, more soluble bases, though with no success. Furthermore, when synthesizing more soluble tetrabutylammonium phosphate bases, such as those employed by Knowles or Nicewicz, yields were highly diminished. This could occur for a number of reasons; a soluble base could inhibit some portion of the reaction, the trace moisture resulting from

synthesis of tetrabutylammonium salts (which cannot be fully removed due to Hofmann elimination) is detrimental to the reaction, or the pK_a of these bases are not poised for this reaction. Regardless, efforts proceeded with these most optimized conditions to evaluate the substrate scope of the reaction.

2.4.3 Reaction Scope of α -Arylation of *N*-Alkyl Benzamides

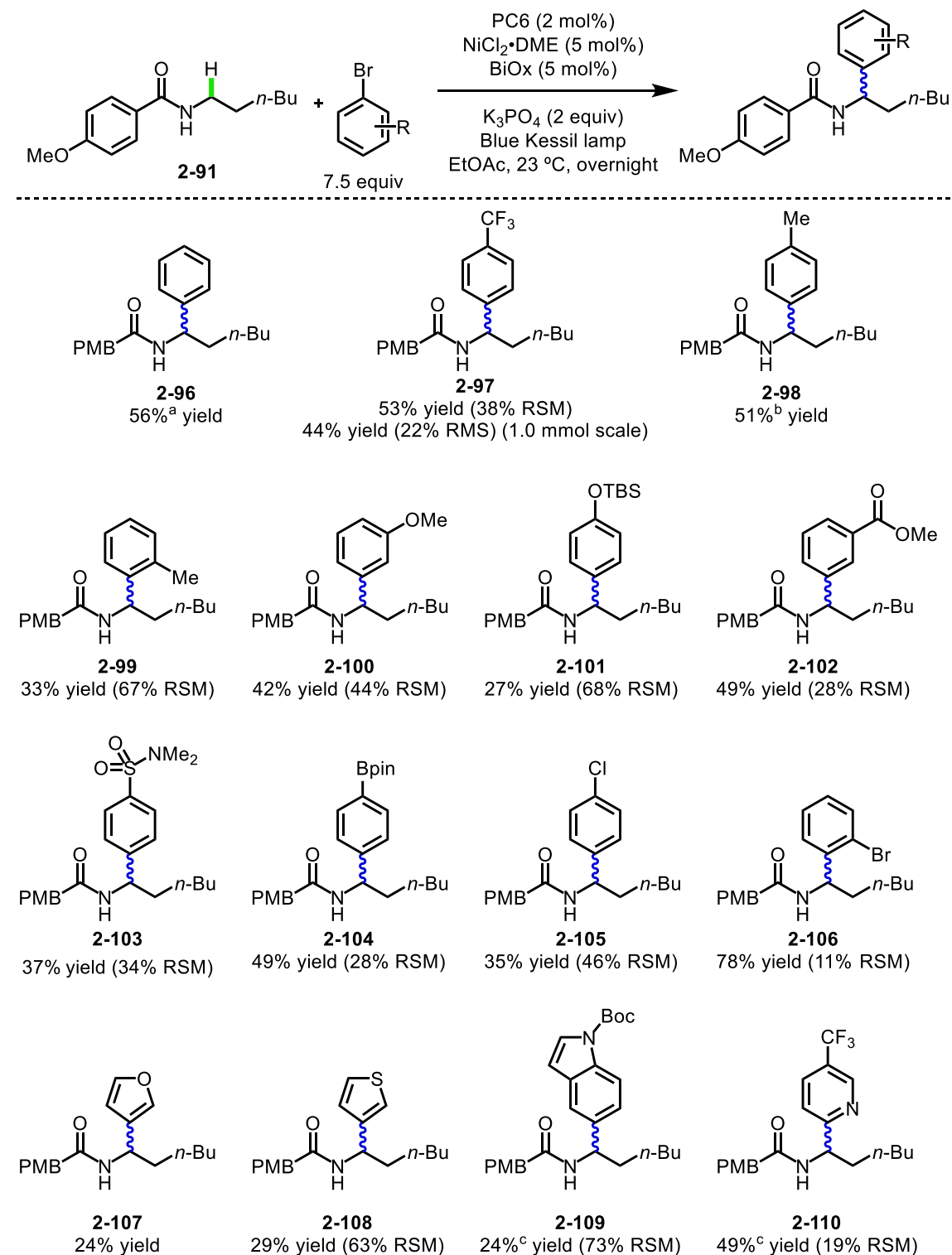


Table 2-11 Aryl bromide scope for the arylation of *N*-alkyl benzamides. All yields are isolated. RSM= recovered starting material. ^a Yield determined by GC/FID. ^b Used *i*-PrBiOx (5 mol%) and EtOAc/DMAc (9:1). ^c Used EtOAc/DMAc (9:1).

With the α -arylation of **2-91** optimized to 56% yield, the substrate scope of this transformation was next explored (Table 2-11). In evaluating aryl bromides with different electronics, sterics, and functional groups, this reaction was found to be compatible with a wide variety of coupling partners. Electron-deficient and electron-rich aryl bromides were well suited for this reaction, giving α -arylation in 53% and 51% (**2-97** and **2-98**). *Ortho*- and *meta*-substitution could be tolerated, though the former provided lower yields (**2-99** and **2-100**). A wide variety of functional groups could be incorporated into the products including protected phenols (**2-101**), which have been shown to be suitable coupling partners in nickel-catalyzed methods developed within our own lab, methyl esters (**2-102**), and sulfonamides (**2-103**) could be incorporated into the product. Additionally, functional groups that can be utilized in further functionalization, such as pinacol boronic esters (**2-104**), aryl chlorides (**2-105**), and bromides (**2-106**) were all well tolerated, highlighting the chemoselectivity of this reaction. Importantly, several heterocyclic aryl bromides including furans (**2-107**), thiophenes (**2-108**), and indoles (**2-109**) could be incorporated in modest yields, though some heterocycles like pyridines (**2-110**) gave synthetically useful yields.

When examining various changes to the aryl region of the benzamide (Table 2-12), it was found that electron-neutral, -donating, and -withdrawing functional groups could be tolerated with minor perturbations in yield from the model substrate (**2-111** to **2-115** and **2-118**). Benzamides with *ortho*- and *meta*-substitution were also tolerated to an extent (**2-116** and **2-117**). It was found that very electron-deficient benzamides performed very well in this chemistry (**2-119**), providing yields better than the model substrate, and that heterocycles on the benzamide could be incorporated (**2-120**). When modifying the alkyl portion of the benzamide, it was found that shorter alkyl chains could be arylated to some

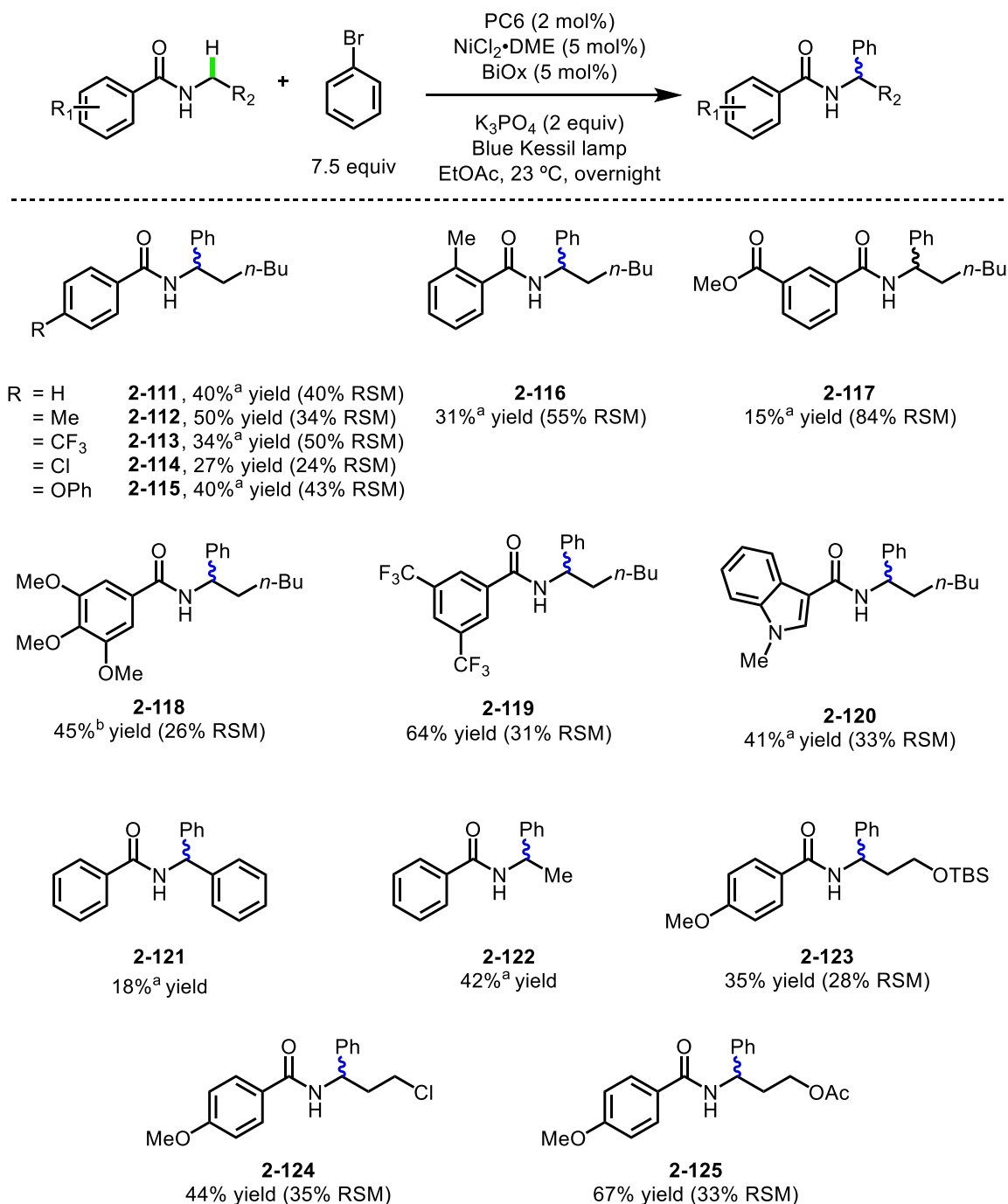


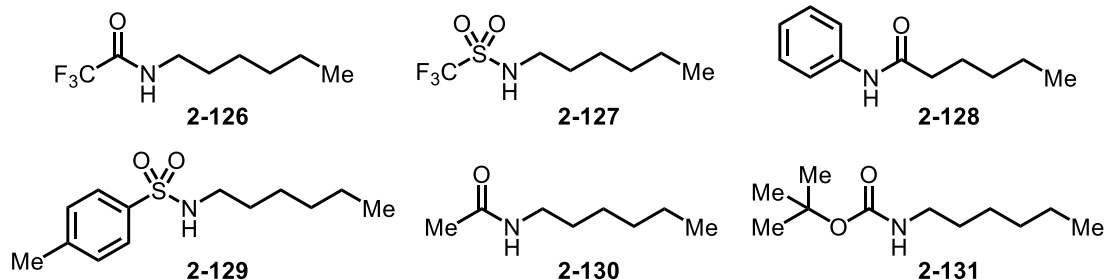
Table 2-12 Benzamide scope for the arylation of *N*-alkyl benzamides. All yields are isolated. RSM= recovered starting material. ^a Yield determined by GC/FID. ^b Used *i*-PrBiOx (5 mol%) and EtOAc/DMAc (9:1).

degree (**2-121** and **2-122**). Pleasingly, other functional groups on the alkyl portion of the benzamide, such as protected alcohols (**2-123**), alkyl chlorides (**2-124**), and acetates (**2-125**) could all be used in this transformation.

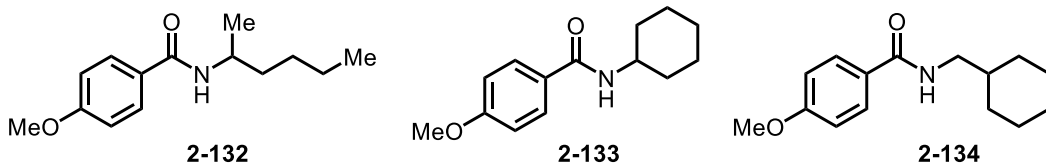
2.4.4 Limitations in the Functionalization of *N*-Alkyl Benzamides

As demonstrated through the exploration of aryl bromide coupling partners and the varied alkyl and aryl portion of the benzamide, this method is quite broad in scope.

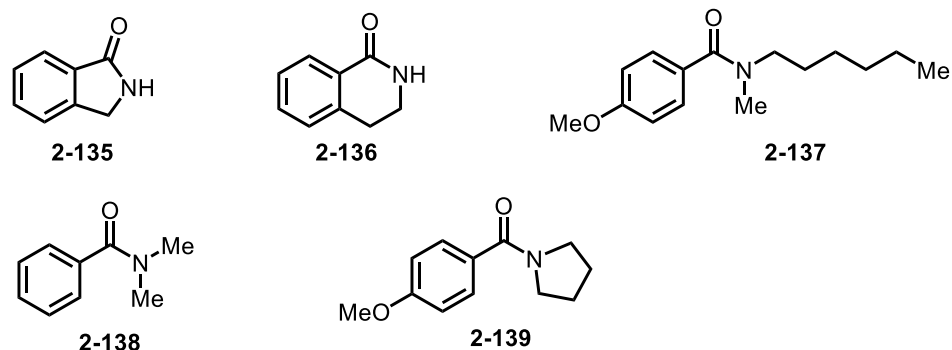
Nitrogen protecting groups:



Branching patterns:

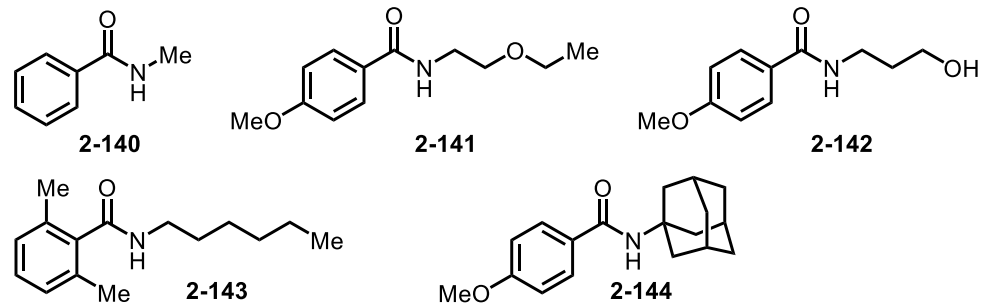


Cyclic and tertiary amides:



multiple products observed in GCMS and NMR

Secondary amides:



product observed, but messy
NMR with multiple products

Table 2-13 Incompatible nitrogen protecting groups and amides.

However, there are some limitations on both the electrophiles and benzamides that can be

used in this reaction. Despite the similarity of our conditions to those of the Rovis report, triflamides and trifluoroacetamides (**2-126** and **2-127**) were unreactive under these conditions. Additionally, other common protecting groups on nitrogen were tested, including tosylates, acetates, and boc-groups, though to no avail (**2-128** to **2-131**). From this data it appears that only benzamides are compatible in this reaction.

Of the benzamides tested, there were several that were unreactive and returned only starting material (Table 2-13). α - and β -branching of benzamides were found to be incompatible (**2-132** to **2-134**), as were cyclic substrates (**2-135** and **2-136**). Tertiary benzamides were also not tolerated (**2-137** and **2-138**), though a pyrrolidino group gave small amounts of product in addition to 2-phenyl pyrrole, possibly through a nickel-

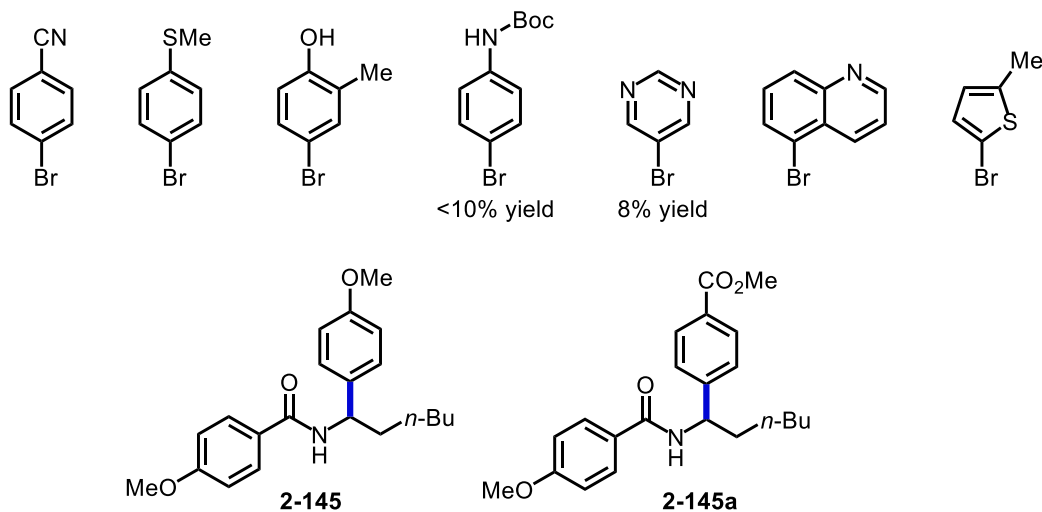


Table 2-14 Incompatible aryl bromides and inseparable products.

mediated oxidation of the substrate via β -hydride elimination and aromatization (**2-139**). This reaction was also not suitable for the arylation of primary C–H bonds (**2-140**) or substrates containing ethers (**2-141**) or alcohols (**2-142**). Interestingly, amides with bis-*ortho*-substitution (**2-143**) gave multiple products by NMR and trace amounts of the desired product. This could explain why other protecting groups, like acetates, were unsuccessful as this substrate too lacks π -overlap due to the large steric profile of the *ortho*-

substituents. Last, but unsurprising, benzamides lacking α -C–H bonds (**2-144**) could not be used in this chemistry.

Turning our attention to the aryl bromide coupling partner, several substrates were found to give either low yields or no reaction (Table 2-14). Among these, aryl nitriles and easily oxidized groups, such as thioethers were unsuccessful in this reaction. Additionally, aryl bromides containing acidic protons, like phenols or Boc-amines were also not tolerated. Although several heterocycles could be used in this reaction, pyrimidines and quinolines did not give appreciable reactivity. Oddly enough, 3-bromothiophene gave the desired product, yet 2-bromon-5-methyl thiophene did not. Lastly, although several functional groups were tolerated in the reaction, some substitution patterns gave inseparable mixtures of product and starting material, such as methyl ether **2-145** and ester **2-145a**, and therefore were not included in the substrate table. Despite these limitations, numerous secondary benzamides and aryl bromides could be used in this reaction, highlighting the robustness of this system.

2.4.5 Enantioselective α -Arylation of N-Alkyl Benzamides

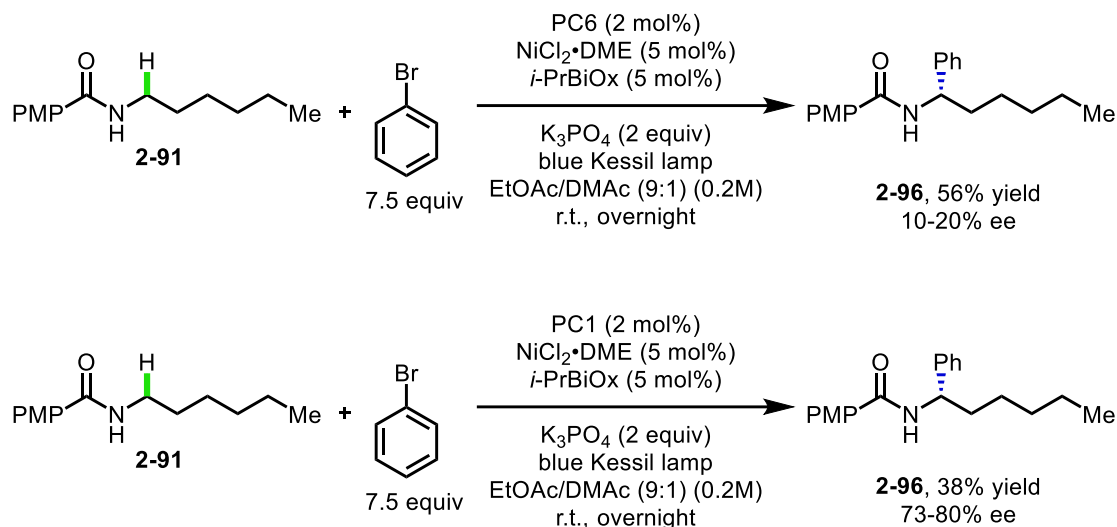


Figure 2-34 Inconsistent enantioselectivity using different photocatalysts.

With a wide substrate scope and compatibility of coupling partners, the enantioselectivity of this reaction was re-examined. Initially, promising results with *i*-PrBiOx gave the desired product in 13% yield and 79% ee. However, when these conditions were repeated, inconsistent results were observed (Figure 2-34). The yields for

photocatalyst properties	PC1	PC6
oxidation potential	1.21 V vs SCE	1.25 V vs SCE
reduction potential	-0.89 V vs SCE	-0.74 V vs SCE
max excitation	380 nm	389 nm

Table 2-15 Comparison of the properties of **PC1** and **PC6**.

the overall reaction were comparable to the racemic reaction, but enantioselectivity ranged vastly. When testing other photocatalysts, such as **PC1**, slightly lower yields were observed, but surprisingly the ees were higher. Prompted by this result, it was hypothesized that the more strongly oxidizing photocatalyst was somehow racemizing either *i*-PrBiOx during the reaction or the product, leading to lower ee (Table 2-15). Efforts were thus

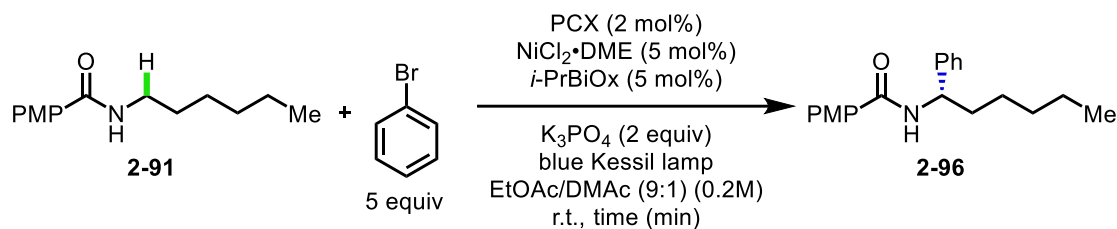
directed at determining the source of racemization and the reason for different enantioselectivities with different photocatalysts.

To probe whether ligand or product racemization were occurring, several control experiments were devised (Table 2-16). Firstly, enantioenriched product was subjected to the reaction conditions using **PC6**, which gave low ee with the model substrate during a

entry	conditions	beginning ee	ending ee	Δ ee
1	as written	71%	71%	0%
2	no NiCl ₂ ·DME or <i>i</i> -PrBiOx	72%	74%	+2%
3	no NiCl ₂ ·DME, <i>i</i> -PrBiOx, or K ₃ PO ₄	74%	70%	-4%
4	no PC6	80%	70%	-10%

Table 2-16 Racemization of enantioenriched arylation product.

productive reaction (Table 2-16, entry 1). Surprisingly, there was very little change in ee under standard conditions or when omitting nickel, ligand, or base (Table 2-16, entries 2 & 3). There was, however, a small change in ee when omitting the photocatalyst, though the ee was still substantially higher than what was observed under standard conditions (70% ee vs. 10-20% ee) (Table 2-16, entry 4). These results suggest that once the product is formed, its ee does not drastically change over the course of the reaction. While informative, these experiments did not elucidate the origin of the lower ee for **PC6** vs. **PC1**, thus further studies were deemed necessary.



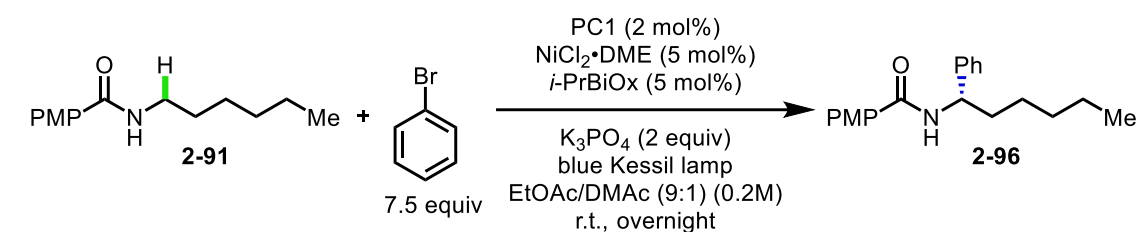
		PC6		PC1	
entry	time	yield	ee	yield	ee
1	30 min	4.9%	ND	3.2%	ND
2	60 min	6.3%	ND	5.6%	ND
3	90 min	7.4%	70%	9.2%	89%
4	150 min	15.3%	57%	16.2%	88%
5	210 min	22.5%	51%	24.8%	82%
6	270 min	30.0%	44%	25.9%	81%
7	330 min	ND	40%	ND	81%

Table 2-17 Change in enantioselectivity over time using different photocatalysts.

Next, to determine if the ee of the reaction was changing over time due to some other pathway, such as ligand decomposition, a time course study was undertaken (Table 2-17). Using **PC1** and **PC6**, aliquots of the reaction mixture were taken periodically over 330 minutes and analyzed by GCMS and SFC for yield and ee. Despite the differences in yield at the end of a standard reaction, both photocatalysts performed similarly, giving approximately the same yield throughout the first 210 minutes (Table 2-17, entry 5). When comparing the ee, these two photocatalysts gave very different results. Due to the small amount of product formed at early time-points, ee could only be determined after 90 minutes. At this time point, both reactions had substantially different ees, **PC1** with 89%

ee and **PC6** with 70% ee (Table 2-17, entry 3). As the reaction with **PC1** progressed, there was a slight drop to 81% ee after 330 minutes (Table 2-17, entry 7). However, the reaction with **PC6**, gave much lower ees throughout the reaction, with the last time point of 330 minutes showing 40% ee (Table 2-17, entry 7).

From these experiments it was clear that ee changes for both catalysts throughout the reaction. Further, **PC6** had a much lower initial ee and also larger drop in ee over time. While the reason for lower ees of the product when comparing **PC6** to **PC1** was not identified, it became clear that **PC1** was a better catalyst for the enantioselective arylation of *N*-alkyl benzamides and was thus used in subsequent studies.



entry	conditions	yield	ee
1	run with a fan	47%	34% ee
2	run without a fan	48%	12% ee
3	run in a water bath	37%	67% ee

Table 2-18 Effects of temperature on α -arylation enantioselectivity.

Having gained a better understanding of the drop in selectivity over time and the erratic ees observed from one photocatalyst to another, the photoreactor setup was next examined (Table 2-18). For the purposes of screening, each reaction was run in a 1-dram vial on a stir-plate, approximately 2 cm away from a blue Kessil lamp, with two reactions per lamp. Above each stir-plate was a 10" fan that was directed straight down on the vials to keep them at uniform temperature during irradiation. Because ee eroded over time, we

hypothesized that the vials slowly heated up over the course of the reaction, leading to lower ees as the reaction progressed. To test this, three reactions were run, one in the manner described above (Table 2-18, entry 1), one in an identical manner but without a fan (Table 2-18, entry 2), and one was placed in a recrystallization dish filled with water (Table 2-18, entry 3). Yield and ee were measured for all three reactions and it was found that the reaction run without a fan gave very low enantioselectivity, while the one run in a

entry	conditions	temperature	time	yield	ee
1	run in ice-bath	4 °C to 0 °C	12 h		85% ee
2	run in jacketed beaker	-5 °C	46 h	30%	68% ee
3	run in jacketed beaker	-10 °C	24 h	31%	89% ee
4	run in recrystallization dish	-10 °C	18 h	22%	88% ee
5	run in recrystallization dish	-20 °C	18 h	25%	80% ee
6	run in recrystallization dish	-20 °C	42 h	32%	71% ee

Table 2-19 Comparison of yield and enantioselectivity for cooled photoreactors.

recrystallization dish filled with water gave substantially better enantioselectivities. After repeating these experiments to confirm reproducibility, it was found that reactions maintained at approximately 25 °C, using the water bath, consistently gave ees (between 65% ee to 70% ee), confirming that indeed the Kessil lamps were causing the reactions to

heat up, despite the cooling fans, thus adversely affecting the ee of the reaction. Further supporting this result, when a reaction was run in an ice-bath, carefully maintained at approximately 4 °C for 12 hours, the ee for the reaction was found to be 85% (Table 2-19,

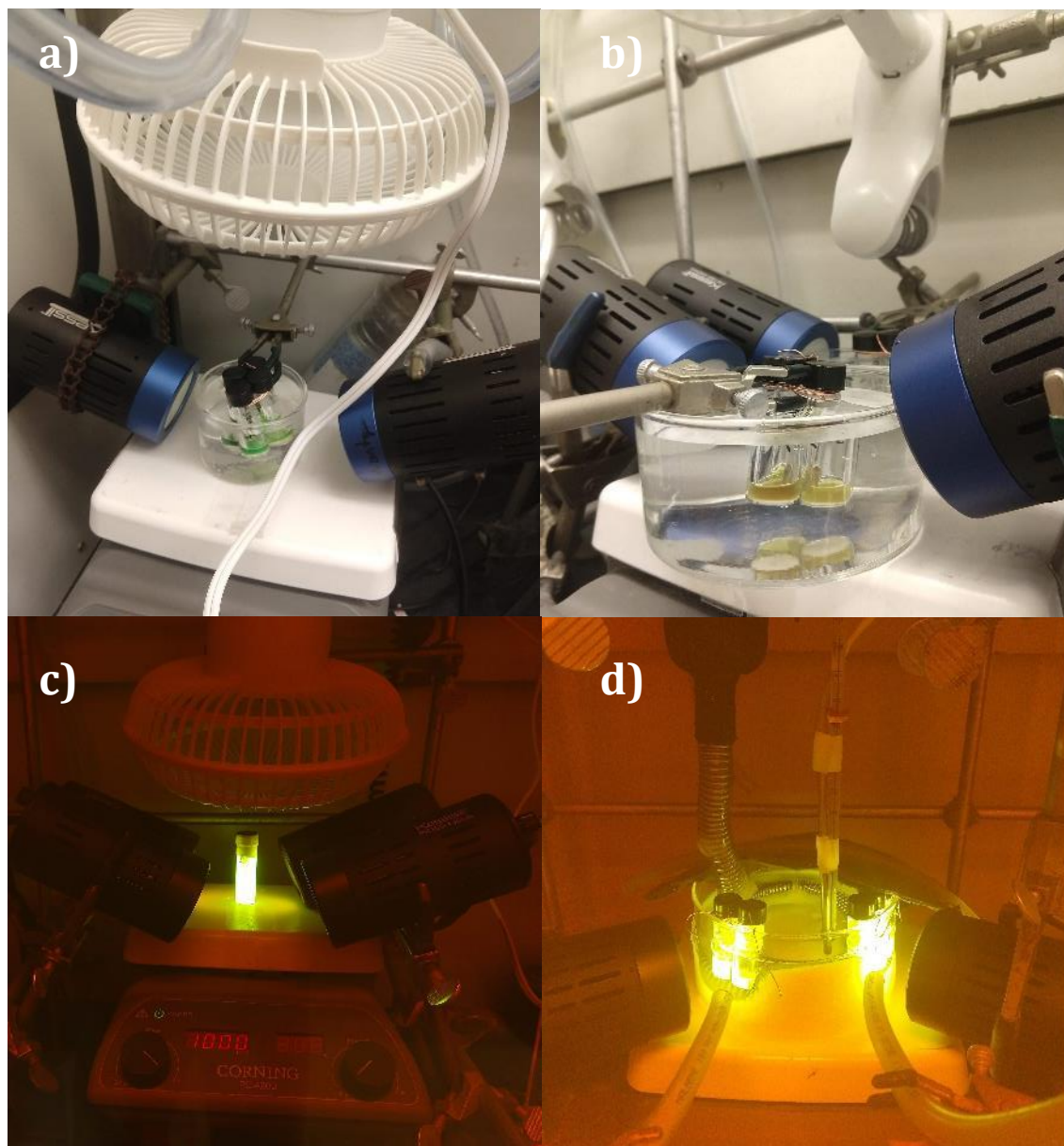


Figure 2-35 Different photoreactor setups used to maintain low temperatures during α -arylation reactions. **a)** Reactions cooled in a water bath, before irradiation, **b)** after 16 hours of irradiation, **c)** reaction cooled using a fan, and **d)** reactions in an IPA bath that is cooled using a cryo-cool. A thermometer is used to monitor the temperature and two air hoses (bottom of the photo) are used to prevent the build-up of ice.

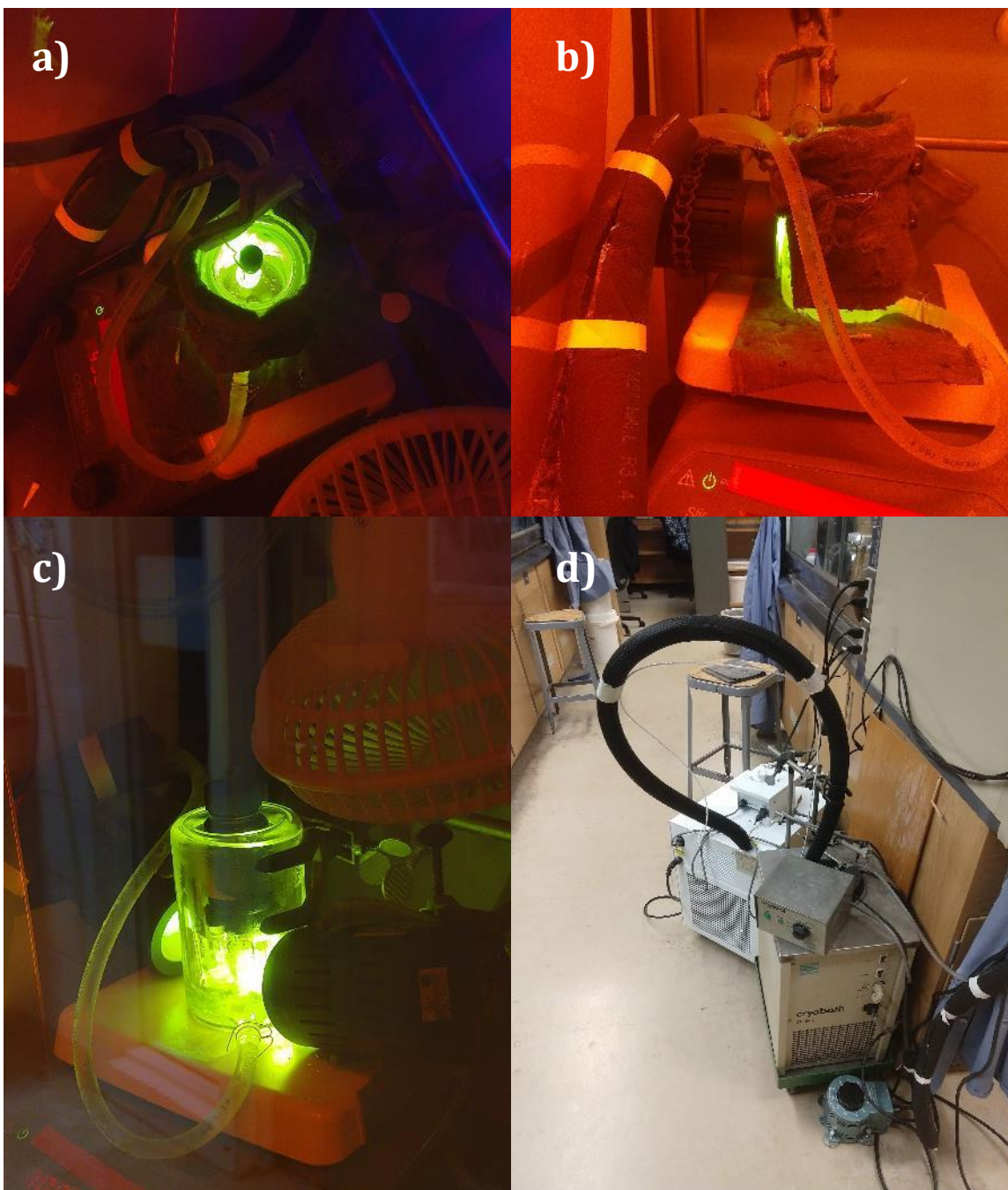


Figure 2-36 Different photoreactor setups used to maintain low temperatures during α -arylation reactions. **a)** Top view, and **b)** side view of an IPA-cooled insulated jacketed beaker using one Kessil lamp, **c)** jacketed beaker using an IPA-cooled jacketed beaker with two Kessil lamps, and **d)** cryo-cooler used to pump cold IPA through the jacketed beaker.

entry 1)! With these results, efforts were directed towards developing a photoreactor capable of maintaining low temperatures over the course of the reaction.

Having discovered the culprit for irregular trends in ee and decreases in enantioselectivity over the course of a reaction, a newly designed photoreactor was

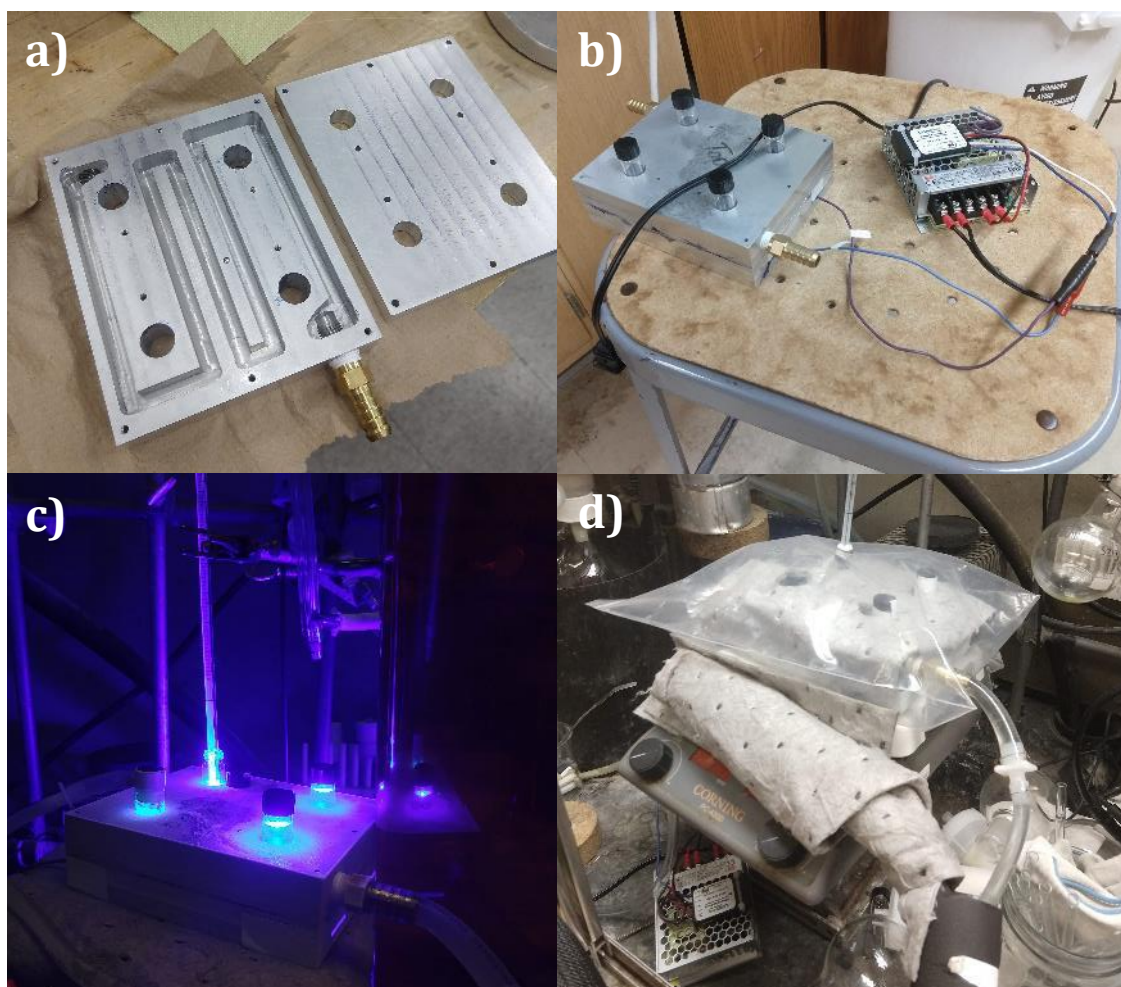


Figure 2-37 Aluminum photoreactor for enantioselective α -arylation. **a)** Cross-section of aluminum photoreactor, **b)** assembled photoreactor and power supply, **c)** photoreaction in progress with three reactions and a thermometer, **d)** photoreactor insulated with pigmat, inside a ziplock filled with N_2 gas to prevent condensation.

targeted. The design of the new photoreactor was challenging and several different setups were explored (Figure 2-35 and Figure 2-36). Importantly, the new photoreactor would have to maintain low temperatures over the course of the reaction. It would also need to allow good light penetration by a light source, as well as being compatible with a stir-plate to ensure even mixing of the reaction. Because the ice-bath method required constant refilling and attention, it was deemed an impractical solution. Various other reactors examined in order to solve our cooling issues. Systems including 1) a jacketed beaker that could be hooked up to a recirculating pump, 2) a setup in which vials were

placed in a Dewar full of a cooled solvent (using either dry ice or a cryo-cool), with a Kessil lamp pointing into the Dewar, and finally, 3) irradiating the vial from below a recrystallizing dish that was cooled by a cryo-cool. All of these setups had one issue or another, including the buildup of condensation (or sometimes ice) that blocked light penetration, problems holding low temperatures, or problems with stirring.

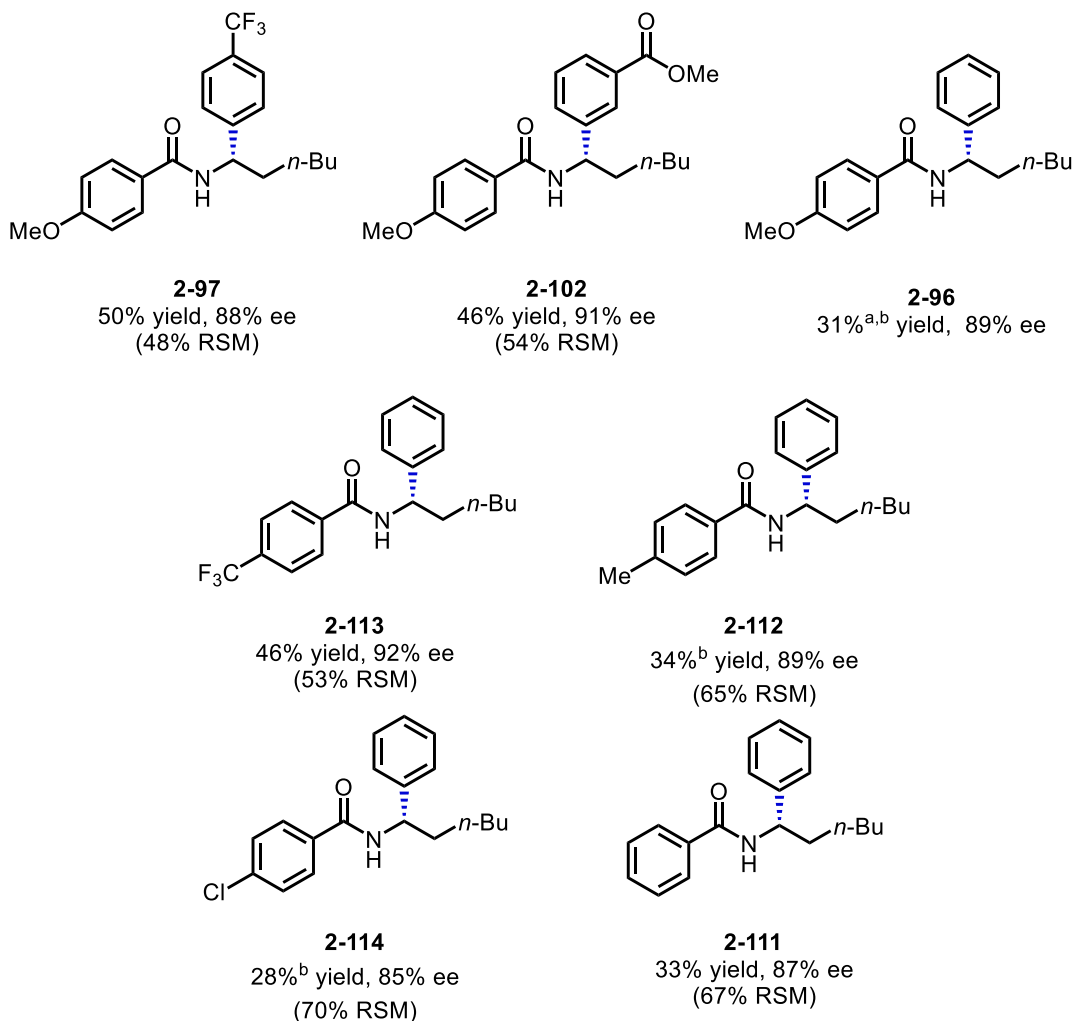
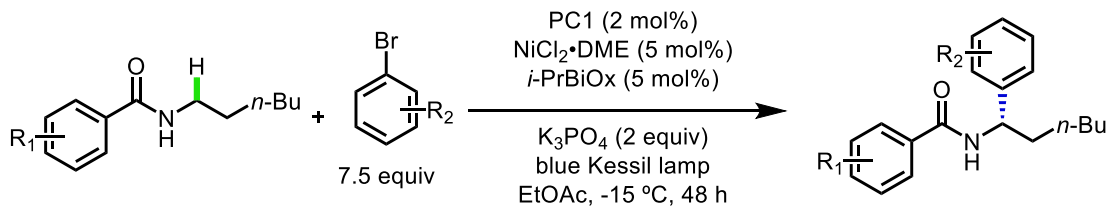


Table 2-20 Reaction scope of enantioselective arylation of benzamides. ^a Yield determined by GCMS. ^b Reaction run for 24 h.

To address the issues with the development of a photoreactor that could maintain low temperatures, light penetration and stirring, Cameron Nubile, who worked in the University of Michigan Electronic Shop was consulted for assistance with the design and construction of a photoreactor. With Cameron's help, a four-well aluminum block, with channels for cooling fluid to run through and high-powered blue Cree LEDs below each well, was built. This new reactor allowed for simultaneous cooling of four reactions by pumping cooled fluid through the channels of the aluminum block, while irradiating each vial (Figure 2-37). Additionally, this reactor was thin enough to allow stirring from a standard stir-plate so that reaction mixtures received consistent mixing. Using a cryo-cool, a recirculating aquarium pump, and the new photoreactor, temperatures as low as $-15\text{ }^{\circ}\text{C}$ could now be maintained for up to 48 hours.

Having developed an efficient photoreactor to maintain low temperature reactions, the enantioselective α -arylation of *N*-alkyl benzamides was explored. Like the racemic reaction, aryl bromides bearing several different functional groups could be used in this reaction (**2-96**, **2-97**, and **2-102**). These reactions were typically slower, though the yields were comparable to the racemic version when substrates were irradiated for 48 hours instead of overnight. Additionally, different groups on the aryl portion of the benzamide could be seamlessly incorporated (**2-111** to **2-114**). In all cases, good to excellent ee was observed when reactions were run between $-10\text{ }^{\circ}\text{C}$ and $-15\text{ }^{\circ}\text{C}$. Unlike the racemic reaction, the mass balance was solely accounted for by starting material. This indicated the potential for longer reaction times to increase yields and conversions.

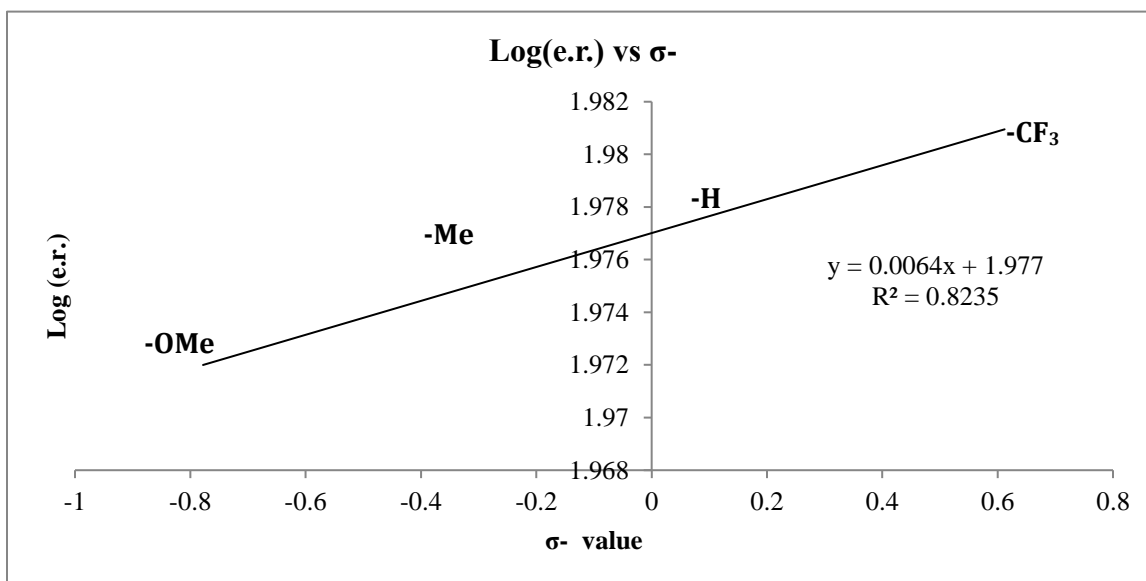
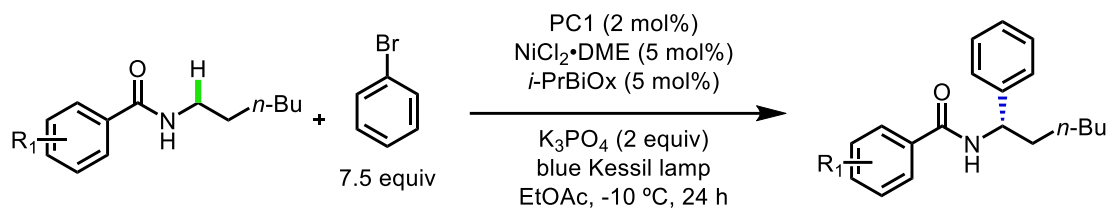


Figure 2-38 Relation between enantioselectivity and σ^- for para-substituted benzamides.

When first analyzing the enantioselectivity of this reaction, it was thought that the electronics of the aryl bromide or benzamide might influence ee. However, when plotting these values against different Hammett parameters, there appeared to be no strong correlation between σ^- (*para*-benzamide) and ee or σ (*para*-aryl bromide) and ee (Figure 2-38 and Figure 2-39). Although preliminary data, this may be useful in studying the mechanism of this and other enantioselective metallaphotoredox reactions.

By examining the factors that affect enantioselectivity in the arylation of benzamides, a new method to access enantioenriched α -aryl *N*-alkyl benzamides was developed. In order to address inconsistencies in ee, a more detailed study of racemization processes was undertaken, which identified increases in temperature due to

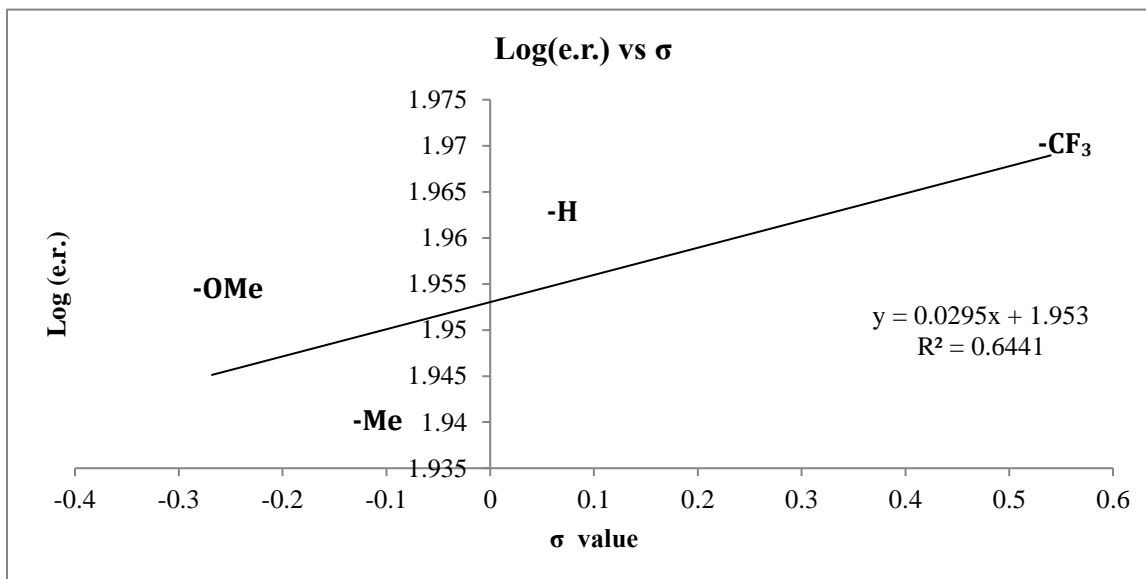
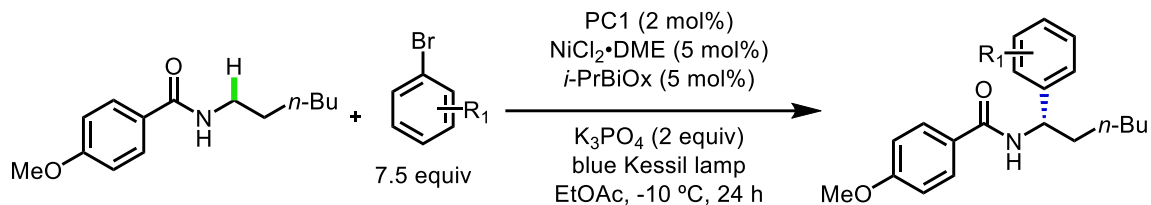


Figure 2-39 Relation between enantioselectivity and σ for para-substituted aryl bromides.

irradiation by Kessil lamps as the cause for racemization over time. This problem was addressed by the design of a photoreactor that could maintain reaction temperatures between $-10\text{ }^{\circ}\text{C}$ and $-15\text{ }^{\circ}\text{C}$ for extended periods of time. In all, this method provides a new way to access enantioenriched amine derivatives and expands the overall understanding of enantioselective metallaphotoredox.

2.4.6 Applications and Synthetic Demonstrations

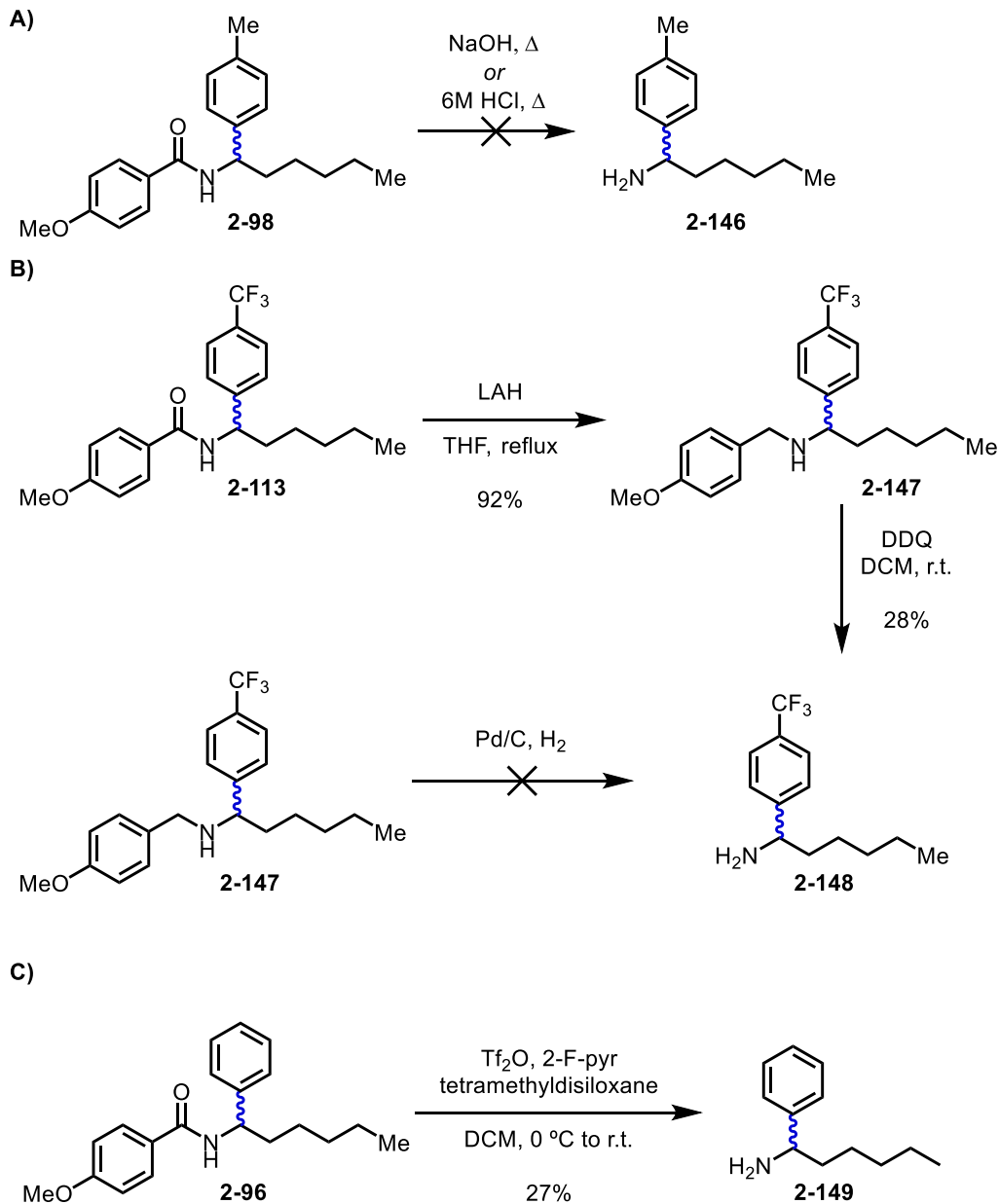


Figure 2-40 Methods for removing *para*-methoxybenzoyl groups

Having established the synthetic scope and limitations of the racemic and enantioselective α -arylation of *N*-alkyl benzamides, a series of experiments designed to highlight the value of this methodology were conducted. Firstly, as this method provided access to α -functionalized amine derivative, the removal of the benzoyl group was attempted in order to access the free α -aryl amines. Despite several attempts to hydrolyze

the benzoyl group under acidic or basic conditions at elevated temperatures, deprotection of the amine was not possible (Figure 2-40a). Turning to a two-step procedure, reduction of the benzamide gave the PMB-protected amine **2-147** in high yields, which could be then be treated with DDQ to remove the PMB group in modest yields **2-148** (Figure 2-40b). Other conditions attempted, such as hydrogenation with Pd/C using 1 atm H₂ were unsuccessful. While yields for this reaction were low, it is expected that further optimization could provide better, more synthetically useful yields of the unprotected amine. Alternatively, using a recent method in the literature, direct one-step deprotection could be achieved, albeit in modest yields as well (Figure 2-40c).

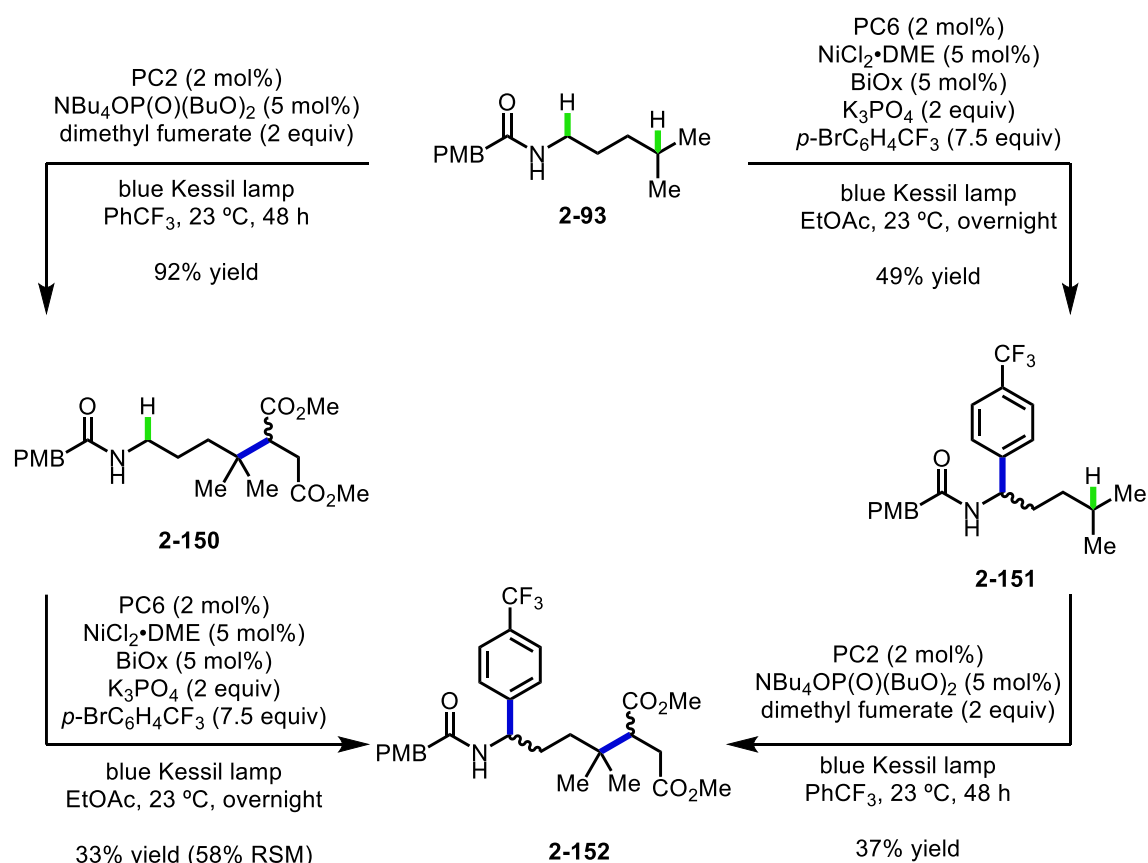


Figure 2-41 Proximal and distal for the divergent/convergent functionalization of amides.

As mentioned earlier, the similarity between this and newly developed methods developed by Rovis, Knowles, and Tambar piqued interest in their observed

regioselectivity. To compare our α -arylation to the distal alkylation of *N*-alkyl benzamides developed by Knowles, a common starting material was subjected to both conditions (Figure 2-41). Gratifyingly, exclusive α -selectivity was observed using the method described above, providing **2-151** in 49% yield. As expected, the Knowles conditions gave comparable yields to their initial report, forming **2-150** in 92% yield. When subjecting **2-150** to our conditions, clean α -arylation to provide **2-152** was observed in 33% yield. In a convergent manner, **2-151** could be converted to **2-152** in 37% yield. This divergent/convergent synthetic sequence exemplifies that high regioselectivity that is imparted by modest changes in base and catalyst structure. Additionally, it highlights the ability to form highly complex products in two synthetic steps using C–H functionalization.

2.4.7 Functionalization of Other Weak C–H Bonds

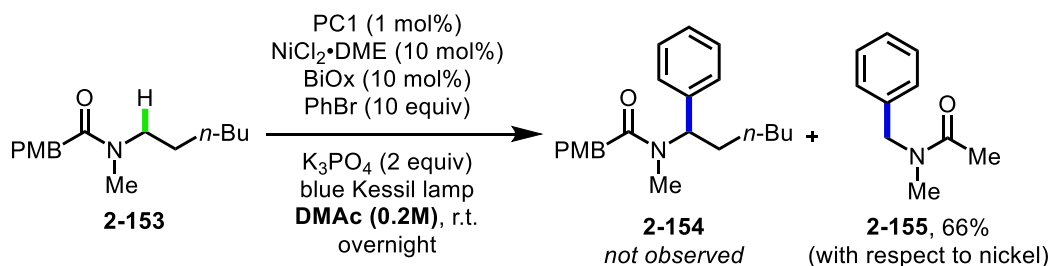
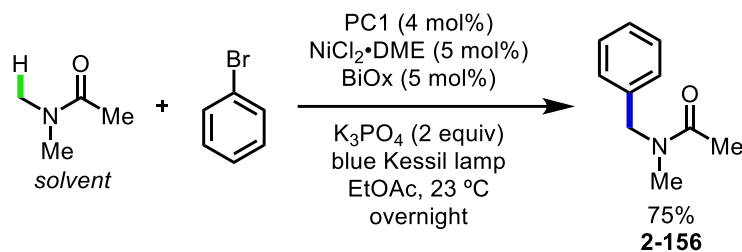


Figure 2-42 Serendipitous discovery of DMAc arylation.

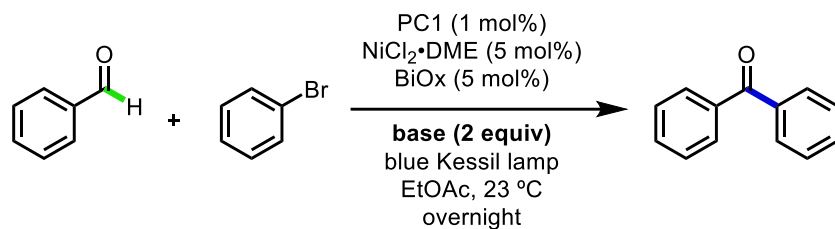
Having demonstrated the versatility of this transformation in functionalizing secondary *N*-alkyl benzamides, it was hypothesized that tertiary amides might also provide useful α -arylation products. To test this, benzamide **2-153** was synthesized and tested under the reaction conditions. While the starting material was quantitatively recovered at the end of the reaction, some arylation of the solvent, DMAc, was observed. Intrigued by



entry	DMAc	PhBr	yield
1	1 equiv	1 equiv	4%
2	0.5 mL (no EtOAc)	1 equiv	75%

Table 2-21 Arylation of DMAc using metallaphotoredox catalysis.

observation, a brief optimization was undertaken, and further optimization for the α -

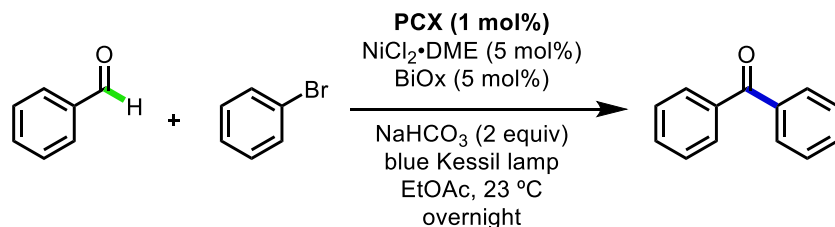


entry	base	yield
1	K ₃ PO ₄	44%
2	K ₃ PO ₄ + quinuclidine (10 mol%)	2%
3	quinuclidine	0%
4	KHCO ₃	33%
5	Cs ₂ CO ₃	14%
6	NaHCO ₃	59%

Table 2-22 Examination of different bases in the arylation of benzaldehyde.

arylation of secondary benzamides was conducted in a less reactive solvent, EtOAc.

After analyzing these reactions by GCMS, it was found that while equal ratios of DMAc and PhBr gave small amounts of product, though synthetically useful yields could be achieved when using DMAc as the solvent (Table 2-21). This provides a complementary method to the work by the Stephenson group,¹⁷⁶ which demonstrated the arylation of simple amides using electron-rich arenes. Although the scope of this method was not fully explored, it is hypothesized that a similar collection of aryl bromides could be used and other amide- or formamide-containing solvents, including those mentioned in the previous section, would be compatible.



entry	photocatalyst	yield
1	PC1	45%
2	PC5	48%
3	PC6	47%
4	PC8	27%
5	PC9	56%
6	4CzIPN	3%

Table 2-23 Examination of different photocatalysts for the arylation of benzaldehyde.

In addition to functionalizing DMAc, other weak C–H bonds, such as those of aldehydes, were examined. Inspired by the work of Newman,¹⁷⁷ a direct synthesis of ketones from aryl bromides and aldehydes was envisioned using a similar method to the arylation of secondary benzamides or DMAc. Initially, subjecting benzaldehyde

and bromobenzene to the most optimized conditions for secondary benzamide arylation yielded 44% of the desired product (Table 2-22, entry 1). Encouraged by this, a simple screen of bases was conducted, and it was determined that NaHCO_3 provided a noticeable increase in yield (Table 2-22, entry 6).

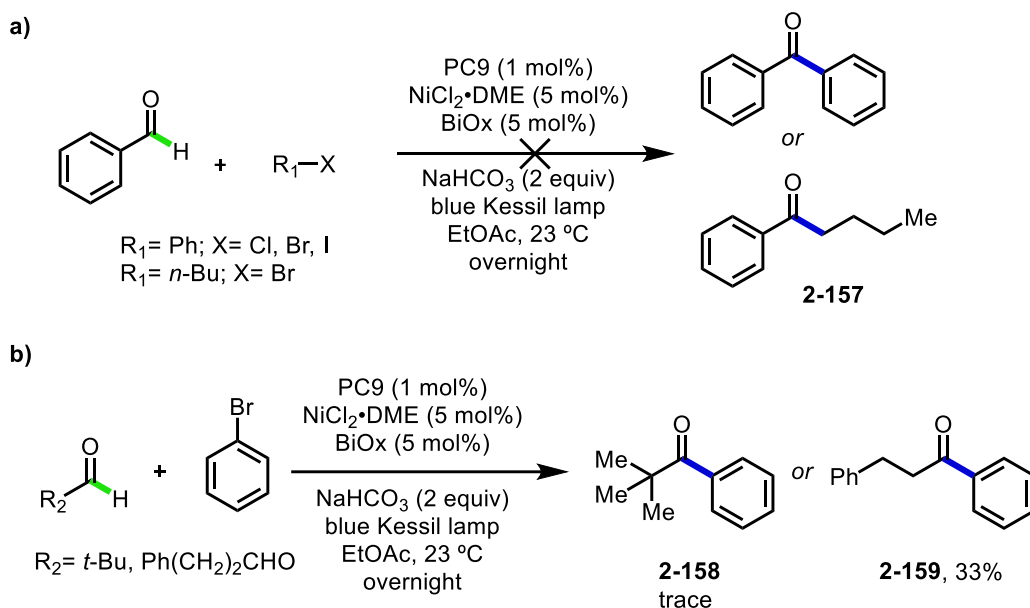
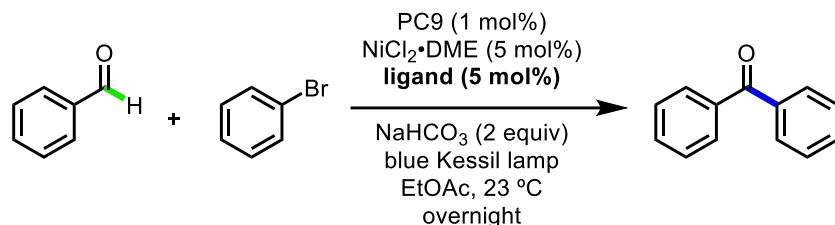


Figure 2-43 Evaluation of different electrophiles and aldehydes for cross-coupling.

After re-examining the identity of the photocatalyst, it was found that **PC9** consistently outperformed **PC1**, providing 56% yield of benzophenone (Table 2-23, entries 1 & 6). Using these most optimized conditions, the identity of the electrophile and aldehyde were explored. It was found that chlorobenzene, iodobenzene and simple alkyl bromides were incompatible under these reaction conditions. Furthermore, it was discovered that aliphatic aldehydes, such as dihydrocinnamaldehyde, provided modest yields of the arylated product, while α -substituted aldehydes did not (Figure 2-43). Lastly, a simple ligand screening revealed that bpy-base ligands, such as dtbbpy, also provided sufficient quantities of the arylated product (Table 2-24). Despite the brief optimization, this

transformation shows the breadth of reactivity that can be conferred when using a metallaphotoredox system.



entry	ligand	yield	entry	ligand	yield
1	bpy	32%	7	dtbbpy	61%
2	2-(4,5,-dihydro-2-oxazolyl)quinoline	22%	8	5,5'-diCF ₃ bpy	47%
3	bpp	36%	9	4,4'-diOMebpy	3%
4	PyBiOx	6%	10	bathocuprine	3%
5	BnBiOx	35%	11	1,10-phen	5%
6	(+)-2,2'-isopropylidenebis[(4R)-4-benzyl-2-oxazoline]	26%	12	terpy	7%

Table 2-24 Ligand screen for the arylation of benzaldehyde with bromobenzene.

2.4.8 Summary of the α -Arylation of Benzamides, Tertiary Amides, and Aldehydes

A new method for the α -arylation of *N*-alkyl benzamides was developed using a nickel/iridium metallaphotoredox system. Through the exploration of different aryl bromides, it was shown that this reaction could enable a wide variety of sterically, electronically, and functionally diverse coupling partners. Additionally, changes to the aryl or alkyl portion of the benzamide were tolerated in most cases, showcasing the ability to diversify highly decorated benzamides. This transformation circumvents the challenges of using amides in non-solvent quantities, allowing more valuable substrates to be functionalized. Furthermore, this reaction provides an orthogonal method to access

enantioenriched amine derivatives under mild conditions using a novel metallaphotoredox system. While there are several limitations to both the electrophile and the benzamides that can be used, the mildness and efficiency of this reaction make it broadly useful for the diversification of amine derivatives.

Additionally, this method was extended to an enantioselective variant, which provided access to enantioenriched α -aryl amine derivatives in modest yields and good to excellent enantioselectivity. Key to the development of an enantioselective reaction were systematic studies regarding the source of ee degradation over the course of the reaction. This work led to important insights into the reactor setup in enantioselective metallaphotoredox, which enabled us to develop a temperature-regulated photoreactor. This new reaction setup provided high levels of reproducibility and excellent selectivity. Further, this new photoreactor allowed for a brief exploration of the substrate scope, which proved similarly tolerant of aryl halides and benzamides as the racemic variant.

Lastly, this metallaphotoredox system was employed in the arylation of other C–H bonds including those of tertiary amides and aldehydes. Slight modifications of the conditions afforded the direct arylation of DMAc in up to 75% yield, and benzaldehyde or dihydrocinnamaldehyde in 61% and 33% yield respectively. Further investigation should be directed at improving the yield for all reactions mentioned above, expanding the scope of enantioselective arylations, and reducing the excess of coupling partners to equimolar quantities.

Chapter 3

Mechanistic Investigations of Metallaphotoredox Catalyzed C–H Arylations

3.1 Overview of PET and Photochemical Thermodynamics

In order to study the role of the photocatalyst in this reaction, a rudimentary understanding of photophysical processes was necessary. While visible light possesses a great deal of energy, it is not readily absorbed by many organic molecules, hindering energy transfer. To circumvent this, a mediator is often necessary to transfer this energy into chemical potential to make and break bonds. Typically, these mediators include polypyridyl transition metal complexes and organic dyes, which are capable of absorbing photons to reach a higher energy excited state. Upon excitation, there are two possible modes of relaxation to the ground state. The first mode, unimolecular relaxation, included emissive processes such as fluorescence, phosphorescence, and non-emissive thermal processes whereupon the catalyst can return to the ground state (S_0).¹⁷⁸ Second, the excited photocatalyst can undergo a bimolecular reaction with another molecule through a photoinduced electron transfer (PET) or energy transfer (Figure 3-1). In the case of most polypyridyl transition metal complexes, this occurs through an excited triplet state (T_1). Although triplet states tend to have lower excited state energies ($E_{0,0}$) compared to singlet states, they tend to have much longer excited state lifetimes ($\tau = 20\text{-}1000$ ns for triplet states and 1-20 ns for singlet states). The longer-lived excited state originates from the

spin-forbidden relaxation associated for $T_1 \rightarrow S_0$. This property is beneficial for a photoredox catalyst where slower relaxation times allow for a higher probability of a bimolecular reaction to occur.

Despite being spin forbidden, there are many pathways for intersystem crossing (ISC) from an excited singlet to triplet state.¹⁷⁹ At its core, these transitions occur through coupling of the spin angular momentum and orbital angular momentum to circumvent quantum mechanical restrictions. In the case of iridium or ruthenium photocatalysts, ISC rates are enhanced through heavy atom effects that allow the spin and orbital quantum numbers to more easily mix. For systems lacking heavy atoms, ISC can be achieved

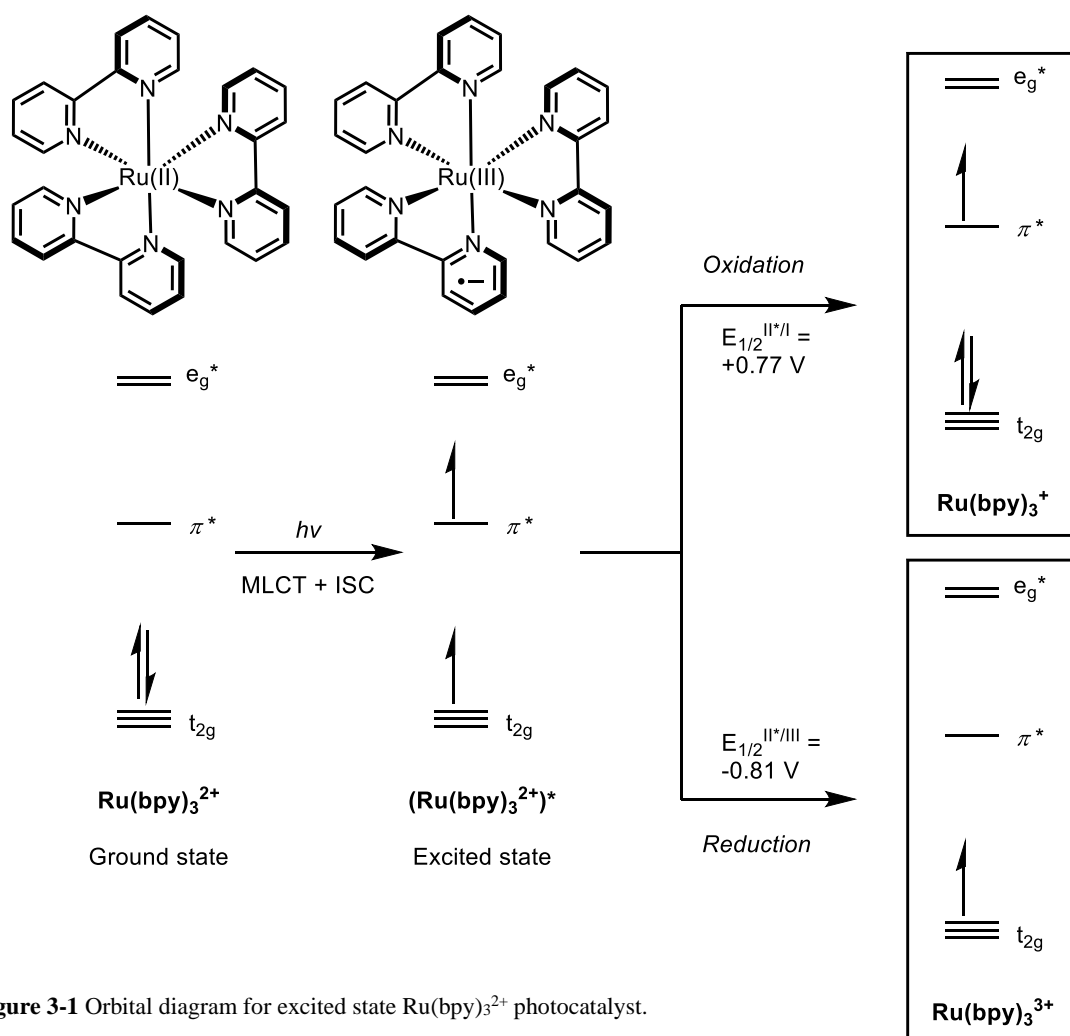


Figure 3-1 Orbital diagram for excited state Ru(bpy)₃²⁺ photocatalyst.

through interconversion of $^1(\pi, \pi^*)$ to $^3(n, \pi^*)$, described by El-Sayed's rule, as changes in orbital angular momentum make this an allowed transition.¹⁷⁹

Having established the fundamentals for excitation and ISC for photocatalysts, the kinetics and thermodynamics of electron transfer will next be discussed. As it was mentioned before, PET is what drives reactivity in photoredox catalysis. Excitation of a molecule drastically changes the redox properties, which can be leveraged to achieve challenging electron transfers that would otherwise not be favorable in the ground state.¹⁷⁹ The thermodynamics of electron transfer of a molecule can be described by Equation 1, where \mathcal{F} = Faraday's constant (23.06 kcal/mol), $E_{\text{red}} = E_{1/2}(\text{A}/\text{A} \cdot -)$ = reduction potential of the acceptor, $E_{\text{ox}} = E_{1/2}(\text{D} \cdot +/\text{D})$ = oxidation potential of the donor.¹⁸⁰ The ground-state oxidation and reduction potential for electron transfer can be determined through cyclic voltammetry (CV).¹⁸¹

Equation 1: Thermodynamics of electron transfer for a molecule in the ground state.

$$\Delta G_{\text{ET}} = -\mathcal{F}(\Delta E) = -\mathcal{F}(E_{\text{red}} - E_{\text{ox}}) = \mathcal{F}(E_{1/2}(\text{A}/\text{A} \cdot -) - E_{1/2}(\text{D} \cdot +/\text{D}))$$

Since the redox properties of a molecule change in the excited state, this must be accounted for when determining if a PET is thermodynamically favorable. The thermodynamics of electron transfer from the excited state of a molecule can be described by Equation 2, where $E_{0,0}$ = the excited state energy, and ω = the energy associated with charge separation induced by coulombic interactions (though this term is highly variable from system to system and often does not have a large effect on the thermodynamics of electron transfer).¹⁸⁰⁻¹⁸¹

Equation 2: Thermodynamics of electron transfer for a molecule in the excited state.

$$\Delta G_{\text{PET}} = \mathcal{F}(E_{1/2}(\text{A}/\text{A} \cdot -) - E_{1/2}(\text{D} \cdot +/\text{D})) - \omega - E_{0,0}$$

Unlike the oxidation and reduction potentials for electron transfer in the ground state, the redox properties of a molecule in the excited state ($E_{1/2}^*$) require additional experimentation to determine. Since the oxidation and reduction potentials change in the excited state, a combination of CV and $E_{0,0}$ is required to accurately determine these values. Using these values, $E_{1/2}^*$ can be calculated by adding the $E_{1/2}(\text{PC}/\text{PC}^{\cdot-})$ and $E_{0,0}$ (Equation 3).¹⁷⁸

Equation 3 Calculating excited-state reduction potentials using CV and $E_{0,0}$.

$$E_{1/2}^* = \mathcal{F}(\text{PC}^*/\text{PC}^{\cdot-}) = E_{1/2}(\text{PC}/\text{PC}^{\cdot-}) + E_{0,0}$$

3.2 Initial Mechanistic Investigations

N-H PCET to from an amidyl radical:

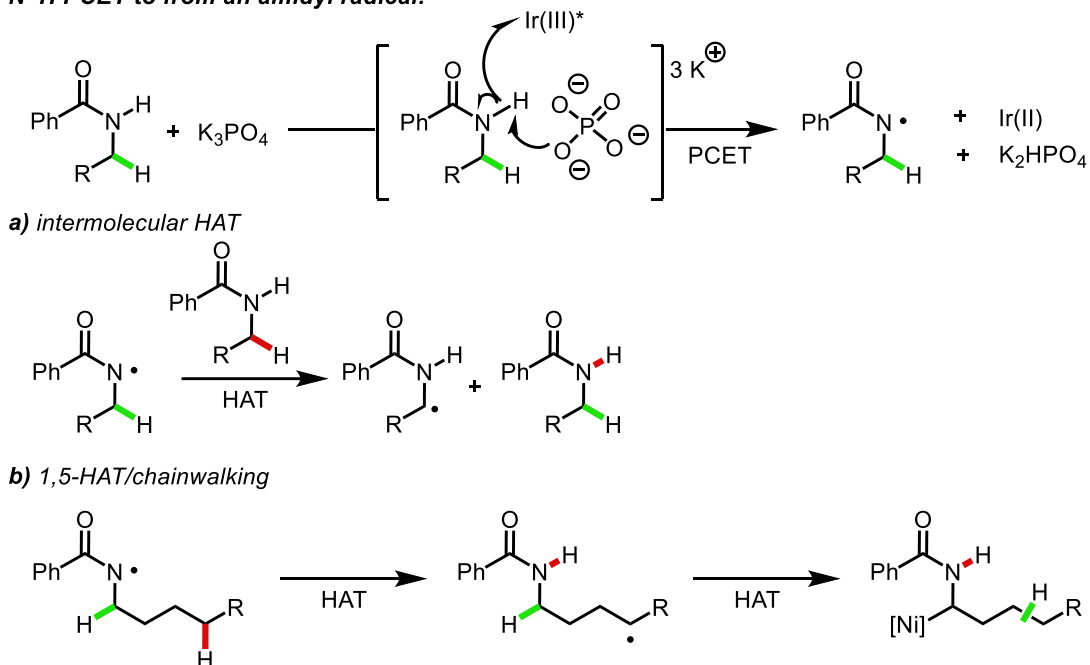


Figure 3-2 *N*-H PCET-mediated α -amidyl radical formation via, **a)** intermolecular HAT, and **b)** 1,5-HAT/chainwalking from an amidyl radical.

Having developed a novel method for the regioselective arylation of *N*-alkylbenzamides, we reasoned that uncovering its mechanism could lead to further developments in metallaphotoredox.¹⁸² Furthermore, we hypothesized a deeper

understanding of the factors that affect site-selectivity and overall reactivity could be leveraged to enable higher yields, lower stoichiometries of coupling partners, and eventually, realization of the initial goal of distal arylation of unactivated C–H bonds.

Stemming from our initial hypothesis, we first explored a mechanism similar to that proposed by Rovis and Knowles involving a PCET to form an amidyl radical (Figure 3-2).¹⁵⁴⁻¹⁵⁵ In their reports, the combination of a weak base and an oxidizing iridium photocatalyst facilitates the formation of a highly reactive amidyl radical. This electron deficient radical performs an intramolecular 1,5-HAT to form a distal carbon-centered radical. In the context of our initial hypothesis, there are two possible mechanisms for the α -arylation stemming from a common amidyl radical intermediate: 1) 1,5-HAT from an amidyl radical could form a carbon-centered radical, which could be captured by a nickel species. This nickel species could then undergo a chain-walking event until it reaches the α -position. 2) The amidyl radical could undergo an intermolecular HAT to abstract the weak α -C–H bond of an amide to give an α -amidyl radical. To study the mechanism of the initial N–H PCET, the Knowles group performed Stern-Volmer experiments that show that both base and photocatalyst are necessary for quenching to occur. Additionally, there have been several reports of chainwalking of carbon-radicals,¹⁸³ most recently by Grevorgian,¹⁸⁴⁻¹⁸⁶ to give site-selective C–H functionalization. In light of these precedents in the chemical literature, we decided both mechanistic pathways have merit in our reaction and thus were explored.

3.2.1 Mechanisms Involving a 1,5-HAT

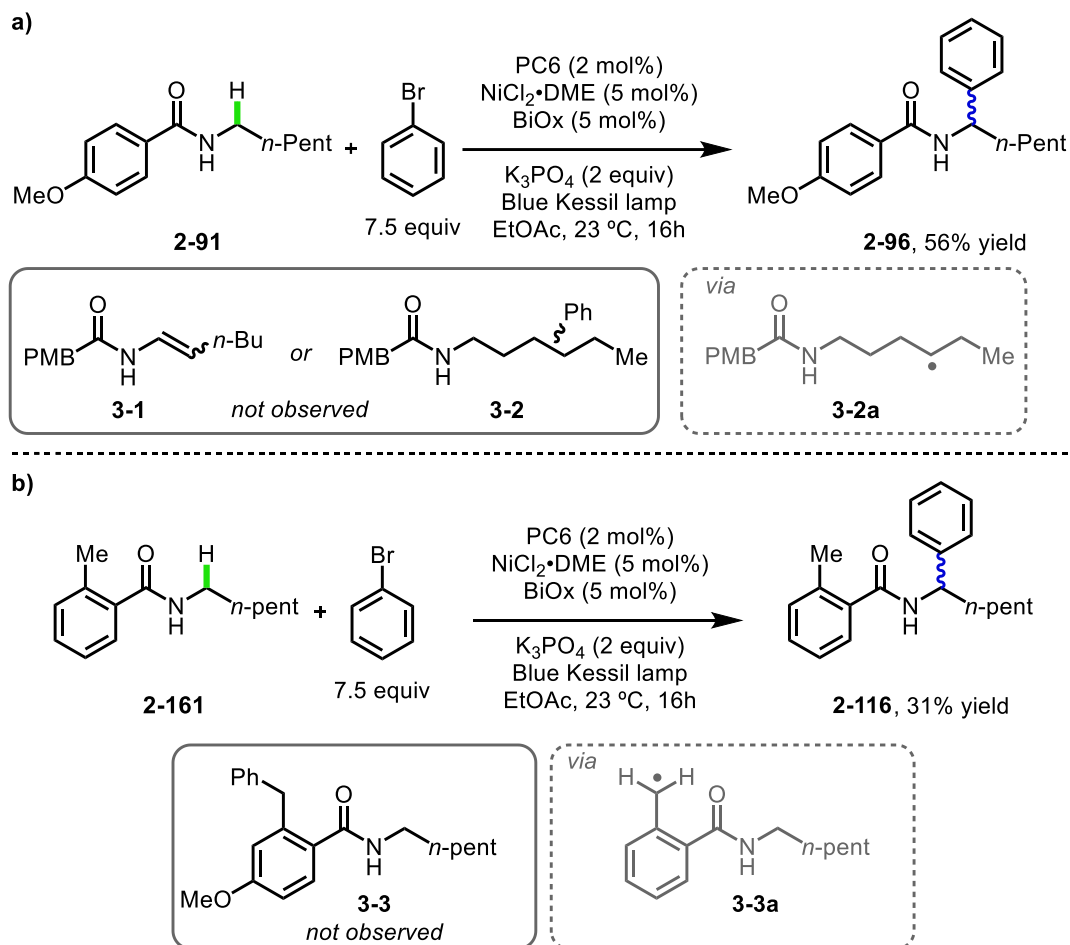


Figure 3-3 Evidence against amidyl radical formation. **a)** potential side-products that could occur from a 1,5-HAT, and **b)** evidence against a 1,5-HAT to benzylic C–H bonds.

Throughout the course of developing the α -arylation of *N*-alkyl benzamides, several experiments proved particularly insightful to the mechanism of this reaction (Figure 3-3). Namely, intermediates or side-products that would arise from an amidyl radical were not observed. Included in this are olefins (**3-1**) and distal arylations along the aliphatic chain (**3-2**) that could arise from a N–H PCET/1,5-HAT, followed by capture and β -hydride elimination by nickel.¹⁸⁷ Other systems that contained weak C–H bonds that could potentially compete with a 1,5-HAT from an amidyl radical, such as benzylic C–H bonds (**3-3**) were left unscathed throughout the reaction. The observation that regioisomers of

arylation or olefins are not observed in this reaction suggest that β -hydride elimination and chain walking are not operable.

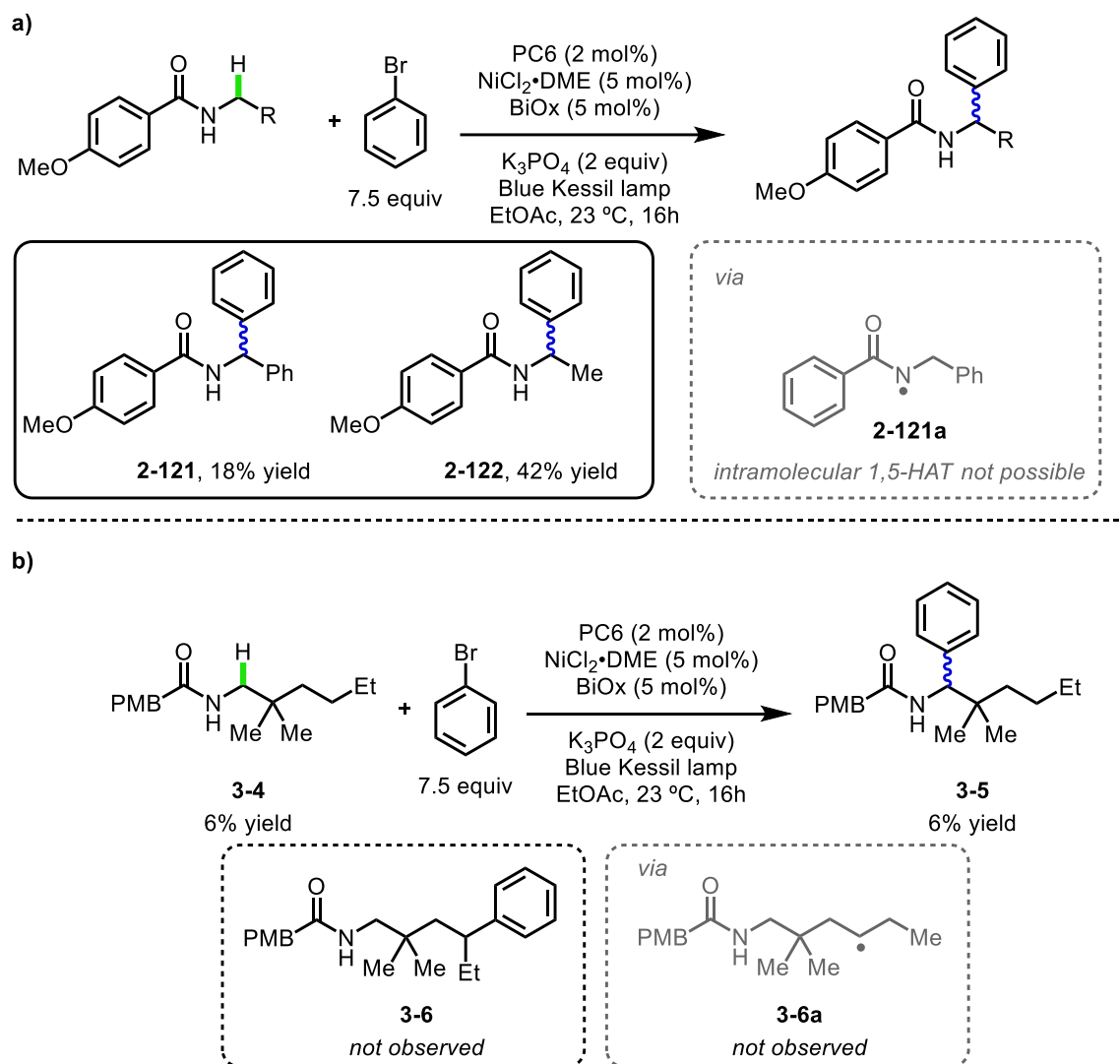


Figure 3-4 Mechanistic evidence against a 1,5-HAT. **a)** α -arylation of substrate with shorter alkyl chains, and **b)** α -arylation of substrates containing a quaternary carbon center.

To gain further information about the feasibility of a mechanism involving a 1,5-HAT, two mechanistic probes specifically aimed at testing this hypothesis were investigated (Figure 3-4a). It was hypothesized that using a substrate that did not possess distal C–H bonds might inhibit this reaction. From a synthetic standpoint, it would be advantageous to be able to functionalize *N*-alkyl chains of various lengths and substitution

patterns, so two different substrates with shorter alkyl chains were synthesized. When subjecting a *N*-benzyl substrate to the reaction conditions 18% of the desired product (**2-121**) was observed. Furthermore, using a less sterically demanding *N*-ethyl substrate, 42% of the desired product (**2-122**) was observed. As this value is close to those observed for our model substrate with an *N*-hexyl chain, it appears that an intramolecular 1,5-HAT is not operable in this reaction, though these experiments do not rule out the possibility of an intermolecular HAT from an amidyl radical.

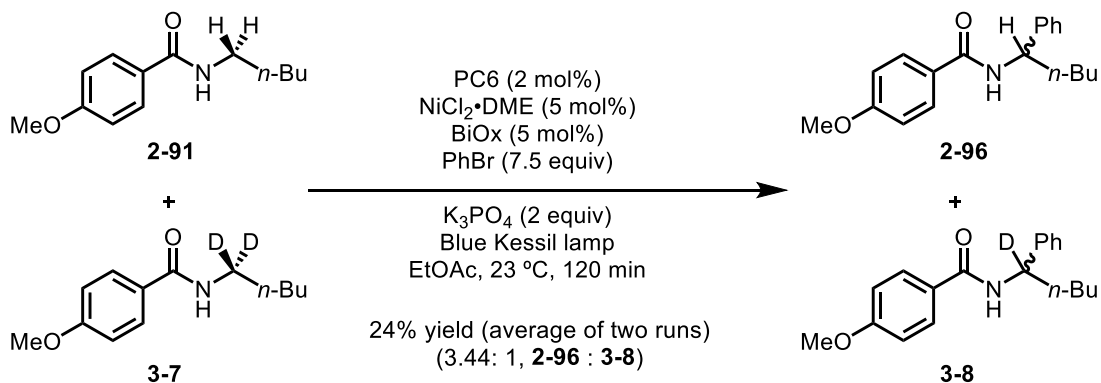


Figure 3-5 Intermolecular competition between α -proteo and α -deutero benzamides. Ratio of **2-96** to **3-8** was determined by ¹H NMR and GCMS analysis of reaction mixture.

Further testing the hypothesis of intramolecular 1,5-HAT, a substrate bearing a quaternary center in the middle of the alkyl chain was synthesized and tested (Figure 3-4b). If a 1,5-HAT were occurring in this reaction, there would be no possibility of chain-walking to the α -position, yielding only distal arylated products. Potentially due to the more sterically demanding nature of this substrate, lower yields were observed, though no distal arylation was observed by ¹H NMR and GCMS. Instead, 6% of the α -arylated product (**3-5**) was isolated, supporting the idea that intramolecular 1,5-HAT is not operable.

Under the mechanistic hypothesis that 1,5-HAT followed by chain walking was not operative in this chemistry, deuterium labeling studies were undertaken (Figure 3-5). An equimolar mixture of α -deutero benzamide and α -proteo benzamide were subjected to the

standard reaction conditions. Stopping the reaction after 120 minutes, two independent runs yielded 26% and 22% (24% average yield) of a mixture of the desired arylated proteo and deuterio product. Using GCMS and ^1H NMR, it was determined that there was a 78:22 and 77:23 ratio of arylated proteo (**2-96**) to deuterio product (**3-8**), which corresponds to a KIE of 3.44. This suggests that C–H cleavage is involved in the rate-determining step. If in this reaction the substrate was to undergo a 1,5-HAT from an amidyl radical followed by chain walking to the α -position, we would expect to observe a small or non-existent KIE. While the exact mechanism for cleavage of the α -C–H is not clear, from this data it seems unlikely that a 1,5-HAT from an amidyl radical is operative.

3.2.2 Testing the Validity of Nitrogen-Centered Radical Formation

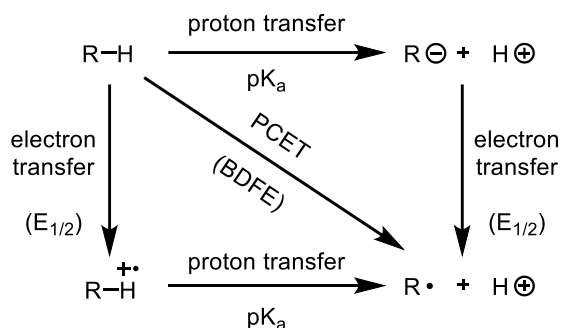


Figure 3-6 Thermodynamic cycle to determine the BDFE of a reaction.

Our experimental evidence refuting intramolecular 1,5-HAT from a nitrogen-centered radical prompted investigation into the possibility of forming an amidyl radical under the reaction conditions. In the reports by Rovis and Knowles, it is proposed that a nitrogen-centered radical forms through a PCET, in which a mild base simultaneously deprotonates an acidic N–H bond while a photocatalyst performs an oxidation.¹⁵² Since our system contains parameters present in both systems (i.e. photocatalyst and base from the Rovis report and benzamide from the Knowles report), we hypothesized that even if an intramolecular 1,5-HAT was not operative, amidyl radical formation still might be feasible.

Previously described by Mayer and Knowles,^{146, 188-190} a thermodynamic cycle in which proton and electron transfer can be used to determine the exergonicity of a PCET (Figure 3-6). Moreover, by breaking up these two steps, experimentally measured values, such as pK_a and oxidation potential, can be used to determine bond dissociation free energy (BDFE) for a specific base/photocatalyst combination (Equation 4), where pK_a(R–H) corresponds to the pK_a of our benzamides, (R[–]/R[•]) is the oxidation potential of the deprotonated amide, and (H[–]/H[•]) is the oxidation potential of hydride.

Equation 4 Bond dissociation free energy.

$$\text{BDFE (kcal/mol)} = 1.37\text{pK}_a(\text{R} - \text{H}) + 23.07\text{E}^\circ(\text{R}^- / \text{R}^\bullet) + 23.07\text{E}^\circ(\text{H}^- / \text{H}^\bullet)$$

Applying BDFE calculations to our photocatalyst/base combination, an approximation of the favorability of nitrogen-centered radical formation can be made. Because K₃PO₄ is insoluble in EtOAc and MeCN, NBu₄OP(O)(OBu)₂, which has a pK_a of 13 in MeCN, was used for this calculation. While NBu₄OP(O)(OBu)₂ does not give substantial amounts of product in our reaction, it merely serves as an approximation for the BDFE of our system. **PC1** (E_{1/2} = +1.21 V vs SCE in MeCN) was used as the photocatalyst in these calculations. Applying Equation 4, these values give a BDFE of approximately 92 kcal/mol. This is well below the average BDE of most amides N–H bonds (102-110 kcal/mol)^{150, 191-192} suggesting that amidyl radical formation is not thermodynamically feasible via PCET with our base/photocatalyst combination. If the more oxidizing photocatalyst **PC2**, developed for N–H PCET by Knowles, is used a BDFE of 102 kcal/mol is attained, which explains why the Knowles group observe much higher reactivity with **PC2** vs **PC1** in the δ-alkylation of benzamides. Despite this compelling evidence that N–H PCET is not thermodynamically favorable, the Knowles groups still observes some

reactivity with **PC1** in their reaction (10% yield for **PC1** vs 79% yield with **PC2**),¹⁵⁵ thus requiring further investigation into the possibility of nitrogen-centered radical formation in our reaction.

In support of their BDFE calculation, the Knowles lab also performed quenching studies of each reaction component to better elucidate the source of the amidyl radical.¹⁵⁵ Using Stern-Volmer analysis, they determined that benzamide alone does not quench **PC2**. Additionally, they observed some quenching with NBu₄OP(O)(OBu)₂ and **PC2**, however, strong quenching was observed when varying the concentration of NBu₄OP(O)(OBu)₂ in the presence of **PC2** and benzamide, or when varying the concentration of benzamide in the presence of **PC2** and NBu₄OP(O)(OBu)₂. This data is congruent with their calculated BDFE and strongly suggests PCET is operative in their system.

Motivated by their delineation of PCET processes using Stern-Volmer analysis, similar studies were undertaken using our system. When measuring the intensity of fluorescence of **PC1** in EtOAc with varied concentrations of PhBr or *N*-alkyl benzamide, no quenching was observed (see Section 4.4.2). Unfortunately, using this system we were

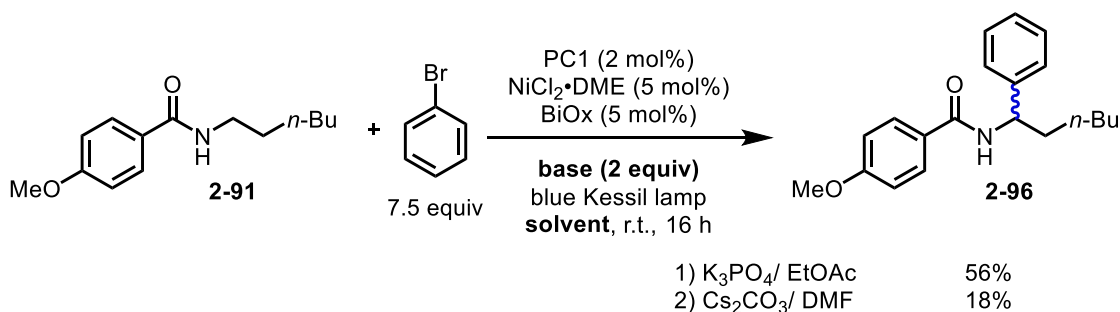


Figure 3-7 Comparison of K₃PO₄ in EtOAc and Cs₂CO₃ in DMF for the α -arylation of benzamides.

unable to perform Stern-Volmer analysis using K₃PO₄ due to its limited solubility in organic solvents.

Unsatisfied by this, a similar system was devised that used a more soluble base/solvent combination that also yielded α -arylation. During optimization it was found that Cs_2CO_3 was competent in the model reaction. Although this base/solvent combination provided lower yields, it was deemed suitable for mechanistic studies, and since Cs_2CO_3 has a known solubility in DMF, this combination was tested (Figure 3-7).

Undertaking Stern-Volmer analysis with Cs_2CO_3 in DMF, quenching with benzamide and PhBr were first tested. It is well known that photophysical properties change drastically in different solvents so this does not bring into question the results with EtOAc.^{179, 193-196} Because of this, it is important that all comparisons should be made within the same solvent. Unsurprisingly, neither of these reaction components quenched **PC1**. Next, when using Cs_2CO_3 , quenching of **PC1** was not observed (this will be further discussed in section 3.3.3.1 when direct oxidation of K_3PO_4 is discussed). Lastly, when varying the concentration of Cs_2CO_3 with constant benzamide and **PC1**, some quenching was observed.

In addition to observing different quenching events in DMF, significant amounts of *N*-arylation was also observed when testing the competency of Cs_2CO_3 in DMF under otherwise standard reaction conditions. The observation of significant side product formation and the limited solubility of K_3PO_4 in EtOAc led us to believe using Cs_2CO_3 in DMF was not a fair comparison to K_3PO_4 in EtOAc. Additionally, the lack of strong quenching with Cs_2CO_3 and benzamide, despite its increased solubility in DMF suggest that this event is not a major contributor in reactions with $\text{K}_3\text{PO}_4/\text{EtOAc}$, where K_3PO_4 is insoluble. Having explored the possibility that K_3PO_4 might play a role in a PCET in our

reaction and by testing Cs₂CO₃ in this system, there is inconclusive data to suggest a N–H PCET is a major pathway in the arylation of *N*-alkyl benzamides.

3.3 Discussion of Mechanistic Hypotheses

Without strong evidence for a PCET/1,5-HAT in our reaction, several mechanistic possibilities derived from other work within this field were examined. Of these studies, three distinct mechanistic pathways were proposed for α -amidyl radical formation: 1) deprotonation followed by HAT, 2) direct α -amidyl radical formation from a photocatalyst via C–H PCET, and 3) α -amidyl radical formation from a HAT agent. By conducting further mechanistic studies we believed that more conclusive data might allow us to better rule out a mechanism involving amidyl radical formation via PCET, while gathering direct evidence for a different mode of reactivity. With the overarching goal of improving upon yields of this reaction, a series of experimental and spectroscopic studies that seek to rule out specific pathways were undertaken in order to elucidate a reasonable mechanistic pathway for the α -arylation of *N*-alkyl benzamides.

3.3.1 Deprotonation of Benzamides for Direct Oxidation

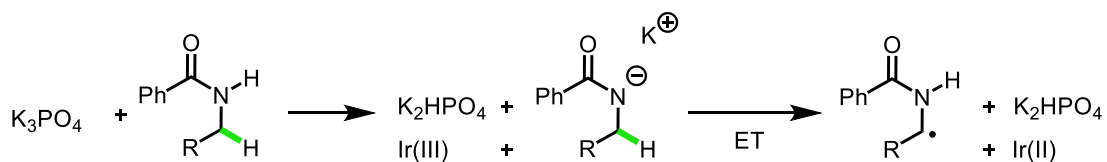


Figure 3-8 Direct oxidation of a deprotonated benzamide to give α -amidyl radicals.

In reports by Rovis, the combination of quinuclidine and an iridium photocatalyst were shown to generate carbon-centered radicals on triflamides¹⁶⁹ or carbamates.¹⁵⁶ Unlike their previous report with trifluoroacetates, which undergo 1,5-HAT from a nitrogen-centered radical, exclusive α -selectivity was observed with triflamides. Mechanistic insights support the formation of a quinuclidine radical cation, generated through the

oxidation of quinuclidine by an iridium photocatalyst, followed by HAT from a deprotonated triflamide to form a carbon-centered radical. Stern-Volmer quenching studies suggest that most of the photocatalyst quenching occurs from quinuclidine, though a non-negligible quenching event is observed from the deprotonated triflamide.

Rovis (2019):

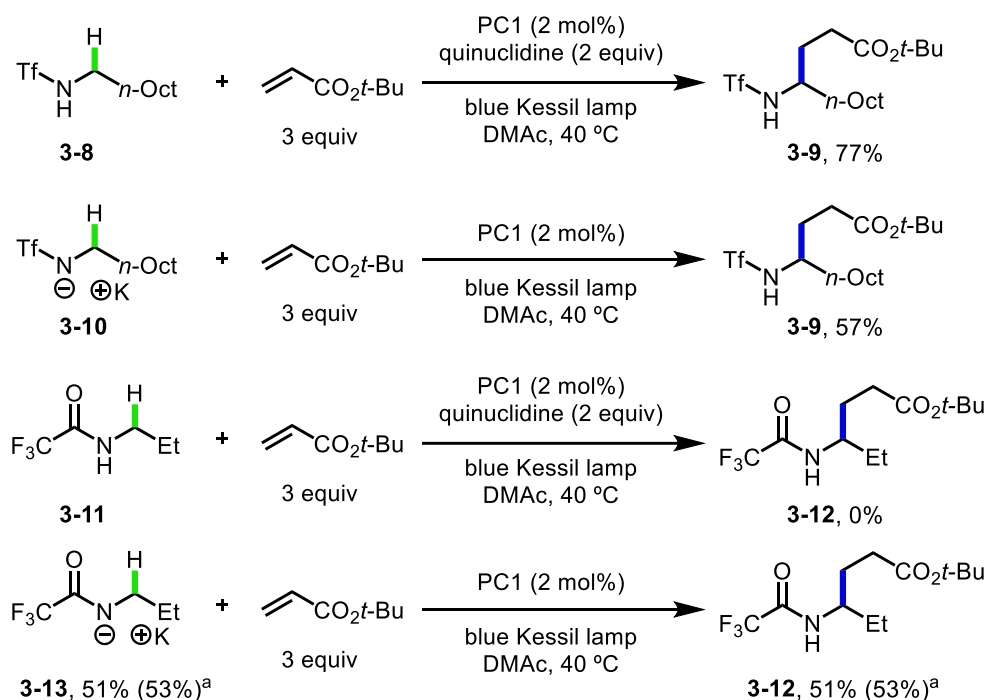


Figure 3-9 Effects of HAT reagents on protonated and deprotonated trifluoroacetamides and triflamides. ^a Reaction run with 2 equiv quinuclidine.

Hypothesizing that the more acidic N–H of the triflamide was responsible for this change in selectivity, they prepared the potassium salts of both triflamides and trifluoroacetates and tested them in their reaction conditions (Figure 3-9). They found that in the case of the deprotonated triflamide, reactivity was observed with and without quinuclidine, suggesting that this component was not necessary for HAT, and perhaps direct oxidation of their substrate by the photocatalyst was occurring. While our system lacks quinuclidine, the possibility of a direct oxidation of a deprotonated benzamide was considered in our mechanistic investigation (Figure 3-8).

Furthermore, when testing the deprotonated trifluoroacetate with and without quinuclidine, exclusively α -functionalization was observed (Figure 3-9). Intriguingly, the reaction of trifluoroacetate and quinuclidine gave no α - or δ -functionalized product. This suggests that highly electron-rich systems, such as deprotonated amine derivatives can be directly oxidized, in a similar manner as tertiary amines, to generate α -radicals via spin-center shift. Inspired by this observation, we set about synthesizing the potassium salt of our model substrate to test it under our standard reaction conditions.

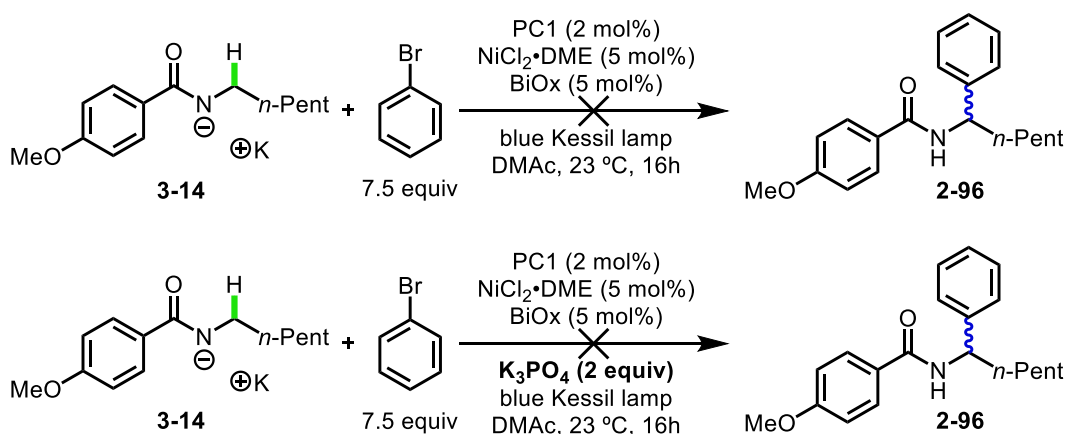


Figure 3-10 Inhibited reactivity of potassium benzamide salts in α -arylation.

Upon deprotonation of our model substrate with KH in DMF, we subjected this species to our most optimized conditions with and without K₃PO₄ (Figure 3-10). To our surprise, neither of these reactions gave any product and the mass balance was all starting material. This suggests that deprotonation by K₃PO₄ is not beneficial under the reaction conditions. This could also explain why bases stronger than K₃PO₄ are not effective in our reaction. Most importantly, this result suggests that deprotonation of benzamide is not a viable pathway for α -amidyl radical formation, prompting further investigations into the source of radical generation.

3.3.2 Direct C–H PCET to Form an α -Amidyl Radical

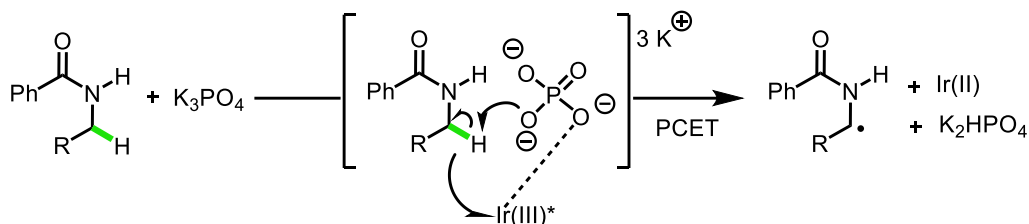


Figure 3-11 C–H PCET of benzamides to give α -amidyl radicals.

With convincing evidence that deprotonation of the benzamide is not operable under our reaction conditions, efforts were next turned to exploring the possibility of a C–H PCET to directly give an amidyl radical (Figure 3-11). As described by Mayer and later Alexanian and Knowles, PCET is not only restricted to polarized systems like heteroatom–H bonds but can be applied to C–H bonds which are less polarized.¹⁹⁷⁻¹⁹⁸ This paradigm was applied to the photoredox catalyzed functionalization of activated C–H bonds, such as THF or benzylic systems, or unactivated C–H bonds, like those found in cyclohexane,

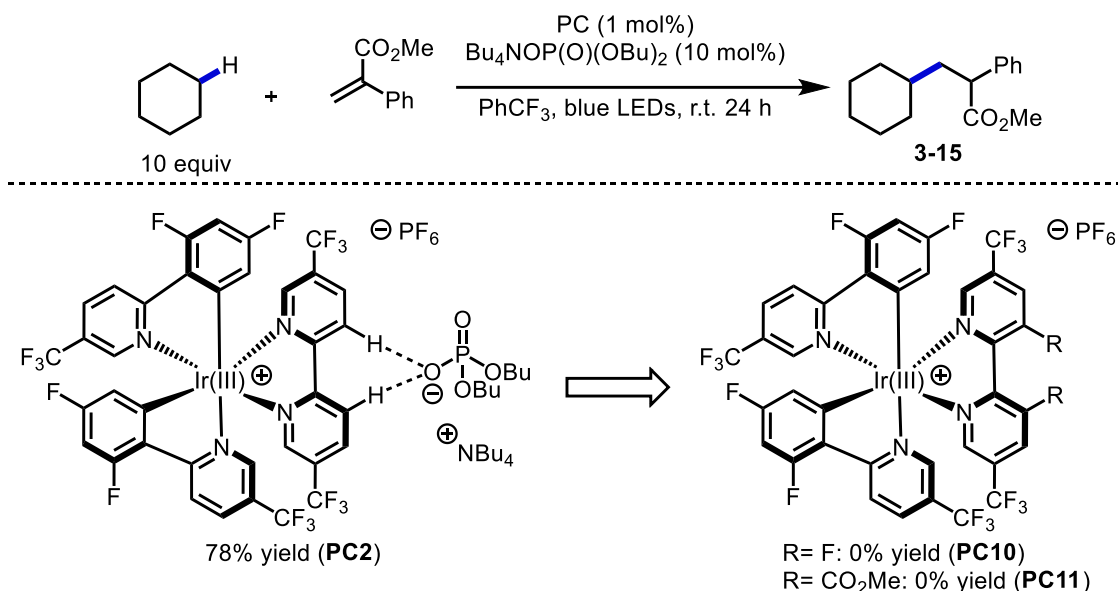


Figure 3-12 Effects of substitution at the 3,3'-position of iridium photocatalysts.

using a potent iridium-phosphate complex. Investigations into this system identified key interactions between the 3,3'-C–H bonds of a bipyridyl ligand on the iridium photocatalyst and a phosphate base (Figure 3-12). This complex promotes greater reactivity by shifting

this reaction from a multi-site PCET to a single-site PCET, thus increasing the likelihood that a productive PCET will occur.¹⁹⁹⁻²⁰¹

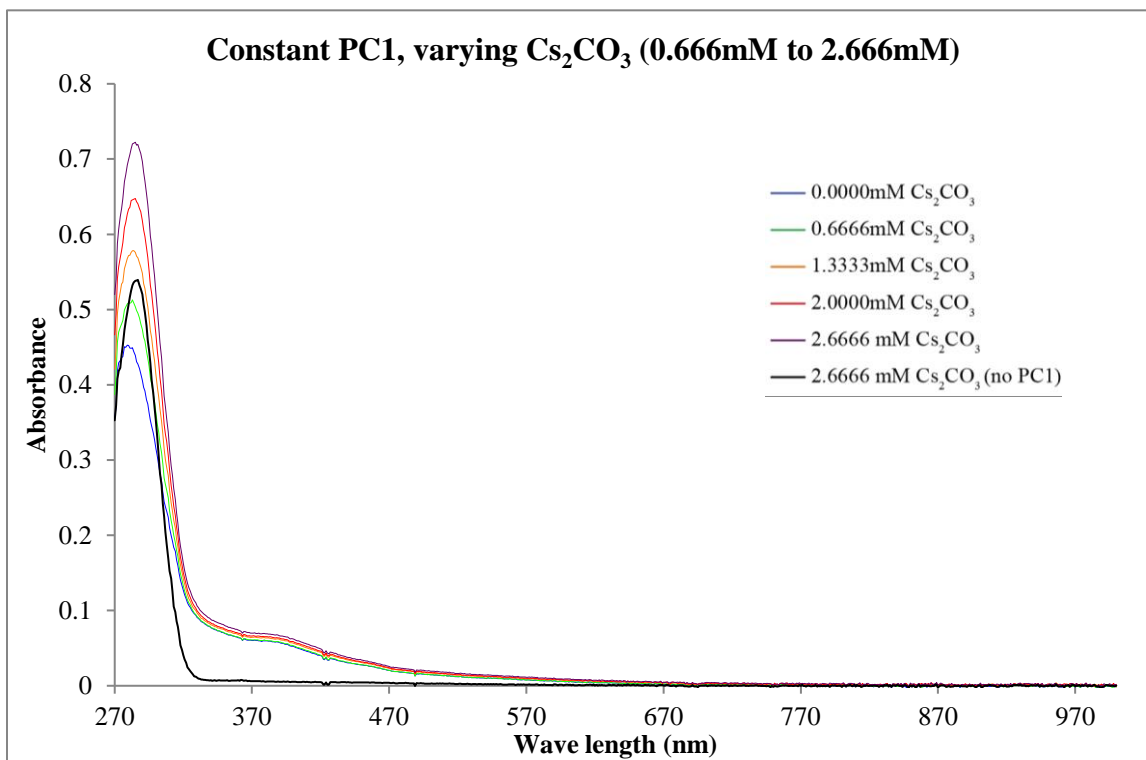


Figure 3-13 UV-Vis titration of Cs₂CO₃ to a solution of PC1.

Having uncovered a new type of reactivity, Alexanian and Knowles were able to corroborate their hypothesis through ¹H NMR and UV-Vis experiments.¹⁹⁸ During their studies, significant shifts in the ¹H NMR of the iridium complex (corresponding to the 3,3'-C-H bonds of the bipyridyl ligand) were seen when a solution of phosphate base was titrated in. Similarly, changes in UV-Vis absorption in the region associated with MLCT for the iridium photocatalyst (380 nm) suggest that a new species is formed in solution when phosphate base is added. These changes in the spectra prompted the authors to isolate a discrete iridium-phosphate complex, resulting from mixing **PC2** with NBu₄OP(O)(OBu)₂, which they were able to confirm key hydrogen bonding interactions through x-ray crystallography. Lastly, they synthesized two different photocatalyst (**PC10**

and **PC11**) that lacked protons at the 3,3'-position of the bipyridyl ligand and tested these catalysts in their reaction (Figure 3-12). Indeed, neither of these complexes were competent in the reaction, though they were shown to be catalytically active in analogous reactions that did not involve a C–H PCET.

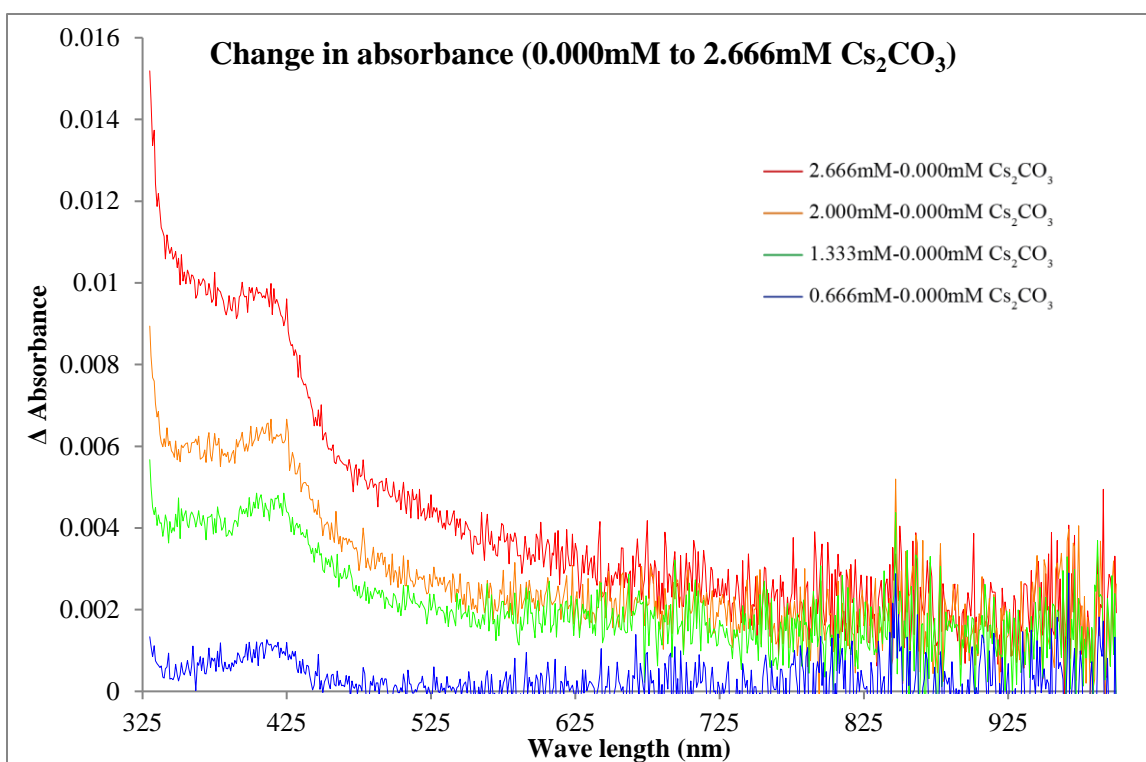


Figure 3-14 Changes in UV-Vis when adding Cs₂CO₃ to a solution of PC1.

Since our system shares many similarities to theirs, including the use of a phosphate base and iridium photocatalyst, this mechanism was next investigated. Building upon the work of Alexanian and Knowles, we set about testing if a complex between our base and photocatalyst was responsible for the formation of an α -amidyl radical. Despite the different reaction profile with Cs₂CO₃ in DMF, the observation of a quenching event when adding increasing concentrations of Cs₂CO₃ to a constant concentration of benzamide and **PC1** prompted further investigation into a C–H PCET by an iridium-base complex. When titrating in increasing concentrations of Cs₂CO₃ to a solution of **PC1**, no significant change

in the MLCT region (381nm) was observed (Figure 3-13). If a new iridium-base complex were forming, we would expect to observe increases and decreases in the absorptivity in the MLCT region (Figure 3-14). The lack of these changes in the UV-Vis suggest that Cs_2CO_3 is not forming a new complex with the photocatalyst. Furthermore, the limited solubility of K_3PO_4 in EtOAc make the possibility of a new iridium-phosphate complex highly unlikely.

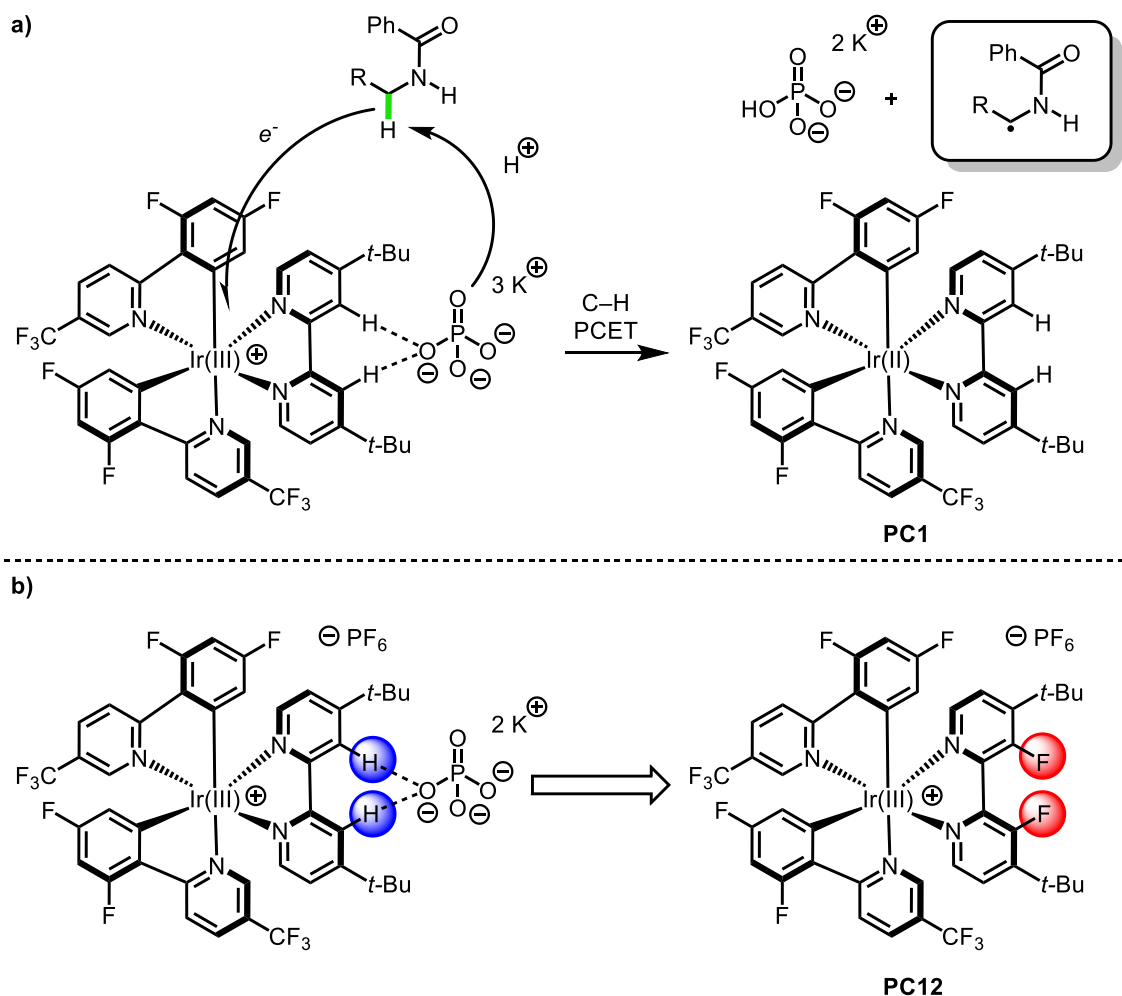


Figure 3-15 a) hydrogen bond-enabled C-H PCET, and b) newly proposed photocatalyst modifications to inhibit hydrogen bonding.

Dissatisfied by our inability to test K_3PO_4 in these quenching studies due to solubility, we decided to pursue alternative methods of probing the formation of an iridium-base complex (Figure 3-15). Like the Alexanian and Knowles report, we decided to study

the effects of blocking the C–H bonds of the bipyridyl ligand on **PC1**. As our reaction did not work well with the highly oxidizing photocatalyst used in the Alexanian and Knowles report, a novel bipyridyl ligand was targeted that had 3,3'-difluoro substituents. Through a 7-step procedure we were able to synthesize a dtbbpy analog that featured 3,3'-difluoro substituents to prohibit hydrogen bonding between the bipyridyl ligand and the base (Figure 3-16). After synthesizing the requisite cationic iridium complex, this new bipyridine was ligated to the iridium to form **PC12** (Figure 3-17).

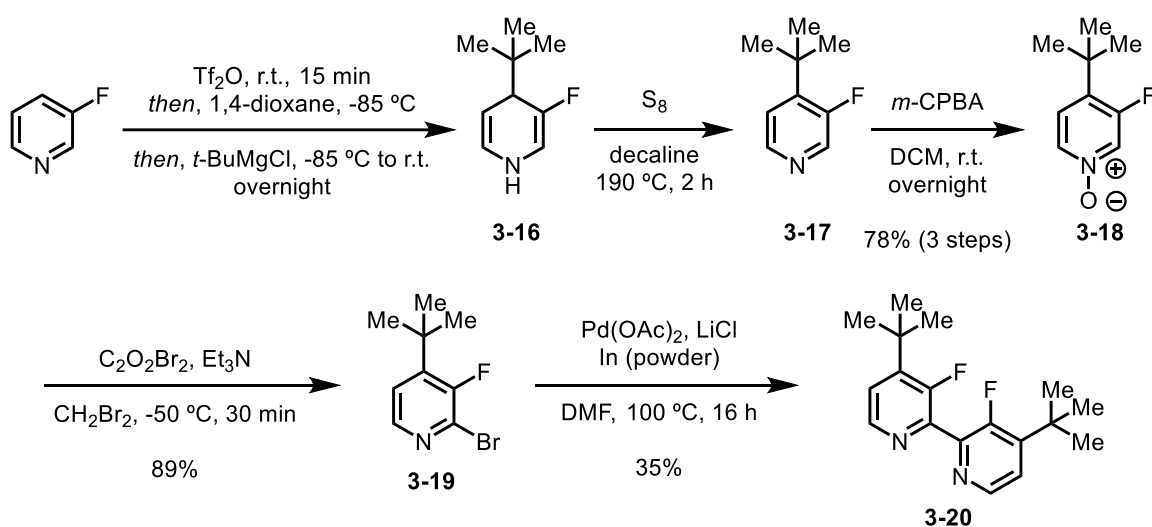


Figure 3-16 Synthesis of a novel bipyridyl ligand with blocked hydrogen bonding sites.

With this new photocatalyst in hand, we tested our model reaction with both K_3PO_4 in EtOAc and Cs_2CO_3 in DMF. While in the Alexanian and Knowles report, complete inhibition of their reaction was observed when using their block photocatalyst, our reaction was only partially inhibited. We observed 6% yield when using K_3PO_4 in EtOAc and 14% yield when using Cs_2CO_3 in DMF, opposed to 56% yield and 18% yield when using **PC1** (Figure 3-18). Although this reaction is partially inhibited by this new photocatalyst, the lack of hydrogen bonding sites might not be the only reason for diminished yield. The

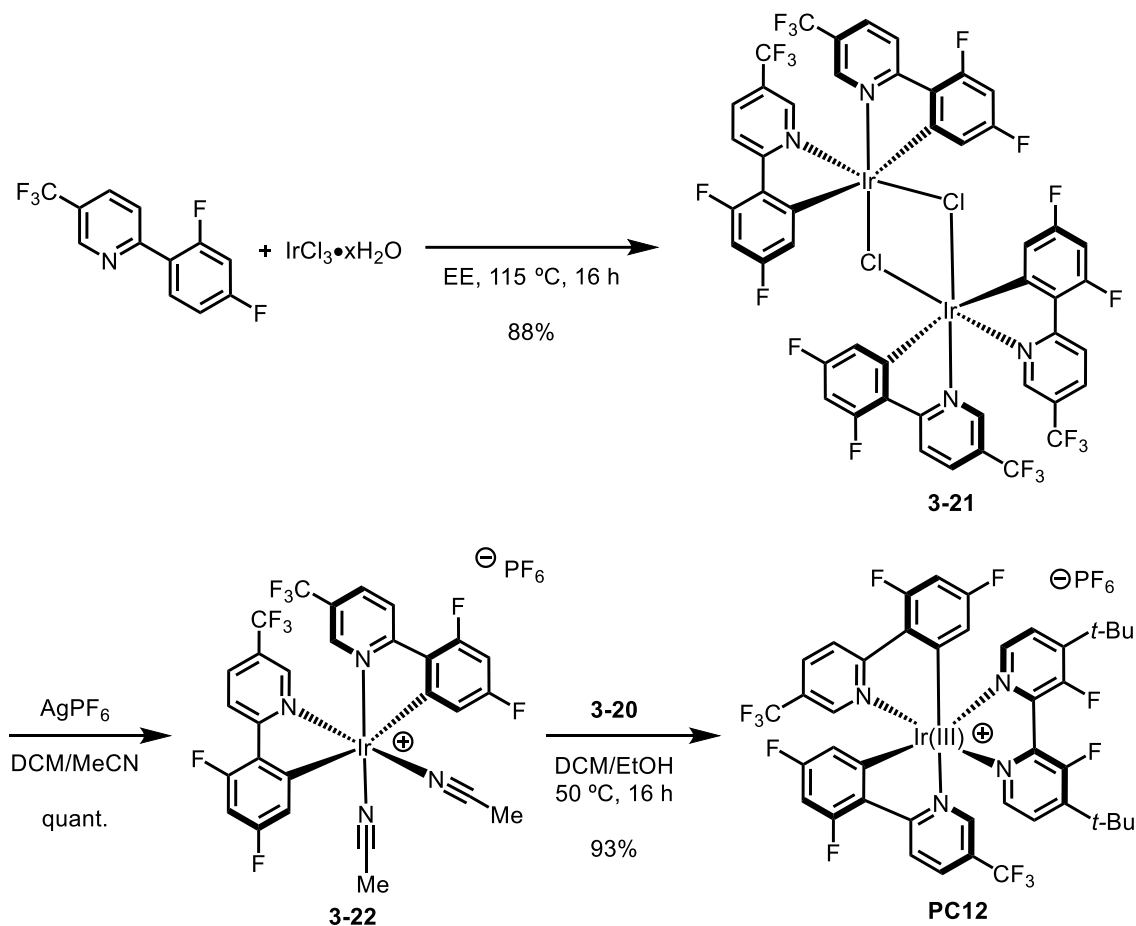


Figure 3-17 Synthesis of a photocatalyst with blocked hydrogen bonding sites.

photophysical properties of this catalyst were measured through CV and $E_{0,0}$ in order to determine the excited state potentials. The ground state redox potentials were determined $E_{1/2} = \text{Ir(III/II)} = -1.12\text{V vs SCE}$ and $E_{1/2} = \text{Ir(III/IV)} = 1.45\text{V vs SCE}$ (Figure 4-33). **PC12** was irradiated at 381 nm and, with an emission observed at 481nm. The excited state potentials were calculated to be $\text{Ir(III}^*/\text{II)} = 1.47\text{V vs SCE}$ and $\text{Ir(III}^*/\text{IV)} = -1.13\text{V vs SCE}$ using Equation 3. When comparing the excited state potentials of **PC1** and **PC12**, the redox properties were drastically different, which could explain the lower reactivity of this photocatalyst in our model system, as it performed similarly to other photocatalyst with similar oxidation potentials (Table 2-7, section 2.4.2).

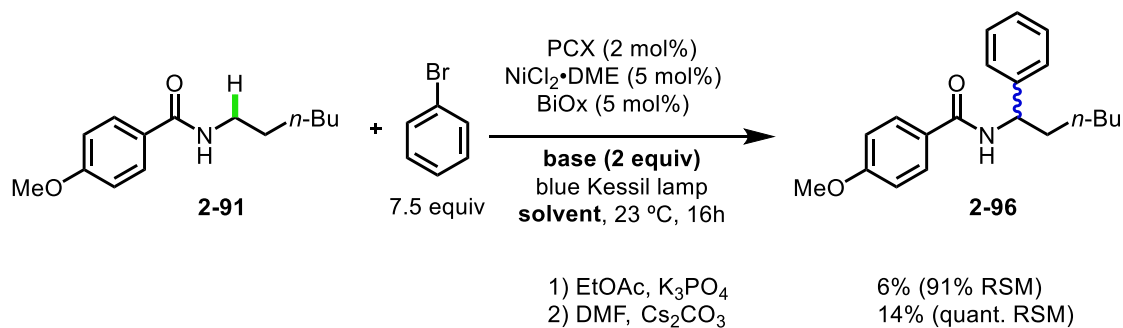


Figure 3-18 α -arylation using a photocatalyst with blocked hydrogen bonding sites. RSM = recovered starting material.

While no one piece of data completely refutes a mechanism where an iridium-base complex is responsible for a C–H PCET, the data acquired in these two experiments suggest other mechanisms may be at play. Neither UV-Vis titrations nor using a photocatalyst with blocked hydrogen-bonding sites gave convincing evidence for an iridium-base complex. Despite the similarities of these two systems, the lack of changes in the UV-Vis and observed reactivity using **PC12** do not support a similar mechanism to that proposed by Alexanian and Knowles. Although not definitive, these pieces of data suggest that further investigations are necessary to make claims about the mechanism for α -amidyl radical formation.

3.3.3 α -Amidyl Radical Formation from a HAT Agent

3.3.3.1 Phosphate and Sulfate Radicals for HAT

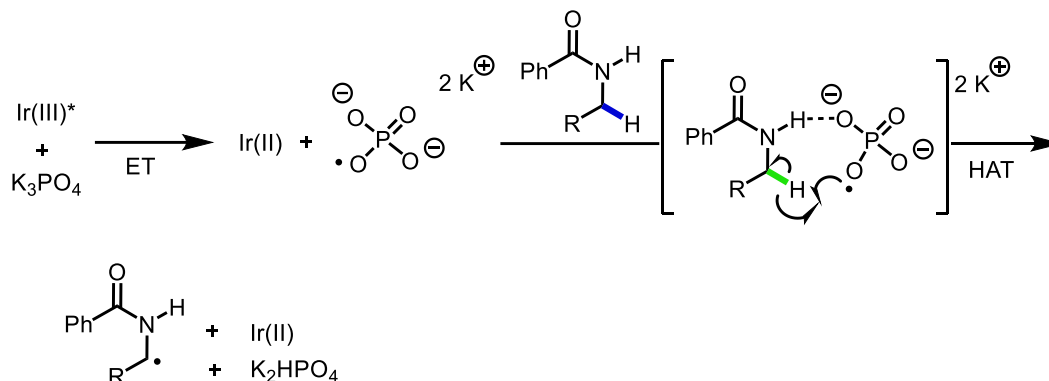


Figure 3-19 Phosphate radical formation to give α -amidyl radicals.

Among the arsenal of C–H functionalization methods, photoredox catalysis has been used to generate reactive HAT mediators capable of abstracting strong C–H bonds (Figure 3-19). Included in these methods, the Stephenson lab were able to show thermal or photogenerated sulfate radicals are capable of functionalizing weak C–H bonds of amides through an intermolecular HAT.¹⁷⁶ More recently, the Nicewicz lab used strongly oxidizing acridinium photocatalyst to generate phosphate radicals from simple phosphate salts, which could be used to functionalize activated and unactivated C–H bonds.²⁰² Other groups have also evoked the use of phosphate as HAT agents and suggest that they are oxidizable using iridium photocatalyst.²⁰³ Similarities between our method and these two systems prompted investigations into HAT agents for C–H cleavage.²⁰⁴⁻²⁰⁷

Initially, it was hypothesized that persulfates, like the ones used by the Stephenson group, could supplant K_3PO_4 in our reaction as the HAT agent.¹⁷⁶ Persulfates are bench stable solids that bear a weak O–O bond and can be easily reduced or homolyzed to give highly reactive sulfate radicals. However, when adding potassium persulfate ($\text{K}_2\text{S}_2\text{O}_8$) to the reaction, no noticeable increase in yield was observed (Figure 3-20). Additionally,

when omitting the photocatalyst and heating the reaction to 55 °C, the point at which the Stephenson group observed reactivity in their chemistry, no reaction was observed. While discouraging, the lack of reactivity in our system could be due to a number of complicating factors including the need to modulate the oxidation state of nickel for oxidative addition, or the use of non-solvent quantities of substrate, which are not explored in the Stephenson report.

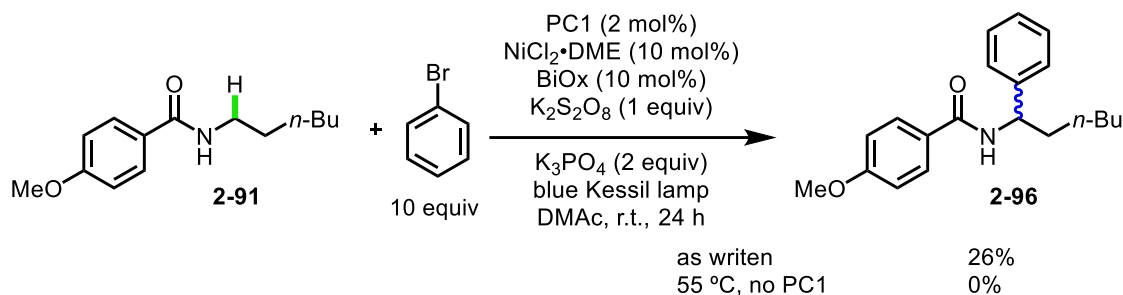


Figure 3-20 Addition of persulfates as HAT agents for the α -arylation of benzamides.

As the stoichiometry and use of K₃PO₄ in the Nicewicz report more closely resembled our system, explorations of this mechanism were undertaken. In their report, the authors evoke an oxidation of K₃PO₄ by an acridinium photocatalyst.²⁰² This highly reactive phosphate radical then abstracts a C–H bond to give a more stable carbon-centered radical which can engage with radicalphiles to give newly functionalized products. Key to their mechanistic findings were CV data and Stern-Volmer quenching studies that implicate oxidation of phosphate (in order to measure these values, the more soluble (NBu₄)₂O₂P(O)(OPh) was prepared and tested) by the photocatalyst. Furthermore, they were able to demonstrate that (NBu₄)₂O₂P(O)(OPh) is competent in this reaction, providing comparable yields to those run with K₃PO₄.

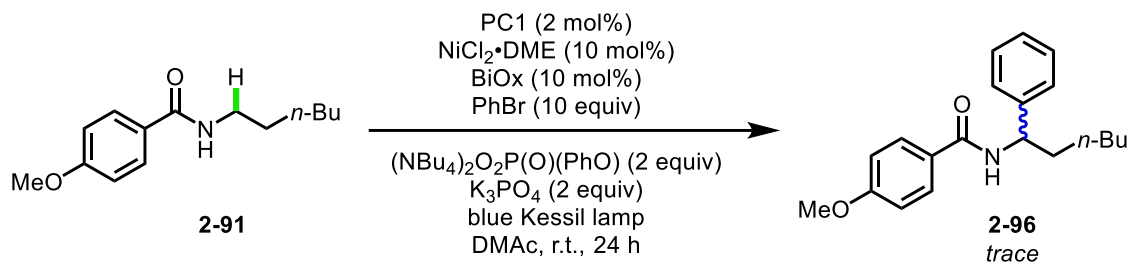


Figure 3-21 Use of a soluble phosphate base for the α -arylation of benzamides.

Comparing the redox properties of (NBu₄)₂O₂P(O)(OPh) to K₃PO₄ cannot be easily done in organic solvents, though it can be assumed that since (NBu₄)₂O₂P(O)(OPh) is dibasic, its oxidation potential will be similar to tribasic K₃PO₄. The oxidation potential of (NBu₄)₂O₂P(O)(OPh) was measured by the Nicewicz lab to be $E_{1/2} = +0.87$ V vs SCE,²⁰² which is well within the range of **PC1** (+1.21 V vs SCE). However, while the Nicewicz lab were able to use (NBu₄)₂O₂P(O)(OPh) in their reaction with only small deviations in yield, we observed only trace product by GCMS when substituting K₃PO₄ for (NBu₄)₂O₂P(O)(OPh) (Figure 3-21).

Throughout the optimization of this reaction it was noted that some inorganic bases worked better than others. Namely, bases with a higher pK_a (i.e. K₃PO₄ > K₂HPO₄ > KH₂PO₄) gave higher yields, as did more soluble bases (i.e. K₃PO₄ > Na₃PO₄ or Cs₂CO₃ > K₂CO₃). As more soluble tetrabutylammonium analogs, such as those described by Knowles¹⁵⁵ and Nicewicz,²⁰² did not give satisfactory results in our reaction, we hypothesized that exploring a base that was both soluble and gave some yields in our chemistry might allow for a better comparison. Since Cs₂CO₃ in DMF gave modest yields in our reaction, we selected this base for further studies. If direct oxidation were an operable pathway in our chemistry, it would be expected that a quenching event would be observed through Stern-Volmer analysis. When adding increasing concentrations of Cs₂CO₃ to a constant concentration of **PC1**, we were surprised that no quenching was observed (see

section 4.4.2). This result definitively shows that direct oxidation of a competent base for the α -arylation of benzamides, Cs_2CO_3 , is not a major pathway in our mechanism.

In summary, the potential of a photocatalytically generated HAT agent in this reaction was explored. Two different systems previously shown to be competent in the functionalization of amides and strong C–H bonds were applied to the α -arylation of *N*-alkyl benzamides with limited success. The reduced yields of arylation observed under thermal or photochemical conditions when using $\text{K}_2\text{S}_2\text{O}_8$ suggest that more complex factors are in play which necessitate careful modulation of both α -amidyl radical formation and the catalytic cycle of nickel. Although a direct comparison between the Nicewicz report and our reaction cannot be made, the insolubility of K_3PO_4 and the lack of observed reactivity with $(\text{NBu}_4)_2\text{O}_2\text{P}(\text{O})(\text{OPh})$ suggest that direct oxidation to give a phosphate HAT agent is not a major pathway in our chemistry. Furthermore, when performing Stern-Volmer analysis on Cs_2CO_3 in DMF, a more soluble base that gives modest yields in our reaction, no quenching was observed. Together, these results indicate that direct oxidation of the base in the reaction by a photocatalyst is not responsible for α -amidyl radical formation, and that a different pathway is responsible for the observed chemo- and regioselectivity.

3.3.3.2 Halide Radicals as HAT Agents for α -Amidyl Radical Formation

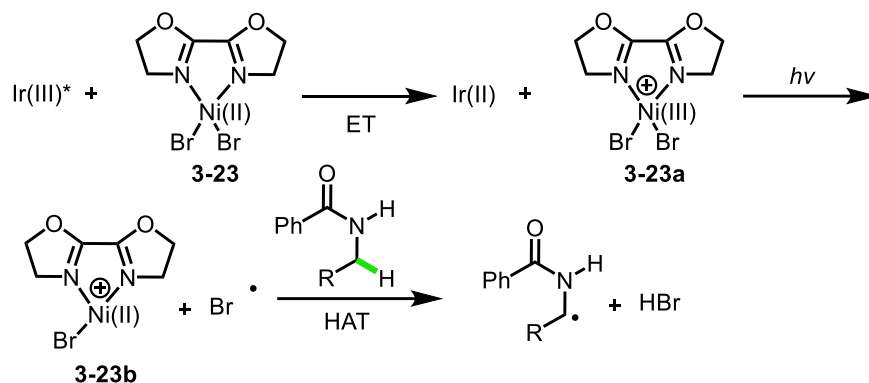


Figure 3-22 Potential mechanism for halide radical formation from a Ni(III) species.

Lastly, several mechanistic studies involving metallaphotoredox have evoked halide radicals as the key HAT species for the functionalization of C–H bonds.^{173, 208-209} First reported by Nocera, the interaction of light and nickel halide complexes can be leveraged to generate halide radicals capable of functionalizing C–H bonds.²¹⁰⁻²¹² Halide radicals have long been known to abstract C–H bonds, though the generation of these species largely hinge on homolysis of Br₂ or Cl₂ under UV irradiation or of weak heteroatom–X bonds, such as the HLF reaction.

Detailed studies by the Doyle group implicate Ni(III)-halide complexes in generating halide radicals upon oxidation of nickel(II) through a interaction between an excited Ir(III) complex,^{208, 213} interaction with a second nickel(II) species,²⁰⁹ or direct absorption of light.²¹⁴ Using stoichiometric oxidants, such as aminium salts, cationic nickel(III) species can be formed, which undergoes homolysis to give halide radicals capable to abstracting C–H bonds. These experiments offer validity to the idea that highly oxidizing iridium photocatalysts are able to generate halide radicals from Ni(II)X₂ or Ni(II)ArX complexes (Figure 3-22).

In reactions where nickel interacts directly with light, the exact identity of the nickel halide species is important for disproportionation, as low lying MLCT bands must be accessible by the wavelength of light being used. Using Ni(II)ArCl complexes, the Doyle group was able to show that ³MLCT bands were readily accessible using blue LEDs.²⁰⁹ Moreover, this type of reactivity was not reserved to Ni(II)ArCl species. Both Ni(II)ArBr and Ni(II)ArI complexes were also competent in generating Ni(III)ArX complexes through a disproportionation with a second equivalent of Ni(II)ArX. Despite this observation, the BDFE of weak C–H bonds, such as THF (92 kcal/mol) and *i*-PrNHC(O)Me (92 kcal/mol), make C–H abstraction by a halide radical thermodynamically unfavorable for iodide radicals and challenging for bromide radicals (BDE for F–H: 136 kcal/mol, Cl–H: 103 kcal/mol, Br–H; 87 kcal/mol, I–H: 71 kcal/mol). Despite the Doyle groups use of Ni(0)

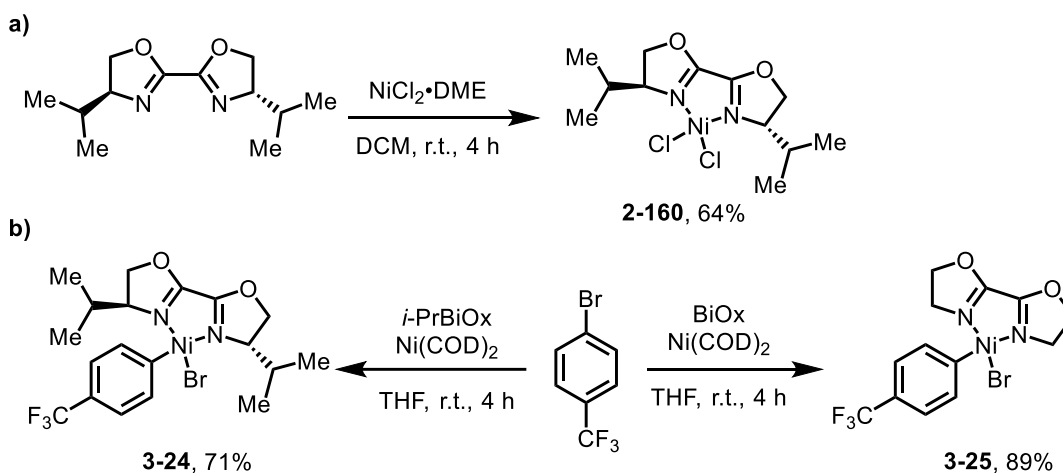


Figure 3-23 Synthesis of BiOxNi(II) complexes.

pre-catalysts, and the lower observed yields for C–H abstraction by Ni(II)ArBr species, we hypothesized that a similar mechanism could arise under our reaction conditions. Initially, oxidation by an excited iridium photocatalyst could form a Ni(III) species, which could fragment to give a halide radical. This halide radical could then perform a HAT to give an α -amidyl radical, as depicted in Figure 3-22.

To test this hypothesis, several nickel(II) complexes including *i*-PrBiOxNi(II)Cl₂,

entry	nickel complex	E _{p/2} (Ni(II/III)) vs SCE	E _{p/2} (Ni(I/II)) vs SCE
1	<i>i</i> -PrBiOxNi(II)Cl ₂	+1.27	-0.88
2	<i>i</i> -PrBiOxNi(II)ArBr	+1.43	-0.43
3	BiOxNi(II)ArBr	+1.52	-0.34

Table 3-1 Redox properties of nickel(II) complexes.

i-PrBiOxNi(II)ArBr, and BiOxNi(II)ArBr were synthesized (Figure 3-23). BiOxNi(II)Cl₂ was also synthesized, but its low solubility in common organic solvents, such as MeCN and EtOAc, prohibited accurate comparison of its redox properties to other Ni(II) complexes or iridium photocatalyst. The redox properties of these complexes were determined using CV and compared to those of **PC1** (Table 3-1). It was found that the redox potentials of each nickel catalyst were unfavorable for oxidation, but accessible for reduction by **PC1** (Ir(III^{*}/II)= +1.21V vs SCE and Ir(III^{*}/IV)= -0.89V vs SCE). This suggests that it is unlikely a cationic nickel(III)X₂ or cationic nickel(III)ArBr species is formed under the reaction conditions, though reduction to give a nickel(I) is feasible, leading us to refine our initial mechanistic hypothesis.

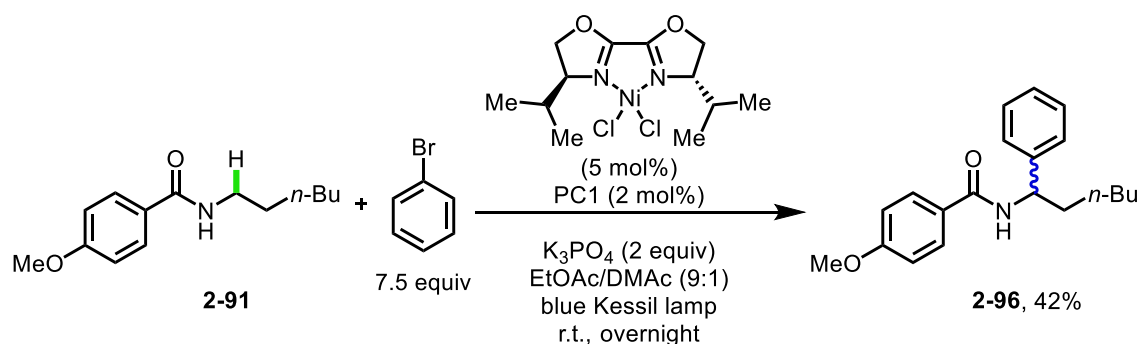


Figure 3-24 α -arylation of benzamides using a discrete *i*-PrBiOxNi(II)Cl₂ complex.

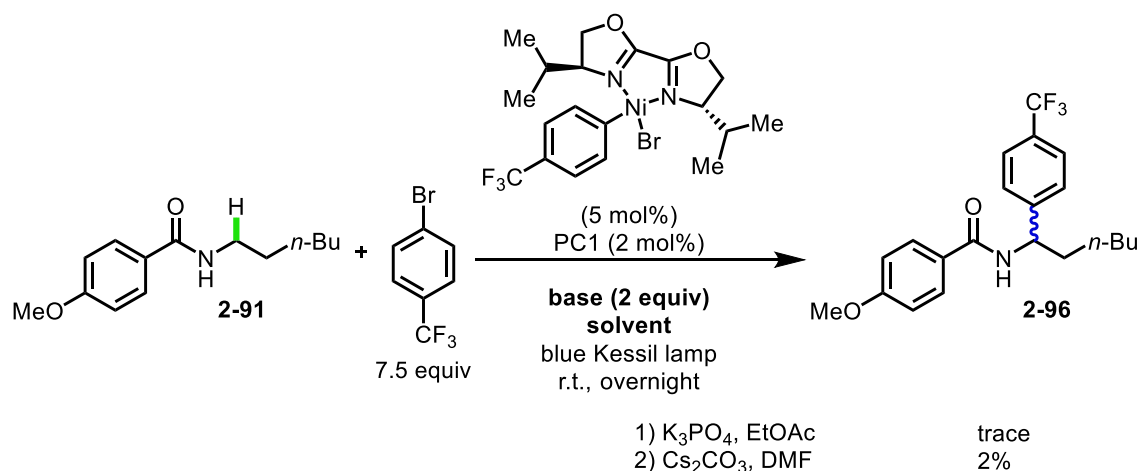


Figure 3-25 α -arylation of benzamides using a discrete *i*-PrBiOxNi(II)ArBr complex.

The favorable reduction potential of nickel species in this reaction may lend insight into the source of amidyl radical formation. Upon reduction, two potential pathways could occur; 1) oxidative addition of PhBr to a nickel(I) species to give a nickel(III) complex that undergoes light-induced homolysis, as in the case described by Doyle, or 2) the chloride or bromide ion generated from reduction of nickel(II) could be oxidized by the Ir(IV) photocatalyst to form a halide radical.²¹⁵⁻²¹⁶ These two hypotheses led us to test *i*-PrBiOxNi(II)Cl₂, *i*-PrBiOxNi(II)ArBr, and BiOxNi(II)ArBr as catalysts in the reaction. Under standard reaction conditions, *i*-PrBiOxNi(II)Cl₂ gave 42% of the desired product, which is similar in yield to the *in situ* protocol (Figure 3-24). However, when testing *i*-PrBiOxNi(II)ArBr in this reaction, trace product was observed (Figure 3-25). Moreover, switching to Cs₂CO₃ in DMF did not restore yields. From this data it can be concluded that this is not a relevant catalytic intermediate.

Interestingly, when testing BiOxNi(II)ArBr under identical conditions, 21% of the desired product (**2-96**) was observed in addition to 19% *N*-arylation (**3-26**) and 19% recovered starting material (Figure 3-26). This result was surprising since BiOxNi(II)ArBr and *i*-PrBiOxNi(II)ArBr are very similar, yet no reactivity was observed in the latter case.

Additionally, catalytic turnover was observed with BiOxNi(II)ArBr, which could mean that this is a relevant catalytic intermediate, though the production of substantial amounts of *N*-arylation product (**3-26**) suggest otherwise, since only trace amounts of this are produced under standard reaction conditions. Furthermore, the poor mass balance could mean that deleterious side reactions from this catalyst result in decomposition, which is contrary to standard reaction conditions in which good mass balance is observed for most substrates. Although mechanistically interesting, the lack of reactivity with *i*-PrBiOxNi(II)ArBr and observation of substantial amounts of a side product not typically observed under standard reaction conditions suggest that BiOxNi(II)ArBr is not a relevant intermediate along the catalytic cycle.

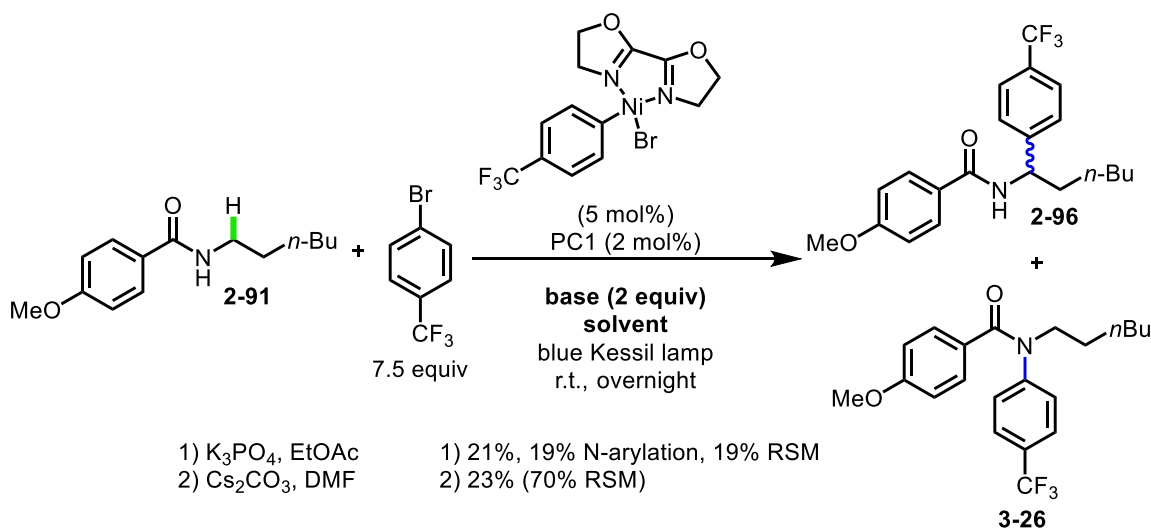


Figure 3-26 α -arylation of benzamides using a discrete BiOxNi(II)ArBr complex. RSM = recovered starting material.

From these observations, we were curious if an interaction between iridium and nickel was responsible for initiating α -amidyl radical formation. Furthermore, since nickel(0) complexes were not found to provide good yields of the desired product, we hypothesized that a reduction event by the photocatalyst may be responsible for both generating a HAT agent and modulating the oxidation state of nickel. To explore this

possibility, Stern-Volmer quenching studies were performed with a discrete nickel pre-catalyst (**2-160**). Interestingly, strong quenching of **PC1** was observed with **2-160** in EtOAc. **2-160** was also tested in DMF tested and it was found that although this quenched **PC1**, the quenching constant was an order of magnitude less than the quenching observed in EtOAc (Table 3-2). As no other quenching event was observed in EtOAc, this suggests that the reaction is initiated through an interaction between the excited-state iridium photocatalyst and a nickel(II) complex.

Halide radical formation from Ni(II):

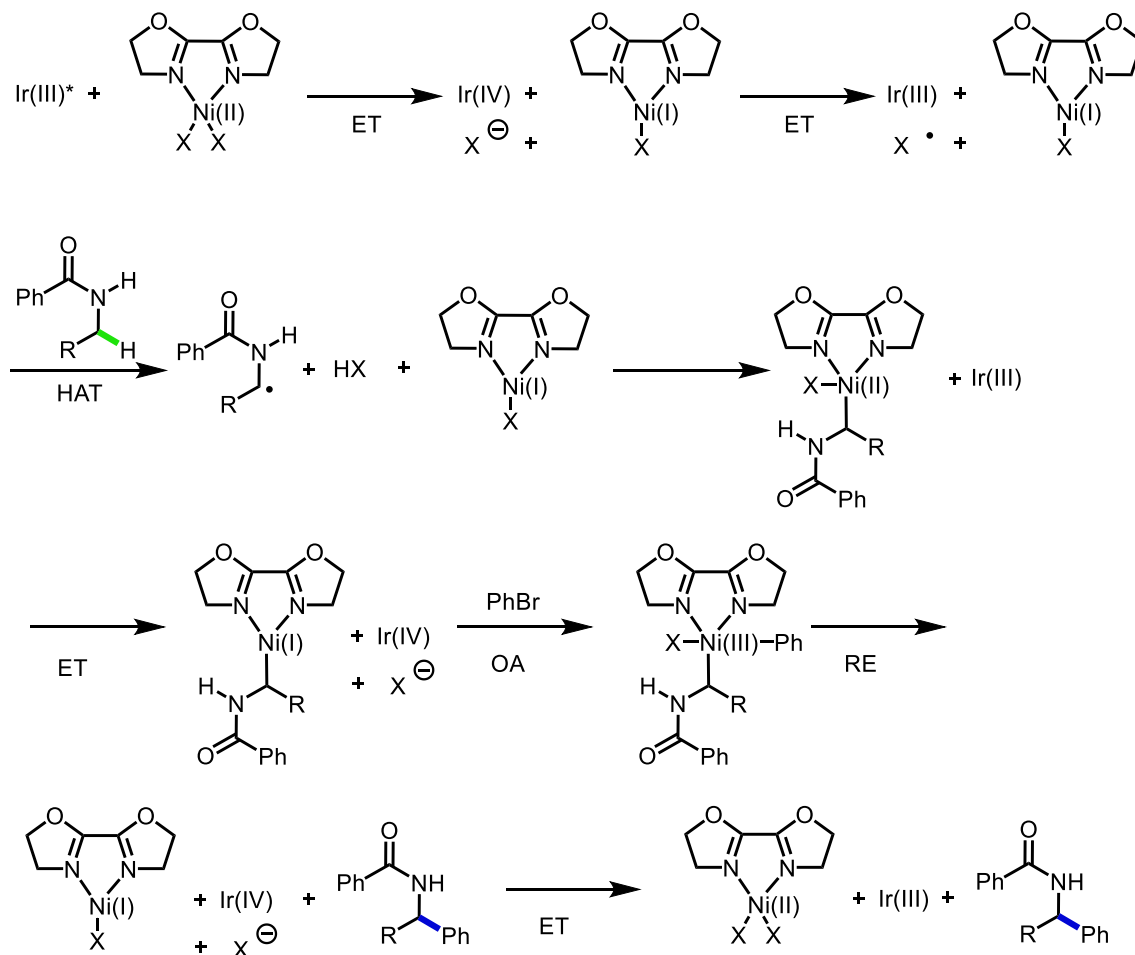


Figure 3-27 Revised mechanistic hypothesis for α -arylation of benzamides.

Based on the results from these newly tested nickel catalysts, a refined mechanistic hypothesis was made (Figure 3-27). Taken together with the Stern-Volmer quenching

studies (Table 3-2), in which *i*-PrBiOxNiCl₂ quenches **PC1**, we believe the reaction initiates from the PET of **PC1** to BiOxNi(II)X₂. Through the reduction of Ni(II) to Ni(I) and oxidation of X⁻ to X[•] by Ir(III)*, a potent halide HAT agent is generated. X[•] can then abstract the α-amidyl C–H bond to form HX, which is sequestered by K₃PO₄. The newly formed Ni(I) species then combines with the α-amidyl radical to form a L₂Ni(II)alkylX species. This L₂Ni(II)alkylX species can then be reduced to a Ni(I)alkyl species, to which PhBr oxidatively adds to form L₂Ni(III)alkylPhBr. This Ni(III) species can then reductively eliminate to form the product and Ni(I)X, which interacts with X⁻ and Ir(IV) to regenerate both catalysts, completing the catalytic cycle.

compound(s)	quenching in EtOAc?	K _{SV} (M ⁻¹)	quenching in DMF?	K _{SV} (M ⁻¹)
PhBr	none		none	–
Benzamide (2-91)	none	–	none	–
K ₃ PO ₄	–	–	–	–
Cs ₂ CO ₃	–	–	none	–
Cs ₂ CO ₃ + benzamide (2-91)	–	–	yes	54
<i>i</i> -PrBiOxNiCl ₂ (2-160)	yes	1125	yes	165

Table 3-2 Summary of Stern-Volmer analysis for alpha-arylation of benzamides.

Critical to this mechanistic hypothesis is the observation that Ni(II)X₂ complexes strongly quench the photocatalyst. Because the Ni(I/II) couple is predicted to be more thermodynamically favorable, it is thought that a Ni(II/I) redox event takes place to generate Br⁻, which can be oxidized by Ir(IV) to give Br[•].²¹⁷ The large primary KIE observed in the competition experiment cannot be ignored, as this supports the direct abstraction of C–H bonds from a HAT agent, such as bromine radical.²¹⁸ Furthermore,

previous studies have shown that halide anions can be oxidized by Ir(III)* complexes,²¹⁹⁻²²³ therefore the more oxidizing Ir(IV) should be able to perform the same transformation ($E_{1/2}^{IV/III} = 1.69$ V vs SCE).

Additionally, we believe that Ni(II)ArX is not generated under the reaction conditions due to the observation that *i*-PrBiOxNi(II)ArBr is not a competent catalyst. This is supported by Molander who concluded that energy transfer, rather than halide radical formation, is operative for the direct functionalization of C–H bonds in THF in systems using Ni(II)ArBr species.¹⁷³ The lack of reactivity using Ni(II)ArBr species in our reaction suggest that a different mechanism than that proposed by Molander. Therefore, we propose the newly formed α -amidyl radical adds into Ni(I)Br to give a Ni(II)alkylBr species. Further studies should be directed at the synthesis of a discrete Ni(II)alkylBr species to test its catalytic competency.

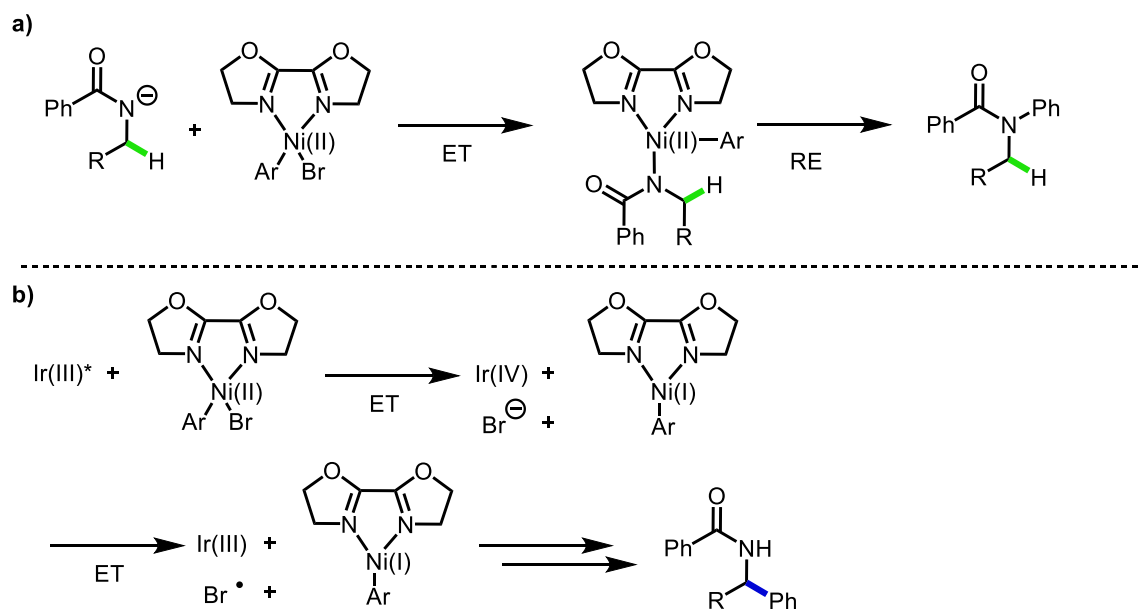
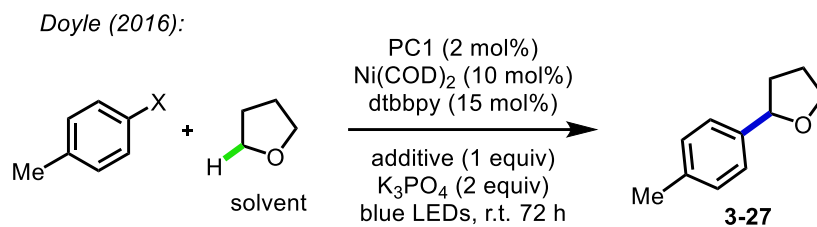


Figure 3-28 Possible competing pathways for, **a)** N-arylation and **b)** C-arylation, when using BiOxNi(II)ArBr.

Intrigued by the observation of N-arylation when using BiOxNi(II)ArBr, a possible mechanism is proposed based on additional data acquired during our studies (Figure 3-28).

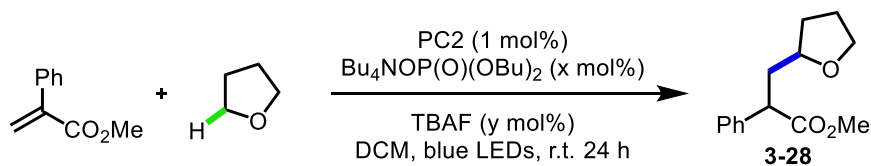
One potential explanation for the N-arylation of benzamide could result from the ligand exchange between deprotonated benzamide and bromide. This would give a $\text{Ni(II)(NR}_1\text{R}_2\text{)Ar}$, which could then reductively eliminated (with or without assistance from the photocatalyst). A competitive rate of exchange of the bromide with deprotonated benzamide could result in reduction of the Ni(II)ArBr species by iridium to yield a bromide radical, similar to the mechanism mentioned above. This could then lead to the desired product through an analogous mechanism and might explain why near equal quantities of N-arylation and C-arylation is observed when using BiOxNi(II)ArBr and not with *i*-Pr BiOxNi(II)Cl_2 . Additional studies are necessary to rule out a competitive energy transfer, such as that proposed by Molander, though the fact that BiOxNiArBr provides some product, whereas *i*-Pr BiOxNiArBr does not suggests that this not a major pathway when using a Ni(II)X_2 pre-catalyst.¹⁷³



entry	X	additive	yield
1	Cl	none	68%
2	Br	none	10%
3	I	none	5%
4	I	TBACl	51%
5	I	TBABr	37%
6	I	TBAI	6%

Table 3-3 Studies by Doyle of restoring reactivity of aryl bromides and iodides by adding TBACl.

Having established that BiOxNi(II)ArBr is not a catalytically relevant intermediate in this reaction, efforts were next turned toward exploring the mode of α -amidyl radical formation using *i*-PrBiOxNi(II)Cl₂. The Doyle group has explored the benefits of adding tetrabutylammonium salts to generate potent HAT mediators (Table 3-3).²⁰⁸ In their work, they observe that only aryl chlorides provide substantial amounts of product despite the well-known facile oxidative addition of aryl bromides and iodides to nickel(0) complexes (Table 3-3, entries 1-3). They provide convincing evidence that the active HAT agent is generated through the homolysis of a nickel(III) halide complex to give halide radicals, which would explain why bromide or iodide radicals are ineffective in this chemistry (BDE for F–H: 136 kcal/mol, Cl–H: 103 kcal/mol, Br–H; 87 kcal/mol,

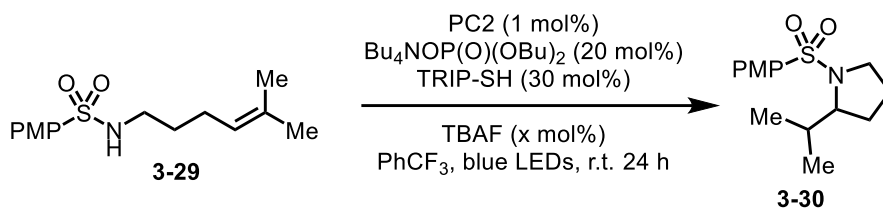


entry	x	y	yield
1	10	0	92%
2	10	5	13%
5	0	5	0%

Table 3-4 Knowles' study on the effects of adding TBAF on yield to C–H PCET reaction that requires hydrogen bonding between the photocatalyst and base.

I–H: 71 kcal/mol, as their BDE is too low to abstract C–H bonds from cyclic ethers (THF BDE: 92 kcal/mol). They go on to show that adding tetrabutylammonium chloride restores reactivity by generating the requisite nickel(III) chloride species for homolysis (Table 3-3, entry 4). As both NiCl₂·DME and NiBr₂·DME gave similar yields in our reaction, and PhBr

was the only aryl halide that provided any product, we were curious to see if the addition of halide salts would have a positive effect on our reaction.



entry	x	yield
1	0	96%
2	5	96%
3	20	92%

Table 3-5 Knowles' study on the effects of adding TBAF on the yield for a N-H PCET reaction that does not require hydrogen bonding to the iridium photocatalyst.

It is well known that iridium photocatalysts are capable of anion exchange, and that these types of photocatalysts can oxidize halogens to give radical species capable of HAT.^{216, 224-225} In studies by the Knowles group, varying concentrations of TBAF were added to a productive reaction containing a phosphate base to show that competitive

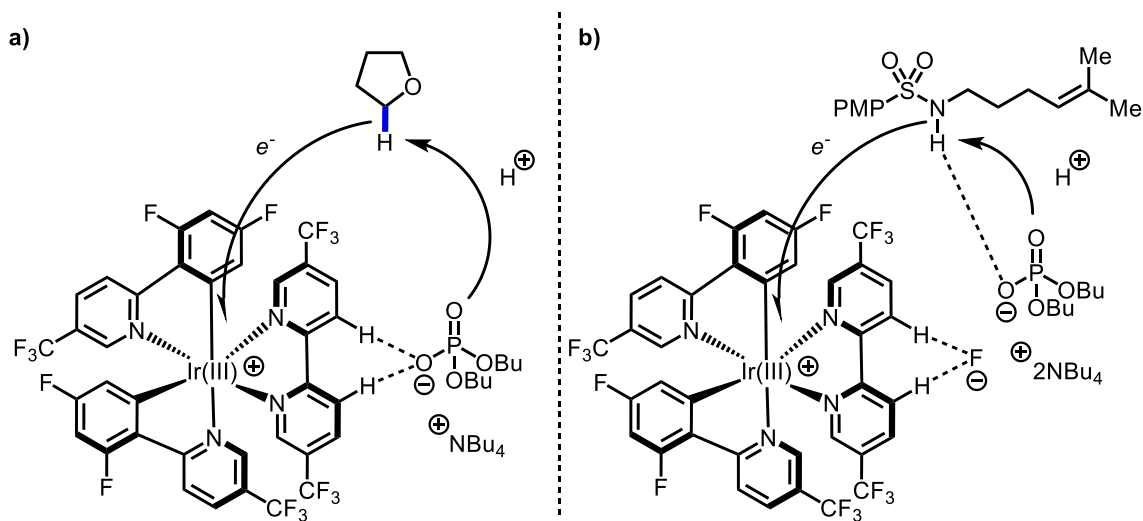
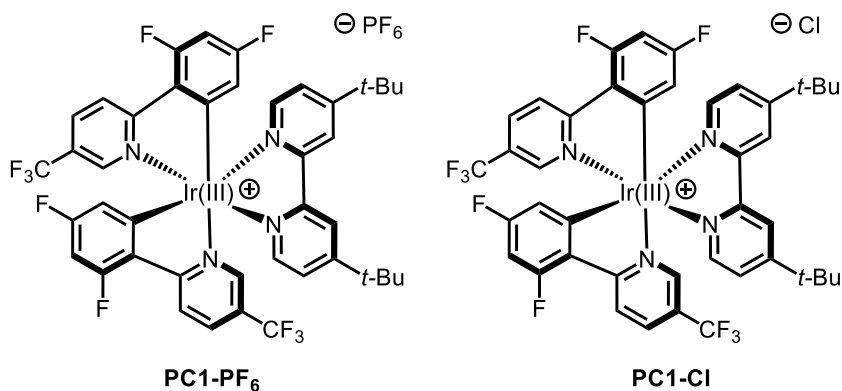
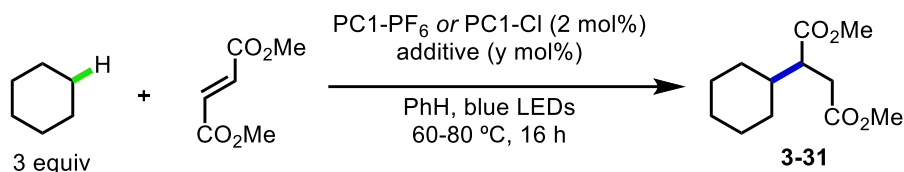


Figure 3-29 Comparison of hydrogen bonding between the photocatalyst and phosphate base in, **a**) single-site PCET and, **b**) multi-site PCET.

binding of certain halides to the photocatalyst have negative effects on reaction rate (Table 3-4).¹⁹⁸



entry	x	additive	yield
1	PC1-PF ₆	TBACl (10 mol%)	80%
2	PC1-PF ₆	TBACl (5 mol%)	84%
3	PC1-PF ₆	none	0%
4	PC1-Cl	none	86%
5	PC1-Cl	none	0% ^a

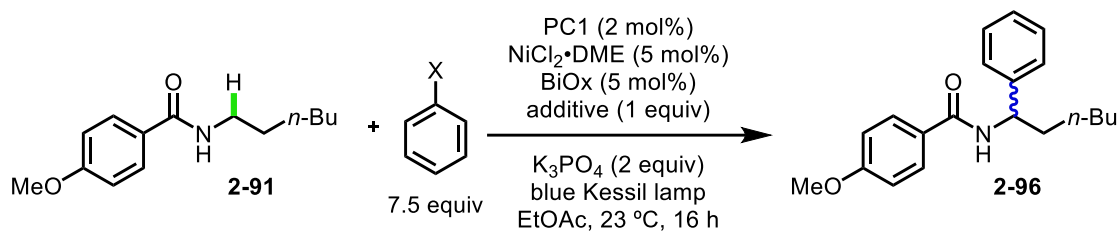
Table 3-6 Studies by Barriault on counterion effects on HAT using iridium photocatalysts. ^a Reaction run at room temp.

This effect is only observed in reactions which involve hydrogen bond pairing of the photocatalyst and the base, where binding of strong hydrogen bond acceptors, like fluoride, out compete iridium-phosphate complexation. The Knowles group were able to show that this is not the case in N–H PCET reactions where the more polarized N–H bond of the

substrate coordinates to the base (Table 3-5).¹⁹⁸ This allows for multi-site PCET to be operative regardless of the inclusion of hydrogen bond acceptors to the reaction (Figure 3-29).

Contrary to this, observations by Barriault and others found that using iridium photocatalysts bearing counterions that are more susceptible to oxidation, such as chloride,²¹⁵ or bromide²¹⁶ were necessary for productive catalysis (Table 3-6). Further studies implicate these oxidizable counter ions as HAT agents. Unlike the fluoride, chloride has a lower oxidation potential and can serve as a HAT agent. The authors were able to show that either photocatalyst with chloride counterions or the inclusion of TBACl enable abstraction of strong C–H bonds (Table 3-6, entries 2-4). However, while the oxidation event is thermodynamically favorable (TBACl $E_{1/2}^{\text{red}} = +1.01$ V vs SCE; TBABr $E_{1/2}^{\text{red}} = +0.71$ V vs SCE; TBAI $E_{1/2}^{\text{red}} = +0.26$ V vs SCE),^{180, 217, 221} the HAT is challenging, which the authors attribute to the lack of reactivity at room temperature observed with TBACl (Table 3-6, entry 5). The strong affinity of halide counterions to iridium photocatalysts and their potential to serve as HAT agents led us to explore tetrabutylammonium halides as additives for our reaction.

Encouraged by the positive results of the Doyle and Barriault groups, we commenced studying the effects of adding tetrabutylammonium halides to our reaction. Since our reaction only worked with aryl bromides, we added tetrabutylammonium bromide (TBABr) to reactions containing PhCl and PhI. Upon adding 1 equivalent of TBABr to a reaction containing PhCl as the aryl source, 30% yield was observed, which is slightly lower than the model reaction (~50%). Nickel-catalyzed halide exchange of tetrabutylammonium salts and aryl halides has been documented by the Doyle group, and



entry	X	additive	yield
1	Cl	none	0%
2	Br	none	49%
3	I	none	0%
4	Cl	TBABr	30%
5	Cl	TBACl	0%
6	I	TBABr	0%
7	Br	TBACl	46%
8	Br	TBAI	30%
9	Cl	TBAI	0%

Table 3-7 Effects of adding tetrabutylammonium salts to the α -arylation of benzamides.

could explain the changes in reactivity.²⁰⁸ Control experiments using PhCl or PhCl/TBACl gave no reaction, suggesting that bromide ions are in some way important for this reaction. Notably, when the same experiment was performed with PhI and TBABr, no reaction was observed. Further experiments were undertaken to see if these counter ion effects were observed when switching tetrabutylammonium salts and aryl sources.

Intrigued by the reactivity with some aryl halides and not with others when adding tetrabutylammonium salts, a reaction with PhBr with 1 equivalent tetrabutylammonium chloride (TBACl) and one with 1 equivalent of tetrabutylammonium iodide (TBAI) were conducted (Table 3-7, entries 7 & 8). In the reaction using PhBr and TBACl, 46% yield

was observed, though in the reaction with TBAI only 30% yield was observed. These

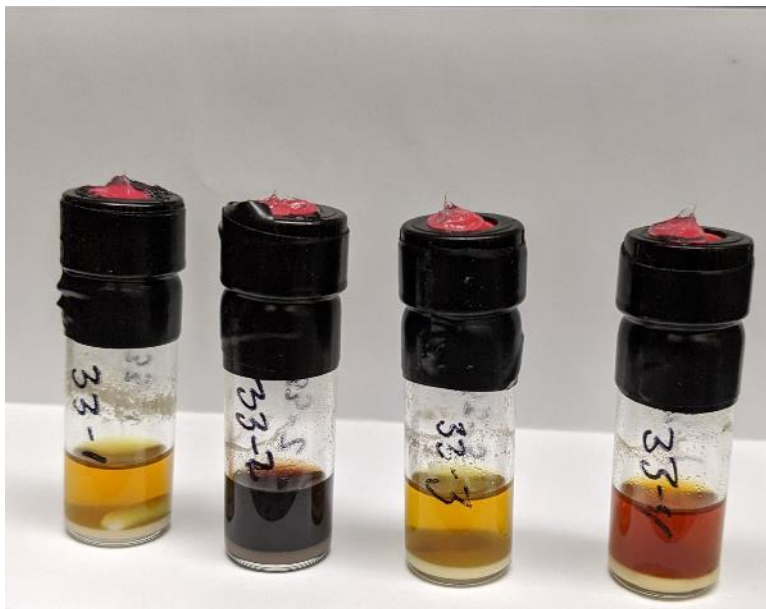


Figure 3-30 Effects on reaction color with and without TBABr. **Left to right:** 1 equiv PhBr with TBABr, 1 equiv PhBr with no TBABr, 7.5 equiv PhBr with TBABr, 7.5 equiv PhBr with no TBABr. Reactions were run for 16 hours under irradiation by blue LEDs using standard reaction conditions for α -arylation of benzamides.

results suggest that chloride ions have less of an effect on the reaction as iodide ions, though both species have no benefit on yields. Together, these results are not supportive of the mechanism proposed by Doyle where a more potent HAT agent can be generated by adding tetrabutylammonium chloride to reactions with aryl bromides or aryl iodides. Instead, we observe either negligible effects or decreases in yield when adding different tetrabutylammonium salts to reactions containing PhBr (Table 3-7, entries 7 & 8). This led us to pursue the hypothesis that halide additives could be used to serve as a HAT agents through the direct oxidation by an iridium photocatalyst rather than the generation of a Ni(II)ArX or intermediate for homolysis.

Early on in our studies of adding tetrabutylammonium salts to reactions with different aryl bromides, it was observed that control reactions with TBABr and PhBr had a drastically different color at the end of the reaction than those without TBABr (Figure 3-

30). We hypothesized that changes in the color of these reactions was the results of degradation of the photocatalyst, nickel catalyst or both. Despite this, portion-wise additions of fresh catalyst(s) or higher catalyst loadings did not have a positive effect on yield, as discussed in the optimization of the reaction (see section 2.4.2, Table 2-10). Since photon absorption is essential for productive catalysis to take place, we hypothesized that the degradation products were competitively absorbing light.²²⁶ While no new species related to catalyst(s) degradation could be isolated or observed spectroscopically, evidence for photocatalyst modification was observed through LCMS analysis of reactions run for 1 hour and 12 hours (see Section 4.4.4). Additionally, modifications of the photocatalyst structure were unfruitful, though there is evidence that photocatalyst modification is not necessarily detrimental to productive catalysis (Figure 4-37).²²⁷ Still we opted to pursue these results in the hope that additions of tetrabutylammonium salts might protect the integrity of the catalyst(s), leading to higher yields.

In line with our goals of improving upon the yields and lowering the equivalents of electrophilic coupling partner in this reaction, systematic experiments were conducted to see if TBABr was beneficial for reactivity. By including 1 equivalent of TBABr and lowering the amount of aryl bromide from 7.5 equivalents to 2 or 1 equivalent, synthetically useful yields could be achieved when running these reaction for 48 hours (Table 3-8, entries 1 & 2). When adding 1 equivalent of TBABr to a reaction with 2 equivalents of benzamide and 1 equivalent of PhBr, 73% arylation was observed, with a high ratio of C-arylation to N-arylation (Table 3-8, entry 3)! Unlike those run without TBABr, these reactions showed no sign of catalyst degradation or color change, indicating

greater catalyst longevity, and therefore give hope that longer reaction times could potentially be used to increase yield.

entry	x	y	C-arylation to N-arylation ^a	yield ^b
1	1	1	4.3:1	47%
2	2	1	3.6:1	52%
3	1	2	7.3:1	73%

Table 3-8 Effects of reaction stoichiometry on yield when adding TBABr. ^a Ratio were determined through GCMS analysis of the crude reaction mixture. ^b Yield refers to total yield of C-arylation and N-arylation and was determined by a calibration curve using tridecane as an internal standard.

It has been documented that halides are competent quenchers for iridium photocatalysts.^{219-220, 223} The reactivity observed with TBABr over TBACl might occur because of a more favorable redox event with **PC1**, as shown by Barriault.²¹⁵ This could explain why TBACl did not provide substantial increases in yield. Additionally, the low BDFE of iodide radical could explain why TBAI did not provide any product, as the C–H bonds of benzamide are too strong to be abstracted by **I•**. These results suggest that TBABr can be used as a HAT agent for the α -arylation of *N*-alkyl benzamides. We hypothesize that the increased concentration of bromide anions results in more facile formation of a HAT agent. Further studies should be conducted to determine the exact role of TBABr in this reaction. Specifically, UV-Vis and fluorescence studies could lend insight into the formation of a new anionic nickel halide complex under the reaction conditions. Additionally, Stern-Volmer studies to explore the rates of quenching between TBABr and

i-PrBiO_xNiCl₂ could elucidate if nickel is necessary for the generation of a HAT agent or if exogenous KBr generated in the reaction is responsible for the observed reactivity when TBABr is not included.

Despite these promising results, control reactions must be undertaken to confirm that TBABr is responsible for the drastic increases in yield for reactions that use near-stoichiometric amount of coupling partners. These preliminary results also open up the possibility for further optimization. Factors that should be initially examined include the stoichiometry of the electrophile, amount of TBABr, reaction time, and catalyst loading for nickel and iridium. Additionally, efforts will be made to extend this to other electrophiles and benzamides as a general method to achieve high yields for α -arylation of *N*-alkyl benzamides.

Chapter 4

Experimental Section

4.1 General Supporting Information

All reagents were used as received unless otherwise noted. Solvents were purified under nitrogen using a solvent purification system (Innovative Technology, Inc. Model # SPS400-3 and PS-400-3). Et₃SiH (Sigma-Aldrich), BnMe₂SiH (Sigma-Aldrich), PhMe₂SiH (Sigma-Aldrich), and (TMSO)MeSiH (TCI Chemicals) were passed through basic alumina and distilled before use and stored under nitrogen. IPr*^{OMe} (made from known procedure²²⁸), IMes·HCl (made from known procedure²²⁹), other *N*-heterocyclic carbenes (Sigma-Aldrich), and NaO-*t*-Bu (Strem Chemicals) were stored and weighed in an inert atmosphere glovebox. Ethyl acetate (Sigma-Aldrich, 99.8% anhydrous) was distilled over CaH₂ (Sigma-Aldrich) and then freeze, pumped, thawed three times before storing under N₂. Aryl bromides (Oakwood) were dried on high vacuum or distilled over CaH₂ prior to use. K₃PO₄ (Strem, anhydrous) was finely ground and then heated under vacuum at 100 °C overnight before transferring to a glove box. Phenylpyridines and bipyridines were synthesized through known procedures.^{155, 230} Iridium photocatalysts were synthesized by modified literature procedures for [Ir(dCF₃(CF₃)ppy)₂(4,4'-di-*t*-bubpy)]PF₆, [Ir(FCF₃(CF₃)ppy)₂(4,4'-di-*t*-bubpy)]PF₆, and [Ir(dF(CF₃)ppy)₂(4,4'-di-*t*-

bubpy)]PF₆,²³¹ [Ir(dF(CF₃)ppy)₂(5,5'-di-CF₃bpy)]PF₆.¹⁵⁵ Bisoxazoline (BiOx) ligands were synthesized through known procedures.²³²

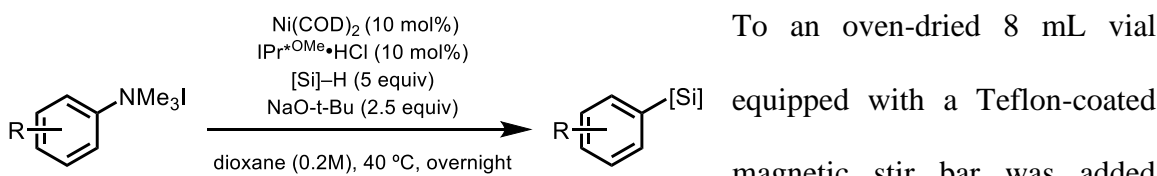
Analytical thin layer chromatography (TLC) was performed on Kieselgel 60 F254 (250 µm silica gel) glass plates and compounds were visualized with UV light and *p*-anisaldehyde, potassium permanganate or ceric ammonium molybdate stains. Flash column chromatography was performed using Kieselgel 60 (230-400 mesh) silica gel. Eluent mixtures are reported as v:v percentages of the minor constituent in the major constituent. All compounds purified by column chromatography were sufficiently pure for use in further experiments unless otherwise indicated. ¹H NMR spectra were collected at 400 MHz on a Varian MR400, at 500 MHz on a Varian Inova 500 or Varian vnmrs 500, or at 700 MHz on a Varian vnmrs 700 instrument. The proton signal of the residual, nondeuterated solvent (δ 7.26 for CHCl₃) was used as the internal reference for ¹H NMR spectra. ¹³C NMR spectra were completely heterodecoupled and measured at 125 MHz or 175 MHz. Chloroform-d (δ 77.00) was used as an internal reference. High resolution mass spectra were recorded on a VG 70-250-s spectrometer manufactured by Micromass Corp. (Manchester UK) at the University of Michigan Mass Spectrometry Laboratory or recorded on an Agilent 6545 Q-TOF LS/MS at the University of Michigan Life Sciences Institute. LCMS traces were recorded on an Agilent 6545 Q-TOF LS/MS at the University of Michigan Life Sciences Institute. GCMS analysis was carried out on a HP 6980 Series GC system with HP-5MS column (30 m x 0.250 mm x 0.25 µm) or on an Agilent 7890B GC system with HP-5MS column (30 m x 0.250 mm x 0.25 µm). GCFID analysis was carried out on a HP 6980N Series GC system with a HP-5 column (30 m x 0.32 mm x 0.25 µm). SFC analysis was carried out on a Waters Investigator SFC using a Waters 2998

photodiode array detector. Samples were run on an OD-H Daicel 5 μ m (4.6mm x 250mm) analytical chiral column using a MeOH/CO₂ gradient. Infrared spectra were recorded using a Nicolet iS10 FT-IR spectrometer as a neat solid.

4.2 Experimental Details for Chapter 1

4.2.1 General Procedures for Chapter 1

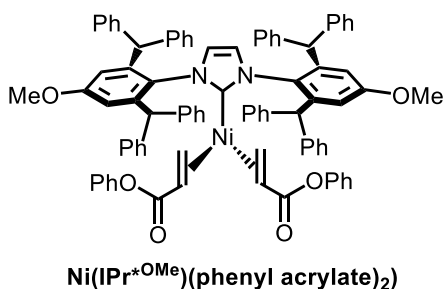
4.2.1.1 General Procedure for Nickel-Catalyzed Silylation of Aryl Trialkylammonium Salts:



To an oven-dried 8 mL vial equipped with a Teflon-coated magnetic stir bar was added

Ni(COD)₂ (2.8 mg, 0.01 mmol, 0.1 equiv), *N,N'*-bis(2,6-bis(diphenylmethyl)-4-methoxyphenyl)imidazolium chloride (IPr*OMe·HCl) (9.8 mg, 0.01 mmol, 0.1 equiv), NaO-*t*-Bu (24 mg, 0.25 mmol, 2.5 equiv), and ammonium salt (0.1 mmol, 1 equiv) were combined under inert atmosphere and suspended in 0.5 mL of dioxane at rt. Silane (0.5 mmol, 5 equiv) was added and the vial was sealed with a Teflon cap before removing from the glovebox to heat to 40 °C overnight. Upon completion, the reaction mixture was quenched with 1 mL EtOAc and run through a silica gel plug with 5 mL EtOAc. The solvent was removed by rotary evaporation and the crude reaction mixture was purified by silica gel chromatography.

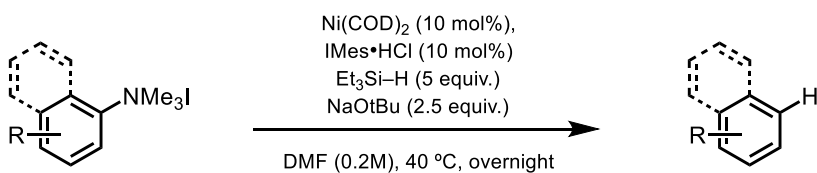
4.2.1.2 Modified General Procedure using Air-Tolerant Nickel(0) Catalyst:



To an oven-dried 8 mL vial equipped with a Teflon-coated magnetic stir bar was added (1,3-bis(2,6-bis(diphenylmethyl)-4-methoxyphenyl)imidazol-2-ylidene)bis(phenyl acrylate)nickel(0) ($\text{Ni}(\text{IPr}^*\text{OMe})(\text{phenyl acrylate})_2$) (**106**) (26 mg, 0.01

mmol, 0.1 equiv), NaO-*t*-Bu (48 mg, 0.50 mmol, 2.5 equiv), and ammonium salt **1-81** (68mg, 0.2 mmol, 1 equiv) were combined under inert atmosphere and suspended in 1.0 mL of dioxane at rt. Triethylsilane (156 μ L, 1.0 mmol, 5 equiv) was added and the vial was sealed with a Teflon cap before removing from the glovebox to heat to 40 °C overnight. Upon completion, the reaction mixture was quenched with 1 mL EtOAc and run through a silica gel plug with 5 mL EtOAc. Analysis of the crude reaction mixture by GCFID using tridecane as an internal standard showed 76% yield of aryl silane **1-81a** and 13% yield of **1-81b**. The solvent was removed by rotary evaporation and the crude reaction mixture was purified by flash chromatography (100% hexanes) to give **1-81a** as a colorless oil in 67% yield (35.9 mg, 0.134 mmol).

4.2.1.3 General Procedure for Nickel-Catalyzed Reduction of Aryl Trialkylammonium Salts:

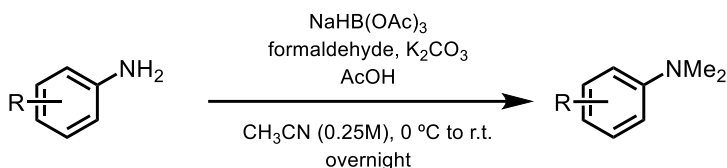


To an oven-dried 8 mL vial equipped with a Teflon-coated magnetic

stir bar was added Ni(COD)₂ (2.8 mg, 0.01 mmol, 0.1 equiv), 1,3-bis(2,4,6-trimethylphenyl)imidazolium chloride (IMes·HCl) (3.4 mg, 0.01 mmol, 0.1 equiv), NaO-

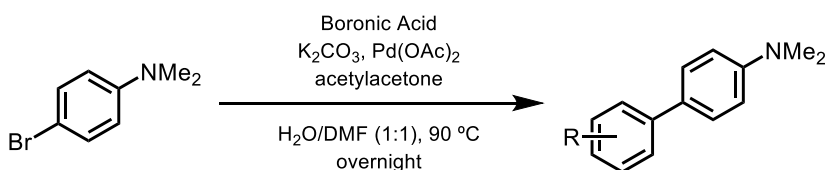
t-Bu (24 mg, 0.25 mmol, 2.5 equiv), and ammonium salt (0.1 mmol, 1 equiv) were combined under inert atmosphere and dissolved in 0.5 mL of DMF at rt. Triethylsilane (80 μ L, 0.5 mmol, 5 equiv) was added and the vial was sealed with a Teflon cap before removing from the glovebox to heat to 40 $^{\circ}$ C overnight. Upon completion, the reaction mixture was quenched with 1 mL EtOAc and run through a silica gel plug with 5 mL EtOAc. The solvent was removed by rotary evaporation and the crude reaction mixture was purified by silica gel chromatography.

4.2.1.4 General Procedures for Reductive Amination:



To an appropriately sized round-bottom flask equipped with a Teflon-coated magnetic stir bar under a nitrogen atmosphere were added aniline (1 equiv) and CH_3CN (0.25M). The flask was cooled to 0 $^{\circ}$ C before adding formaldehyde solution (37%) (6 equiv) and K_2CO_3 (2 equiv). After 1 hour of stirring NaHB(OAc)_3 (3 equiv) was added followed by the slow addition of AcOH (11 equiv). The solution was warmed to room temperature after 30 min and stirred overnight. The reaction was quenched with H_2O and EtOAc. The solution was basified with sat. NaHCO_3 and extracted with 3xEtOAc. The organics were dried over brine, then Na_2SO_4 and concentrated before purifying by silica gel column chromatography.

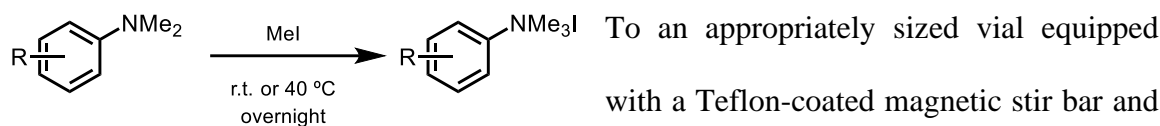
4.2.1.5 General Procedures for Suzuki-Miura Coupling:



To an appropriately sized round-bottom flask equipped with a

Teflon-coated magnetic stir bar and a reflux condenser was added 4-bromo-dimethylaniline (1.00 equiv), arylboronic acid (1.50 equiv), K_2CO_3 (2.00 equiv), $Pd(OAc)_2$ (0.01 equiv), and acetylacetone (0.02 equiv). The flask was backfilled with N_2 three times before adding H_2O (0.66M) and DMF (0.66M). The reaction was heated to 90 °C overnight. The reaction was cooled and quenched with Et_2O and the organics were washed 1x H_2O , 2x brine. The organics were then dried over $MgSO_4$ and concentrated before purifying by silica gel column chromatography.²³³

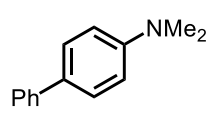
4.2.1.6 General Procedures for Aryl Trialkylammonium Salt Formation:



a reflux condenser was added *N,N*-dimethylaniline (1.00 equiv) and MeI (10.00 equiv). The vial was sealed and stirred until a white precipitate formed. Electron deficient aniline typically required heating to 40 °C overnight while electron rich anilines reached full conversion in a few hours. The solid was then filtered washed copiously with Et_2O and rigorously dried on high vac for several hours. The trimethylammonium salts were used as is in subsequent chemistry.²³⁴

4.2.2 Starting Material Synthesis:

N,N-dimethyl-[1,1'-biphenyl]-4-amine



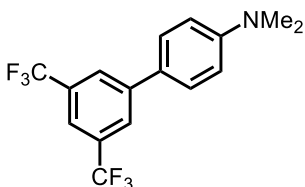
The general procedure for Suzuki-Miura coupling was followed using 4-bromo-dimethylaniline (1.00 g, 5.00 mmol, 1.00 equiv), phenylboronic acid (914 mg, 7.5 mmol, 1.50 equiv), K_2CO_3 (1.38 g, 10.00 mmol, 2.00 equiv), $Pd(OAc)_2$ (11 mg, 0.05 mmol, 0.01 equiv), acetylacetone (10 mg, 0.10 mmol, 0.02 equiv), H_2O (7.5

mL), and DMF (7.5 mL). Purification by flash chromatography (90:10 hexanes/EtOAc) gave the title compound as a white solid in 87% yield (690 mg, 3.49 mmol). The spectral data matches that previously reported in the literature.^[3]

¹H NMR (401 MHz, Chloroform-*d*) δ 7.61 – 7.53 (m, 2H), 7.51 (d, *J* = 8.8 Hz, 2H), 7.39 (t, *J* = 7.6 Hz, 2H), 7.26 (m, 1H), 6.81 (d, *J* = 8.8 Hz, 2H), 3.00 (s, 6H).

¹³C NMR (126 MHz, Chloroform-*d*) δ 150.11, 141.36, 129.38, 128.77, 127.83, 126.42, 126.11, 112.90, 40.71.

***N,N*-dimethyl-3',5'-bis(trifluoromethyl)-[1,1'-biphenyl]-4-amine**



To an oven-dried 25-mL round-bottom flask containing a Teflon-coated magnetic stir bar were brought into a N₂ glovebox and Pd(PPh₃)₄ (34.7 mg, 0.03 mmol, 3 mol%) was added. The round bottom was sealed with a septa and removed from the glovebox. 4-bromo-*N,N*-dimethylaniline (200 mg, 1.00 mmol, 1.00 equiv) and 3,5-bis(trifluoromethyl)phenylboronic acid (257 mg, 1.00 mmol, 1.00 equiv) were added, followed by toluene (10 mL, 0.1M), EtOH (3 mL, 0.33M), and Sat. Na₂CO₃ (5 mL). A reflux condenser was added and the reaction was heated to 80 °C overnight. The reaction was cooled to room temperature and quenched with H₂O (20 mL) and Et₂O (20 mL). The mixture was then extracted 2x20 mL Et₂O. The organic layers were washed with 50 mL brine, then dried over MgSO₄. The organics were concentrate and purification by flash chromatography (100% to 95:5 hexanes/EtOAc) gave the title compound as a white solid in quantitative yield (333 mg, 1.00 mmol).²³⁵

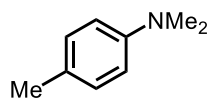
¹H NMR (400 MHz, Chloroform-*d*) δ 7.97 (s, 2H), 7.74 (s, 1H), 7.63 – 7.47 (m, 2H), 6.90

– 6.74 (m, 2H), 3.04 (s, 6H).

^{13}C NMR (100 MHz, Chloroform-*d*) δ 150.98, 143.38, 132.01 (q, $J = 32.9$ Hz), 127.96, 126.04, 123.74 (q, $J = 273.6$ Hz), 119.56 – 118.93 (m), 112.76, 40.45.

^{19}F NMR (376 MHz, Chloroform-*d*) δ -62.91.

N,N,4-trimethylaniline

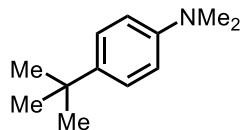


The general procedure for reductive amination was followed using *p*-toluidine (107 mg, 1.00 mmol, 1.00 equiv), NaHB(OAc)₃ (636 mg, 3.00 mmol, 3.00 equiv), formaldehyde solution (37%) (0.45 mL, 6.00 mmol, 6.00 equiv), K₂CO₃ (276 mg, 2.00 mmol, 2.00 equiv), AcOH (0.7 mL, 11.00 mmol, 11.00 equiv), CH₃CN (4 mL, 0.25M). Purification by flash chromatography (100% to 95:5 hexanes/EtOAc) gave the title compound as a colorless oil in 23% yield (31 mg, 0.23 mmol). The spectral data matches that previously reported in the literature.²³⁶

^1H NMR (500 MHz, Chloroform-*d*) δ 7.08 (d, $J = 8.0$ Hz, 2H), 6.71 (d, $J = 8.0$ Hz, 2H), 2.92 (s, 6H), 2.28 (s, 3H).

^{13}C NMR (126 MHz, Chloroform-*d*) δ 148.97, 129.71, 126.22, 113.34, 41.21, 20.39.

4-(*tert*-butyl)-*N,N*-dimethylaniline



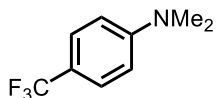
The general procedure for reductive amination was followed using 4-(*tert*-butyl)aniline (597 mg, 4.00 mmol, 1.00 equiv), NaHB(OAc)₃ (2.54 g, 12.00 mmol, 3.00 equiv), formaldehyde solution (37%) (1.05 mL, 14.00 mmol, 3.52 equiv), K₂CO₃ (1.11 g, 8.00 mmol, 2.00 equiv), AcOH (2 mL, 34.70 mmol, 8.70 equiv), CH₃CN (8 mL, 0.2M). Purification by flash chromatography (100% to 95:5

hexanes/EtOAc) gave the title compound as a colorless oil in quantitative yield (710 mg, 4.00 mmol). The spectral data matches that previously reported in the literature.²³⁷

¹H NMR (500 MHz, Chloroform-*d*) δ 7.34 – 7.26 (m, 2H), 6.81 – 6.71 (m, 2H), 2.93 (s, 6H), 1.31 (s, 9H).

¹³C NMR (126 MHz, Chloroform-*d*) δ 148.71, 139.51, 125.98, 112.76, 40.99, 33.89, 31.67.

***N,N*-dimethyl-4-(trifluoromethyl)aniline**



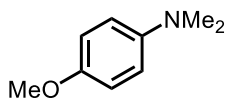
The general procedure for reductive amination was followed using 4-aminobenzotrifluoride (1.40 mL, 11.18 mmol, 1.00 equiv), NaHB(OAc)₃ (7.00 g, 34.54 mmol, 3.0 equiv), formaldehyde solution (37%) (4.99 mL, 67.08 mmol, 6.00 equiv), K₂CO₃ (3 g, 22.36 mmol, 2.00 equiv), AcOH (5 mL, 79.99 mmol, 7.09 equiv), CH₃CN (56 mL, 0.2M). Purification by flash chromatography (95:5 hexanes/EtOAc) gave the title compound as a white solid in 36% yield (751 mg, 4.02 mmol). The spectral data matches that previously reported in the literature.²³⁸

¹H NMR (500 MHz, Chloroform-*d*) δ 7.45 (d, *J* = 8.4 Hz, 2H), 6.70 (d, *J* = 8.4 Hz, 2H), 3.01 (s, 6H).

¹³C NMR (126 MHz, Chloroform-*d*) δ 152.45, 126.44 (q, *J* = 3.8 Hz), 117.59 (q, *J* = 32.6 Hz), 111.28, 40.19.

¹⁹F NMR (471 MHz, Chloroform-*d*) δ -60.86.

4-methoxy-*N,N*-dimethylaniline



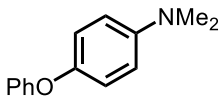
The general procedure for reductive amination was followed using *p*-

anisidine (493mg, 4.00 mmol, 1.00 equiv), NaHB(OAc)₃ (2.54 g, 12.00 mmol, 3.00 equiv), formaldehyde solution (37%) (1.05 mL, 14.00 mmol, 3.52 equiv), K₂CO₃ (1.11 g, 8.00 mmol, 2.00 equiv), AcOH (2 mL, 34.70 mmol, 8.70 equiv), CH₃CN (8 mL, 0.2M). Purification by flash chromatography (90:10 hexanes/EtOAc) gave the title compound as a light yellow solid in 99% yield (600 mg, 3.97 mmol). The spectral data matches that previously reported in the literature.²³⁹

¹H NMR (500 MHz, Chloroform-*d*) δ 6.86 (d, *J* = 9.2 Hz, 2H), 6.80 – 6.74 (m, 2H), 3.78 (s, 3H), 2.88 (s, 6H).

¹³C NMR (126 MHz, Chloroform-*d*) δ 152.08, 145.90, 115.01, 114.74, 55.87, 41.95.

***N,N*-dimethyl-4-phenoxyaniline**

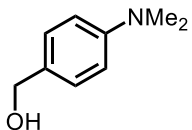


The general procedure for reductive amination was followed using 4-phenoxyaniline (741mg, 4.00 mmol, 1.00 equiv), NaHB(OAc)₃ (2.54 g, 12.00 mmol, 3.00 equiv), formaldehyde solution (37%) (1.05 mL, 14.00 mmol, 3.52 equiv), K₂CO₃ (1.11 g, 8.00 mmol, 2.00 equiv), AcOH (2 mL, 34.70 mmol, 8.70 equiv), CH₃CN (8 mL, 0.2M). Purification by flash chromatography (95:5 hexanes/EtOAc) gave the title compound as a clear oil in 94% yield (600 mg, 3.75 mmol). The spectral data matches that previously reported in the literature.²⁴⁰

¹H NMR (500 MHz, Chloroform-*d*) δ 7.28 (d, *J* = 7.5 Hz, 1H), 7.03 – 6.99 (m, 1H), 6.96 (d, *J* = 9.0 Hz, 2H), 6.95 – 6.91 (m, 2H), 6.74 (d, *J* = 9.0 Hz, 2H), 2.94 (s, 6H).

¹³C NMR (126 MHz, Chloroform-*d*) δ 159.23, 147.80, 147.43, 129.62, 122.05, 121.06, 117.28, 114.08, 41.36.

(4-(dimethylamino)phenyl)methanol

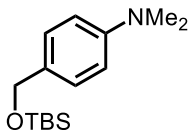


To an oven-dried 10-mL round-bottom flask containing a Teflon-coated magnetic stir bar under a nitrogen atmosphere was added 4-dimethylaminobenzaldehyde (149 mg, 1.00 mmol, 1.00 equiv) and THF (2.5 mL, 0.25M). The flask was cooled to 0 °C and LiAlH₄ (38 mg, 1.00 mmol, 1.00 equiv) was added. The reaction was stirred for 4 hours at 0 °C before quenching with MeOH (2 mL) and H₂O (2 mL). The reaction was diluted with 10 mL H₂O and extracted 3x10 mL Et₂O. The organic layers were dried with 20 mL brine and then MgSO₄ before concentrating. Purification by flash chromatography (90:10 hexanes/EtOAc) gave the title compound as a clear oil in 95% yield (144 mg, 0.952 mmol). The spectral data matches that previously reported in the literature.²⁴¹

¹H NMR (400 MHz, Chloroform-*d*) δ 7.25 (d, *J* = 8.3 Hz, 2H), 6.84 – 6.62 (m, 2H), 4.57 (s, 2H), 2.96 (s, 6H).

¹³C NMR (100 MHz, Chloroform-*d*) δ 150.51, 129.02, 128.77, 112.76, 65.51, 40.79.

4-(((*tert*-butyldimethylsilyl)oxy)methyl)-*N,N*-dimethylaniline



To an oven-dried 25-mL round-bottom flask containing a Teflon-coated magnetic stir bar under a nitrogen atmosphere were added (4-(dimethylamino)phenyl)methanol (1.00 g, 6.61 mmol, 1.00 equiv) and DCM (6.60 mL, 1M). The solution was cooled to 0 °C before adding TBSCl (1.00 g, 6.61 mmol, 1.00 equiv) and imidazole (900 mg, 13.22 mmol, 2.00 equiv). The reaction was then warmed to room temperature and stirred for 15 min. The reaction was quenched with sat. NaHCO₃ and extracted 3x30 mL hexanes. The organics were dried 1x30 mL brine and Na₂SO₄ before

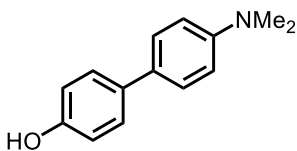
concentrating. The title compound was obtained in yield as a clear oil in 94% yield (1.65 g, 6.23 mmol) pure by NMR.

¹H NMR (401 MHz, Chloroform-*d*) δ 7.19 (d, *J* = 8.6 Hz, 2H), 6.72 (d, *J* = 8.7 Hz, 2H), 4.64 (s, 2H), 2.93 (s, 6H), 0.93 (s, 9H), 0.08 (s, 6H).

¹³C NMR (126 MHz, Chloroform-*d*) δ 150.07, 129.66, 127.66, 112.76, 65.15, 40.95, 26.17, 25.80, -4.97.

HRMS (ESI) (m/z): [M+H] calculated for C₁₅H₂₇NOSi, 266.1940, found, 266.1945.

4'-(dimethylamino)-[1,1'-biphenyl]-4-ol



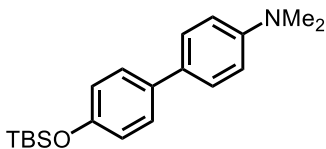
The general procedure for Suzuki-Miura coupling was followed using 4-bromo-dimethylaniline (200 mg, 1.00 mmol, 1.00 equiv), 4-hydroxyphenylboronic acid (207mg, 1.5 mmol, 1.50 equiv), K₂CO₃ (275 mg, 2.00 mmol, 2.00 equiv), Pd(OAc)₂ (2.2 mg, 0.01 mmol, 0.01 equiv), acetylacetone (2 mg, 0.02 mmol, 0.02 equiv), H₂O (2 mL), and DMF (2 mL). Purification by flash chromatography (70:30 hexanes/EtOAc) gave the title compound as a white solid in 95% yield (203 mg, 0.952 mmol). The spectral data matches that previously reported in the literature.²⁴²

¹H NMR (500 MHz, Chloroform-*d*) δ 9.74 (br), 7.52 – 7.34 (m, 4H), 6.95 – 6.72 (m, 4H), 2.97 (s, 6H).

¹³C NMR (126 MHz, Chloroform-*d*) δ 154.30, 149.76, 134.27, 129.54, 127.69, 127.44, 115.68, 113.33, 40.95.

HRMS (EI) (m/z): [M] calculated for C₂₀H₂₉NOSi, 328.2091, found, 328.2096.

4'-((*tert*-butyldimethylsilyl)oxy)-*N,N*-dimethyl-[1,1'-biphenyl]-4-amine

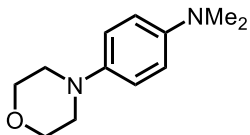


To an oven-dried 25-mL round-bottom flask containing a Teflon-coated magnetic stir bar under a nitrogen atmosphere were added 4'-(dimethylamino)-[1,1'-biphenyl]-4-ol (670 mg, 3.14 mmol, 1.00 equiv) and DCM (6.28 mL, 0.5M). The solution was cooled to 0 °C before adding TBSCl (473 mg, 3.14 mmol, 1.00 equiv) and imidazole (428 mg, 6.28 mmol, 2.00 equiv). The reaction was then warmed to room temperature and stirred for 15 min. The reaction was quenched with sat. NaHCO₃ and extracted 3x30 mL hexanes. The organics were dried 1x30 mL brine and Na₂SO₄ before concentrating. The title compound was obtained in yield as an off-white crystalline solid in 76% yield (780 mg, 2.39 mmol) pure by NMR.

¹H NMR (500 MHz, Chloroform-*d*) δ 7.45 (d, *J* = 8.7 Hz, 2H), 7.41 (d, *J* = 8.6 Hz, 2H), 6.87 (d, *J* = 8.5 Hz, 2H), 6.80 (d, *J* = 8.3 Hz, 2H), 2.98 (s, 6H), 1.01 (s, 9H), 0.23 (s, 6H).

¹³C NMR (126 MHz, Chloroform-*d*) δ 154.40, 149.73, 134.57, 129.41, 127.45, 127.34, 120.34, 113.04, 40.83, 25.88, 18.39, -4.22.

N,N-dimethyl-4-morpholinoaniline



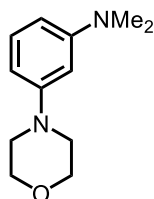
To an oven-dried 25-mL round-bottom flask containing a Teflon-coated magnetic stir bar were brought into a N₂ glovebox and Pd₂(dba)₃ (11.4 mg, 0.0125 mmol, 0.5 mol%), P(*t*-Bu)₃ (5.1 mg, 0.05 mmol, 1 mol%), and NaO-*t*-Bu (250 mg, 2.50 mmol, 1.00 equiv) were added. The round bottom was sealed with a septa and removed from the glovebox. Toluene (5 mL, 0.5M) and morpholine (0.27 mL, 3.12 mmol, 1.25 equiv) were added, followed by 3-bromo-*N,N*-dimethylaniline (500 mg,

2.50 mmol, 1.00 equiv). The reaction was stirred at room temperature overnight. The reaction was quenched with 20 mL H₂O and extracted 3x30 mL Et₂O. The organics were washed with 60 mL brine and dried over MgSO₄ before concentrating. Purification by flash chromatography (90:10 to 1:1 hexanes/EtOAc) gave the title compound as a yellowish powder in 62% yield (320 mg, 1.55 mmol). The spectral data matches that previously reported in the literature.²⁴³

¹H NMR (500 MHz, Chloroform-*d*) δ 6.90 (d, *J* = 8.9 Hz, 2H), 6.76 (d, *J* = 9.0 Hz, 2H), 3.89 – 3.84 (m, 4H), 3.08 – 3.01 (m, 4H), 2.88 (s, 6H).

¹³C NMR (126 MHz, Chloroform-*d*) δ 151.98, 138.24, 120.93, 115.53, 66.59, 58.13, 47.97.

***N,N*-dimethyl-3-morpholinoaniline**



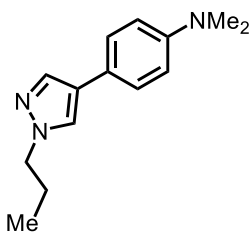
To an oven-dried 25-mL round-bottom flask containing a Teflon-coated magnetic stir bar were brought into a N₂ glovebox and Pd₂(dba)₃ (22.9 mg, 0.025 mmol, 0.5 mol%), P(*t*-Bu)₃ (10.1 mg, 0.05 mmol, 1 mol%), and NaO-*t*-Bu (481 mg, 5.00 mmol, 1.00 equiv) were added. The round bottom was sealed with a septa and removed from the glovebox. Toluene (10 mL, 0.5M) and morpholine (0.54 mL, 6.25 mmol, 1.25 equiv) were added, followed by 3-bromo-*N,N*-dimethylaniline (1.00 g, 5.00 mmol, 1.00 equiv). The reaction was stirred at room temperature overnight. The reaction was quenched with 20 mL H₂O and extracted 3x30 mL Et₂O. The organics were washed with 60 mL brine and dried over MgSO₄ before concentrating. Purification by flash chromatography (70:30 hexanes/EtOAc) gave the title compound as a yellowish oil in 35% yield (360 mg, 1.80 mmol). The spectral data matches that previously reported in the

literature.²⁴³

¹H NMR (500 MHz, Chloroform-*d*) δ 7.15 (t, J = 8.1 Hz, 1H), 6.34 (dd, J = 8.2, 2.1 Hz, 2H), 6.28 (s, 1H), 3.86 (t, J = 4.7 Hz, 4H), 3.16 (t, J = 4.7 Hz, 4H), 2.94 (s, 6H).

¹³C NMR (126 MHz, Chloroform-*d*) δ 152.66, 151.83, 129.76, 105.63, 105.11, 100.89, 67.21, 50.00, 40.90.

***N,N*-dimethyl-4-(1-propyl-1*H*-pyrazol-4-yl)aniline**



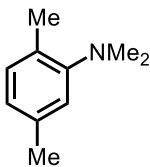
The general procedure for Suzuki-Miura coupling was followed using 4-bromo-dimethylaniline (400 mg, 2.00 mmol, 1.00 equiv), 1-propylpyrazole-4-boronic acid (462mg, 3.00 mmol, 1.50 equiv), K₂CO₃ (553 mg, 4.00 mmol, 2.00 equiv), Pd(OAc)₂ (4.5 mg, 0.02 mmol, 0.01 equiv), acetylacetone (4 mg, 0.04 mmol, 0.02 equiv), H₂O (7 mL), and DMF (7 mL). Purification by flash chromatography (80:20 hexanes/EtOAc) gave the title compound as a white solid in 76% yield (350 mg, 1.52 mmol).

¹H NMR (500 MHz, Chloroform-*d*) δ 7.69 (d, J = 0.8 Hz, 1H), 7.52 (d, J = 0.8 Hz, 1H), 7.36 (d, J = 8.8 Hz, 2H), 6.75 (d, J = 8.8 Hz, 2H), 4.09 (t, J = 7.1 Hz, 2H), 2.96 (s, 6H), 1.92 (q, J = 7.3 Hz, 2H), 0.95 (t, J = 7.4 Hz, 3H).

¹³C NMR (126 MHz, Chloroform-*d*) δ 149.45, 136.17, 126.49, 125.09, 123.07, 121.47, 113.18, 54.08, 40.86, 23.93, 11.34.

HRMS (ESI) (m/z): [M+H] calculated for C₁₄H₁₉N₃, 230.1657, found, 230.1649.

***N,N*,2,5-tetramethylaniline**

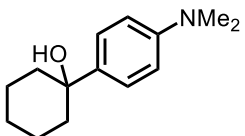


The general procedure for reductive amination was followed using 2,5-dimethylaniline (0.5 mL, 4.06 mmol, 1.00 equiv), NaHB(OAc)₃ (2.59 g, 12.20 mmol, 3.00 equiv), formaldehyde solution (37%) (1.05 mL, 14.00 mmol, 3.52 equiv), K₂CO₃ (1.12 g, 8.12 mmol, 2.00 equiv), AcOH (2 mL, 34.70 mmol, 8.70 equiv), CH₃CN (8 mL, 0.2M). Aqueous workup gave the title compound as a clear oil, pure by NMR, in 76% yield (450 mg, 3.09 mmol). The spectral data matches that previously reported in the literature.²⁴⁴

¹H NMR (500 MHz, Chloroform-*d*) δ 7.04 (d, *J* = 7.5 Hz, 1H), 6.84 (s, 1H), 6.77 (d, *J* = 7.6 Hz, 1H), 2.69 (s, 6H), 2.31 (s, 3H), 2.28 (s, 3H).

¹³C NMR (126 MHz, Chloroform-*d*) δ 153.46, 136.07, 131.12, 128.97, 123.33, 119.26, 44.39, 21.36, 18.10.

1-(4-(dimethylamino)phenyl)cyclohexan-1-ol



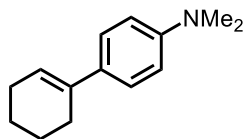
To an oven-dried 10--mL round-bottom flask containing a Teflon-coated magnetic stir bar were added freshly ground magnesium metal (64 mg, 2.62 mmol, 1.05 equiv) and 4-bromodimethylaniline (500 mg, 2.50 mmol, 1.00 equiv). THF (4 mL) was added along with a small crystal of I₂ (to activate the magnesium) and the mixture was stirred until nearly all of the magnesium was consumed. The mixture was cooled in a salt/ice bath for 10 minutes before adding cyclohexanone (0.23 mL, 2.25 mmol, 0.90 equiv) dropwise. The reaction was then stirred for 1 hour before warming to room temperature overnight. The solution was poured into a sat. NH₄Cl solution and extracted 3x20 mL DCM. The organics were dried over Na₂SO₄ and concentrated. Purification by flash chromatography (90:10 to 80:20 hexanes/EtOAc) gave the title

compound as a white solid in 45% yield (224 mg, 1.02 mmol). The spectral data matches that previously reported in the literature.²⁴⁵

¹H NMR (500 MHz, Chloroform-*d*) δ 7.42 (dd, $J = 8.9, 2.2$ Hz, 2H), 6.78 (dd, $J = 8.9, 2.2$ Hz, 2H), 2.98 (s, 6H), 1.93 – 1.72 (m, 8H), 1.64 (dd, $J = 11.1, 4.7$ Hz, 2H), 1.40 – 1.26 (m, 1H).

¹³C NMR (126 MHz, Chloroform-*d*) δ 149.36, 137.50, 125.46, 112.41, 72.48, 40.66, 38.80, 25.66, 22.38.

***N,N*-dimethyl-2',3',4',5'-tetrahydro-[1,1'-biphenyl]-4-amine**

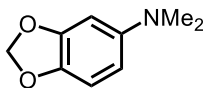


To an oven-dried 8-mL vial containing a Teflon-coated magnetic stir bar were added 1-(4-(dimethylamino)phenyl)cyclohexan-1-ol (224 mg, 1.02 mmol, 1.00 equiv) and trifluoroacetic acid (1.30 mL, 0.8M). The vial was sealed with a Teflon cap and stirred at room temperature for 15 min. The reaction was then poured into a flask containing 20 mL of a sat. NaHCO₃. The contents were then transferred to a separatory funnel and extracted 3x10 mL Et₂O. The organic layers were dried over Mg₂SO₄ and concentrated to give the title compound as a white solid in quantitative yield (210 mg, 1.02 mmol), which was pure by NMR. The spectral data matches that previously reported in the literature.²⁴⁵

¹H NMR (400 MHz, Chloroform-*d*) δ 7.30 (d, $J = 8.4$ Hz, 2H), 6.71 (d, $J = 8.4$ Hz, 2H), 6.01 (s, 1H), 2.94 (s, 6H), 2.39 (q, $J = 5.2$ Hz, 2H), 2.19 (dq, $J = 6.4, 3.2$ Hz, 2H), 1.77 (q, $J = 5.9$ Hz, 2H), 1.66 (q, $J = 5.9$ Hz, 2H).

¹³C NMR (100 MHz, Chloroform-*d*) δ 149.64, 136.12, 131.33, 125.67, 121.70, 112.63, 40.87, 27.48, 26.01, 23.36, 22.50.

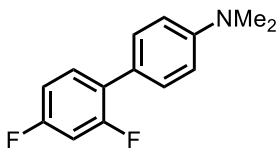
***N,N*-dimethylbenzo[*d*][1,3]dioxol-5-amine**



A modified general procedure for reductive amination was followed using 3,4-(dimethyleneoxy)aniline (2 g, 14.06 mmol, 1.00 equiv), NaH₃BCN (917 mg, 14.06 mmol, 1.00 equiv), formaldehyde solution (37%) (3.60 mL, 45.2 mmol, 3.10 equiv), ZnCl₂ (1 g, 7.30 mmol, 0.50 equiv), MeOH (70 mL, 0.2M). Aqueous workup gave the title compound as a clear oil, pure by NMR, in 14% yield (340 mg, 1.97 mmol). The spectral data matches that previously reported in the literature.²⁴⁶

¹H NMR (401 MHz, Chloroform-*d*) δ 6.72 (d, *J* = 8.5 Hz, 1H), 6.42 (d, *J* = 2.5 Hz, 1H), 6.17 (dd, *J* = 8.5, 2.5 Hz, 1H), 5.87 (s, 2H), 2.86 (s, 6H).

2',4'-difluoro-*N,N*-dimethyl-[1,1'-biphenyl]-4-amine



The general procedure for Suzuki-Miura coupling was followed using 4-bromo-dimethylaniline (400 mg, 2.00 mmol, 1.00 equiv), 2,4-difluorophenylboronic acid (472mg, 3.00 mmol, 1.50 equiv), K₂CO₃ (553 mg, 4.00 mmol, 2.00 equiv), Pd(OAc)₂ (4.5 mg, 0.02 mmol, 0.01 equiv), acetylacetone (4 mg, 0.04 mmol, 0.02 equiv), H₂O (7 mL), and DMF (7 mL). Purification by flash chromatography (95:5 to 90:10 hexanes/EtOAc) gave the title compound as an off-white solid in quantitative yield.

¹H NMR (400 MHz, Chloroform-*d*) δ 7.42 – 7.38 (m, 2H), 7.36 (dd, *J* = 8.9, 6.6 Hz, 1H), 6.89 (dddd, *J* = 13.3, 11.3, 8.5, 2.7 Hz, 2H), 6.82 – 6.76 (m, 2H), 3.00 (s, 6H).

¹³C NMR (126 MHz, Chloroform-*d*) δ 162.63, 162.54, 150.14, 130.90 (q, *J* = 5.3 Hz) 129.70 (d, *J* = 3.2 Hz), 122.88, 112.45, 111.43 (dd, *J* = 3.6 Hz), 104.43 (d, *J* = 25.4 Hz),

104.22 (d, $J = 25.3$ Hz), 40.62.

^{19}F NMR (471 MHz, Chloroform-*d*) δ -113.56 (p, $J = 7.6$ Hz), -114.04 (q, $J = 9.0$ Hz).

HRMS (ESI) (m/z): [M+H] calculated for $\text{C}_{14}\text{H}_{13}\text{F}_2\text{N}$, 234.1094, found, 234.1090.

4.2.3 Calibration Curves:

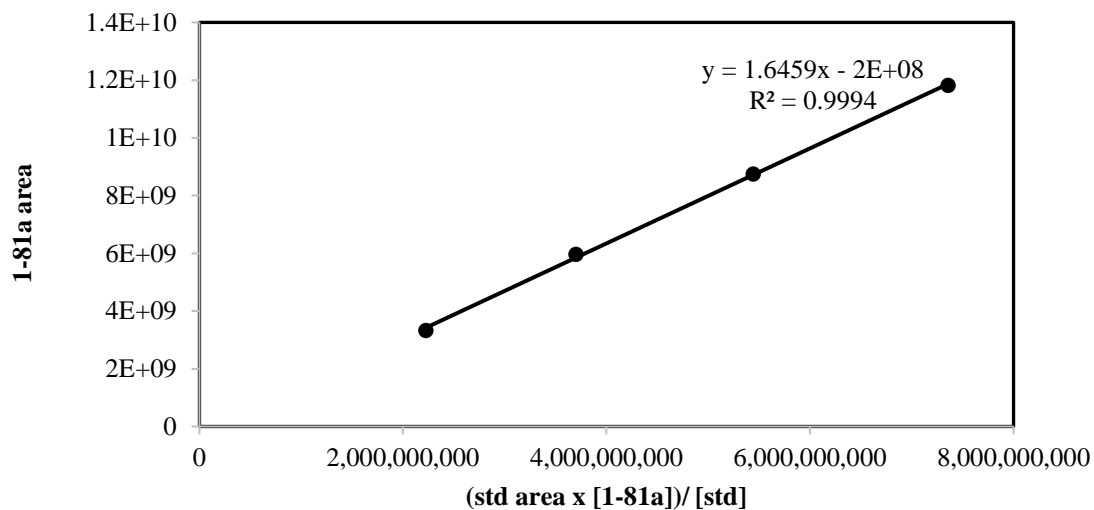
Solutions containing a constant concentration of an internal standard (tridecane (0.164 M) and varying concentrations of the desired product (0.05, 0.10, 0.15 and 0.20 M) were prepared in ethyl acetate. Each was analyzed by GC-FID and the response factor (F) calculated by solving equation S1 for the area of product to give equation S2, where the response factor (F) is the slope. Yields of crude reactions mixtures, containing a known amount of internal standard, were then determined by solving Equation S1 for the concentration of the product to give Equation S3 and filling in the known data from a crude reaction.

$$\frac{\textit{(Area of Product)}}{\textit{(Concentration of Product)}} = F * \frac{\textit{(Area of Standard)}}{\textit{(Concentration of Standard)}}$$

$$\textit{(Area of Product)} = F * \left(\frac{\textit{(Area of Standard)}}{\textit{(Concentration of Standard)}} \right) \textit{(Concentration of Product)}$$

$$\textit{(Concentration of Product)} = \frac{\textit{(Concentration of Standard)} \textit{(Area of Product)}}{F * \textit{(Area of Standard)}}$$

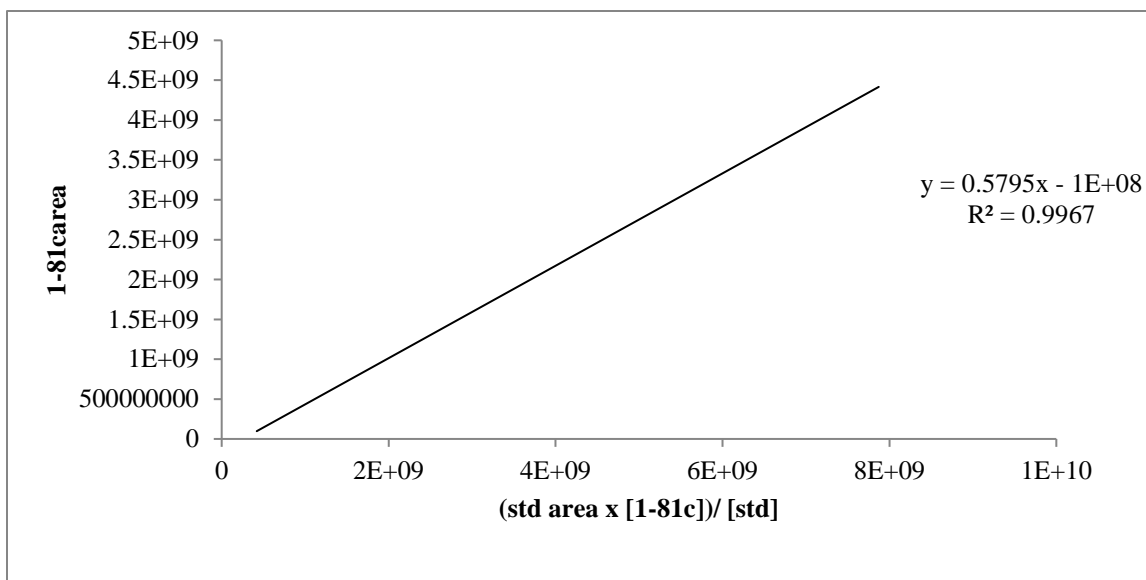
Calibration curve for [1,1'-biphenyl]-4-yltriethylsilane (Compound 1-81a):



mmol 1-81a	mmol tridecane	area IS	area product
0.048420739	0.16403	7535226346	3329460100
0.08715733	0.16403	6961574030	5961048038
0.143027414	0.16403	6242681983	8751150218
0.192938021	0.16403	6254367926	11816631504

Figure 4-1 Plot of **1-81a** area versus (std area x [1-81a]) / [std] fitted to $y = mx + b$ where $m = 1.6459$ and $b = -2 \times 10^8$ with a R^2 of 0.9994.

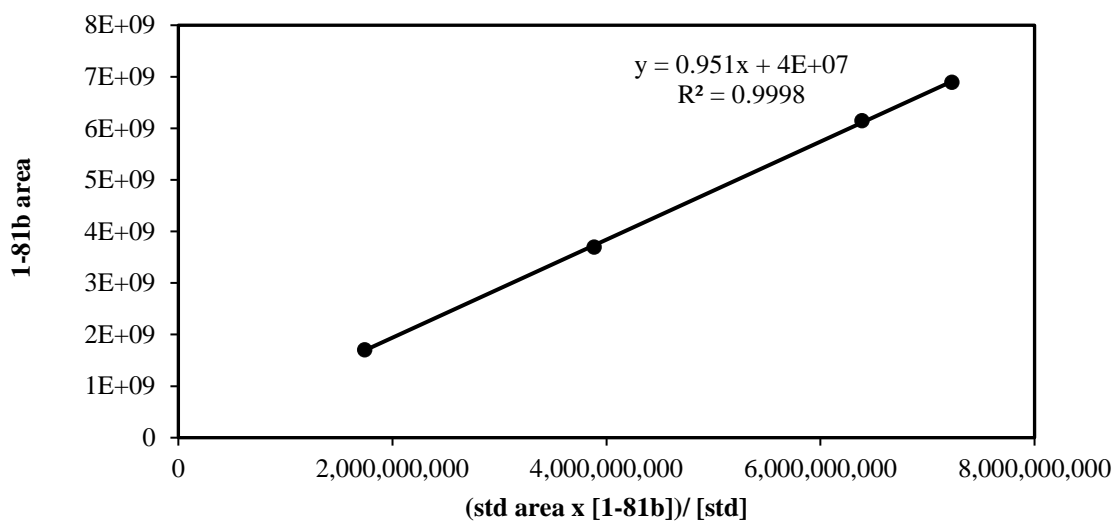
Calibration curve for [1,1'-biphenyl]-4-yl(benzyl)dimethylsilane (1-81c):



mmol 1-81c	mmol tridecane	area IS	area product
9.91768E-06	0.164026904	3947284982	419876796
0.049919006	0.164026904	3315120257	1789461089
0.102152137	0.164026904	3575670979	3999385208
0.150418196	0.164026904	3564399649	6087760854
0.199345433	0.164026904	3665141539	7872337807

Figure 4-2 Plot of 1-81c area versus (std area x [1-81c]) / [std] fitted to $y = mx + b$ where $m = 0.5795$ and $b = -1 \times 10^8$ with a R^2 of 0.99674.

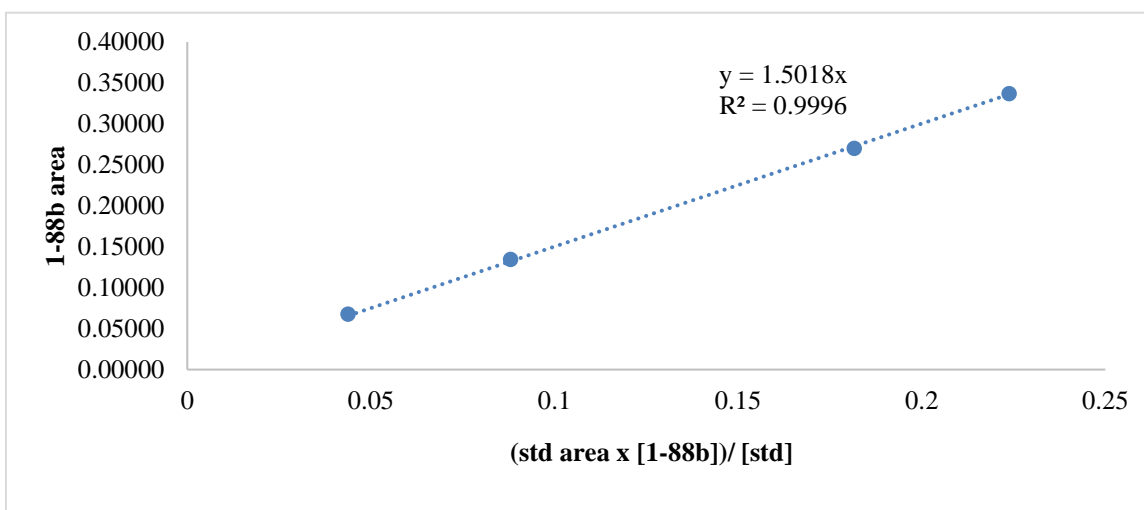
Calibration curve for biphenyl (1-81b):



mmol 1-81b	mmol tridecane	area IS	area product
0.0509	0.16403	5647778523	1707314294
0.0966	0.16403	6596748815	3699921557
0.1582	0.16403	6622184645	6149186696
0.192	0.16403	6176751384	6891778392
0.0509	0.16403	5647778523	1707314294

Figure 4-3 Plot of **1-81b** area versus (std area x [1-81b]) / [std] fitted to $y = mx + b$ where $m = 0.951$ and $b = 4 \times 10^7$ with a R^2 of 0.9998.

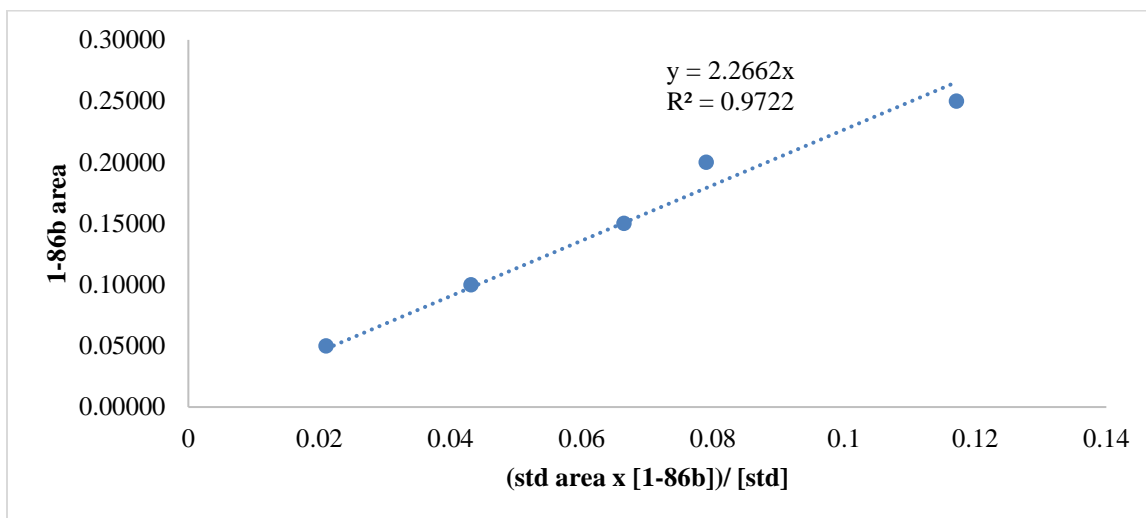
Calibration curve for diphenyl ether (1-88b):



mmol 1-88b	mmol tridecane	area IS	area product
0.067830908	0.164026904	3611778993	964667595
0.134567768	0.164026904	3522436673	1891415126
0.202398676	0.164026904	3360770109	3112052070
0.270229584	0.164026904	3320105098	3676856664
0.336966444	0.164026904	3504987328	4783168130

Figure 4-4 Plot of **1-88b** area versus (std area x [1-88b]) / [std] fitted to $y = mx + b$ where $m = 1.5018$ and $b = 0$ with a R^2 of 0.99963.

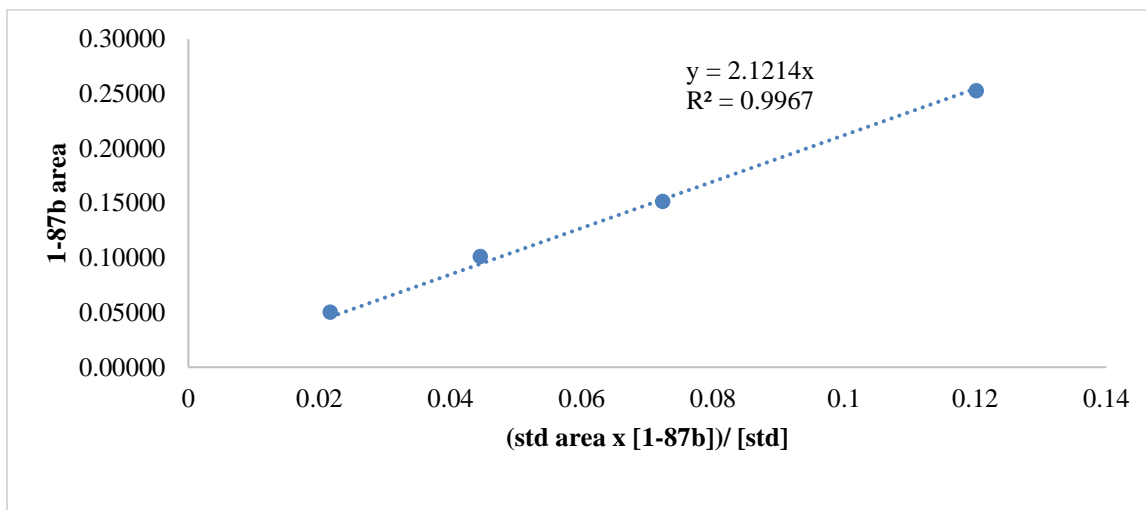
Calibration curve for trifluorotolunene (1-86b):



mmol 1-86b	mmol tridecane	area IS	area product
0.050030799	0.16403	4492524320	574994724
0.100061597	0.16403	3927418367	1032274349
0.150092396	0.16403	4914023783	1990948584
0.200123195	0.16403	3902305473	1878381691
0.250153994	0.16403	4893566950	3494602386

Figure 4-5 Plot of **1-86b** area versus (std area x [1-86b]) / [std] fitted to $y = mx + b$ where $m = 2.2662$ and $b = 0$ with a R^2 of 0.97223.

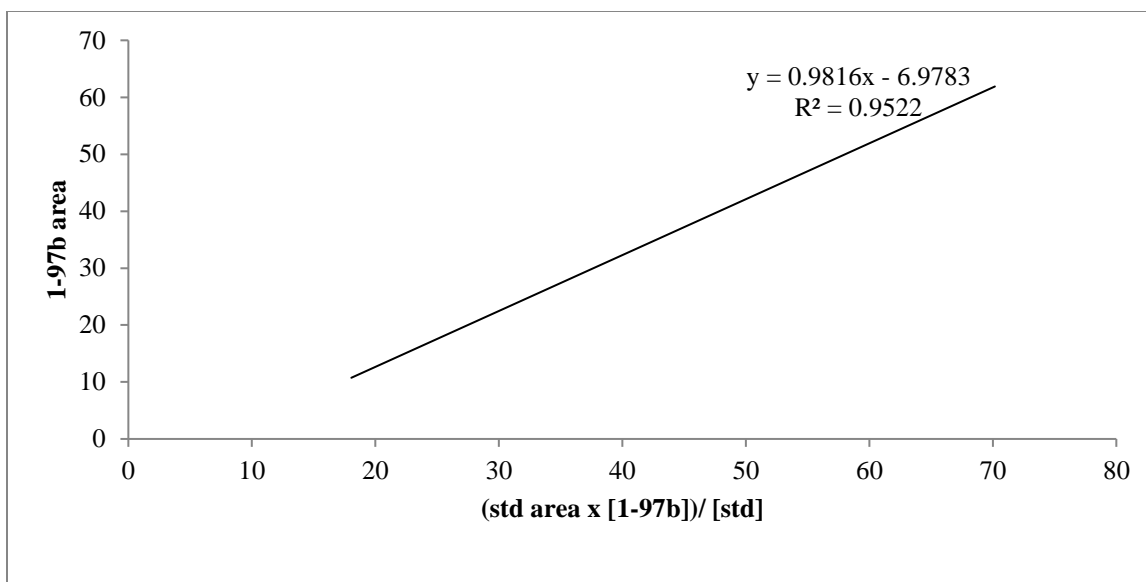
Calibration curve for anisole (1-87b):



mmol 1-87b	mmol tridecane	area IS	area product
0.0501862	0.164026904	4000104738	527950383
0.101301774	0.164026904	3537739243	960449091
0.151487974	0.164026904	3236629289	1427195136
0.201674174	0.164026904	3602495138	1828214896
0.252789749	0.164026904	3975653755	2912617178

Figure 4-6 Plot of **1-87b** area versus (std area x [1-87b]) / [std] fitted to $y = mx + b$ where $m = 2.1214$ and $b = 0$ with a R^2 of 0.99673.

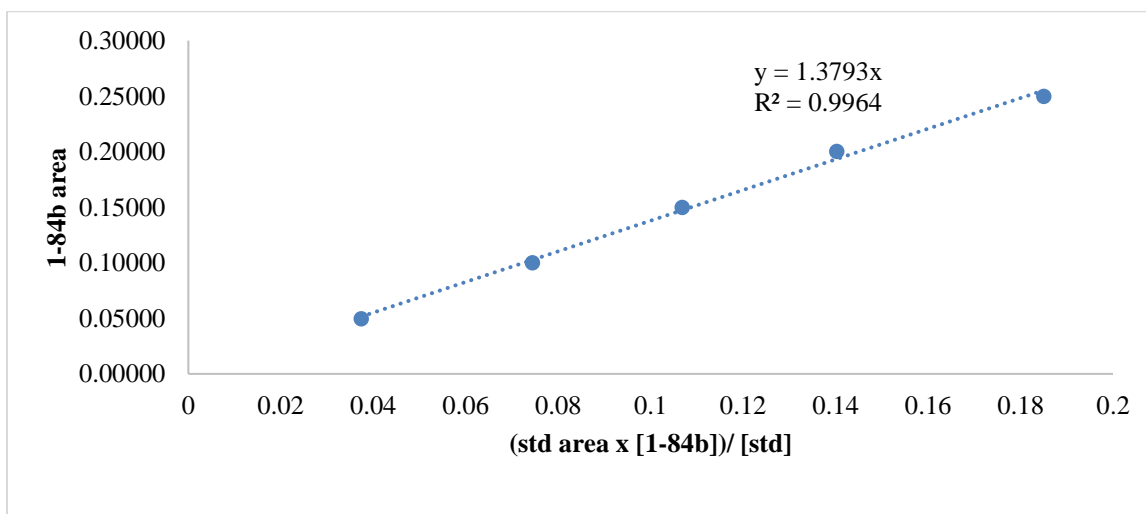
Calibration curve for naphthalene (1-97):



mmol 1-97b	mmol tridecane	area IS	area product
0.049153468	0.16403	5560584759	1352944750
0.103768433	0.16403	7185032978	3353404616
0.154482328	0.16403	6904005775	4614671198
0.201295155	0.16403	6790282011	6296395603

Figure 4-7 Plot of **1-97b** area versus (std area x [1-97b]) / [std] fitted to $y = mx + b$ where $m = 0.9816$ and $b = -6.9783$ with a R^2 of 0.95217.

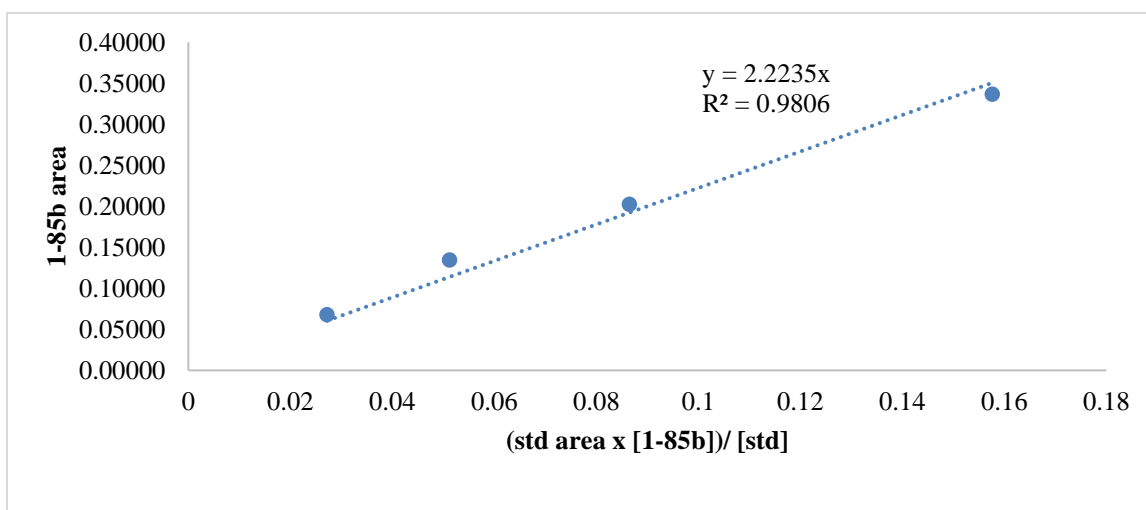
Calibration curve for *t*-butylbenzene (1-84b):



mmol 1-84b	mmol tridecane	area IS	area product
0.049738489	0.16403	2518295474	574090525
0.100122932	0.16403	3255077022	1477595029
0.149861422	0.16403	3930989531	2559730260
0.200245865	0.16403	3546712147	3032026099
0.249984354	0.16403	3479578042	3925217274

Figure 4-8 Plot of **1-84b** area versus (std area x [1-84b]) / [std] fitted to $y = mx + b$ where $m = 1.3793$ and $b = 0$ with a R_2 of 0.99639.

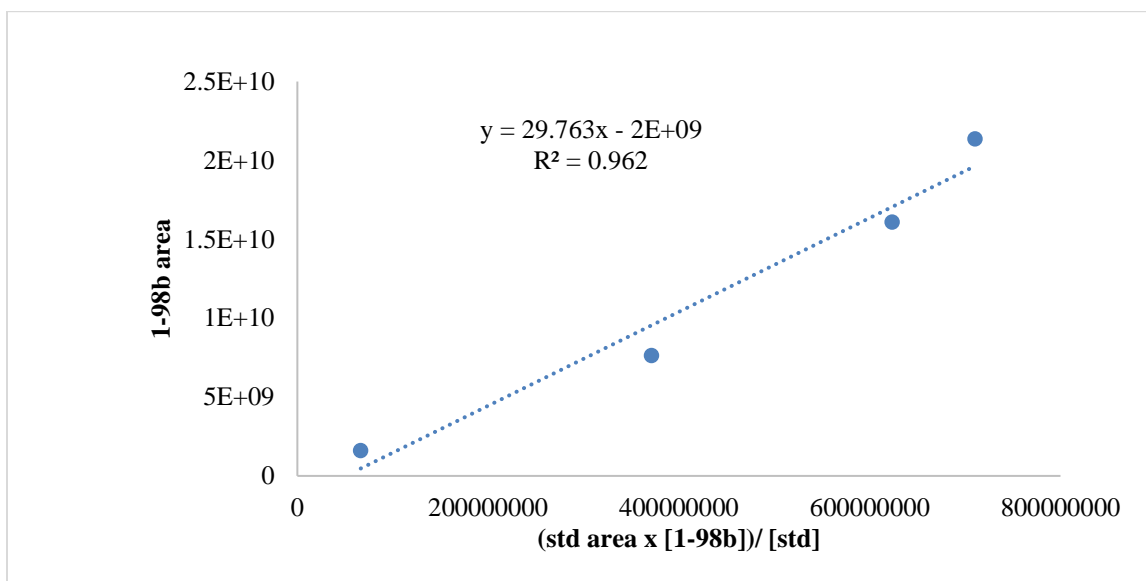
Calibration curve for *p*-xylene (1-85b)



mmol 1-85b	mmol tridecane	area IS	area product
0.067830908	0.164026904	3288937475	545232412
0.134567768	0.164026904	3669199995	1145416244
0.202398676	0.164026904	3546770818	1870406001
0.270229584	0.164026904	3601846681	2352337673
0.336966444	0.164026904	2666629964	2562696982

Figure 4-9 Plot of **1-85b** area versus (std area x [1-85b]) / [std] fitted to $y = mx + b$ where $m = 2.2235$ and $b = 0$ with a R_2 of 0.98064

Calibration curve for pyridine (1-98b):

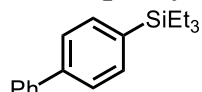


mmol 1-98b	mmol tridecane	area IS	area product
0.062134632	0.164026904	4233992225	66403740
0.31067316	0.164026904	4031783804	371135414
0.62134632	0.164026904	4249091608	623374155
0.93201948	0.164026904	3760306370	710497433

Figure 4-10 Plot of **1-98b** area versus (std area x [1-98b]) / [std] fitted to $y = mx + b$ where $m = 29.763$ and $b = -2 \times 10^9$ with a R^2 of 0.96197.

4.2.4 Silylation Substrates:

[1,1'-biphenyl]-4-yltriethylsilane (1-81a)



1-81a

The general procedure for silylation was followed using *N,N,N*-trimethylanilinium iodide **1-81** (73 mg, 0.215 mmol) and triethylsilane (160 μ L, 1 mmol). Purification by flash chromatography (100% hexanes)

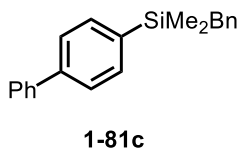
gave the title compound as a colorless oil in 86% yield (50 mg, 0.186 mmol). The spectral

data matches that previously reported in the literature.¹¹⁵

¹H NMR (401 MHz, Chloroform-*d*) δ 7.62 (m, 6H), 7.59 (d, $J = 1.5$ Hz, 2H), 7.45 (dd, $J = 8.3, 6.9$ Hz, 1H), 7.40 – 7.30 (m, 1H), 1.01 (t, $J = 7.8$ Hz, 9H), 0.84 (q, $J = 7.3$ Hz, 6H).

¹³C NMR (126 MHz, Chloroform-*d*) δ 141.56, 141.33, 136.38, 134.83, 128.88, 127.41, 127.27, 126.52, 7.60, 3.57.

[1,1'-biphenyl]-4-yl(benzyl)dimethylsilane (**1-81c**)

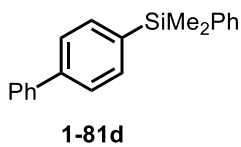


The general procedure for silylation was followed using *N,N,N*-trimethylanilinium iodide **1-81** (66 mg, 0.194 mmol) and dimethylbenzylsilane (160 μ L, 1 mmol). Purification by flash chromatography (100% hexanes to 98:2 hex/EtOAc) gave the title compound as a white solid in 85% yield (50 mg, 0.165 mmol). The spectral data matches that previously reported in the literature.¹¹⁵

¹H NMR (400MHz, Chloroform-*d*) δ 7.68-7.57 (m, 4H), 7.54 (d, $J = 8.0$ Hz, 2H), 7.46 (dd, $J = 8.3, 6.8$ Hz, 2H), 7.4-7.33 (m, 1H), 7.20 (t, $J = 7.5$ Hz, 2H), 7.13-7.02 (m, 2H), 6.98 (d, $J = 7.3$ Hz, 2H), 2.35 (s, 2H), 0.29 (s, 6H).

¹³C NMR (100 MHz, Chloroform-*d*) δ 141.92, 141.18, 139.76, 137.37, 134.36, 128.92, 128.28, 128.13, 127.54, 127.29, 126.58, 124.25, 26.35, -3.24.

[1,1'-biphenyl]-4-yl(dimethyl(phenyl)silane (**1-81d**)



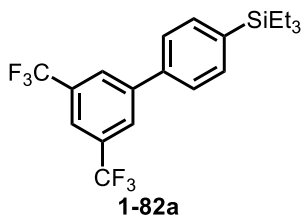
The general procedure for silylation was followed using *N,N,N*-trimethylanilinium iodide **1-81** (73 mg, 0.215 mmol), 30 mg of 4Å molecular sieves powder, IPr*^{OMe}: (free carbene) (9.4 mg, 0.1 equiv,

0.01 mmol), and dimethylphenylsilane (156 μ L, 1 mmol). Purification by flash chromatography (100% hexanes) gave the title compound in an inseparable mixture with phenyldimethyldisilane as a colorless oil. 65% yield (41 mg, 0.14 mmol) by NMR analysis. The spectral data matches that previously reported in the literature.²⁴⁷

¹H NMR (500MHz, Chloroform-*d*) δ 7.65-7.53 (m, 8H), 7.45 (t, *J*= 7.7 Hz, 2H), 7.41-7.32 (m, 4H), 0.60 (s, 6H).

¹³C NMR (126 MHz, Chloroform-*d*) δ 142.01, 141.20, 138.30, 137.13, 134.81, 134.33, 129.29, 128.90, 127.99, 127.53, 127.31, 126.70, 32.22, -2.19.

(3',5'-bis(trifluoromethyl)-[1,1'-biphenyl]-4-yl)triethylsilane (**1-82a**)

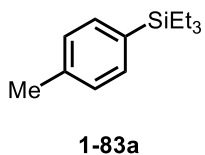


The general procedure for silylation was followed using *N,N,N*-trimethylanilinium iodide **1-82** (45.7 mg, 0.100 mmol) and triethylsilane (80 μ L, 1 mmol). Yield determined by NMR of the crude reaction mixture using fluorobenzene as an internal standard (98%). The spectral data matches that previously reported in the literature.²⁴⁸

¹H NMR (500MHz, Chloroform-*d*) δ 8.02 (d, *J*=1.6Hz, 2H), 7.85 (s, 1H), 7.63 (d, *J*=8.1Hz, 2H), 7.59 (d, *J*=8.1Hz, 2H), 0.99 (t, *J*= 7.8 Hz, 9H), 0.84 (q, *J*=7.8 Hz, 6H).

¹³C NMR (176 MHz, Chloroform-*d*) δ 143.51, 138.79, 138.52, 132.23 (q, *J*= 33.3Hz), 127.35, 126.55, 123.55 (q, *J*= 272.8Hz), 121.04 (m), 7.52, 3.46.

triethyl(*p*-tolyl)silane (**1-83a**)



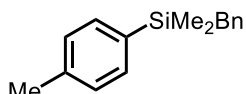
The general procedure for silylation was followed using *N,N,N*-trimethylanilinium iodide **1-83** (54 mg, 0.195 mmol) and triethylsilane

(160 μ L, 1 mmol). Yield determined by NMR of the crude reaction mixture using CH_2Br_2 as an internal standard (90%). The spectral data matches that previously reported in the literature.²⁴⁸

^1H NMR (400MHz, Chloroform-*d*) δ 7.39 (d, J = 7.9 Hz), 2H), 7.17 (d, J = 7.5 Hz, 2H), 2.35 (s, 3H), 0.96 (t, J = 7.7 Hz, 9H), 0.77 (q, J =7.6 Hz, 6H).

^{13}C NMR (126 MHz, Chloroform-*d*) δ 138.62, 134.38, 133.38, 128.67, 7.58, 3.56.

benzyl dimethyl(*p*-tolyl)silane (**1-83c**)



1-83c

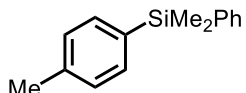
The general procedure for silylation was followed using *N,N,N*-trimethylanilinium iodide **1-83** (28 mg, 0.101 mmol) and dimethylbenzylsilane (80 μ L, 0.5 mmol). Yield determined by NMR of the crude reaction mixture using CH_2Br_2 as an internal standard (79%).

^1H NMR (400 MHz, Chloroform-*d*) δ 7.38 (d, J = 7.6 Hz, 2H), 7.19 (d, J = 7.3 Hz, 4H), 7.08 (t, J = 7.3 Hz, 1H), 7.03 – 6.91 (m, 2H), 2.38 (s, 3H), 2.31 (s, 2H), 0.24 (s, 5H).

^{13}C NMR (126 MHz, Chloroform-*d*) δ 139.94, 139.03, 134.96, 133.89, 128.71, 128.45, 128.22, 124.16, 26.42, 21.62, -3.22.

HRMS (EI) (m/z): [M] calculated for $\text{C}_{16}\text{H}_{20}\text{Si}$, 240.1334, found, 240.1343.

dimethyl(phenyl)(*p*-tolyl)silane (**1-83d**)



1-83d

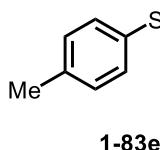
The general procedure for silylation was followed using *N,N,N*-trimethylanilinium iodide **1-83** (56 mg, 0.202 mmol) and dimethylphenylsilane (156 μ L, 1 mmol). Yield determined by NMR of the crude reaction mixture using CH_2Br_2 as an internal standard (74%). The spectral data

matches that previously reported in the literature.²⁴⁷

¹H NMR (400 MHz, Chloroform-*d*) δ 7.54 (dt, $J = 4.7, 2.3$ Hz, 2H), 7.44 (d, $J = 7.5$ Hz, 2H), 7.42 – 7.31 (m, 3H), 7.20 (d, $J = 7.5$ Hz, 2H), 2.37 (s, 3H), 0.56 (s, 6H).

¹³C NMR (126 MHz, Chloroform-*d*) δ 134.38, 134.32, 134.30, 129.23, 129.15, 128.80, 127.94, 127.91, 21.62, -2.16.

1,1,1,3,5,5,5-heptamethyl-3-(*p*-tolyl)trisiloxane (**1-83e**)



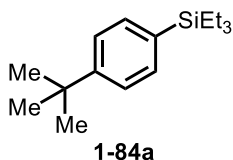
The general procedure for silylation was followed using *N,N,N*-trimethylanilinium iodide **1-83** (57 mg, 0.206 mmol) and 1,1,1,3,5,5,5-heptamethyltrisiloxane (272 μ L, 1 mmol). Yield determined by NMR of the crude reaction mixture using CH₂Br₂ as an internal standard (81%).

¹H NMR (400MHz, Chloroform-*d*) δ 7.44 (d, $J = 7.8$ Hz), 2H), 7.17 (d, $J = 7.5$ Hz, 2H), 2.35 (s, 3H), 0.25 (s, 3H), 0.10 (s, 18H).

¹³C NMR (100 MHz, Chloroform-*d*) δ 139.36, 135.17, 133.43, 128.54, 21.70, 2.03, 0.28.

HRMS (EI) (m/z): [M] calculated for C₁₄H₂₈O₂Si₃, 312.1397, found, 312.1409.

(4-(*tert*-butyl)phenyl)triethylsilane (**1-84a**)

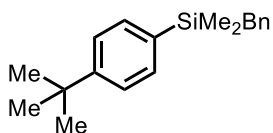


The general procedure for silylation was followed using *N,N,N*-trimethylanilinium iodide **1-84** (62 mg, 0.194 mmol) and triethylsilane (160 μ L, 1 mmol). Purification by flash chromatography (100% hexanes) gave the title compound as a colorless oil in 76% yield (37 mg, 0.149 mmol). The spectral data matches that previously reported in the literature.¹¹⁵

¹H NMR (500 MHz, Chloroform-*d*) δ 7.43 (d, J = 8.2 Hz, 2H), 7.37 (d, J = 6.5 Hz, 2H), 1.32 (s, 9H), 0.97 (t, J = 7.8 Hz, 9H), 0.78 (q, J = 8.0 Hz, 6H).

¹³C NMR (126 MHz, Chloroform-*d*) δ 151.64, 134.19, 133.97, 124.74, 34.74, 31.42, 7.63, 3.61.

benzyl(4-(*tert*-butyl)phenyl)dimethylsilane (**1-84c**)



1-84c

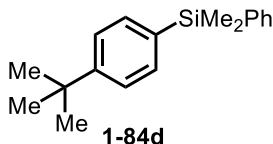
The general procedure for silylation was followed using *N,N,N*-trimethylanilinium iodide **1-84** (64 mg, 0.200 mmol) and dimethylbenzylsilane (160 μ L, 1 mmol). Purification by flash chromatography (100% hexanes) gave the title compound as a white solid in 41% yield (23 mg, 0.081 mmol).

¹H NMR (500 MHz, Chloroform-*d*) δ 7.42 (d, J = 8.0 Hz, 2H), 7.38 (d, J = 8.1 Hz, 2H), 7.19 (t, J = 7.5 Hz, 2H), 7.07 (t, J = 7.3 Hz, 1H), 6.97 (d, J = 7.0 Hz, 2H), 2.30 (s, 2H), 1.33 (s, 9H), 0.22 (s, 6H).

¹³C NMR (126 MHz, Chloroform-*d*) δ 152.16, 140.01, 135.15, 133.73, 128.47, 128.24, 124.85, 124.16, 34.80, 31.40, 26.36, -3.23.

HRMS (EI) (m/z): [M] calculated for C₁₉H₂₆Si, 282.1804, found, 282.1814.

(4-(*tert*-butyl)phenyl)dimethyl(phenyl)silane (**1-84d**)



1-84d

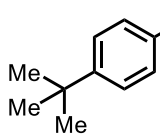
The general procedure for silylation was followed using *N,N,N*-trimethylanilinium iodide **1-84** (67 mg, 0.210 mmol) and dimethylphenylsilane (156 μ L, 1 mmol). Purification by flash chromatography (100% hexanes) gave the title compound as a white solid in 93% yield (53

mg, 0.198 mmol). The spectral data matches that previously reported in the literature.²⁴⁷

¹H NMR (401 MHz, Chloroform-*d*) δ 7.53 (ddd, $J = 7.5, 4.9, 2.3$ Hz, 2H), 7.47 (d, $J = 8.2$ Hz, 2H), 7.38 (d, $J = 8.2$ Hz, 2H), 7.36 (dd, $J = 4.7, 2.7$ Hz, 3H), 1.32 (s, 9H), 0.54 (s, 6H).

¹³C NMR (126 MHz, Chloroform-*d*) δ 152.15, 138.65, 134.76, 134.31, 134.20, 129.14, 127.90, 124.92, 34.79, 31.39, -2.18.

3-(4-(*tert*-butyl)phenyl)-1,1,1,3,5,5,5-heptamethyltrisiloxane (1-84e)



1-84e

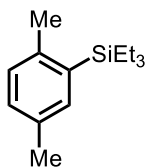
The general procedure for silylation was followed using *N,N,N*-trimethylanilinium iodide **1-84** (68 mg, 0.213 mmol) and 1,1,1, 3, 5, 5, 5-heptamethyltrisiloxane (272 μ L, 1 mmol).

Purification by flash chromatography (100% hexanes) gave the title compound as a colorless oil in 46% yield (34 mg, 0.096 mmol).

¹H NMR (500 MHz, Chloroform-*d*) δ 7.50 (d, $J = 7.5$ Hz, 2H), 7.38 (d, $J = 7.6$ Hz, 2H), 1.33 (s, 9H), 0.26 (s, 3H), 0.12 (s, 18H).

¹³C NMR (126 MHz, Chloroform-*d*) δ 152.43, 135.16, 133.83, 133.27, 124.65, 34.82, 31.41, 2.04, 0.41.

(2,5-dimethylphenyl)triethylsilane (1-85a)



1-85a

The general procedure for silylation was followed using *N,N,N*-trimethylanilinium iodide **1-85** (58 mg, 0.198 mmol) and triethylsilane (160 μ L, 1 mmol). Yield determined by NMR of the crude reaction mixture using

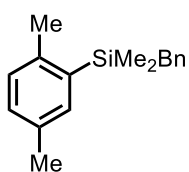
CH₂Br₂ as an internal standard (35%). The spectral data matches that

previously reported in the literature.²⁴⁹

¹H NMR (500MHz, Chloroform-*d*) δ 7.22 (s, 1H), 7.05 (q, *J*= 7.8 Hz, 2H), 2.39 (s, 3H), 2.31 (s, 3H), 0.95 (t, *J*= 8 Hz, 9H), 0.85 (q, *J*= 7.9 Hz, 6H).

¹³C NMR (126 MHz, Chloroform-*d*) δ 140.81, 136.30, 135.31, 133.83, 129.84, 129.78, 22.61, 21.30, 7.78, 4.16.

benzyl(2,5-dimethylphenyl)dimethylsilane (1-85c)



1-85c

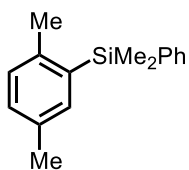
The general procedure for silylation was followed using *N,N,N*-trimethylanilinium iodide **1-85** (58 mg, 0.198 mmol) and dimethylbenzylsilane (160 μL, 1 mmol). Yield determined by NMR of the crude reaction mixture using CH₂Br₂ as an internal standard (65%).

¹H NMR (500MHz, Chloroform-*d*) δ 7.22 (d, *J*= 1.8 Hz, 1H), 7.19 (t, *J*= 7.5 Hz, 2H), 7.08 (qd, *J*= 8.1, 7.5, 4.9 Hz, 3H), 7.00- 6.92 (m, 2H), 2.40 (s, 3H), 2.38 (s, 3H), 0.28 (s, 6H).

¹³C NMR (126 MHz, Chloroform-*d*) δ 140.58, 140.11, 136.60, 135.57, 134.17, 130.20, 130.01, 128.48, 128.25, 124.21, 26.36, 22.84, 21.20, -1.95.

HRMS (EI) (m/z): [M] calculated for C₁₇H₂₂Si, 254.1491, found, 254.1489.

(2,5-dimethylphenyl)dimethyl(phenyl)silane (1-85d)



1-85d

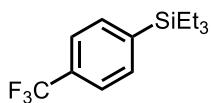
The general procedure for silylation was followed using *N,N,N*-trimethylanilinium iodide **1-85** (58 mg, 0.198 mmol) and dimethylphenylsilane (156 μL, 1 mmol). Yield determined by NMR of the crude reaction mixture using CH₂Br₂ as an internal standard (47%).

¹H NMR (500MHz, Chloroform-*d*) δ 7.56- 7.44 (m, 2H), 7.41- 7.28 (m, 4H), 7.13 (dd, *J*= 7.7, 2.1 Hz, 1H), 7.05 (dd, *J*= 7.7, 2.0 Hz, 1H), 2.33 (s, 3H), 2.22 (s, 3H), 0.58 (s, 6H).

¹³C NMR (126 MHz, Chloroform-*d*) δ 141.07, 139.24, 136.15, 134.32, 134.15, 134.11, 130.43, 129.99, 128.99, 127.93, 22.77, 21.24, -1.18.

HRMS (EI) (m/z): [M] calculated for C₁₆H₂₀Si, 240.1334, found, 240.1344.

triethyl(4-(trifluoromethyl)phenyl)silane (**1-86a**)



1-86a

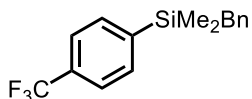
The general procedure for silylation was followed using *N,N,N*-trimethylanilinium iodide **1-86** (68 mg, 0.205 mmol) and triethylsilane (160 μ L, 1 mmol). Yield determined by NMR of the crude reaction mixture using fluorobenzene as an internal standard (50%). The spectral data matches that previously reported in the literature.⁹⁴

¹H NMR (401 MHz, Chloroform-*d*) δ 7.60 (d, *J* = 8.5 Hz, 2H), 7.58 (d, *J* = 8.4 Hz, 2H), 0.96 (t, *J* = 7.7 Hz, 9H), 0.81 (q, *J* = 7.7 Hz, 6H).

¹³C NMR (126 MHz, Chloroform-*d*) δ 155.84, 142.74, 134.56, 130.82 (q, *J* = 31.8 Hz), 124.28 (q, *J* = 3.7 Hz), 7.43, 3.32.

¹⁹F NMR (377 MHz, Chloroform-*d*) δ -62.91.

benzyl(dimethyl)(4-(trifluoromethyl)phenyl)silane (**1-86c**)



1-86c

The general procedure for silylation was followed using *N,N,N*-trimethylanilinium iodide **1-86** (66 mg, 0.199 mmol) and dimethylbenzylsilane (63 μ L, 0.4 mmol). Yield determined by NMR of the crude reaction mixture using fluorobenzene as an internal standard (52%). Purification by preparative TLC (100% hexanes) gave the title compound as a clear oil.

¹H NMR (500 MHz, Chloroform-*d*) δ 7.58 (d, *J* = 7.8 Hz, 2H), 7.55 (d, *J* = 7.9 Hz, 2H),

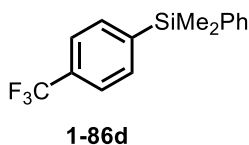
7.19 (t, $J = 7.4$ Hz, 2H), 7.08 (t, $J = 7.4$ Hz, 1H), 6.92 (d, $J = 7.6$ Hz, 2H), 2.32 (s, 2H), 0.29 (s, 6H).

^{13}C NMR (126 MHz, Chloroform- d) δ 143.57, 139.11, 134.14, 131.02, 128.41, 128.37, 124.48, 124.34 (q, $J = 3.8$ Hz), 26.00, -3.42.

^{19}F NMR (471 MHz, Chloroform- d) δ -62.92.

HRMS (EI) (m/z): [M] calculated for $\text{C}_{16}\text{H}_{17}\text{F}_3\text{Si}$, 294.1052, found, 294.1062.

dimethyl(phenyl)(4-(trifluoromethyl)phenyl)silane (**1-86d**)



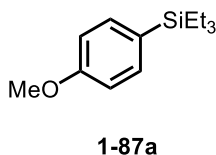
The general procedure for silylation was followed using *N,N,N*-trimethylanilinium iodide **1-86d** (65 mg, 0.196 mmol) and dimethylphenylsilane (62 μL , 0.4 mmol). Yield determined by NMR of the crude reaction mixture using fluorobenzene as an internal standard (47%). Purification by preparative TLC (100% hexanes) gave the title compound as a clear oil. The spectral data matches that previously reported in the literature.²⁴⁷

^1H NMR (401 MHz, Chloroform- d) δ 7.64 (d, $J = 7.9$ Hz, 1H), 7.59 (d, $J = 7.9$ Hz, 1H), 7.55 – 7.48 (m, 1H), 7.45 – 7.33 (m, 1H), 0.59 (s, 3H).

^{13}C NMR (126 MHz, Chloroform- d) δ 143.54, 137.21, 134.57, 134.26, 131.19 (d, $J = 32.4$ Hz), 129.61, 128.14, 124.45 (q, $J = 3.7$ Hz), -2.45.

^{19}F NMR (471 MHz, Chloroform- d) δ -62.95.

triethyl(4-methoxyphenyl)silane (**1-87a**)



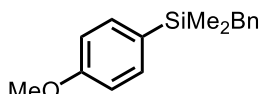
The general procedure for silylation was followed using *N,N,N*-trimethylanilinium iodide **1-87** (58 mg, 0.198 mmol) and triethylsilane

(160 μL , 1 mmol). Yield determined by NMR of the crude reaction mixture using CH_2Br_2 as an internal standard (98%). The spectral data matches that previously reported in the literature.²⁵⁰

^1H NMR (500MHz, Chloroform-*d*) δ 7.42 (d, $J= 8.6$ Hz), 2H), 6.91(d, $J= 8.6$ Hz, 2H), 3.81 (s, 3H), 0.96 (t, $J= 7.9$ Hz, 9H), 0.76 (q, $J= 7.9$ Hz, 6H).

^{13}C NMR (100 MHz, Chloroform-*d*) δ 160.30, 135.70, 128.28, 113.59, 55.11, 7.34, 3.65.

benzyl(4-methoxyphenyl)dimethylsilane (**1-87c**)



1-87c

The general procedure for silylation was followed using *N,N,N*-trimethylanilinium iodide **1-87** (58 mg, 0.198 mmol) and dimethylbenzylsilane (160 μL , 1 mmol). Yield determined by NMR

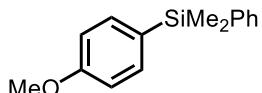
of the crude reaction mixture using CH_2Br_2 as an internal standard (98%).

^1H NMR (400 MHz, Chloroform-*d*) δ 7.42 – 7.33 (m, 2H), 7.23 – 7.14 (m, 2H), 7.12 – 7.04 (m, 1H), 7.00 – 6.88 (m, 3H), 3.83 (s, 3H), 2.29 (s, 2H), 0.24 (s, 6H).

^{13}C NMR (100 MHz, Chloroform-*d*) δ 160.57, 139.96, 135.29, 129.39, 128.44, 128.20, 124.14, 113.63, 55.16, 26.61, -3.12.

HRMS (ESI) (m/z): $[\text{M}+\text{Na}]$ calculated for $\text{C}_{16}\text{H}_{20}\text{OSi}$, 279.1176, found, 279.1179.

(4-methoxyphenyl)dimethyl(phenyl)silane (**1-87d**)



1-87d

The general procedure for silylation was followed using *N,N,N*-trimethylanilinium iodide **1-87** (58 mg, 0.198 mmol) and dimethylphenylsilane (156 μL , 1 mmol). Yield determined by NMR of the crude reaction

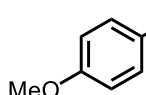
mixture using CH_2Br_2 as an internal standard (92%). The spectral data matches that

previously reported in the literature.²⁴⁷

¹H NMR (500 MHz, Chloroform-*d*) δ 7.58 – 7.51 (m, 2H), 7.48 (d, $J = 8.0$ Hz, 2H), 7.37 (m, $J = 5.8$ Hz, 3H), 6.94 (d, $J = 8.0$ Hz, 2H), 3.83 (s, 3H), 0.56 (s, 6H).

¹³C NMR (126 MHz, Chloroform-*d*) δ 160.63, 138.82, 135.78, 134.27, 129.13, 127.91, 113.74, 55.16, -2.04.

3-(4-methoxyphenyl)-1,1,1,3,5,5,5-heptomethyltrisiloxane (1-87e)



1-87e

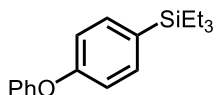
The general procedure for silylation was followed using *N,N,N*-trimethylanilinium iodide **1-87** (29 mg, 0.096 mmol) and 1,1,1,3,5,5,5-heptomethyltrisiloxane (136 μ L, 0.5 mmol). Yield

determined by NMR of the crude reaction mixture using CH_2Br_2 as an internal standard (59%). The spectral data matches that previously reported in the literature.⁹⁷

¹H NMR (500 MHz, Chloroform-*d*) δ 7.48 (d, $J = 8.5$ Hz, 2H), 6.90 (d, $J = 8.5$ Hz, 2H), 3.82 (s, 3H), 0.25 (s, 3H), 0.10 (s, 18H).

¹³C NMR (126 MHz, Chloroform-*d*) δ 160.79, 134.91, 129.96, 113.42, 55.13, 2.02, 0.33.

triethyl(4-phenoxyphenyl)silane (1-88a)



1-88a

The general procedure for silylation was followed using *N,N,N*-trimethylanilinium iodide **1-88** (70 mg, 0.197 mmol) and triethylsilane (160 μ L, 1 mmol). Purification by flash chromatography (100%

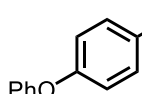
hexanes) gave the title compound as a colorless oil in 89% yield (50 mg, 0.176 mmol).

¹H NMR (500 MHz, Chloroform-*d*) δ 7.44 (d, $J = 7.4$ Hz, 2H), 7.39 – 7.31 (m, 2H), 7.11 (t, $J = 7.4$ Hz, 1H), 7.04 (d, $J = 8.7$ Hz, 2H), 6.98 (d, $J = 7.4$ Hz, 2H), 0.97 (t, $J = 7.9$ Hz, 9H), 0.78 (q, $J = 7.9$ Hz, 6H).

¹³C NMR (126 MHz, Chloroform-*d*) δ 158.24, 156.98, 135.85, 129.86, 123.53, 119.43, 119.02, 118.01, 7.56, 3.63.

HRMS (EI) (m/z): [M] calculated for C₁₈H₂₄OSi, 284.1596, found, 284.1609.

benzyltrimethyl(4-phenoxyphenyl)silane (**1-88c**)



1-88c

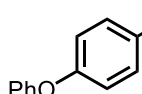
The general procedure for silylation was followed using *N,N,N*-trimethylanilinium iodide **1-88** (73 mg, 0.206 mmol) and dimethylbenzylsilane (64 μ L, 0.4 mmol). Purification by flash chromatography (100% hexanes) gave the title compound as a white solid in 72% yield (47 mg, 0.148 mmol).

¹H NMR (500 MHz, Chloroform-*d*) δ 7.42 (d, $J = 7.2$ Hz, 2H), 7.37 (t, $J = 8.1$ Hz, 2H), 7.20 (t, $J = 6.6$ Hz, 29H), 7.15 (t, $J = 7.9$, 1H), 7.09 (d, $J = 6.9$ Hz, 1H), 7.05 (d, $J = 7.8$ Hz, 2H), 7.00 (d, $J = 6.6$ Hz, 2H), 6.96 (d, $J = 7.1$ Hz, 2H), 2.31 (s, 0H), 0.27 (s, 1H).

¹³C NMR (126 MHz, Chloroform-*d*) δ 158.46, 156.95, 139.77, 135.46, 132.53, 129.90, 128.44, 128.24, 124.22, 123.59, 119.37, 118.10, 26.50, -3.16.

HRMS (ESI) (m/z): [M+Na] calculated for C₂₁H₂₂OSi, 341.1332, found, 341.1338.

dimethyl(4-phenoxyphenyl)(phenyl)silane (**1-88d**)



1-88d

The general procedure for silylation was followed using *N,N,N*-trimethylanilinium iodide **1-88** (70 mg, 0.197 mmol), 30 mg of 4Å

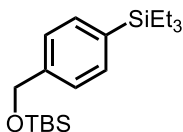
molecular sieves powder, IPr*^{OMe}: (free carbene) (9.4 mg, 0.1 equiv, 0.01 mmol), and dimethylphenylsilane (156 μ L, 1 mmol). Purification by flash chromatography (100% hexanes) gave the title compound in an inseparable mixture with phenyldimethyldisilane as a colorless oil. 68% yield (41 mg, 0.1348 mmol) by NMR analysis.

¹H NMR (401 MHz, Chloroform-*d*) δ 7.53 (ddd, $J = 7.4, 5.1, 2.1$ Hz, 3H), 7.47 (d, $J = 8.1$ Hz, 2H), 7.41 – 7.30 (m, 5H), 7.12 (t, $J = 7.4$ Hz, 1H), 7.03 (d, $J = 8.1$ Hz, 2H), 6.98 (d, $J = 8.4$ Hz, 2H), 0.54 (s, 6H).

¹³C NMR (126 MHz, Chloroform-*d*) δ 158.60, 156.84, 138.44, 135.93, 134.27, 132.24, 129.89, 129.25, 127.97, 123.65, 119.49, 118.08, -2.09.

HRMS (EI) (m/z): [M] calculated for C₂₀H₂₀OSi, 304.1283, found, 304.1294.

***tert*-butyldimethyl((4-(triethylsilyl)benzyl)oxy)silane (1-89a)**



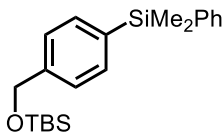
The general procedure for silylation was followed using *N,N,N*-trimethylanilinium iodide **1-89** (80 mg, 0.196 mmol), 30 mg of 4 \AA molecular sieves powder, IPr*^{OMe}: (free carbene) (18.8 mg, 0.1 equiv, 0.01 mmol), triethylsilane (160 μ L, 1 mmol). Purification by flash chromatography (100% hexanes) gave the title compound as a yellow solid in 46% yield (31 mg, 0.091 mmol).

¹H NMR (401 MHz, Chloroform-*d*) δ 7.46 (d, $J = 7.6$ Hz, 2H), 7.31 (d, $J = 7.5$ Hz, 2H), 4.74 (s, 2H), 0.96 (t, $J = 7.8$ Hz, 9H), 0.95 (s, 9H), 0.78 (q, $J = 7.8$ Hz, 6H), 0.10 (s, 3H).

¹³C NMR (100 MHz, Chloroform-*d*) δ 142.05, 135.80, 134.29, 125.46, 65.08, 26.13, 18.60, 7.56, 3.54, -5.11.

HRMS (ESI) (m/z): [M+Na] calculated for C₁₉H₃₆OSi₂, 359.2197, found, 359.2197.

***tert*-butyl((4-(dimethyl(phenyl)silyl)benzyl)oxy)dimethylsilane (1-89d)**



1-89d

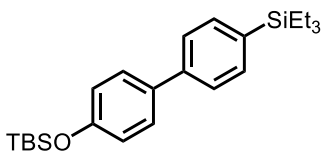
The general procedure for silylation was followed using *N,N,N*-trimethylanilinium iodide **1-89** (81 mg, 0.199 mmol), 30 mg of 4Å molecular sieves powder, IPr^{OMe} : (free carbene) (9.4 mg, 0.1 equiv, 0.01 mmol), and dimethyphenylsilane (156 μL , 1 mmol). Purification by flash chromatography (100% hexanes) gave the title compound as an off white solid in 57% yield (40 mg, 0.113 mmol).

^1H NMR (400 MHz, Chloroform-*d*) δ 7.51 (dd, $J = 3.0, 1.6$ Hz, 2H), 7.49 (d, $J = 8.6$ Hz, 2H), 7.34 (m, 3H), 7.31 (d, $J = 7.7$ Hz, 2H), 4.74 (s, 2H), 0.94 (s, 9H), 0.54 (s, 6H), 0.10 (s, 6H).

^{13}C NMR (126 MHz, Chloroform-*d*) δ 142.57, 138.54, 136.60, 134.31, 134.29, 129.18, 127.92, 125.57, 65.01, 26.12, 18.59, -2.18, -5.11.

HRMS (ESI) (m/z): $[\text{M}+\text{Na}]$ calculated for $\text{C}_{21}\text{H}_{32}\text{OSi}_2$, 379.1884, found, 379.1895.

***tert*-butyldimethyl((4'-(triethylsilyl)-[1,1'-biphenyl]-4-yl)oxy)silane (1-90a)**



1-90a

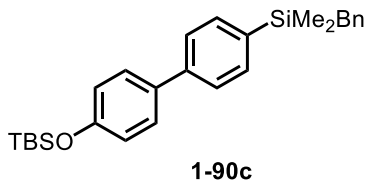
The general procedure for silylation was followed using *N,N,N*-trimethylanilinium iodide **1-90** (97 mg, 0.207 mmol) and triethylsilane (160 μL , 1 mmol). Purification by flash chromatography (100% hexanes) gave the title compound as a colorless oil in 56% yield (46 mg, 0.115 mmol).

^1H NMR (400 MHz, Chloroform-*d*) δ 7.54 (m, 4H), 7.48 (d, $J = 8.6$ Hz, 2H), 6.90 (d, $J = 8.6$ Hz, 2H), 1.00 (s, 9), 0.82 (q, $J = 7.4$ Hz, 6H), 0.23 (s, 6H).

¹³C NMR (100 MHz, Chloroform-*d*) δ 155.46, 141.23, 135.52, 134.78, 134.37, 128.19, 126.10, 120.47, 25.86, 18.40, 7.60, 3.59, -4.21.

HRMS (EI) (m/z): [M] calculated for C₂₄H₃₈OSi₂, 398.2461, found, 398.2473.

benzyl(4'-((*tert*-butyldimethylsilyl)oxy)-[1,1'-biphenyl]-4-yl)dimethylsilane (1-90c)



The general procedure for silylation was followed using *N,N,N*-trimethylanilinium iodide **1-90** (251 mg, 0.535 mmol) and dimethylbenzylsilane (421 μL, 2.66 mmol).

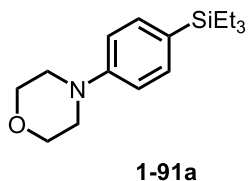
Purification by flash chromatography (100% hexanes to 98:2 hexanes/EtOAc) gave the title compound as a colorless oil in 76% yield (175 mg, 0.404 mmol).

¹H NMR (400 MHz, Chloroform-*d*) δ 7.54 (d, *J* = 7.7 Hz, 2H), 7.52 – 7.44 (m, 4H), 7.19 (t, *J* = 7.5 Hz, 2H), 7.07 (t, *J* = 7.3 Hz, 1H), 6.96 (d, *J* = 7.6 Hz, 2H), 6.91 (d, *J* = 8.3 Hz, 2H), 2.33 (s, 2H), 1.01 (s, 9H), 0.27 (s, 6H), 0.23 (s, 6H).

¹³C NMR (126 MHz, Chloroform-*d*) δ 155.57, 141.61, 139.83, 136.55, 134.32, 134.21, 128.48, 128.27, 128.23, 126.16, 124.22, 120.50, 26.40, 25.86, -3.22, -4.21.

HRMS (ESI) (m/z): [M+Na] calculated for C₂₇H₃₆OSi₂, 455.2197, found, 455.2200.

4-(4-(triethylsilyl)phenyl)morpholine (1-91a)



The general procedure for silylation was followed using *N,N,N*-trimethylanilinium iodide **1-91** (73 mg, 0.210 mmol) and triethylsilane (160 μL, 1 mmol). Purification by flash

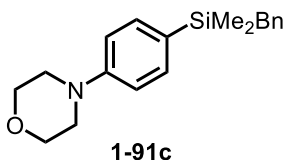
chromatography (95:5 hexanes/EtOAc) gave the title compound as a white solid in 86% yield (51 mg, 0.184 mmol).

¹H NMR (500 MHz, Chloroform-*d*) δ 7.41 (d, J = 8.4 Hz, 2H), 6.91 (d, J = 8.6 Hz, 2H), 3.86 (dd, J = 5.8, 3.9 Hz, 4H), 3.20 (dd, J = 5.9, 3.8 Hz, 4H), 0.97 (t, J = 7.8 Hz, 9H), 0.77 (q, J = 7.6 Hz, 6H).

¹³C NMR (126 MHz, Chloroform-*d*) δ 151.55, 135.44, 127.01, 114.78, 67.08, 48.83, 7.59, 3.66.

HRMS (ESI) (m/z): [M+H] calculated for C₁₆H₂₇NOSi, 278.1940, found, 278.1936.

4-(4-(benzyltrimethylsilyl)phenyl)morpholine (1-91c)



The general procedure for silylation was followed using *N,N,N*-trimethylanilinium iodide **1-91** (70 mg, 0.201 mmol) and dimethylbenzylsilane (160 μ L, 1 mmol). Purification by flash

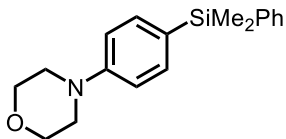
chromatography (95:5 to 90:10 hexanes/EtOAc) gave the title compound as a white solid in 76% yield (47 mg, 0.151 mmol).

¹H NMR (500 MHz, Chloroform-*d*) δ 7.36 (d, J = 7.8 Hz, 2H), 7.18 (t, J = 7.5 Hz, 2H), 7.06 (t, J = 7.3 Hz, 1H), 6.94 (d, J = 7.6 Hz, 2H), 6.90 (d, J = 8.2 Hz, 2H), 3.89 – 3.84 (m, 4H), 3.20 (t, J = 4.9 Hz, 4H), 2.28 (s, 2H), 0.21 (s, 6H).

¹³C NMR (126 MHz, Chloroform-*d*) δ 151.86, 140.08, 135.01, 128.46, 128.19, 128.08, 124.10, 114.80, 67.04, 48.85, 26.61, -3.15.

HRMS (ESI) (m/z): [M+H] calculated for C₁₉H₂₅NOSi, 312.1784, found, 312.1786.

4-(4-(dimethyl(phenyl)silyl)phenyl)morpholine (1-91d)



1-91d

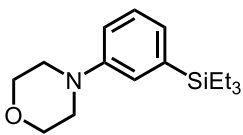
The general procedure for silylation was followed using *N,N,N*-trimethylanilinium iodide **1-91** (67 mg, 0.198 mmol) and dimethylphenylsilane (156 μ L, 1 mmol). Purification by flash chromatography (95:5 hexanes/EtOAc) gave the title compound as a white solid in 78% yield (46 mg, 0.155 mmol).

^1H NMR (500 MHz, Chloroform-*d*) δ 7.55 – 7.48 (m, 2H), 7.43 (d, J = 8.0 Hz, 2H), 7.34 (d, J = 6.2 Hz, 3H), 6.90 (d, J = 8.0 Hz, 2H), 3.85 (t, J = 4.6 Hz, 4H), 3.19 (t, J = 4.7 Hz, 4H), 0.52 (s, 6H).

^{13}C NMR (126 MHz, Chloroform-*d*) δ 151.89, 138.99, 135.49, 134.28, 129.06, 127.86, 127.66, 114.84, 67.02, 48.77, -2.07.

HRMS (ESI) (m/z): [$M+\text{Na}$] calculated for $\text{C}_{18}\text{H}_{23}\text{NOSi}$, 298.1622, found, 298.1628.

4-(3-(triethylsilyl)phenyl)morpholine (**1-92a**)



1-92a

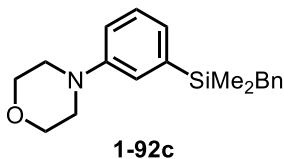
The general procedure for silylation was followed using *N,N,N*-trimethylanilinium iodide **1-92** (70 mg, 0.201 mmol) and triethylsilane (160 μ L, 1 mmol). Purification by flash chromatography (100% hexanes to 95:5 hexanes/EtOAc) gave the title compound as a white solid in 81% yield (45 mg, 0.162 mmol). The spectral data matches that previously reported in the literature.¹¹⁵

^1H NMR (401 MHz, Chloroform-*d*) δ 7.29 (d, J = 7.7 Hz, 1H), 7.06 (d, J = 2.6 Hz, 1H), 7.03 (dd, J = 7.2, 1.1 Hz, 1H), 6.91 (dd, J = 8.2, 2.6 Hz, 1H), 3.92 – 3.84 (m, 4H), 3.17 (dd, J = 5.8, 3.8 Hz, 4H), 0.97 (t, J = 7.7 Hz, 9H), 0.79 (q, J = 7.8 Hz, 6H).

^{13}C NMR (100 MHz, Chloroform-*d*) δ 150.71, 138.52, 128.61, 126.25, 121.76, 116.37, 67.17, 49.73, 7.61, 3.55.

HRMS (ESI) (m/z): [M+H] calculated for C₁₈H₂₃NOSiO, 298.1627, found, 298.1628.

4-(3-(benzylidimethylsilyl)phenyl)morpholine (**1-92c**)



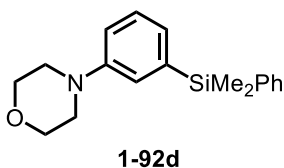
The general procedure for silylation was followed using *N,N,N*-trimethylanilinium iodide **1-92c** (69 mg, 0.198 mmol) and dimethylbenzylsilane (160 μ L, 1 mmol). Purification by flash chromatography (95:5 hexanes/EtOAc) gave the title compound as a white solid in 85% yield (53 mg, 0.167 mmol).

¹H NMR (400 MHz, Chloroform-*d*) δ 7.29 (d, *J* = 7.5 Hz, 1H), 7.23 – 7.13 (m, 2H), 7.06 (t, *J* = 7.2 Hz, 1H), 7.00 (d, *J* = 7.1 Hz, 1H), 6.98 – 6.88 (m, 4H), 3.90 – 3.82 (m, 4H), 3.16 – 3.10 (m, 4H), 2.29 (s, 2H), 0.24 (s, 6H).

¹³C NMR (100 MHz, Chloroform-*d*) δ 150.66, 139.88, 139.48, 128.73, 128.49, 128.24, 125.62, 121.32, 116.73, 67.13, 49.66, 26.38, -3.20.

HRMS (ESI) (m/z): [M+H] calculated for C₁₉H₂₅NOSi, 312.1784, found, 312.1791.

4-(3-(dimethyl(phenyl)silyl)phenyl)morpholine (**1-92d**)



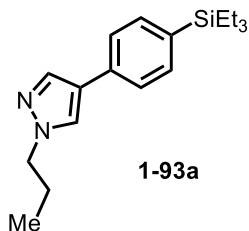
The general procedure for silylation was followed using *N,N,N*-trimethylanilinium iodide **1-92** (70 mg, 0.201 mmol) and dimethylphenylsilane (156 μ L, 1 mmol). Purification by flash chromatography (95:5 hexanes/EtOAc) gave the title compound as a white solid in 70% yield (42 mg, 0.141 mmol).

¹H NMR (400 MHz, Chloroform-*d*) δ 7.56 – 7.49 (m, 2H), 7.40 – 7.32 (m, 3H), 7.29 (d, *J* = 7.6 Hz, 1H), 7.11 – 7.02 (m, 2H), 6.97 – 6.88 (m, 1H), 3.89 – 3.81 (m, 4H), 3.17 – 3.10

(m, 4H), 0.54 (s, 6H).

^{13}C NMR (100 MHz, Chloroform-*d*) δ 150.78, 139.21, 138.42, 134.32, 129.21, 128.83, 127.92, 126.19, 121.65, 116.69, 67.12, 49.59, -2.17.

1-propyl-4-(4-(triethylsilyl)phenyl)-1*H*-pyrazole (1-93a)



The general procedure for silylation was followed using *N,N,N*-trimethylanilinium iodide **1-93** (73 mg, 0.197 mmol) and triethylsilane (160 μL , 1 mmol). Purification by flash chromatography (90:10 hexanes/EtOAc) gave the title compound as

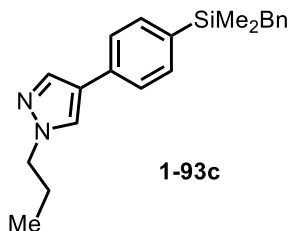
a white solid in 81% yield (48 mg, 0.160 mmol).

^1H NMR (500 MHz, Chloroform-*d*) δ 7.80 (s, 1H), 7.64 (s, 1H), 7.49 (d, $J = 8.1$ Hz, 2H), 7.47 (d, $J = 8.1$ Hz, 2H), 4.11 (t, $J = 7.0$ Hz, 2H), 1.93 (h, $J = 7.2$ Hz, 2H), 0.98 (t, $J = 7.8$ Hz, 9H), 0.94 (t, $J = 7.4$ Hz, 3H), 0.80 (q, $J = 7.9$ Hz, 6H).

^{13}C NMR (126 MHz, Chloroform-*d*) δ 136.76, 135.23, 134.90, 133.19, 126.14, 124.87, 122.89, 54.20, 23.89, 11.30, 7.56, 3.53.

HRMS (ESI) (m/z): [M+H] calculated for $\text{C}_{18}\text{H}_{28}\text{N}_2\text{OSi}$, 301.2100, found, 301.2092.

4-(4-(benzyl dimethylsilyl)phenyl)-1-propyl-1*H*-pyrazole (1-93c)



The general procedure for silylation was followed using *N,N,N*-trimethylanilinium iodide **1-93** (36 mg, 0.097 mmol) and dimethylbenzylsilane (80 μL , 0.5 mmol). Purification by flash chromatography (90:10 hexanes/EtOAc) gave the title compound

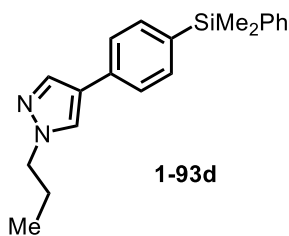
as a white solid in 93% yield (30 mg, 0.090 mmol).

¹H NMR (500 MHz, Chloroform-*d*) δ 7.80 (s, 1H), 7.65 (s, 1H), 7.47 (d, *J* = 8.0 Hz, 2H), 7.44 (d, *J* = 7.8 Hz, 2H), 7.18 (t, *J* = 7.6 Hz, 2H), 7.10 – 7.04 (m, 1H), 6.95 (d, *J* = 7.5 Hz, 2H), 4.12 (t, *J* = 7.1 Hz, 2H), 2.31 (s, 2H), 1.94 (q, *J* = 7.2 Hz, 2H), 0.96 (dd, *J* = 7.9, 6.8 Hz, 3H), 0.26 (s, 6H).

¹³C NMR (126 MHz, Chloroform-*d*) δ 139.78, 136.76, 136.18, 134.43, 133.53, 128.45 (d, *J* = 2.5 Hz), 128.23, 126.18, 124.86, 124.19, 54.21, 26.38, 23.88, 11.31, -3.26.

HRMS (ESI) (m/z): [M+H] calculated for C₂₁H₂₆N₂Si, 335.1944, found, 335.1938.

4-(4-(dimethyl(phenyl)silyl)phenyl)-1-propyl-1*H*-pyrazole (1-93d)



The general procedure for silylation was followed using *N,N,N*-trimethylanilinium iodide **1-93** (36 mg, 0.097 mmol) and dimethylphenylsilane (78 μL, 0.5 mmol). Purification by flash chromatography (90:10 hexanes/EtOAc) gave the title compound

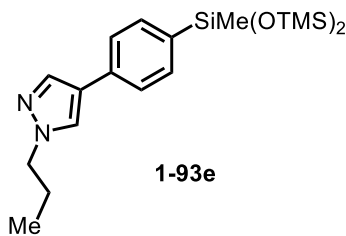
as a white solid in 72% yield (22 mg, 0.069 mmol).

¹H NMR (500 MHz, Chloroform-*d*) δ 7.79 (s, 1H), 7.64 (s, 1H), 7.57 – 7.49 (m, 4H), 7.49 – 7.45 (m, 2H), 7.40 – 7.33 (m, 3H), 4.11 (t, *J* = 7.1 Hz, 2H), 1.93 (q, *J* = 7.3 Hz, 2H), 0.95 (t, *J* = 7.4 Hz, 3H), 0.57 (s, 6H).

¹³C NMR (126 MHz, Chloroform-*d*) δ 138.44, 136.78, 135.93, 134.90, 134.29, 133.62, 129.21, 128.96, 127.94, 126.20, 124.98, 54.20, 23.87, 11.29, -2.21.

HRMS (ESI) (m/z): [M+H] calculated for C₂₀H₂₄N₂Si, 321.1787, found, 321.1781.

4-(4-(1,1,1,3,5,5,5-heptamethyltrisiloxan-3-yl)phenyl)-1-propyl-1*H*-pyrazole (1-93e)



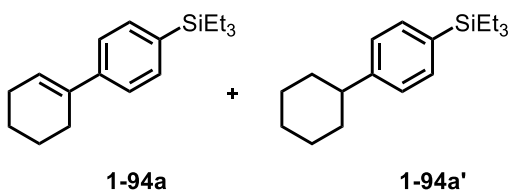
The general procedure for silylation was followed using *N,N,N*-trimethylanilinium iodide **1-93** (35 mg, 0.094 mmol) and 1,1,1, 3, 5, 5, 5-heptamethyltrisiloxane (136 μ L, 0.5 mmol). Purification by flash chromatography (90:10 to 80:20 hexanes/EtOAc) gave the title compound as a white solid in 27% yield (10 mg, 0.018 mmol).

^1H NMR (500 MHz, Chloroform-*d*) δ 7.80 (s, 1H), 7.65 (s, 1H), 7.54 (d, $J = 7.8$ Hz, 2H), 7.47 (d, $J = 7.8$ Hz, 2H), 4.11 (t, $J = 7.1$ Hz, 2H), 1.93 (h, $J = 7.3$ Hz, 2H), 0.95 (t, $J = 7.4$ Hz, 3H), 0.27 (s, 3H), 0.11 (s, 18H).

^{13}C NMR (126 MHz, Chloroform-*d*) δ 136.80, 136.35, 133.96, 133.83, 126.19, 124.75, 122.86, 54.22, 23.90, 11.32, 2.03, 0.22.

HRMS (ESI) (m/z): [$M+H$] calculated for $\text{C}_{19}\text{H}_{34}\text{N}_2\text{O}_2\text{Si}_3$, 407.2006, found, 407.2003.

triethyl(2',3',4',5'-tetrahydro-[1,1'-biphenyl]-4-yl)silane (**1-94a**)



The general procedure for silylation was followed using *N,N,N*-trimethylanilinium iodide **1-94** (137 mg, 0.399 mmol) and triethylsilane (192 μ L, 1.2 mmol). Reaction was run under a stream of nitrogen in order to prevent hydrogenation of the product. Purification by flash chromatography (100% hexanes) gave the title compound as a white solid in 45% yield (49 mg, 0.180 mmol) and the hydrogenated product in 10% yield (11mg, 0.040 mmol).

1-94a: **^1H NMR** (500 MHz, Chloroform-*d*) δ 7.43 (d, $J = 7.8$ Hz, 2H), 7.37 (d, $J = 7.7$ Hz, 2H), 6.16 (tt, $J = 3.9, 1.7$ Hz, 1H), 2.42 (tq, $J = 6.5, 2.3$ Hz, 2H), 2.21 (dh, $J = 6.1, 2.8$ Hz,

2H), 1.81 – 1.73 (m, 2H), 1.70 – 1.62 (m, 2H), 0.96 (t, $J = 7.8$ Hz, 9H), 0.78 (q, $J = 7.8$ Hz, 6H).

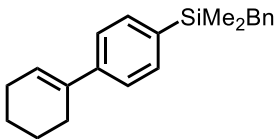
^{13}C NMR (100 MHz, Chloroform- d) δ 142.94, 136.61, 135.42, 134.33, 125.04, 124.25, 27.36, 26.08, 23.23, 22.35, 7.58, 3.56.

1-94a': ^1H NMR (500 MHz, Chloroform- d) δ 7.41 (d, $J = 6.6$ Hz, 2H), 7.19 (d, $J = 6.9$ Hz, 2H), 2.58 – 2.42 (m, 1H), 1.96 – 1.80 (m, 3H), 1.74 (d, $J = 13.1$ Hz, 1H), 1.41 (h, $J = 12.4$ Hz, 3H), 1.31 – 1.18 (m, 1H), 0.96 (t, $J = 7.7$ Hz, 9H), 0.77 (q, $J = 8.0$ Hz, 7H).

^{13}C NMR (126 MHz, Chloroform- d) δ 148.64, 134.37, 134.34, 126.37, 44.66, 34.48, 27.10, 26.36, 7.62, 3.62.

HRMS (EI) (m/z): [M] calculated for $\text{C}_{18}\text{H}_{30}\text{Si}$, 274.2117, found, 274.2125.

benzyl dimethyl(2',3',4',5'-tetrahydro-[1,1'-biphenyl]-4-yl)silane (**1-94c**)



1-94c

The general procedure for silylation was followed using *N,N,N*-trimethylanilinium iodide **1-94** (136 mg, 0.396 mmol) and dimethylbenzylsilane (190 μL , 1.2 mmol). Reaction was run under

a stream of nitrogen in order to prevent hydrogenation of the product. Purification by flash chromatography (100% hexanes to 98:2 hexanes/EtOAc) gave the title compound as a white solid in 59% yield (72 mg, 0.234 mmol).

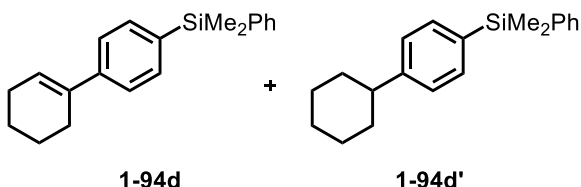
^1H NMR (400 MHz, Chloroform- d) δ 7.40 (d, $J = 8.2$ Hz, 2H), 7.36 (d, $J = 8.1$ Hz, 2H), 7.18 (t, $J = 7.5$ Hz, 2H), 7.06 (t, $J = 7.3$ Hz, 1H), 6.94 (d, $J = 7.3$ Hz, 2H), 6.16 (tt, $J = 4.1$, 1.7 Hz, 1H), 2.42 (dq, $J = 6.1$, 3.8, 3.1 Hz, 2H), 2.30 (s, 2H), 2.22 (dq, $J = 6.3$, 3.5 Hz, 2H), 1.79 (ddt, $J = 12.0$, 8.6, 4.5 Hz, 1H), 1.71 – 1.62 (m, 2H), 0.23 (s, 6H).

^{13}C NMR (100 MHz, Chloroform- d) δ 143.40, 139.91, 136.60, 133.84, 128.46, 128.23,

125.30, 124.37, 124.17, 27.39, 26.39, 26.08, 23.20, 22.32, -3.24.

HRMS (EI) (m/z): [M] calculated for C₂₁H₂₆Si, 306.1804, found, 306.1811.

dimethyl(phenyl)(2',3',4',5'-tetrahydro-[1,1'-biphenyl]-4-yl)silane (1-94d)



The general procedure for silylation was followed using *N,N,N*-trimethylanilinium iodide **1-94** (138 mg, 0.402 mmol) and

dimethylphenylsilane (187 μ L, 1.2 mmol). Reaction was run under a stream of nitrogen in order to prevent hydrogenation of the product. Purification by flash chromatography (100% hexanes to 98:2 hexanes/EtOAc) gave the title compound as a white solid in 56% yield (65 mg, 0.222 mmol) and the hydrogenated product in 27% yield (32mg, 0.109 mmol).

1-94d: ¹H NMR (500 MHz, Chloroform-*d*) δ 7.58 – 7.49 (m, 2H), 7.47 (d, *J* = 8.2 Hz, 2H), 7.36 (dt, *J* = 10.5, 3.6 Hz, 5H), 6.15 (tt, *J* = 5.7, 2.6 Hz, 1H), 2.41 (tq, *J* = 6.4, 2.1 Hz, 2H), 2.21 (dddd, *J* = 8.9, 6.6, 4.4, 2.5 Hz, 2H), 1.78 (ddt, *J* = 8.4, 6.1, 3.8 Hz, 2H), 1.70 – 1.61 (m, 2H), 0.54 (s, 6H).

¹³C NMR (126 MHz, Chloroform-*d*) δ 143.48, 136.10, 134.31, 133.14, 129.39, 129.16, 127.91, 127.84, 125.34, 124.47, 27.38, 26.06, 23.19, 22.30, -2.19.

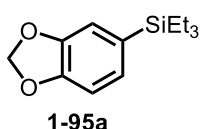
HRMS (EI) (m/z): [M] calculated for C₂₀H₂₄Si, 292.1647, found, 292.1646.

1-94d': ¹H NMR (500 MHz, Chloroform-*d*) δ 7.53 (dd, *J* = 4.8, 2.5 Hz, 2H), 7.45 (d, *J* = 7.7 Hz, 2H), 7.40 – 7.32 (m, 5H), 7.20 (d, *J* = 7.5 Hz, 2H), 2.49 (dt, *J* = 11.6, 5.7 Hz, 1H), 1.93 – 1.79 (m, 4H), 1.74 (d, *J* = 13.1 Hz, 1H), 1.49 – 1.32 (m, 4H), 1.32 – 1.19 (m, 1H), 0.54 (s, 6H).

^{13}C NMR (126 MHz, Chloroform-*d*) δ 149.16, 134.38, 134.32, 129.23, 129.13, 127.94, 127.89, 126.55, 44.70, 34.45, 27.05, 26.32, -2.15.

HRMS (EI) (m/z): [M] calculated for $\text{C}_{20}\text{H}_{26}\text{Si}$, 294.1804, found, 294.1812.

benzo[*d*][1,3]dioxol-5-yltriethylsilane (**1-95a**)

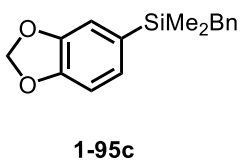


The general procedure for silylation was followed using *N,N,N*-trimethylanilinium iodide **1-95** (60 mg, 0.195 mmol) and triethylsilane (160 μL , 1 mmol). Purification by flash chromatography (100% hexanes) gave the title compound as a colorless oil in 68% yield (32 mg, 0.135 mmol). The spectral data matches that previously reported in the literature.²⁴⁸

^1H NMR (400 MHz, Chloroform-*d*) δ 6.96 (d, $J = 7.6$ Hz, 1H), 6.94 (s, 1H), 6.84 (d, $J = 7.6$ Hz, 1H), 5.93 (s, 2H), 0.95 (t, $J = 7.8$ Hz, 9H), 0.75 (q, $J = 7.9$ Hz, 6H).

^{13}C NMR (100 MHz, Chloroform-*d*) δ 148.26, 147.42, 130.44, 128.18, 113.57, 108.66, 100.55, 7.52, 3.66.

benzo[*d*][1,3]dioxol-5-yl(benzyl)dimethylsilane (**1-95c**)



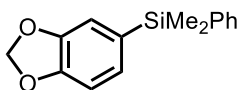
The general procedure for silylation was followed using *N,N,N*-trimethylanilinium iodide **1-95c** (60 mg, 0.195 mmol) and dimethylbenzylsilane (160 μL , 1 mmol). Purification by flash chromatography (100% hexanes) gave the title compound as a colorless oil in 79% yield (42 mg, 0.155 mmol).

¹H NMR (500 MHz, Chloroform-*d*) δ 7.19 (t, $J = 7.6$ Hz, 2H), 7.07 (t, $J = 7.3$ Hz, 1H), 6.97 – 6.90 (m, 4H), 6.90 (s, 1H), 6.84 (d, $J = 7.6$ Hz, 1H), 5.95 (s, 2H), 2.27 (s, 2H), 0.22 (s, 6H).

¹³C NMR (126 MHz, Chloroform-*d*) δ 148.54, 147.45, 139.75, 128.42, 128.24, 127.86, 124.23, 113.19, 108.65, 100.67, 26.54, -3.08.

HRMS (EI) (m/z): [M] calculated for C₁₆H₁₈O₂Si, 270.1076, found, 270.1084.

benzo[*d*][1,3]dioxol-5-yl(dimethyl(phenyl)silane (**1-95d**)



1-95d

The general procedure for silylation was followed using *N,N,N*-trimethylanilinium iodide **1-95** (61 mg, 0.199 mmol) and dimethylphenylsilane (156 μ L, 1 mmol). Purification by flash chromatography (100% hexanes) gave the title compound as a colorless oil in 60% yield (31 mg, 0.119 mmol).

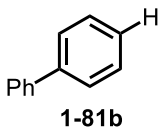
¹H NMR (400 MHz, Chloroform-*d*) δ 7.56 – 7.47 (m, 2H), 7.40 – 7.31 (m, 3H), 7.01 (d, $J = 7.6$ Hz, 1H), 6.96 (s, 1H), 6.84 (d, $J = 7.6$ Hz, 1H), 5.93 (s, 2H), 0.53 (s, 6H).

¹³C NMR (100 MHz, Chloroform-*d*) δ 148.63, 147.53, 138.45, 134.24, 131.36, 129.25, 128.39, 127.96, 113.65, 108.74, 100.69, -2.05.

HRMS (EI) (m/z): [M] calculated for C₁₅H₁₆O₂Si, 256.0920, found, 256.0921.

4.2.5 Reduction Substrates:

biphenyl (**1-81b**)

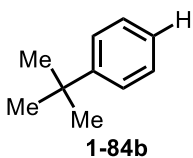


1-81b

The general procedure for reduction was followed using *N,N,N*-trimethylanilinium iodide **1-81** (36 mg, 0.100 mmol) and triethylsilane (80 μ L, 0.5 mmol) in DMF at room temperature for overnight. The crude reaction mixture was

passed through a short silica gel plug with EtOAc. The yield was determined by GC-FID analysis using tridecane as an internal standard due to volatility of the product (98%).

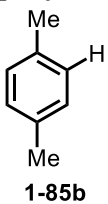
tert-butylbenzene (1-84b)



The general procedure for reduction was followed using *N,N,N*-trimethylanilinium iodide **1-84** (32 mg, 0.100 mmol) and triethylsilane (80 μ L, 0.5 mmol) in dioxane at 40 $^{\circ}$ C. The crude reaction mixture was

passed through a short silica gel plug with EtOAc. The yield was determined by GC-FID analysis using tridecane as an internal standard due to volatility of the product (75%).

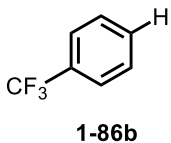
***p*-xylene (1-85b)**



The general procedure for reduction was followed using *N,N,N*-trimethylanilinium iodide **1-85** (29 mg, 0.100 mmol) and triethylsilane (80 μ L, 0.5 mmol) in dioxane at 60 $^{\circ}$ C. The crude reaction mixture was passed through

a short silica gel plug with EtOAc. The yield was determined by GC-FID analysis using tridecane as an internal standard due to volatility of the product (15%).

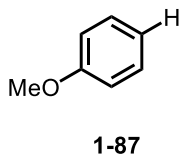
trifluorotoluene (1-86b)



The general procedure for reduction was followed using *N,N,N*-trimethylanilinium iodide **1-86** (33 mg, 0.100 mmol) and triethylsilane (80 μ L, 0.5 mmol) in dioxane at 40 $^{\circ}$ C. The crude reaction mixture was passed

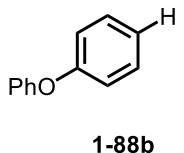
through a short silica gel plug with EtOAc. The yield was determined by GC-FID analysis using tridecane as an internal standard due to volatility of the product (67%).

anisole (1-87c)



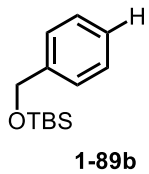
The general procedure for reduction was followed using *N,N,N*-trimethylanilinium iodide **1-87** (29 mg, 0.989 mmol) and triethylsilane (80 μ L, 0.5 mmol) in DMF at room temperature for 2 hours. The crude reaction mixture was passed through a short silica gel plug with EtOAc. The yield was determined by GC-FID analysis using tridecane as an internal standard due to volatility of the product (20%).

diphenylether (1-88b)



The general procedure for reduction was followed using *N,N,N*-trimethylanilinium iodide **1-88** (36 mg, 0.101 mmol) and triethylsilane (80 μ L, 0.5 mmol) in DMF at room temperature for 2 hours. The crude reaction mixture was passed through a short silica gel plug with EtOAc. The yield was determined by GC-FID analysis using tridecane as an internal standard due to volatility of the product (60%).

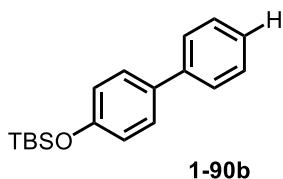
(benzyloxy)(*tert*-butyl)dimethylsilane (1-89b)



The general procedure for reduction was followed using *N,N,N*-trimethylanilinium iodide **1-89** (41 mg, 0.101 mmol) and triethylsilane (80 μ L, 0.5 mmol) in dioxane at 60 $^{\circ}$ C. The crude reaction mixture was passed through a short silica gel plug with EtOAc and the solution was evaporated under reduced pressure. The yield was determined using CH_2Br_2 (7 μ L) as an internal standard (68%) by ^1H NMR. The spectral data matches that previously reported in the literature.²⁵¹

$^1\text{H NMR}$ (401 MHz, Chloroform-*d*) δ 7.33 (d, $J = 4.4$ Hz, 5H), 4.75 (s, 2H), 1.24 (s, 9H), 0.10 (s, 6H).

([1,1'-biphenyl]-4-yloxy)(*tert*-butyl)dimethylsilane (1-90b)

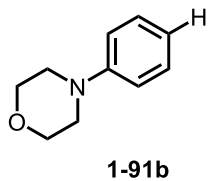


The general procedure for reduction was followed using *N,N,N*-trimethylanilinium iodide **1-90** (48 mg, 0.102 mmol) and triethylsilane (80 μL , 0.5 mmol) in dioxane at 40 $^\circ\text{C}$. The crude reaction mixture was passed through a short silica gel plug with EtOAc and the solution was evaporated under reduced pressure. The yield was determined using CH_2Br_2 (7 μL) as an internal standard (80%) by $^1\text{H NMR}$. The spectral data matches that previously reported in the literature.¹¹⁵

$^1\text{H NMR}$ (500 MHz, Chloroform-*d*) δ 7.59 – 7.51 (m, 2H), 7.50 – 7.45 (m, 2H), 7.41 (t, $J = 7.7$ Hz, 2H), 7.35 – 7.27 (m, 1H), 6.91 (d, $J = 8.6$ Hz, 1H), 1.01 (s, 9H), 0.24 (s, 6H).

$^{13}\text{C NMR}$ (126 MHz, Chloroform-*d*) δ 155.42, 141.04, 134.43, 128.81, 128.22, 126.88, 126.78, 120.46, 25.86, 18.39, -4.22.

4-phenylmorpholine (1-91b)

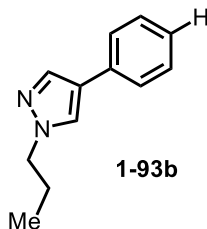


The general procedure for reduction was followed using *N,N,N*-trimethylanilinium iodide **1-91** (67 mg, 0.192 mmol) and triethylsilane (160 μL , 1 mmol) at 60 $^\circ\text{C}$. Purification by flash chromatography (95:5% hexanes/EtOAc) gave the title compound as a white solid in 90% yield (20 mg, 0.150 mmol). The spectral data matches that previously reported in the literature.²⁵²

¹H NMR (500 MHz, Chloroform-*d*) δ 7.29 (t, *J* = 7.8 Hz, 2H), 6.93 (d, *J* = 8.1 Hz, 2H), 6.89 (t, *J* = 7.3 Hz, 1H), 3.87 (t, *J* = 4.8 Hz, 4H), 3.17 (t, *J* = 4.8 Hz, 4H).

¹³C NMR (126 MHz, Chloroform-*d*) δ 151.42, 129.32, 120.18, 115.85, 67.09, 49.51.

4-phenyl-1-propyl-1*H*-pyrazole (1-93b)



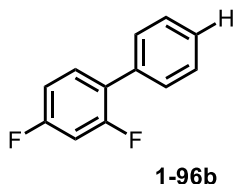
The general procedure for reduction was followed using *N,N,N*-trimethylanilinium iodide **1-98** (77 mg, 0.207 mmol) and triethylsilane (160 μL, 1 mmol). Purification by flash chromatography (90:10% hexanes/EtOAc) gave the title compound as a white solid in 90% yield (35 mg, 0.189 mmol).

¹H NMR (500 MHz, Chloroform-*d*) δ 7.78 (s, 1H), 7.63 (s, 1H), 7.48 (d, *J* = 8.3 Hz, 2H), 7.43 – 7.30 (m, 2H), 7.25 – 7.16 (m, 1H), 4.11 (t, *J* = 7.1 Hz, 2H), 2.35 – 1.83 (m, 2H), 0.95 (t, *J* = 7.4 Hz, 3H).

¹³C NMR (126 MHz, Chloroform-*d*) δ 136.71, 132.93, 128.97, 126.40, 126.07, 125.61, 122.89, 54.22, 23.91, 11.33.

HRMS (ESI) (*m/z*): [M+H] calculated for C₁₂H₁₄N₂, 187.1235, found, 187.1226.

2,4-difluoro-1,1'-biphenyl (1-96b)



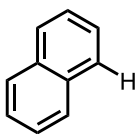
The general procedure for reduction was followed using *N,N,N*-trimethylanilinium iodide **1-96** (75 mg, 0.200 mmol) and triethylsilane (160 μL, 1 mmol) at room temperature. Purification by flash chromatography (100% hexanes/) gave the title compound as a white solid in 67% yield (25 mg, 0.134 mmol) with approximately 10% of an impurity that could not be

separated by silica chromatography. The spectral data matches that previously reported in the literature.²⁵³

¹H NMR (400 MHz, Chloroform-*d*) δ 7.51 (d, $J = 7.9$ Hz, 2H), 7.49 – 7.41 (m, 3H), 7.41 – 7.34 (m, 1H), 7.01 – 6.83 (m, 2H).

¹⁹F NMR (376 MHz, Chloroform-*d*) δ -111.62 (p, $J = 8.0$ Hz), -113.66 (q, $J = 9.2$ Hz).

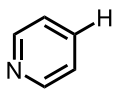
naphthalene (1-97b)



1-97b

The general procedure for reduction was followed using *N,N,N*-trimethylanilinium iodide **1-97** (63 mg, 0.201 mmol) and triethylsilane (160 μ L, 1 mmol) in DMF at 40 °C. The crude reaction mixture was passed through a short silica gel plug with EtOAc. The yield was determined by GC-FID analysis using tridecane as an internal standard due to volatility of the product (81%).

pyridine (1-98b)

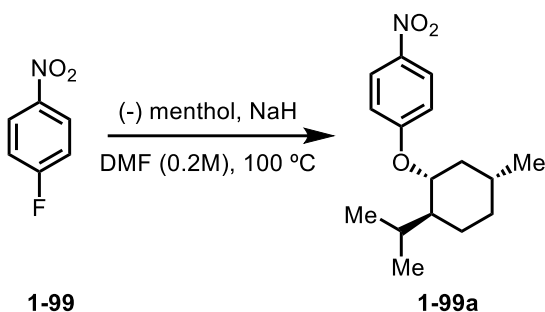


1-98b

The general procedure for reduction was followed using *N,N,N*-trimethylanilinium iodide **1-98** (26 mg, 0.098 mmol) and triethylsilane (80 μ L, 0.5 mmol) in dioxane at 90 °C. The crude reaction mixture was passed through a short silica gel plug with EtOAc. The yield was determined by GC-FID analysis using tridecane as an internal standard due to volatility of the product (37%).

4.2.6 Synthetic Demonstrations:

1-(((1*R*,2*S*,5*R*)-2-isopropyl-5-methylcyclohexyl)oxy)-4-nitrobenzene (1-99a)



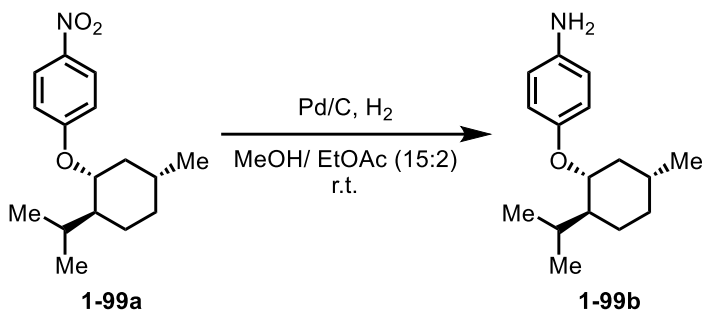
A solution of (-)-menthol (3.4g, 21.7 mmol, 2.0 equiv) in DMF (4 mL) was added dropwise to a flame dried 20 mL scintillation vial equipped with a stir bar containing a solution of NaH (60% dispersion in mineral oil) (120mg, 30 mmol, 3.0 equiv) in DMF (1 mL) at 0 °C. After 30min the vial was allowed to warm to room temperature. 4-fluoro-nitrobenzene (1.06 mL, 10 mmol, 1.0 equiv) was added slowly and the vial was sealed with a Teflon cap and headed to 90 °C for 48 hours. The solution was then cooled to room temperature, transferred to a separatory funnel, and diluted with 30 mL diethyl ether. The organics were then washed 2x50 mL 5M NaOH solution and 1x50 mL brine. The organic layer was dried with sodium sulfate before concentrating. The product can be obtained *via* Kugelrohr distillation at 0.5 bar at 80 °C through the removal of unreacted 4-fluoro-nitrobenzene and excess menthol. The product was obtained as a yellow crystalline solid. The discoloration was removed through Purification by flash chromatography (90:10 hexanes/EtOAc) to give the title compound as a white crystalline solid in 30% yield (1.72 g, 6.2 mmol).

¹H NMR (401 MHz, Chloroform-*d*) δ 8.18 (d, *J* = 8.9 Hz, 2H), 6.93 (d, *J* = 9.0 Hz, 2H), 4.16 (td, *J* = 10.6, 4.2 Hz, 1H), 2.20 – 2.04 (m, 2H), 1.85 – 1.69 (m, 2H), 1.63 – 1.46 (m, 2H), 1.18 – 1.01 (m, 3H), 0.93 (t, *J* = 7.5 Hz, 6H), 0.75 (d, *J* = 6.9 Hz, 3H).

¹³C NMR (176 MHz, Chloroform-*d*) δ 163.85, 141.13, 126.22, 115.13, 78.53, 47.96, 40.00, 34.43, 31.54, 26.38, 23.90, 22.19, 20.74, 16.77.

HRMS (ESI) (*m/z*): [*M*+Na] calculated for C₁₆H₂₃NO₃, 300.1570, found, 300.1580.

4-(((1*R*,2*S*,5*R*)-2-isopropyl-5-methylcyclohexyl)oxy)aniline (**1-99b**)



To a round bottom equipped with a stir bar was added **1-99a** (400 mg, 1.44 mmol) and palladium on carbon (10%) (40 mg, 2.5 mol%). The flask was backfilled

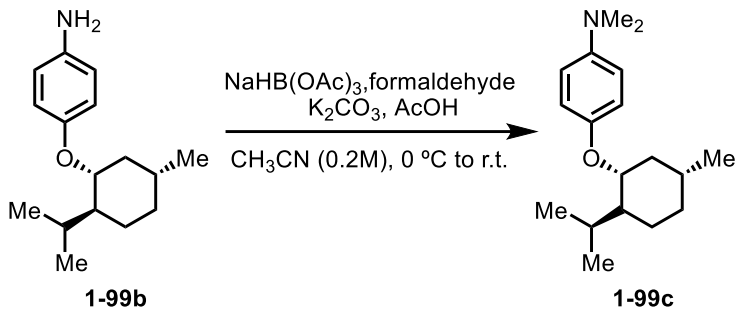
three times with nitrogen before adding methanol (15 mL) and EtOAc (2 mL). The flask was then backfilled three times with H₂ before attaching a H₂ balloon. The reaction was left to stir at room temperature overnight. The contents of the flask were then filtered through Celite with EtOAc. The filtrate was concentrated to give the title compound as a reddish solid in 97% yield (344 mg, 1.39 mmol).

¹H NMR (700 MHz, Chloroform-*d*) δ 6.75 (d, *J* = 8.6 Hz, 2H), 6.63 (d, *J* = 8.7 Hz, 1H), 3.82 (td, *J* = 10.5, 4.2 Hz, 1H), 3.42 (s, 2H), 2.28 (pd, *J* = 7.0, 2.7 Hz, 1H), 2.11 (dtd, *J* = 12.6, 3.8, 1.9 Hz, 1H), 1.69 (dt, *J* = 14.3, 3.7 Hz, 2H), 1.45 (ddt, *J* = 13.3, 10.4, 3.2 Hz, 1H), 1.39 (tdq, *J* = 12.6, 6.6, 3.3 Hz, 1H), 1.10 – 1.02 (m, 1H), 1.01 – 0.94 (m, 1H), 0.92 (dd, *J* = 24.6, 6.8 Hz, 7H), 0.80 (d, *J* = 6.9 Hz, 3H).

¹³C NMR (176 MHz, Chloroform-*d*) δ 151.50, 140.24, 118.09, 116.51, 79.17, 48.34, 40.73, 34.70, 31.60, 26.03, 23.70, 22.32, 21.02, 16.58.

HRMS (ESI) (*m/z*): [*M*+*H*] calculated for C₁₆H₂₅NO, 248.2009, found, 248.2016.

4-(((1*R*,2*R*,5*R*)-2-isopropyl-5-methylcyclohexyl)oxy)-*N,N*-dimethylaniline (**1-99c**)



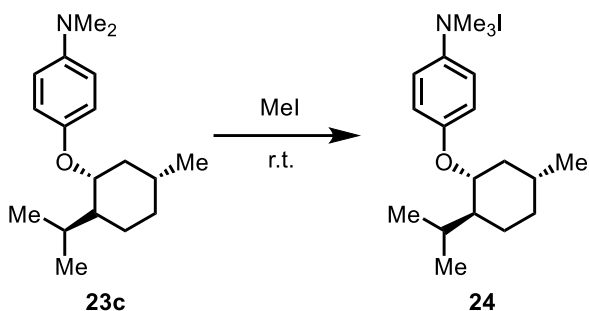
To a round bottom equipped with a stir bar was dissolved **1-99b** (344 mg, 1.39 mmol, 1.0 equiv) in acetonitrile (5 mL). K_2CO_3 (384 mg, 2.78 mmol, 2.0 equiv) and an aqueous formaldehyde solution (37%) (0.62 mL, 8.34 mmol, 6.0 equiv) were added and the reaction was stirred for 30 min. The reaction was then cooled in an ice bath for 5 min before adding sodium triacetoxyborohydride (883 mg, 4.17 mmol, 3.0 equiv) in 200 mg portions over 5 min. Acetic acid (1 mL) was slowly added and the reaction was warmed and allowed to stir at room temperature overnight. Quench the reaction with 15 mL H_2O and 15 mL EtOAc. Basify with sat. NaHCO_3 and extract 3x25 mL EtOAc. Wash organic layers with 1x25 mL brine and dry over sodium sulfate before concentrating. The product was obtained as a light brown crystalline solid in 88% yield (336 mg, 1.21 mmol) with no need for further purification.²⁵⁴

^1H NMR (400 MHz, Chloroform-*d*) δ 6.84 (d, $J = 9.0$ Hz, 2H), 6.72 (d, $J = 8.9$ Hz, 2H), 3.85 (td, $J = 10.5, 4.2$ Hz, 1H), 2.87 (s, 6H), 2.29 (pd, $J = 7.1, 2.7$ Hz, 1H), 2.12 (d, $J = 12.4$ Hz, 1H), 1.70 (dt, $J = 14.6, 3.8$ Hz, 2H), 1.55 – 1.33 (m, 3H), 1.07 (td, $J = 13.2, 9.6$ Hz, 2H), 0.98 (m, 1H), 0.92 (dd, $J = 15.7, 6.7$ Hz, 6H), 0.80 (d, $J = 6.9$ Hz, 3H).

^{13}C NMR (100 MHz, Chloroform-*d*) δ 150.57, 145.97, 117.81, 114.88, 79.02, 48.34, 41.91, 40.76, 34.73, 31.61, 26.06, 23.74, 22.34, 21.04, 16.62.

HRMS (ESI) (m/z): $[\text{M}+\text{H}]$ calculated for $\text{C}_{18}\text{H}_{29}\text{NO}$, 276.2327, found, 276.2323.

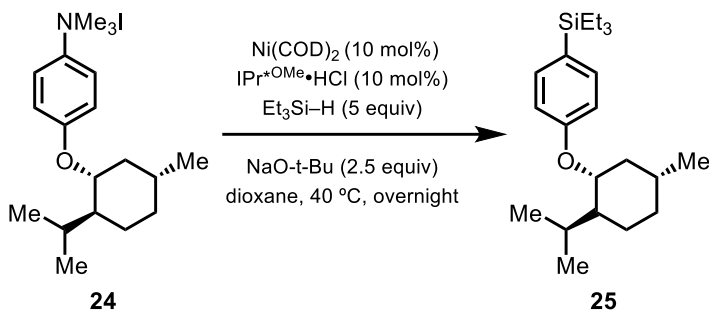
4-(((1*R*,2*R*,5*R*)-2-isopropyl-5-methylcyclohexyl)oxy)-*N,N,N*-trimethylammoniumaniline iodide (1-100)



To a dry vial with a stirbar was added **1-99c** (336 mg, 1.21 mmol, 1 equiv) and MeI (0.75 mL, 12.10 mmol, 10 equiv). The vial was sealed with a Teflon cap and stirred until the reaction solidified (~5 hours).

The contents were suspended in Et₂O and filtered, washing with 3x10 mL Et₂O to remove any unreacted starting material. The ammonium salt was dried on high vac for ~2 hours and used as is for subsequent reactions. The product was obtained as a white powder in 83% yield (419 mg, 1.00 mmol) and used without further purification.

triethyl(4-(((1*R*,2*R*,5*R*)-2-isopropyl-5-methylcyclohexyl)oxy)phenyl)silane (1-100a)



The general procedure for silylation was followed using *N,N,N*-trimethylanilinium iodide **1-100** (87 mg, 0.208 mmol) and triethylsilane (160

μL, 1 mmol). Purification by flash chromatography (100% hexanes) gave the title compound as a clear oil in 58% yield (40 mg, 0.121 mmol).

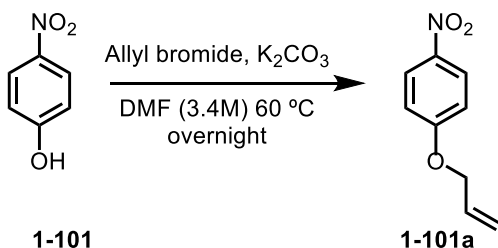
¹H NMR (500 MHz, Chloroform-*d*) δ 7.38 (d, *J* = 8.1 Hz, 1H), 6.89 (d, *J* = 8.4 Hz, 1H), 4.06 (td, *J* = 10.5, 4.3 Hz, 1H), 2.20 (ddt, *J* = 16.5, 12.8, 3.7 Hz, 1H), 1.72 (dd, *J* = 11.8,

3.1 Hz, 1H), 1.60 – 1.38 (m, 1H), 1.10 (qd, $J = 12.6, 2.9$ Hz, 1H), 1.05 – 0.87 (m, 12H), 0.84 – 0.71 (m, 7H).

^{13}C NMR (126 MHz, Chloroform-*d*) δ 159.10, 135.73, 127.87, 115.28, 77.04, 48.18, 40.46, 34.70, 31.58, 26.17, 23.87, 22.30, 20.96, 16.76, 7.61, 3.71.

HRMS (EI) (m/z): [M] calculated for $\text{C}_{22}\text{H}_{38}\text{OSi}$, 346.2692, found, 346.2682.

1-(allyloxy)-4-nitrobenzene (1-101a)

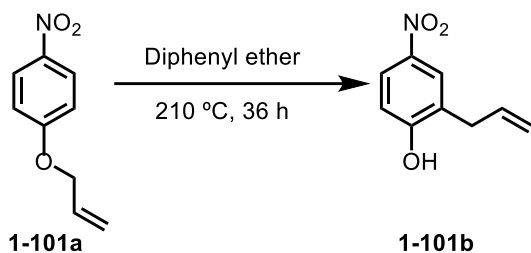


To a solution of **1-101** (1g, 7.19 mmol, 1.00 equiv) in DMF (3 mL, 2.4M) was added K₂CO₃ (1g, 7.19 mmol, 1.00 equiv). Allylbromide (0.68 mL, 7.90 mmol, 1.10 equiv) was added and a reflux condenser was added before heating to 60 °C overnight. Upon cooling to room temperature, 20 mL H₂O and 20 mL Et₂O were added and the reaction mixture was extracted 2x20 mL Et₂O. The combined organics were then washed 2x20 mL 1M NaOH, 1x20 mL brine, and dried over MgSO₄ before concentrating. The product was obtained via Kugelrohr distillation to give a yellow oil that was carried on to the next step without further purification.²⁵⁵

^1H NMR (401 MHz, Chloroform-*d*) δ 8.20 (d, $J = 9.3$ Hz, 1H), 6.97 (d, $J = 9.2$ Hz, 1H), 6.04 (ddt, $J = 17.4, 10.6, 5.3$ Hz, 1H), 5.44 (dt, $J = 17.3, 1.5$ Hz, 1H), 5.35 (dt, $J = 10.6, 1.4$ Hz, 1H), 4.64 (dt, $J = 5.4, 1.6$ Hz, 2H).

^{13}C NMR (100 MHz, Chloroform-*d*) δ 163.71, 141.73, 132.01, 126.03, 118.82, 114.84, 69.54.

2-allyl-4-nitrophenol (**1-101b**)

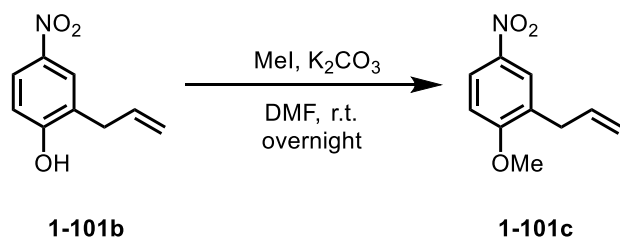


Crude **1-101a** (~1.3g) and an equal weight of diphenylether were added to a round bottom equipped with a reflux condenser. The mixture was heated to 210 °C for 36 hours. The reaction was cooled to room temperature and diluted with 30 mL Et₂O. The organics were extracted 3x30 mL 6M NaOH. The combined aqueous layers were acidified with conc. HCl. The acidic aqueous solution was then extracted 3X30 mL Et₂O. The ether layers were combined and dried over MgSO₄. The product can be recrystallized. Product was obtained as a yellow crystalline solid in 46% over two steps (593 mg, 3.31 mmol).²⁵⁵

¹H NMR (500 MHz, Chloroform-*d*) δ 8.06 (m, 2H), 6.89 (d, *J* = 8.7 Hz, 1H), 6.01 (ddt, *J* = 16.8, 10.4, 6.6 Hz, 1H), 5.88 (br, 1H), 5.30 – 5.16 (m, 2H), 3.47 (d, *J* = 6.4 Hz, 2H).

¹³C NMR (126 MHz, Chloroform-*d*) δ 159.90, 141.77, 134.72, 126.60, 126.54, 124.44, 118.19, 116.01, 34.79.

2-allyl-1-methoxy-4-nitrobenzene (**1-101c**)



In a dry round bottom, **1-101b** (1.00 g, 5.58 mmol, 1 equiv) was dissolved in DMF (10 mL). K₂CO₃ (1.77g, 12.84 mmol, 2.3 equiv) was added followed by MeI (0.80 mL, 12.84 mmol, 2.3 equiv). The mixture was stirred at room temperature overnight. The reaction was quenched with 50 ml Et₂O and 50 ml H₂O. The organics were washed 2x40 mL 1M NaOH, then 1x40 mL brine followed by drying of the organics over

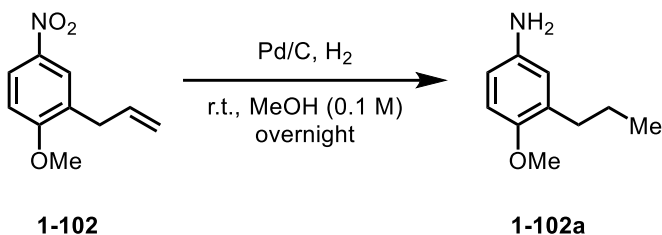
MgSO₄. The product was obtained as pure a yellow oil in 97% yield (1.05 g, 5.41 mmol) with no need for further purification.²⁵⁶

¹H NMR (500 MHz, Chloroform-*d*) δ 8.14 (dd, *J* = 9.0, 2.8 Hz, 1H), 8.05 (d, *J* = 2.8 Hz, 1H), 6.90 (d, *J* = 9.0 Hz, 1H), 5.96 (ddt, *J* = 16.9, 10.1, 6.7 Hz, 1H), 5.21 – 5.03 (m, 2H), 3.94 (s, 3H), 3.41 (d, *J* = 6.6 Hz, 2H).

¹³C NMR (176 MHz, Chloroform-*d*) δ 162.41, 141.44, 135.16, 130.04, 125.44, 124.16, 117.14, 109.80, 56.23, 34.07.

HRMS (ESI) (*m/z*): [M+H] calculated for C₁₀H₁₅NO, 194.0812, found, 194.0811.

4-methoxy-3-propylaniline (1-102a)



To a round bottom equipped with a stir bar was added **1-102** (1.05 g, 5.43 mmol) and palladium on carbon (10%) (144 mg, 2.5 mol%). The

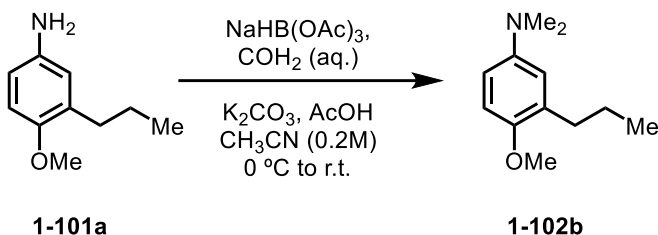
flask was backfilled three times with nitrogen before adding methanol (50 mL). The flask was then backfilled three times with H₂ before attaching a H₂ balloon. The reaction was left to stir at room temperature overnight. The contents of the flask were then filtered through Celite with DCM. The filtrate was concentrated to give the title compound in quantitative yield as an off-white crystalline solid.

¹H NMR (400 MHz, Chloroform-*d*) δ 6.68 (d, *J* = 8.3 Hz, 1H), 6.57 – 6.47 (m, 2H), 3.75 (s, 3H), 3.37 (s, 2H), 2.55 – 2.47 (m, 3H), 1.58 (h, *J* = 7.3 Hz, 3H), 0.95 (t, *J* = 7.3 Hz, 3H).

¹³C NMR (100 MHz, Chloroform-*d*) δ 151.02, 139.68, 132.35, 117.86, 113.26, 111.96, 56.21, 32.40, 23.24, 14.26.

HRMS (ESI) (m/z): [M+H] calculated for C₁₀H₁₅NO, 166.1226, found, 166.1225.

4-methoxy-*N,N*-dimethyl-3-propylaniline (1-102b)



To a round bottom equipped with a stir bar was dissolved **1-102a** (897 mg, 5.43 mmol, 1.0 equiv) in acetonitrile (25 mL). K₂CO₃ (1.5 g,

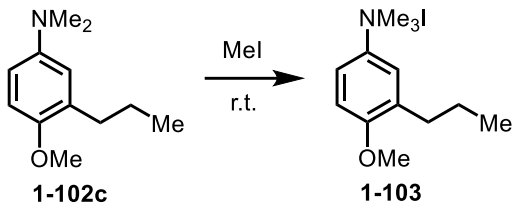
10.86 mmol, 2.0 equiv) and an aqueous formaldehyde solution (37%) (2.42 mL, 32.58 mmol, 6.0 equiv) were added and the reaction was stirred for 30 min. The reaction was then cooled in an ice bath for 5 min before adding sodium triacetoxyborohydride (3.45 mg, 16.29 mmol, 3.0 equiv) in 500 mg portions over 5 min. Acetic acid (2.5 mL) was slowly added and the reaction was warmed and allowed to stir at room temperature overnight. Quench the reaction with 50 mL H₂O and 50 mL EtOAc. Basify with sat. NaHCO₃ and extract 3x50 mL EtOAc. Wash organic layers with 1x25 mL brine and dry over sodium sulfate before concentrating. The product was obtained as a crystalline solid in 83% yield (876 mg, 4.51 mmol) with no need for further purification.

¹H NMR (400 MHz, Chloroform-*d*) δ 6.78 (d, *J* = 8.8 Hz, 1H), 6.66 (d, *J* = 3.2 Hz, 1H), 6.60 (dd, *J* = 8.8, 3.1 Hz, 1H), 3.77 (s, 3H), 2.86 (s, 6H), 2.57 (dd, *J* = 8.8, 6.7 Hz, 2H), 1.62 (h, *J* = 7.4 Hz, 2H), 0.97 (t, *J* = 7.3 Hz, 3H).

¹³C NMR (100 MHz, Chloroform-*d*) δ 150.36, 145.66, 132.02, 116.69, 111.85, 111.83, 56.24, 42.06, 32.93, 23.49, 14.33.

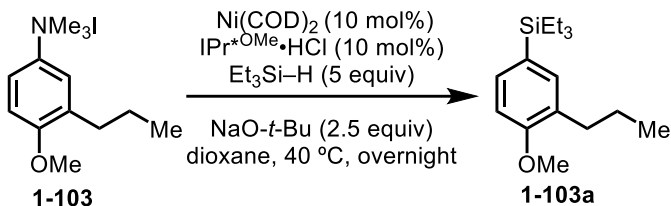
HRMS (ESI) (m/z): [M+H] calculated for C₁₂H₁₉NO, 194.1545, found, 194.1536.

4-methoxy-3-propyl-*N,N,N*-trimethylammoniumaniline iodide (**1-103**)



To a dry vial with a stirbar was added **1-102c** (860 mg, 4.53 mmol, 1 equiv) and MeI (2.82 mL, 45.30 mmol, 10 equiv). The vial was sealed with a Teflon cap and stirred until the reaction solidified (~5 hours). The contents were suspended in Et₂O and filtered, washing with 3x15 mL Et₂O to remove any unreacted starting material. The ammonium salt was dried on high vac for ~2 hours and used as is for subsequent reactions. The product was obtained as a white crystalline powder in 88% yield (1.33g, 3.99 mmol) and used without further purification.

triethyl(4-methoxy-3-propylphenyl)silane (**1-103a**)



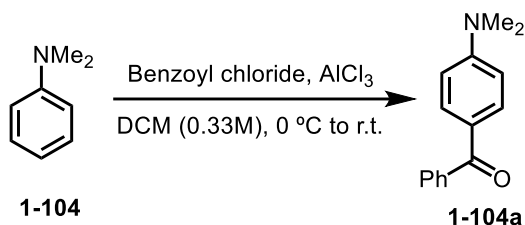
The general procedure for silylation was followed using *N,N,N*-trimethylanilinium iodide **1-103** (67 mg, 0.200 mmol) and triethylsilane (160 μL, 1 mmol). Purification by flash chromatography (100% hexanes) gave the title compound as a clear oil in 77% yield (41 mg, 0.154 mmol).

¹H NMR (401 MHz, Chloroform-*d*) δ 7.30 (dd, *J* = 8.0, 1.6 Hz, 1H), 7.22 (d, *J* = 1.7 Hz, 1H), 6.85 (d, *J* = 8.1 Hz, 1H), 3.82 (s, 3H), 2.75 – 2.36 (m, 2H), 1.61 (q, *J* = 7.5 Hz, 2H), 1.11 – 0.87 (m, 9H), 0.76 (q, *J* = 7.9 Hz, 3H).

¹³C NMR (126 MHz, Chloroform-*d*) δ 158.31, 136.02, 133.28, 130.39, 127.70, 109.84, 55.18, 32.60, 23.20, 14.27, 7.63, 3.72.

HRMS (ESI) (*m/z*): [M+Na] calculated for C₁₆H₂₈OSi, 287.1802, found, 287.1802.

(4-(dimethylamino)phenyl)(phenyl)methanone (**1-104a**)

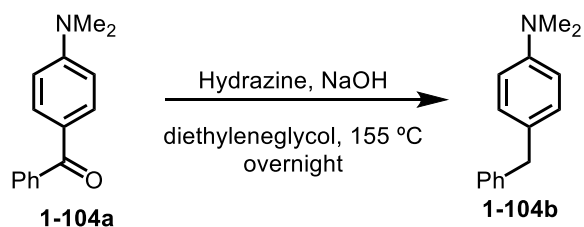


To a suspension of AlCl_3 (520 mg, 3.92 mmol, 1.00 equiv) in DCM (12.5 mL) at 0°C was slowly added benzoylchloride (0.46 mL, 3.92 mmol, 1.00 equiv). Dimethylaniline (0.52 mL, 4.12 mmol, 1.05 equiv) was then added dropwise and the reaction was stirred at 0°C for 4 hours before stirring at room temperature for 3 hours. Dilute reaction mixture with DCM and add ~15 mL H_2O . Wash organic layer 2x20 mL H_2O , 2x20 mL sat. NaHCO_3 , 1x20 mL brine. Dry organic layer over Na_2SO_4 and concentrate. Purification by flash chromatography (90:10 hexanes/ EtOAc) gave the title compound as a yellow solid in 43% yield (401 mg, 1.69 mmol) (*p*-/*o*- benzylation observed in ~2:1 ratio).²⁵⁷

$^1\text{H NMR}$ (401 MHz, Chloroform-*d*) δ 7.80 (d, $J = 9.0$ Hz, 2H), 7.75 – 7.68 (m, 2H), 7.57 – 7.50 (m, 1H), 7.48 – 7.42 (m, 2H), 6.68 (d, $J = 9.0$ Hz, 2H), 3.08 (s, 6H).

$^{13}\text{C NMR}$ (100 MHz, Chloroform-*d*) δ 195.26, 153.42, 139.44, 132.86, 131.22, 129.57, 128.12, 124.91, 110.67, 40.19.

4-benzyl-*N,N*-dimethylaniline (**1-104b**)



NaOH (1.02g, 25.5 mmol, 5 equiv) and hydrazine hydrate (1.25g, 25.5 mmol, 5 equiv) were added to a round bottom containing **1-104a** (1.17g, 5.1 mmol, 1 equiv) in ethylene glycol (30 mL). A reflux condenser was attached, and the mixture was

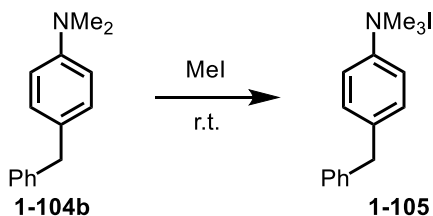
heated to 155 °C overnight. The reaction mixture was cooled to room temperature and diluted with 50 mL EtOAc and 50 mL H₂O. The mixture was then extracted 2x50 mL EtOAc. The organic layers were dried over Na₂SO₄ and concentrated. Purification by flash chromatography (95:5 hexanes/EtOAc) gave the title compound as a clear oil in 80% yield (860 mg, 4.08 mmol).²⁵⁷

¹H NMR (500 MHz, Chloroform-*d*) δ 7.28 (d, *J* = 8.0 Hz, 2H), 7.20 – 7.15 (m, 3H), 7.07 (d, *J* = 8.9 Hz, 2H), 6.70 (d, *J* = 8.8 Hz, 2H), 3.90 (s, 2H), 2.91 (s, 6H).

¹³C NMR (126 MHz, Chloroform-*d*) δ 149.28, 142.20, 129.67, 129.38, 128.94, 128.47, 113.09, 41.06, 40.98.

HRMS (EI) (*m/z*): [M] calculated for C₁₇H₃₄O₂Si, 377.1759, found, 377.1764.

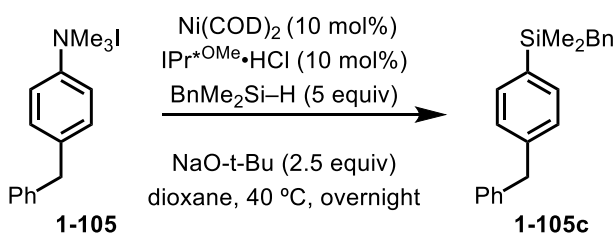
4-benzyl-*N,N,N*-trimethylammoniumaniline iodide (1-105)



To a dry vial with a stirbar was added **1-104b** (860 mg, 4.07 mmol, 1 equiv) and MeI (2.55 mL, 41.00 mmol, 10 equiv). The vial was sealed with a Teflon cap and stirred until the reaction solidified (~5 hours). The

contents were suspended in Et₂O and filtered, washing with 3x15 mL Et₂O to remove any unreacted starting material. The ammonium salt was dried on high vac for ~2 hours and used as is for subsequent reactions. The product was obtained as a white crystalline powder in 83% yield (1.2g, 2.80 mmol) and used without further purification.

benzyl(4-benzylphenyl)dimethylsilane (1-104c)



The general procedure for silylation was followed using *N,N,N*-trimethylanilinium iodide **1-105** (76 mg, 0.215 mmol) and

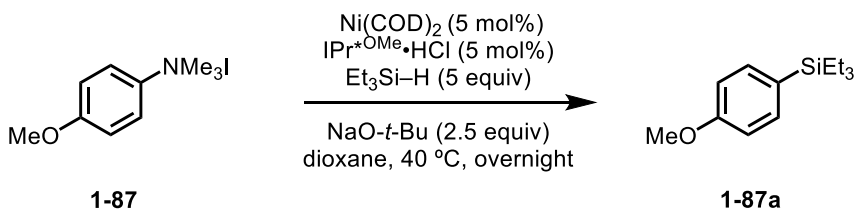
benzyl(dimethyl)silane (158 μ L, 1 mmol). Purification by flash chromatography (100% hexanes) gave an inseparable mixture of the title compound in 66% yield (45 mg, 0.142 mmol) and 1,2-dibenzyl-1,1,2,2-tetramethyldisilane (12 mg, 0.040 mmol).

$^1\text{H NMR}$ (500 MHz, Chloroform-*d*) δ 7.39 (dd, $J = 8.1, 2.6$ Hz, 2H), 7.31 (td, $J = 7.7, 7.2, 2.3$ Hz, 2H), 7.20 (dq, $J = 14.3, 6.1$ Hz, 7H), 7.11 – 7.03 (m, 2H), 6.95 (dd, $J = 8.0, 2.7$ Hz, 2H), 4.00 (s, 2H), 2.30 (d, $J = 2.7$ Hz, 2H), 0.23 (d, $J = 2.8$ Hz, 6H).

$^{13}\text{C NMR}$ (126 MHz, Chloroform-*d*) δ 142.15, 141.07, 139.88, 135.93, 134.06, 129.11, 128.61, 128.50, 128.45, 128.23, 128.14, 126.24, 124.18, 124.04, 42.09, 32.20, 28.99, 26.37, 0.74, -3.25.

HRMS (EI) (m/z): [M] calculated for $\text{C}_{22}\text{H}_{24}\text{Si}$, 316.1647, found, 316.1641.

4.2.7 Large Scale Silylation:



To a 50 mL round bottom was added $\text{Ni}(\text{COD})_2$ (45 mg,

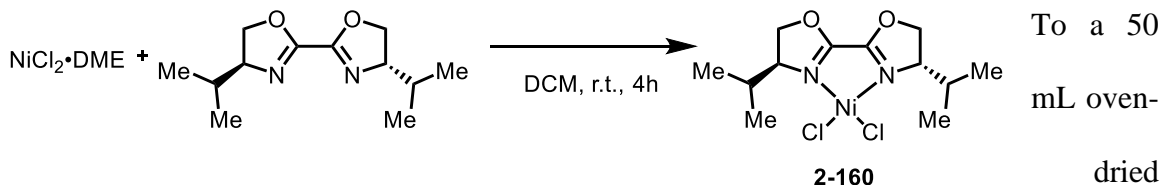
0.16 mmol, 0.05 equiv), *N,N'*-bis(2,6-bis(diphenylmethyl)-4-methoxyphenyl)imidazolium chloride ($\text{IPr}^*\text{OMe}\cdot\text{HCl}$) (160 mg, 0.16 mmol, 0.05 equiv), $\text{NaO-}t\text{-Bu}$ (787 mg, 8.17 mmol, 2.5 equiv), and **1-87** (3.27 mmol, 1 equiv) were combined under inert atmosphere and suspended in 15 mL of dioxane at rt. Silane (2.61 mL, 16.35 mmol, 5 equiv) was added and the vial was sealed with a Teflon cap before removing from the glovebox to heat to 40

°C overnight. Upon completion, the reaction mixture was filtered through Celite with DCM, the solvent was removed by rotary evaporation, and the crude reaction mixture was purified by silica gel chromatography (100% hexanes to 95:5 hexanes/ EtOAc) to give the title compound as a clear oil in 78% yield (569 mg, 2.55 mmol).

4.3 Experimental Details for Chapter 2

4.3.1 Synthesis of Catalysts and Ligands:

Synthesis of discrete *i*-PrBiOxNiCl₂ catalyst:



round-bottom flask with a Teflon-coated magnetic stir bar in a glovebox was added NiCl₂·DME (91.6 mg, 0.42 mmol, 1.0 equiv) and *i*-PrBiOx (112 mg, 0.5 mmol, 1.2 equiv) and DCM (15 mL, 0.03 M). The mixture turned homogenous and reaction was stirred for 4 hours before stripping the solvent by high vacuum. The brownish residue was then taken up in 3 mL DCM and Et₂O was added to precipitate a white solid, which was filtered off. Pentanes were then added to the mother liquor resulting in further precipitation. This precipitate was then washed with pentanes and Et₂O and dried under high vacuum for 1 hour to give an off-white powder (94.8 mg, 0.267 mmol, 64%). The powder was dissolved in C₆D₆ and was observed to be paramagnetic by NMR.

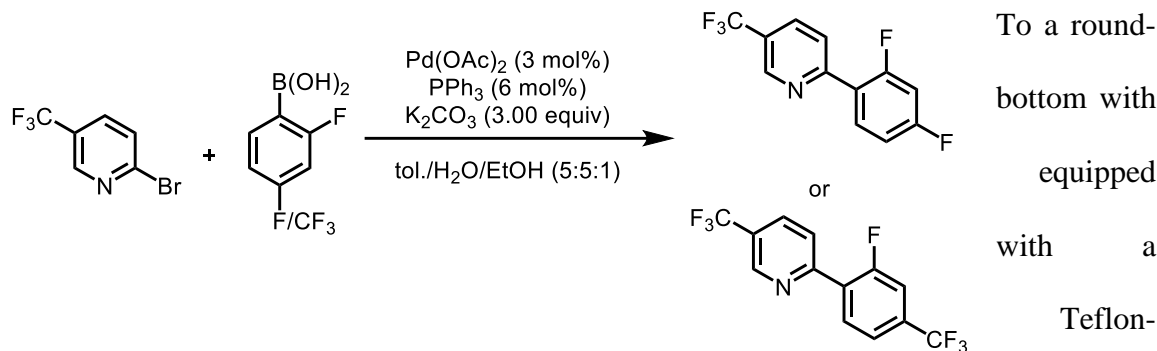
¹H NMR (401 MHz, Chloroform-*d*) δ 23.03 ppm (br, 2H) 19.02 ppm, (br, 2H) 2.63 ppm (br, 3H), 2.00 (br, 4H), 1.70 ppm (br, 6H), and 0.87 ppm (br, 1H).

UV-Vis (EtOAc, ambient temperature): $\lambda_{\text{max}} = 272 \text{ nm}$ ($4,100 \text{ M}^{-1}\text{cm}^{-1}$)

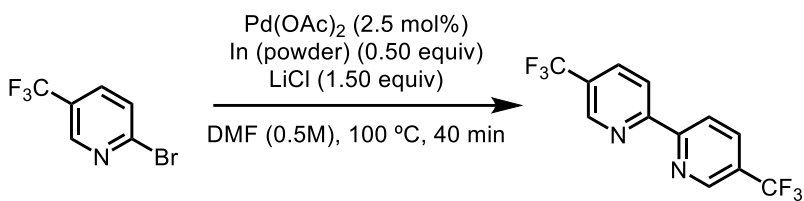
and 228 nm ($3,600 \text{ M}^{-1}\text{cm}^{-1}$)

IR (neat, ambient temperature): 1651 cm^{-1} (C=N)

Synthesis of bpy and ppy ligands for photocatalysts:



coated magnetic stir bar and a reflux condenser was added 2-bromo-5-trifluoromethylpyridine (1.51 g, 6.70 mmol, 1.0 equiv), boronic acid (8.02 mmol, 1.2 equiv), Pd(OAc)₂ (45 mg, 0.201 mmol, 3 mol%), PPh₃ (105 mg, 0.402 mmol, 6 mol%), and K₂CO₃ (2.78 g, 20.10 mmol, 3.0 equiv). The flask was backfilled with N₂ three times before adding toluene (6.7 mL, 1 M), H₂O (6.7 mL, 1 M), and EtOH (1.2 mL, 5.6 M) and heating to reflux overnight. The flask was cooled to room temperature and diluted with 20 mL H₂O and extracted 3 x 30 mL EtOAc. The organic layers were dried with 50 mL brine and then Na₂SO₄ before removing the solvent by rotary evaporation. The crude reaction mixture was purified by silica gel chromatography (100% hexanes to 97.5:2.5 hexanes/EtOAc to 80:20 hexanes/EtOAc) to give a white crystalline solid (1.307 g, 4.489 mmol 67% yield for FCF₃(CF₃)ppy or 1.389g, 5.36 mmol, 80% yield for dF(CF₃)ppy). The spectral data matched that previously reported in the literature.¹⁵⁵



To a round-bottom with equipped with a Teflon-coated magnetic stir bar

and equipped to a reflux condenser was added Pd(OAc)_2 (25 mg, 0.11 mmol, 2.5 mol%), indium powder (255 mg, 2.22 mmol, 0.5 equiv), 2-bromo-4-trifluoromethylpyridine (1.0 g, 4.44 mmol, 1.0 equiv), and LiCl (283 mg, 6.66 mmol, 1.5 equiv). The flask was backfilled with N_2 three times before adding DMF (10 mL, 0.44 M). The reaction was heated to 100 °C for 40 minutes. The flask was cooled to room temperature and the mixture diluted with 25 mL H_2O and extracted 3 x 30 mL Et_2O , the organics were washed 2 x 50 mL H_2O , then dried with 50 mL brine and then MgSO_4 before removing the solvent by rotary evaporation. The crude reaction mixture was purified by silica gel chromatography (100% hexanes to 90:10 hexanes/ EtOAc) to give a white solid (450 mg, 1.54 mmol, 69% yield). The spectral data matched that previously reported in the literature.²³⁰

^1H NMR (401 MHz, Chloroform-*d*) δ 8.96 (s, 1H), 8.63 (d, J = 8.3 Hz, 1H), 8.09 (d, J = 8.4 Hz, 1H).

^{13}C NMR (126 MHz, Chloroform-*d*) δ 157.85, 146.46 (q, J = 4.2 Hz), 134.46 (q, J = 3.6 Hz), 127.43, 127.17, 123.66 (q, J = 272.3 Hz), 121.41.

^{19}F NMR (471 MHz, Chloroform-*d*) δ -62.53.

4.3.2 General Procedures for PCET Reactions:

To an oven-dried 1 dram vial equipped with a Teflon-coated magnetic stir bar in a N_2 filled glovebox was added benzamide (0.200 mmol, 1.00 equiv), $[\text{Ir}(\text{dF}(\text{CF}_3)\text{ppy})_2(5,5'-(\text{dCF}_3)\text{bpy})]\text{PF}_6$ (4.6 mg, 0.004 mmol, 0.02 equiv), $(\text{BuO})_2\text{OP}(\text{O})(\text{NBu}_4)$ (4.5 mg, 0.004 mmol, 0.02 equiv), and dimethylfumerate (58 mg, 0.4 mmol, 2 equiv) were combined and

suspended in 1.0 mL of dry, degassed PhCF₃ at room temperature. The vial was sealed with a Teflon cap before removing from the glovebox. The reaction was stirred at 900 rpm overnight in a recrystallization dish filled with water (for cooling) and irradiated with a 34 W blue LED lamp placed 1 cm away. Upon completion, the reaction mixture was quenched with 1 mL EtOAc and run through a silica gel plug with 5 mL EtOAc. The solvent was removed by rotary evaporation and the crude reaction mixture was purified by silica gel chromatography.¹⁵⁵

4.3.3 Synthesis of Phosphate Bases:

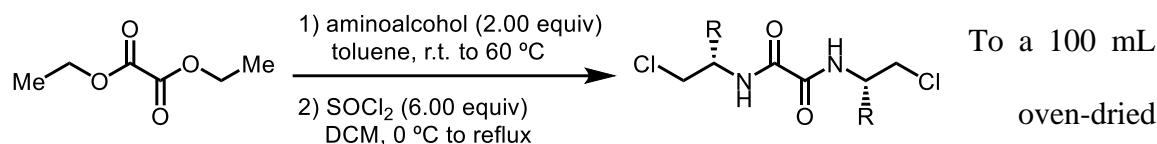
$$\text{Bu}_4\text{NOH} \text{ (37\% in MeOH) } + \text{BuO-P(=O)(OH)-BuO} \xrightarrow{\text{r.t., overnight}} \text{BuO-P(=O)(O}^-\text{)-BuO}^{\oplus} \text{NBu}_4$$
 To a 25 mL oven-dried round-bottom flask under N₂ equipped with a Teflon-coated magnetic stir bar was added dibutylphosphate (1.41 mL, 7.13 mmol, 1.0 equiv) and tetrabutylammonium hydroxide (37% in methanol) (6.31 mL, 7.13 mmol, 1.0 equiv). The reaction was stirred overnight. The next day the solvent was stripped, and the gooey residue dried under high vacuum in a heating block set to 50 °C for several days or until the goo solidified. The solid was then finely ground and further dried under high vacuum overnight. The product was then stored in the glovebox (very hygroscopic!). The spectral data matched that previously reported in the literature.²⁵⁸

$$\text{Bu}_4\text{NOH} \text{ (37\% in MeOH) } + \text{PhO-P(=O)(OH)-OH} \xrightarrow{\text{r.t., overnight}} \text{PhO-P(=O)(O}^-\text{)-O}^-\text{NBu}_4$$
 To a 25 mL oven-dried round-bottom flask under N₂ equipped with a Teflon-coated magnetic stir bar was added phenyldihydrogenphosphate (587 mg,

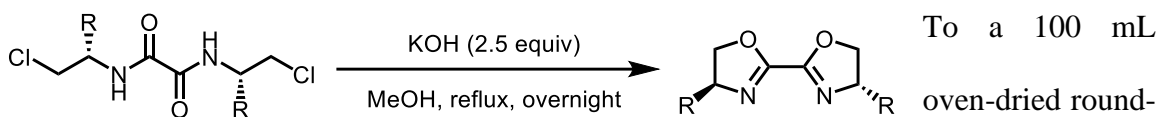
3.37 mmol, 1.0 equiv) and tetrabutylammonium hydroxide (37% in methanol) (5.20 mL, 6.75 mmol, 2.0 equiv). The reaction was stirred overnight. The next day the solvent was stripped, and the gooey residue dried under high vacuum in a heating block set to 50 °C for a week. The product was then stored in the glovebox (very hygroscopic!). The spectral data matched that previously reported in the literature.²⁰²

4.3.4 General Procedures for the Synthesis of BiOx Ligands:

Method A:

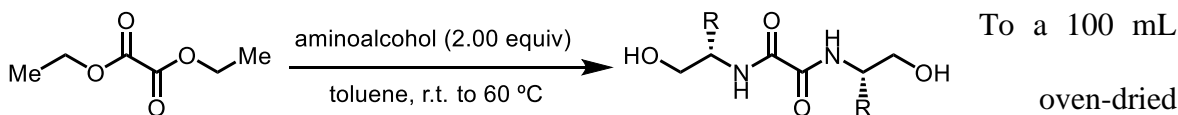


round-bottom flask under N₂ equipped with a reflux condenser and a Teflon-coated magnetic stir bar was added diethyl oxalate (0.56 mL, 4.14 mmol, 1.0 equiv) and dry toluene (32 mL, 0.12 M). Amino alcohol (8.28 mmol, 2.0 equiv) was added and the reaction was heated to 60 °C for 4 hours. A white precipitate formed, and the reaction was cooled to room temperature before filtering. The white precipitate was then washed with toluene and dried under high vacuum in a 100 mL round-bottom flask. The flask was backfilled with N₂ three times before adding DCM (32 mL, 0.13 M) and cooling to 0 °C in an ice bath. SOCl₂ (1.80 mL, 24.80 mmol, 6.0 equiv) was added slowly and the reaction was warmed to reflux and stirred overnight. The reaction was then carefully concentrated under reduced pressure using rotary evaporation. Residual SOCl₂ was removed by taking up the residue with benzene and concentrating under reduced pressure using rotary evaporation. The crude product was carried on to the next step without further purification.

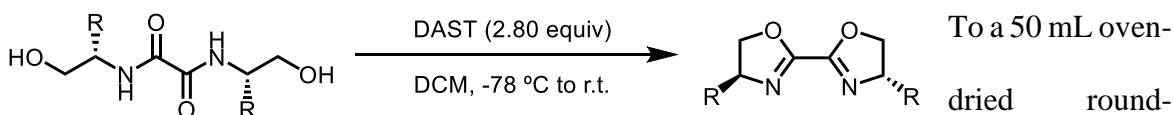


bottom flask equipped with a Teflon-coated magnetic stir bar was added crude dichloride (4.14 mmol, 1.0 equiv) and KOH (580 mg, 10.35 mmol, 2.5 equiv). The flask was backfilled with N₂ three times before adding MeOH (32 mL, 0.13 M). The mixture was then stirred at reflux overnight. The reaction was then cooled to room temperature and concentrated under reduced pressure using rotary evaporation. The residue was taken up in 50 mL DCM and washed with 50 mL H₂O and then 50 mL brine before drying the organic layer with Na₂SO₄. The solvent was removed by rotary evaporation and the white solid was then purified by silica gel chromatography.

Method B:



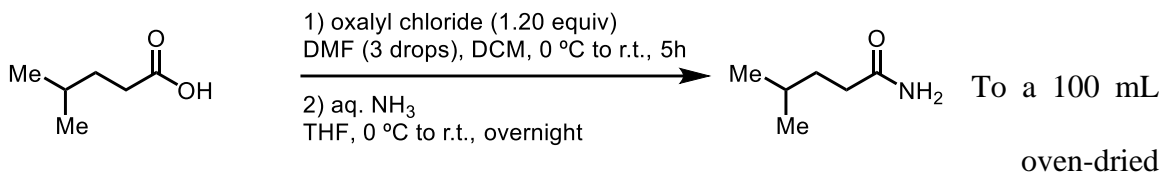
round-bottom flask under N₂ equipped with a Teflon-coated magnetic stir bar and a reflux condenser was added diethyl oxalate (0.56 mL, 4.14 mmol, 1.0 equiv) and dry toluene (32 mL, 0.12 M). Amino alcohol (8.28 mmol, 2.0 equiv) was added and the reaction was heated to 60 °C for 4 hours. A white precipitate formed, and the reaction was cooled to room temperature before filtering. The white precipitate was then washed with toluene and dried under high vacuum in a 100 mL round-bottom flask. The crude reaction was carried on to the next step without further purification.



bottom flask equipped with a Teflon-coated magnetic stir bar was added crude diol (1.00 mmol, 1.0 equiv) and the flask was backfilled with N₂ three times before adding DCM (20 mL, 0.05 M). The mixture was cooled to -78 °C in a dryice/ acetone bath and DAST (0.37 mL, 2.80 mmol, 2.8 equiv) was added dropwise. The reaction was stirred for 1 hour before adding K₂CO₃ (553 mg, 4.00 mmol, 4.0 equiv). The reaction was then warmed to room temperature and stirred for 2 hours. The reaction was quenched with 20 mL H₂O and extracted 3 x 20 mL DCM. The organics were dried with 50 mL brine before drying with Na₂SO₄. The solvent was removed by rotary evaporation and the crude reaction mixture was purified by silica gel chromatography.²³²

4.3.5 Synthesis of Starting Materials:

4-methylpentanamide



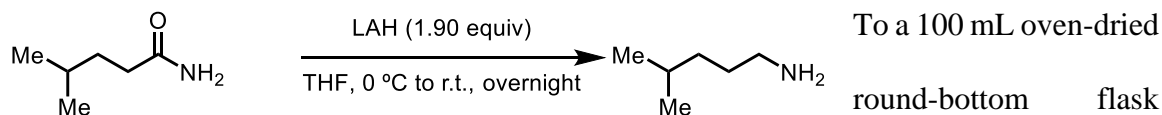
round-bottom flask equipped with a Teflon-coated magnetic stir bar was added 4-methyl valeric acid (2.0 mL, 15.90 mmol, 1.0 equiv). The flask was backfilled with N₂ three times before adding DCM (30 mL, 0.5 M) and cooling to 0 °C in an ice bath. Oxalyl chloride (1.6 mL, 19.08 mmol, 1.2 equiv) was then added followed by DMF (3-5 drops). The reaction was then allowed to warm to room temperature and stirred for 4 hours. The reaction was then concentrated under reduced pressure using rotary evaporation and used in the following step without further purification.

To a 250 mL round-bottom flask equipped with a Teflon-coated magnetic stir bar was added the crude acid chloride and THF (32 mL, 0.5 M). The flask was cooled to 0 °C in an ice bath and aq. ammonium (28%) (32 mL) was added dropwise. After the addition of aq. ammonium, the reaction was stirred for 1 hour and then extracted 3 x 100 mL EtOAc. The organic layers were dried with 150 mL brine and then Na₂SO₄. The solvent was removed by rotary evaporation to give the title compound as a white flakey solid (1.65 g, 14.31 mmol, 90% yield).

¹H NMR (400 MHz, Chloroform-*d*) δ 6.00 (s, 1H), 5.59 (s, 1H), 2.20 (t, *J* = 7.8 Hz, 2H), 1.55 (m, 3H), 0.89 (d, *J* = 6.2 Hz, 6H).

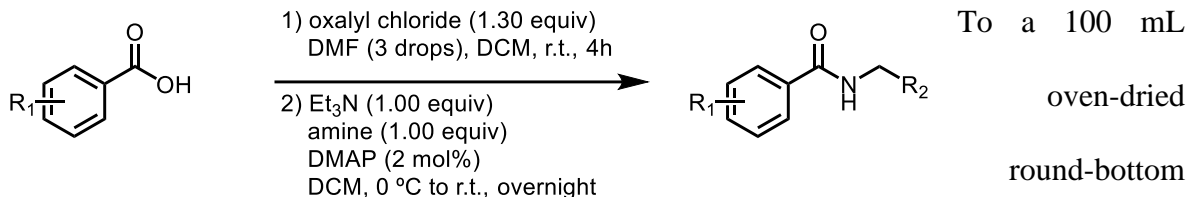
¹³C NMR (176 MHz, Chloroform-*d*) δ 176.66, 34.44, 34.03, 27.79, 22.34.

4-methylpentan-1-amine



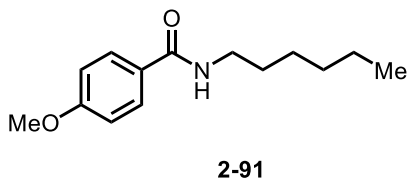
To a 100 mL oven-dried round-bottom flask equipped with a Teflon-coated magnetic stir bar was added 4-methylpentanamide (1.65 g, 14.31 mmol, 1.0 equiv) and THF (48 mL, 0.3 M). The reaction was cooled to 0 °C and LAH (1.03 g, 27.19 mmol, 1.9 equiv) in 250 mg portions. The reaction was then warmed to room temperature and stirred overnight. The reaction was cooled to 0 °C and carefully quenched with 1 mL H₂O/ 1 g LAH, then 1 mL 1 M NaOH/ 1 g LAH. The reaction was stirred for 30 minutes and then filtered and the solvent removed by rotary evaporation to give the crude amine (approximately 45% yield), which was used as is in subsequent steps.¹⁵⁴

4.3.6 General Procedures for the Synthesis of Benzamides:



flask equipped with a Teflon-coated magnetic stir bar was added benzoic acid (5.00 mmol, 1.00 equiv). The flask was backfilled with N₂ three times before adding DCM (25 mL, 0.2 M) and cooling to 0 °C in an ice bath. Oxalyl chloride (0.55 mL, 6.50 mmol, 1.30 equiv) was then added followed by DMF (3-5 drops). The reaction was then allowed to warm to room temperature and stirred for 4 hours. The reaction was then concentrated under reduced pressure using rotary evaporation. The residue was then taken up in fresh DCM (25 mL, 0.2 M) and cooled to 0 °C. Et₃N (0.70 mL, 5.00 mmol, 1.00 equiv) was added dropwise followed by amine (5.00 mmol, 1.00 equiv) and DMAP (12 mg, 0.1 mmol, 0.02 equiv). The reaction was then allowed to warm to room temperature and stirred overnight. The reaction was quenched with 10 mL H₂O and 25 mL DCM and the organics were washed 2 x 25 mL 1M HCl, 2 x 25 mL 1M NaOH, dried with 25 mL brine, and then over Na₂SO₄. The solvent was removed by rotary evaporation and the crude reaction mixture was purified by silica gel chromatography.²⁵⁹

N-hexyl-4-methoxybenzamide (2-91)



The general procedure for benzamide synthesis coupling was followed using 4-methoxybenzoic acid (600 mg, 3.94 mmol, 1.00 equiv), oxalyl chloride (0.43 mL, 5.13 mmol, 1.30 equiv), DCM (20 mL, 0.2 M), DMF (3 drops), Et₃N (0.55 mL, 3.94 mmol, 1.00

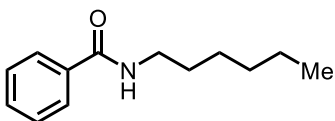
equiv), *n*-hexylamine (0.52 mL, 3.94 mmol, 1.00 equiv) and DMAP (10 mg, 0.10 mmol, 0.02 equiv). Purification by aqueous work-up gave the title compound as a white solid (870 mg, 3.70 mmol, 94% yield over two steps). The spectral data matches that previously reported in the literature.

Rf: 0.20 (70:30 hexanes/EtOAc)

¹H NMR (400 MHz, Chloroform-*d*) δ 7.72 (d, *J* = 8.7 Hz, 2H), 6.92 (d, *J* = 8.5 Hz, 2H), 6.02 (s, 1H), 3.84 (s, 3H), 3.43 (q, *J* = 6.7 Hz, 2H), 1.60 (p, *J* = 7.2 Hz, 2H), 1.53 – 1.19 (m, 6H), 1.06 – 0.79 (t, *J* = 6.5 Hz, 3H).

¹³C NMR (126 MHz, Chloroform-*d*) δ 167.12, 162.04, 128.73, 127.26, 113.70, 55.43, 40.15, 31.62, 29.79, 26.78, 22.65, 14.10.

***N*-hexylbenzamide**



To a 100 mL oven-dried round-bottom flask equipped with a Teflon-coated magnetic stir bar under N₂ was added benzoylchloride (1 mL, 8.60 mmol, 1.00 equiv) and DCM (25 ml, 0.2 M). The flask was cooled to 0 °C and Et₃N (1.20 mL, 8.60 mmol, 1.00 equiv) was added dropwise followed by *n*-hexylamine (1.14 mL, 8.60 mmol, 1.00 equiv) and DMAP (20 mg, 0.17 mmol, 0.02 equiv). The reaction was then allowed to warm to room temperature and stirred overnight. The reaction was quenched with quenched with 10 ml H₂O and 25 mL DCM and the organics were washed 2 x 25 mL 1M HCl, 2 x 25 mL 1M NaOH, dried with 25 mL brine, and then over Na₂SO₄. The solvent was removed by rotary evaporation and the crude reaction mixture was purified by silica gel chromatography (100% hexanes to 80:20

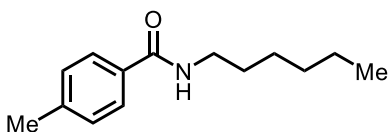
hexanes/EtOAc) to give the title compound as a white solid (1.628 g, 7.91 mmol, 92% yield).

Rf: 0.15 (80:20 hexanes/EtOAc)

¹H NMR (400 MHz, Chloroform-*d*) δ 7.76 (d, $J = 7.3$ Hz, 2H), 7.61 – 7.38 (m, 3H), 6.09 (s, 1H), 3.46 (q, $J = 6.7$ Hz, 2H), 1.61 (h, $J = 7.2$ Hz, 2H), 1.48 – 1.16 (m, 6H), 0.95 – 0.84 (t, $J = 6.5$ Hz, 3H).

¹³C NMR (126 MHz, Chloroform-*d*) δ 167.64, 134.89, 131.17, 128.40, 126.97, 40.17, 31.54, 29.64, 26.71, 22.58, 14.03.

***N*-hexyl-4-methylbenzamide**



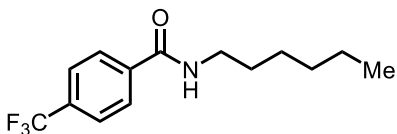
The general procedure for benzamide synthesis coupling was followed using 4-methylbenzoic acid (681 mg, 5.00 mmol, 1.00 equiv), oxalyl chloride (0.55 mL, 6.50 mmol, 1.30 equiv), DCM (25 mL, 0.2 M), DMF (3 drops), Et₃N (0.70 mL, 5.00 mmol, 1.00 equiv), *n*-hexylamine (0.66 mL, 5.00 mmol, 1.00 equiv) and DMAP (12 mg, 0.10 mmol, 0.02 equiv). Purification by silica gel chromatography (80:20 hexanes/EtOAc) gave the title compound as a white solid (1.024 g, 4.65 mmol, 93% yield over two steps).

Rf: 0.25 (80:20 hexanes/EtOAc)

¹H NMR (700 MHz, Chloroform-*d*) δ 7.65 (s, 1H), 7.21 (d, $J = 7.8$ Hz, 2H), 6.15 (s, 1H), 3.43 (td, $J = 7.3, 5.8$ Hz, 2H), 2.38 (s, 3H), 1.59 (p, $J = 7.4$ Hz, 2H), 1.37 (dq, $J = 12.1, 6.9, 6.5$ Hz, 2H), 1.33 – 1.28 (m, 4H), 0.88 (t, $J = 6.6$ Hz, 3H).

¹³C NMR (126 MHz, Chloroform-*d*) δ 167.55, 141.48, 132.05, 129.06, 126.96, 40.11, 31.56, 29.68, 26.73, 22.59, 21.40, 14.04.

***N*-hexyl-4-(trifluoromethyl)benzamide**



The general procedure for benzamide synthesis coupling was followed using 4-trifluoromethylbenzoic acid (500 mg, 2.63 mmol, 1.00 equiv), oxalyl chloride (0.29 mL, 3.42 mmol, 1.30 equiv), DCM (11 mL, 0.2 M), DMF (3 drops), Et₃N (0.48 mL, 3.42 mmol, 1.00 equiv), *n*-hexylamine (0.45 mL, 3.42 mmol, 1.00 equiv) and DMAP (10 mg, 0.1 mmol, 0.02 equiv). Purification by aqueous work-up followed by silica gel chromatography (80:20 hexanes/EtOAc) gave the title compound as a yellowish crystalline solid (573 mg, 2.74 mmol, 80% yield over two steps).

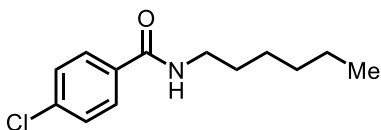
Rf: 0.20 (80:20 hexanes/EtOAc)

¹H NMR (400 MHz, Chloroform-*d*) δ 7.87 (d, $J = 8.0$ Hz, 2H), 7.70 (d, $J = 8.0$ Hz, 2H), 6.11 (s, 1H), 3.47 (q, $J = 6.9$ Hz, 2H), 1.63 (p, $J = 7.4$ Hz, 2H), 1.56 – 1.21 (m, 6H), 0.91 (t, $J = 6.5$ Hz, 3H).

¹³C NMR (126 MHz, Chloroform-*d*) δ 166.52 (d, $J = 3.3$ Hz), 138.25, 133.07 (q, $J = 32.5$ Hz), 127.51, 125.54 (q, $J = 3.8$ Hz), 123.77 (q, $J = 272.5$ Hz), 40.45, 31.58, 29.61, 26.77, 22.63, 14.04.

¹⁹F NMR (471 MHz, Chloroform-*d*) δ -63.05.

4-chloro-*N*-hexylbenzamide



The general procedure for benzamide synthesis coupling was followed using 4-chlorobenzoic acid (783 mg, 5.00 mmol, 1.00 equiv), oxalyl chloride (0.55 mL, 6.50 mmol, 1.30 equiv), DCM (25 mL, 0.2

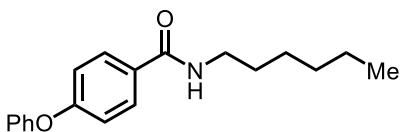
M), DMF (3 drops), Et₃N (0.70 mL, 5.00 mmol, 1.00 equiv), *n*-hexylamine (0.66 mL, 5.00 mmol, 1.00 equiv) and DMAP (12 mg, 0.10 mmol, 0.02 equiv). Purification by silica gel chromatography (80:20 hexanes/EtOAc) gave the title compound as a white solid (1.079 g, 4.50 mmol, 93% yield over two steps).

Rf: 0.20 (80:20 hexanes/EtOAc)

¹H NMR (400 MHz, Chloroform-*d*) δ 7.69 (d, *J* = 8.4 Hz, 2H), 7.37 (dd, *J* = 8.6, 2.3 Hz, 2H), 6.28 (s, 1H), 3.41 (q, *J* = 7.5, 6.7 Hz, 2H), 1.59 (p, *J* = 7.3 Hz, 2H), 1.49 – 1.09 (m, 6H), 0.87 (t, *J* = 6.5 Hz, 3H).

¹³C NMR (126 MHz, Chloroform-*d*) δ 166.64, 137.51, 133.31, 128.75, 128.46, 40.33, 31.59, 29.66, 26.77, 22.64, 14.09.

***N*-hexyl-4-phenoxybenzamide**



The general procedure for benzamide synthesis coupling was followed using 4-phenoxybenzoic acid (1.07 g, 5.00 mmol, 1.00 equiv), oxalyl chloride (0.55 mL, 6.50 mmol,

1.30 equiv), DCM (25 mL, 0.2 M), DMF (3 drops), Et₃N (0.70 mL, 5.00 mmol, 1.00 equiv), *n*-hexylamine (0.66 mL, 5.00 mmol, 1.00 equiv) and DMAP (12 mg, 0.10 mmol, 0.02 equiv). Purification by silica gel chromatography (90:10 hexanes/EtOAc) gave the title compound as a white solid (1.367 g, 4.60 mmol, 92% yield over two steps).

Rf: 0.20 (90:10 hexanes/EtOAc)

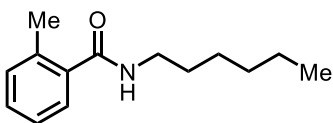
¹H NMR (500 MHz, Chloroform-*d*) δ 7.75 (dd, *J* = 13.6, 8.5 Hz, 2H), 7.39 (dt, *J* = 13.5, 7.9 Hz, 2H), 7.30 – 7.23 (m, 1H), 7.18 (dt, *J* = 14.6, 7.4 Hz, 1H), 7.04 (ddd, *J* = 19.7, 13.3,

8.2 Hz, 3H), 6.02 (s, 1H), 3.45 (dp, $J = 11.4, 5.9, 4.8$ Hz, 2H), 1.77 – 1.51 (m, 2H), 1.44 – 1.22 (m, 6H), 0.90 (m, 3H).

^{13}C NMR (126 MHz, Chloroform-*d*) δ 166.94, 160.32, 156.16, 130.05, 129.44, 128.87, 124.26, 119.79, 117.89, 40.24, 31.63, 29.79, 26.79, 22.67, 14.13.

HRMS: (ESI) (m/z): $[\text{M}+\text{H}]$ calculated for $\text{C}_{19}\text{H}_{23}\text{NO}_2$, 298.1807, found 298.1859.

***N*-hexyl-2-methylbenzamide (2-161)**



2-161

The general procedure for benzamide synthesis coupling was followed using 2-methylbenzoic acid (681 mg, 5.00 mmol, 1.00 equiv), oxalyl chloride (0.55 mL, 6.50 mmol, 1.30 equiv),

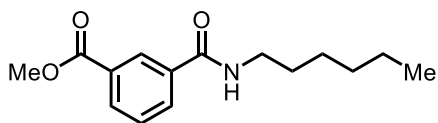
DCM (25 mL, 0.2 M), DMF (3 drops), Et_3N (0.70 mL, 5.00 mmol, 1.00 equiv), *n*-hexylamine (0.66 mL, 5.00 mmol, 1.00 equiv) and DMAP (12 mg, 0.10 mmol, 0.02 equiv). Purification by silica gel chromatography (80:20 hexanes/EtOAc) gave the title compound as a white solid (992 mg, 4.50 mmol, 90% yield over two steps).

Rf: 0.35 (70:30 hexanes/EtOAc)

^1H NMR (500 MHz, Chloroform-*d*) δ 7.36 – 7.26 (m, 2H), 7.23 – 7.15 (m, 2H), 5.77 (s, 1H), 3.41 (dd, $J = 7.0, 3.4$ Hz, 2H), 2.43 (s, 1H), 1.58 (q, $J = 7.1, 6.5$ Hz, 2H), 1.35 (m, 6H), 0.89 (t, $J = 6.8$ Hz, 3H).

^{13}C NMR (126 MHz, Chloroform-*d*) δ 170.13, 136.88, 135.83, 130.85, 129.60, 126.65, 125.62, 39.82, 31.52, 29.64, 26.66, 22.60, 19.71, 14.05.

methyl 3-(hexylcarbamoyl)benzoate



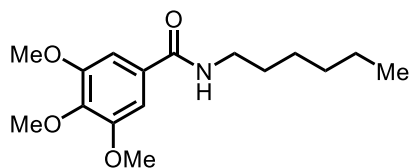
The general procedure for benzamide synthesis coupling was followed using 3-(methoxycarbonyl)benzoic acid (900 mg, 5.00 mmol, 1.00 equiv), oxalyl chloride (0.55 mL, 6.50 mmol, 1.30 equiv), DCM (25 mL, 0.2 M), DMF (3 drops), Et₃N (0.70 mL, 5.00 mmol, 1.00 equiv), *n*-hexylamine (0.66 mL, 5.00 mmol, 1.00 equiv) and DMAP (12 mg, 0.10 mmol, 0.02 equiv). Purification by silica gel chromatography (70:30 hexanes/EtOAc to 1:1 hexanes/EtOAc) gave the title compound as a white solid (1.119 g, 4.25 mmol, 85% yield over two steps).

Rf: 0.10 (70:30 hexanes/EtOAc)

¹H NMR (700 MHz, Chloroform-*d*) δ 8.34 (s, 1H), 8.10 (d, *J* = 7.8 Hz, 1H), 8.00 (d, *J* = 7.8 Hz, 1H), 7.46 (t, *J* = 7.7 Hz, 1H), 6.57 – 6.34 (m, 1H), 3.89 (s, 3H), 3.42 (d, *J* = 6.9 Hz, 2H), 1.58 (q, *J* = 7.5 Hz, 2H), 1.40 – 1.15 (m, 6H), 0.85 (t, *J* = 6.5 Hz, 3H).

¹³C NMR (176 MHz, Chloroform-*d*) δ 166.56, 166.47, 135.24, 132.25, 131.89, 130.41, 128.87, 127.60, 52.42, 40.35, 31.58, 29.67, 26.76, 22.64, 14.11.

***N*-hexyl-3,4,5-trimethoxybenzamide**



The general procedure for benzamide synthesis coupling was followed using 3,4,5-trimethoxybenzoic acid (910 mg, 5.00 mmol, 1.00 equiv), oxalyl chloride (0.55 mL, 6.50 mmol, 1.30 equiv), DCM (25 mL, 0.2 M), DMF (3 drops), Et₃N (0.70 mL, 5.00 mmol, 1.00 equiv), *n*-hexylamine (0.66 mL, 5.00 mmol, 1.00 equiv) and DMAP (12 mg, 0.10 mmol, 0.02 equiv). Purification by aqueous work-up gave the title compound as a white solid (1.255 g, 4.25 mmol, 92% yield over two steps).

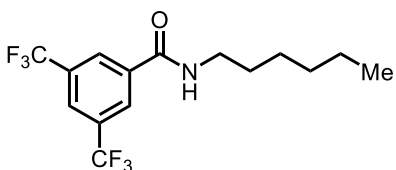
Rf: 0.20 (70:30 hexanes/EtOAc)

¹H NMR (400 MHz, Chloroform-*d*) δ 6.98 (s, 2H), 6.13 (t, $J = 5.6$ Hz, 1H), 3.89 (s, 3H), 3.87 (s, 6H), 3.42 (q, $J = 6.8$ Hz, 3H), 1.60 (p, $J = 7.3$ Hz, 2H), 1.48 – 1.19 (m, 6H), 0.88 (t, $J = 6.7$ Hz, 3H).

¹³C NMR (176 MHz, Chloroform-*d*) δ 167.26, 153.11, 140.61, 130.36, 104.30, 60.90, 56.23, 40.32, 31.56, 29.69, 26.73, 22.59, 14.07.

HRMS: (ESI) (m/z): [M+H] calculated for C₁₆H₂₅NO₄, 296.1862, found 296.1879.

***N*-hexyl-3,5-bis(trifluoromethyl)benzamide**



The general procedure for benzamide synthesis coupling was followed using 2-methylbenzoic acid (681 mg, 5.00 mmol, 1.00 equiv), oxalyl chloride (0.55 mL, 6.50 mmol, 1.30 equiv), DCM (25 mL, 0.2 M), DMF (3 drops), Et₃N (0.70 mL, 5.00 mmol, 1.00 equiv), *n*-hexylamine (0.66 mL, 5.00 mmol, 1.00 equiv) and DMAP (12 mg, 0.10 mmol, 0.02 equiv). Purification by silica gel chromatography (80:20 hexanes/EtOAc) gave the title compound as a clear oil (1.280 g, 3.75 mmol, 70% yield over two steps).

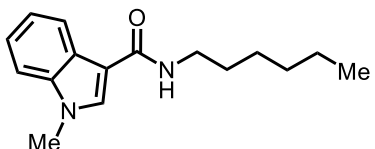
Rf: 0.15 (95:5 hexanes/EtOAc)

¹H NMR (400 MHz, Chloroform-*d*) δ 8.20 (s, 2H), 7.98 (s, 1H), 6.47 (s, 1H), 3.47 (q, $J = 6.6$ Hz, 2H), 1.63 (p, $J = 7.3$ Hz, 2H), 1.51 – 1.17 (m, 6H), 0.88 (t, $J = 6.6$ Hz, 3H).

¹³C NMR (126 MHz, Chloroform-*d*) δ 165.16, 136.95, 132.09 (q, $J = 33.9$ Hz), 127.55 (q, $J = 3.8$ Hz), 124.98 – 124.63 (m), 123.03 (q, $J = 272.9$ Hz), 40.76, 31.57, 29.50, 26.79, 22.61, 13.96.

¹⁹F NMR (471 MHz, Chloroform-*d*) δ -63.25.

***N*-hexyl-1-methyl-1*H*-indole-3-carboxamide**



The general procedure for benzamide synthesis coupling was followed using 1-methylindole-3-carboxylic acid (876 mg, 5.00 mmol, 1.00 equiv), oxalyl chloride (0.55 mL, 6.50 mmol, 1.30 equiv), DCM (25 mL, 0.2 M), DMF (3 drops), Et₃N (0.70 mL, 5.00 mmol, 1.00 equiv), *n*-hexylamine (0.66 mL, 5.00 mmol, 1.00 equiv) and DMAP (12 mg, 0.10 mmol, 0.02 equiv). Purification by silica gel chromatography (80:20 hexanes/EtOAc) gave the title compound as a white solid (1.245 g, 4.80 mmol, 96% yield over two steps).

Rf: 0.25 (80:20 hexanes/EtOAc)

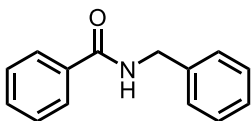
¹H NMR (500 MHz, Chloroform-*d*) δ 7.91 (dd, *J* = 8.2, 3.4 Hz, 1H), 7.65 (s, 1H), 7.36 (d, *J* = 7.9 Hz, 1H), 7.32 – 7.24 (m, 1H), 5.91 (s, 1H), 3.82 (s, 3H), 3.60 – 3.39 (m, 2H), 1.70 – 1.52 (m, 2H), 1.50 – 1.19 (m, 6H), 0.96 – 0.81 (m, 3H).

¹³C NMR (100 MHz, Chloroform-*d*) δ 165.27, 137.14, 131.95, 125.60, 122.38, 121.25, 120.34, 110.92, 109.92, 39.55, 33.08, 31.60, 29.98, 26.80, 22.61, 14.07.

IR (neat, cm⁻¹): 3303, 2951, 2924, 2855, 1608, 1540, 1522, 1461, 1125, 741.

HRMS: (ESI) (*m/z*): [*M*+Na⁺] calculated for C₁₆H₂₂N₂O, 259.1810, found 281.1626.

***N*-benzylbenzamide (2-162)**



2-162

To a 100 mL oven-dried round-bottom flask equipped with a Teflon-coated magnetic stir bar under N₂ was added benzoylchloride (0.5 mL, 4.30 mmol, 1.00 equiv) and DCM (20 mL, 0.2 M). The flask was cooled to 0 °C and Et₃N (0.60 mL, 4.30 mmol, 1.00 equiv) was added dropwise followed

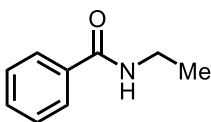
by benzylamine (0.47 mL, 4.30 mmol, 1.00 equiv) and DMAP (12 mg, 0.10 mmol, 0.02 equiv). The reaction was then allowed to warm to room temperature and stirred overnight. The reaction was quenched with quenched with 10 mL H₂O and 25 mL DCM and the organics were washed 2 x 25 mL 1M HCl, 2 x 25 mL 1M NaOH, dried with 25 mL brine, and then over Na₂SO₄. The solvent was removed by rotary evaporation to give the title compound as a white powder (845 mg, 4.00 mmol, 93% yield).

Rf: 0.15 (90:10 hexanes/EtOAc)

¹H NMR (401 MHz, Chloroform-*d*) δ 7.83 – 7.77 (m, 2H), 7.55 – 7.48 (m, 1H), 7.43 (dd, $J = 8.2, 6.9$ Hz, 2H), 7.36 (d, $J = 4.3$ Hz, 4H), 7.31 (p, $J = 4.6$ Hz, 1H), 6.40 (s, 1H), 4.66 (d, $J = 5.6$ Hz, 2H).

¹³C NMR (126 MHz, Chloroform-*d*) δ 167.51, 138.36, 134.45, 131.56, 128.79, 128.60, 127.91, 127.58, 127.10, 44.11.

***N*-ethylbenzamide (2-163)**



2-163

To an oven-dried 100-mL round-bottom flask containing a Teflon-coated magnetic stir bar and equipped to a reflux condenser was added benzamide (500 mg, 4.10 mmol, 1.00 equiv). The flask was backfilled with N₂ three times before adding cyclopentyl ether (20 mL, 0.2 M) and triethylphosphate (2.10 mL, 12.40 mmol, 3.00 equiv). *n*-BuLi (2.5 M in hexanes) (3.0 mL, 7.40 mmol, 1.80 equiv) was added dropwise and the reaction was heated to 115 °C for 24 hours. The reaction was carefully quenched with 20 mL brine and then extracted 3 x 30 mL EtOAc. The organics were then dried over Na₂SO₄ and the solvent was removed by rotary evaporation. Purification by silica gel chromatography (70:30 hexanes/EtOAc to 1:1 hexanes/EtOAc)

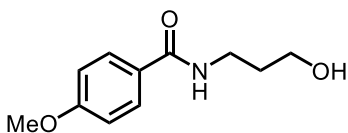
gave the title compound as a white sticky solid (274 mg, 1.84 mmol, 45% yield). The spectral data matched that previously reported in the literature.²⁶⁰

Rf: 0.10 (1:1 hexanes/EtOAc)

¹H NMR (401 MHz, Chloroform-*d*) δ 7.76 (d, $J = 7.1$ Hz, 2H), 7.54 – 7.35 (m, 3H), 6.11 (s, 1H), 3.51 (qd, $J = 7.3, 5.6$ Hz, 2H), 1.26 (t, $J = 7.3$ Hz, 2H).

¹³C NMR (126 MHz, Chloroform-*d*) δ 167.56, 134.62, 128.14, 126.90, 34.74, 14.62.

***N*-(3-hydroxypropyl)-4-methoxybenzamide**



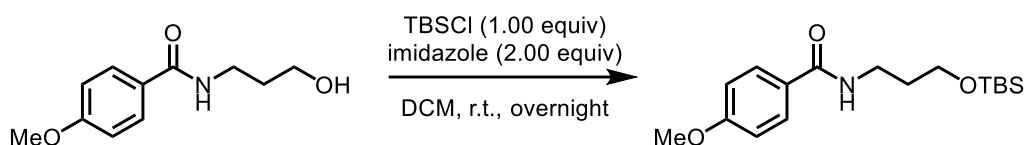
The general procedure for benzamide synthesis coupling was followed using 4-methoxybenzoic acid (5.00 g, 32.86 mmol, 1.00 equiv), oxalyl chloride (3.62 mL, 42.72 mmol, 1.30 equiv), DCM (150 mL, 0.2 M), DMF (5 drops), Et₃N (4.58 mL, 32.86 mmol, 1.00 equiv), 3-aminopropane (2.51 mL, 32.86 mmol, 1.00 equiv) and DMAP (80 mg, 0.66 mmol, 0.02 equiv). The reaction was then allowed to warm to room temperature and stirred overnight. The reaction was quenched with quenched with 100 mL H₂O and 100 mL DCM the organics were washed 2 x 100 mL 1M HCl, 2 x 100 mL 1M NaOH, dried with 150 mL brine, and then over Na₂SO₄. The solvent was removed by rotary evaporation and the crude reaction mixture was purified by silica gel chromatography (1:1 hexanes/EtOAc, then 95:5 DCM/MeOH to 90:10 DCM/MeOH) to give a white powder (1.987 g, 9.53 mmol, 29% yield).

Rf: 0.15 (95:5 DCM/MeOH)

¹H NMR (400 MHz, Methanol-*d*₄) δ 7.77 (d, *J* = 8.8 Hz, 2H), 6.96 (dt, *J* = 9.1, 3.2 Hz, 2H), 3.82 (s, 3H), 3.63 (t, *J* = 6.3 Hz, 2H), 3.45 (t, *J* = 6.9 Hz, 2H), 1.81 (p, *J* = 6.6 Hz, 2H).

¹³C NMR (176 MHz, Methanol-*d*₄) δ 169.91, 163.82, 130.02, 127.66, 114.67, 60.60, 55.88, 38.03, 33.29.

***N*-(3-((*tert*-butyldimethylsilyl)oxy)propyl)-4-methoxybenzamide**



To an oven-dried 25-mL round-bottom flask containing a Teflon-coated magnetic stir bar was added *N*-(3-hydroxypropyl)-4-methoxybenzamide (300 mg, 1.43 mmol, 1.00 equiv) and DCM (7 mL, 0.2 M). TBSCl (215 mg, 1.43 mmol, 1.00 equiv) and imidazole (195 mg, 2.86 mmol, 2.0 equiv) were added and the reaction was stirred overnight. The reaction was quenched with sat. NaHCO₃ and extracted 3 x 30 mL DCM. The organics were dried 1 x 30 mL brine and Na₂SO₄. The solvent was removed by rotary evaporation and the crude reaction mixture was purified by silica gel chromatography (70:30 hexanes/EtOAc) to give the product as a white solid (302 mg, 0.930 mmol, 65% yield).

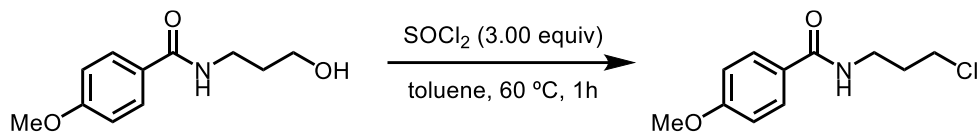
Rf: 0.45 (1:1 hexanes/EtOAc)

¹H NMR (400 MHz, Chloroform-*d*) δ 7.72 (d, *J* = 8.2 Hz, 1H), 6.90 (d, *J* = 8.0 Hz, 1H), 6.82 (s, 1H), 3.84 (s, 1H), 3.81 (d, *J* = 5.5 Hz, 1H), 3.58 (q, *J* = 5.9 Hz, 1H), 1.83 (p, *J* = 5.8 Hz, 1H), 0.90 (s, 5H), 0.08 (s, 2H).

¹³C NMR (126 MHz, Chloroform-*d*) δ 167.02, 161.99, 128.73, 127.30, 113.61, 63.04, 55.40, 39.09, 31.62, 26.04, 18.45, -5.27.

HRMS: (ESI) (*m/z*): [M+H] calculated for C₁₇H₂₉NO₃Si, 324.1995, found 324.2050.

***N*-(3-chloropropyl)-4-methoxybenzamide**



To an oven-dried 25-mL round-bottom flask containing a Teflon-coated magnetic stir bar was added *N*-(3-hydroxypropyl)-4-methoxybenzamide (300 mg, 1.43 mmol, 1.00 equiv). The flask was backfilled with N₂ three times before adding toluene (7 mL, 0.2 M) and SOCl₂ (0.31 mL, 4.29 mmol, 3.00 equiv). The reaction was heated to 60 °C and stirred for 1 hour. The reaction was carefully quenched with sat. NaHCO₃ and H₂O and extracted 3 x 30 mL DCM. The organics were dried 1 x 30 mL brine and Na₂SO₄. The solvent was removed by rotary evaporation and the crude reaction mixture was purified by silica gel chromatography (1:1 hexanes/EtOAc to 90:10 DCM/MeOH) to give the product as a white powder (151 mg, 0.658 mmol, 46% yield).

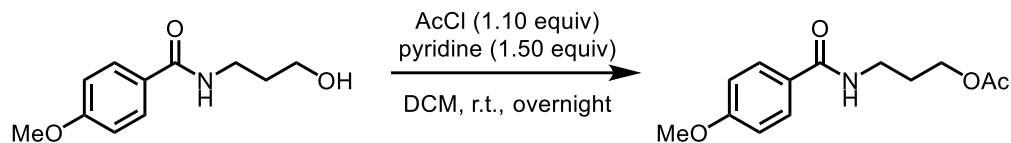
Rf: 0.2 (1:1 hexanes/EtOAc)

¹H NMR (400 MHz, Chloroform-*d*) δ 7.73 (d, *J* = 8.5 Hz, 2H), 6.93 (d, *J* = 8.5 Hz, 2H), 6.25 (s, 1H), 3.85 (s, 3H), 3.63 (m, 4H), 2.12 (p, *J* = 6.5 Hz, 2H).

¹³C NMR (126 MHz, Chloroform-*d*) δ 167.42, 162.28, 128.81, 126.75, 113.83, 55.50, 42.87, 37.68, 32.26.

HRMS: (ESI) (*m/z*): [M+H] calculated for C₁₁H₁₄ClNO₂, 228.0791, found 228.0788.

3-(4-methoxybenzamido)propyl acetate



To a 25 mL oven-dried round-bottom flask equipped with a Teflon-coated magnetic stir bar was added *N*-(3-hydroxypropyl)-4-methoxybenzamide (300 mg, 1.43 mmol, 1.00 equiv). The flask was backfilled with N₂ three times before adding DCM (7 mL, 0.2 M) and cooling to 0 °C in an ice bath. Acetyl chloride (0.11 mL, 1.57 mmol, 1.10 equiv) was then added followed by pyridine (0.17 mL, 2.14 mmol, 1.50 equiv). The reaction was then allowed to warm to room temperature and stirred overnight. The reaction was quenched with water and extracted 3 x 20 mL DCM, washed 1 x 40 mL brine, then the organics were dried over Na₂SO₄. The solvent was removed by rotary evaporation and the crude reaction mixture was purified by silica gel chromatography (1:1 hexanes/EtOAc to 100% EtOAc) to give the title compound as an off-white solid (252 mg, 1.00 mmol, 70% yield).²⁶¹

Rf: 0.10 (1:1 hexanes/EtOAc)

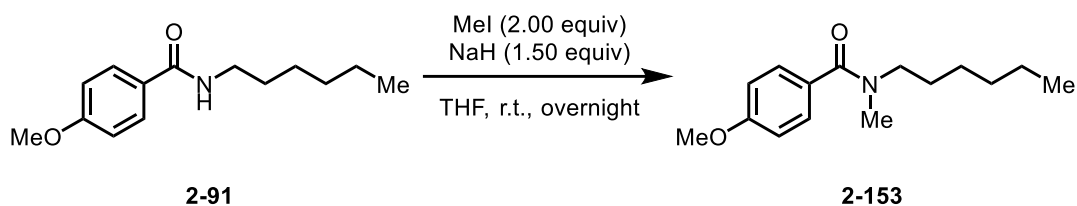
¹H NMR (400 MHz, Chloroform-*d*) δ 7.75 (d, *J* = 8.7 Hz, 2H), 6.92 (d, *J* = 8.5 Hz, 2H), 6.47 (s, 1H), 4.22 (t, *J* = 6.0 Hz, 2H), 3.85 (s, 3H), 3.50 (q, *J* = 6.4 Hz, 2H), 2.08 (s, 3H), 1.94 (p, *J* = 6.3 Hz, 2H).

¹³C NMR (126 MHz, Chloroform-*d*) δ 171.54, 167.11, 162.20, 128.75, 126.88, 113.78, 62.16, 55.46, 36.71, 28.89, 21.05.

IR (neat, cm⁻¹): 3324, 2970, 2898, 2845, 1723, 1652, 1627, 1606, 1505, 1475, 1246, 1189, 1021, 849.

HRMS: (ESI) (*m/z*): [M+H] calculated for C₁₃H₁₇NO₄, 252.1236, found 252.1231.

***N*-hexyl-4-methoxy-*N*-methylbenzamide (2-153)**



To an oven-dried 25-mL round-bottom flask containing a Teflon-coated magnetic stir bar and equipped to a reflux condenser was added **2-91** (348 mg, 1.48 mmol, 1.00 equiv). The flask was backfilled with N₂ three times before adding THF (5 mL, 0.2 M) and NaH (60% in mineral oil) (89 mg, 2.21 mmol, 1.50 equiv). MeI (1.8 mL, 2.96 mmol, 2.00 equiv) was added dropwise and the reaction was stirred at room temperature for 24 hours. The reaction was carefully quenched with 10 mL brine and then extracted 3 x 30 mL EtOAc. The organics were then dried over Na₂SO₄ and the solvent was removed by rotary evaporation. Purification by silica gel chromatography (80:20 hexanes/EtOAc) gave the title compound as a yellow oil (219 mg, 0.873 mmol, 59% yield). Rotamers caused line broadening of the methyl and alkyl chain in the proton NMR spectra as well as unresolved peaks in the carbon NMR despite heating to 52 °C.²⁶²

Rf: 0.20 (80:20 hexanes/EtOAc)

¹H NMR (401 MHz, Chloroform-*d*) δ 7.36 (d, *J* = 8.2 Hz, 3H), 6.90 (d, *J* = 8.7 Hz, 2H), 3.83 (s, 3H), 3.45 (br s, 1H), 3.27 (br s, 1H), 3.01 (br s, 3H), 1.73 – 1.46 (br m, 2H), 1.38 – 1.08 (br m, 6H), 0.86 (br s, 3H).

¹³C NMR (100 MHz, Chloroform-*d*, **52 °C**) δ 160.58, 129.34, 128.80, 113.72, 55.37, 31.53, 27.77, 26.40, 22.57, 13.96.

HRMS: (ESI) (*m/z*): [M+H] calculated for C₁₅H₂₃NO₂, 250.1807, found 250.1875.

4.3.7 Controls and Additive Screening:

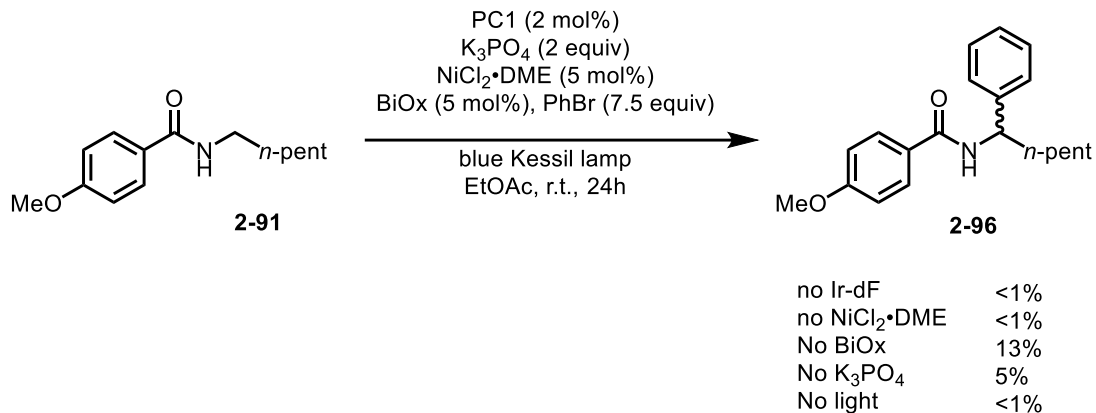


Figure 4-12 Controls for α -arylation of benzamides.

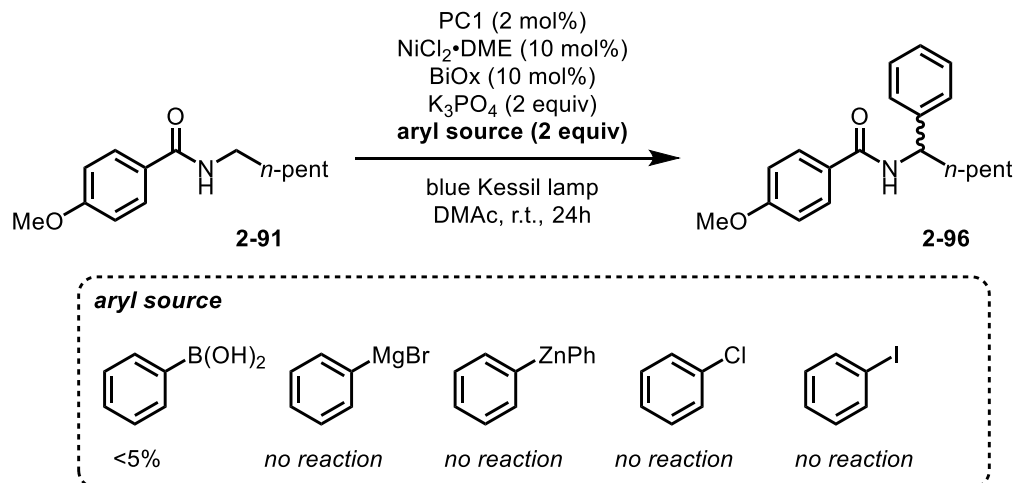


Figure 4-11 Evaluation of different aryl sources in the α -arylation of benzamides.

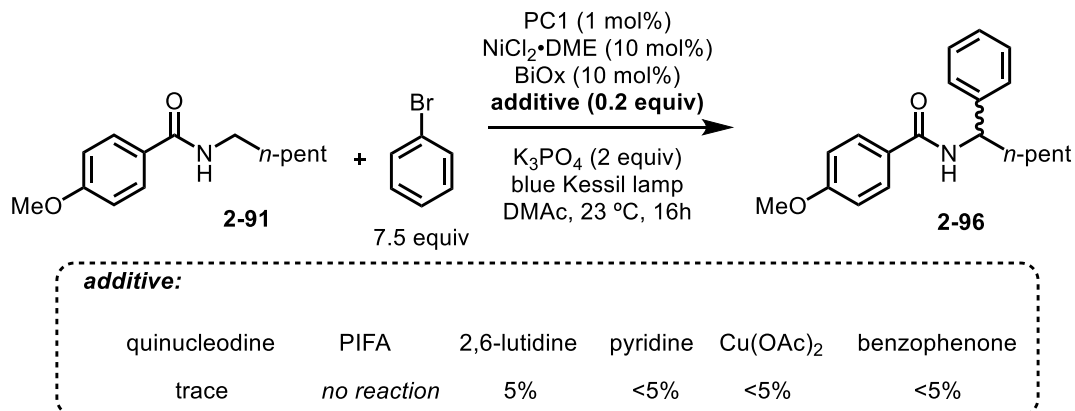


Figure 4-13 Evaluation of sub-stoichiometric additives. PIFA= [Bis(trifluoroacetoxy)iodo]benzene

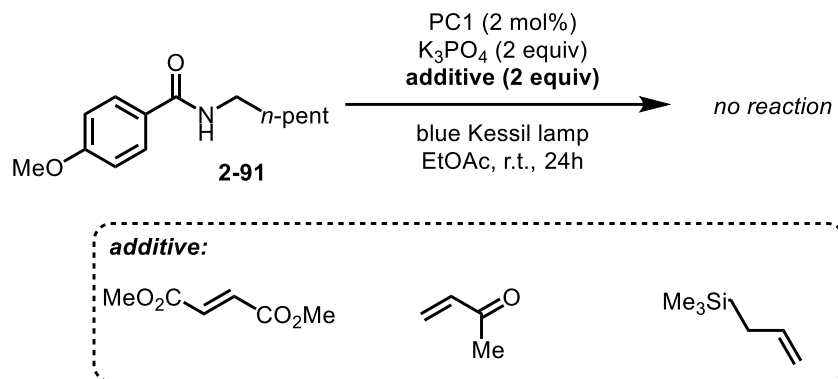
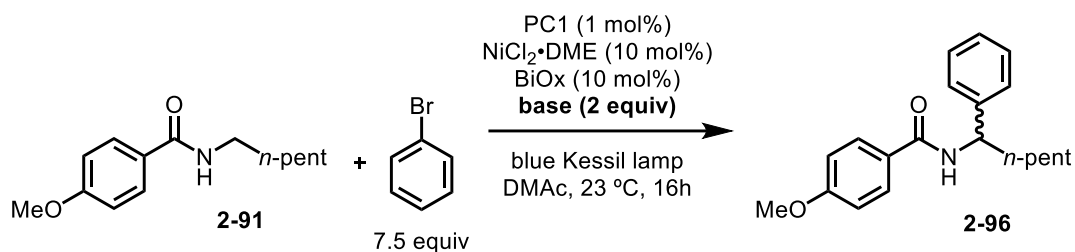


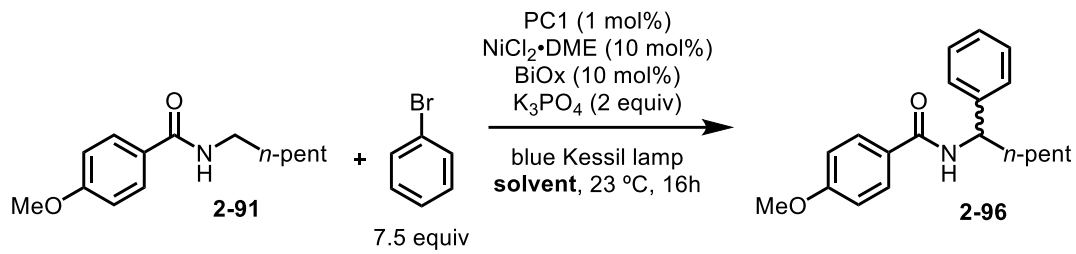
Figure 4-14 Attempted trapping of carbocation or radical intermediates.



Base	Yields^a
K ₃ PO ₄	20%
K ₂ HPO ₄	11%
KH ₂ PO ₄	5%
Na ₃ PO ₄	10%
K ₂ CO ₃	14%
KHCO ₃	14%
Bu ₄ NOP(O)(OBu) ₂	trace

^aYields determined by GC/FID.

Figure 4-15 Examination of different bases in the α -arylation of benzamides.



Solvent

EtOAc
*t*BuCN
*t*AmylOH
 MeCN
 DMF
 EtOH/DMAc (1:1)
 diphenyl ether

Yields^a

33%
 35%
 33%
 28%
 32%
 19%
 6%

^aYields determined by GC/FID.

Figure 4-16 Evaluation of different solvents in the α -arylation of benzamides.

4.3.8 UV-Vis Data:

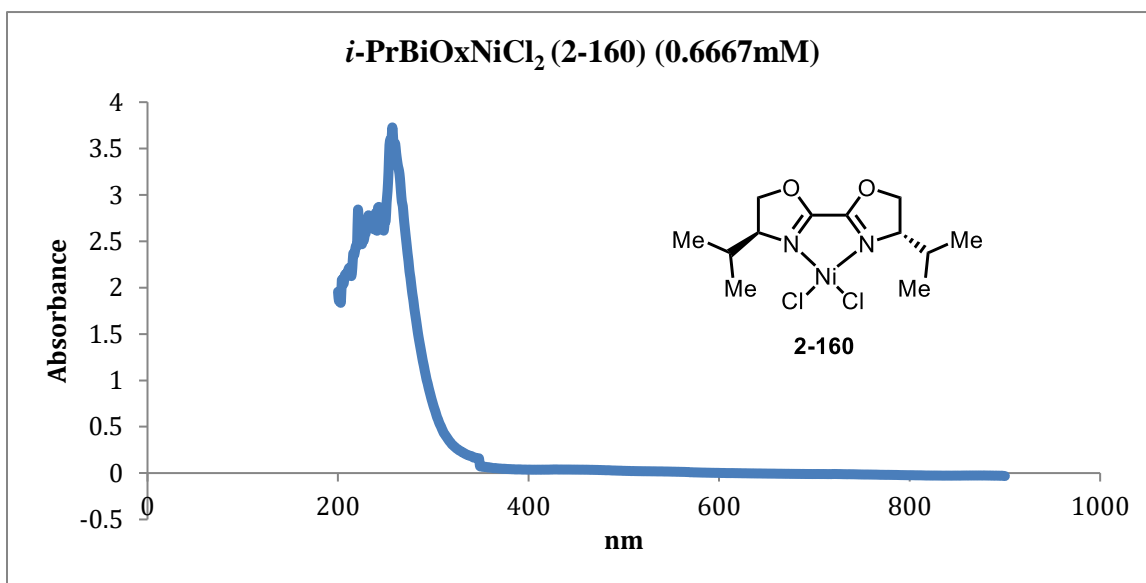


Figure 4-18 UV-Vis of 2-160.

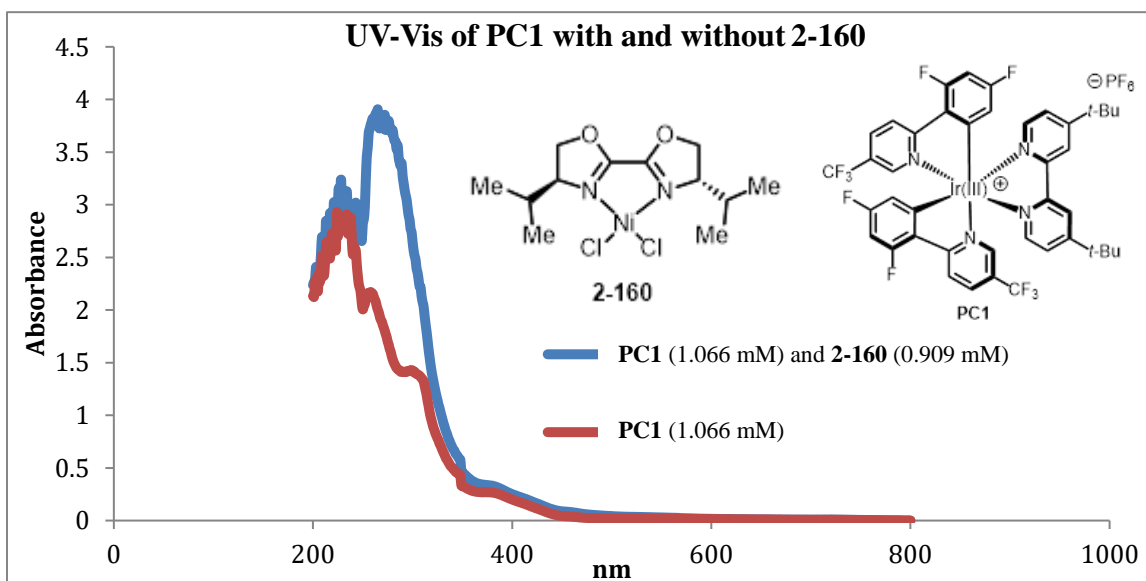


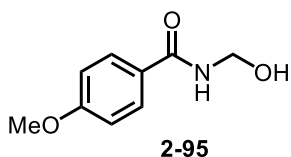
Figure 4-17 UV-Vis of PC1 with and without 2-160.

4.3.9 General Procedures for the α -Arylation of Benzamides:

To an oven-dried 1 dram vial equipped with a Teflon-coated magnetic stir bar in a N₂ filled glovebox was added [Ir(FCF₃(CF₃)ppy)₂(4,4'-di-*t*-bubpy)]PF₆ (PC6) (5.1mg,

0.004 mmol, 0.02 equiv), NiCl₂•DME (2.2 mg, 0.01 mmol, 0.05 equiv), bisoxazoline (BiOx) (1.4 mg, 0.01 mmol, 0.05 equiv), K₃PO₄ (85 mg, 0.4 mmol, 2.0 equiv), and benzamide (0.2 mmol, 1.00 equiv) were combined and suspended in 1.0 mL of dry, degassed EtOAc at room temperature. The mixture was stirred for 10 minutes before adding aryl bromide (1.5 mmol, 7.50 equiv). The vial was sealed with a Teflon cap before removing from the glovebox. The reaction was stirred at 900 rpm overnight in a recrystallization dish filled with water (for cooling) and irradiated with a 34 W blue LED lamp placed 1 cm away. Upon completion, the reaction mixture was quenched with 1 mL EtOAc and run through a silica gel plug with 5 mL EtOAc. The solvent was removed by rotary evaporation and the crude reaction mixture was purified by silica gel chromatography.

N-(hydroxymethyl)-4-methoxybenzamide (2-95)

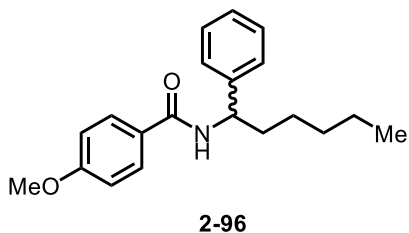


¹H NMR (300 MHz, CDCl₃): δ (ppm) = 3.67-3.77 (bm, 1H), 3.85 (s, 3H), 4.94 (t, 2H, *J* = 6.79 Hz), 6.92 (d, 2H, *J* = 8.30 Hz), 7.12 (bs, 2H), 7.76 (d, 2H, *J* = 9.06 Hz).

¹³C NMR (75 MHz, CDCl₃ + DMSO-*d*₆): δ (ppm) = 54.5, 63.4, 112.6, 125.7, 128.4, 161.3, 166.5.

HRMS: (ESI) (*m/z*): calculated for C₉H₁₁O₃N (M⁺ + Na) 204.06328, found 204.06325

4-methoxy-N-(1-phenylhexyl)benzamide (2-96)



The general procedure for the α -arylation of benzamides was followed using **2-91** (47 mg, 0.200 mmol, 1.00 equiv), **PC6** (5.1 mg, 0.004 mmol, 0.02 equiv), $\text{NiCl}_2\cdot\text{DME}$ (2.2 mg, 0.010 mmol, 0.05 equiv), BiOx (1.4 mg, 0.010 mmol, 0.05 equiv), K_3PO_4 (85 mg, 0.400 mmol, 2.00 equiv), and bromobenzene (156 μL , 1.500 mmol, 7.50 equiv) in 1.0 mL EtOAc. Analysis by GCFID using tridecane as an internal standard showed 56% yield of the desired product. Purification by silica gel chromatography (70:30 hexanes/EtOAc) gave the title compound as a white solid (32.0 mg, 0.102 mmol, 51% yield).

Rf: 0.35 (70:30 hexanes/EtOAc)

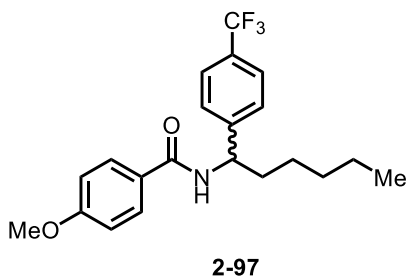
^1H NMR (500 MHz, Chloroform-*d*) δ 7.73 (d, $J = 8.5$ Hz, 2H), 7.49 – 7.14 (m, 5H), 6.91 (d, $J = 8.6$ Hz, 2H), 6.21 (d, $J = 8.1$ Hz, 1H), 5.15 (q, $J = 7.6$ Hz, 1H), 3.84 (s, 3H), 2.01 – 1.76 (m, 2H), 1.50 – 1.20 (m, 6H), 0.86 (t, $J = 6.8$ Hz, 3H).

^{13}C NMR (126 MHz, Chloroform-*d*) δ 166.27, 162.28, 142.74, 128.83 (two overlapping peaks), 127.46, 127.12, 126.78, 113.87, 55.58, 53.96, 36.45, 31.75, 26.13, 22.65, 14.16.

IR (neat, cm^{-1}): 3317, 2953, 2931, 2855, 1623, 1609, 1505, 1259, 1025, 843, 701.

HRMS: (ESI) (m/z): $[\text{M}+\text{H}]$ calculated for $\text{C}_{20}\text{H}_{25}\text{NO}_2$, 312.1963, found 312.1994.

4-methoxy-*N*-(1-(4-(trifluoromethyl)phenyl)hexyl)benzamide (**2-97**)



The general procedure for the α -arylation of benzamides was followed using **2-91** (47 mg, 0.200 mmol, 1.00 equiv), **PC1** (4.5 mg, 0.004 mmol, 0.02 equiv), $\text{NiCl}_2\cdot\text{DME}$ (2.2 mg, 0.010 mmol, 0.05 equiv), BiOx

(1.4 mg, 0.010 mmol, 0.05 equiv), K₃PO₄ (85 mg, 0.400 mmol, 2.00 equiv), and 4-bromobenzotrifluoride (210 μ L, 1.500 mmol, 7.50 equiv) in 1 mL EtOAc. Purification by silica gel chromatography (90:10 to 80:20 hexanes/EtOAc) gave the title compound as a white solid (40.5 mg, 0.106 mmol, 53% yield) and recovered **2-91** (18.0 mg, 0.076 mmol, 38% recovery).

Rf: 0.40 (70:30 hexanes/EtOAc)

¹H NMR (500 MHz, Chloroform-*d*) δ 7.85 (d, *J* = 8.0 Hz, 2H), 7.77 – 7.57 (m, 2H), 7.28 (q, *J* = 4.5 Hz, 1H), 6.45 (d, *J* = 7.9 Hz, 1H), 5.15 (q, *J* = 7.7 Hz, 1H), 2.04 – 1.82 (m, 2H), 1.44 – 1.14 (m, 8H), 0.86 (t, *J* = 6.7 Hz, 3H).

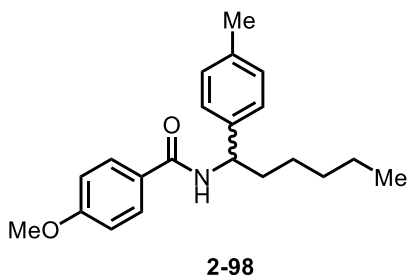
¹³C NMR (126 MHz, Chloroform-*d*) δ 166.54, 162.45, 147.07, 129.94, 129.68, 129.42, 129.16, 128.90, 127.50, 127.50, 127.01, 126.64, 125.72, 125.69, 125.66, 125.34, 123.18, 121.01, 113.91, 55.54, 53.77, 36.38, 31.64, 26.08, 22.60, 14.10.

¹⁹F NMR (377 MHz, Chloroform-*d*) δ -62.50.

IR (neat, cm⁻¹): 3306, 2954, 2868, 1628, 1606, 1540, 1505, 1326, 1253, 1116, 1068, 847.

HRMS: (ESI) (*m/z*): [M+H] calculated for C₂₁H₂₄F₃NO₂, 380.1837, found 380.1893.

4-methoxy-*N*-(1-(*p*-tolyl)hexyl)benzamide (**2-98**)



The general procedure for the α -arylation of benzamides was followed using **2-98** (24 mg, 0.100 mmol, 1.00 equiv), **PC6** (2.5 mg, 0.002 mmol, 0.02 equiv), NiCl₂•DME (1.1 mg, 0.005 mmol, 0.05 equiv), *i*-PrBiOx

(1.1 mg, 0.005 mmol, 0.05 equiv), K₃PO₄ (43 mg, 0.200 mmol, 2.00 equiv), and 4-methylbromobenzene (92.3 μ L, 0.750 mmol, 7.50 equiv) in 0.5 mL EtOAc/DMAc (9:1).

Purification by silica gel chromatography (90:10 to 80:20 hexanes/EtOAc) gave the title compound as a white solid (16.6 mg, 0.051 mmol, 51% yield).

Rf: 0.45 (70:30 hexanes/EtOAc)

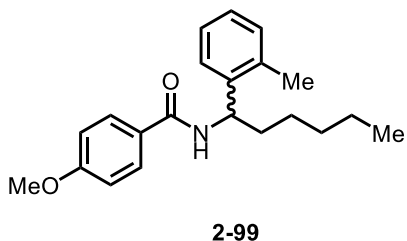
¹H NMR (500 MHz, Chloroform-*d*) δ 7.73 (d, *J* = 6.6 Hz, 2H), 7.25 (d, *J* = 6.8 Hz, 2H), 7.15 (d, *J* = 7.3 Hz, 2H), 6.89 (d, *J* = 7.7 Hz, 2H), 6.31 (d, *J* = 7.9 Hz, 1H), 5.11 (q, *J* = 7.9 Hz, 1H), 3.83 (s, 3H), 2.33 (s, 3H), 2.02 – 1.71 (m, 2H), 1.52 – 1.08 (m, 6H), 0.87 (t, *J* = 6.6 Hz, 3H).

¹³C NMR (126 MHz, Chloroform-*d*) δ 166.22, 162.18, 139.75, 137.00, 129.44, 128.81, 127.17, 126.69, 113.77, 55.49, 53.70, 36.35, 31.74, 26.14, 22.63, 21.19, 14.14.

IR (neat, cm⁻¹): 3299, 2926, 2856, 1626, 1606, 1503, 1251, 1175, 1030, 842.

HRMS: (ESI) (m/z): [M+H] calculated for C₂₁H₂₇NO₂, 326.2120, found 326.2132.

4-methoxy-*N*-(1-(*o*-tolyl)hexyl)benzamide (**2-99**)



The general procedure for the α -arylation of benzamides was followed using **2-91** (47 mg, 0.200 mmol, 1.00 equiv), **PC6** (5.1 mg, 0.004 mmol, 0.02 equiv), NiCl₂·DME (2.2 mg, 0.010 mmol, 0.05 equiv), BiOx (1.4 mg, 0.010 mmol, 0.05 equiv), K₃PO₄ (85 mg, 0.400 mmol, 2.00 equiv), and 2-methylbromobenzene (180 μ L, 1.500 mmol, 7.50 equiv) in 1 mL EtOAc. Purification by silica gel chromatography (90:10 to 80:20 hexanes/EtOAc) gave the title compound as a white solid (21.4 mg, 0.066 mmol, 33% yield) and recovered **2-91** (35.7 mg, 0.152 mmol, 76% recovery).

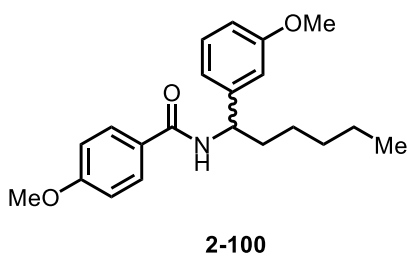
Rf: 0.40 (70:30 hexanes/EtOAc)

¹H NMR (400 MHz, Chloroform-*d*) δ 7.70 (d, J = 9.0 Hz, 2H), 7.28 (d, J = 7.4 Hz, 2H), 7.23 – 7.10 (m, 3H), 6.88 (d, J = 8.8 Hz, 2H), 6.17 (d, J = 8.1 Hz, 1H), 5.36 (q, J = 7.6 Hz, 1H), 3.81 (s, 3H), 2.43 (s, 3H), 1.84 (tdd, J = 15.3, 11.3, 5.7 Hz, 1H), 1.28 (p, J = 11.8 Hz, 6H), 0.84 (t, 6.6 Hz, 3H).

¹³C NMR (100 MHz, Chloroform-*d*) δ 166.12, 162.24, 140.89, 136.44, 130.89, 128.79, 127.26, 127.03, 126.40, 125.04, 113.84, 55.54, 50.03, 36.20, 31.84, 26.20, 22.67, 19.63, 14.18.

HRMS: (ESI) (m/z): [M+H] calculated for C₂₁H₂₇NO₂, 326.2120, found 326.2125.

4-methoxy-*N*-(1-(3-methoxyphenyl)hexyl)benzamide (2-100)



The general procedure for the α -arylation of benzamides was followed **2-91** (47 mg, 0.200 mmol, 1.00 equiv), **PC6** (5.1 mg, 0.004 mmol, 0.02 equiv), NiCl₂•DME (2.2 mg, 0.010 mmol, 0.05 equiv), BiOx (1.4 mg, 0.010 mmol, 0.05 equiv), K₃PO₄ (85 mg, 0.400 mmol, 2.00 equiv), and methyl-3-bromoanisole (190 μ L, 1.500 mmol, 7.50 equiv) in 1 mL EtOAc. Purification by silica gel chromatography (99:1 DCM/acetone to 97:3 DCM/acetone) gave the title compound as a white solid (28.9 mg, 0.084 mmol, 42% yield) and recovered **2-91** (20.7 mg, 0.088 mmol, 44% recovery).

Rf: 0.20 (99:1 DCM/acetone)

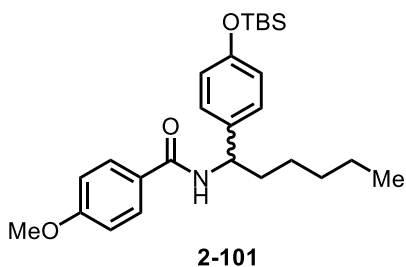
¹H NMR (700 MHz, Chloroform-*d*) δ 7.73 (d, J = 8.7 Hz, 2H), 7.34 – 7.18 (m, 1H), 7.01 – 6.91 (m, 1H), 6.91 – 6.83 (m, 3H), 6.80 (d, J = 8.3 Hz, 1H), 6.26 (d, J = 8.2 Hz, 1H),

5.11 (q, $J = 7.6$ Hz, 1H), 3.83 (s, 2H), 3.80 (s, 3H), 1.99 – 1.78 (m, 2H), 1.44 – 1.16 (m, 6H), 0.86 (t, $J = 6.9$ Hz, 3H).

^{13}C NMR (176 MHz, Chloroform- d) δ 166.28, 162.26, 159.95, 144.44, 129.83, 128.82, 127.08, 119.02, 113.84, 112.84, 112.50, 55.44 (d, $J = 30.3$ Hz), 53.97, 36.44, 31.74, 26.12, 22.64, 14.16.

HRMS: (ESI) (m/z): [M+H] calculated for $\text{C}_{21}\text{H}_{27}\text{NO}_3$, 342.2069, found 342.2095.

***N*-(1-(4-((*tert*-butyldimethylsilyl)oxy)phenyl)hexyl)-4-methoxybenzamide (2-101)**



The general procedure for the α -arylation of benzamides was followed using **2-91** (47 mg, 0.200 mmol, 1.00 equiv), **PC6** (5.1 mg, 0.004 mmol, 0.02 equiv), $\text{NiCl}_2 \cdot \text{DME}$ (2.2 mg, 0.010 mmol, 0.05 equiv), BiOx (1.4 mg, 0.010 mmol, 0.05 equiv), K_3PO_4 (85 mg, 0.400 mmol, 2.00 equiv), and (4-bromophenoxy)(*tert*-butyl)dimethylsilane (431 mg, 1.500 mmol, 7.50 equiv) in 1 mL EtOAc . Purification by silica gel chromatography (25:75 Et_2O /hexanes to 1:1 Et_2O /hexanes) gave the title compound as a clear oil (23.6 mg, 0.054 mmol, 27% yield) and recovered **2-91** (32.1 mg, 0.136 mmol, 68% recovery).

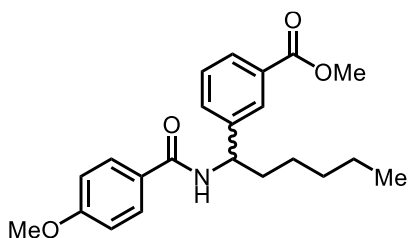
Rf: 0.25 (25:75 Et_2O /hexanes)

^1H NMR (700 MHz, Chloroform- d) δ 7.72 (d, $J = 8.7$ Hz, 2H), 7.20 (d, $J = 8.2$ Hz, 2H), 6.90 (d, $J = 8.8$ Hz, 2H), 6.80 (d, $J = 8.5$ Hz, 2H), 6.18 (d, $J = 8.2$ Hz, 1H), 5.09 (q, $J = 7.6$ Hz, 1H), 3.83 (s, 3H), 1.94 – 1.78 (m, 2H), 1.39 – 1.23 (m, 6H), 0.97 (s, 9H), 0.85 (t, $J = 6.9$ Hz, 3H), 0.18 (s, 6H).

^{13}C NMR (176 MHz, Chloroform-*d*) δ 166.18, 162.21, 154.95, 135.34, 128.80, 127.86, 127.22, 120.24, 113.83, 55.53, 53.37, 36.33, 31.74, 26.12, 25.81, 22.65, 18.31, 14.15, -4.27 (d, $J = 1.4$ Hz).

HRMS: (ESI) (m/z): [M+H] calculated for $\text{C}_{26}\text{H}_{39}\text{NO}_3\text{Si}$, 442.2777, found 442.2788.

methyl 3-(1-(4-methoxybenzamido)hexyl)benzoate (2-102)



2-102

The general procedure for the α -arylation of benzamides was followed using **2-91** (47 mg, 0.200 mmol, 1.00 equiv), **PC6** (5.1 mg, 0.004 mmol, 0.02 equiv), $\text{NiCl}_2 \cdot \text{DME}$ (2.2 mg, 0.010 mmol, 0.05 equiv), BiOx (1.4 mg, 0.010 mmol, 0.05 equiv), K_3PO_4 (85 mg, 0.400 mmol, 2.00 equiv), and methyl-3-bromobenzoate (323 mg, 1.500 mmol, 7.50 equiv) in 1 mL EtOAc. Purification by silica gel chromatography (100% hexanes to 80:20 hexanes/EtOAc) gave the title compound as a white solid (36.3 mg, 0.098 mmol, 49% yield) and recovered **2-91** (13.4 mg, 0.056 mmol, 28% recovery).

Rf: 0.20 (2.5:97.5 acetone/DCM)

^1H NMR (700 MHz, Chloroform-*d*) δ 8.02 (s, 1H), 7.91 (d, $J = 7.8$ Hz, 1H), 7.79 – 7.65 (m, 2H), 7.54 (d, $J = 7.8$ Hz, 1H), 7.38 (t, $J = 7.7$ Hz, 1H), 6.88 (d, $J = 8.8$ Hz, 2H), 6.45 (d, $J = 7.9$ Hz, 1H), 5.16 (q, $J = 7.5$ Hz, 1H), 3.89 (s, 3H), 3.82 (s, 3H), 1.95 – 1.81 (m, 2H), 1.45 – 1.22 (m, 6H), 0.84 (t, $J = 6.8$ Hz, 3H).

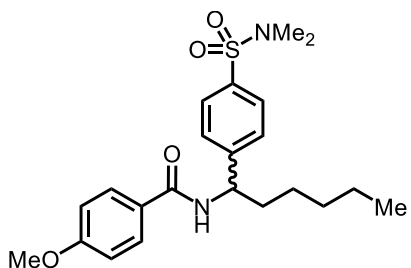
¹³C NMR (176 MHz, Chloroform-*d*) δ 167.12, 166.41, 162.31, 143.49, 131.83, 130.62, 128.88, 128.79, 128.59, 127.44, 126.80, 55.51, 53.78, 52.24, 36.46, 31.63, 29.39, 26.11, 22.59, 14.10.

IR (neat, cm⁻¹): 3300, 2931, 2857, 1719, 1629, 1606, 1502, 1251, 1176, 1029, 843.

HRMS: (ESI) (m/z): [M+H] calculated for C₂₂H₂₇NO₄, 370.2018, found 370.1994

N-(1-(4-(*N,N*-dimethylsulfonyl)phenyl)hexyl)-4-methoxybenzamide (**2-103**)

The general procedure for the α-arylation of benzamides was followed using **2-91** (23 mg,



2-103

0.100 mmol, 1.00 equiv), **PC1** (2.2 mg, 0.004 mmol, 0.02 equiv), NiCl₂•DME (1.1 mg, 0.010 mmol, 0.05 equiv), *b*-PrBiOx (1.1 mg, 0.010 mmol, 0.05 equiv), K₃PO₄ (43 mg, 0.200 mmol, 2.00 equiv), and 4-bromo-*N,N*-dimethylbenzenesulfonamide (212 mg, 0.750

mmol, 7.50 equiv) in 0.5 mL EtOAc. Purification by silica gel chromatography (70:30 hexanes/EtOAc to 100% EtOAc) gave the title compound as a white solid (22.1 mg, 0.053 mmol, 53% yield).

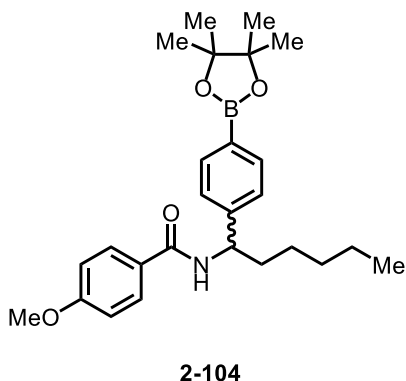
Rf: 0.15 (1:1 hexanes/EtOAc)

¹H NMR (500 MHz, Chloroform-*d*) δ 7.76 (d, *J* = 8.5 Hz, 2H), 7.69 (d, *J* = 8.1 Hz, 2H), 7.50 (d, *J* = 8.0 Hz, 2H), 6.89 (d, *J* = 8.4 Hz, 2H), 6.59 (d, *J* = 7.9 Hz, 1H), 5.18 (q, *J* = 7.5 Hz, 1H), 3.82 (s, 3H), 2.68 (s, 6H), 1.86 (tt, *J* = 8.8, 4.2 Hz, 2H), 1.51 – 1.17 (m, 6H), 0.85 (t, *J* = 6.7 Hz, 4H).

¹³C NMR (126 MHz, Chloroform-*d*) δ 166.59, 162.46, 148.42, 134.34, 128.94, 128.15, 127.28, 126.46, 113.89, 55.54, 53.62, 37.99, 36.37, 31.56, 26.07, 22.55, 14.08.

HRMS: (ESI) (m/z): [M+H] calculated for C₂₂H₃₀N₂O₄S, 419.2004, found 419.2014.

4-methoxy-N-(1-(4-(4,4,5,5-tetramethyl-1,3,2-dioxaborolan-2-yl)phenyl)hexyl)benzamide (2-104)



The general procedure for the α -arylation of benzamides was followed using **2-91** (47 mg, 0.200 mmol, 1.00 equiv), **PC6** (5.1 mg, 0.004 mmol, 0.02 equiv), NiCl₂•DME (2.2 mg, 0.010 mmol, 0.05 equiv), BiOx (1.4 mg, 0.010 mmol, 0.05 equiv), K₃PO₄ (85 mg, 0.400 mmol, 2.0 equiv), and 2-(4-bromophenyl)-4,4,5,5-tetramethyl-1,3,2-dioxaborolane (424 mg, 1.500 mmol, 7.5 equiv) in 1 mL EtOAc. Reaction was stopped at 12 hours to avoid Suzuki-Miura coupling of the product with a second equivalent of aryl bromide. Purification by silica gel chromatography (90:10 to 70:30 hexanes/EtOAc) gave the title compound as a white solid (30.5 mg, 0.098 mmol, 49% yield) and recovered **2-91** (13.1 mg, 0.056 mmol, 28% recovery).

Rf: 0.25 (70:30 hexanes/EtOAc)

¹H NMR (700 MHz, Chloroform-*d*) δ 7.78 (d, *J* = 7.6 Hz, 2H), 7.71 (d, *J* = 8.3 Hz, 2H), 7.35 (d, *J* = 7.5 Hz, 2H), 6.87 (d, *J* = 8.7 Hz, 2H), 6.40 (d, *J* = 8.1 Hz, 1H), 5.14 (q, *J* = 7.8 Hz, 1H), 3.81 (s, 3H), 1.87 (m, 2H), 1.51 – 1.20 (m, 18H), 0.84 (t, *J* = 6.6 Hz, 3H).

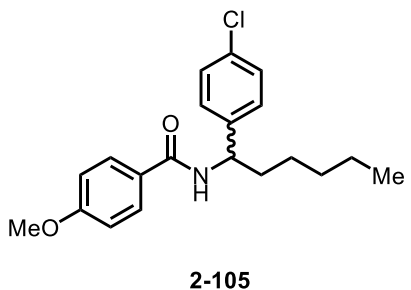
¹³C NMR (176 MHz, Chloroform-*d*) δ 166.33, 162.18, 145.89, 136.39, 135.28, 128.82, 126.96, 126.12, 113.76, 83.84, 55.47, 54.05, 36.29, 31.68, 26.06, 24.94, 22.60, 14.13.

¹¹B NMR (225 MHz, Chloroform-*d*) δ 30.86.

IR (neat, cm⁻¹): 3289, 2930, 2858, 1629, 1607, 1503, 1358, 1252, 1143, 1088, 730.

HRMS: (ESI) (m/z): [M+H] calculated for C₂₆H₃₆BNO₄, 438.2815, found 438.2863.

***N*-(1-(4-chlorophenyl)hexyl)-4-methoxybenzamide (2-105)**



The general procedure for the α -arylation of benzamides was followed using **2-91** (47 mg, 0.200 mmol, 1.00 equiv), **PC6** (5.1 mg, 0.004 mmol, 0.02 equiv), NiCl₂•DME (2.2 mg, 0.010 mmol, 0.05 equiv), BiOx (1.4 mg, 0.010 mmol, 0.05 equiv), K₃PO₄ (85 mg, 0.400 mmol, 2.00 equiv), and 4-bromo-1-chlorobenzene (287 mg, 1.500 mmol, 7.50 equiv) in 1 mL EtOAc. Purification by silica gel chromatography (90:10 to 80:20 hexanes/EtOAc) gave the title compound as a white solid (24.2 mg, 0.070 mmol, 35% yield) and recovered **2-91** (21.5 mg, 0.092 mmol, 46% recovery).

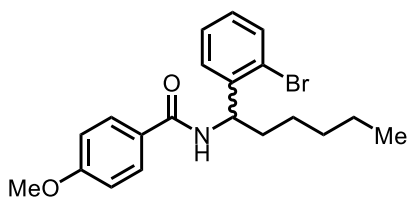
Rf: 0.40 (70:30 hexanes/EtOAc)

¹H NMR (400 MHz, Chloroform-*d*) δ 7.71 (d, *J* = 8.7 Hz, 2H), 7.37 – 7.23 (m, 4H), 6.90 (d, *J* = 8.8 Hz, 2H), 6.15 (d, *J* = 7.8 Hz, 1H), 5.08 (q, *J* = 7.5 Hz, 1H), 3.83 (s, 3H), 1.84 (m, 2H), 1.26 (m, 2H), 0.85 (t, *J* = 6.8 Hz, 3H).

¹³C NMR (176 MHz, Chloroform-*d*) δ 166.36, 162.37, 141.41, 133.06, 128.89, 128.84, 128.13, 126.82, 113.89, 55.55, 53.42, 36.32, 31.67, 26.07, 22.62, 14.13.

HRMS: (ESI) (m/z): [M+H] calculated for C₂₀H₂₄ClNO₂, 346.1574, found 346.1569.

***N*-(1-(2-bromophenyl)hexyl)-4-methoxybenzamide (2-106)**



2-106

The general procedure for the α -arylation of benzamides was followed **2-91** (47 mg, 0.200 mmol, 1.00 equiv), **PC6** (5.1 mg, 0.004 mmol, 0.02 equiv), NiCl₂•DME (2.2 mg, 0.010 mmol, 0.05 equiv), BiOx (1.4 mg, 0.010 mmol, 0.05 equiv), K₃PO₄ (85 mg, 0.400 mmol, 2.00 equiv), and 1,2-dibromobenzene (181 μ L, 1.500 mmol, 7.50 equiv) in 1 mL EtOAc. Purification by silica gel chromatography (90:10 to 80:20 hexanes/EtOAc) gave the title compound as a white solid (61.1 mg, 0.156 mmol, 78% yield) and recovered **2-91** (5.2 mg, 0.022 mmol, 11% recovery).

Rf: 0.30 (70:30 hexanes/EtOAc)

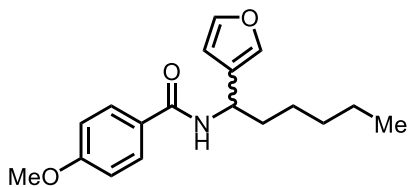
¹H NMR (400 MHz, Chloroform-*d*) δ 7.76 (d, *J* = 8.5 Hz, 2H), 7.56 (d, *J* = 7.9 Hz, 1H), 7.36 – 7.23 (m, 2H), 7.11 (t, *J* = 7.9 Hz, 1H), 6.93 (d, *J* = 8.5 Hz, 2H), 6.54 (d, *J* = 7.8 Hz, 1H), 5.41 (q, *J* = 7.6 Hz, 1H), 3.85 (s, 3H), 1.90 (m, 2H), 1.48 – 1.15 (m, 6H), 0.87 (t, *J* = 6.6 Hz, 3H).

¹³C NMR (176 MHz, Chloroform-*d*) δ 166.19, 162.30, 141.72, 133.62, 128.89, 128.74, 128.38, 127.75, 126.87, 123.08, 113.86, 55.52, 54.27, 35.48, 31.61, 26.25, 22.63, 14.13.

IR (neat, cm⁻¹): 3304, 2958, 2930, 2857, 1633, 1505, 1250, 1188, 1024, 754.

HRMS: (ESI) (*m/z*): [M+H] calculated for C₂₀H₂₄BrNO₂, 390.1068, found 390.1078.

***N*-(1-(furan-3-yl)hexyl)-4-methoxybenzamide (2-107)**



2-107

The general procedure for the α -arylation of benzamides was followed **2-91** (47 mg, 0.200 mmol, 1.00 equiv), **PC6** (5.1 mg, 0.004 mmol, 0.02 equiv), NiCl₂•DME (2.2 mg, 0.010 mmol, 0.05 equiv), BiOx (1.4 mg, 0.010

mmol, 0.05 equiv), K₃PO₄ (85 mg, 0.400 mmol, 2.00 equiv), and 3-bromofurane (135 uL, 1.500 mmol, 7.50 equiv) in 1 mL EtOAc. Purification by silica gel chromatography (80:20 hexanes/EtOAc to 70:30 hexanes/EtOAc) gave the title compound as a white solid (14.2 mg, 0.048 mmol, 24% yield).

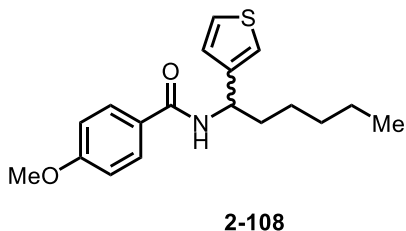
Rf: 0.30 (70:30 hexanes/EtOAc)

¹H NMR (401 MHz, Chloroform-*d*) δ 7.73 (d, *J* = 8.2 Hz, 2H), 7.39 (d, *J* = 5.0 Hz, 2H), 6.91 (d, *J* = 8.3 Hz, 2H), 6.38 (s, 1H), 6.05 (d, *J* = 8.6 Hz, 1H), 5.17 (q, *J* = 7.6 Hz, 1H), 3.84 (s, 3H), 2.18 – 1.72 (m, 2H), 1.52 – 1.09 (m, 6H), 0.87 (t, *J* = 5.2 Hz, 3H).

¹³C NMR (100 MHz, Chloroform-*d*) δ 166.32, 162.31, 143.47, 139.46, 128.80, 127.12, 127.02, 113.89, 109.29, 55.55, 45.85, 35.40, 31.73, 25.93, 22.67, 14.16.

HRMS: (ESI) (*m/z*): [M+H] calculated for C₁₈H₂₃NO₃, 302.1756, found 302.1756.

4-methoxy-*N*-(1-(thiophen-3-yl)hexyl)benzamide (2-108)



The general procedure for the α-arylation of benzamides was followed **2-91** (47 mg, 0.200 mmol, 1.00 equiv), **PC6** (5.1 mg, 0.004 mmol, 0.02 equiv), NiCl₂•DME (2.2 mg, 0.010 mmol, 0.05 equiv), BiOx (1.4 mg, 0.010 mmol, 0.05 equiv), K₃PO₄ (85 mg, 0.400 mmol, 2.00 equiv), and 3-bromothiophene (140 uL, 1.500 mmol, 7.50 equiv) in 1 mL EtOAc. Purification by silica gel chromatography (100% hexanes to 80:20 hexanes/EtOAc) gave the title compound as a white solid (18.4 mg, 0.058 mmol, 29% yield) and recovered **2-91** (29.3 mg, 0.126 mmol, 63% recovery).

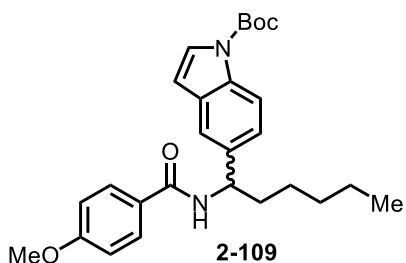
Rf: 0.30 (70:30 hexanes/EtOAc)

¹H NMR (400 MHz, Chloroform-*d*) δ 7.73 (d, J = 8.7 Hz, 2H), 7.30 (dd, J = 5.0, 3.0 Hz, 1H), 7.19 (s, 1H), 7.08 (d, J = 5.0 Hz, 1H), 6.92 (d, J = 8.6 Hz, 2H), 6.10 (d, J = 8.6 Hz, 1H), 5.30 (q, J = 7.8 Hz, 1H), 3.84 (s, 3H), 2.04 – 1.80 (m, 2H), 1.48 – 1.20 (m, 6H), 0.88 (t, J = 6.9 Hz, 3H).

¹³C NMR (176 MHz, Chloroform-*d*) δ 166.25, 162.29, 143.81, 128.83, 127.03, 126.53, 126.26, 121.17, 113.86, 55.54, 49.50, 35.93, 31.75, 26.01, 22.66, 14.16.

HRMS: (ESI) (m/z): [M+H] calculated for C₁₈H₂₃NO₂S, 318.1527, found 318.1537.

***tert*-butyl-5-(1-(4-methoxybenzamido)hexyl)-1*H*-indole-1-carboxylate (2-109)**



The general procedure for the α -arylation of benzamides was followed **2-91** (47 mg, 0.200 mmol, 1.00 equiv), **PC6** (5.1 mg, 0.004 mmol, 0.02 equiv), NiCl₂•DME (2.2 mg, 0.010 mmol, 0.05 equiv), BiOx (1.4 mg, 0.010 mmol, 0.05 equiv), K₃PO₄ (85 mg, 0.400 mmol, 2.00 equiv), and 5-bromo-N-boc-indole (444 mg, 1.500 mmol, 7.50 equiv) in 1 mL EtOAc/DMAc (9:1). Purification by silica gel chromatography (90:10 to 80:20 hexanes/EtOAc) gave the title compound as a white solid (21.7 mg, 0.048 mmol, 24% yield) and recovered **2-91** (34.3 mg, 0.146 mmol, 73% recovery).

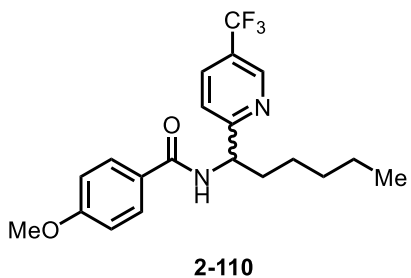
Rf: 0.35 (70:30 hexanes/EtOAc)

¹H NMR (400 MHz, Chloroform-*d*) δ 8.10 (d, J = 8.6 Hz, 1H), 7.72 (d, J = 8.4 Hz, 2H), 7.66 – 7.51 (m, 2H), 7.31 (d, J = 8.7 Hz, 1H), 6.90 (d, J = 8.5 Hz, 2H), 6.54 (d, J = 3.7 Hz, 1H), 6.24 (d, J = 8.0 Hz, 1H), 5.22 (q, J = 7.6 Hz, 1H), 3.83 (s, 3H), 2.04 – 1.86 (m, 1H), 1.66 (s, 9H), 1.29 (m, 6H), 0.85 (t, J = 6.7 Hz, 3H).

¹³C NMR (126 MHz, Chloroform-*d*) δ 166.22, 162.18, 149.81, 137.13, 134.53, 130.91, 128.81, 126.47, 123.07, 119.20, 115.48, 113.79 (d, *J* = 3.6 Hz), 83.82, 55.49, 54.14, 36.54, 31.76, 28.30, 26.21, 22.64, 14.15.

HRMS: (ESI) (*m/z*): [*M*+*H*] calculated for C₂₇H₃₄N₂O₄, 451.2597, found 451.2607.

4-methoxy-*N*-(1-(6-(trifluoromethyl)pyridin-3-yl)hexyl)benzamide (**2-110**)



The general procedure for the α -arylation of benzamides was followed **2-91** (47 mg, 0.200 mmol, 1.00 equiv), **PC6** (5.1 mg, 0.004 mmol, 0.02 equiv), NiCl₂•DME (2.2 mg, 0.010 mmol, 0.05 equiv), BiOx (1.4 mg, 0.010 mmol, 0.05 equiv), K₃PO₄ (85 mg, 0.400 mmol, 2.00 equiv), and 5-bromo-2-trifluoromethylpyridine (339 mg, 1.500 mmol, 7.50 equiv) in 1 mL EtOAc/DMAc (9:1). Purification by silica gel chromatography (90:10 to 80:20 hexanes/EtOAc) gave the title compound as a white solid (37.2 mg, 0.098 mmol, 49% yield) and recovered **2-91** (9.0 mg, 0.038 mmol, 19% recovery).

Rf: 0.40 (70:30 hexanes/EtOAc)

¹H NMR (400 MHz, Chloroform-*d*) δ 8.84 (s, 1H), 7.97 – 7.85 (m, 1H), 7.80 (d, *J* = 8.4 Hz, 2H), 7.42 (d, *J* = 8.2 Hz, 1H), 7.24 (s, 1H), 6.93 (d, *J* = 8.4 Hz, 2H), 5.33 (q, *J* = 7.3 Hz, 1H), 3.85 (s, 3H), 1.92 (dd, *J* = 15.1, 7.5 Hz, 2H), 1.27 (m, 6H), 0.85 (d, *J* = 6.6 Hz, 3H).

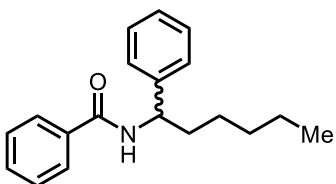
¹³C NMR (100 MHz, Chloroform-*d*) δ 166.40, 164.62, 162.39, 146.44 (q, *J* = 4.3 Hz), 133.89, 128.96, 126.77, 122.18, 113.88, 55.55, 54.34, 36.57, 31.73, 25.45, 22.60, 14.12.

¹⁹F NMR (376 MHz, Chloroform-*d*) δ -62.33.

IR (neat, cm^{-1}): 3293, 2933, 2856, 1633, 1608, 1331, 1257, 1119, 1080, 1018, 853.

HRMS: (ESI) (m/z): $[M+H]$ calculated for $\text{C}_{20}\text{H}_{23}\text{F}_3\text{N}_2\text{O}_2$, 381.1790, found 381.1783.

***N*-(1-phenylhexyl)benzamide (2-111)**



2-111

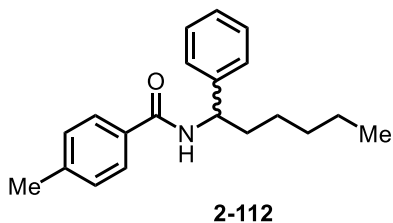
The general procedure for the α -arylation of benzamides was followed using *N*-hexylbenzamide (43 mg, 0.200 mmol, 1.00 equiv), **PC6** (5.1 mg, 0.004 mmol, 0.02 equiv), $\text{NiCl}_2 \cdot \text{DME}$ (2.2 mg, 0.010 mmol, 0.05 equiv), BiOx (1.4 mg, 0.010 mmol, 0.05 equiv), K_3PO_4 (85 mg, 0.400 mmol, 2.00 equiv), and bromobenzene (156 μL , 1.500 mmol, 7.50 equiv) in 1 mL EtOAc/DMAc (9:1). Purification by silica gel chromatography (100% hexanes to 85:15 hexanes/EtOAc) gave the title compound as a white solid (22.5 mg, 0.080 mmol, 40% yield) and recovered *N*-hexylbenzamide (16.3 mg, 0.080 mmol, 40% recovery).

Rf: 0.60 (70:30 hexanes/EtOAc)

^1H NMR (500 MHz, Chloroform-*d*) δ 7.76 (d, $J = 7.6$ Hz, 2H), 7.48 (t, $J = 7.5$ Hz, 1H), 7.41 (t, $J = 7.5$ Hz, 2H), 7.38 – 7.31 (m, 5H), 7.27 (d, $J = 8.0$ Hz, 1H), 6.40 (d, $J = 9.2$ Hz, 1H), 5.16 (q, $J = 7.7$ Hz, 1H), 1.90 (ddt, $J = 23.5, 16.9, 8.3$ Hz, 2H), 1.33 (q, $J = 19.6, 11.8$ Hz, 6H), 0.86 (t, $J = 6.3$ Hz, 3H).

^{13}C NMR (126 MHz, Chloroform-*d*) δ 166.79, 142.56, 134.82, 131.53, 128.81, 128.65, 127.48, 127.03, 126.75, 54.06, 36.38, 31.71, 26.12, 22.63, 14.15.

4-methyl-*N*-(1-phenylhexyl)benzamide (2-112)



The general procedure for the α -arylation of benzamides was followed using *N*-hexyl-4-methylbenzamide (44 mg, 0.200 mmol, 1.00 equiv), **PC1** (4.5 mg, 0.004 mmol, 0.02 equiv), $\text{NiCl}_2\cdot\text{DME}$ (2.2 mg, 0.010 mmol, 0.05 equiv), BiOx (1.4 mg, 0.010 mmol, 0.05 equiv), K_3PO_4 (85 mg, 0.400 mmol, 2.00 equiv), and bromobenzene (156 μL , 1.500 mmol, 7.50 equiv) in 1 mL EtOAc. Purification by silica gel chromatography (95:5 to 80:20 hexanes/EtOAc) gave the title compound as a white solid (29.7 mg, 0.100 mmol, 50% yield) and recovered *N*-hexyl-4-methylbenzamide (14.7 mg, 0.068 mmol, 34% recovery).

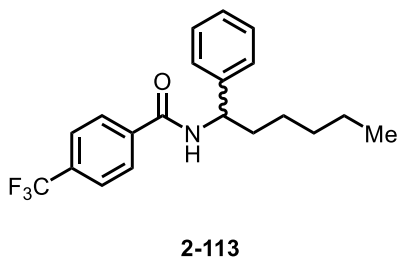
Rf: 0.35 (70:30 hexanes/EtOAc)

^1H NMR (401 MHz, Chloroform-*d*) δ 7.67 (d, $J = 8.1$ Hz, 2H), 7.37 – 7.26 (m, 5H), 7.19 (d, $J = 7.7$ Hz, 2H), 6.43 (t, $J = 7.1$ Hz, 1H), 5.16 (q, $J = 7.7$ Hz, 1H), 2.37 (s, 3H), 1.89 (dq, $J = 15.5, 8.3, 6.7$ Hz, 2H), 1.30 (q, $J = 10.4, 8.9$ Hz, 6H), 0.87 (t, $J = 7.0$ Hz, 3H).

^{13}C NMR (176 MHz, Chloroform-*d*) δ 166.71, 142.69, 141.85, 131.92, 129.24, 128.74, 127.37, 127.03, 126.73, 53.94, 36.37, 31.70, 26.11, 22.61, 21.53, 14.13.

HRMS: (ESI) (m/z): $[\text{M}+\text{H}]$ calculated for $\text{C}_{20}\text{H}_{25}\text{NO}$, 296.2014, found 296.2022.

***N*-(1-phenylhexyl)-4-(trifluoromethyl)benzamide (2-113)**



The general procedure for the α -arylation of benzamides was followed using *N*-hexyl-4-(trifluoromethyl)benzamide (54 mg, 0.200 mmol, 1.00 equiv), **PC6** (5.1 mg, 0.004 mmol, 0.02 equiv), $\text{NiCl}_2\cdot\text{DME}$ (2.2 mg, 0.010 mmol, 0.05 equiv), BiOx (1.4 mg, 0.010 mmol, 0.05 equiv),

K₃PO₄ (85 mg, 0.400 mmol, 2.0 equiv), and bromobenzene (156 μ L, 1.500 mmol, 7.5 equiv) in 1 mL EtOAc/DMAc (9:1). Purification by silica gel chromatography (90:10 to 80:20 hexanes/EtOAc) gave the title compound as a white solid (24.1 mg, 0.068 mmol, 34% yield) and recovered *N*-hexyl-4-(trifluoromethyl)benzamide (27.4 mg, 0.100 mmol, 50% recovery).

Rf: 0.45 (80:20 hexanes/EtOAc)

¹H NMR (500 MHz, Chloroform-*d*) δ 7.85 (d, *J* = 8.0 Hz, 2H), 7.75 – 7.42 (m, 2H), 7.35 (d, *J* = 4.4 Hz, 4H), 7.28 (q, *J* = 4.5 Hz, 1H), 6.45 (d, *J* = 7.9 Hz, 1H), 5.15 (q, *J* = 7.7 Hz, 1H), 2.04 – 1.79 (m, 2H), 1.49 – 1.19 (m, 6H), 0.86 (t, *J* = 6.7 Hz, 3H).

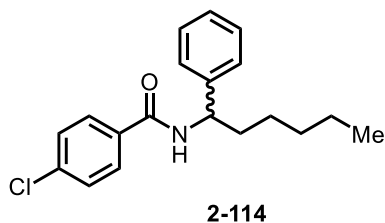
¹³C NMR (126 MHz, Chloroform-*d*) δ 165.58, 142.14, 138.09, 133.41, 133.15, 128.93, 127.71, 127.54, 126.76, 125.71 (q, *J* = 3.6 Hz), 123.78 (q, *J* = 272.3 Hz), 54.40, 36.26, 31.68, 26.13, 22.63, 14.13.

¹⁹F NMR (377 MHz, Chloroform-*d*) δ -63.03.

IR (neat, cm⁻¹): 3316, 2930, 2858, 1623, 1635, 1548, 1327, 1127, 1067, 860.

HRMS: (ESI) (*m/z*): [M+H] calculated for C₂₀H₂₂F₃NO, 350.1731, found 350.1745.

4-chloro-*N*-(1-phenylhexyl)benzamide (2-114)



The general procedure for the α -arylation of benzamides was followed using 4-chloro-*N*-hexylbenzamide (48 mg, 0.200 mmol, 1.00 equiv), **PC1** (4.5 mg, 0.004 mmol, 0.02 equiv), NiCl₂•DME (2.2 mg, 0.010 mmol, 0.05 equiv), BiOx (1.4 mg, 0.010 mmol, 0.05 equiv), K₃PO₄ (85 mg, 0.400 mmol, 2.00 equiv), and bromobenzene (156 μ L, 1.500 mmol, 7.50 equiv) in 1.0 mL EtOAc. Purification by silica

gel chromatography (70:30 hexanes/EtOAc) gave the title compound as a white solid (16.9 mg, 0.054 mmol, 27% yield) and recovered 4-chloro-*N*-hexylbenzamide (11.5 mg, 0.048 mmol, 24% recovery).

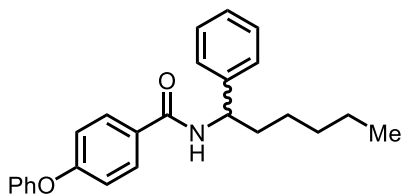
Rf: 0.35 (70:30 hexanes/EtOAc)

¹H NMR (400 MHz, Chloroform-*d*) δ 7.70 (d, $J = 8.1$ Hz, 2H), 7.40 (s, 1H), 7.37 – 7.26 (m, 5H), 6.26 (d, $J = 8.0$ Hz, 1H), 5.13 (q, $J = 7.7$ Hz, 1H), 1.90 (dt, $J = 15.8, 9.3$ Hz, 2H), 1.54 – 1.16 (m, 7H), 0.87 (d, $J = 7.0$ Hz, 3H).

¹³C NMR (100 MHz, Chloroform-*d*) δ 165.76, 142.36, 137.74, 133.18, 128.88, 128.86, 128.50, 127.59, 126.76, 54.24, 36.29, 31.69, 26.13, 22.62, 14.13.

HRMS: (ESI) (m/z): [M+H] calculated for C₁₉H₂₂ClNO, 316.1468, found 316.1466.

4-phenoxy-*N*-(1-phenylhexyl)benzamide (2-115)



2-115

The general procedure for the α -arylation of benzamides was followed *N*-hexyl-4-phenoxybenzamide (60 mg, 0.200 mmol, 1.00 equiv), **PC6** (5.1 mg, 0.004 mmol, 0.02 equiv), NiCl₂•DME (2.2 mg, 0.010 mmol, 0.05 equiv),

BiOx (1.4 mg, 0.010 mmol, 0.05 equiv), K₃PO₄ (85 mg, 0.400 mmol, 2.00 equiv), and bromobenzene (156 μ L, 1.500 mmol, 7.50 equiv) in 1 mL EtOAc/DMAc (9:1). Purification by silica gel chromatography (100% toluene to 96:4 toluene/Et₂O) gave the title compound as a white solid (30.1 mg, 0.080 mmol, 40% yield) and recovered *N*-hexyl-4-phenoxybenzamide (25.5 mg, 0.086 mmol, 43% recovery).

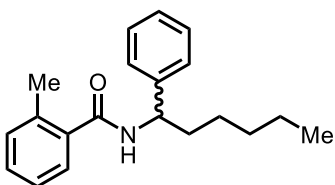
Rf: 0.35 (95:5 toluene/Et₂O)

¹H NMR (401 MHz, Chloroform-*d*) δ 7.74 (d, J = 8.4 Hz, 2H), 7.41 – 7.30 (m, 5H), 7.27 (d, J = 6.4 Hz, 2H), 7.16 (t, J = 7.5 Hz, 1H), 7.03 (d, J = 8.1 Hz, 2H), 6.99 (d, J = 8.9 Hz, 2H), 6.27 (d, J = 8.1 Hz, 1H), 5.15 (q, J = 7.6 Hz, 1H), 1.90 (dt, J = 14.9, 8.5 Hz, 2H), 1.55 – 1.12 (m, 6H), 0.87 (t, J = 6.5 Hz, 3H).

¹³C NMR (176 MHz, Chloroform-*d*) δ 166.11, 160.49, 156.14, 142.59, 130.09, 129.21, 128.95, 128.84, 127.50, 126.75, 124.32, 119.82, 117.97, 54.06, 36.39, 31.72, 26.13, 22.65, 14.17.

HRMS: (ESI) (m/z): [M+H] calculated for C₂₅H₂₇NO₂, 374.2120, found 374.2150.

2-methyl-*N*-(1-phenylhexyl)benzamide (2-116)



2-116

The general procedure for the α -arylation of benzamides was followed using *N*-hexyl-2-methylbenzamide (46 mg, 0.200 mmol, 1.00 equiv), **PC6** (5.1 mg, 0.004 mmol, 0.02 equiv), NiCl₂•DME (2.2 mg, 0.010 mmol, 0.05 equiv), BiOx (1.4 mg, 0.010 mmol, 0.05 equiv), K₃PO₄ (85 mg, 0.400 mmol, 2.00 equiv), and bromobenzene (156 μ L, 1.500 mmol, 7.50 equiv) in 1 mL EtOAc/DMAc (9:1). Purification by silica gel chromatography (90:10 to 80:20 hexanes/EtOAc) gave the title compound as a white solid (18.6 mg, 0.062 mmol, 31% yield) and recovered *N*-hexyl-2-methylbenzamide (24.0 mg, 0.110 mmol, 55% recovery).

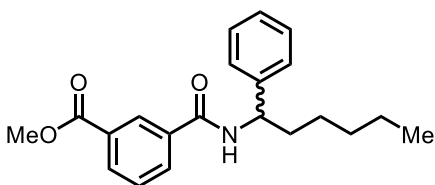
Rf: 0.25 (80:20 hexanes/EtOAc)

¹H NMR (500 MHz, Chloroform-*d*) δ 7.47 – 7.11 (m, 9H), 6.00 (d, J = 8.3 Hz, 1H), 5.15 (p, J = 7.4 Hz, 1H), 2.39 (s, 2H), 1.86 (p, J = 7.4, 6.8 Hz, 3H), 1.51 – 1.17 (m, 6H), 0.88 (t, J = 6.4 Hz, 3H).

¹³C NMR (126 MHz, Chloroform-*d*) δ 169.37, 142.57, 136.78, 136.17, 131.07, 129.89, 128.81, 128.62, 127.47, 126.66, 125.81, 53.80, 36.44, 31.68, 26.12, 22.66, 19.86, 14.14.

HRMS: (ESI) (m/z): [M+H] calculated for C₂₀H₂₅NO, 296.2014, found 296.2026.

methyl 3-((1-phenylhexyl)carbamoyl)benzoate (2-117)



2-117

The general procedure for the α -arylation of benzamides was followed using methyl 3-(hexylcarbamoyl)benzoate (53 mg, 0.200 mmol, 1.00 equiv), **PC6** (5.1 mg, 0.004 mmol, 0.02 equiv), NiCl₂•DME (2.2 mg, 0.010 mmol, 0.05 equiv), BiOx (1.4 mg, 0.010 mmol, 0.05 equiv), K₃PO₄ (85 mg, 0.400 mmol, 2.00 equiv), and bromobenzene (156 μ L, 1.500 mmol, 7.50 equiv) in 1 mL EtOAc/DMAc (9:1). Purification by silica gel chromatography (70:30 hexanes/EtOAc) gave the title compound as a white solid (10.5 mg, 0.030 mmol, 15% yield) and recovered methyl 3-(hexylcarbamoyl)benzoate (39.0 mg, 0.148 mmol, 74% recovery).

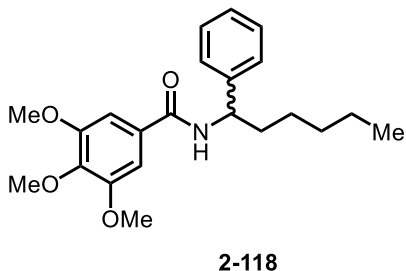
Rf: 0.35 (80:20 hexanes/EtOAc)

¹H NMR (400 MHz, Chloroform-*d*) δ 8.35 (s, 1H), 8.14 (d, *J* = 7.6 Hz, 1H), 8.03 (d, *J* = 7.8 Hz, 1H), 7.51 (t, *J* = 7.8 Hz, 1H), 7.40 – 7.30 (m, 5H), 7.28 (d, *J* = 3.1 Hz, 1H), 6.44 (d, *J* = 8.2 Hz, 2H), 5.17 (q, *J* = 7.6 Hz, 2H), 3.93 (s, 3H), 1.93 (dq, *J* = 16.4, 9.4, 7.1 Hz, 2H), 1.33 (m, 6H), 0.86 (t, *J* = 6.7 Hz, 3H).

¹³C NMR (176 MHz, Chloroform-*d*) δ 166.55, 165.69, 142.26, 135.08, 132.52, 132.14, 130.54, 129.08, 128.91, 127.66, 127.48, 126.84, 54.30, 52.57, 36.26, 31.71, 26.16, 22.65, 14.17.

HRMS: (ESI) (m/z): [M+H] calculated for C₂₁H₂₅NO₃, 340.1912, found 340.1913.

3,4,5-trimethoxy-N-(1-phenylhexyl)benzamide (2-118)



The general procedure for the α -arylation of benzamides was followed using *N*-hexyl-3,4,5-trimethoxybenzamide (59 mg, 0.200 mmol, 1.00 equiv), **PC6** (5.1 mg, 0.004 mmol, 0.02 equiv), NiCl₂•DME (2.2 mg, 0.010 mmol, 0.05 equiv), BiOx (1.4 mg, 0.010 mmol, 0.05 equiv), K₃PO₄ (85 mg, 0.400 mmol, 2.00 equiv), and bromobenzene (156 μ L, 1.500 mmol, 7.50 equiv) in 1 mL EtOAc/DMAc (9:1). Purification by silica gel chromatography (80:20% hexanes/EtOAc) gave the title compound as a white solid (33.8 mg, 0.091 mmol, 45% yield) and recovered *N*-hexyl-3,4,5-trimethoxybenzamide (16.9 mg, 0.057 mmol, 29% recovery).

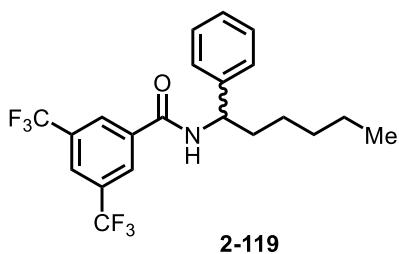
Rf: 0.35 (70:30 hexanes/EtOAc)

¹H NMR (400 MHz, Chloroform-*d*) δ 7.61 – 7.18 (m, 5H), 6.98 (d, *J* = 2.0 Hz, 2H), 6.26 (d, *J* = 8.2 Hz, 1H), 5.14 (q, *J* = 8.6 Hz, 1H), 3.87 (m, 9H), 1.92 (h, *J* = 8.2, 6.8 Hz, 2H), 1.52 – 1.14 (m, 6H), 0.87 (t, *J* = 7.1, 3H).

¹³C NMR (176 MHz, Chloroform-*d*) δ 166.50, 153.14, 142.58, 140.86, 130.07, 128.67, 127.36, 126.75, 104.52, 60.91, 56.28, 54.21, 36.09, 31.62, 26.16, 22.56, 14.08.

HRMS: (ESI) (m/z): [M+H] calculated for C₂₂H₂₉NO₄, 372.2175, found 372.2097.

***N*-(1-phenylhexyl)-3,5-bis(trifluoromethyl)benzamide (2-119)**



The general procedure for the α -arylation of benzamides was followed using *N*-hexyl-3,5-bis(trifluoromethyl)benzamide (68 mg, 0.200 mmol, 1.00 equiv), **PC1** (4.5 mg, 0.004 mmol, 0.02 equiv), NiCl₂•DME (2.2 mg, 0.010 mmol, 0.05 equiv), BiOx (1.4 mg, 0.010 mmol, 0.05 equiv), K₃PO₄ (85 mg, 0.400 mmol, 2.00 equiv), and bromobenzene (156 μ L, 1.500 mmol, 7.50 equiv) in 1 mL EtOAc. Purification by silica gel chromatography (100% hexanes to 95:5 hexanes/EtOAc) gave the title compound as a clear sticky oil (53.3 mg, 0.128 mmol, 64% yield) and recovered *N*-hexyl-3,5-bis(trifluoromethyl)benzamide (21.5 mg, 0.062 mmol, 31% recovery).

Rf: 0.35 (95:5 hexanes/EtOAc)

¹H NMR (401 MHz, Chloroform-*d*) δ 8.18 (s, 2H), 7.98 (s, 1H), 7.36 (d, $J = 4.3$ Hz, 4H), 7.30 (m, 1H), 6.52 (d, $J = 8.0$ Hz, 1H), 5.15 (q, $J = 7.7$ Hz, 1H), 2.04 – 1.79 (m, 2H), 1.34 (m, 6H), 0.87 (t, $J = 6.7$ Hz, 3H).

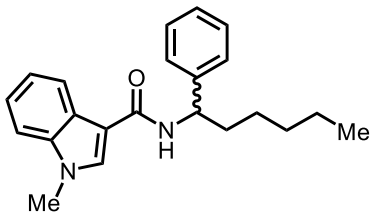
¹³C NMR (126 MHz, Chloroform-*d*) δ 163.89, 141.66, 136.83, 132.31 (q, $J = 33.8$ Hz), 129.03, 127.94, 127.58 – 126.91 (m), 126.88, 125.48 – 124.80 (m), 124.11, 121.94, 54.80, 35.99, 31.65, 26.15, 22.61, 14.12.

¹⁹F NMR (471 MHz, Chloroform-*d*) δ -62.93.

IR (neat, cm⁻¹): 3296, 2931, 2860, 1639, 1615, 1545, 1275, 1176, 1131, 1109, 907.

HRMS: (ESI) (m/z): [M+H] calculated for C₂₁H₂₁F₆NO, 418.1605, found 418.1621.

1-methyl-*N*-(1-phenylhexyl)-1*H*-indole-3-carboxamide (2-120)



2-120

The general procedure for the α -arylation of benzamides was followed. *N*-hexyl-1-methyl-1*H*-indole-3-carboxamide (52 mg, 0.200 mmol, 1.00 equiv), **PC6** (5.1 mg, 0.004 mmol, 0.02 equiv), NiCl₂•DME (2.2 mg, 0.010 mmol, 0.05 equiv), BiOx (1.4 mg, 0.010 mmol, 0.05 equiv), K₃PO₄ (85 mg, 0.400 mmol, 2.00 equiv), and bromobenzene (156 μ L, 1.500 mmol, 7.50 equiv) in 1 mL EtOAc/DMAc (9:1). Purification by silica gel chromatography (90:10 to 80:20 hexanes/EtOAc) gave the title compound as a white solid (27.4 mg, 0.082 mmol, 41% yield) and recovered *N*-hexyl-1-methyl-1*H*-indole-3-carboxamide (16.8 mg, 0.066 mmol, 33% recovery).

Rf: 0.15 (70:30 hexanes/EtOAc)

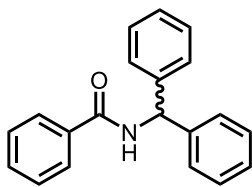
¹H NMR (400 MHz, Chloroform-*d*) δ 7.91 (d, $J = 7.5$ Hz, 1H), 7.63 (s, 1H), 7.31 (m, 8H), 6.18 (d, $J = 8.2$ Hz, 1H), 5.22 (q, $J = 7.6$ Hz, 1H), 3.77 (s, 3H), 1.92 (m, 2H), 1.51 – 1.15 (m, 6H), 0.85 (t, $J = 6.8$ Hz, 3H).

¹³C NMR (126 MHz, Chloroform-*d*) δ 164.46, 143.21, 137.37, 132.53, 128.76, 127.26, 126.75, 125.42, 122.60, 121.54, 120.11, 111.07, 110.23, 53.41, 36.77, 33.35, 31.79, 26.17, 22.66, 14.16.

IR (neat, cm⁻¹): 3288, 2953, 2930, 2858, 1724, 1635, 1482, 1261, 730.

HRMS: (ESI) (m/z): [M+H] calculated for C₂₂H₂₆N₂O, 335.2123, found 335.2167.

N-benzhydrylbenzamide (2-121)



2-121

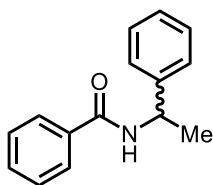
The general procedure for the α -arylation of benzamides was followed using *N*-benzylbenzamide (42 mg, 0.200 mmol, 1.00 equiv), **PC1** (2.2 mg, 0.002 mmol, 0.01 equiv), NiCl₂•DME (4.4 mg, 0.020 mmol, 0.10 equiv), BiOx (2.8 mg, 0.020 mmol, 0.10 equiv), K₃PO₄ (85 mg, 0.400 mmol, 2.00 equiv), and bromobenzene (156 μ L, 1.500 mmol, 7.50 equiv) in 1.0 mL DMAc. Purification by silica gel chromatography (100% hexanes to 90:10 hexanes/EtOAc) gave the title compound as a white solid (24.1 mg, 0.068 mmol, 18% yield).

Rf: 0.25 (80:20 hexanes/EtOAc)

¹H NMR (700 MHz, Chloroform-*d*) δ 7.88 – 7.79 (m, 2H), 7.53 – 7.48 (m, 1H), 7.44 (td, $J = 7.8, 1.9$ Hz, 2H), 7.39 – 7.34 (m, 5H), 7.34 – 7.27 (m, 5H), 6.73 (d, $J = 7.9$ Hz, 1H), 6.46 (d, $J = 7.8$ Hz, 1H).

¹³C NMR (176 MHz, Chloroform-*d*) δ 166.61, 141.56, 134.34, 131.82, 128.87, 128.75, 127.70, 127.63, 127.18, 57.57.

N-(1-phenylethyl)benzamide (**2-122**)



2-122

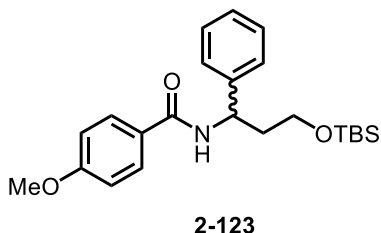
The general procedure for the α -arylation of benzamides was followed using *N*-ethylbenzamide (32 mg, 0.200 mmol, 1.00 equiv), **PC6** (5.1 mg, 0.004 mmol, 0.02 equiv), NiCl₂•DME (2.2 mg, 0.010 mmol, 0.05 equiv), BiOx (1.4 mg, 0.010 mmol, 0.05 equiv), K₃PO₄ (85 mg, 0.400 mmol, 2.00 equiv), and bromobenzene (156 μ L, 1.500 mmol, 7.50 equiv) in 1 mL EtOAc/DMAc (9:1). Purification by silica gel chromatography (80:20 hexanes/EtOAc) gave the title compound as a white solid (18.9 mg, 0.084 mmol, 42% yield).

Rf: 0.40 (70:30 hexanes/EtOAc)

¹H NMR (700 MHz, Chloroform-*d*) δ 7.79 – 7.75 (m, 2H), 7.48 (t, $J = 7.5$ Hz, 1H), 7.40 (dd, $J = 14.2, 7.5$ Hz, 3H), 7.35 (t, $J = 7.6$ Hz, 3H), 7.28 (d, $J = 7.5$ Hz, 1H), 6.48 (d, $J = 11.1$ Hz, 1H), 5.34 (p, $J = 7.1$ Hz, 1H), 1.60 (d, $J = 6.9$ Hz, 3H).

¹³C NMR (176 MHz, Chloroform-*d*) δ 166.69, 143.25, 134.67, 131.55, 128.83, 128.63, 127.53, 127.05, 126.36, 49.31, 21.84.

***N*-(3-((*tert*-butyldimethylsilyl)oxy)-1-phenylpropyl)-4-methoxybenzamide (2-123)**



The general procedure for the α -arylation of benzamides was followed using *N*-(3-((*tert*-butyldimethylsilyl)oxy)propyl)-4-methoxybenzamide (32 mg, 0.100 mmol, 1.00 equiv), **PC1** (2.2 mg, 0.002 mmol, 0.02 equiv), NiCl₂•DME (1.1 mg, 0.005 mmol, 0.05 equiv), BiOx (0.7 mg, 0.005 mmol, 0.05 equiv), K₃PO₄ (43 mg, 0.200 mmol, 2.00 equiv), and bromobenzene (78 μ L, 0.750 mmol, 7.50 equiv) in 1 mL EtOAc. Purification by silica gel chromatography (80:20 to 70:30 hexanes/EtOAc) gave the title compound as a white solid (13.8 mg, 0.035 mmol, 35% yield) and recovered *N*-(3-((*tert*-butyldimethylsilyl)oxy)propyl)-4-methoxybenzamide (8.9 mg, 0.028 mmol, 28% recovery).

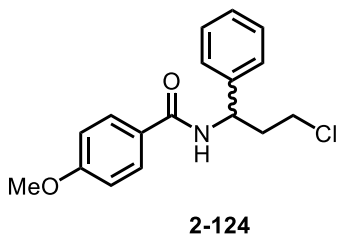
Rf: 0.30 (70:30 hexanes/EtOAc)

¹H NMR (500 MHz, Chloroform-*d*) δ 7.78 (d, $J = 8.6$ Hz, 2H), 7.65 (d, $J = 7.0$ Hz, 1H), 7.37 – 7.28 (m, 3H), 7.23 (d, $J = 6.4$ Hz, 1H), 6.90 (d, $J = 8.3$ Hz, 2H), 5.36 (q, $J = 6.3$ Hz, 1H), 3.84 (s, 3H), 3.76 – 3.38 (m, 2H), 2.20 (ddt, $J = 13.8, 9.0, 4.6$ Hz, 1H), 2.02 (dq, $J = 15.1, 4.7$ Hz, 1H), 0.90 (s, 9H), 0.06 (d, $J = 11.2$ Hz, 6H).

¹³C NMR (126 MHz, Chloroform-*d*) δ 166.29, 162.17, 142.09, 128.96, 128.54, 127.21, 127.03, 126.38, 113.67, 61.00, 55.49, 53.05, 38.07, 26.12, 18.57, -5.24 (d, *J* = 2.7 Hz).

HRMS: (ESI) (*m/z*): [*M*+*H*] calculated for C₂₃H₃₃NO₃Si, 400.2308, found 400.2296.

N-(3-chloro-1-phenylpropyl)-4-methoxybenzamide (2-124)



The general procedure for the α -arylation of benzamides was followed using *N*-(3-chloropropyl)-4-methoxybenzamide (23 mg, 0.100 mmol, 1.00 equiv), **PC1** (2.2 mg, 0.002 mmol, 0.02 equiv), NiCl₂•DME (1.1 mg, 0.005 mmol, 0.05 equiv), BiOx (0.7 mg, 0.005 mmol, 0.05 equiv), K₃PO₄ (43 mg, 0.200 mmol, 2.00 equiv), and bromobenzene (78 μ L, 0.750 mmol, 7.50 equiv) in 1 mL EtOAc. Purification by silica gel chromatography (80:20 to 70:30 hexanes/EtOAc) gave the title compound as a white solid (13.5 mg, 0.044 mmol, 44% yield) and recovered *N*-(3-chloropropyl)-4-methoxybenzamide (7.5 mg, 0.035 mmol, 35% recovery).

Rf: 0.60 (1:1 hexanes/EtOAc)

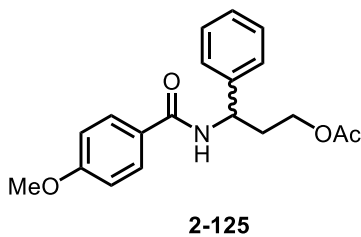
¹H NMR (700 MHz, Chloroform-*d*) δ 7.74 (d, *J* = 8.7 Hz, 2H), 7.37 (d, *J* = 4.4 Hz, 4H), 7.30 (dt, *J* = 8.8, 4.3 Hz, 1H), 6.91 (d, *J* = 8.9 Hz, 2H), 6.48 (dd, *J* = 16.7, 8.1 Hz, 1H), 5.38 (q, *J* = 7.5 Hz, 1H), 3.84 (s, 3H), 3.57 (dt, *J* = 11.1, 6.8 Hz, 1H), 3.51 (dt, *J* = 11.1, 6.8 Hz, 1H), 2.46 (dq, *J* = 14.2, 7.0 Hz, 1H), 2.35 (dq, *J* = 13.7, 6.8 Hz, 1H).

¹³C NMR (176 MHz, Chloroform-*d*) δ 166.39, 162.42, 140.99, 129.12, 128.91, 128.00, 126.72, 126.57, 113.91, 55.57, 52.10, 41.72, 38.98.

IR (neat, cm⁻¹): 3327, 2968, 1623, 1609, 1505, 1260, 1180, 1025, 859.

HRMS: (ESI) (*m/z*): [*M*+*H*] calculated for C₁₇H₁₈ClNO₂, 304.1104, found 304.1102.

3-(4-methoxybenzamido)-3-phenylpropyl acetate (2-125)



The general procedure for the α -arylation of benzamides was followed using 3-(4-methoxybenzamido)propyl acetate (50 mg, 0.200 mmol, 1.00 equiv), **PC1** (4.5 mg, 0.004 mmol, 0.02 equiv), NiCl₂•DME (2.2 mg, 0.010 mmol, 0.05 equiv), BiOx (1.4 mg, 0.010 mmol, 0.05 equiv), K₃PO₄ (85 mg, 0.400 mmol, 2.00 equiv), and bromobenzene (156 μ L, 1.500 mmol, 7.50 equiv) in 1 mL EtOAc. Purification by silica gel chromatography (70:30 to 1:1 hexanes/EtOAc) gave the title compound as a white solid (43.6 mg, 0.134 mmol, 67% yield) and recovered 3-(4-methoxybenzamido)propyl acetate (17.3 mg, 0.066 mmol, 34% recovery).

Rf: 0.35 (1:1 hexanes/EtOAc)

¹H NMR (500 MHz, Chloroform-*d*) δ 7.75 (d, J = 7.3 Hz, 2H), 7.50 – 7.13 (m, 5H), 6.89 (d, J = 7.3 Hz, 2H), 6.68 (d, J = 8.2 Hz, 1H), 5.32 (q, J = 6.5 Hz, 1H), 4.12 (td, J = 7.1, 6.4, 3.3 Hz, 2H), 3.82 (s, 3H), 2.25 (m, 2H), 1.99 (s, 3H).

¹³C NMR (126 MHz, Chloroform-*d*) δ 171.11, 166.40, 162.34, 141.52, 128.92, 128.88, 127.69, 126.73, 126.58, 113.84, 61.73, 55.50, 51.34, 34.94, 21.03.

IR (neat, cm⁻¹): 3359, 2974m 1731, 1633, 1607, 1531, 1504, 1304, 1250, 1180, 1109.

HRMS: (ESI) (m/z): [M+H] calculated for C₁₉H₂₁NO₄, 328.1549, found 328.1522.

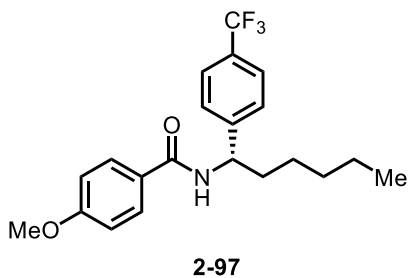
4.3.10 Enantioselective α -Arylation of Benzamides:

General Procedures for the Enantioselective α -Arylation of Benzamides:

To an oven-dried 1 dram vial equipped with a Teflon-coated magnetic stir bar in a N₂ filled glovebox was added [Ir(dF(CF₃)ppy)₂(4,4'-di-*t*-bubpy)]PF₆ (**PC1**) (2.3 mg, 0.002

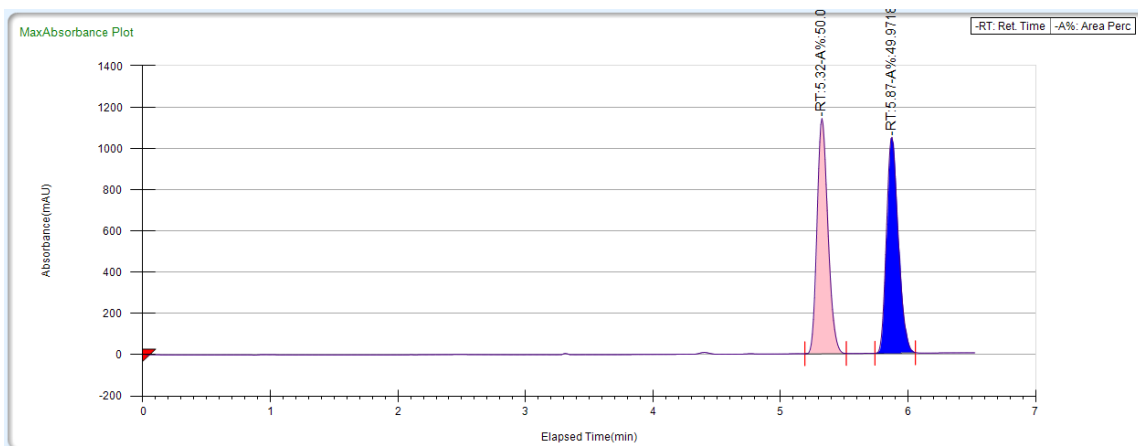
mmol, 0.02 equiv), NiCl₂•DME (1.1 mg, 0.005 mmol, 0.05 equiv), (4*S*,4'*S*)-4,4'-diisopropyl-4,4',5,5'-tetrahydro-2,2'-bioxazole (*i*-PrBiOx) (1.1 mg, 0.01 mmol, 0.05 equiv), K₃PO₄ (43 mg, 0.2 mmol, 2.00 equiv), and benzamide (0.1 mmol, 1 equiv) were combined and suspended in 1.0 mL of dry, degassed EtOAc at room temperature. The mixture was stirred for 10 minutes before adding aryl bromide (1.5 mmol, 7.50 equiv). The vial was sealed with a Teflon cap before removing from the glovebox. The reaction was stirred at 900 rpm for 48 hours in an aluminum block equipped with a 34 W blue LED placed 1 cm away and cooled to approximately -10 °C using a cryocool and a recirculating pump. Upon completion, the reaction mixture was quenched with 1 mL EtOAc and run through a silica gel plug with 5 mL EtOAc. The solvent was removed by rotary evaporation and the crude reaction mixture was purified by silica gel chromatography.

(*S*)-4-methoxy-*N*-(1-(4-(trifluoromethyl)phenyl)hexyl)benzamide (2-97)



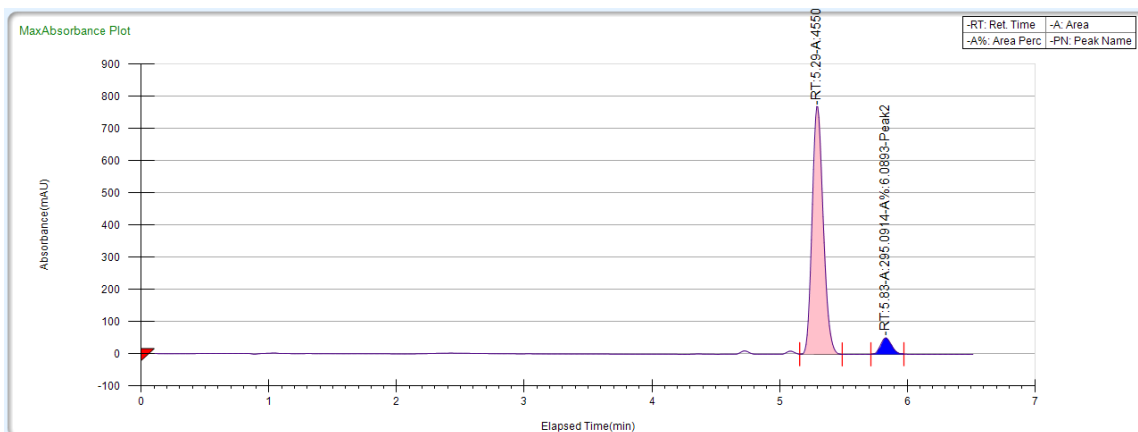
The general procedure for the enantioselective α -arylation of benzamides was followed using **2-91** (47 mg, 0.200 mmol, 1.00 equiv), **PC1** (4.5 mg, 0.004 mmol, 0.02 equiv), NiCl₂•DME (2.2 mg, 0.010 mmol, 0.05 equiv), *i*-PrBiOx (2.2 mg, 0.010 mmol, 0.05 equiv), K₃PO₄ (85 mg, 0.400 mmol, 2.00 equiv), and 4-bromobenzotrifluoride (210 μ L, 1.500 mmol, 7.50 equiv) in 1 mL EtOAc at -15 °C for 48 hours. Purification by silica gel chromatography (90:10 to 80:20 hexanes/EtOAc) gave the title compound as a white solid (37.8 mg, 0.100 mmol, 50% yield, 88% ee) and recovered **2-91** (22.4 mg, 0.095 mmol, 48% recovery).

SFC: Racemic standard



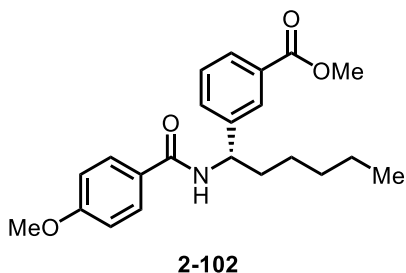
	area percent	area	time
peak 1	50.0282%	6590.599	5.32min
peak 2	49.9718%	6583.1598	5.89min

SFC: Enantioenriched product



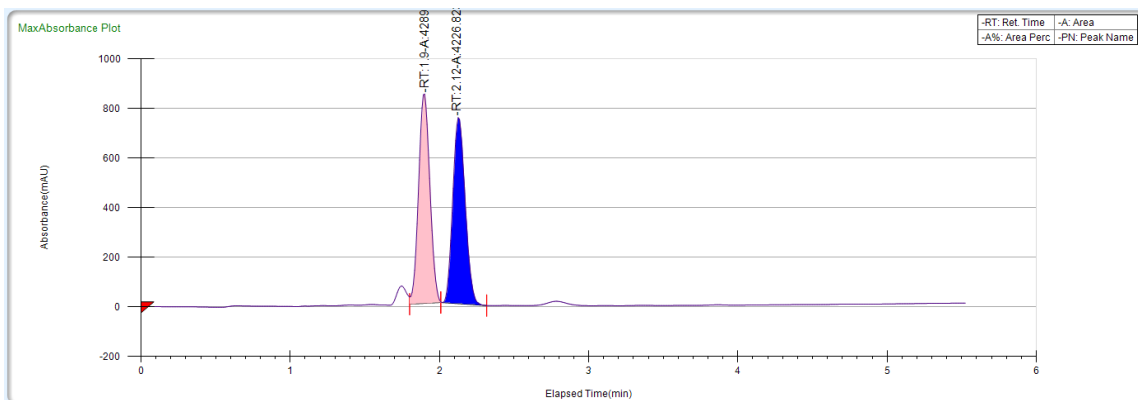
	area percent	area	time
peak 1	93.9107%	4550.9786	5.29min
peak 2	6.0893%	295.0914	5.83min

methyl (S)-3-(1-(4-methoxybenzamido)hexyl)benzoate (2-102)



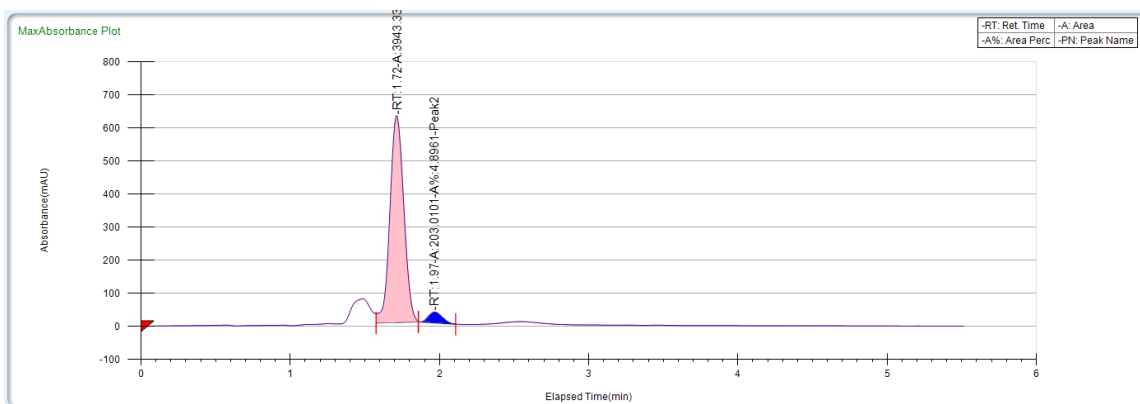
The general procedure for the enantioselective α -arylation of benzamides was followed using **2-91** (47 mg, 0.200 mmol, 1.00 equiv), **PC1** (4.5 mg, 0.004 mmol, 0.02 equiv), NiCl₂•DME (2.2 mg, 0.010 mmol, 0.05 equiv), *i*-PrBiOx (2.2 mg, 0.010 mmol, 0.05 equiv), K₃PO₄ (85 mg, 0.400 mmol, 2.00 equiv), and methyl-3-bromobenzoate (323 mg, 1.500 mmol, 7.50 equiv) in 1 mL EtOAc at -15 °C for 48 hours. Purification by silica gel chromatography (100% hexanes to 80:20 hexanes/EtOAc) gave the title compound as a white solid (34.0 mg, 0.092 mmol, 46% yield, 91% ee) and recovered **2-91** (25.4 mg, 0.108 mmol, 54% recovery).

SFC: Racemic standard



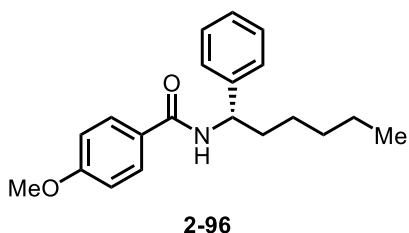
	area percent	area	time
peak 1	50.3684%	4289.5713	1.9 min
peak 2	49.6316%	4226.8231	2.12 min

SFC: Enantioenriched product



	area percent	area	time
peak 1	95.1039%	3943.3333	1.72 min
peak 2	4.8961%	203.0101	1.97 min

(S)-4-methoxy-N-(1-phenylhexyl)benzamide (**2-96**)



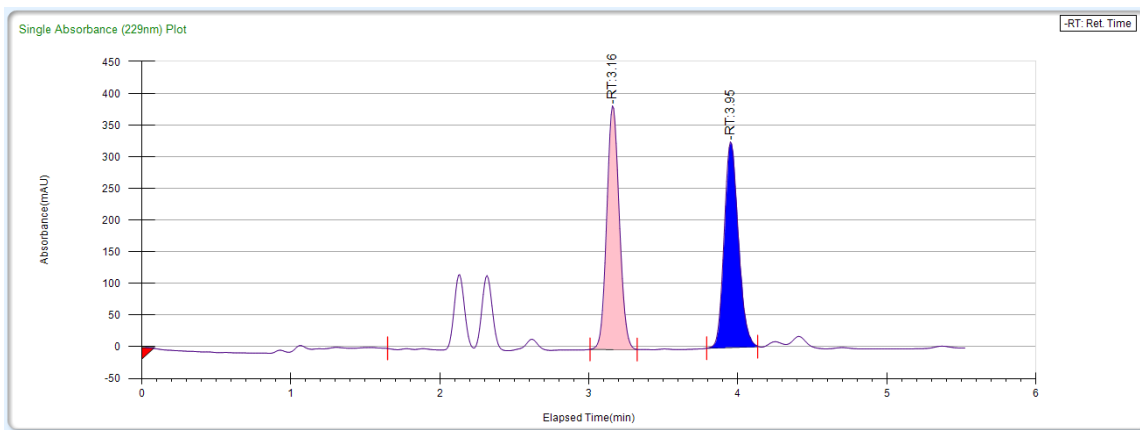
Using an in situ generated nickel catalyst:

The general procedure for the enantioselective α -arylation of benzamides was followed using **2-91** (47 mg, 0.200 mmol, 1.00 equiv), **PC1** (4.5 mg, 0.004 mmol, 0.02 equiv), NiCl₂•DME (2.2 mg, 0.010 mmol, 0.05 equiv), *i*-PrBiOx (2.2 mg, 0.010 mmol, 0.05 equiv), K₃PO₄ (85 mg, 0.400 mmol, 2.00 equiv), and methyl-3-bromobenzoate (323 mg, 1.500 mmol, 7.50 equiv) in 1 mL EtOAc at -10 °C for 48 hours. Purification by silica gel chromatography (70:30 hexanes/EtOAc) gave the title compound as a white solid (24.9 mg, 0.080 mmol, 40% yield, 77% ee) and recovered **2-91** (26.3 mg, 0.112 mmol, 56% recovery).

Using a discrete nickel catalyst: The general procedure for the enantioselective α -arylation of benzamides was followed **2-91** (23 mg, 0.100 mmol, 1.00 equiv), **PC1** (2.2 mg, 0.002 mmol, 0.02 equiv), *i*-PrBiOxNiCl₂ (**2-160**) (1.7 mg, 0.005 mmol, 0.05 equiv), K₃PO₄ (43

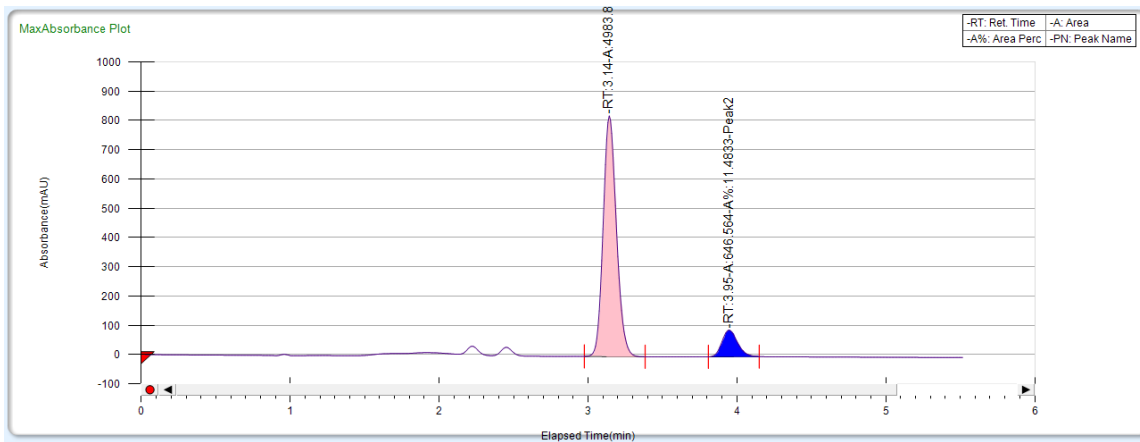
mg, 0.200 mmol, 2.00 equiv), and bromobenzene (78 μ L, 0.750 mmol, 7.50 equiv) in 0.5 mL EtOAc at -10 $^{\circ}$ C for 24 hours. Purification by silica gel chromatography (70:30 hexanes/EtOAc) gave the title compound as a white solid (9.7 mg, 0.031 mmol, 31% yield, 88% ee).

SFC: Racemic standard

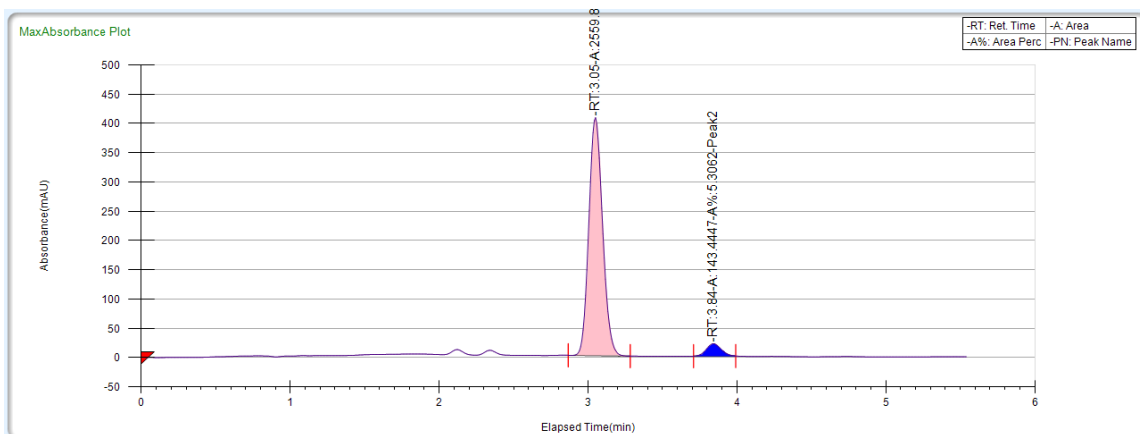


	area percent	area	time
peak 1	51.0861%	2190.4958	3.16 min
peak 2	48.9139%	2097.3522	3.95 min

SFC: Enantioenriched product

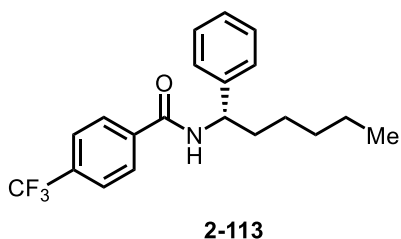


	area percent	area	time
peak 1	88.5167%	4983.895	3.14min
peak 2	11.4833%	646.564	3.95min



	area percent	area	time
peak 1	94.6938%	2559.8757	3.05min
peak 2	5.3062%	143.4447	3.84min

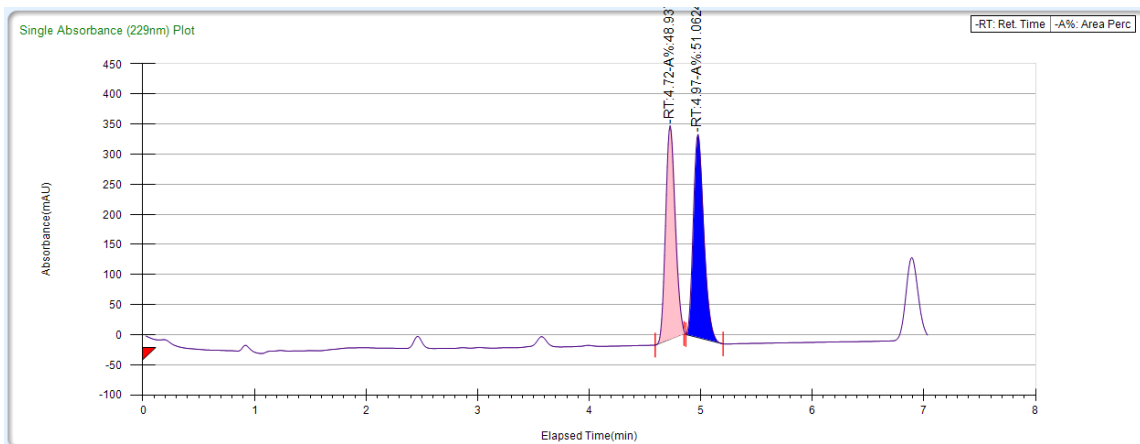
(S)-N-(1-phenylhexyl)-4-(trifluoromethyl)benzamide (2-113)



The general procedure for the enantioselective α -arylation of benzamides was followed using *N*-hexyl-4-(trifluoromethyl)benzamide (55 mg, 0.200 mmol, 1.00 equiv), **PC1** (4.5 mg, 0.004 mmol, 0.02 equiv), $\text{NiCl}_2 \cdot \text{DME}$ (2.2 mg, 0.010 mmol, 0.05 equiv), *i*-PrBiOx (2.2 mg, 0.010 mmol, 0.05 equiv), K_3PO_4 (85 mg, 0.400 mmol, 2.00 equiv), and bromobenzene (156 μL , 1.500 mmol, 7.50 equiv) in 1 mL EtOAc at -15°C for 48 hours. Purification by silica gel chromatography (100% hexanes to 80:20 hexanes/EtOAc) gave the title compound as a white solid (32.0

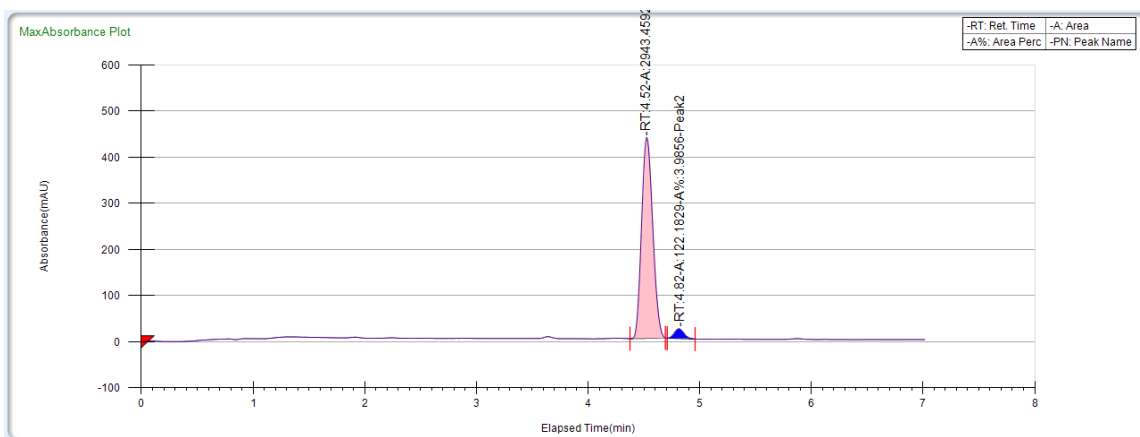
mg, 0.092 mmol, 46% yield, 92% ee) and recovered *N*-hexyl-4-(trifluoromethyl)benzamide (29.0 mg, 0.106 mmol, 53% recovery).

SFC: Racemic standard



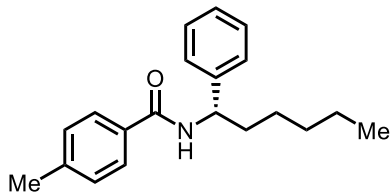
	area percent	area	time
peak 1	48.9376%	2072.4988	4.72min
peak 2	51.0624%	2162.4811	4.97min

SFC: Enantioenriched product



	area percent	area	time
peak 1	96.0144%	2943.4592	4.52 min
peak 2	3.9856	122.1829	4.82 min

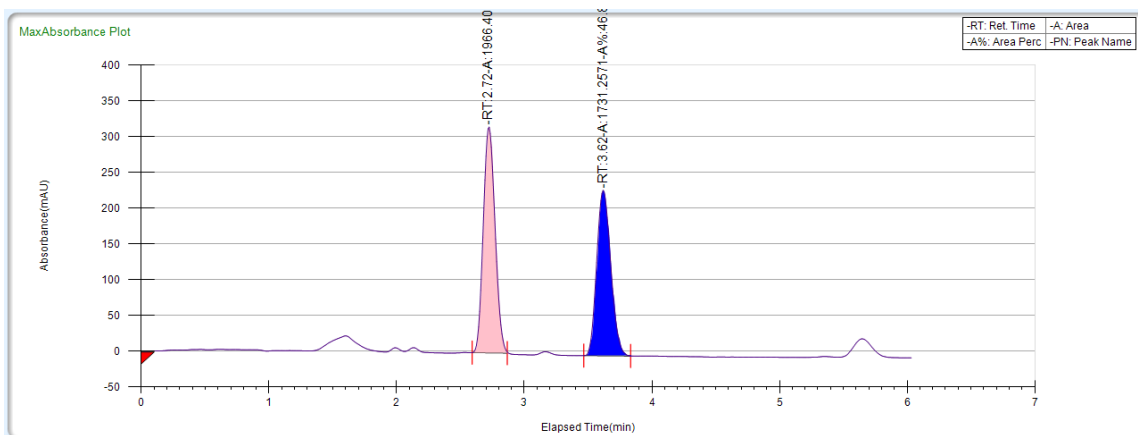
(S)-4-methyl-N-(1-phenylhexyl)benzamide (2-112)



2-112

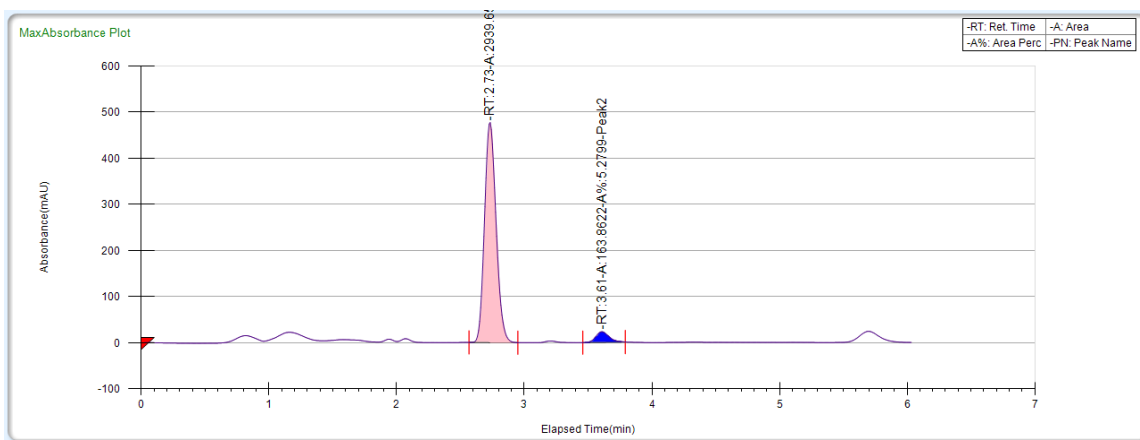
The general procedure for the enantioselective α -arylation of benzamides was followed using *N*-hexyl-4-methylbenzamide (44 mg, 0.200 mmol, 1.00 equiv), **PC1** (4.5 mg, 0.004 mmol, 0.02 equiv), NiCl₂•DME (2.2 mg, 0.010 mmol, 0.05 equiv), *i*-PrBiOx (2.2 mg, 0.010 mmol, 0.05 equiv), K₃PO₄ (85 mg, 0.400 mmol, 2.00 equiv), and bromobenzene (156 μ L, 1.500 mmol, 7.50 equiv) in 1 mL EtOAc at -10 °C for 24 hours. Purification by silica gel chromatography (100% hexanes to 80:20 hexanes/EtOAc) gave the title compound as a white solid (20.3 mg, 0.068 mmol, 34% yield, 89% ee) and recovered *N*-hexyl-4-methylbenzamide (28.4 mg, 0.130 mmol, 65% recovery).

SFC: Racemic standard



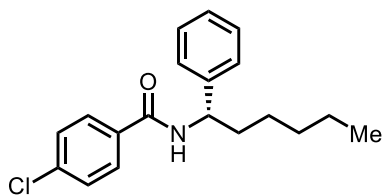
	area percent	area	time
peak 1	53.1797%	1966.4067	2.72 min
peak 2	46.8203%	1731.2571	3.62 min

SFC: Enantioenriched product



	area percent	area	time
peak 1	94.7201%	2939.6525	2.73 min
peak 2	5.2799%	163.8622	3.61 min

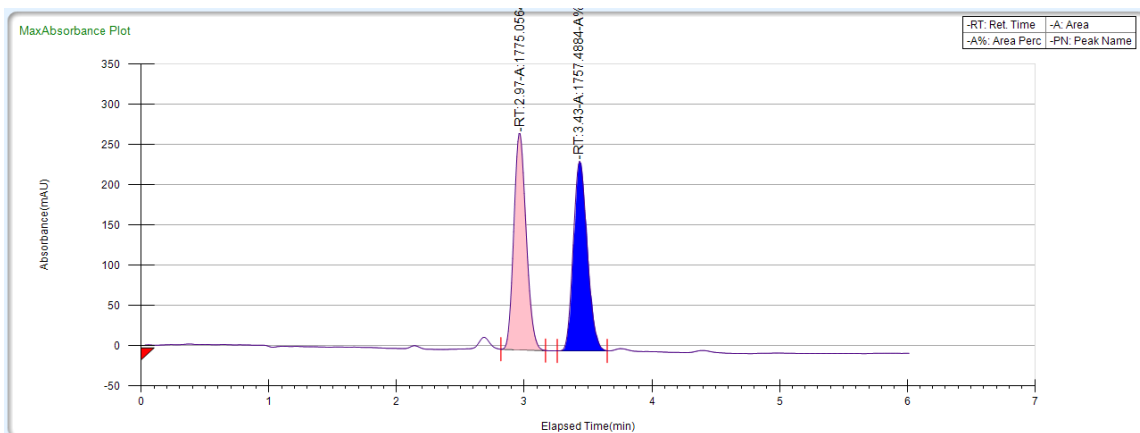
(S)-4-chloro-N-(1-phenylhexyl)benzamide (2-114)



2-114

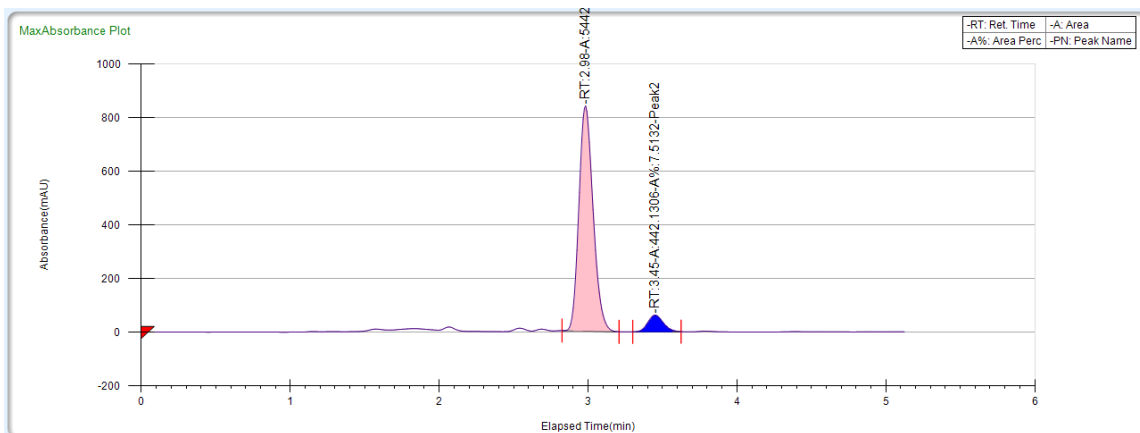
The general procedure for the enantioselective α -arylation of benzamides was followed using *N*-hexyl-4-methylbenzamide (48 mg, 0.200 mmol, 1.00 equiv), **PC1** (4.5 mg, 0.004 mmol, 0.02 equiv), NiCl₂•DME (2.2 mg, 0.010 mmol, 0.05 equiv), *i*-PrBiOx (2.2 mg, 0.010 mmol, 0.05 equiv), K₃PO₄ (85 mg, 0.400 mmol, 2.00 equiv), and bromobenzene (156 μ L, 1.500 mmol, 7.50 equiv) in 1 mL EtOAc at -10 °C. for 24 hours. Purification by silica gel chromatography (100% hexanes to 70:30 hexanes/EtOAc) gave the title compound as a white solid (17.5 mg, 0.054 mmol, 28% yield, 85% ee) and recovered *N*-hexyl-4-methylbenzamide (33.7 mg, 0.140 mmol, 70% recovery).

SFC: Racemic standard



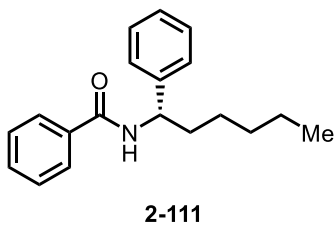
	area percent	area	time
peak 1	50.2487%	1775.0564	2.97 min
peak 2	49.7513%	1757.4884	3.43 min

SFC: Enantioenriched product



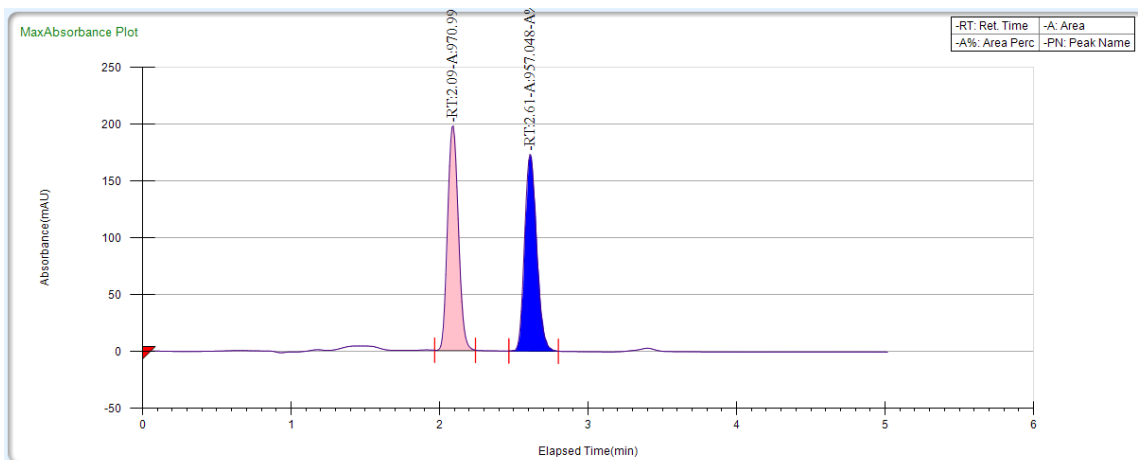
	area percent	area	time
peak 1	92.4868%	5442.5628	2.98 min
peak 2	7.5132%	442.1306	3.45 min

(S)-N-(1-phenylhexyl)benzamide (2-111)



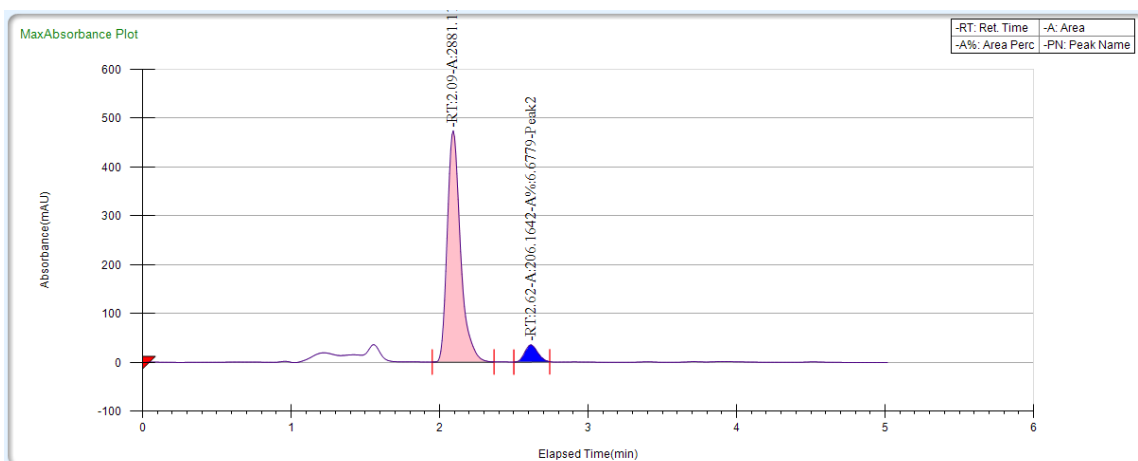
The general procedure for the enantioselective α -arylation of benzamides was followed using *N*-hexylbenzamide (41 mg, 0.200 mmol, 1.00 equiv), **PC1** (4.5 mg, 0.004 mmol, 0.02 equiv), $\text{NiCl}_2 \cdot \text{DME}$ (2.2 mg, 0.010 mmol, 0.05 equiv), *i*-PrBiOx (2.2 mg, 0.010 mmol, 0.05 equiv), K_3PO_4 (85 mg, 0.400 mmol, 2.00 equiv), and bromobenzene (156 μL , 1.500 mmol, 7.50 equiv) in 1 mL EtOAc at $-15\text{ }^\circ\text{C}$ for 48 hours. Purification by silica gel chromatography (100% hexanes to 85:15 hexanes/EtOAc) gave the title compound as a white solid (18.3 mg, 0.066 mmol, 33% yield, 86% ee) and recovered *N*-hexylbenzamide (27.5 mg, 0.134 mmol, 67% recovery).

SFC: Racemic standard



	area percent	area	time
peak 1	50.3616%	970.9913	2.09 min
peak 2	49.6384%	957.048	2.61 min

SFC: Enantioenriched product



	area percent	area	time
peak 1	93.3221%	2881.1128	2.09 min
peak 2	6.6779%	206.1642	2.62 min

4.3.11 Absolute Stereochemistry of Benzamides

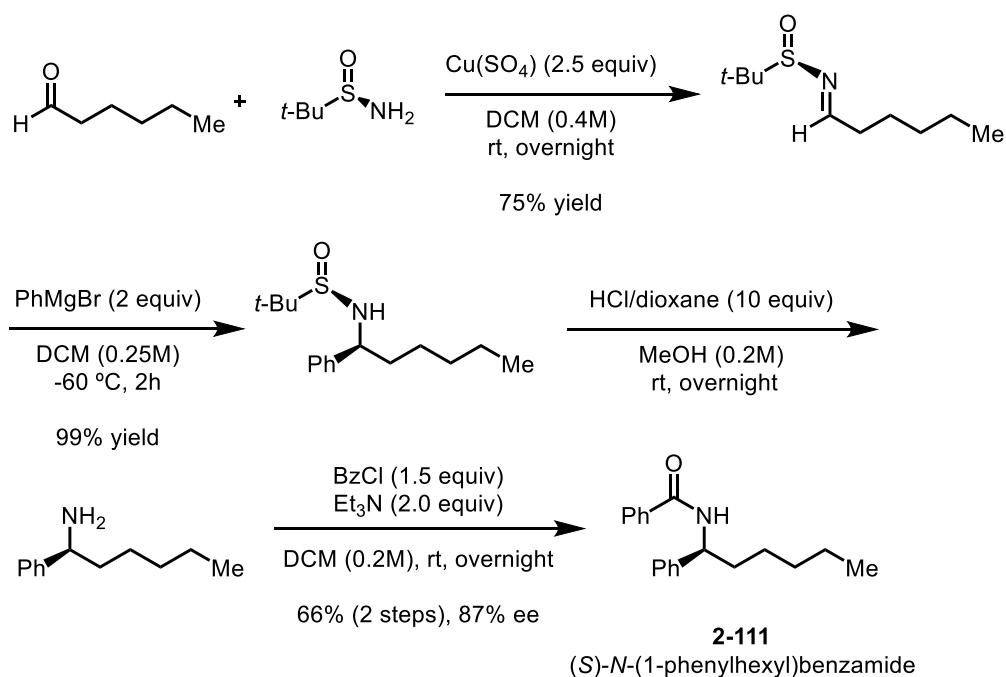
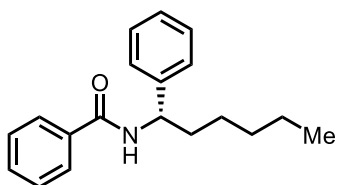


Figure 4-19 Synthesis of enantiopure **2-111**.

The absolute stereochemistry of **2-111** was assigned through a modified synthesis of enantiopure material, using hexanal and (R)-(+)-*tert*-butyl sulfonamide, reported by

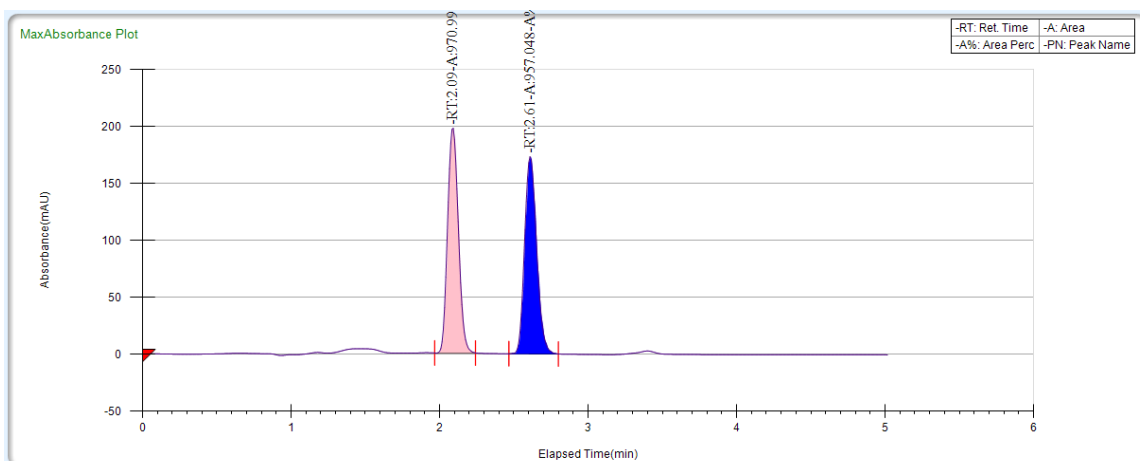
Ellman *et al* and outlined below.²⁶³⁻²⁶⁴ The stereochemistry of **2-96**, **2-97**, **2-102**, **2-111**, **2-112**, **2-113**, and **2-114** were assigned by analogy.

(S)-N-(1-phenylhexyl)benzamide (2-111)



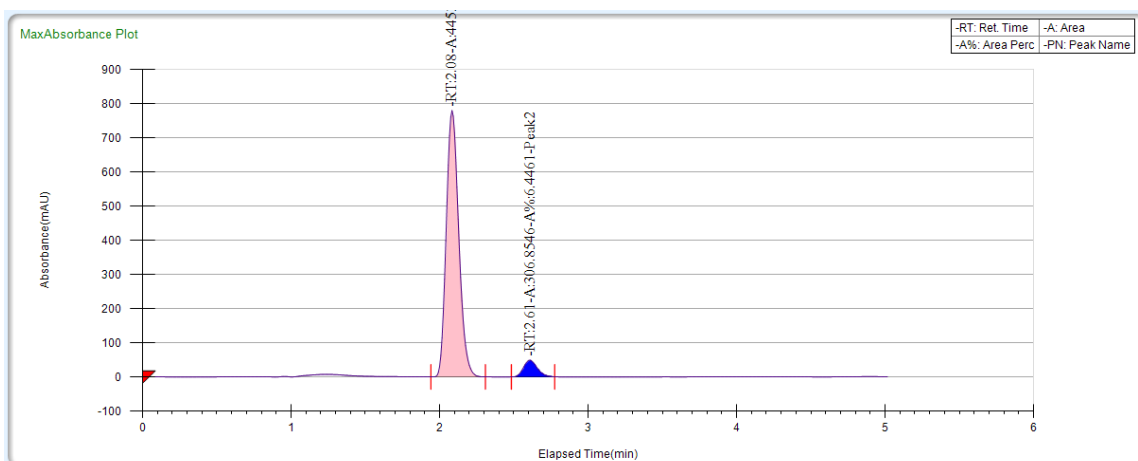
2-111

SFC: Racemic standard



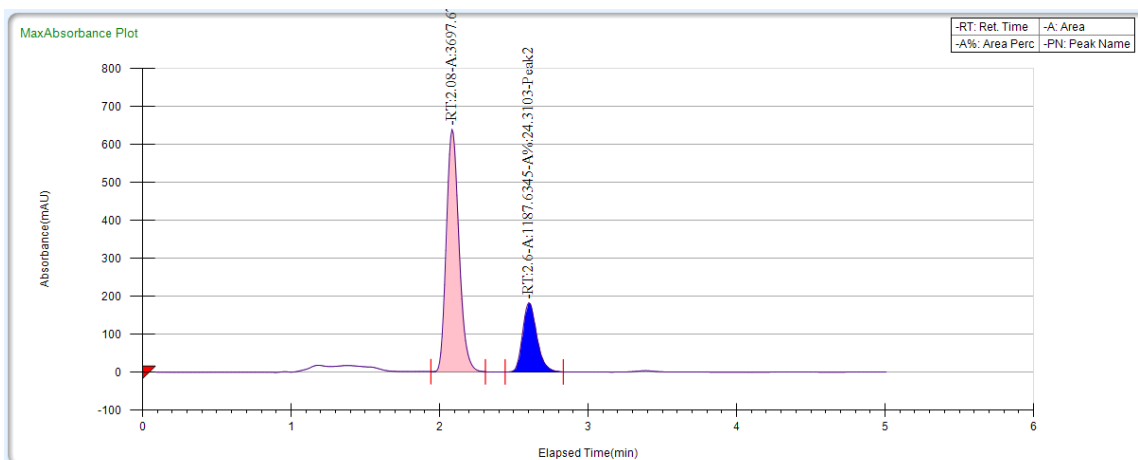
	area percent	area	time
peak 1	50.3616%	970.9913	2.09 min
peak 2	49.6384%	957.048	2.61 min

SFC: Enantioenriched product



	area percent	area	time
peak 1	93.5539%	4453.4291	2.08 min
peak 2	6.4461%	306.8546	2.61 min

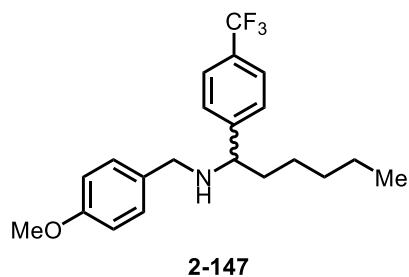
SFC: Co-injection of racemic and enantioenriched product



	area percent	area	time
peak 1	75.6897%	3697.6717	2.08 min
peak 2	24.3103%	1187.6345	2.6 min

4.3.12 Synthetic demonstrations:

N-(4-methoxybenzyl)-1-(4-(trifluoromethyl)phenyl)hexan-1-amine (2-147)



To an oven-dried 1 dram vial equipped with a Teflon-coated magnetic stir bar was added LAH (22 mg, 0.57 mmol, 5.00 equiv) and THF (1 mL). The suspension was cooled to 0 °C and **2-97** (43.2 mg, 0.114 mmol, 1.00 equiv) was added slowly as a solution in 1 mL THF. The

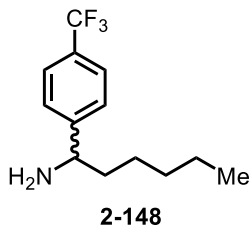
reaction was then warmed to room temperature and stirred for 3 hours. The reaction was then cooled to 0 °C and carefully quenched with 1 M NaOH until a white precipitate formed. The slurry was then filtered through celite and the precipitate washed with Et₂O. The organics were then concentrated by rotary evaporation to give the title compound as a clear oil (38.2 mg, 0.101 mmol, 92% yield)

¹H NMR (401 MHz, Chloroform-*d*) δ 7.58 (d, *J* = 8.0 Hz, 2H), 7.43 (d, *J* = 8.0 Hz, 2H), 3.95 (t, *J* = 6.9 Hz, 1H), 1.81 – 1.44 (m, 2H), 1.44 – 1.04 (m, 6H), 1.00 – 0.64 (m, 3H).

¹³C NMR (176 MHz, Chloroform-*d*) δ 150.93, 126.85, 125.66 – 125.20 (m), 56.11, 39.78, 31.88, 26.24, 22.69, 14.17.

¹⁹F NMR (658 MHz, Chloroform-*d*) δ -62.37.

1-(4-(trifluoromethyl)phenyl)hexan-1-amine (**2-148**)



To a vial with (**2-147**) (20 mg, 0.053 mmol, 1 equiv) was added 0.5 mL of DCM. The vial was cooled in an ice bath and DDQ (14 mg, 0.612 mmol, 1.20 equiv) was added, followed by 0.1 mL H₂O. The reaction was run overnight, then poured into a flask containing Sat.

NaHCO₃. The organic layer was extracted 3 x DCM, then the combined organics were washed 3 x 1 M HCl (aq). The combined aqueous layers were basified with 1 M NaOH

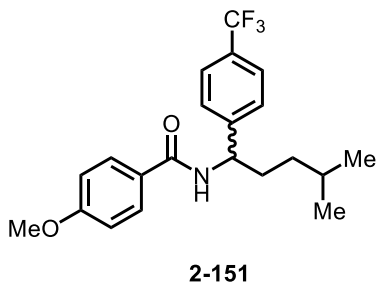
and then extracted 3 x DCM. The organic layers were dried with brine and then Na₂SO₄. The organic layers were concentrated to give the title compound as a clear oil (3.8 mg, 0.016 mmol, 28% yield).

¹H NMR (401 MHz, Chloroform-*d*) δ 7.59 (d, *J* = 7.3 Hz, 2H), 7.44 (d, *J* = 6.8 Hz, 2H), 7.16 (d, *J* = 6.2 Hz, 1H), 6.84 (d, *J* = 5.8 Hz, 1H), 3.79 (s, 2H), 3.65 (t, *J* = 6.3 Hz, 1H), 3.55 (d, *J* = 12.1 Hz, 1H), 3.44 (d, *J* = 14.2 Hz, 1H), 1.63 (m, 2H), 1.31 – 1.03 (m, 6H), 0.83 (t, *J* = 5.7 Hz, 1H).

¹³C NMR (176 MHz, Chloroform-*d*) δ 158.77, 149.01, 132.67, 129.37, 127.82, 125.42 (q, *J* = 3.8 Hz), 124.47 (q, *J* = 271.8 Hz), 113.92, 62.38, 55.40, 51.14, 38.54, 31.90, 25.99, 22.64, 14.14.

¹⁹F NMR (377 MHz, Chloroform-*d*) δ -62.32.

4-methoxy-*N*-(4-methyl-1-(4-(trifluoromethyl)phenyl)pentyl)benzamide (2-151)



The general procedure for the α-arylation of benzamides was followed using **2-93** (117 mg, 0.500 mmol, 1.00 equiv), **PC1** (11.2 mg, 0.010 mmol, 0.02 equiv), NiCl₂•DME (5.5 mg, 0.025 mmol, 0.05 equiv), BiOx (3.5 mg, 0.025 mmol, 0.05 equiv), K₃PO₄ (212 mg, 1.000 mmol, 2.00 equiv), and 4-bromobenzotrifluoride (525 μL, 3.750 mmol, 7.50 equiv) in 5 mL EtOAc. Purification by silica gel chromatography (90:10 to 80:20 hexanes/EtOAc) gave the title compound as a white solid (93 mg, 0.245 mmol, 49% yield).

Rf: 0.30 (70:30 hexanes/EtOAc)

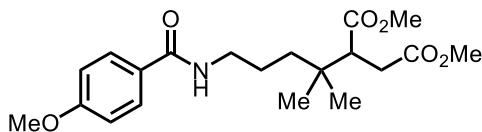
¹H NMR (400 MHz, Chloroform-*d*) δ 7.74 (d, J = 8.4 Hz, 2H), 7.59 (d, J = 7.9 Hz, 2H), 7.46 (d, J = 8.0 Hz, 2H), 6.92 (d, J = 8.4 Hz, 2H), 6.31 (d, J = 7.8 Hz, 1H), 5.14 (q, J = 7.5 Hz, 1H), 3.84 (s, 3H), 1.88 (q, J = 7.9 Hz, 2H), 1.77 – 1.46 (m, 2H), 1.38 – 1.07 (m, 3H), 0.88 (d, J = 6.6 Hz, 6H).

¹³C NMR (176 MHz, Chloroform-*d*) δ 166.47, 162.44, 146.99, 128.88, 127.02, 126.59, 125.75 (q, J = 3.8 Hz), 124.24 (q, J = 272.3 Hz), 113.92, 55.56, 53.99, 35.40, 34.28, 28.00, 22.60.

¹⁹F NMR (658 MHz, Chloroform-*d*) δ -62.48.

HRMS: (ESI) (m/z): [M+H] calculated for C₂₁H₂₄F₃NO₂, 380.1837, found 380.1838.

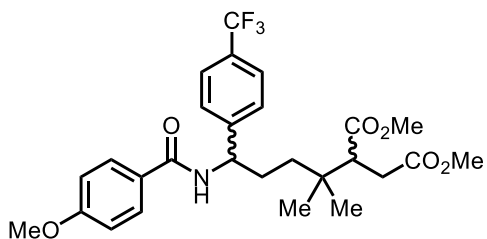
dimethyl 2-(5-(4-methoxybenzamido)-2-methylpentan-2-yl)succinate (2-150)



2-150

The title compound was synthesized using the general procedures for PCET using **2-93** (47 mg, 0.200 mmol, 1.00 equiv), [Ir(dF(CF₃)ppy)₂(5,5'-(dCF₃)bpy)]PF₆ (**PC2**) (4.6 mg, 0.004 mmol, 0.02 equiv), (BuO)₂OP(O)(NBu₄) (4.5 mg, 0.004 mmol, 0.02 equiv), and dimethylfumarate (58 mg, 0.4 mmol, 2 equiv) were combined and suspended in 1.0 mL of dry, degassed PhCF₃ at room temperature. Purification by silica gel chromatography (70:30 to 1:1 hexanes/EtOAc) gave the title compound as a brown sticky oil (69.7 mg, 0.184 mmol, 92% yield) which matched the reported spectra.¹⁵⁵

dimethyl-2-(5-(4-methoxybenzamido)-2-methyl-5-(4-(trifluoromethyl)phenyl)pentan-2-yl)succinate (2-152)



2-152

Method A: The title compound was synthesized using the general procedure for the α -arylation of benzamides with **2-150** (69 mg, 0.182 mmol, 1.00 equiv), **PC6** (4.2 mg, 0.036 mmol, 0.02 equiv), NiCl₂•DME (2.0 mg, 0.093 mmol, 0.05 equiv),

BiOx (1.3 mg, 0.093 mmol, 0.05 equiv), K₃PO₄ (77 mg, 0.364 mmol, 2.00 equiv), and 4-bromobenzotrifluoride (195 μ L, 1.395 mmol, 7.50 equiv) in 2 mL EtOAc. Purification by silica gel chromatography (70:30 to 1:1 hexanes/EtOAc) gave the title compound as a brown oil (31.7 mg, 0.060 mmol, 33% yield) and recovered **2-150** (40.4 mg, 0.106 mmol, 58% recovery).

Method B: The title compound was synthesized using the general procedures for PCET using **2-151** (76 mg, 0.200 mmol, 1.00 equiv), [Ir(dF(CF₃)ppy)₂(5,5'-(dCF₃)Bpy)]PF₆ (**PC2**) (4.6 mg, 0.004 mmol, 0.02 equiv), (BuO)₂OP(O)(NBu₄) (4.5 mg, 0.004 mmol, 0.02 equiv), and dimethylfumarate (58 mg, 0.4 mmol, 2.00 equiv) were combined and suspended in 1.0 mL of dry, degassed PhCF₃ at room temperature. Purification by silica gel chromatography (70:30 to 1:1 hexanes/EtOAc) gave the title compound as a brown oil (39.0 mg, 0.074 mmol, 37% yield). The title compound was isolated as a 1:1.1 (A to B) mixture of inseparable diastereomers. Although the absolute configuration of each diastereomer could not be determined, several resonances in ¹H and ¹³C NMR could be assigned through HSQC and TOCSY experiments.

Rf: 0.20 (70:30 hexanes/EtOAc)

¹H NMR (700 MHz, Chloroform-*d*) δ 7.91 (d, *J* = 8.5 Hz, 1H), 7.79 (d, *J* = 8.5 Hz, 1H), 7.55 (dd, *J* = 8.5, 3.3 Hz, 2H), 7.45 (d, *J* = 7.9 Hz, 1H), 7.43 (d, *J* = 7.9 Hz, 1H), 7.15 (d, *J*

= 7.0 Hz, 1H, *diastereomer A*), 6.89 (dd, $J = 8.6, 6.1$ Hz, 2H), 6.81 (s, 1H, *diastereomer B*), 5.09 (q, $J = 7.1$ Hz, 1H, *diastereomer B*), 5.01 – 4.94 (m, 1H, *diastereomer A*), 3.82 (d, $J = 2.1$ Hz, 3H), 3.68 – 3.53 (m, 6H), 2.85 (dd, $J = 12.1, 3.0$ Hz, 1H), 2.81 – 2.72 (m, 2H), 2.47 – 2.31 (m, 1H), 2.11 – 1.93 (m, 1H, *diastereomer A*), 1.89 – 1.80 (m, 1H, *diastereomer B*), 1.75 (tt, $J = 13.2, 5.1$ Hz, 1H, *diastereomer A*), 1.51 (td, $J = 13.5, 13.0, 2.8$ Hz, 1H, *diastereomer A*), 1.36 – 1.20 (m, 3H, *diastereomer B*), 0.89 (dd, $J = 23.2, 18.4$ Hz, 7H).

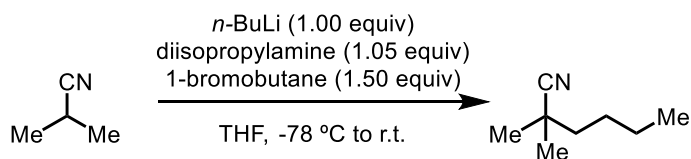
^{13}C NMR (176 MHz, Chloroform-*d*) δ 174.48, 174.44, 173.20, 173.14, 166.60, 162.39, 162.36, 147.74, 146.67, 129.17, 129.03, 126.95, 126.71, 126.40, 126.22, 125.65 (q, $J = 3.6$ Hz), 124.19 (q, $J = 272.0$ Hz) 124.23 (q, $J = 271.7$ Hz), 113.79, 113.67, 55.47, 55.46, 54.36 (*diastereomer A*), 54.18 (*diastereomer B*), 51.98, 51.96, 51.86, 51.63, 48.82, 48.78, 38.66 (*diastereomer A*), 37.60 (*diastereomer B*), 35.02, 34.92, 32.26, 31.90, 30.93 (*diastereomer A*), 30.40 (*diastereomer B*), 25.55, 25.38, 25.34, 25.07.

IR (neat, cm^{-1}): 3299, 2954, 1733, 1629, 1606, 1503, 1324, 1254, 1162, 1119, 1067, 844.

HRMS: (ESI) (m/z): [M+H] calculated for $\text{C}_{27}\text{H}_{32}\text{F}_3\text{NO}_6$, 524.2260, found 524.2182.

4.4 Experimental Details for Chapter 3

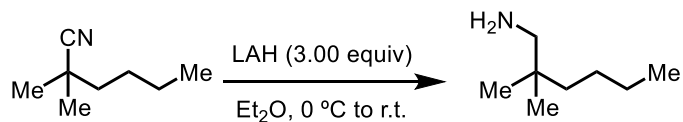
2,2-dimethylhexanenitrile



To a 25 mL oven-dried round-bottom flask equipped with a Teflon-coated magnetic stir bar

was added diisopropylamine (1.40 mL, 10.00 mmol, 1.05 equiv) and THF (40 mL, 0.25 M). The reaction was cooled to $-78\text{ }^\circ\text{C}$ and *n*-BuLi (2.5 M in hexanes) (3.81 mL, 9.52 mmol, 1.00 equiv) was added and then the reaction was stirred for 1 hour before adding isobutyronitrile (0.85 mL, 9.52 mmol, 1.00 equiv). The reaction was stirred for 1 hour before adding 1-bromobutane (1.53 mL, 14.28 mmol, 1.50 equiv). The reaction was then warmed to room temperature and stirred overnight. The reaction was cooled to $0\text{ }^\circ\text{C}$ and carefully quenched with sat. NH_4Cl and extracted 3 x 50 mL DCM. The organic layers were dried with 100 mL brine, then Na_2SO_4 and the solvent was removed by rotary evaporation to give the title compound as a yellow oil (1.05 g, 8.00 mmol, 84% yield), which was used without further purification in subsequent steps.²⁶⁵

2,2-dimethylhexan-1-amine

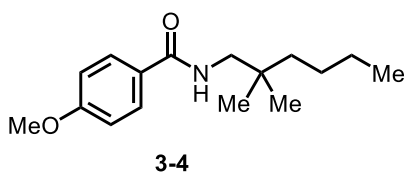


To a 100 mL oven-dried round-bottom flask equipped with a

Teflon-coated magnetic stir bar was added LAH (0.95 g, 25.10 mmol, 3.00 equiv) and Et_2O (40 mL, 0.21 M). The suspension was cooled to $0\text{ }^\circ\text{C}$ and 2,2-dimethylhexanenitrile (1.05 g, 8.39 mmol, 1.00 equiv) was added slowly as a solution in 10 mL Et_2O . The reaction was then warmed to room temperature and stirred for 3 hours. The reaction was

then cooled to 0 °C and carefully quenched with 1 M NaOH until a white precipitate formed. The slurry was then filtered through celite and the precipitate washed with Et₂O. The organics were then concentrated by rotary evaporation to give the title compound as a clear oil (867 mg, 6.71 mmol, 80% yield), which was used without further purification in subsequent steps.²⁶⁵

N-(2,2-dimethylhexyl)-4-methoxybenzamide (3-4)



The general procedure for benzamide synthesis coupling was followed using 4-methoxybenzoic acid (1.40 g, 9.23 mmol, 1.10 equiv), oxalyl chloride (1.01 mL, 12.00 mmol, 1.43 equiv), DCM (37 mL, 0.2 M), DMF (3 drops), Et₃N (1.17 mL, 8.39 mmol, 1.0 equiv), 2,2-dimethylhexan-1-amine (8.39 mmol, 1.00 equiv) and DMAP (15 mg, 0.15 mmol, 0.02 equiv). Purification by aqueous work-up followed by silica gel chromatography (80:20 to 70:30 hexanes/EtOAc) gave the title compound as a white crystalline solid (1.954 mg, 6.71 mmol, 80% yield over 4 steps) that was one spot by TLC and GCMS. NMR showed an equilibrium of rotamers.

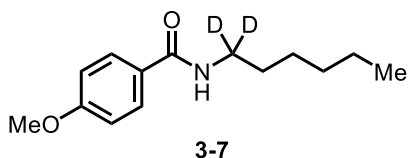
Rf: 0.30 (70:30 hexanes/EtOAc)

¹H NMR (401 MHz, Chloroform-*d*) δ 8.10 (d, *J* = 8.5 Hz, 1H), 7.73 (d, *J* = 8.4 Hz, 2H), 6.98 (d, *J* = 8.7 Hz, 1H), 6.93 (d, *J* = 8.5 Hz, 2H), 6.01 (s, 1H), 3.90 (s, 1H), 3.85 (s, 3H), 3.28 (d, *J* = 6.2 Hz, 2H), 1.39 – 1.10 (m, 6H), 0.92 (d, *J* = 11.7 Hz, 9H).

¹³C NMR (126 MHz, Chloroform-*d*) δ 167.21, 162.05, 132.85, 128.65, 127.44, 114.19, 113.75, 55.64, 55.42, 49.59, 39.91, 34.54, 26.20, 25.11, 23.62, 14.18.

HRMS: (ESI) (*m/z*): [M+H] calculated for C₁₆H₂₅NO₂, 264.1963, found 264.1988.

***N*-(hexyl-1,1-*d*₂)-4-methoxybenzamide (3-7)**



To a 25 mL oven-dried round-bottom flask equipped with a Teflon-coated magnetic stir bar was added LiAlD₄ (0.100 mg, 2.38 mmol, 3.00 equiv) and Et₂O (4 mL, 0.20 M). The suspension was cooled to 0 °C and *n*-hexyl nitrile (0.10 mL, 0.79 mmol, 1.0 equiv) was added slowly as a solution in 1 mL Et₂O. The reaction was then warmed to room temperature and stirred for 3 hours. The reaction was then cooled to 0 °C and carefully quenched with 1 M NaOH until a white precipitate formed. The slurry was then filtered through celite and the precipitate washed with Et₂O. The organics were then concentrated by rotary evaporation to give the desired product as a clear oil which was used without further purification in subsequent steps.²⁶⁵

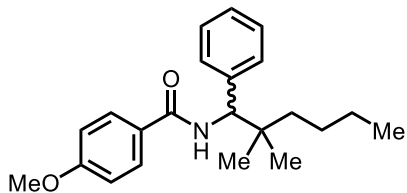
The general procedure for benzamide synthesis coupling was followed using 4-methoxybenzoic acid (132 mg, 0.87 mmol, 1.10 equiv), oxalyl chloride (0.09 mL, 1.05 mmol, 1.4 equiv), DCM (5 mL, 0.2 M), DMF (1 drops), Et₃N (0.11 mL, 0.79 mmol, 1.0 equiv), *N*-(hexyl-1,1-*d*₂) amine (0.79 mmol, 1.00 equiv) and DMAP (5 mg, 0.10 mmol, 0.02 equiv). Purification by silica gel chromatography (70:30 hexanes/EtOAc) gave the title compound as a white powder (126 mg, 0.53 mmol, 67% yield over three steps)

¹H NMR (700 MHz, Chloroform-*d*) δ 7.72 (d, *J* = 8.8 Hz, 1H), 6.89 (d, *J* = 8.8 Hz, 1H), 6.19 (d, *J* = 13.3 Hz, 1H), 3.82 (s, 2H), 1.56 (dd, *J* = 8.9, 6.3 Hz, 2H), 1.32 (m, 6H), 0.87 (td, *J* = 5.7, 4.6, 2.3 Hz, 3H).

¹³C NMR (176 MHz, Chloroform-*d*) δ 167.13, 162.08, 128.72, 127.27, 113.76, 55.48, 39.56 (p, *J* = 22.2, 21.4 Hz), 31.65, 29.62, 26.75, 22.68, 14.15.

HRMS: (ESI) (m/z): [M+H] calculated for C₁₄H₁₉D₂NO₂, 238.1776, found 238.1774.

***N*-(2,2-dimethyl-1-phenylhexyl)-4-methoxybenzamide (3-5)**



3-5

The general procedure for the α -arylation of benzamides was followed **3-4** (50 mg, 0.200 mmol, 1.00 equiv), **PC1** (4.5 mg, 0.004 mmol, 0.02 equiv), NiCl₂•DME (2.2 mg, 0.010 mmol, 0.05 equiv), BiOx

(1.4 mg, 0.010 mmol, 0.05 equiv), K₃PO₄ (85 mg, 0.400 mmol, 2.00 equiv), and bromobenzene (156 μ L, 1.500 mmol, 7.50 equiv) in 1 mL EtOAc. Purification by silica gel chromatography (90:10 to 70:30 hexanes/EtOAc) gave the title compound as a white solid (3.8 mg, 0.011 mmol, 6% yield) and recovered **3-4** (38.6 mg, 0.154 mmol, 77% recovery).

Rf: 0.25 (70:30 hexanes/EtOAc)

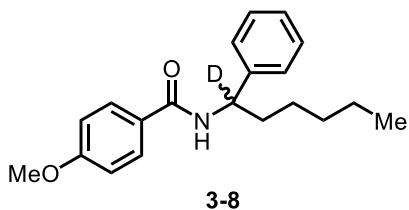
¹H NMR (700 MHz, Chloroform-*d*) δ 7.75 – 7.68 (m, 2H), 7.42 (d, *J* = 8.3 Hz, 1H), 7.32 – 7.18 (m, 5H), 6.93 (d, *J* = 8.5 Hz, 2H), 6.63 (d, *J* = 8.4 Hz, 1H), 6.59 (d, *J* = 9.1 Hz, 1H), 5.05 (d, *J* = 9.1 Hz, 1H), 3.84 (s, 3H), 3.72 (s, 1H), 1.37 – 1.22 (m, 4H), 1.00 – 0.85 (m, 9H).

¹³C NMR (176 MHz, Chloroform-*d*) δ 166.21, 162.23, 140.30, 131.14, 128.73, 128.40, 127.94, 127.47, 127.12, 113.93, 113.56, 60.85, 55.56, 55.45, 41.14, 39.62, 37.55, 29.85, 26.23, 26.20, 24.22, 23.89, 23.68, 14.28.

HRMS: (ESI) (m/z): [M+H] calculated for C₂₂H₂₉NO₂, 340.2276, found 340.2329.

4.4.1 Deuterium Studies:

4-methoxy-*N*-(1-phenylhexyl-1-*d*)benzamide (3-8)



The general procedure for the α -arylation of benzamides was followed using **3-7** (23.7 mg, 0.100 mmol, 1.00 equiv), **PC1** (2.3 mg, 0.002 mmol, 0.02 equiv), NiCl₂•DME (1.1 mg, 0.005 mmol, 0.05 equiv), BiOx (0.7 mg, 0.005 mmol, 0.05 equiv), K₃PO₄ (42 mg, 0.200 mmol, 2.00 equiv), and bromobenzene (78 μ L, 0.750 mmol, 7.50 equiv) in 0.5 mL EtOAc. Reaction was stopped after 2 hours. Purification by silica gel chromatography (70:30 hexanes/EtOAc) gave the title compound as a white solid.

Rf: 0.35 (70:30 hexanes/EtOAc)

¹H NMR (700 MHz, Chloroform-*d*) δ 7.73 (d, *J* = 8.4 Hz, 2H), 7.34 (d, *J* = 6.6 Hz, 4H), 6.90 (d, *J* = 9.0 Hz, 2H), 6.26 (s, 1H), 3.83 (s, 3H), 1.98 – 1.75 (m, 2H), 1.53 – 1.19 (m, 9H), 0.86 (t, *J* = 7.0 Hz, 3H).

¹³C NMR (176 MHz, Chloroform-*d*) δ 166.28, 162.24, 142.67, 129.82, 128.82, 128.80, 127.44, 127.07, 126.75, 114.35, 113.83, 55.53, 36.31, 31.73, 29.85 (t, *J* = 2.7 Hz), 26.10, 22.64, 14.16.

HRMS: (ESI) (*m/z*): [M+H] calculated for C₂₀H₂₄DNO₂, 313.2026, found 313.2046.

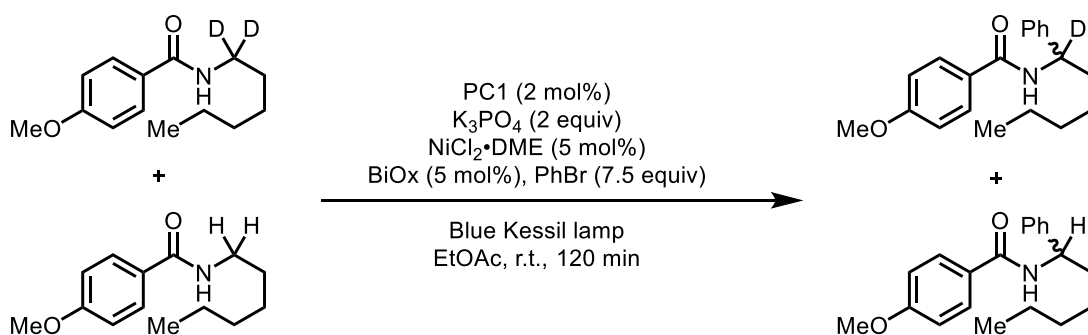


Figure 4-20 Competition experiment between **2-91** and **3-7**.

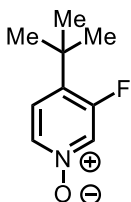
The general procedure for the α -arylation of benzamides was followed using **3-7** (11.9 mg, 0.050 mmol, 0.50 equiv) and **2-91** (11.8 mg, 0.050 mmol, 0.50 equiv), **PC1** (2.3 mg, 0.002 mmol, 0.02 equiv), NiCl₂•DME (1.1 mg, 0.005 mmol, 0.05 equiv), BiOx (0.7 mg, 0.005 mmol, 0.05 equiv), K₃PO₄ (42 mg, 0.200 mmol, 2.00 equiv), and bromobenzene (78 μ L, 0.750 mmol, 7.50 equiv) in 0.5 mL EtOAc. Reaction was stopped after 2 hours. Purification by silica gel chromatography (70:30 hexanes/EtOAc).

Run #1: **2-96** + **3-8** (8.0 mg, 0.026 mmol, 26% yield) and recovered **2-91+3-7** (15.7 mg, 0.067 mmol, 67% recovery).

Run #2: **2-96** + **3-8** (6.9 mg, 0.022 mmol, 22% yield) and recovered **2-91+3-7** (17.9 mg, 0.076 mmol, 76% recovery)

4.4.2 Synthesis of New Compounds

4-(tert-butyl)-3-fluoropyridine 1-oxide (**3-18**)



To an oven-dried round bottom flask under an N₂ atmosphere with a Teflon stir bar was added 3-fluoropyridine (0.26 mL, 3.0 mmol, 1.0 equiv) and DCM (18 mL). TIPSOTf (0.87 mL, 3.2 mmol, 1.05 equiv) was added dropwise and the reaction was stirred for 15 minutes at room temperature. Cool solution to -78 °C and 1,4-dioxane (1.14 mL) was added. Then, *t*-BuMgCl (1.7 M in THF) (7 mL, 12.0 mmol, 4.0 equiv) was added and the reaction was warmed to room temperature overnight. Reaction was quenched with H₂O and sat. NaHCO₃ and then extracted 3x25 mL DCM. The organic layers were dried with 50 mL brine, then over Na₂SO₄. Organics were concentrated and the crude oil was carried on without further purification.

The crude oil was then added to a 25 mL round bottom flask under an N₂ atmosphere with a Teflon stir bar and reflux condenser and dissolved in decaline (6 mL).

S₈ (110 mg, 3.3 mmol, 1.1 equiv) was added, and the reaction was placed under an N₂ atmosphere. The solution was stirred at 190 °C for 2 hours. Cool reaction and load directly on to silica gel chromatography (2:1 pentane/Et₂O, Rf: 0.15). Fractions were carefully concentrated via rotary evaporation (product is volatile!) and the clear oil was carried on directly to the next step.

Crude oil from the previous step was added to a 25 mL round bottom flask under an N₂ atmosphere with a Teflon stir bar and DCM (7.5 mL) was added. *m*-CPBA (1.00g, 3.0 mmol, 1.0 equiv) was added in a single portion and the reaction was stirred overnight. The reaction was partially concentrated (avoid concentrating to dryness since *m*-CPBA should not be completely dry) and then loaded on silica gel chromatography (100% EtOAc, then 100% DCM to 90:10 DCM/MeOH) to give 396 mg (78% yield over 3 steps) of an off-white powder.

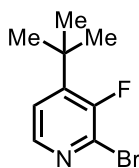
¹H NMR (401 MHz, Methanol-*d*₄) δ 8.34 (dd, *J* = 7.0, 2.0 Hz, 1H), 8.17 – 8.08 (m, 1H), 7.50 (dd, *J* = 9.5, 6.8 Hz, 1H), 1.40 (s, 9H).

¹³C NMR (126 MHz, Methanol-*d*₄) δ 136.68 (d, *J* = 3.0 Hz), 130.80, 130.66 – 129.77 (m), 125.71 (d, *J* = 7.2 Hz), 35.59, 29.47 (d, *J* = 3.1 Hz).

¹⁹F NMR (377 MHz, Methanol-*d*₄) δ -118.66.

HRMS: (ESI) (m/z): [M+H] calculated for C₉H₁₂FNO, 170.0981, found 170.0976.

2-bromo-4-(tert-butyl)-3-fluoropyridine (3-19)



To an oven-dried 1-dram vial under an N₂ atmosphere with a Teflon stir bar was added **3-18** (194 mg, 1.15 mmol, 1.0 equiv), triethylamine (0.32 mL, 2.3 mmol, 2.0 equiv), and dibromomethane (2 mL). The reaction was then

cooled to -50 °C and oxalyl bromide (0.22 mL, 2.3 mmol, 2.0 equiv) was added dropwise and the reaction was stirred for 30 minutes. The reaction was then quenched with MeOH (0.5 mL) and warmed to room temperature. The organics were washed with sat. NH₄Cl (3 mL), H₂O (3 mL), then dried over MgSO₄ and the organics were concentrated.

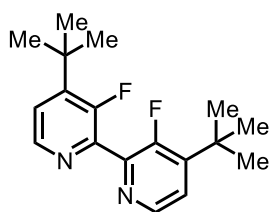
Purification by silica gel chromatography (1:1 hexanes/DCM) gave the title compound as a clear oil (238 mg, 89% yield).

Rf: 0.20 (1:1 hexanes/DCM)

¹H NMR (401 MHz, Chloroform-*d*) δ 8.09 (d, *J* = 5.0 Hz, 1H), 7.18 (t, *J* = 5.4 Hz, 1H), 1.39 (s, 9H).

¹⁹F NMR (377 MHz, Chloroform-*d*) δ -109.27.

4,4'-di-tert-butyl-3,3'-difluoro-2,2'-bipyridine (3-20)



To a round-bottom with equipped with a Teflon-coated magnetic stir bar and equipped to a reflux condenser was added Pd(OAc)₂ (5.6 mg, 0.025 mmol, 2.5 mol%), indium powder (57 mg, 0.6 mmol, 0.5 equiv), **2-19** (232 mg, 1.0 mmol, 1.0 equiv), and LiCl (64 mg, 1.5 mmol, 1.5 equiv). The flask was backfilled with N₂ three times before adding DMF (2.3 mL, 0.44 M). The reaction was heated to 100 °C for 40 minutes. The flask was cooled to room temperature and the mixture diluted with 25 mL H₂O and extracted 3 x 30 mL Et₂O, the organics were washed 2 x 50 mL H₂O, then dried with 50 mL brine and then MgSO₄ before removing the solvent by rotary evaporation. The crude reaction mixture was purified by silica gel chromatography (90:10 hexanes/EtOAc to 1:1 hexanes/EtOAc) to give a tan solid (53 mg, 35% yield).

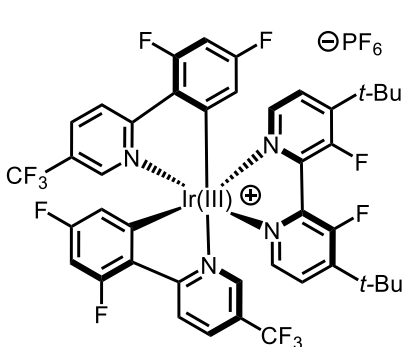
¹H NMR (400 MHz, Chloroform-*d*) δ 8.46 (d, J = 5.0 Hz, 1H), 7.50 – 7.28 (m, 1H), 1.42 (s, 9H).

¹³C NMR (126 MHz, Chloroform-*d*) δ 158.35, 146.62, 145.73 (t, J = 2.9 Hz), 122.63, 34.80, 29.45.

¹⁹F NMR (376 MHz, Chloroform-*d*) δ -121.46.

HRMS: (ESI) (m/z): [M+H] calculated for C₁₈H₂₂F₂N₂, 305.1829, found 305.1827.

[Ir(dF(CF₃)ppy)₂(4,4'-di-tert-butyl-3,3'-difluoro-2,2'-bipyridine)]PF₆ (PC12)



Using the general procedure for iridium photocatalyst synthesis, cationic iridium acetonitrile adduct (168 mg, 0.18 mmol, 1.0 equiv) and **3-20** (56 mg, 0.189 mmol, 1.05 equiv) were added to a Schlenk flask with a Teflon stir bar. DCM (1.8 mL) and EtOH (0.6 mL) were added

and the reaction was stirred at 50 °C for 36 hours. After the reaction was complete, the solution was filtered through Celite and concentrated. Purification by silica gel chromatography (100% DCM to 95:5 DCM/acetone) gave the title compound as a yellow powder (193 mg, 93% yield).

¹H NMR (401 MHz, Acetone-*d*₆) δ 8.61 (dd, J = 8.9, 2.6 Hz, 1H), 8.42 (dd, J = 8.8, 2.1 Hz, 1H), 8.15 (dd, J = 5.6, 1.2 Hz, 1H), 7.87 (dt, J = 6.2, 3.3 Hz, 1H), 7.72 (d, J = 2.0 Hz, 1H), 6.86 (ddd, J = 12.9, 9.3, 2.3 Hz, 1H), 5.94 (dd, J = 8.5, 2.3 Hz, 1H), 1.49 (s, 9H).

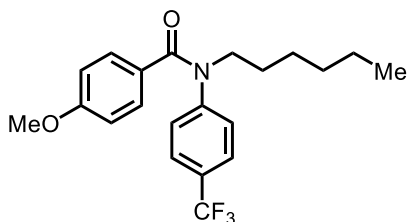
¹³C NMR (176 MHz, Acetone-*d*₆) δ 168.40, 165.98, 164.51, 163.93 (d, J = 13.3 Hz), 162.48, 161.91 – 160.37 (m), 159.11, 153.99, 152.79, 149.12, 147.22, 144.48, 138.31,

129.23, 127.81, 126.35, 126.15, 124.77 (d, $J = 20.9$ Hz), 123.81, 122.27, 115.54 (d, $J = 18.0$ Hz), 102.07 – 98.38 (m), 36.46, 29.14.

^{19}F NMR (377 MHz, Acetone- d_6) δ -63.48 (d, $J = 2.4$ Hz), -71.72, -73.60, -104.46, -104.68 (d, $J = 12.0$ Hz), -106.68 – -108.71 (m).

HRMS: (ESI) (m/z): [M+H] calculated for $\text{C}_{42}\text{H}_{32}\text{F}_{12}\text{IrN}_4$, 1013.2065, found 1013.2069.

***N*-hexyl-4-methoxy-*N*-(4-(trifluoromethyl)phenyl)benzamide (3-26)**



^1H NMR (500 MHz, Chloroform- d) δ 8.01 (dd, $J = 8.3$, 4.6 Hz, 2H), 7.91 (td, $J = 5.4$, 2.3 Hz, 2H), 7.72 (dd, $J = 8.5$, 4.6 Hz, 2H), 7.01 – 6.78 (m, 2H), 3.87 (s, 3H), 2.74 (dt, $J = 10.5$, 5.2 Hz, 2H), 1.56 (q, $J = 6.0$, 4.9 Hz, 2H),

1.25 (qd, $J = 11.9$, 7.9, 6.5 Hz, 6H), 0.80 (t, $J = 6.3$ Hz, 3H).

^{13}C NMR (126 MHz, Chloroform- d) δ 179.40, 168.87, 163.84, 131.55, 129.44, 128.36, 125.81 (d, $J = 5.5$ Hz), 114.00, 55.64, 34.43, 31.86, 29.86, 27.61, 22.29, 13.90, 1.18.

^{19}F NMR (471 MHz, Chloroform- d) δ -62.97.

GCMS Analysis of KIE Experiments:²⁶⁶

Run

#1:

	Authentic Proteo Sample of Product		Authentic Deutero Sample of Product		KIE Experiment #1		Results	
Mass	311	312	311	312	311	312	% Molecule proteo	% Molecule deutero
Percent	73.39	18.8 7	3.13	75.5 6	59.08	31.44	78.05	21.95

Run

#2:

	Authentic Proteo Sample of Product		Authentic Deutero Sample of Product		KIE Experiment #2		Results	
Mass	311	312	311	312	311	312	% Molecule proteo	% Molecule deutero
Percent	73.39	18.8 7	3.13	75.5 6	58.62	32.11	77.08	22.92

Table 4-1 GCMS analysis of competition experiments between **2-91** and **3-7**.

4.4.3 Stern-Volmer Analysis

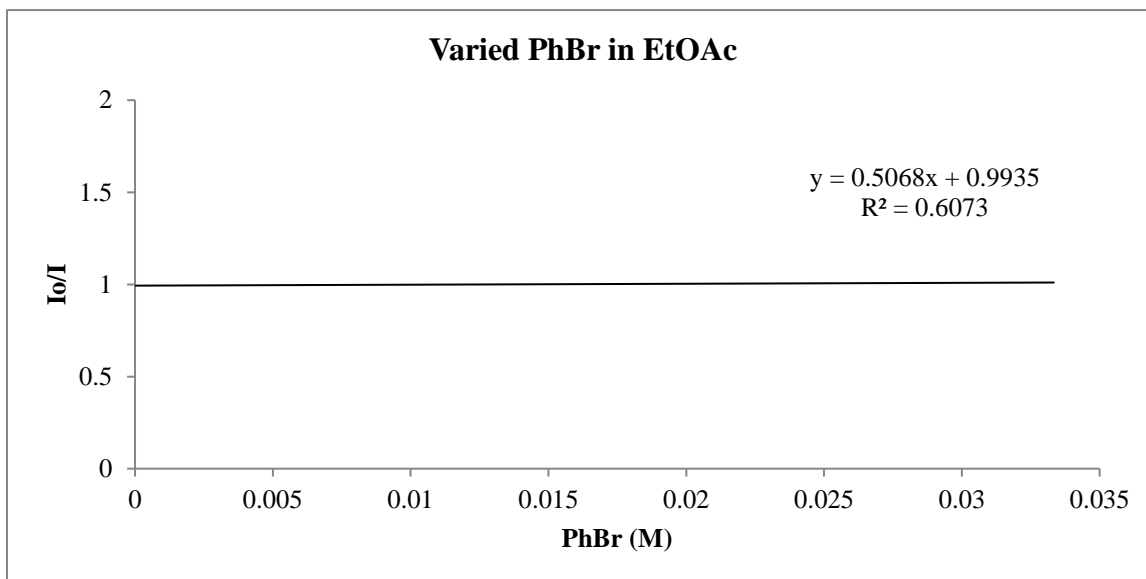


Figure 4-21 Quenching experiment with PC1 and varied PhBr in EtOAc.

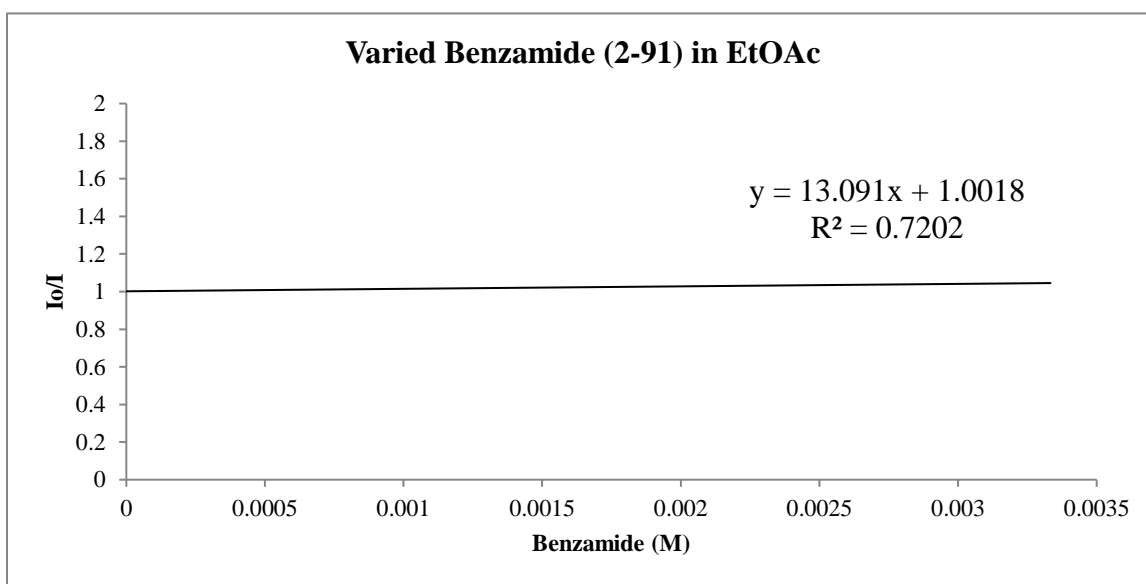


Figure 4-22 Quenching experiment with PC1 and varied 2-91 in EtOAc.

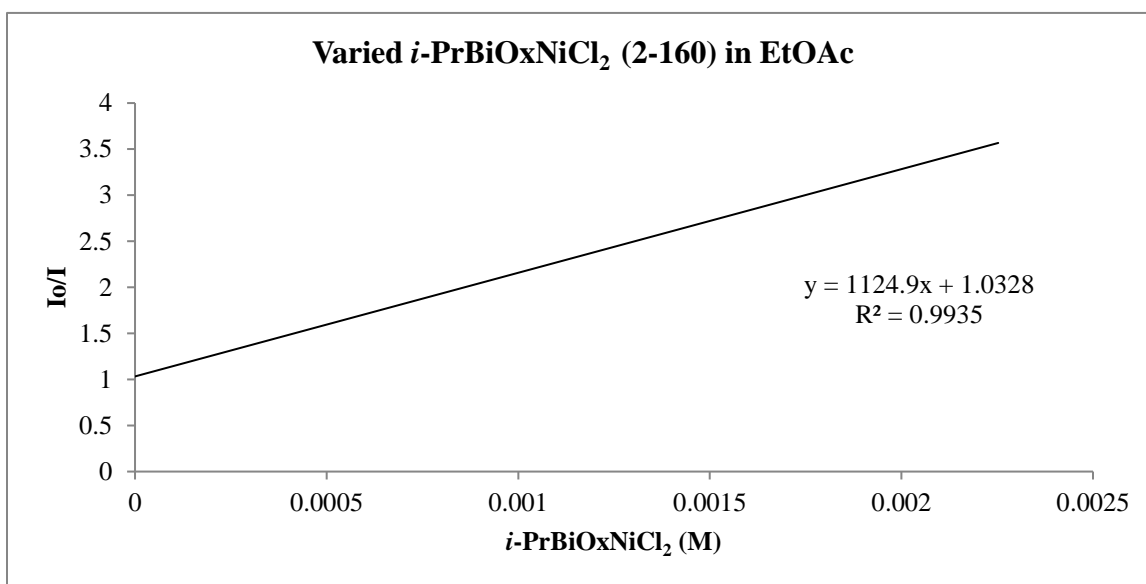


Figure 4-23 Quenching experiment with **PC1** and varied *i*-PrBiOxNiCl₂ in EtOAc.

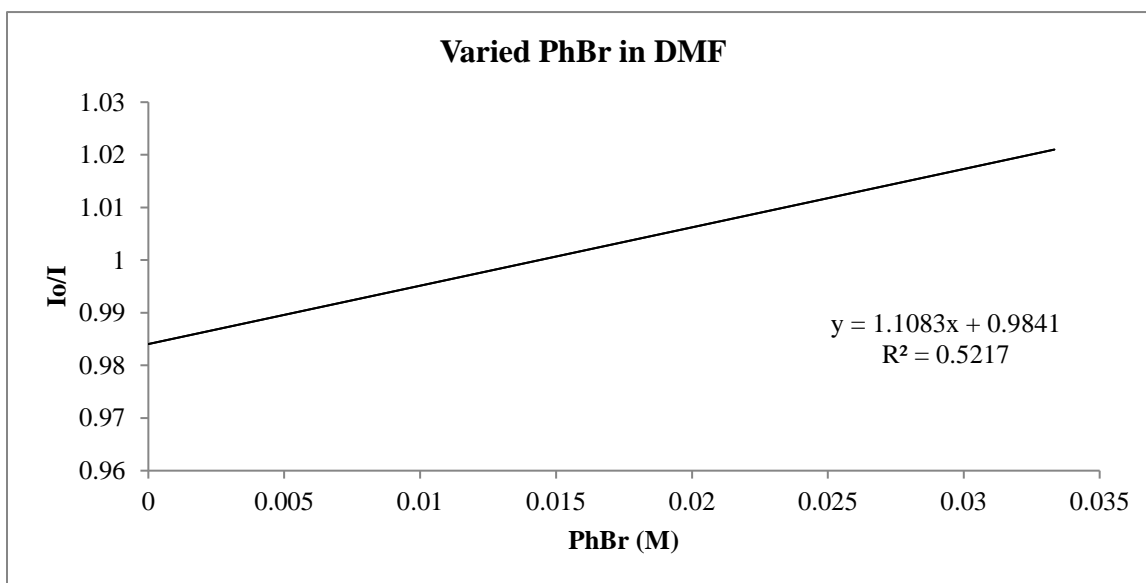


Figure 4-24 Quenching experiment with **PC1** and varied PhBr in DMF.

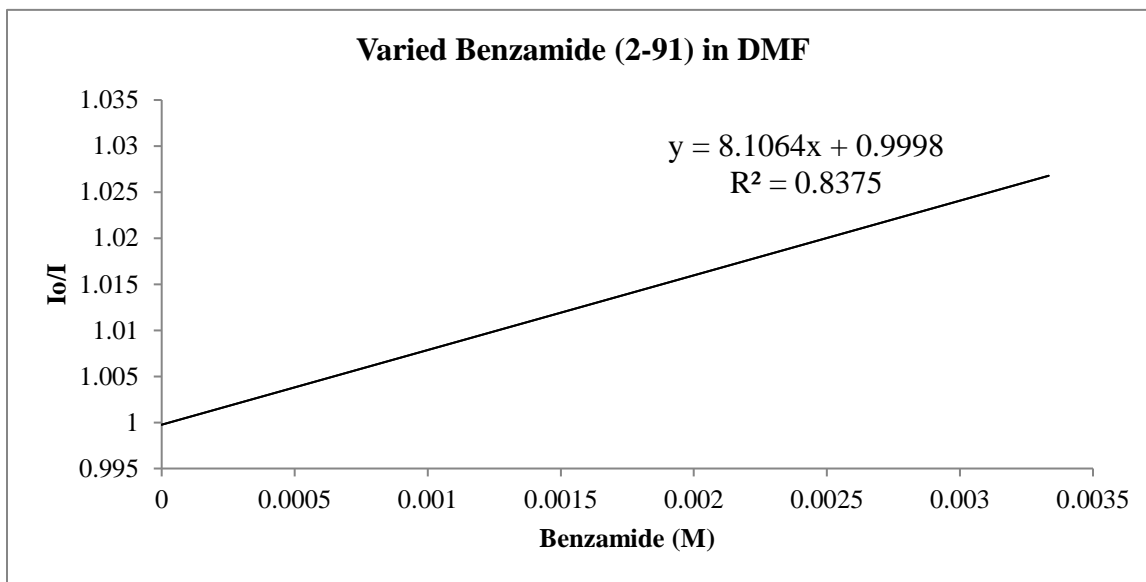


Figure 4-25 Quenching experiment with **PC1** and varied benzamide in DMF.

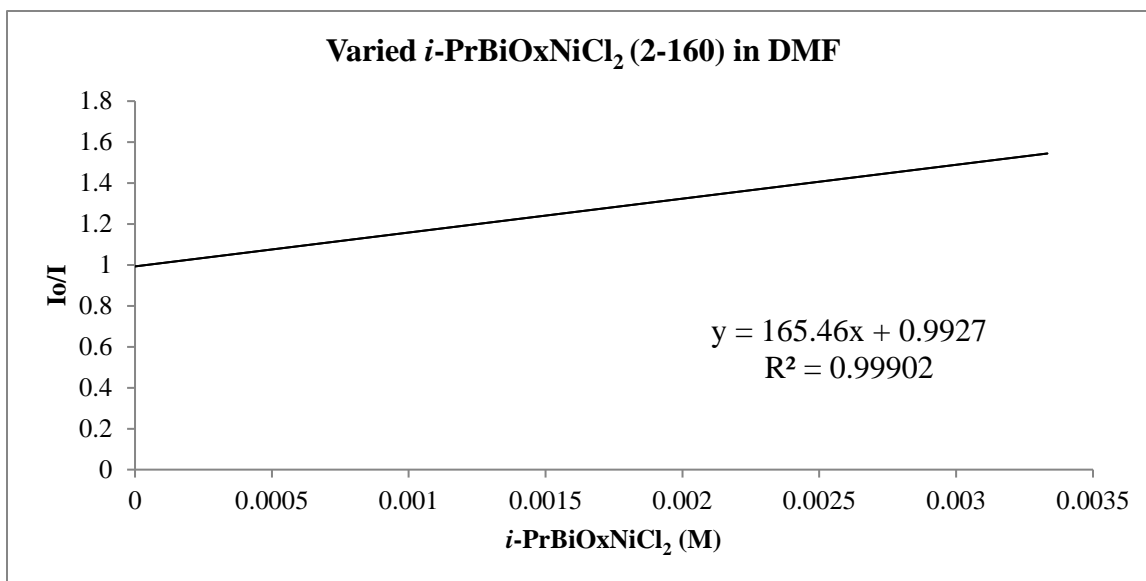


Figure 4-26 Quenching experiment with **PC1** and varied *i*-PrBiOxNiCl₂ in DMF.

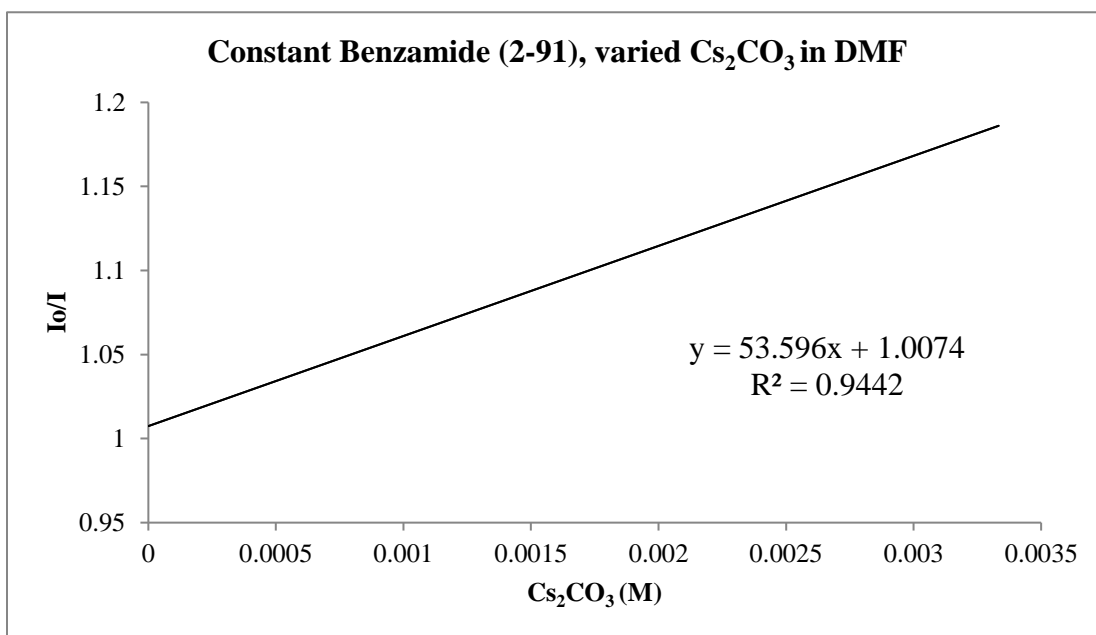


Figure 4-28 Quenching experiment with PC1 and benzamide, and varied Cs_2CO_3 in DMF.

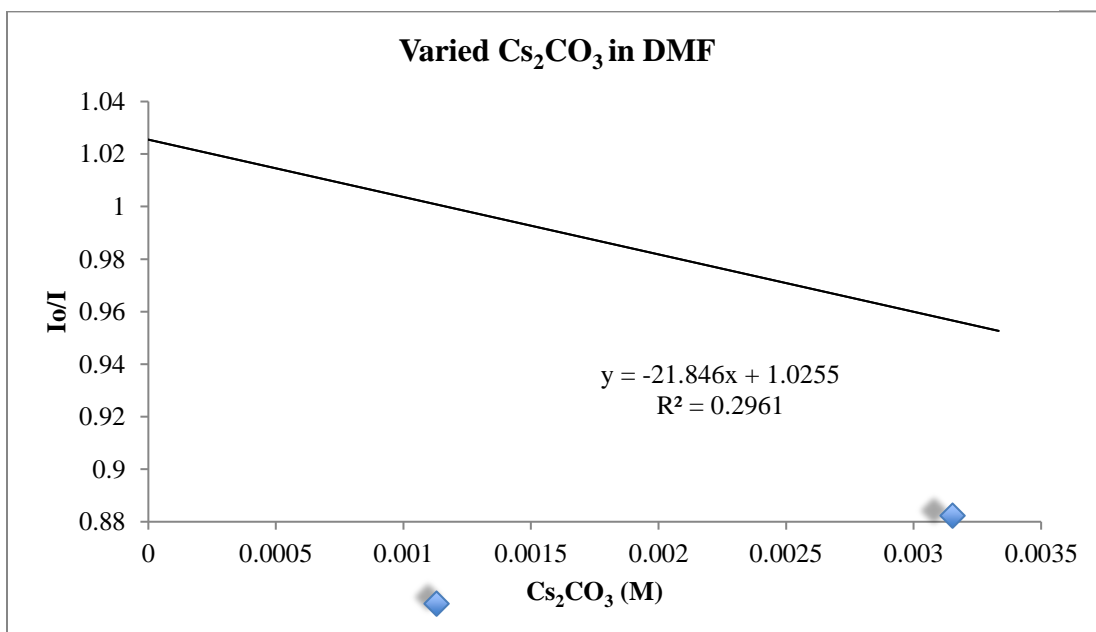


Figure 4-27 Quenching experiment with PC1 and varied Cs_2CO_3 in DMF

4.4.4 CV Data:

Cyclic voltammetry was performed in a nitrogen-filled glovebox with a Biologic VSP multichannel potentiostat/galvanostat using a three electrode electrochemical cell, consisting of a glassy carbon disk working electrode (0.07 cm^2 , BASi), a Ag/Ag⁺ quasi-reference electrode (BASi) with 0.01 M AgBF₄ (Sigma) in acetonitrile, and a platinum wire counter electrode (ALS). The glassy carbon disk electrode was polished in a nitrogen-filled glovebox using aluminum oxide polishing paper (9 micron and 0.3 micron, Fiber Instrument) and anhydrous acetonitrile. All experiments were run in the 0.5 M TBAPF₆ stock electrolyte.

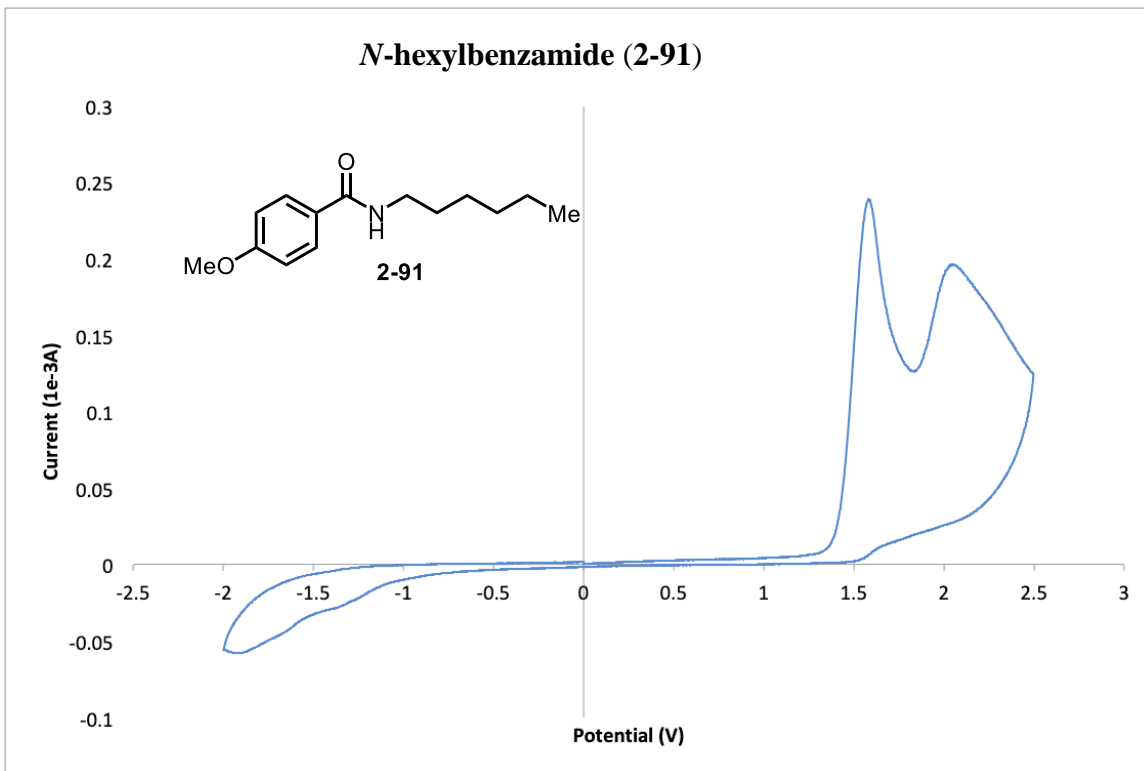


Figure 4-29 CV of benzamide 2-91.

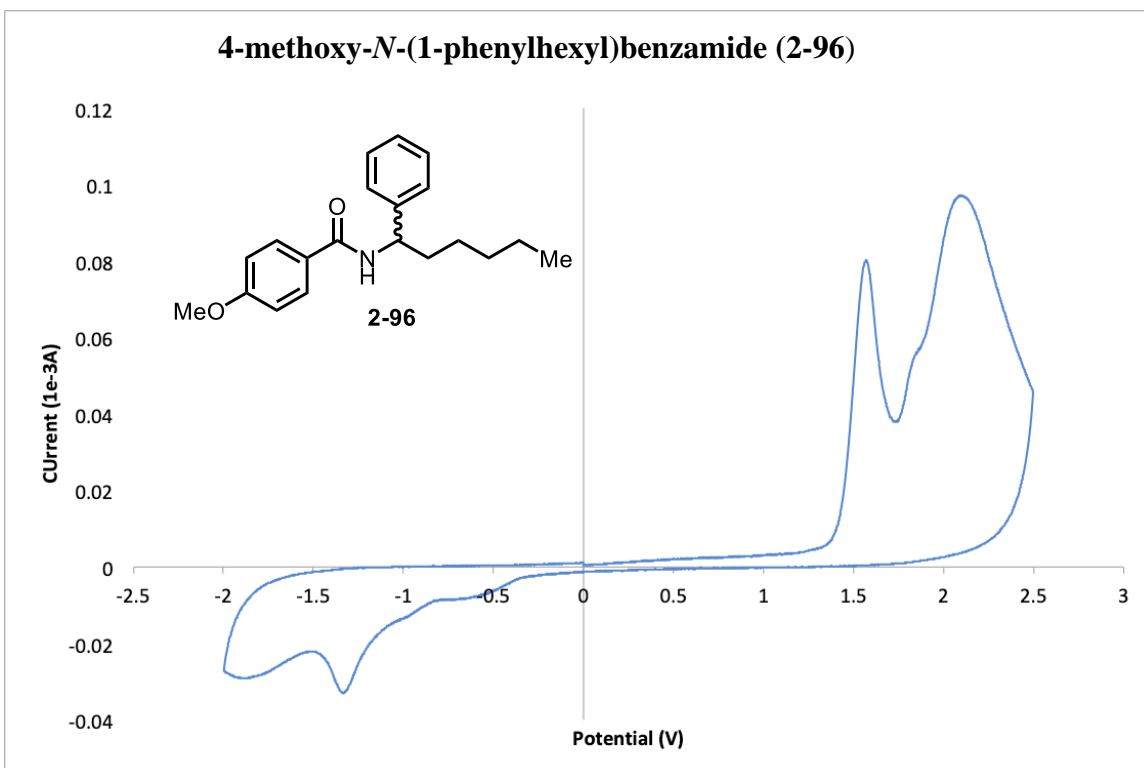


Figure 4-30 CV of benzamide 2-96.

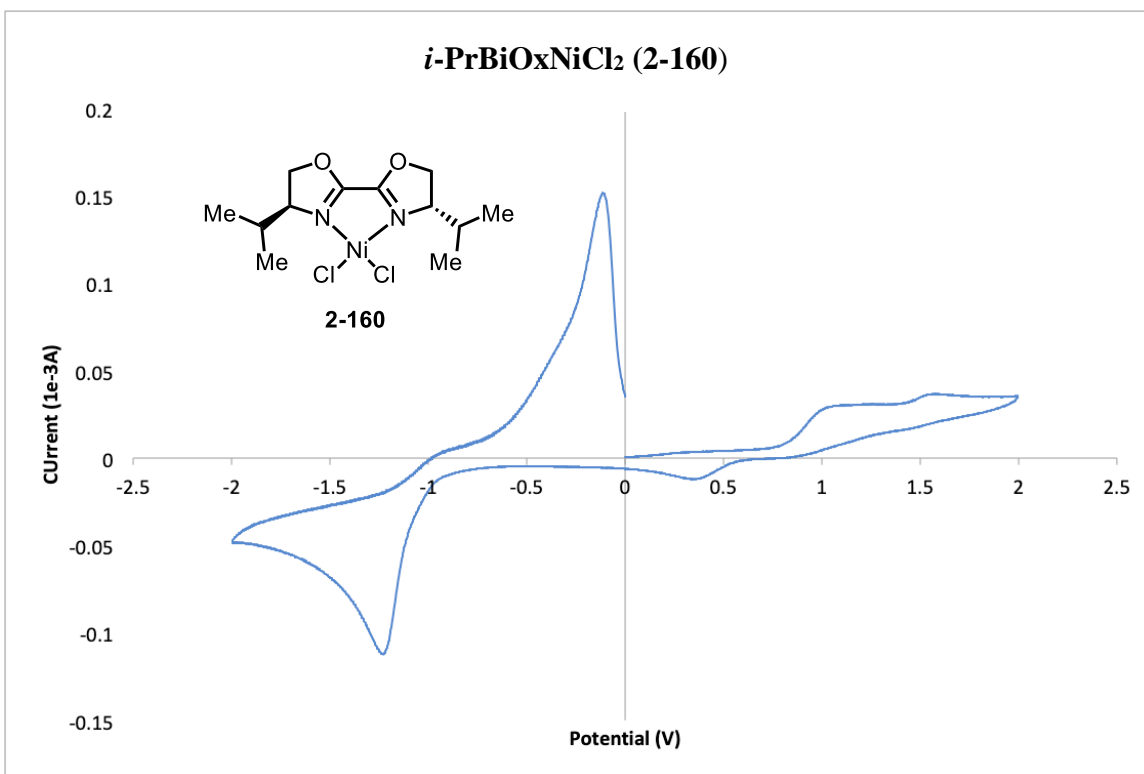


Figure 4-31 CV of benzamide 2-160.

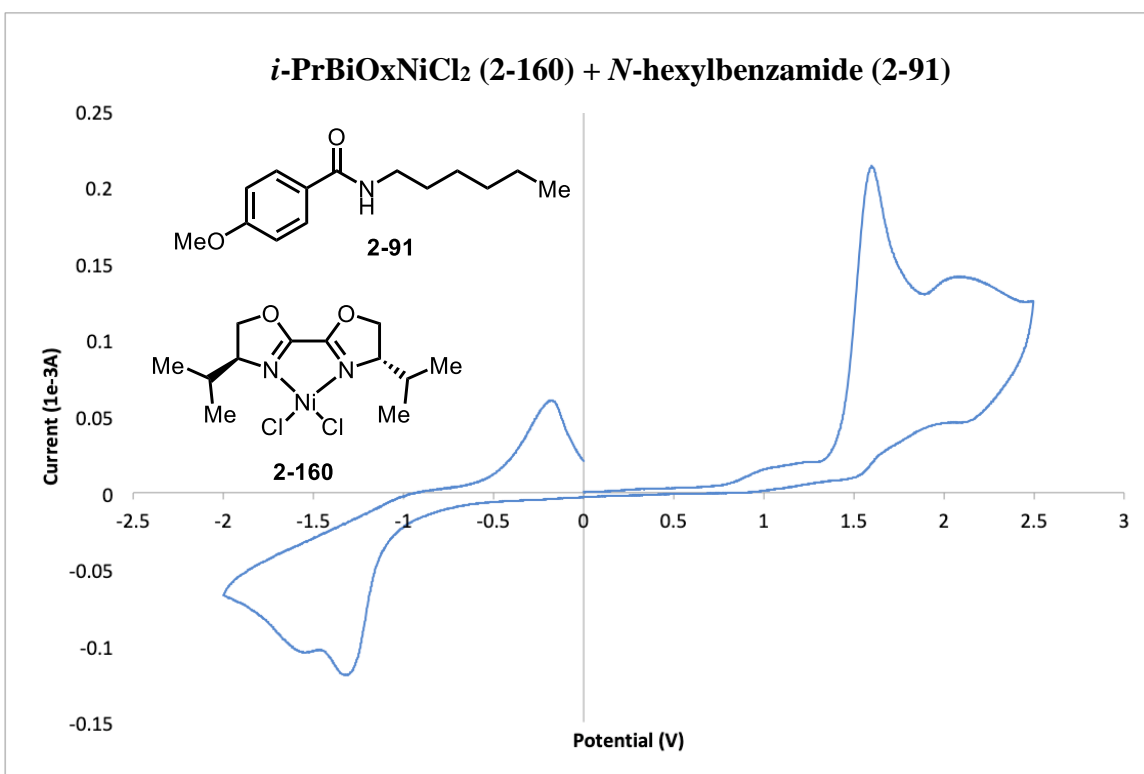


Figure 4-32 CV of benzamide 2-91 and 2-160.

Discussion:

The starting material, **2-91**, and product, **2-96**, are both outside the oxidation potential of our photocatalyst, suggesting that a direct oxidation of **2-91** or **2-96** to yield an α -amidyl radical is not feasible. The oxidation potential of **2-91** does not change when an equal concentration of catalyst, **2-160**, was added. Lastly, **2-160** was shown to be within the range of reduction for our photocatalyst, though its electrochemical potential does not change drastically when in solution with an equal amount of **2-91**.

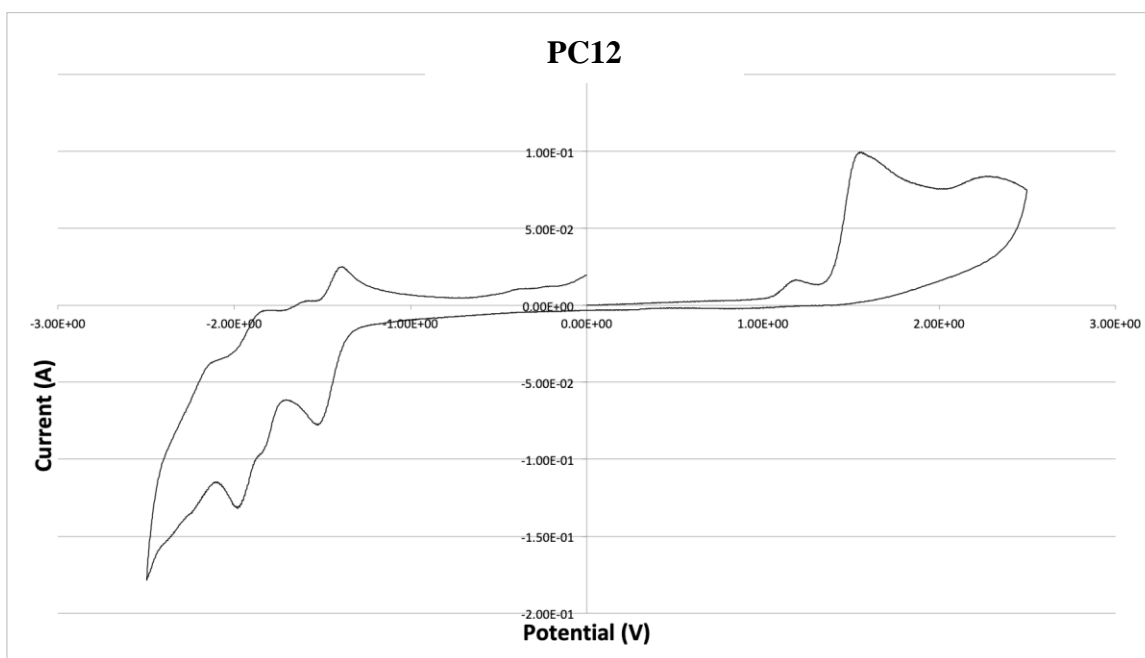


Figure 4-33 CV of PC12.

$\text{Ir(III/II)} = -1.42\text{V vs Ag/Ag}^+ (-1.12\text{V vs SCE})$

$\text{Ir(III/IV)} = 1.15\text{V vs Ag/Ag}^+ (1.45\text{V vs SCE})$

$\text{Ir(III}^*/\text{II)} = 1.16\text{V vs Ag/Ag}^+ (1.47\text{V vs SCE})$

$\text{Ir(III}^*/\text{IV)} = -1.43\text{ vs Ag/Ag}^+ (-1.13\text{V vs SCE})$

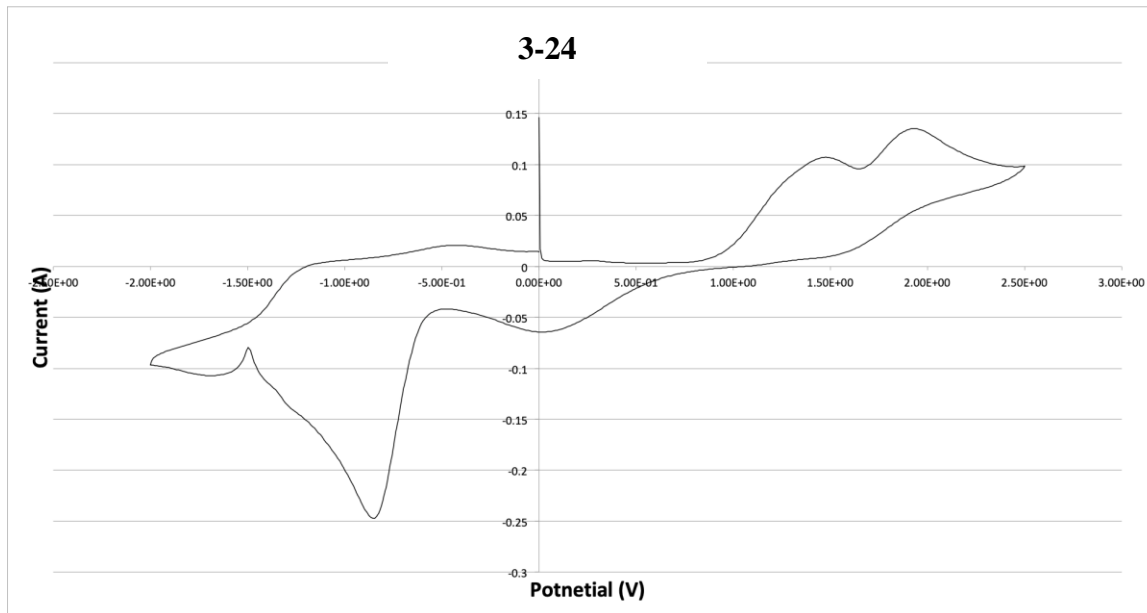


Figure 4-34 CV of 3-24.

Ni(II/III) $E_p=1.45\text{V}$ vs Ag/Ag⁺ (1.75V vs SCE)

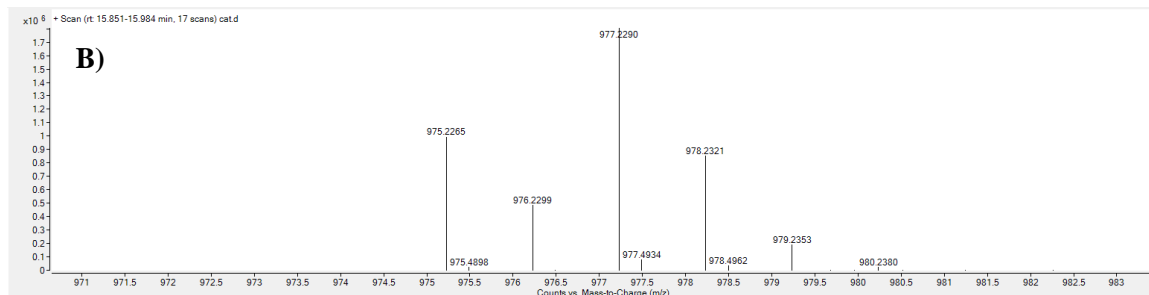
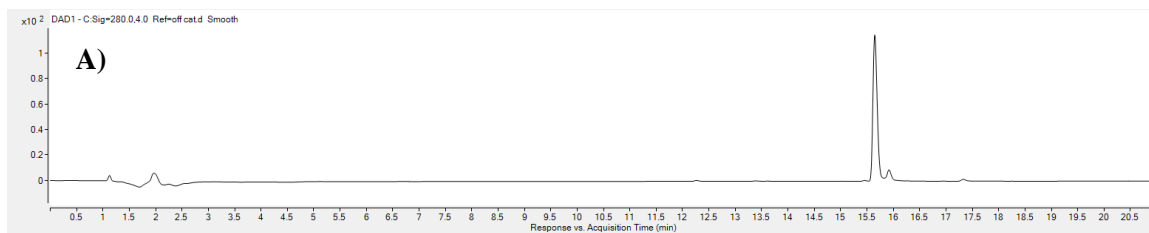
Ni(II/I) $E_p = -0.84\text{V}$ vs Ag/Ag⁺ (-0.54V vs SCE)

4.4.5 Catalyst Degradation Studies

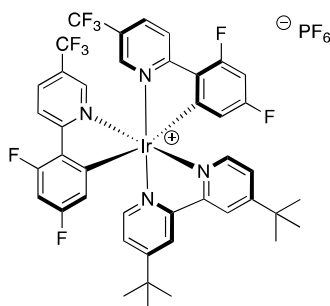
A recent report in showed that LCMS analysis of photoredox reaction mixtures was an effective tool for determining the amount of photocatalyst present at any time during the reaction.²²⁶ Based on this report, analysis of the photocatalyst throughout the reaction was undertaken using LCMS QTOF. It was found that irradiation of **PC1** in EtOAc/DMAc (9:1) did not degrade the photocatalyst (Figure 4-35), suggesting that the photocatalyst were stable in solution. When subjecting the photocatalyst to the standard reaction conditions for 1 hour, a large amount of photocatalyst was still present in the reaction mixture (by LCMS). However, after 12 hour of irradiation under standard reaction conditions, the mass of the photocatalyst could not be detected in the reaction mixture (Figure 4-36). It was found that the photocatalyst decomposition products eluted with the

same retention time as the starting catalyst, though analysis of the mass spec showed that these peaks were indeed different species. Several peaks were identified as molecules containing iridium (characteristic isotope patterns of iridium allowed for the assignment of peaks that contained this metal), though no definitive structure or molecular formula could be isolated or deduced by NMR. Although we were unable to isolate and completely characterize the structure of the newly formed iridium species, these studies show that **PC1** is completely consumed throughout the reaction, which prompted us to examine other photocatalysts.

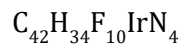
As **PC6** consistently gave higher yields than **PC1** in the racemic α -arylation of benzamides, it was hypothesized that the lifetime of this photocatalyst in the reaction was much longer than the latter. Under this assumption, and since the oxidation potentials are nearly the same (1.21 V and 1.25 V vs SFC), it was hypothesized that under the reaction conditions the phenyl portion of the ppy ligands on the iridium center were being modified;^{227, 267} this hypothesis would explain why **PC6** gave higher yields, since it has two less sp^2 C–F bonds. Under this hypothesis, a new catalyst was designed and synthesized which contained no sp^2 C–F bonds. Despite this modification, no noticeable increase in yield was observed and no photocatalyst was observed by LCMS QTOF at the end of the reaction suggesting that this catalyst also suffered from degradation under the reaction conditions (Figure 4-37).



C)



Chemical Formula:



Exact Mass: 977.2253

m/z: 977.2253

(100.0%), 975.2230

(59.5%), 978.2287

(45.4%), 976.2263

(27.0%), 979.2320

(7.4%), 977.2297

(4.4%), 979.2320

(2.7%), 977.2297

(1.6%), 978.2223

(1.5%), 980.2354 (1.5%)

Figure 4-35 LCMS and analysis of PC1. **A)** LCMS trace of Ir-dF, **B)** mass spec analysis of LCMS trace of PC1 from 15.85-15.98 minutes, and **C)** structure of PC1 and expected ratio of isotopes based on natural abundance.

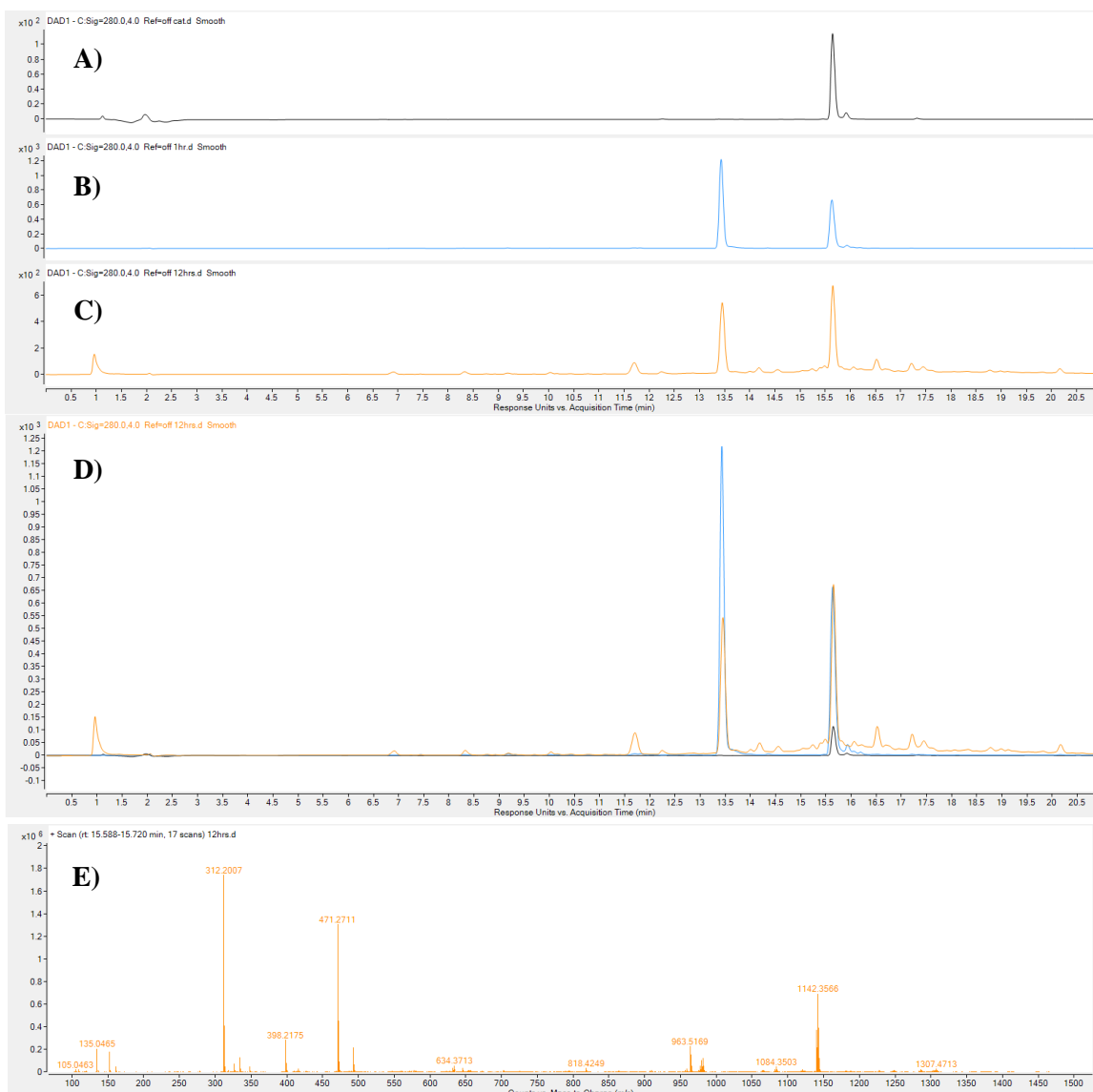


Figure 4-36 LCMS analysis of Ir-dF before and after subjecting to reaction conditions. **A)** LCMS trace of Ir-dF, **B)** LCMS trace of productive reaction using Ir-dF after irradiating for 1 hour, **C)** LCMS trace of productive reaction using Ir-dF after irradiating for 12 hours, **D)** Overlay of LCMS traces of Ir-dF, reaction after irradiating for 1 hour, and reaction after irradiating for 12 hours, and **E)** mass spec analysis of LCMS trace of productive reaction using Ir-dF after 12 hours of irradiation from 15.85-15.98 minutes. No mass of the starting photocatalyst was detected, however, peaks with similar isotopic patterns to Ir-dF were observed.

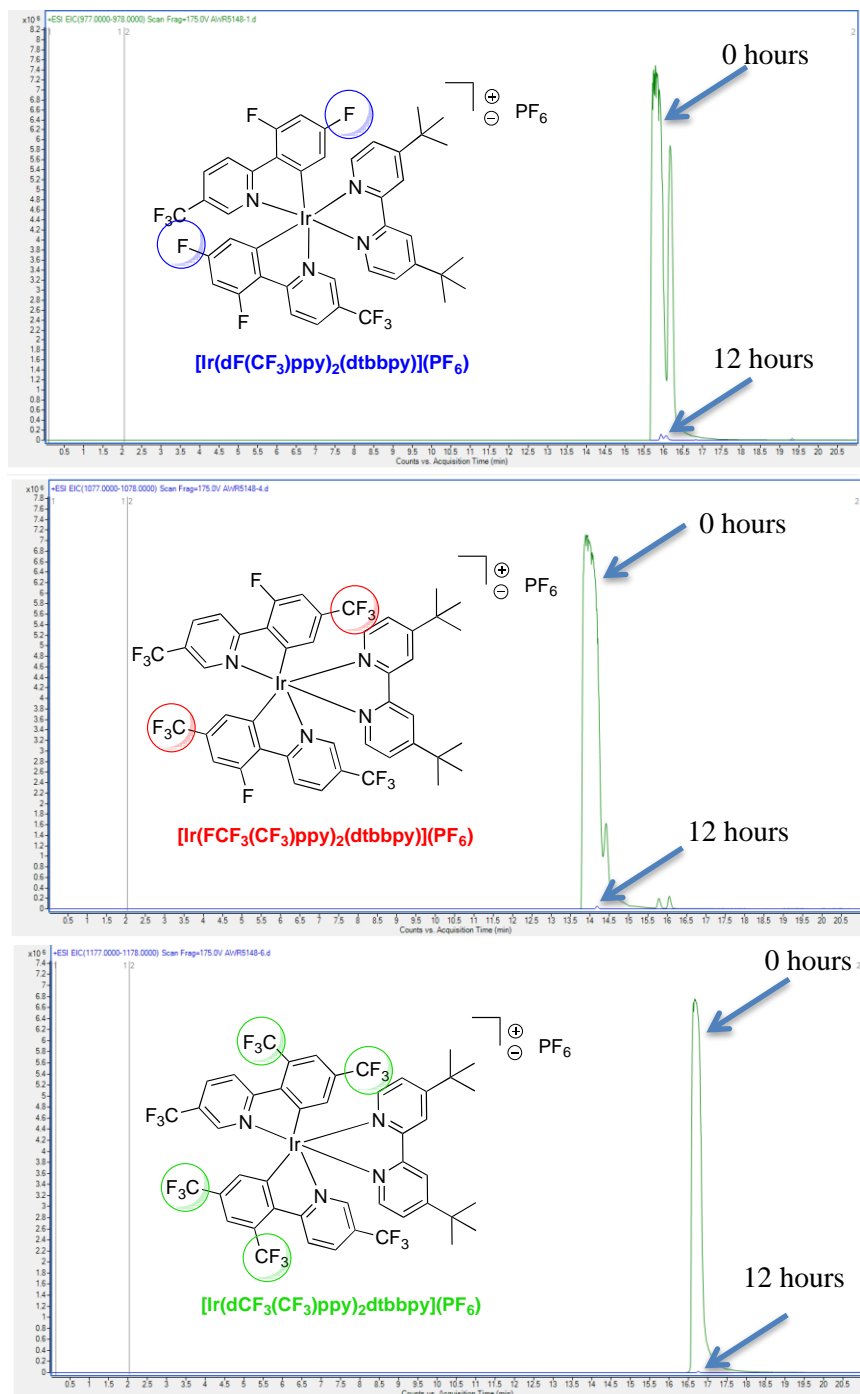
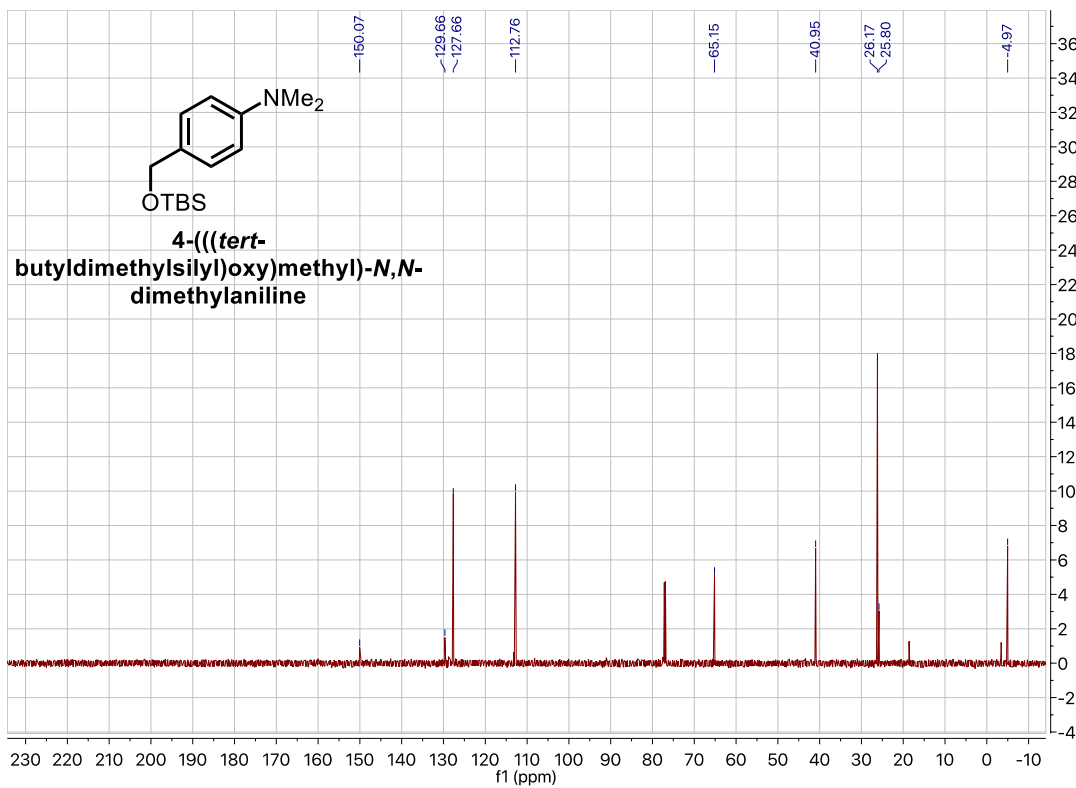
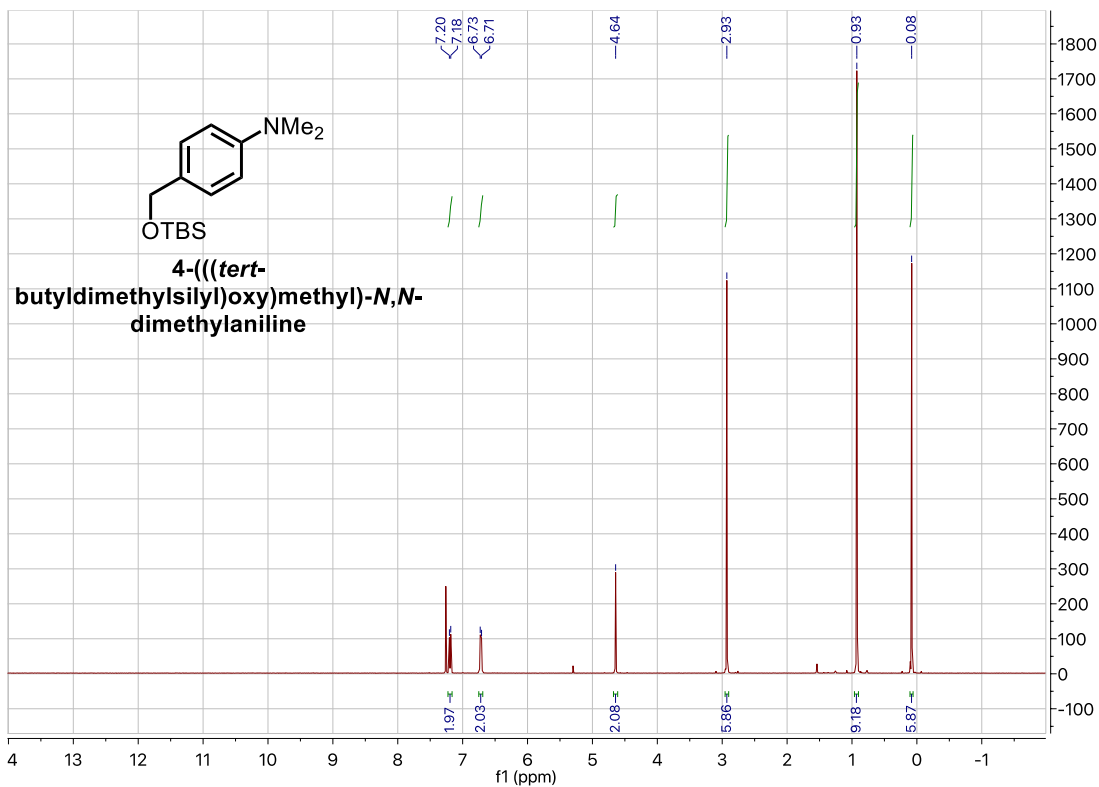
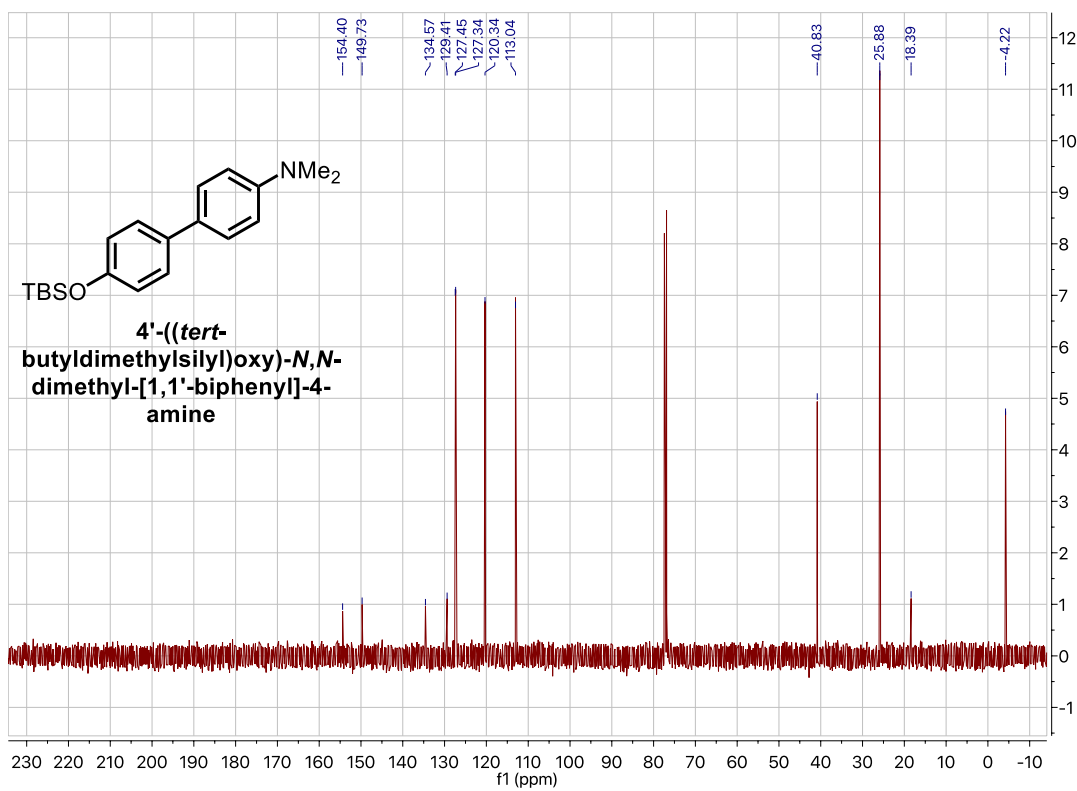
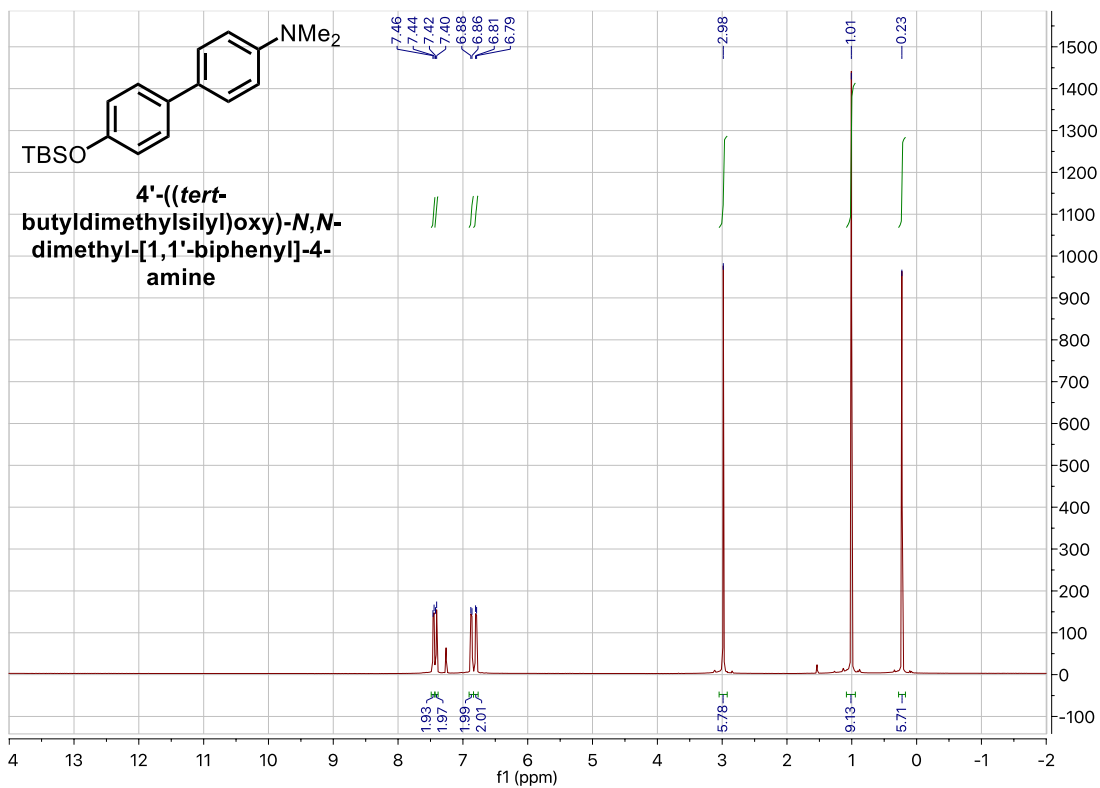
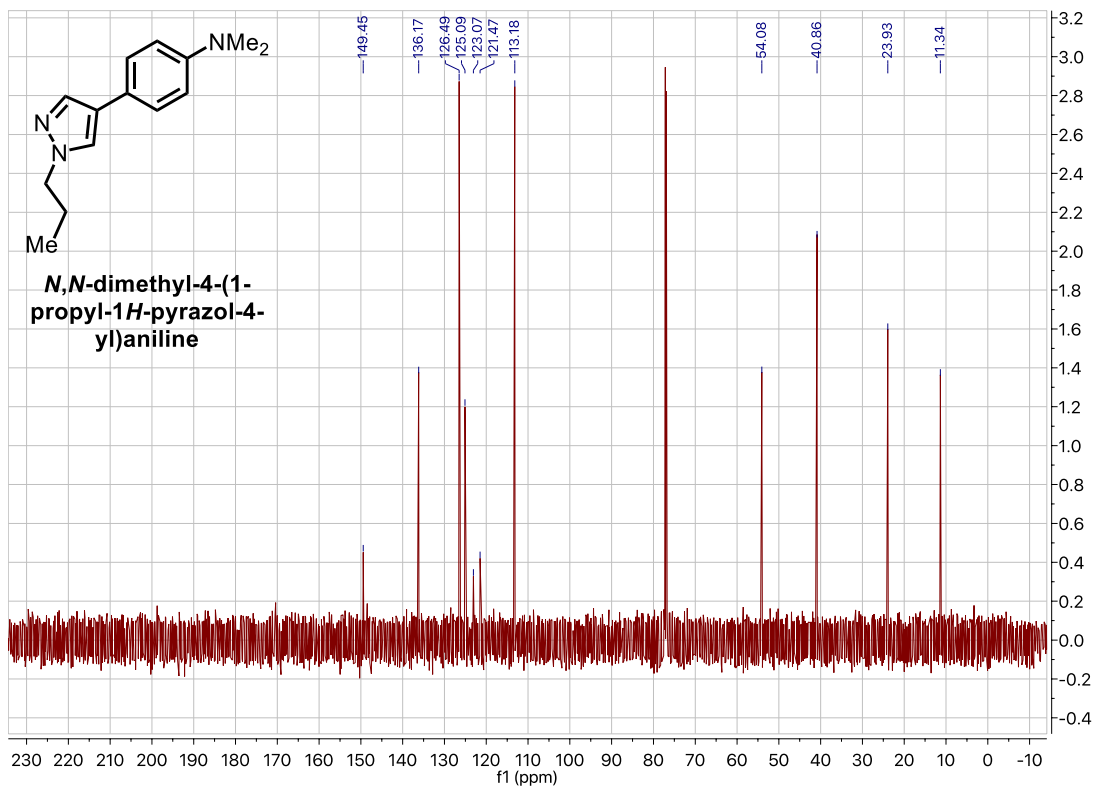
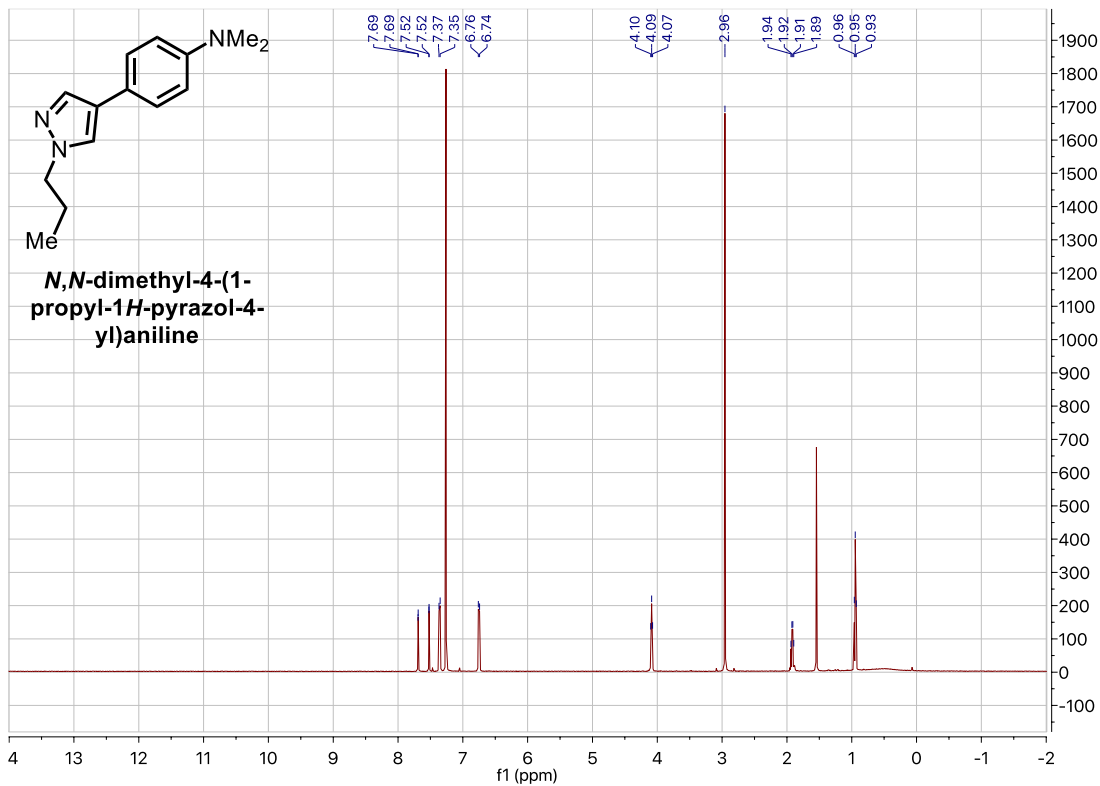


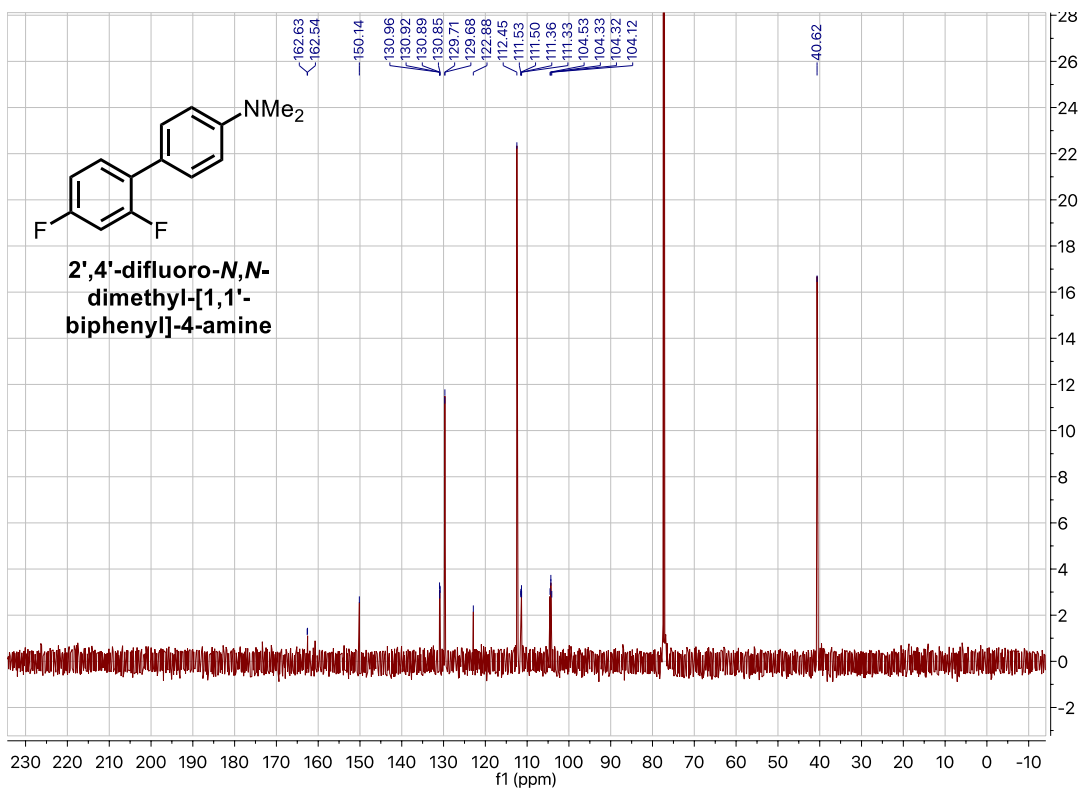
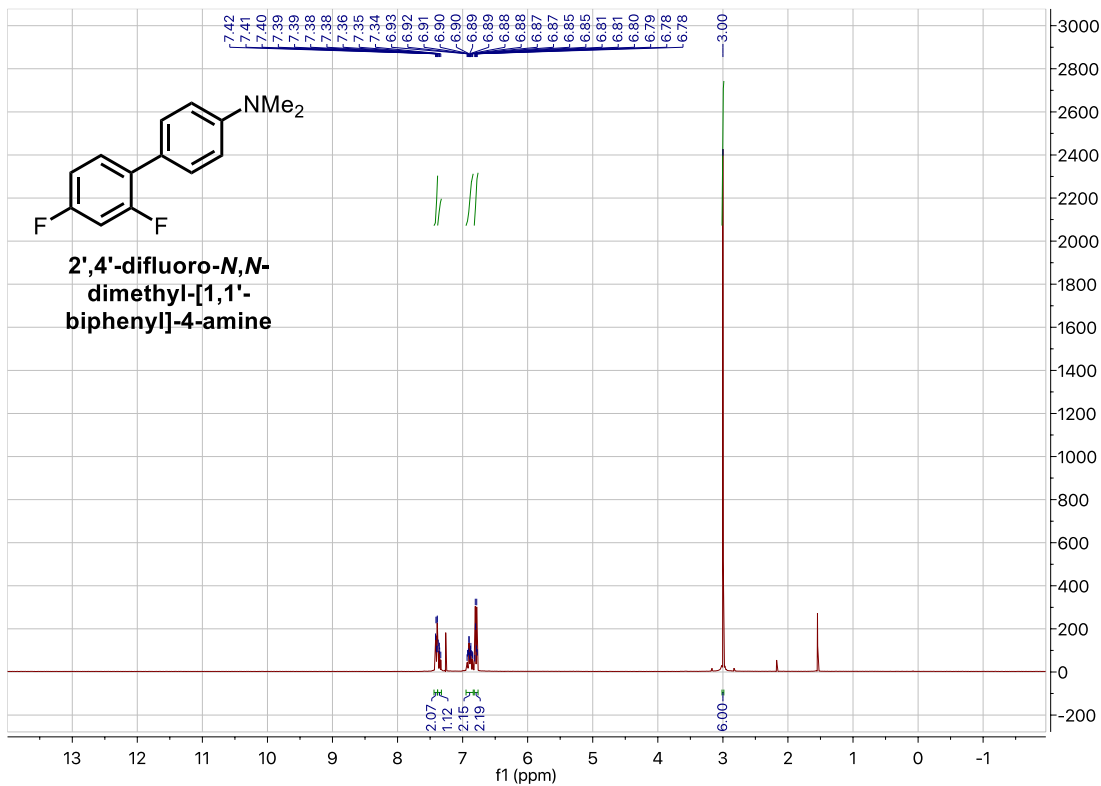
Figure 4-37 LCMS Q-TOF traces for three different photocatalyst at 0 hours (in green) and 12 hours (in blue), overlaid. LCMS traces were analyzed for the mass of each respective photocatalyst before and after irradiation for 12 hours in a productive reaction. In each case the photocatalyst is completely consumed at the end of the reaction.

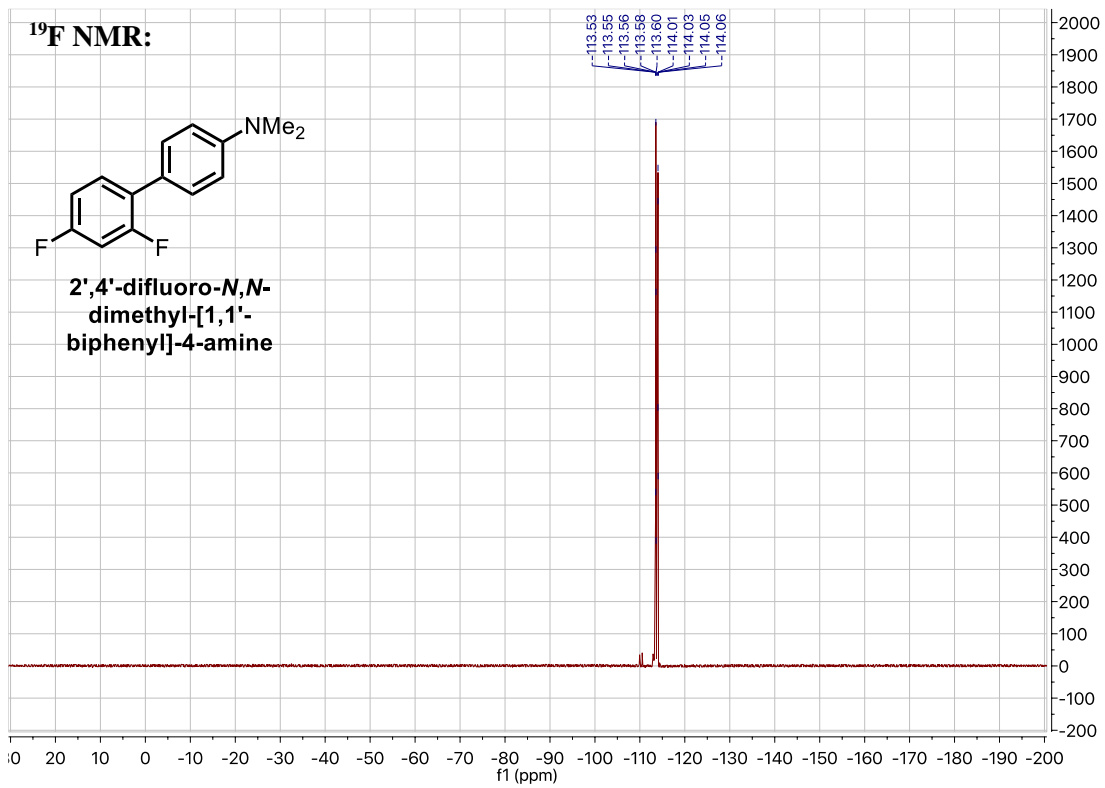
4.5 Spectra of New Compounds

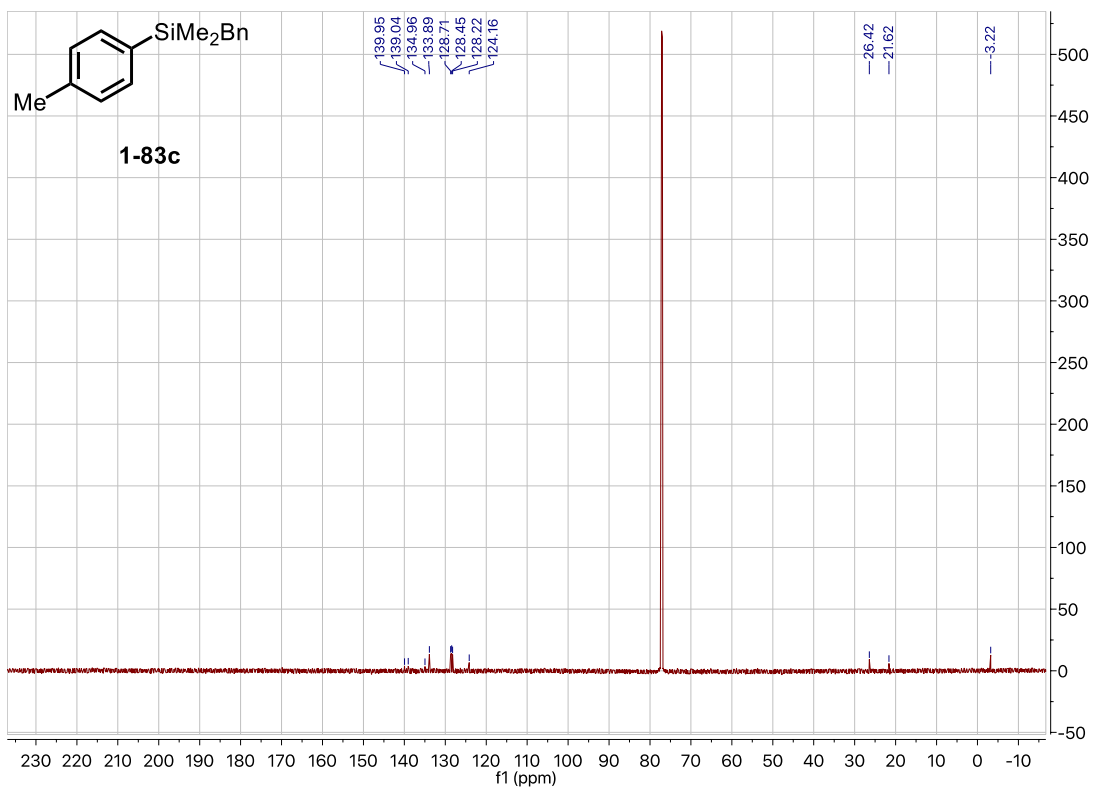
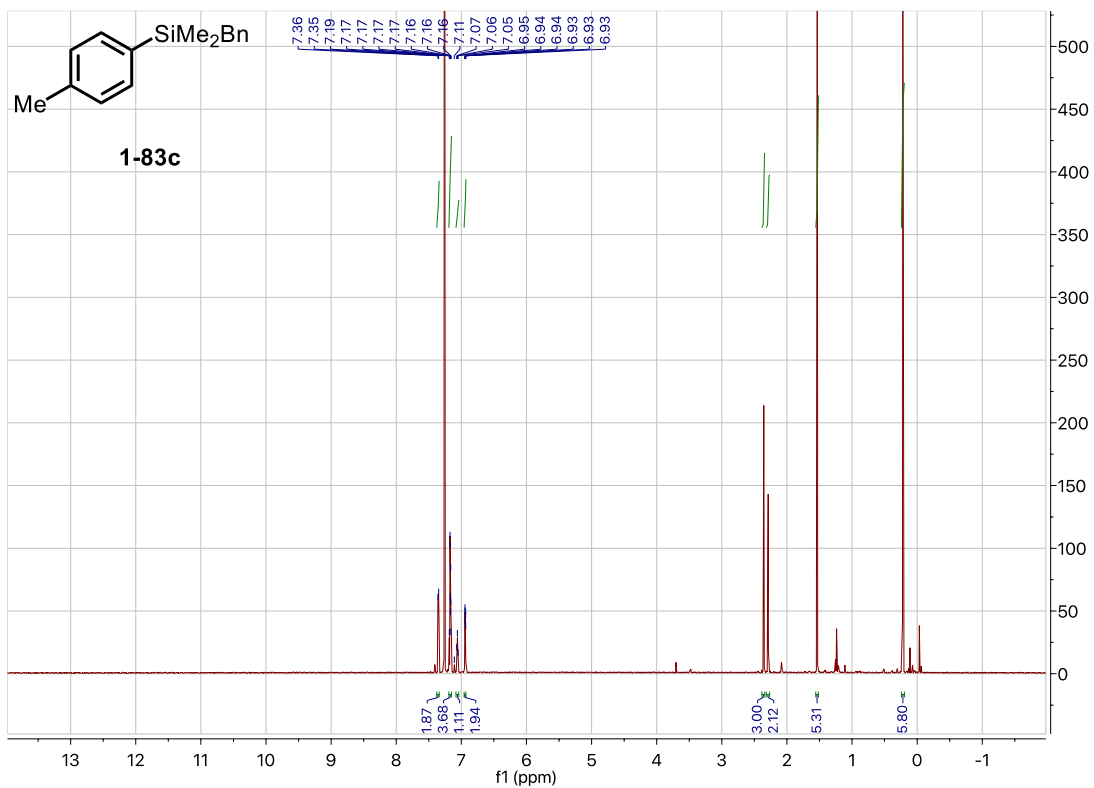


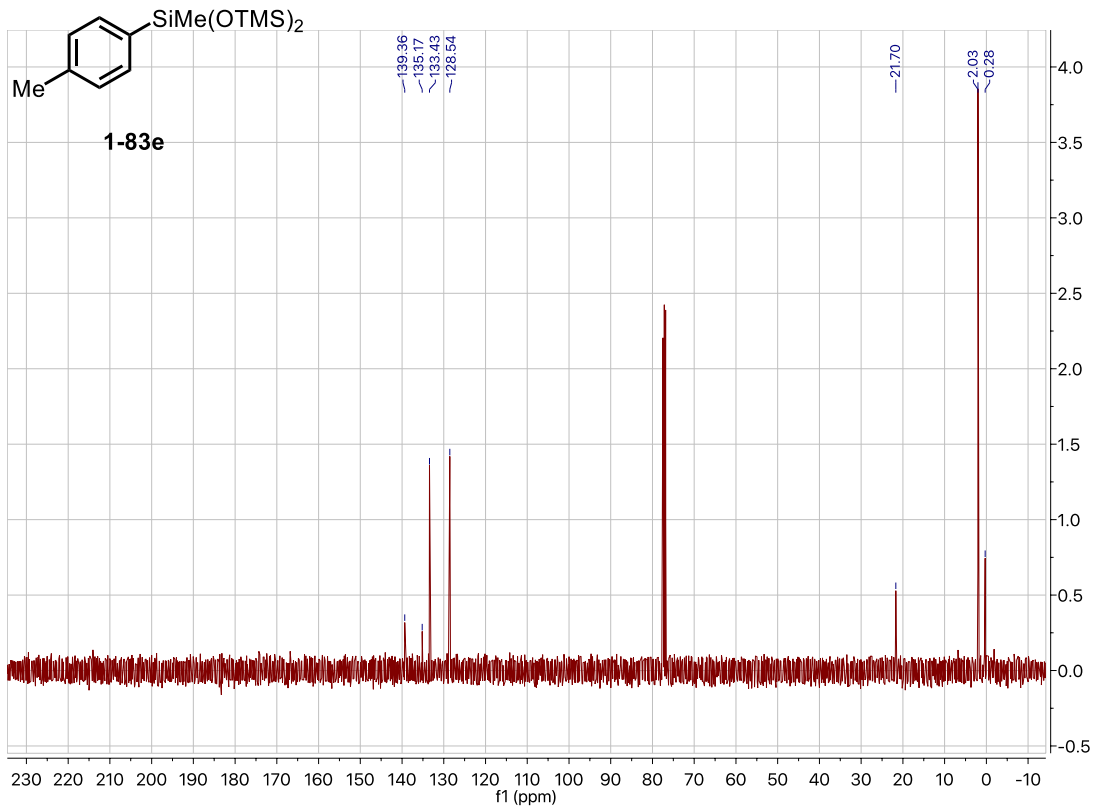
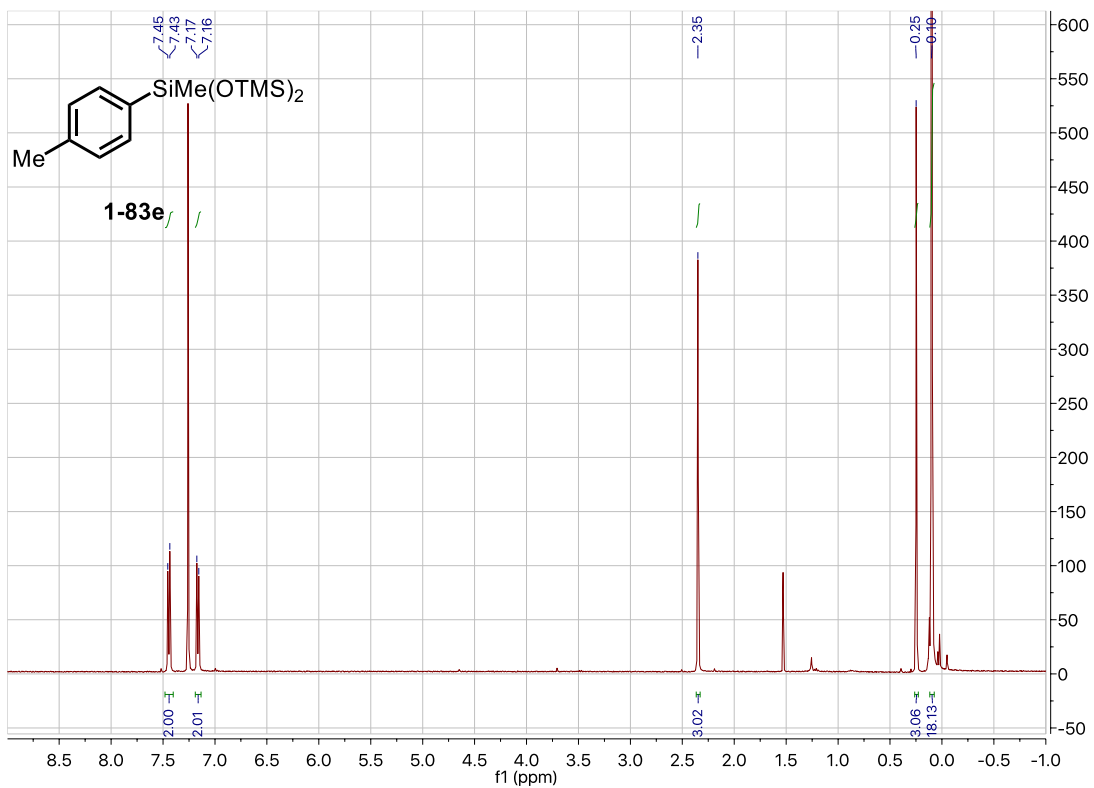


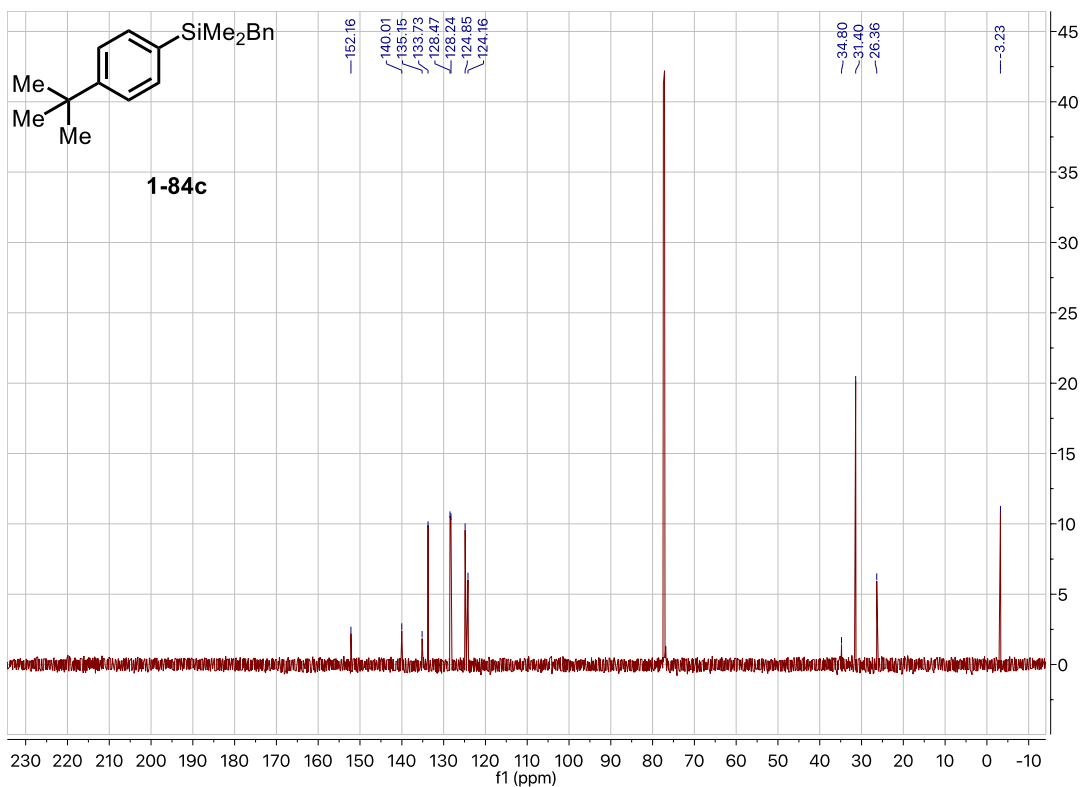
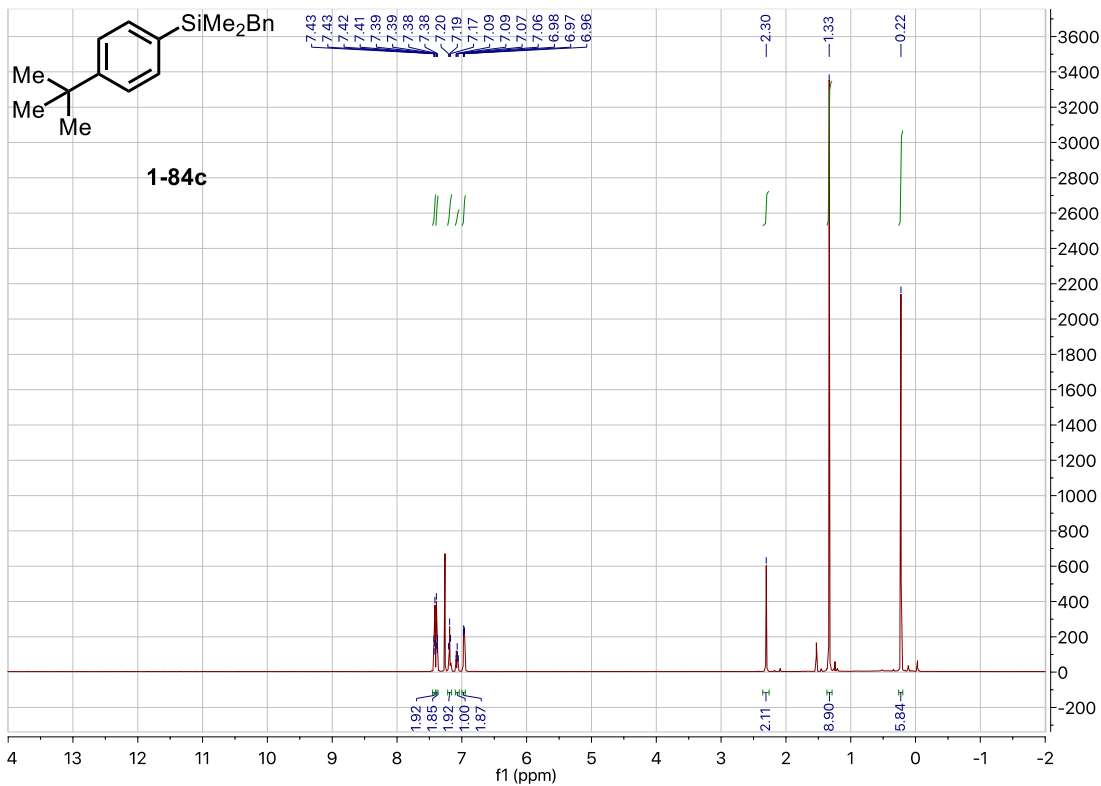


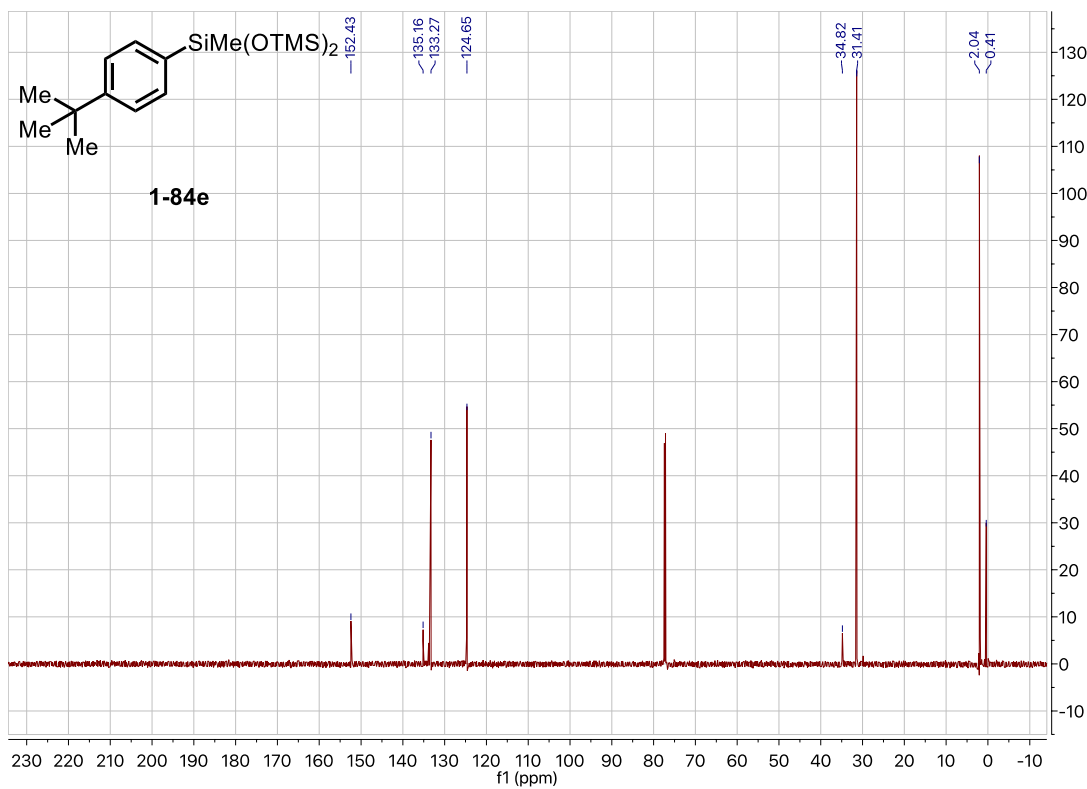
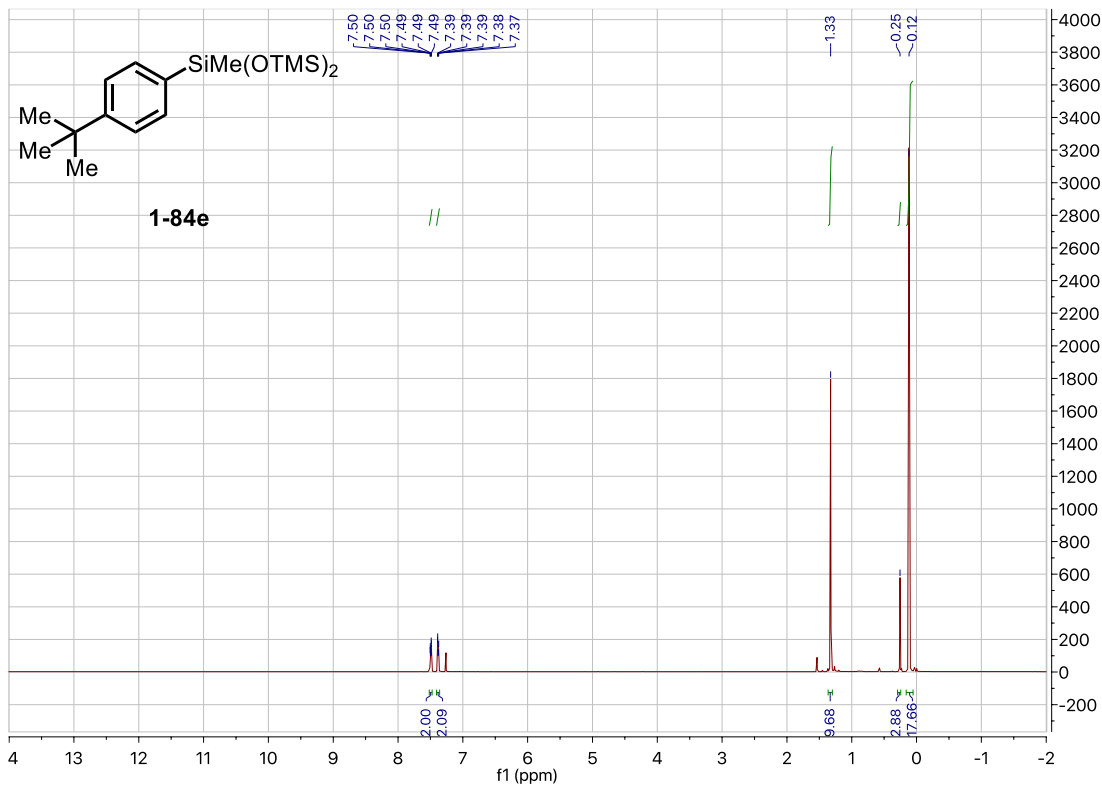


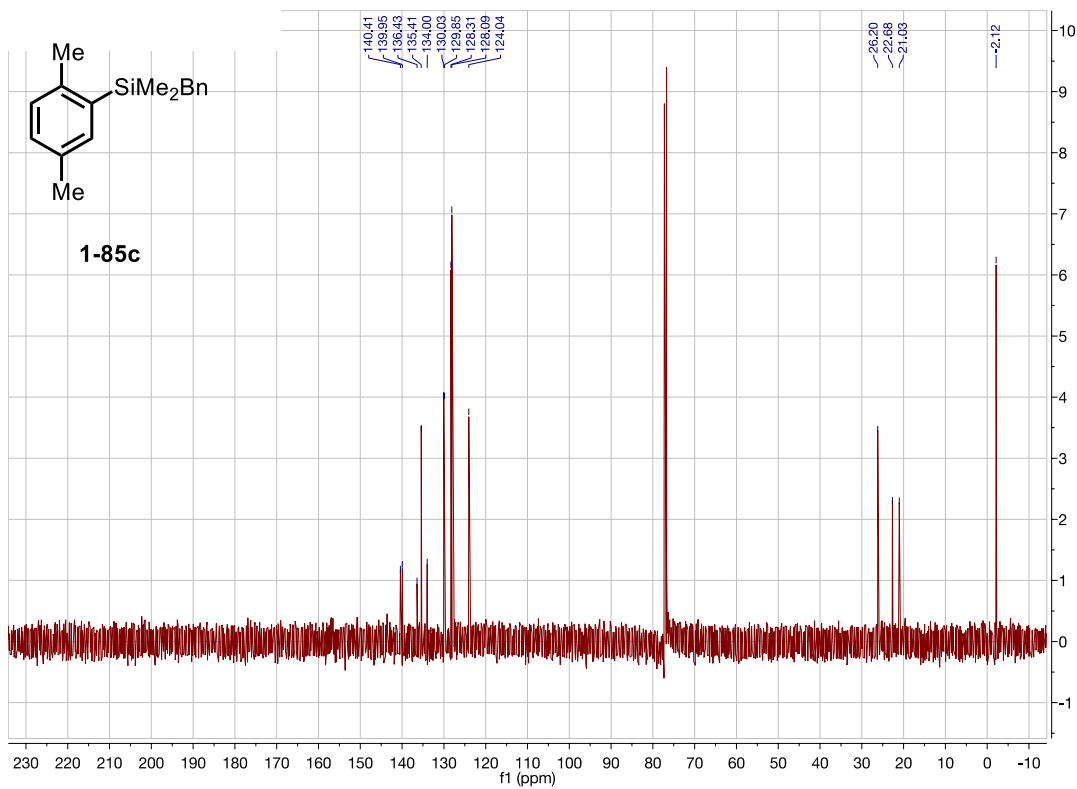
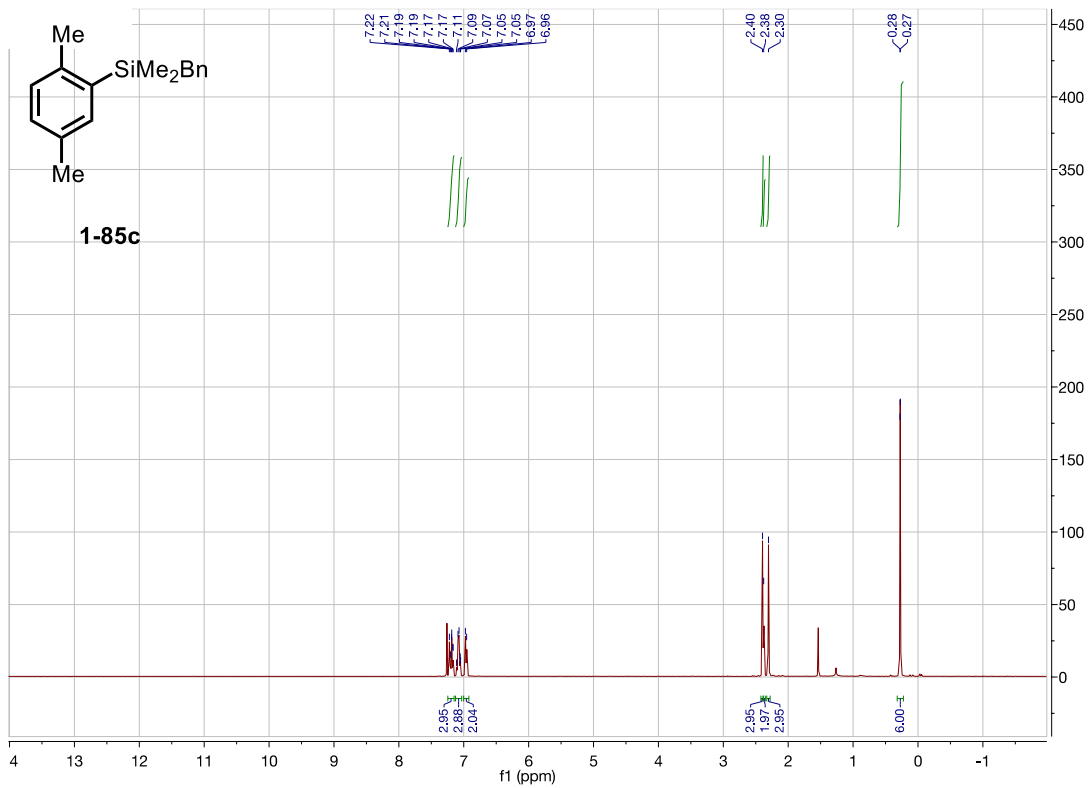


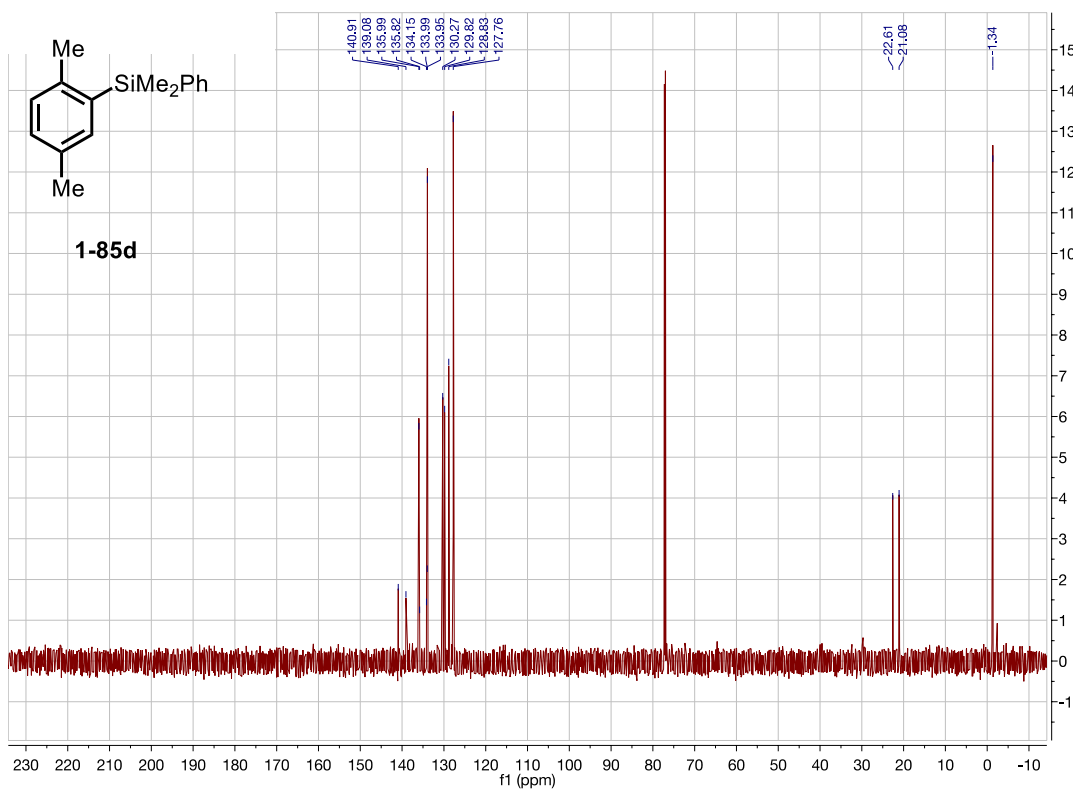
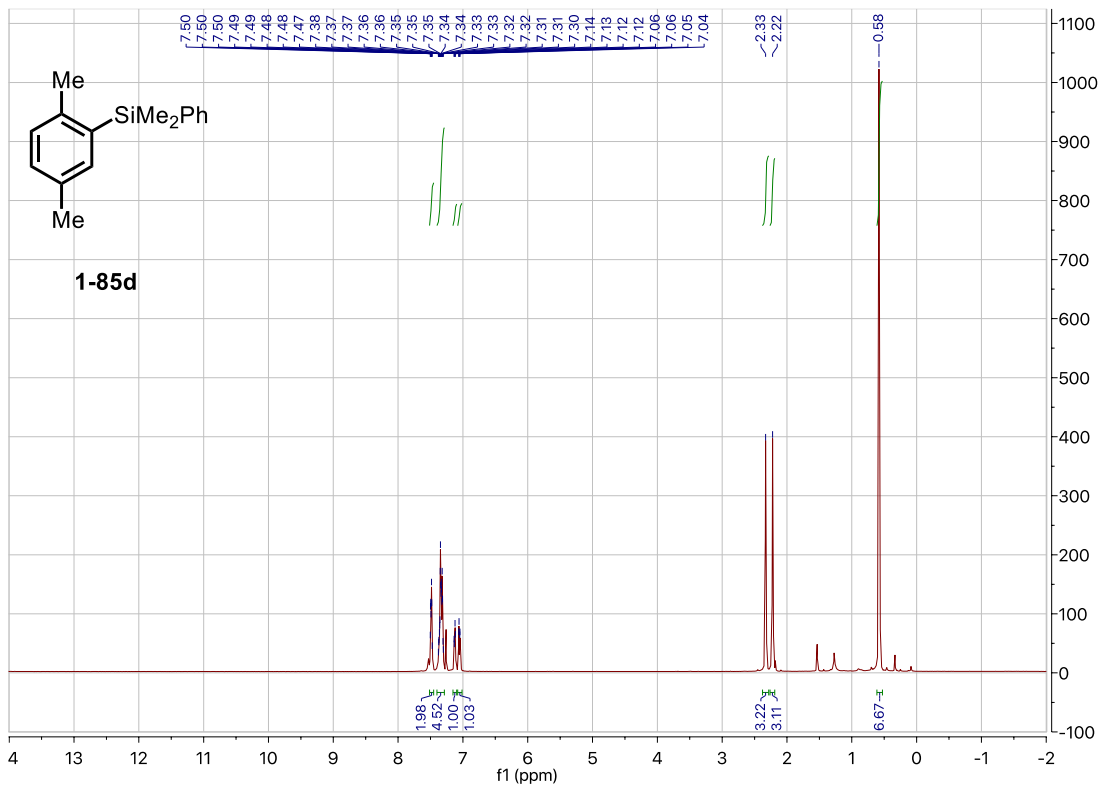


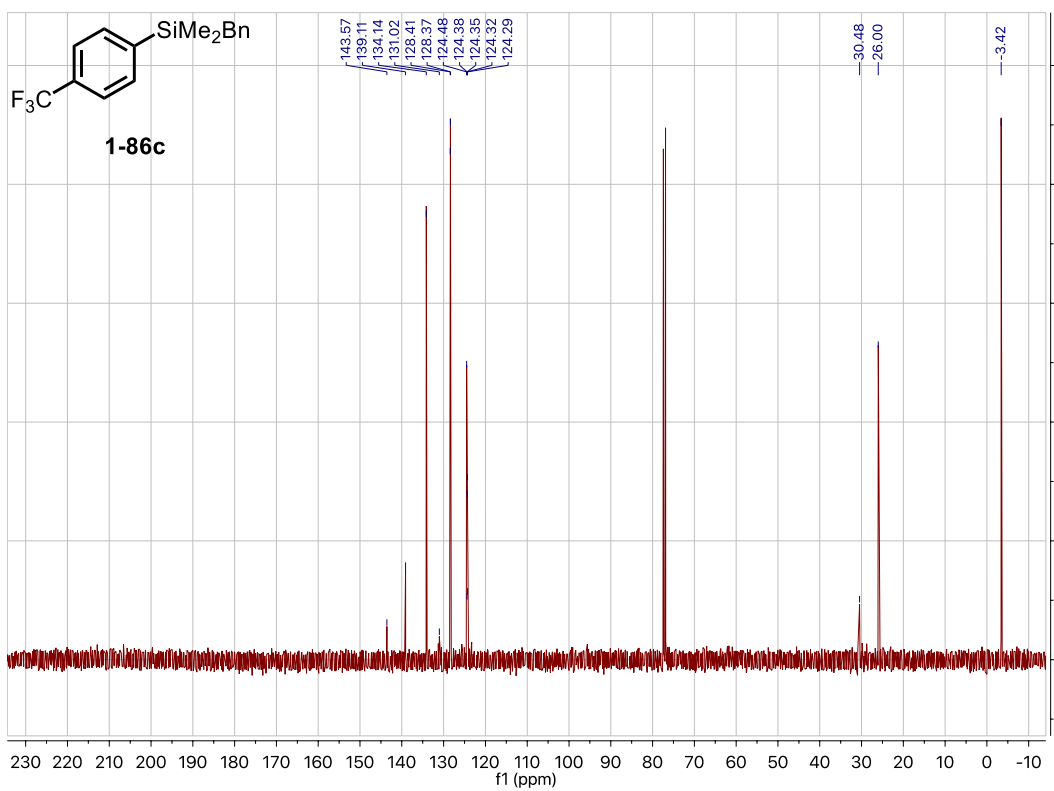
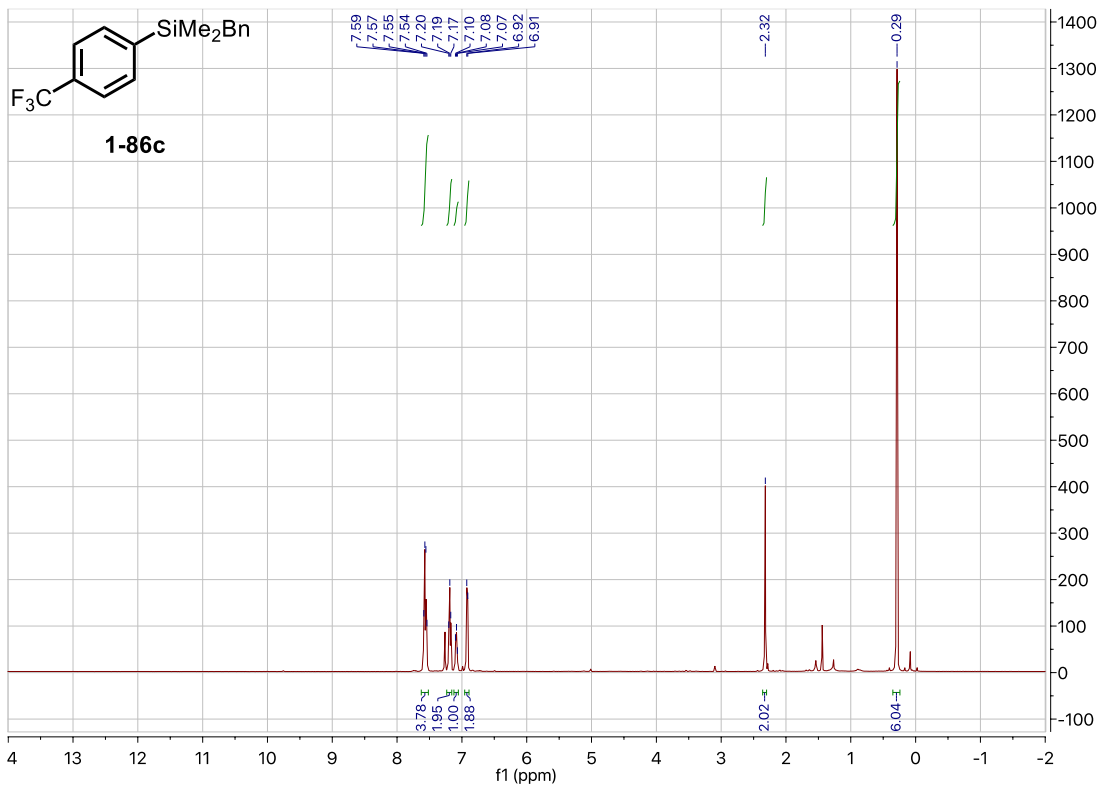


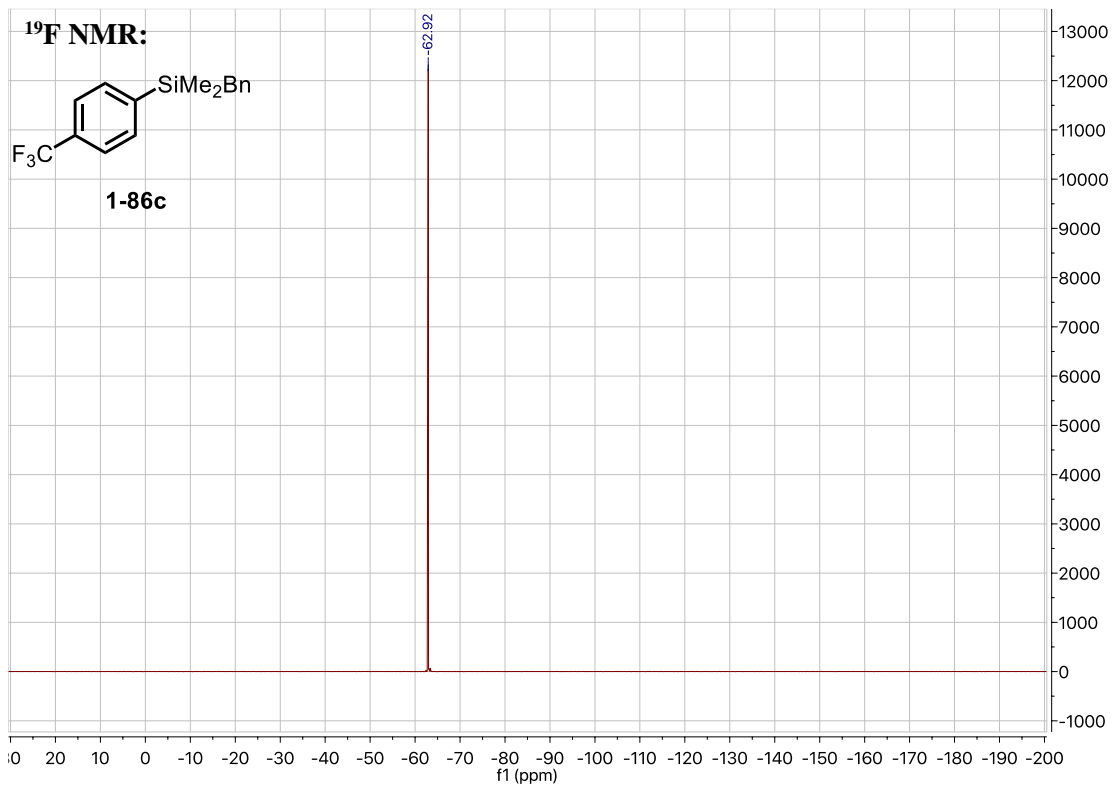


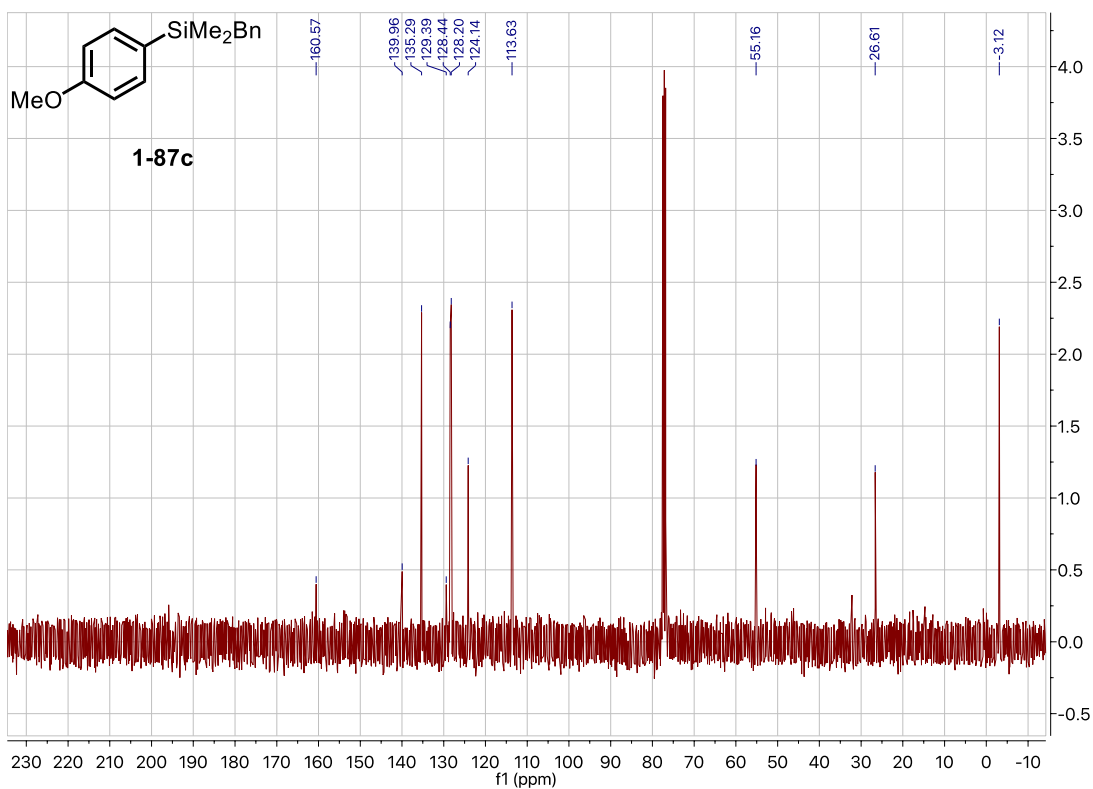
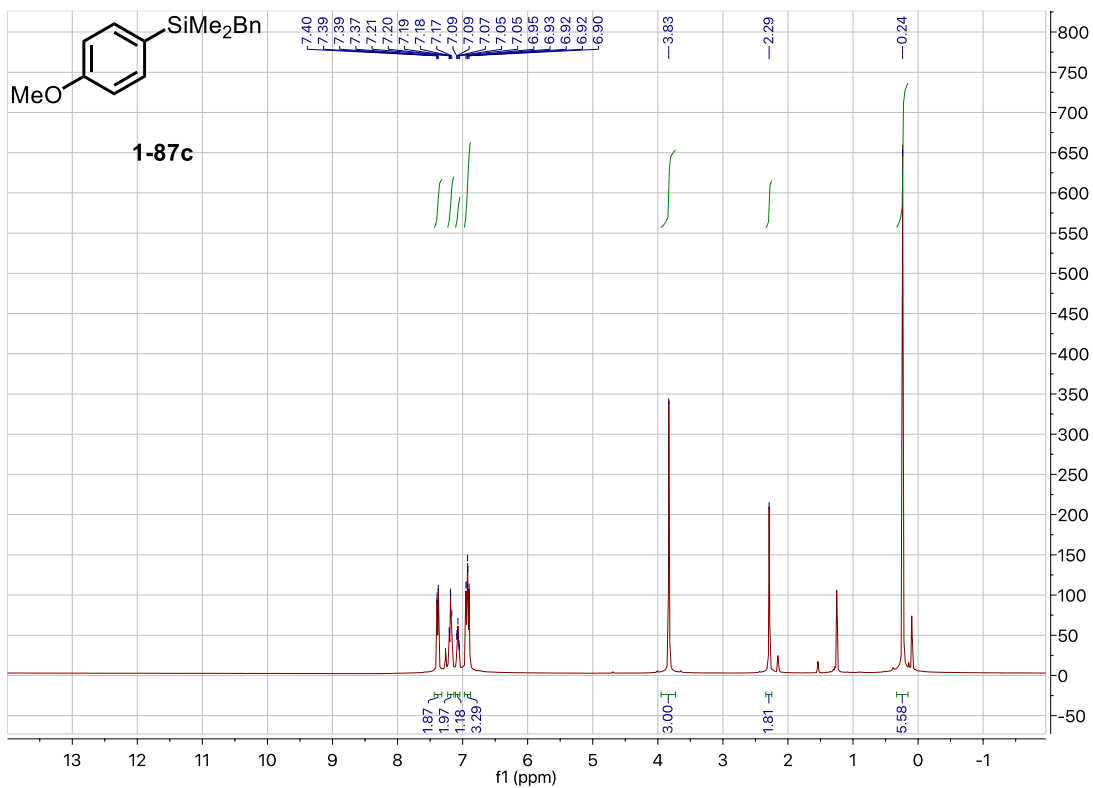


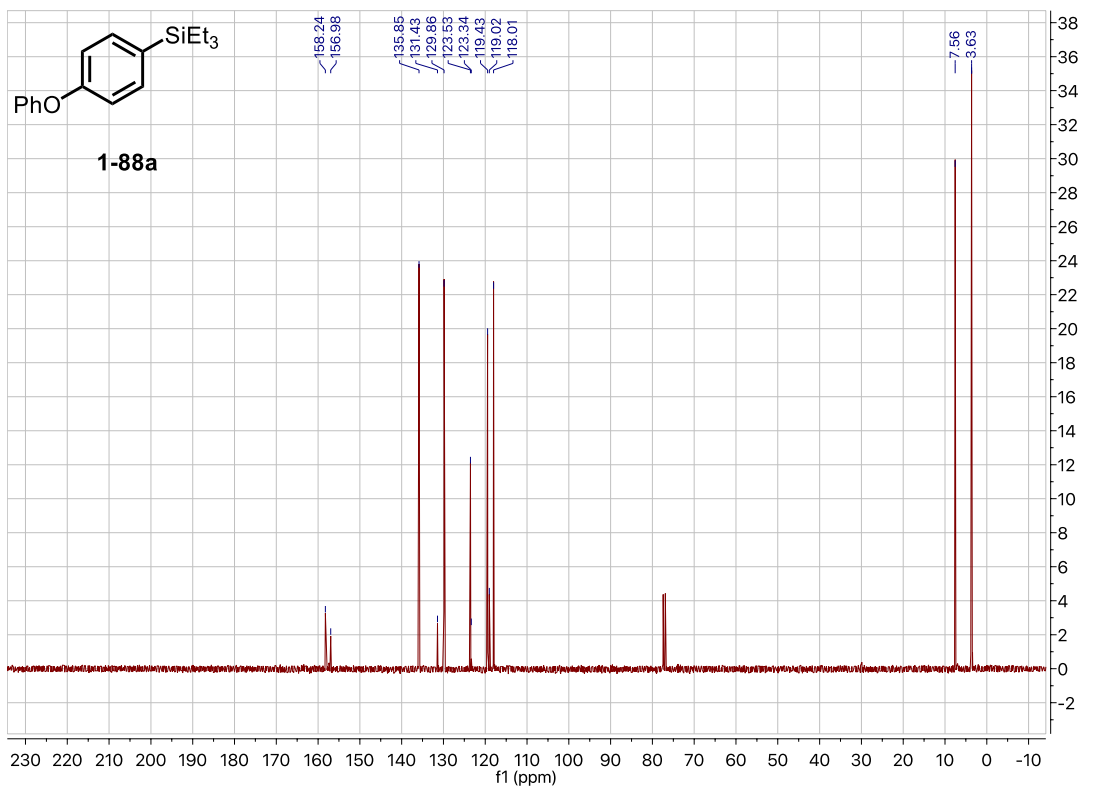
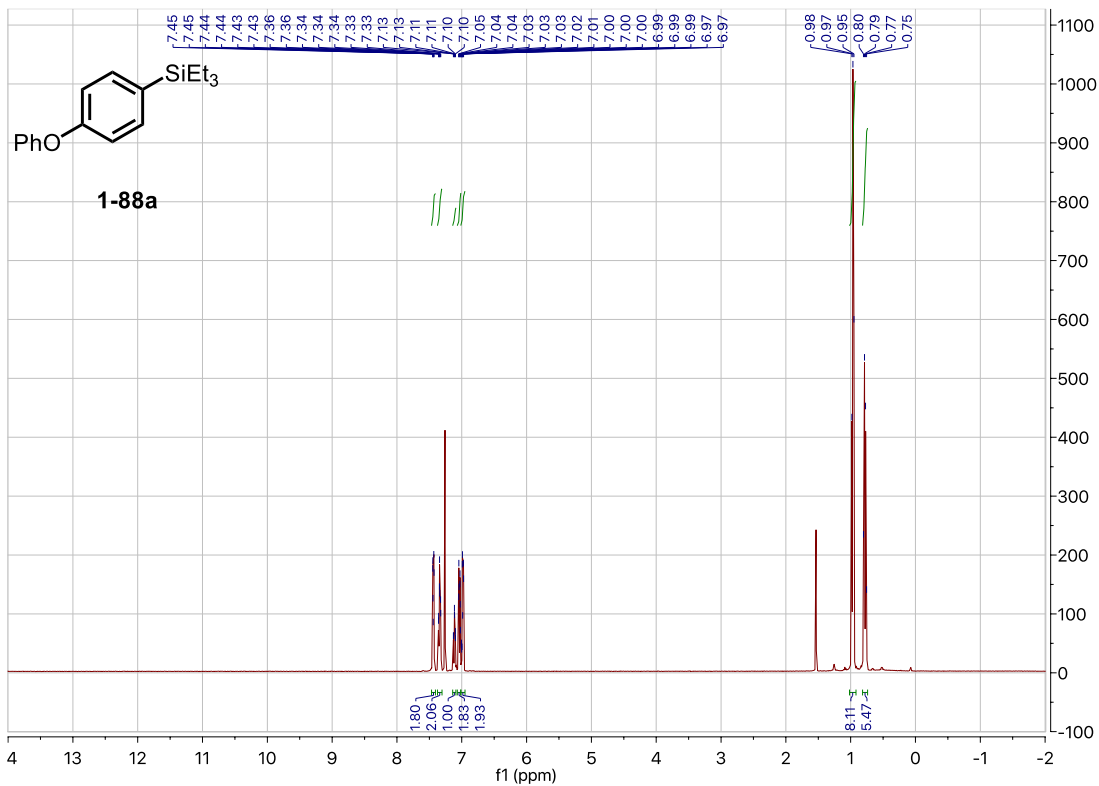


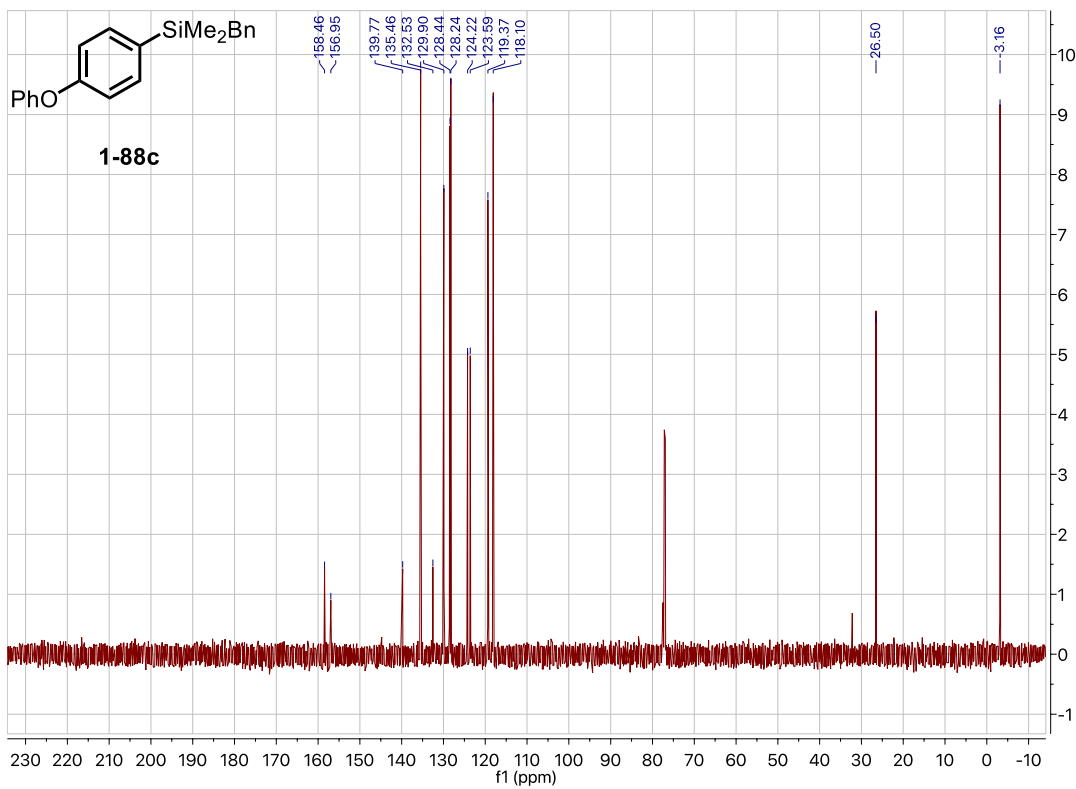
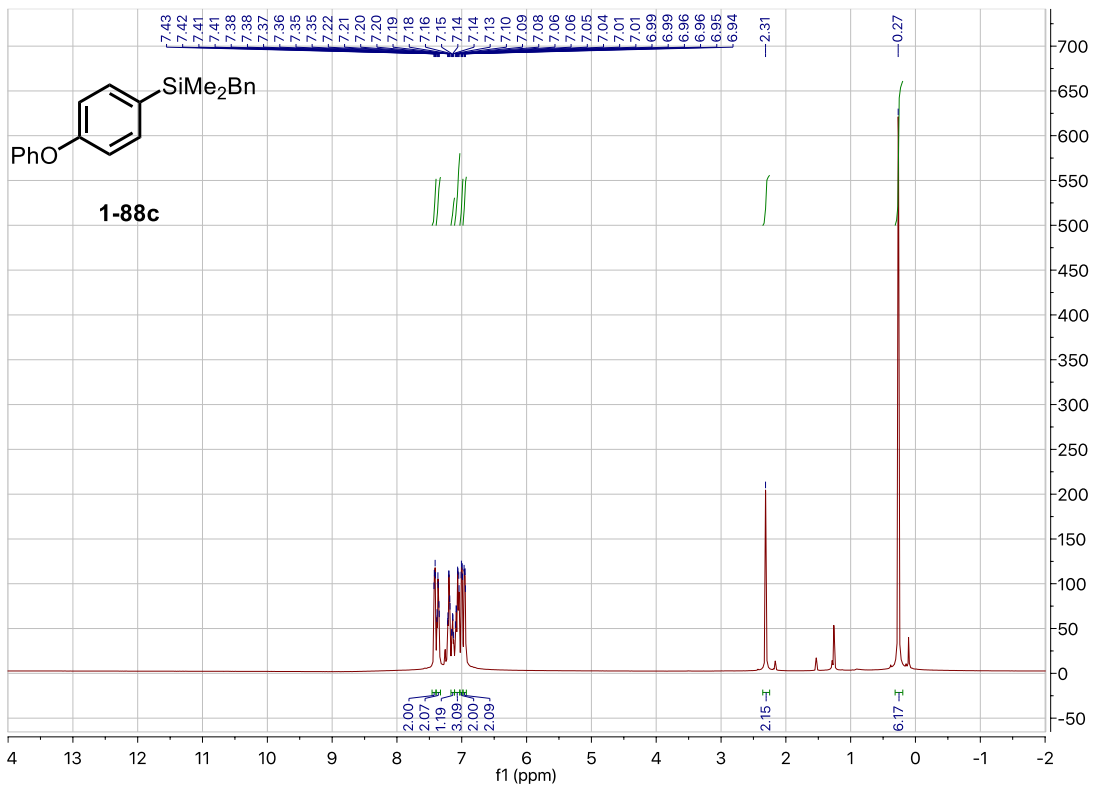


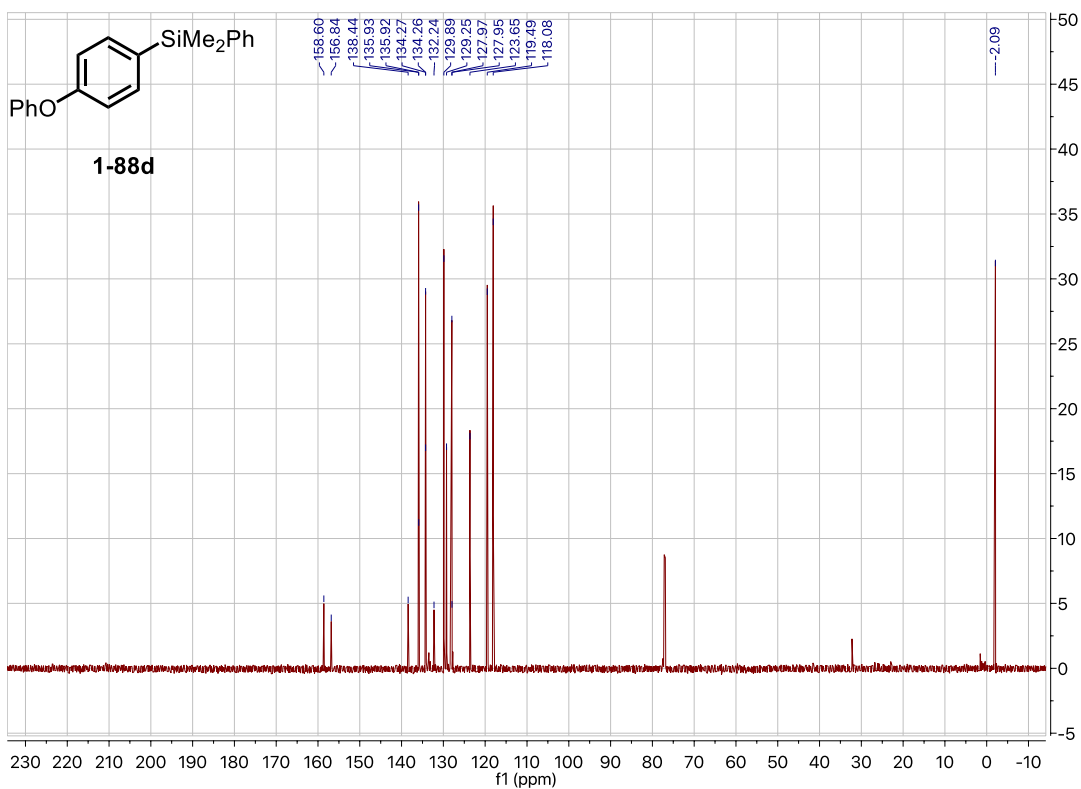
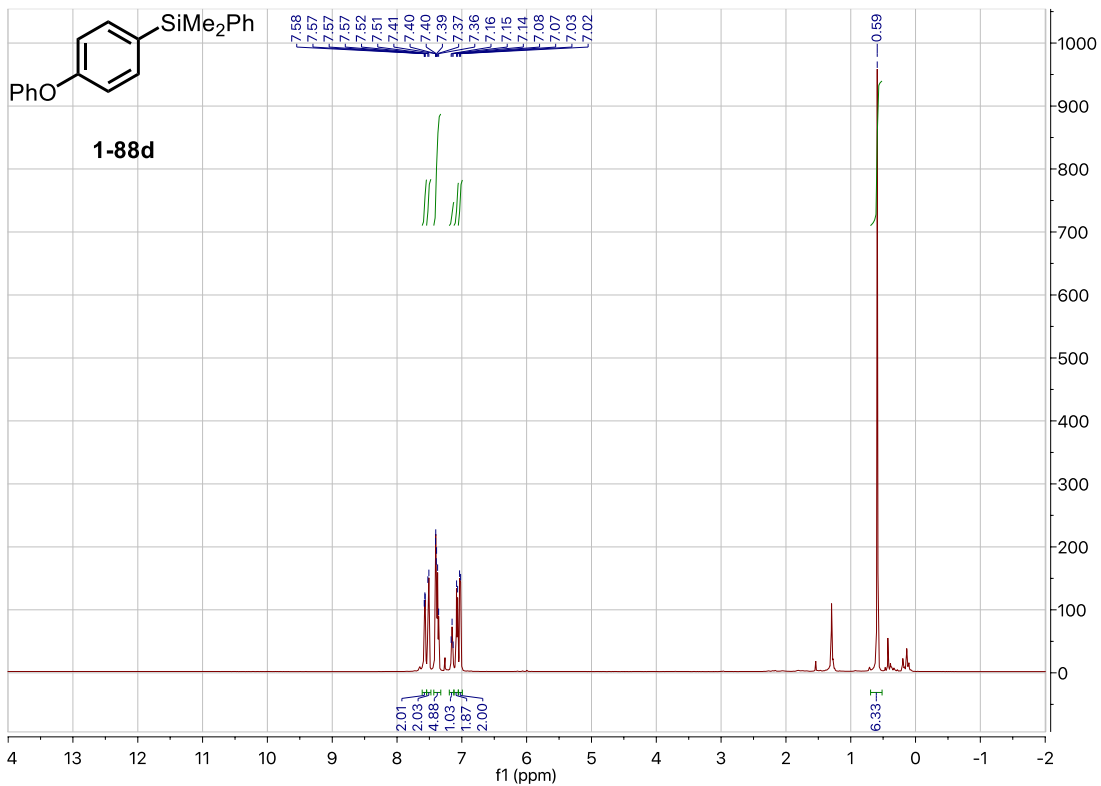


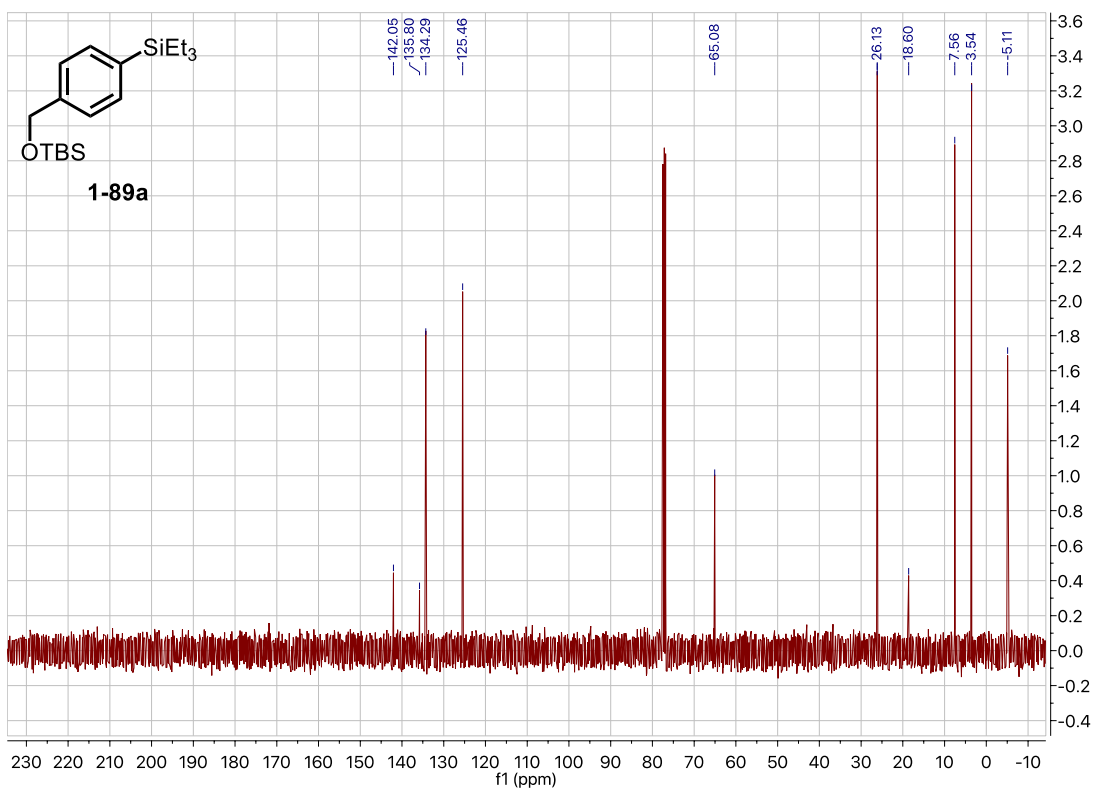
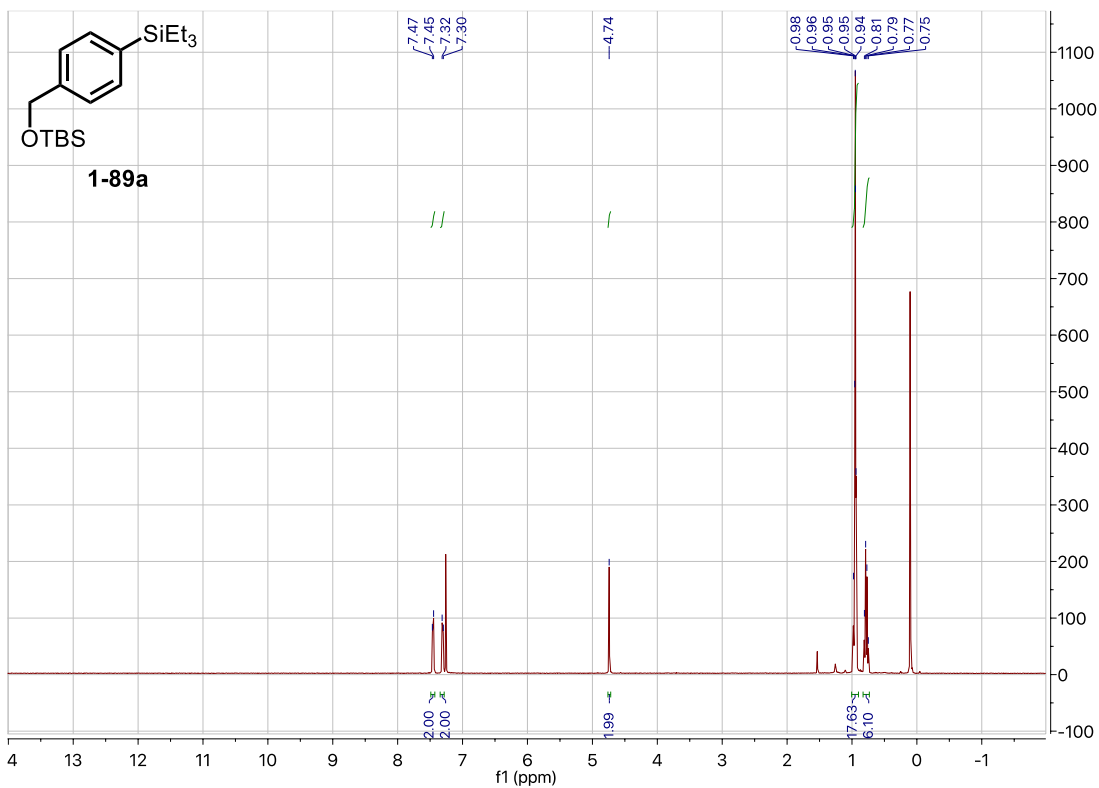


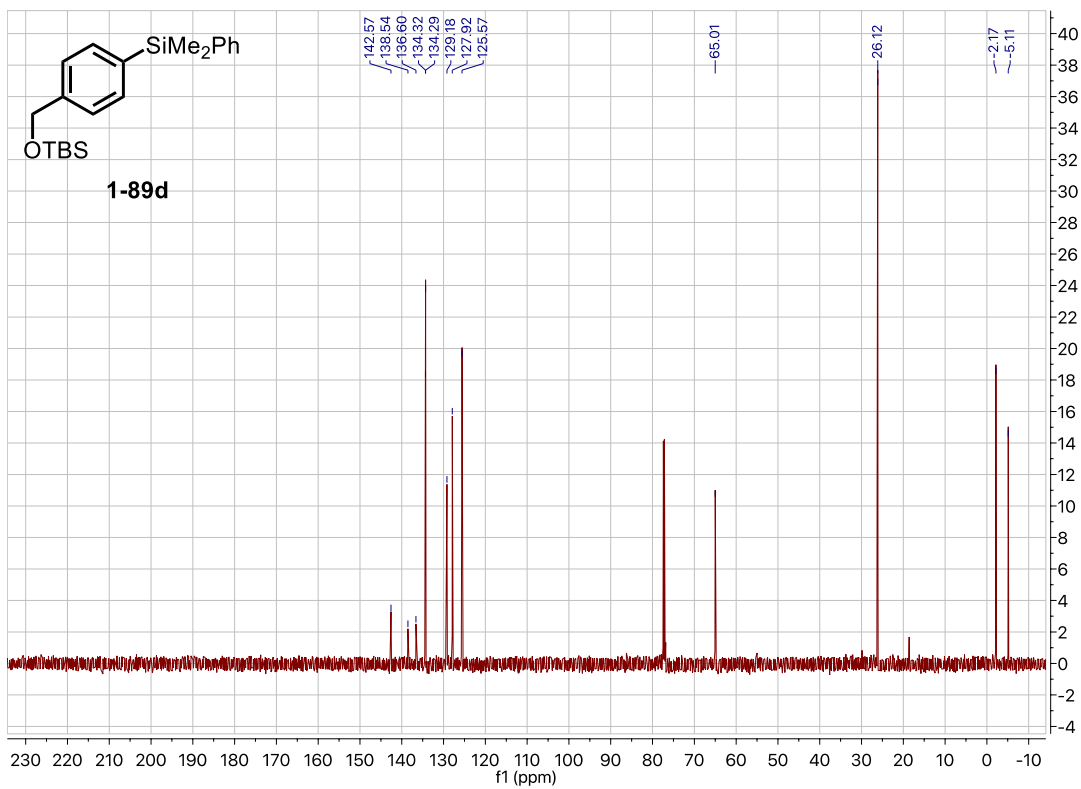
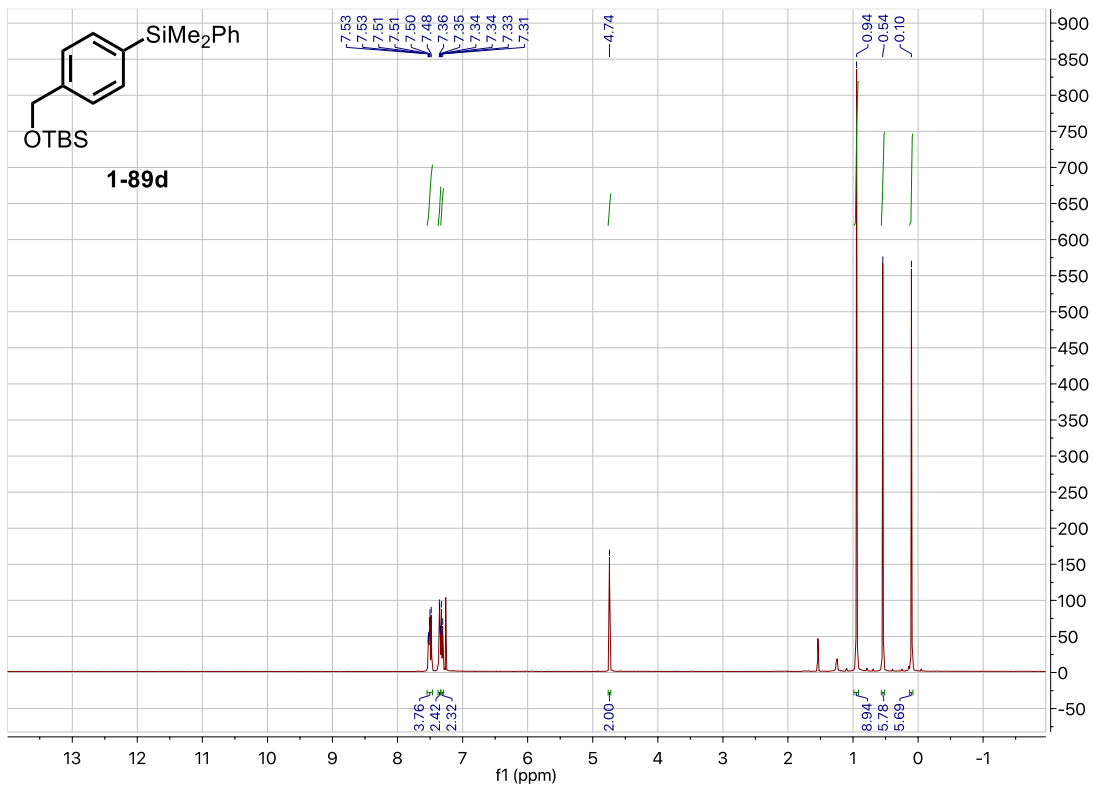


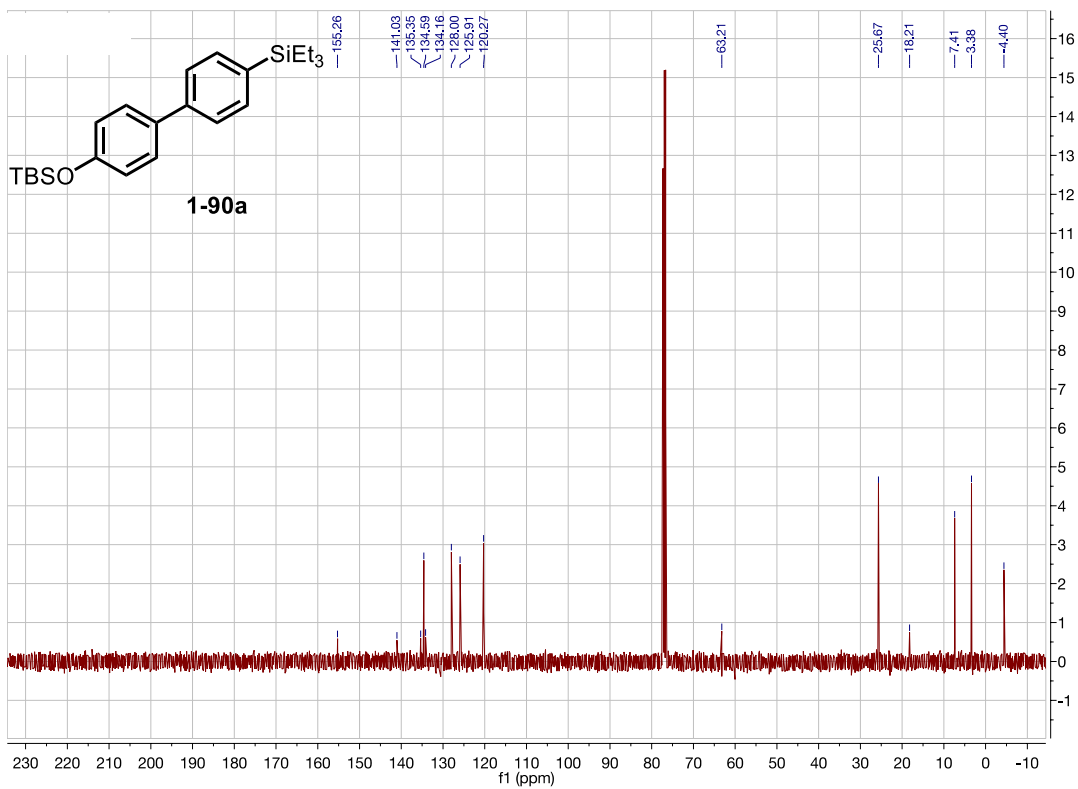
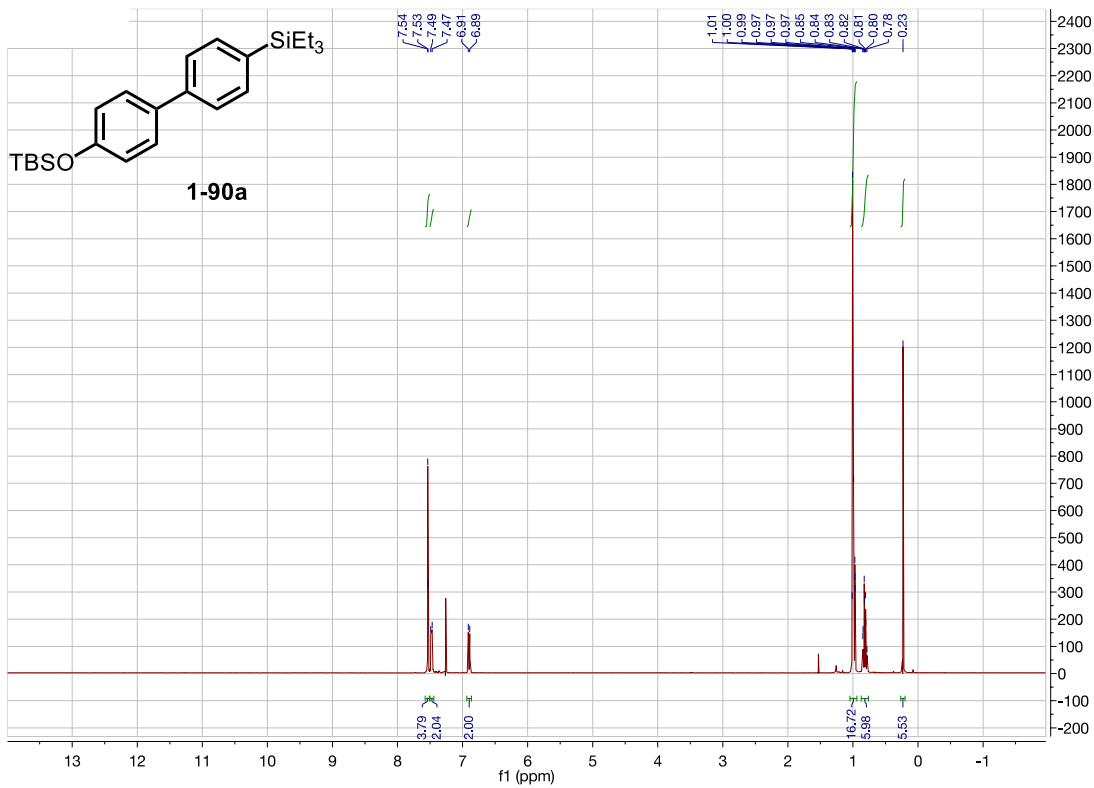


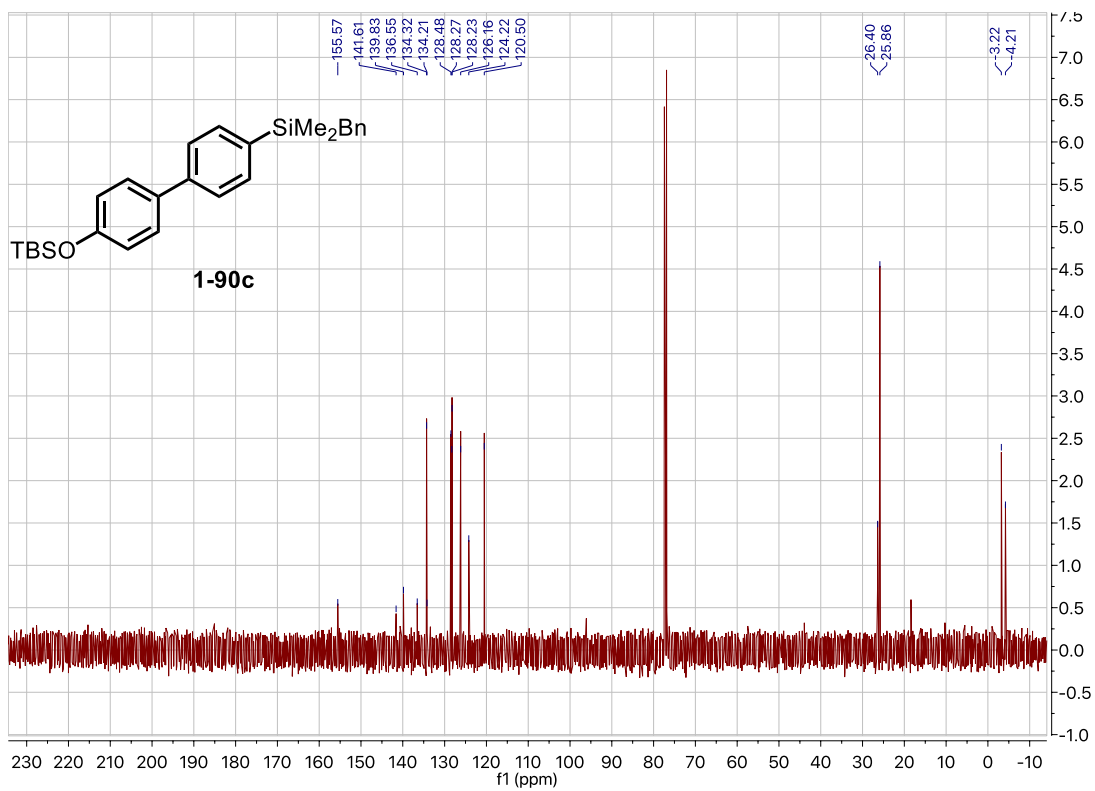
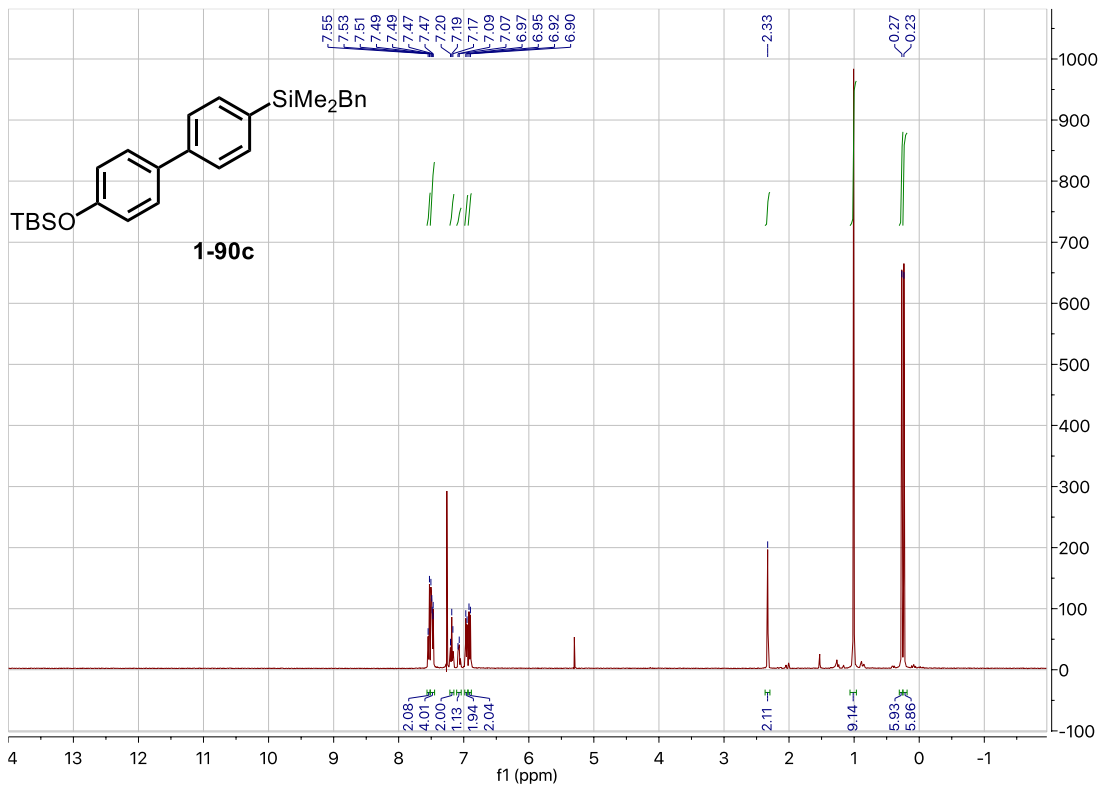


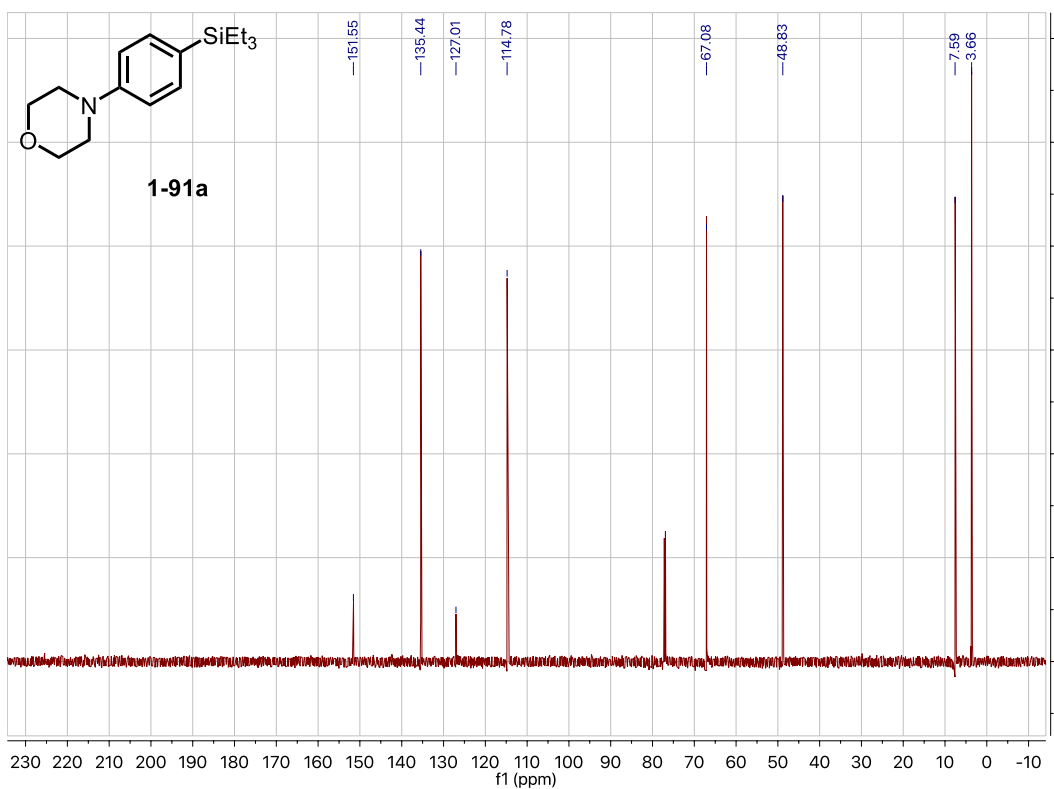
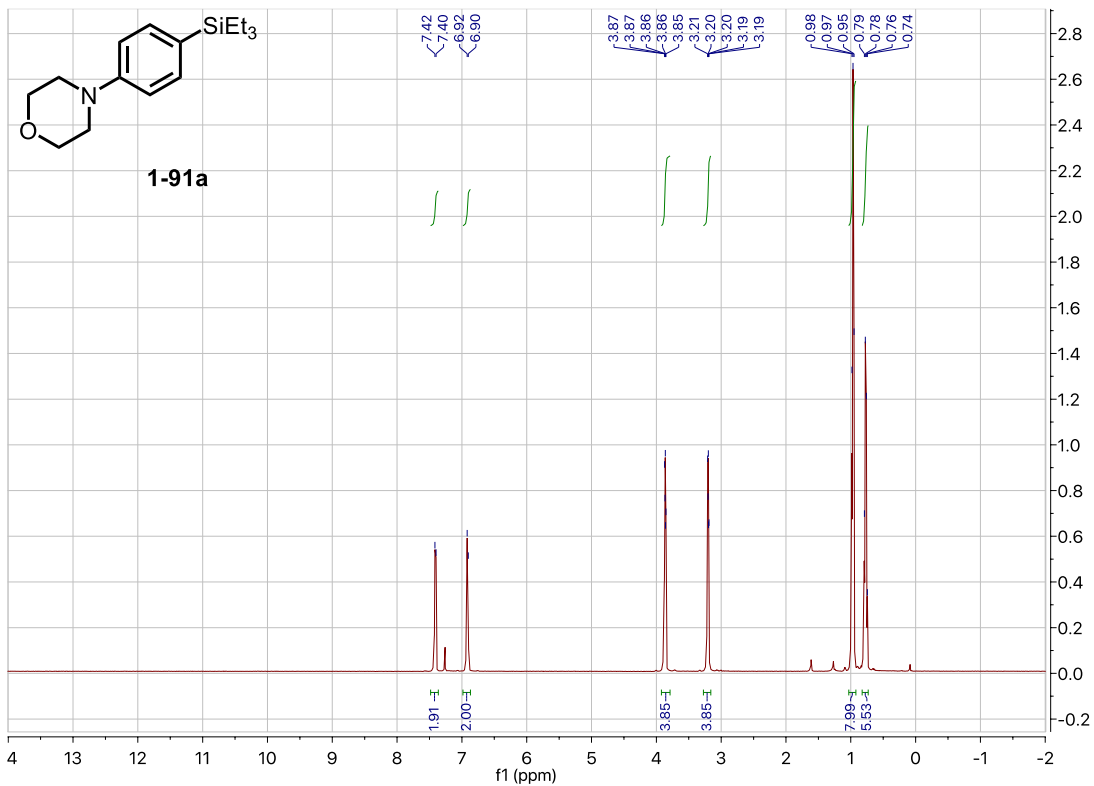


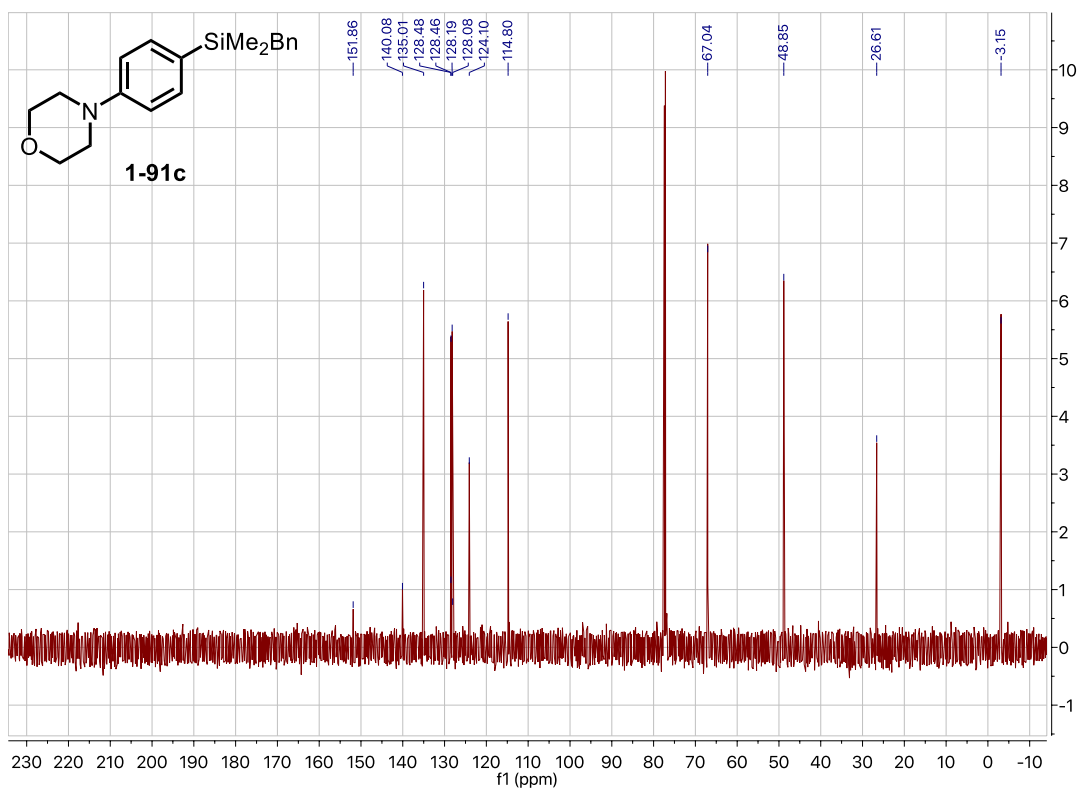
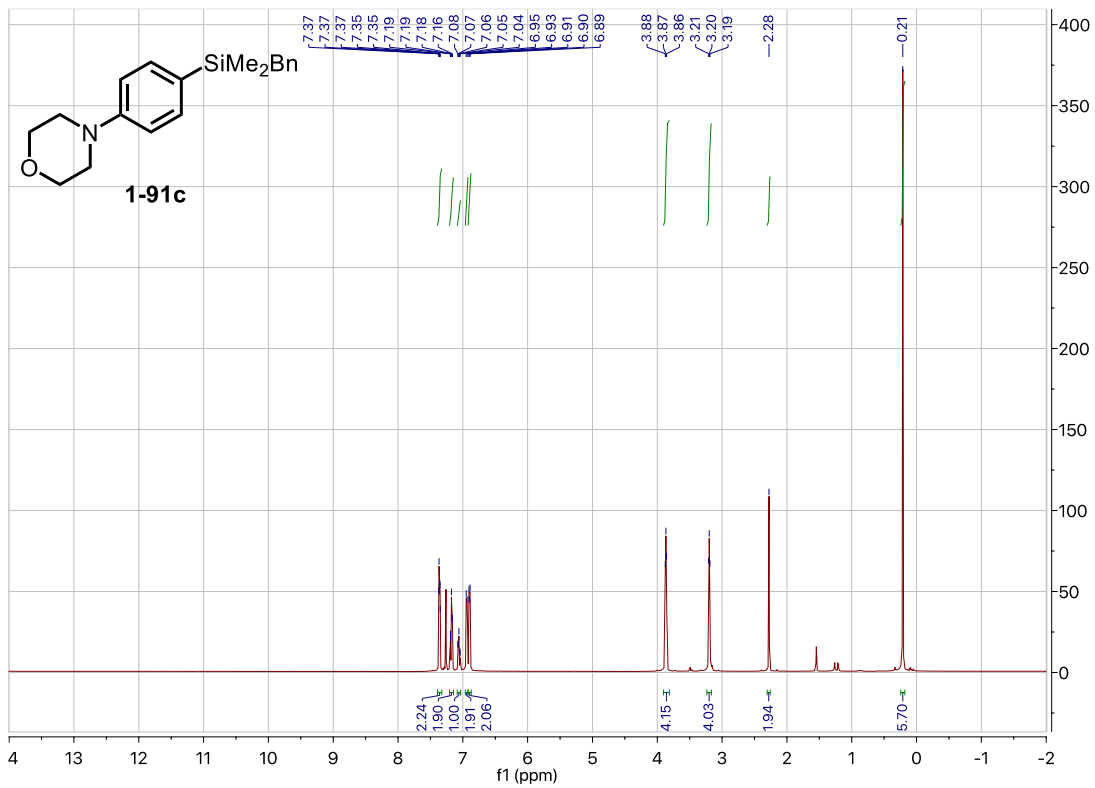


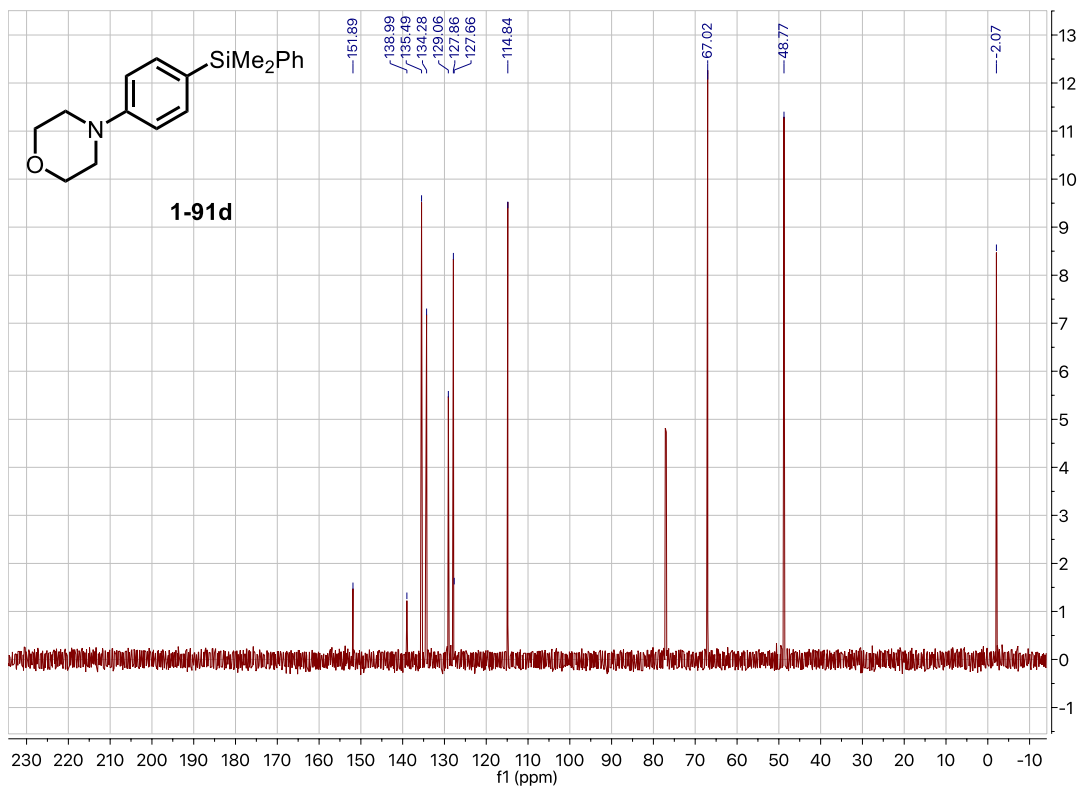
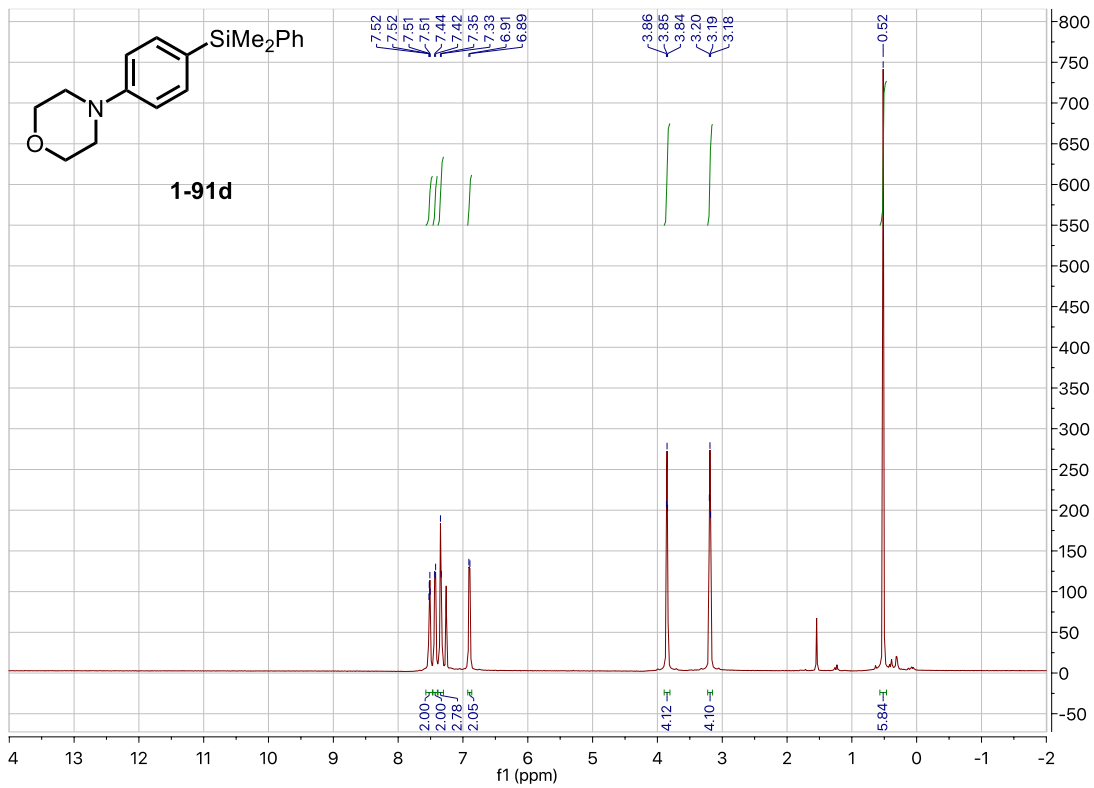


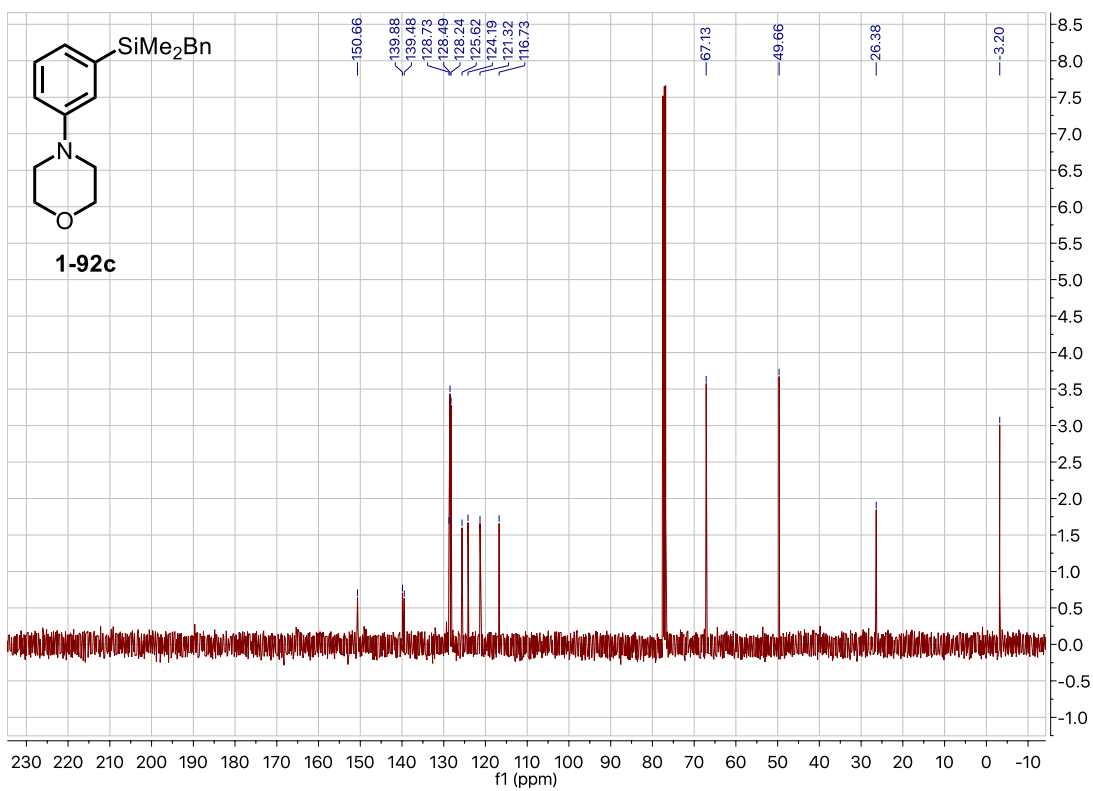
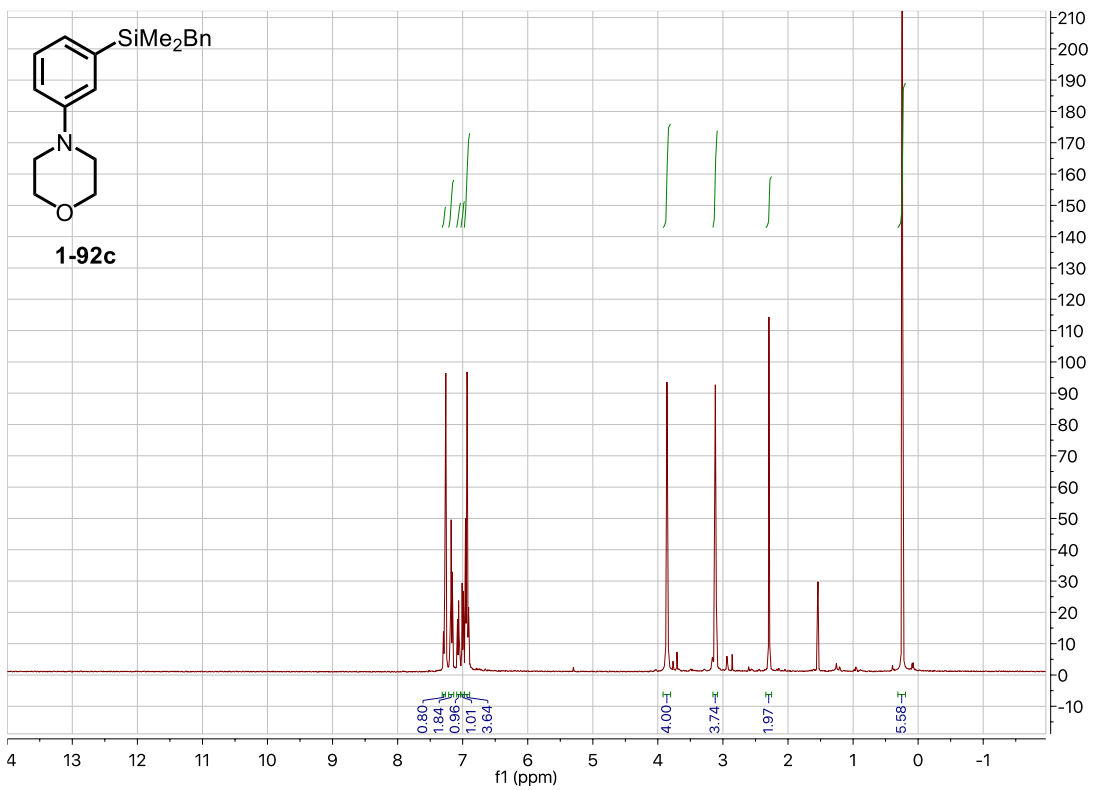


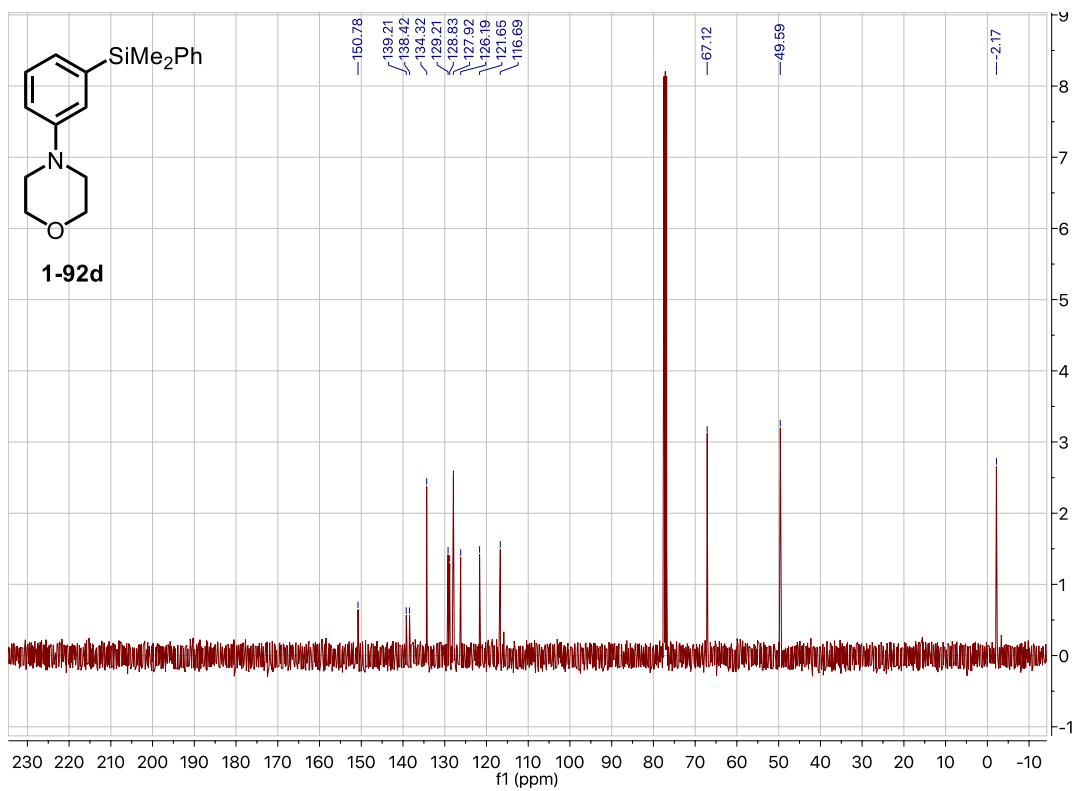
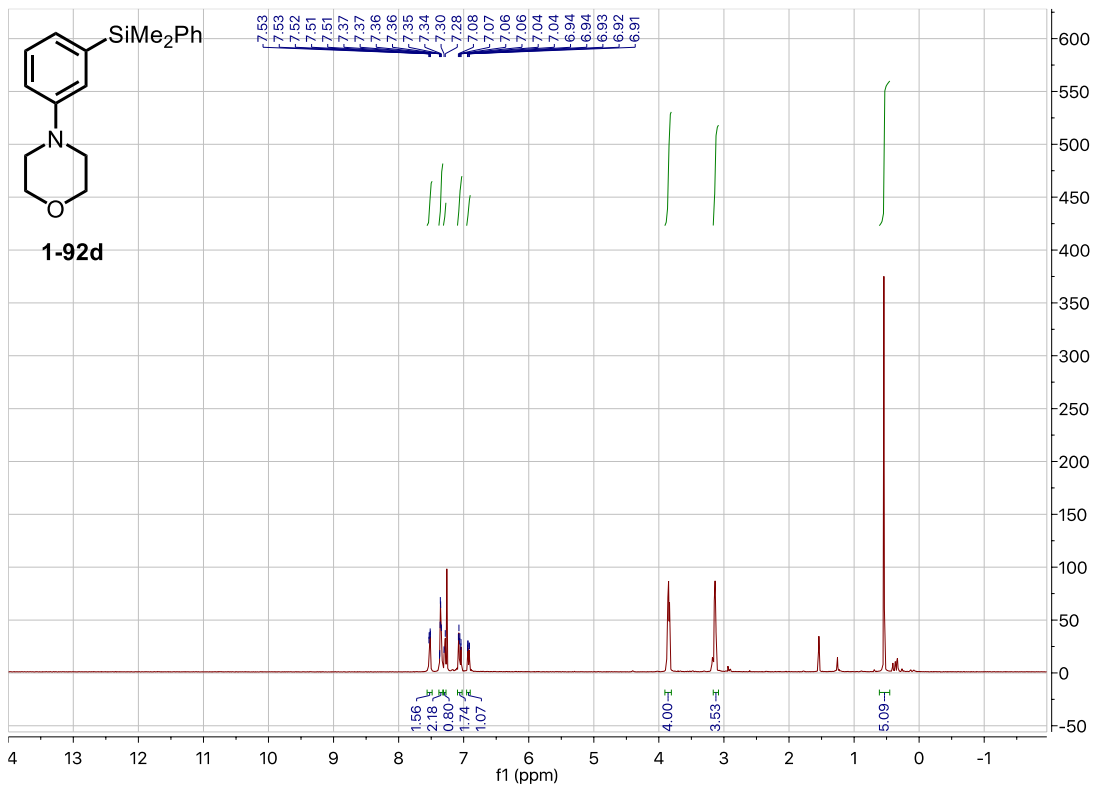


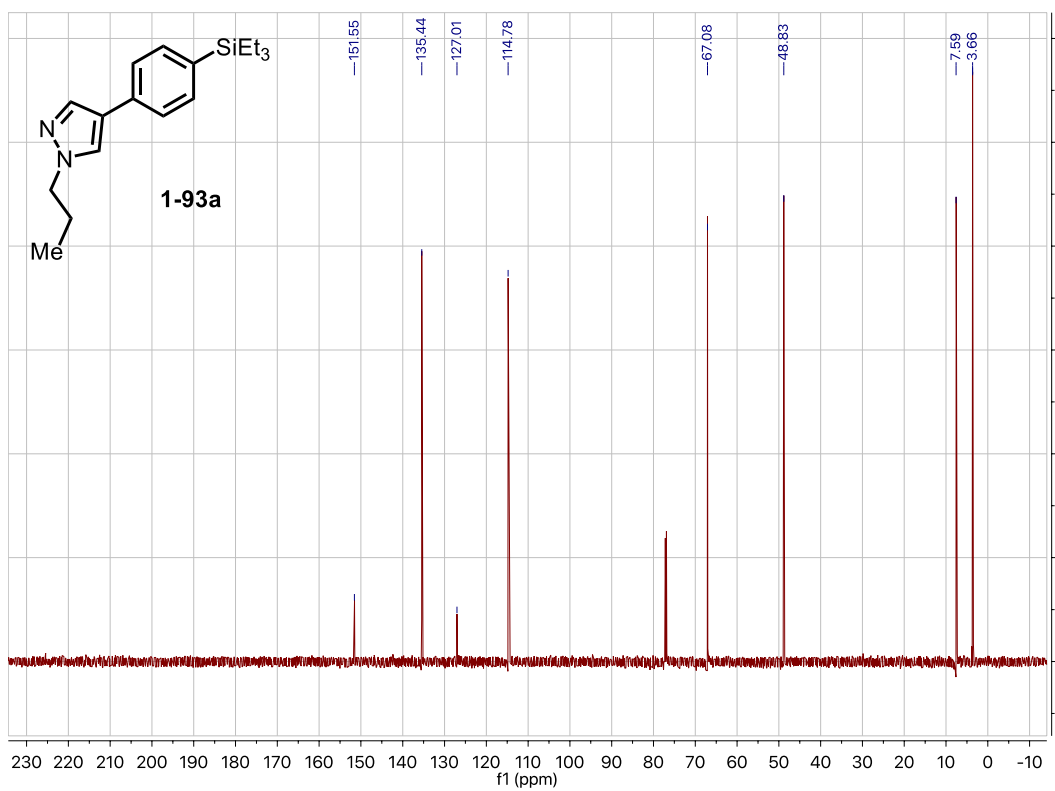
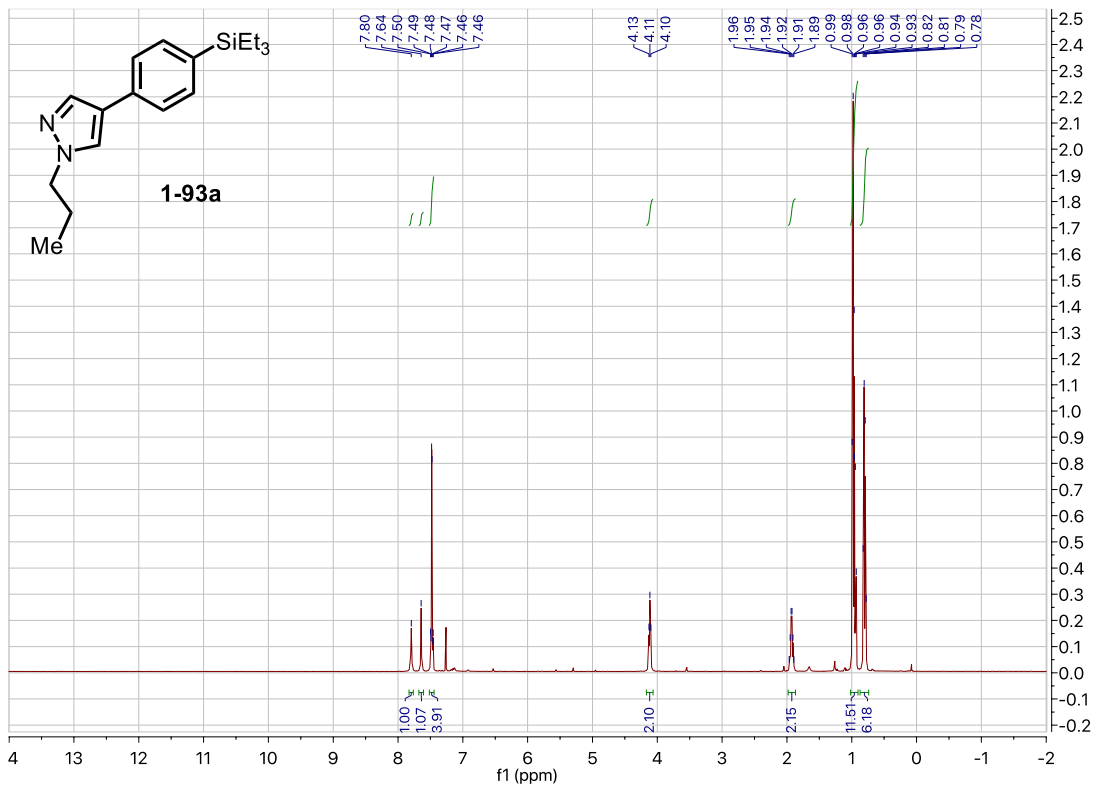


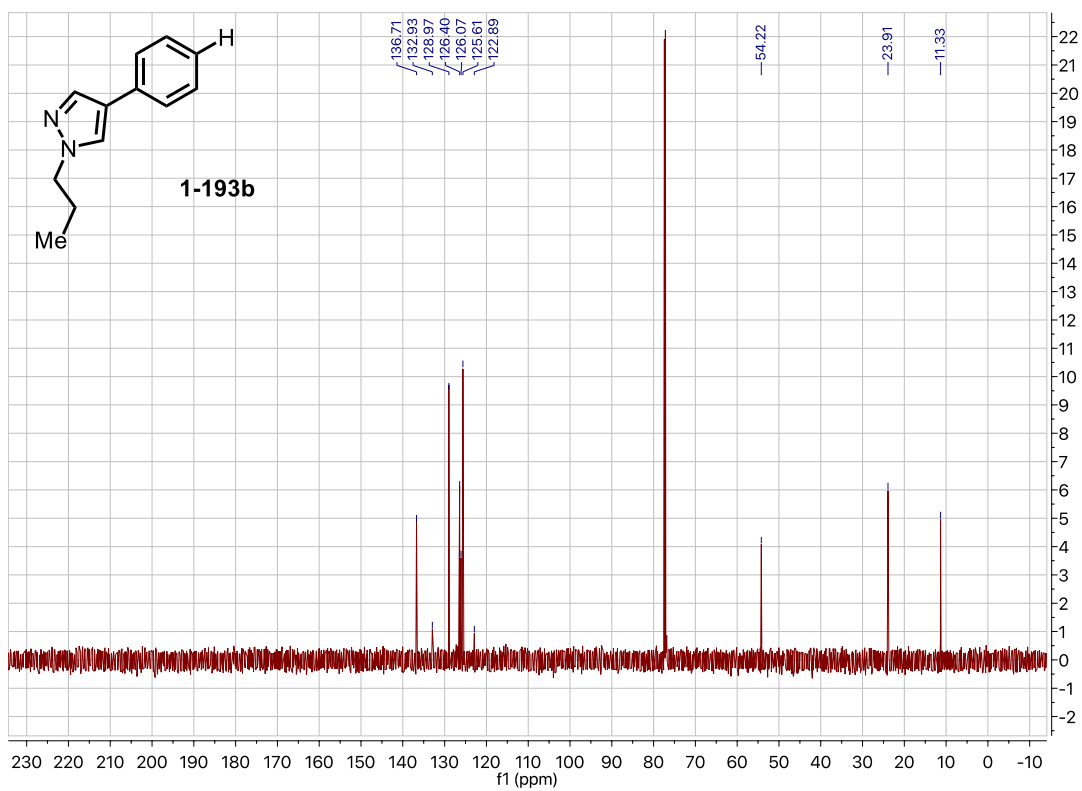
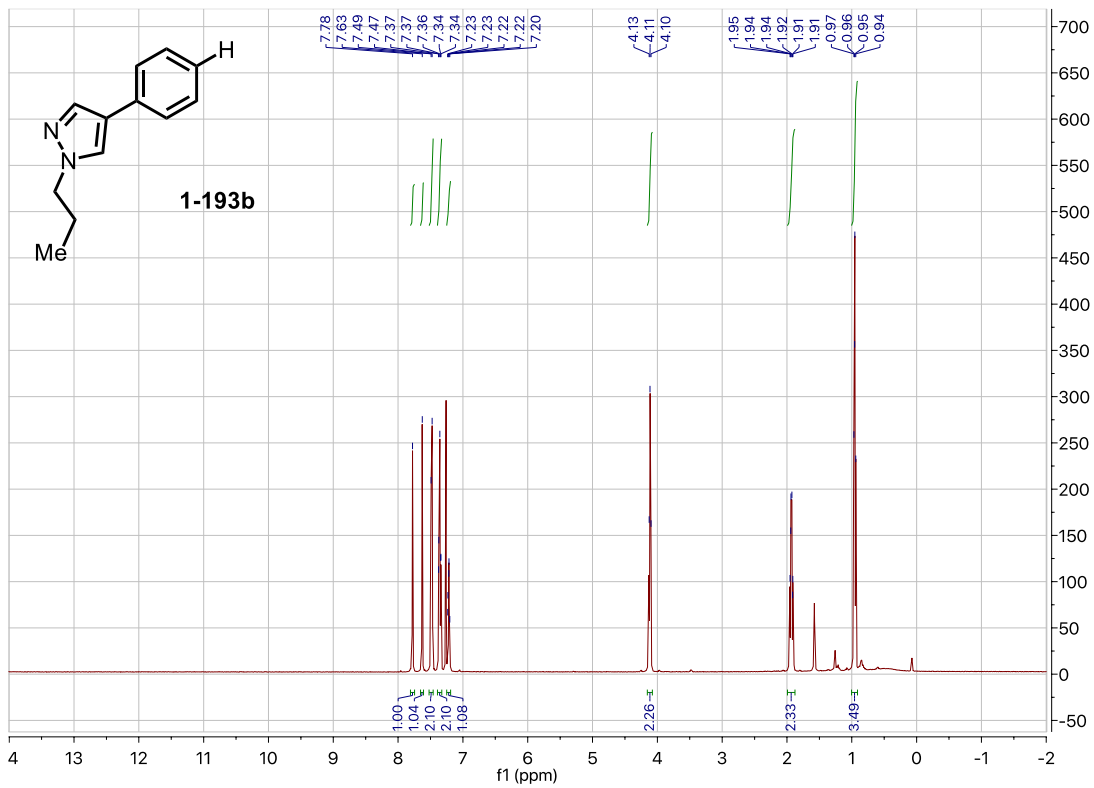


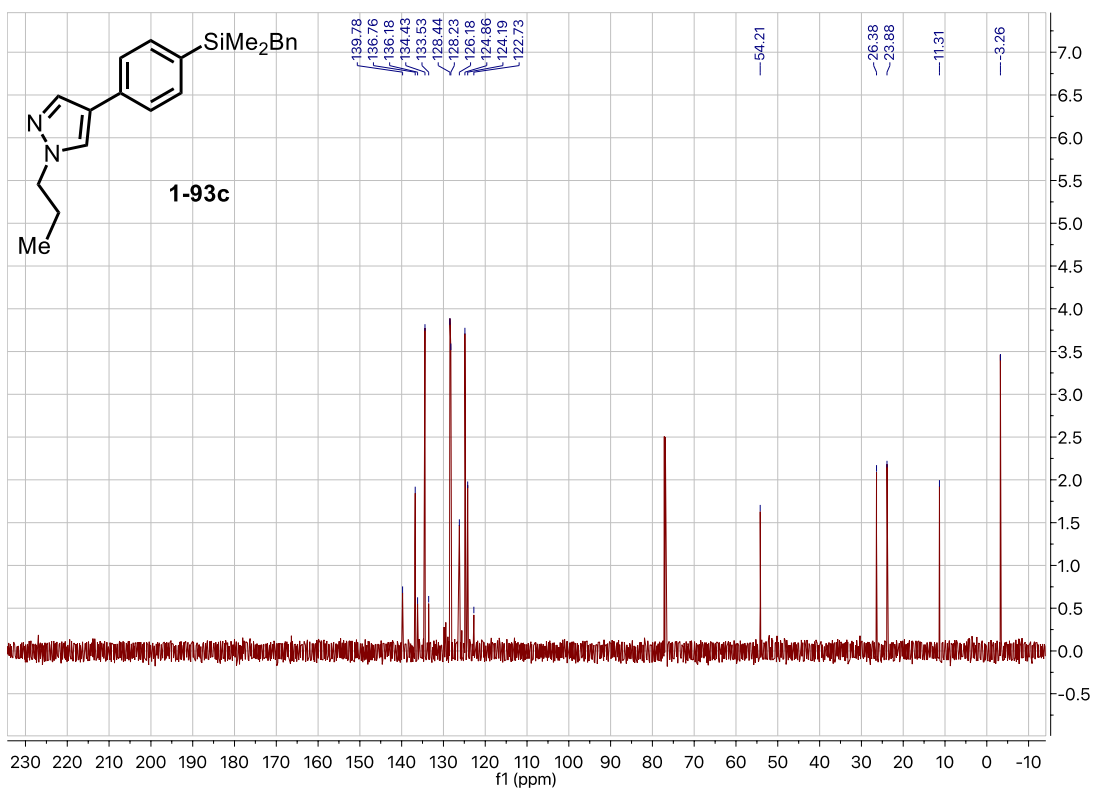
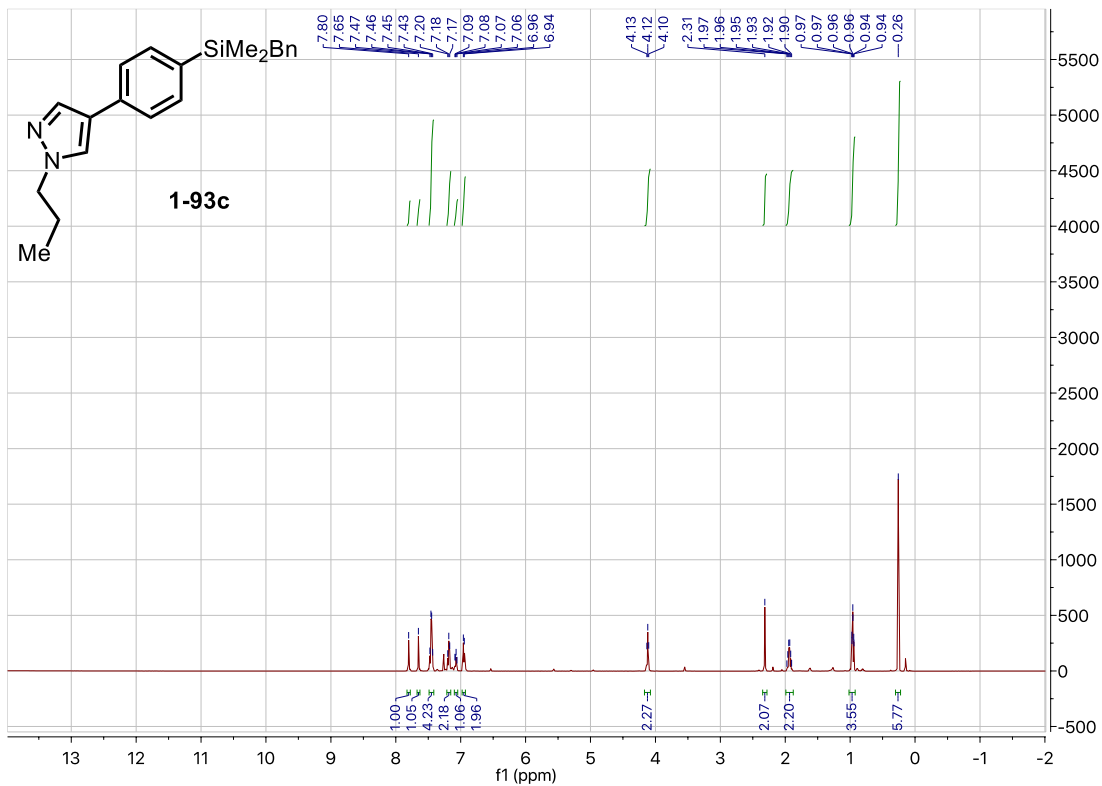


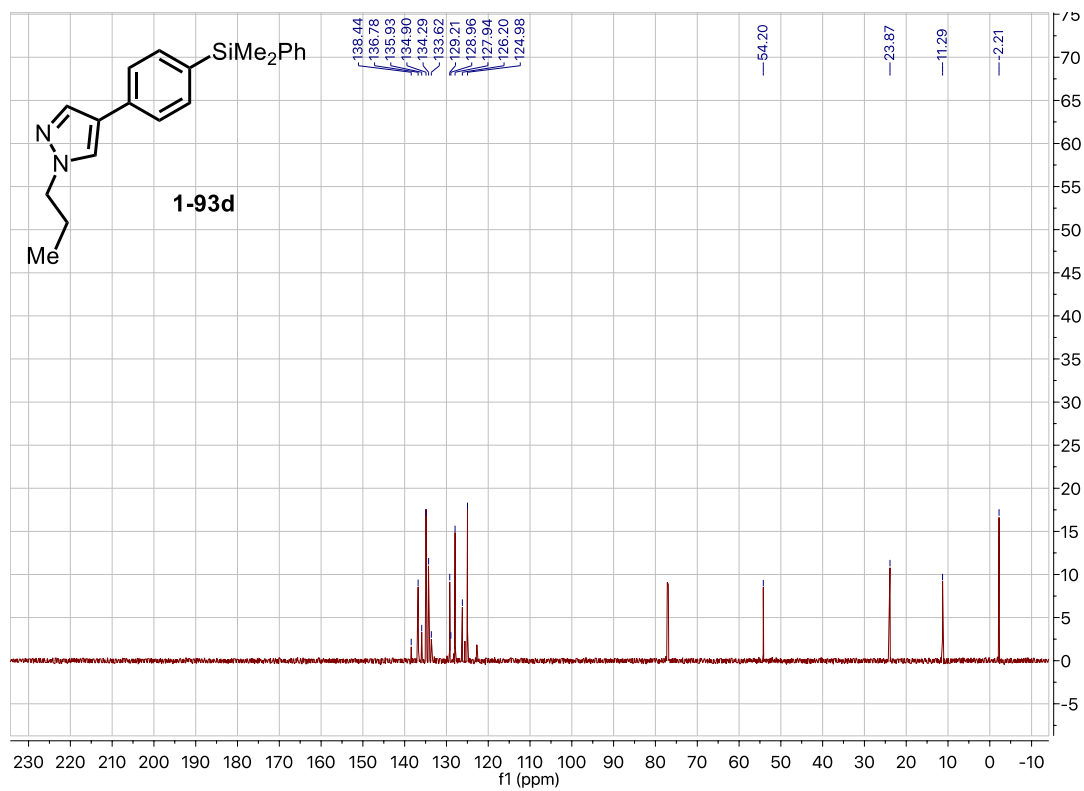
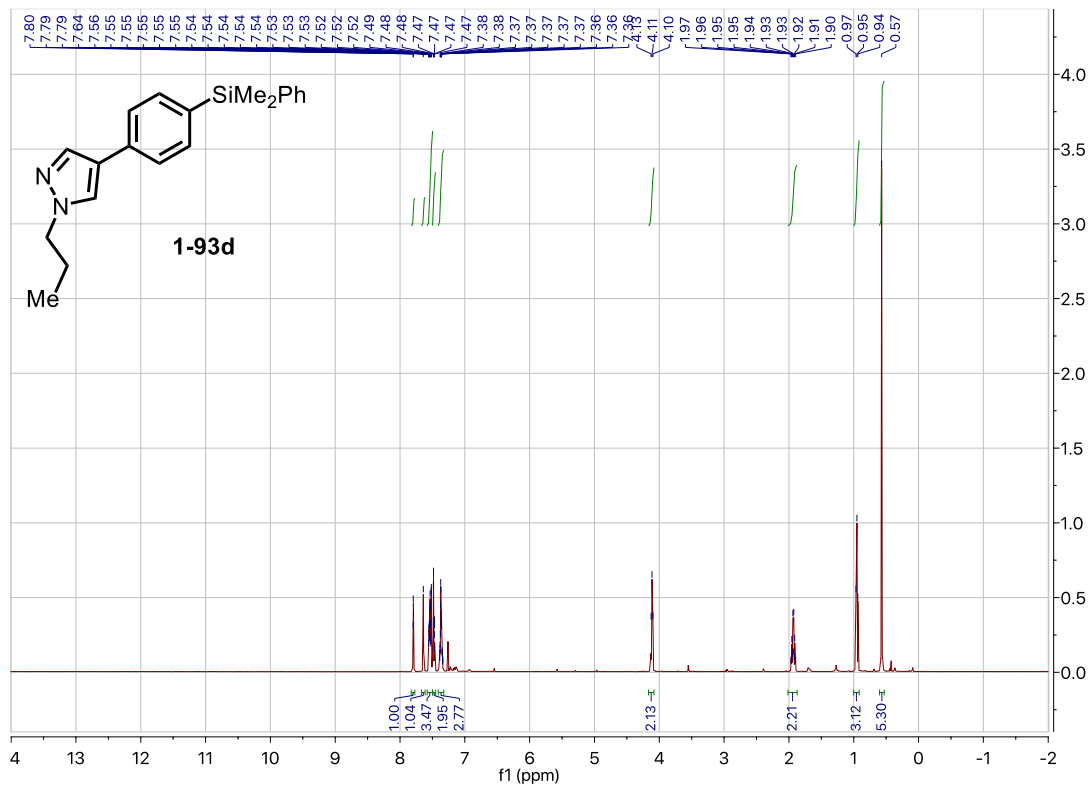


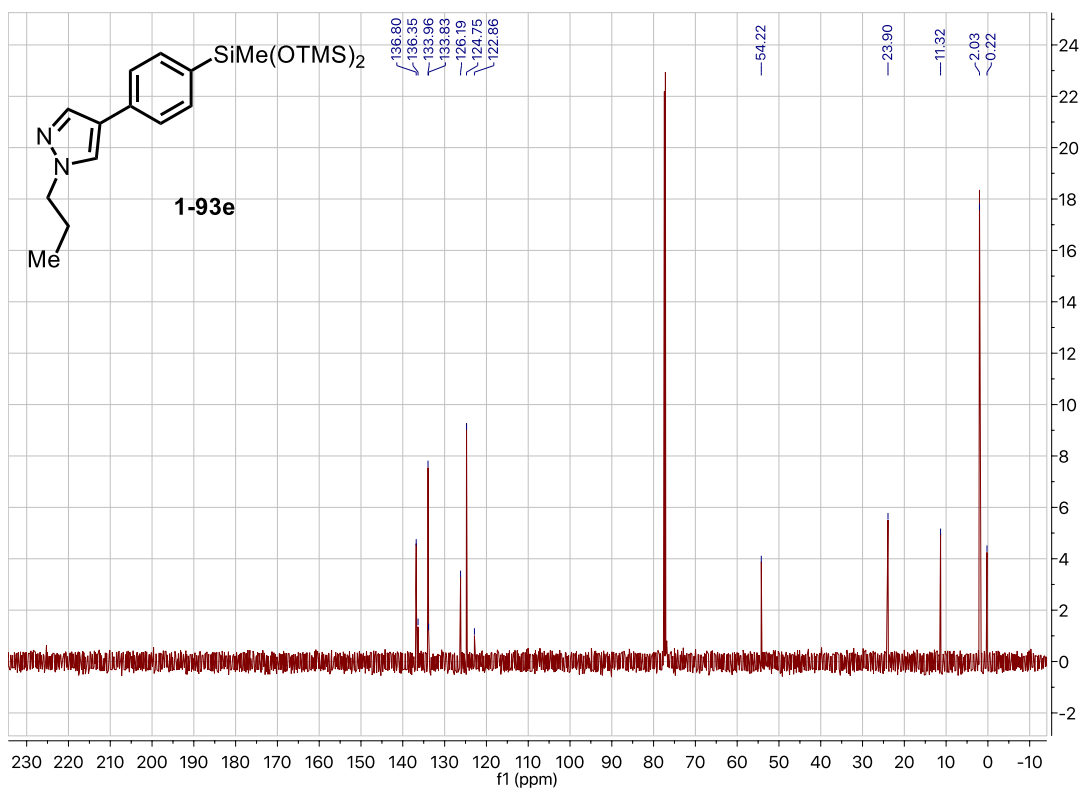
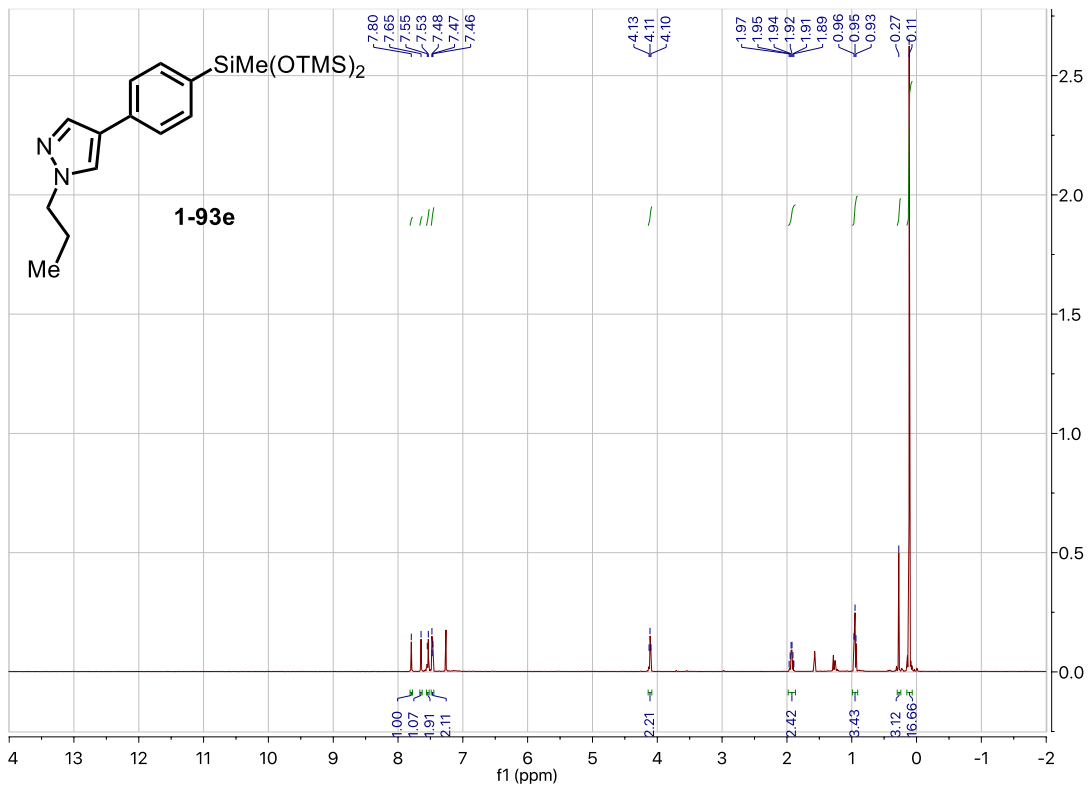


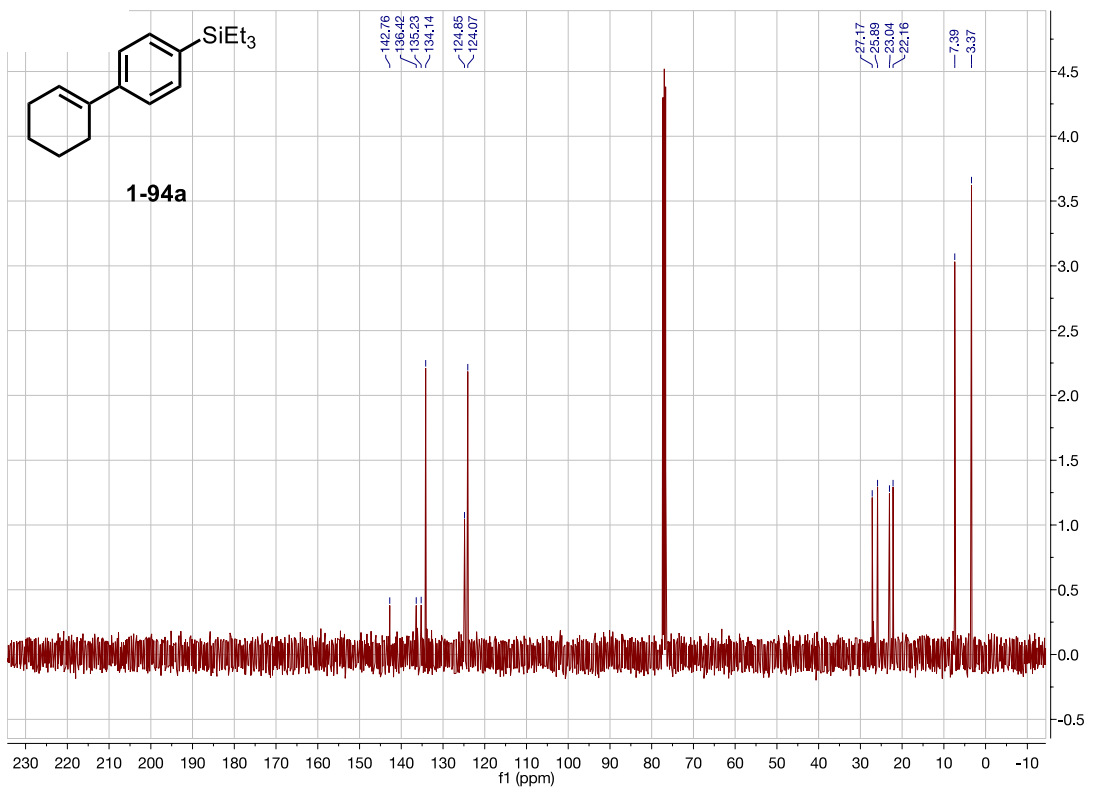
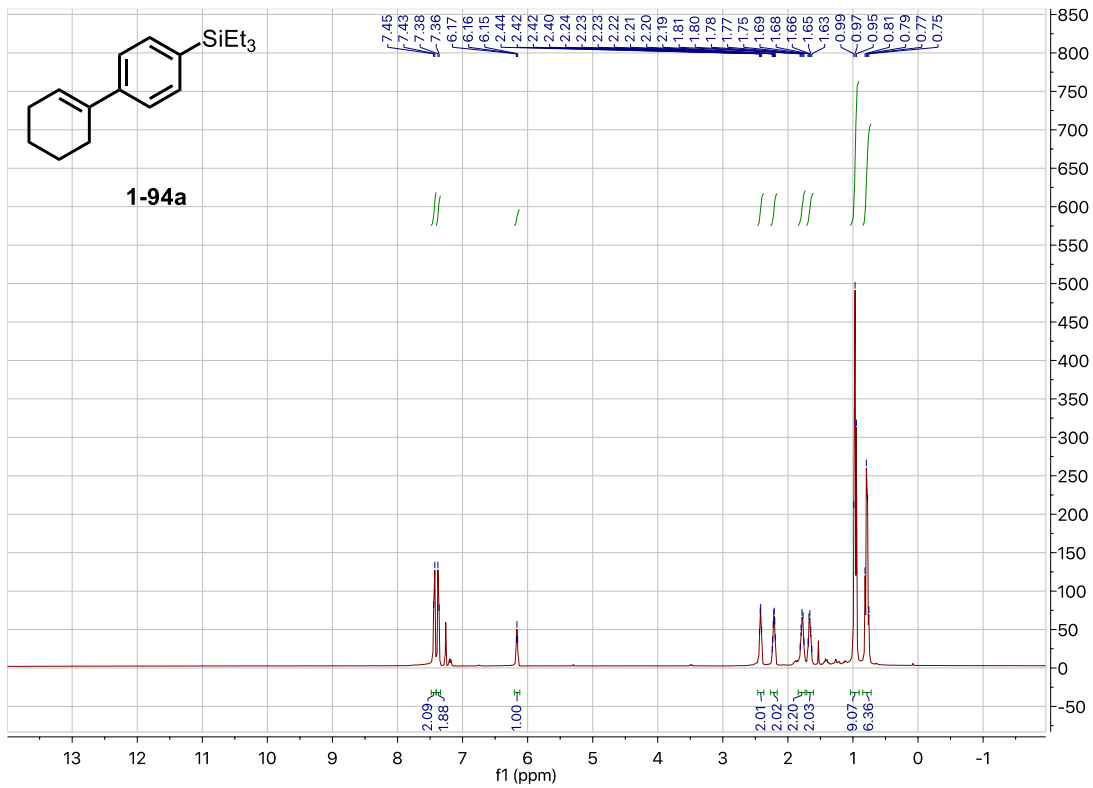


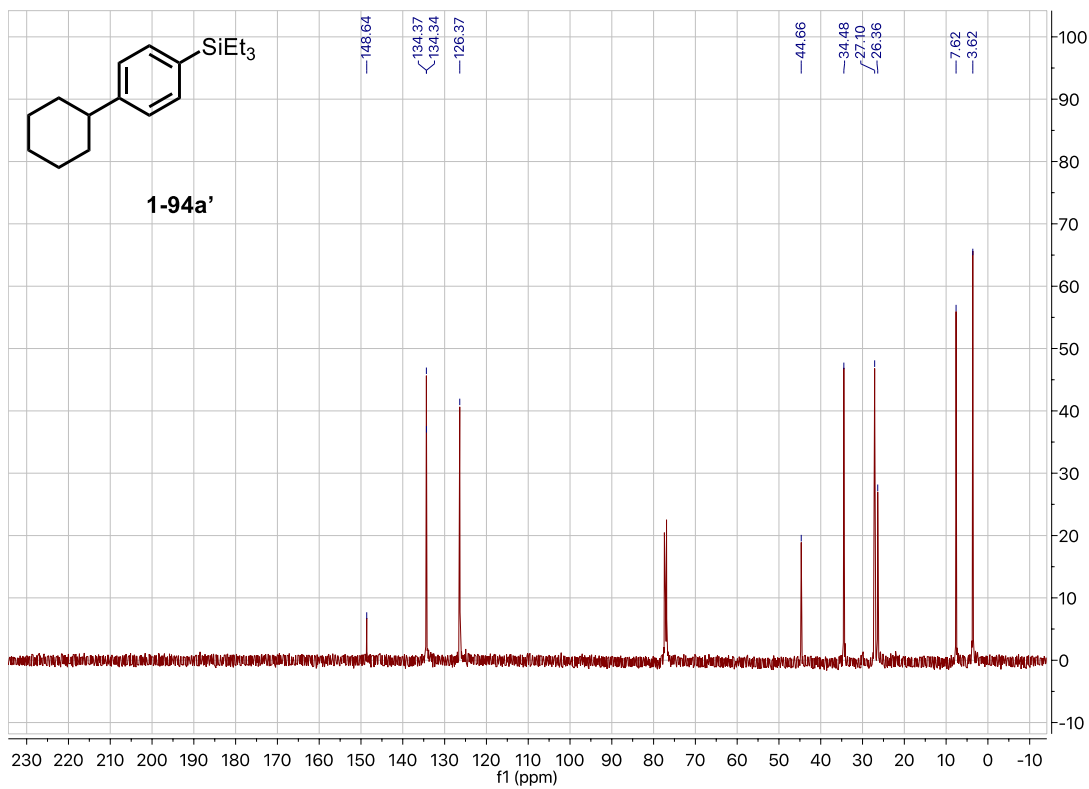
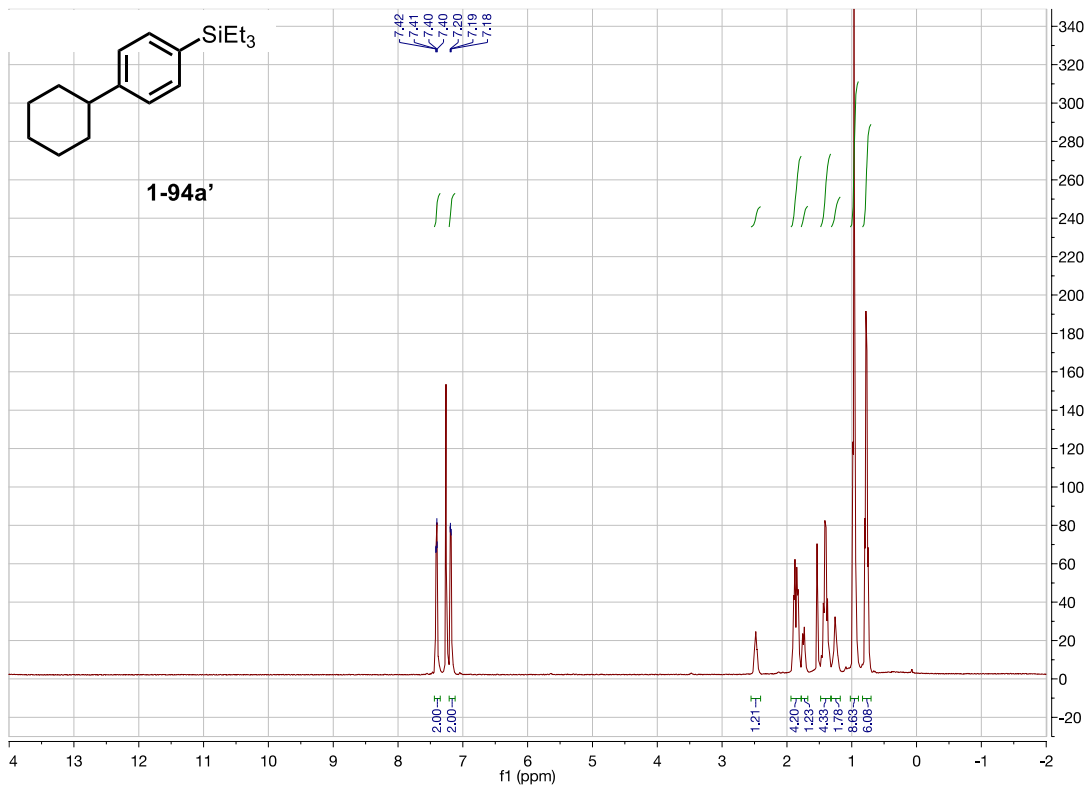


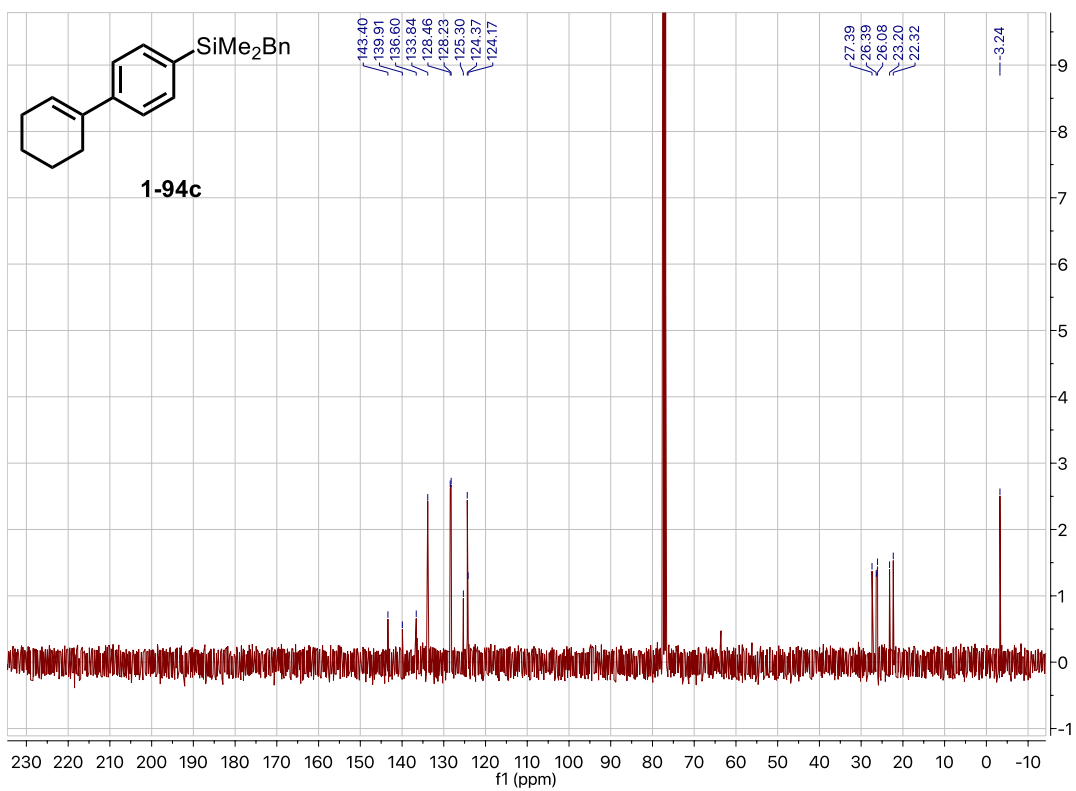
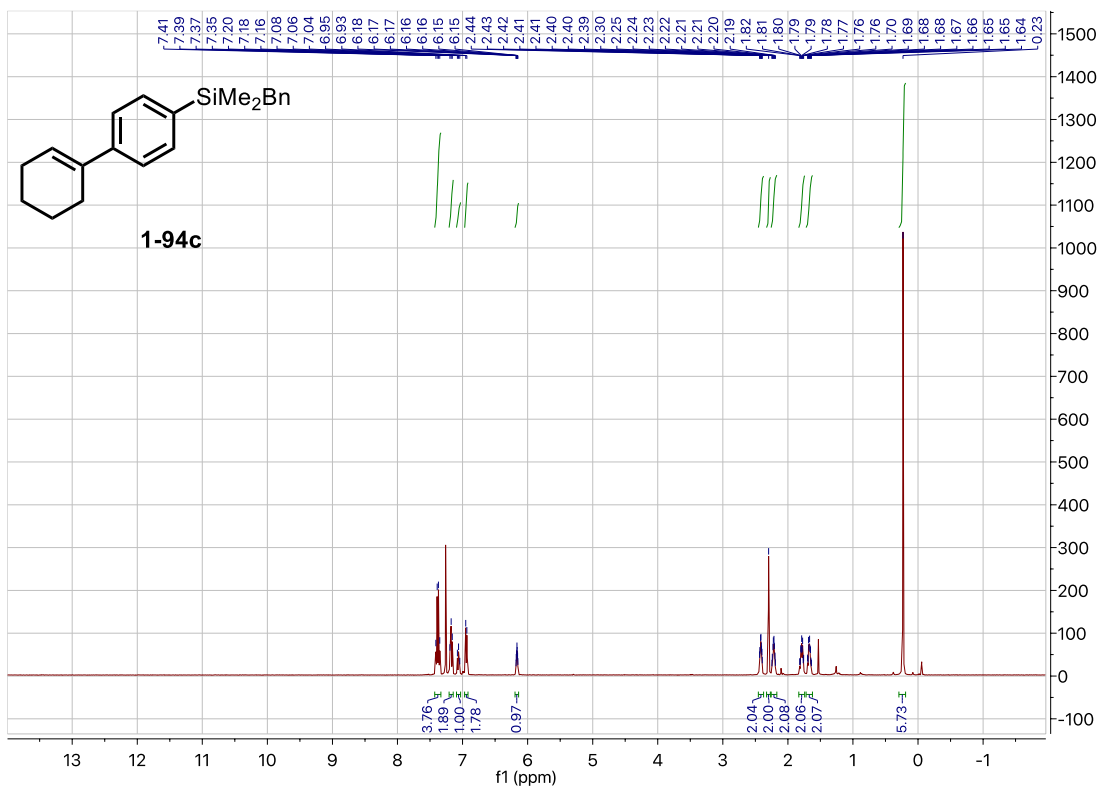


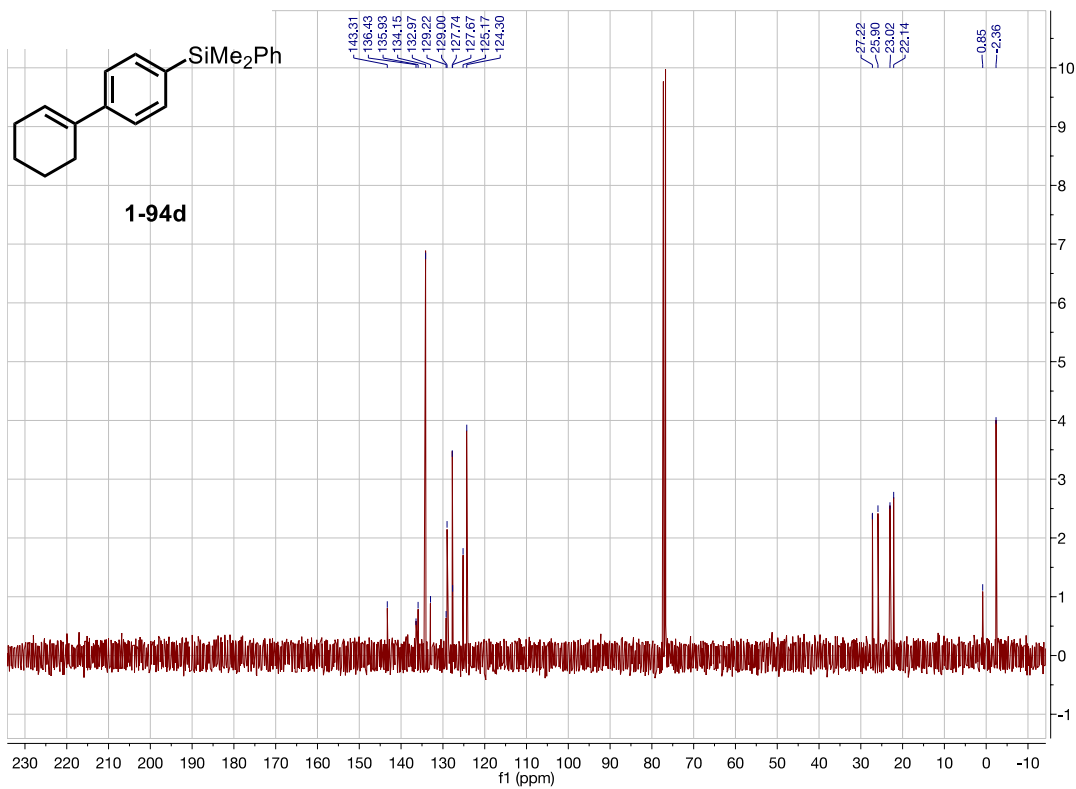
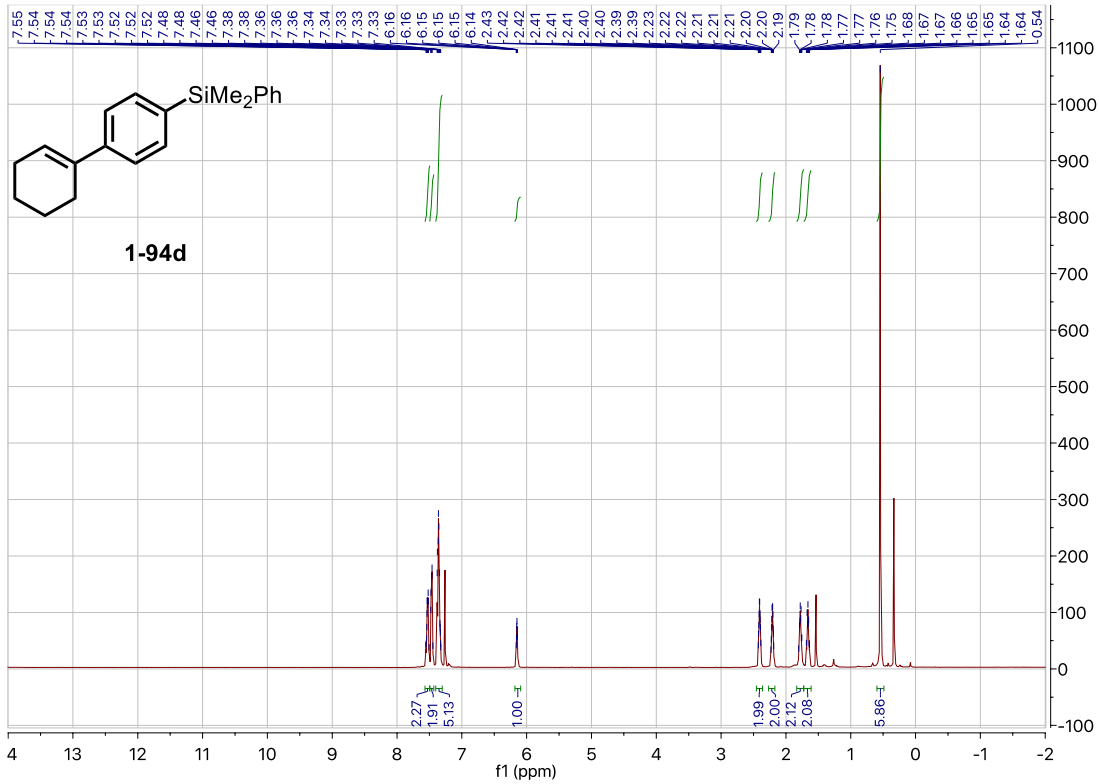


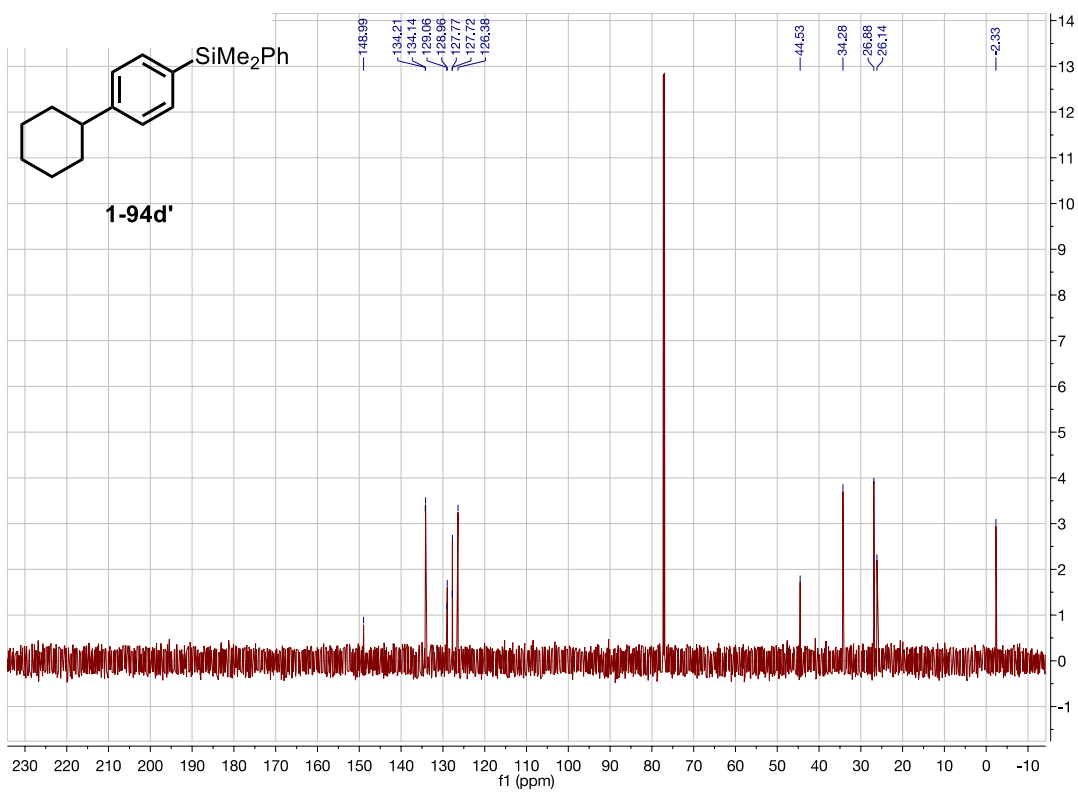
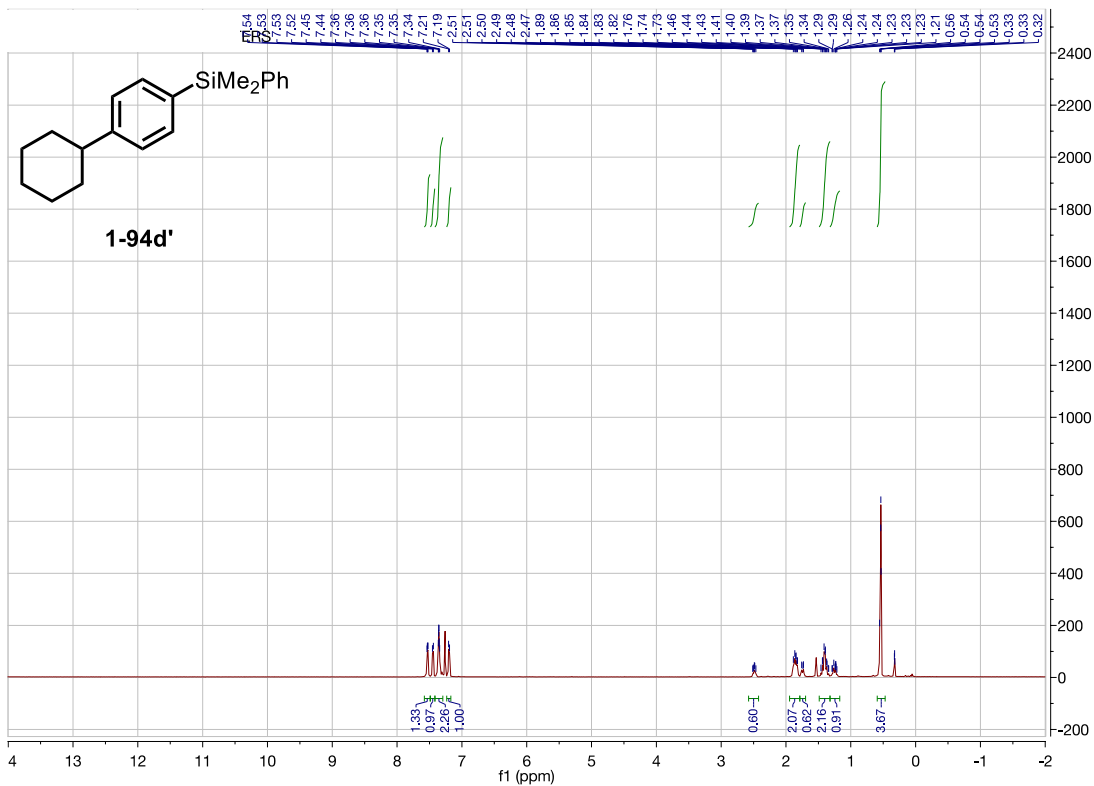


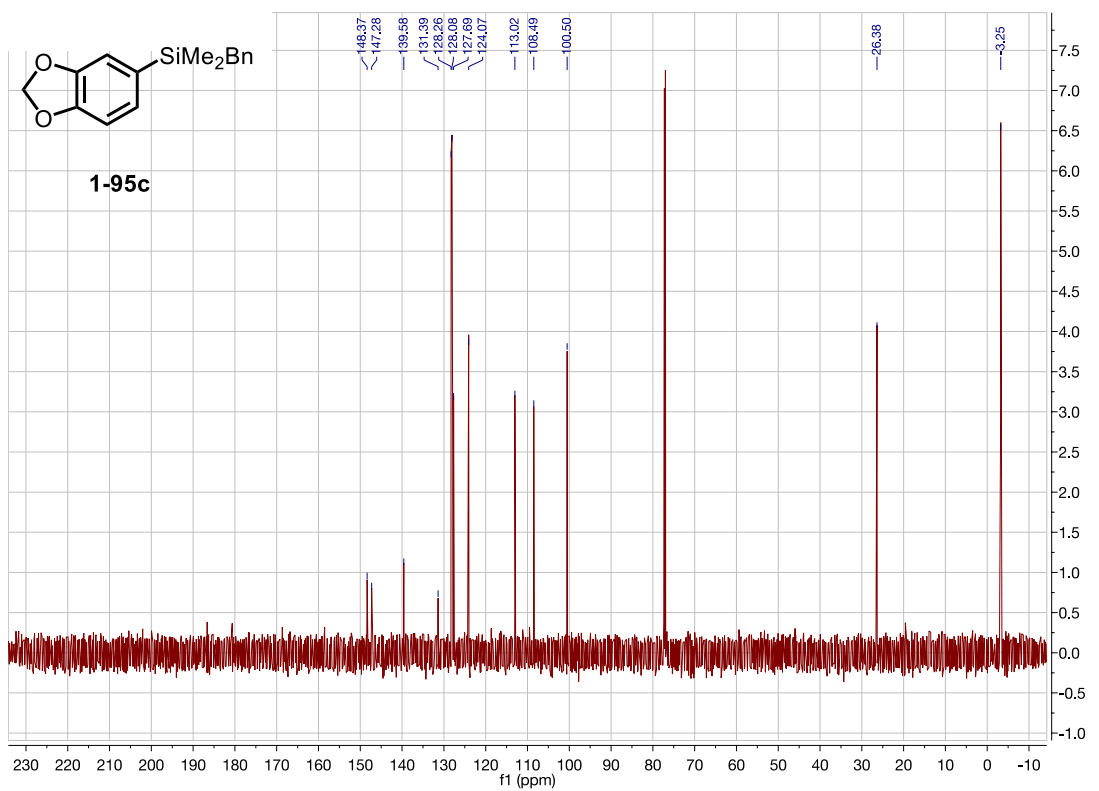
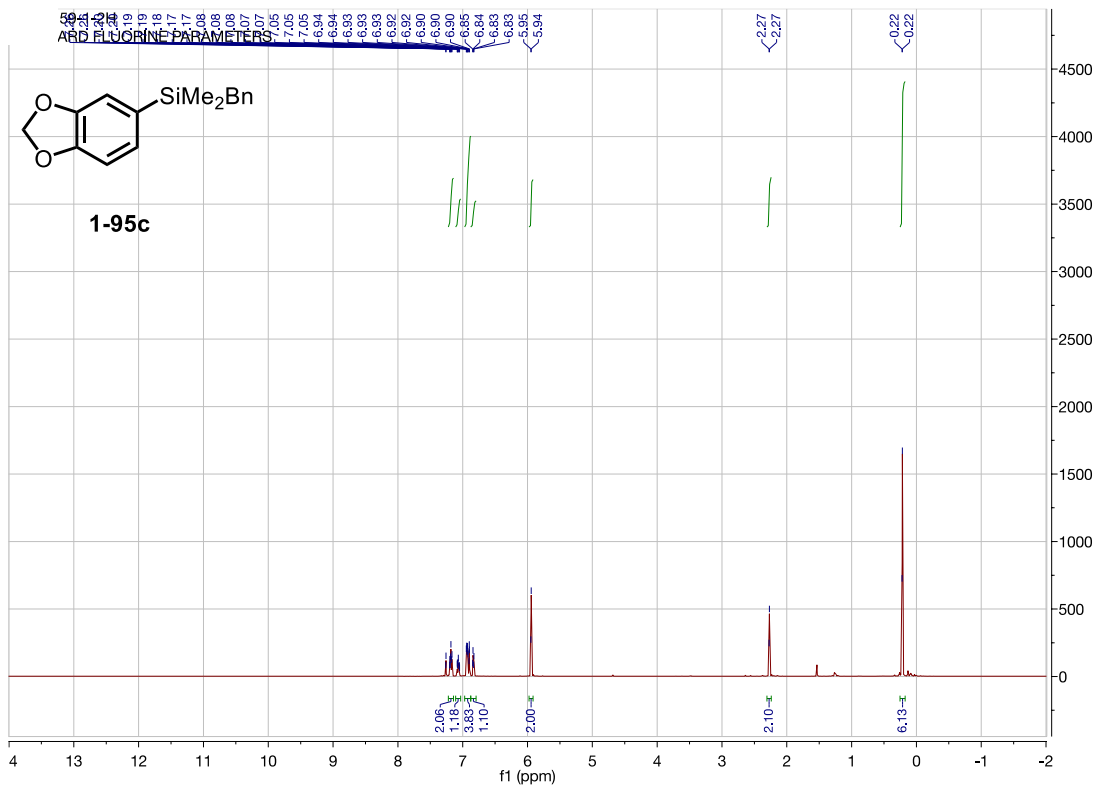


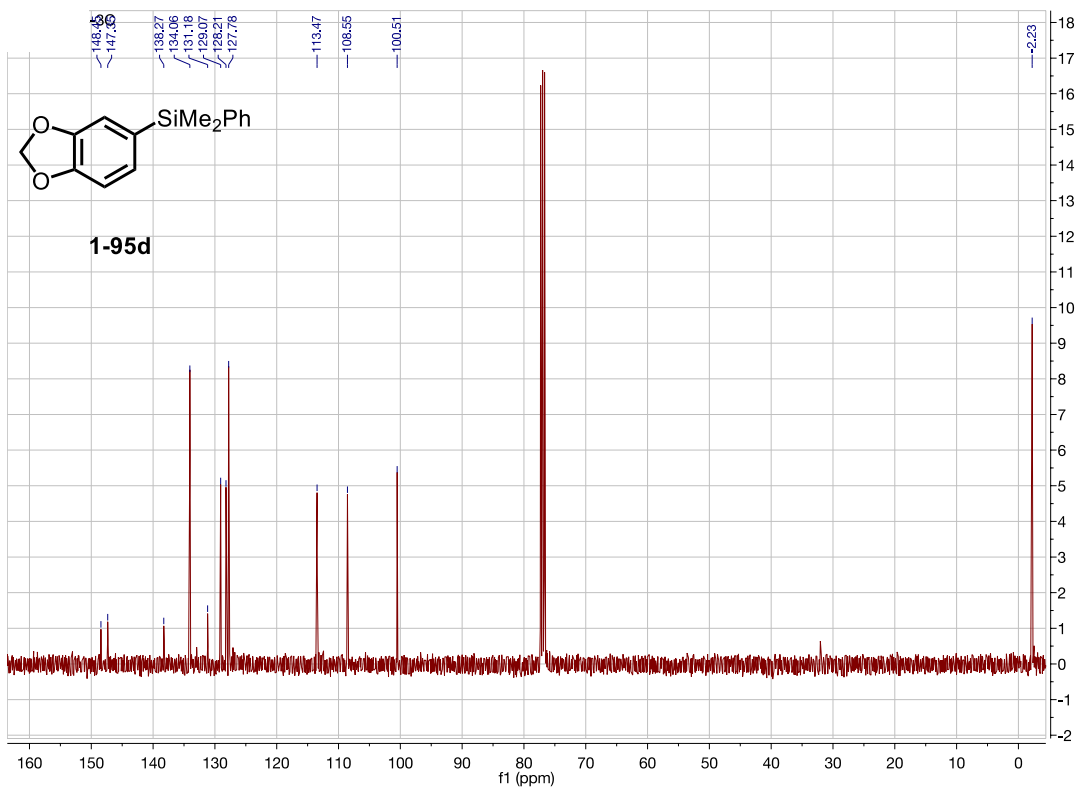
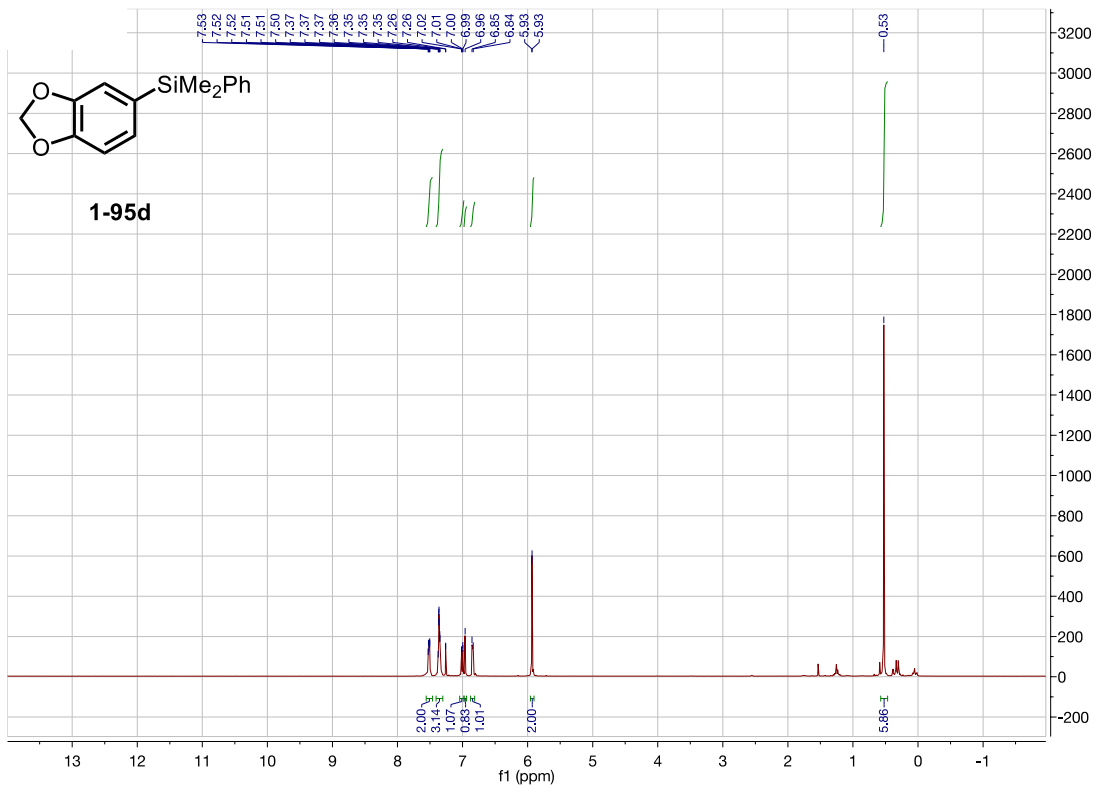


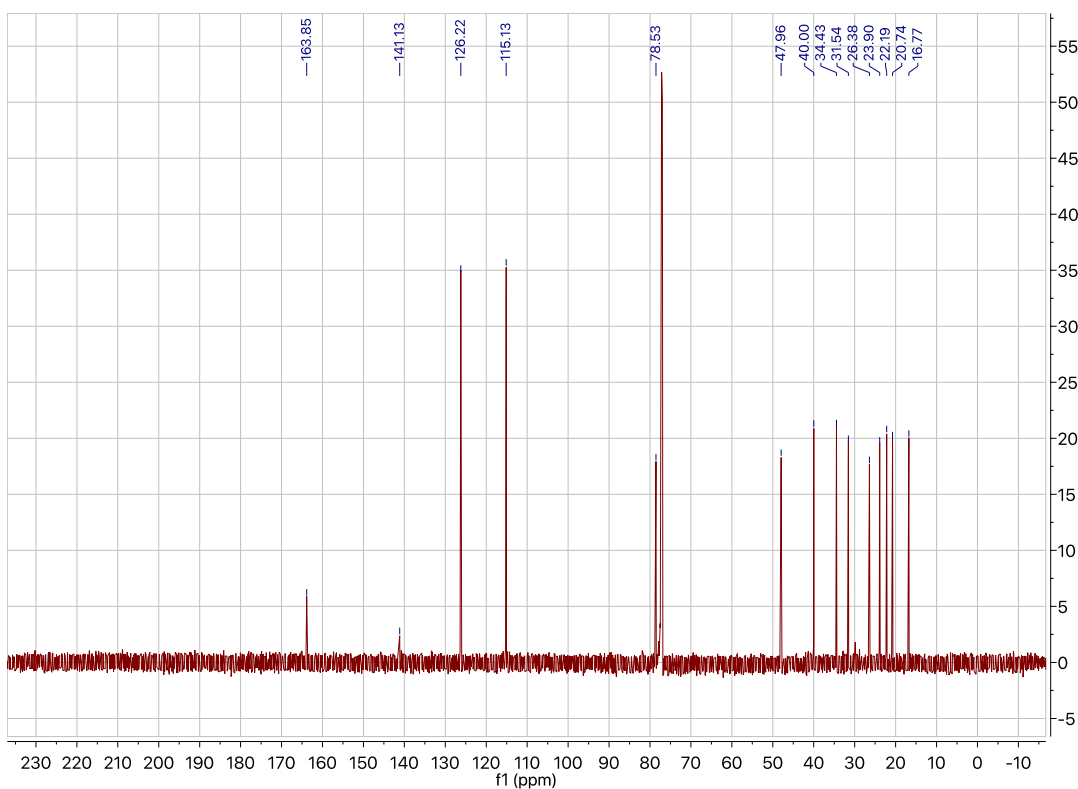
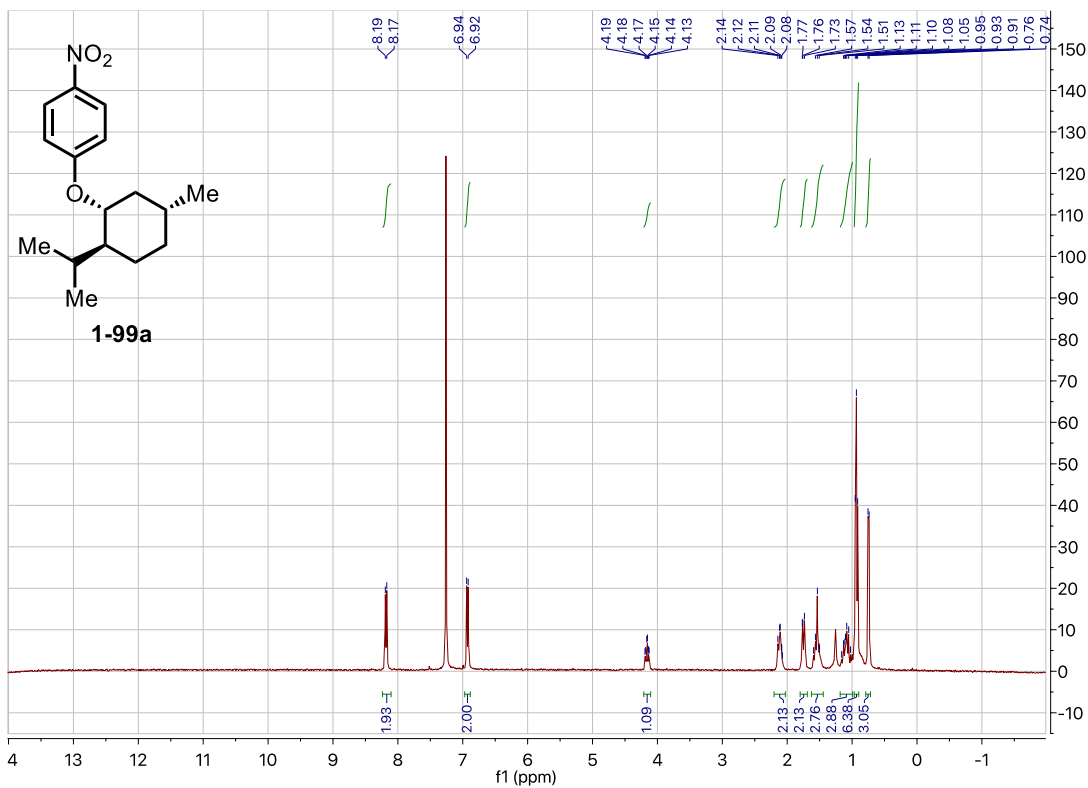


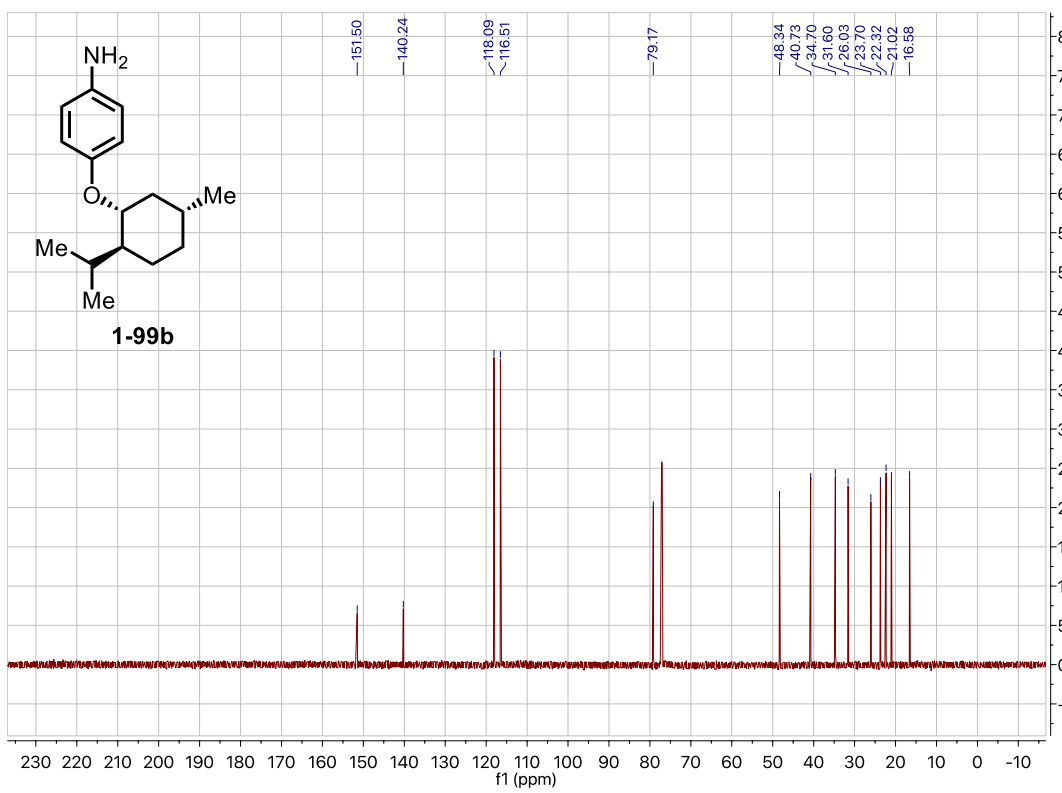
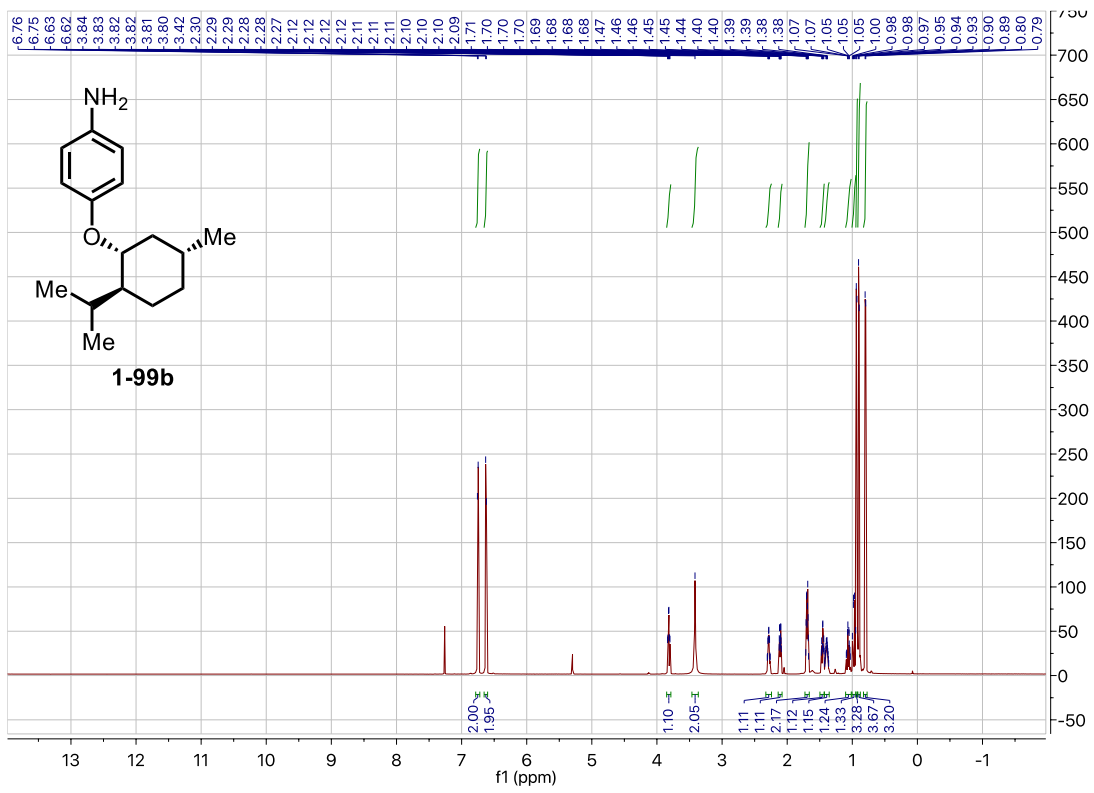


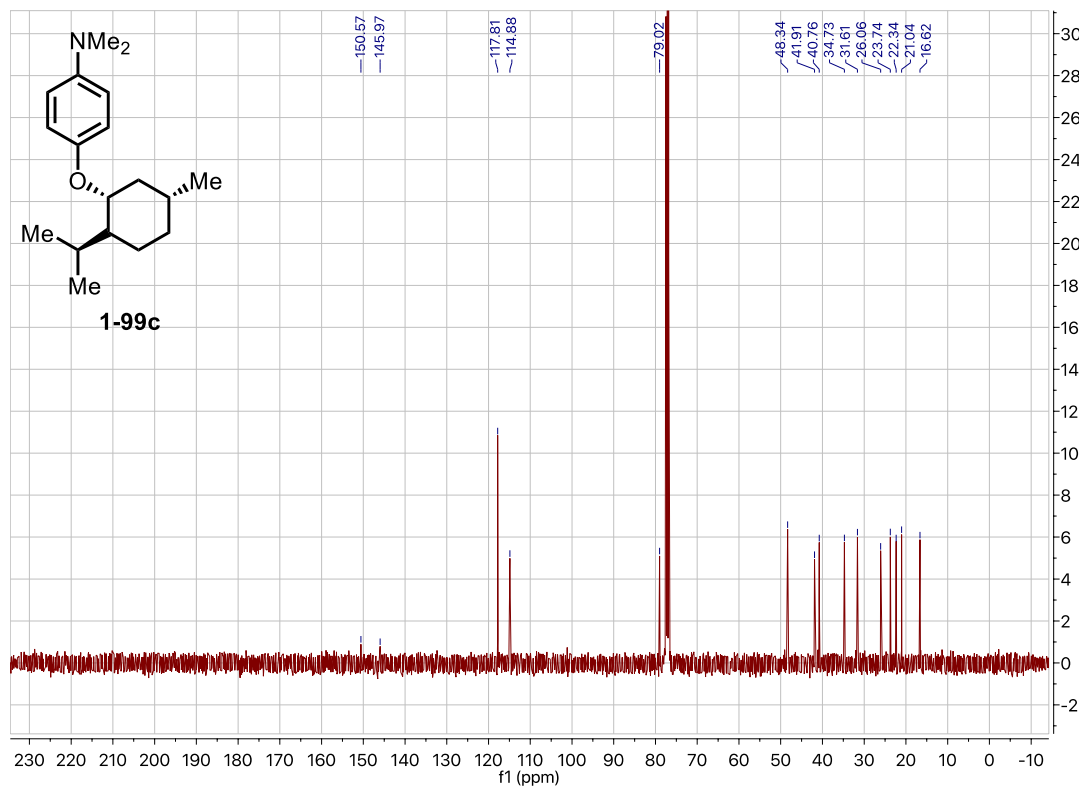
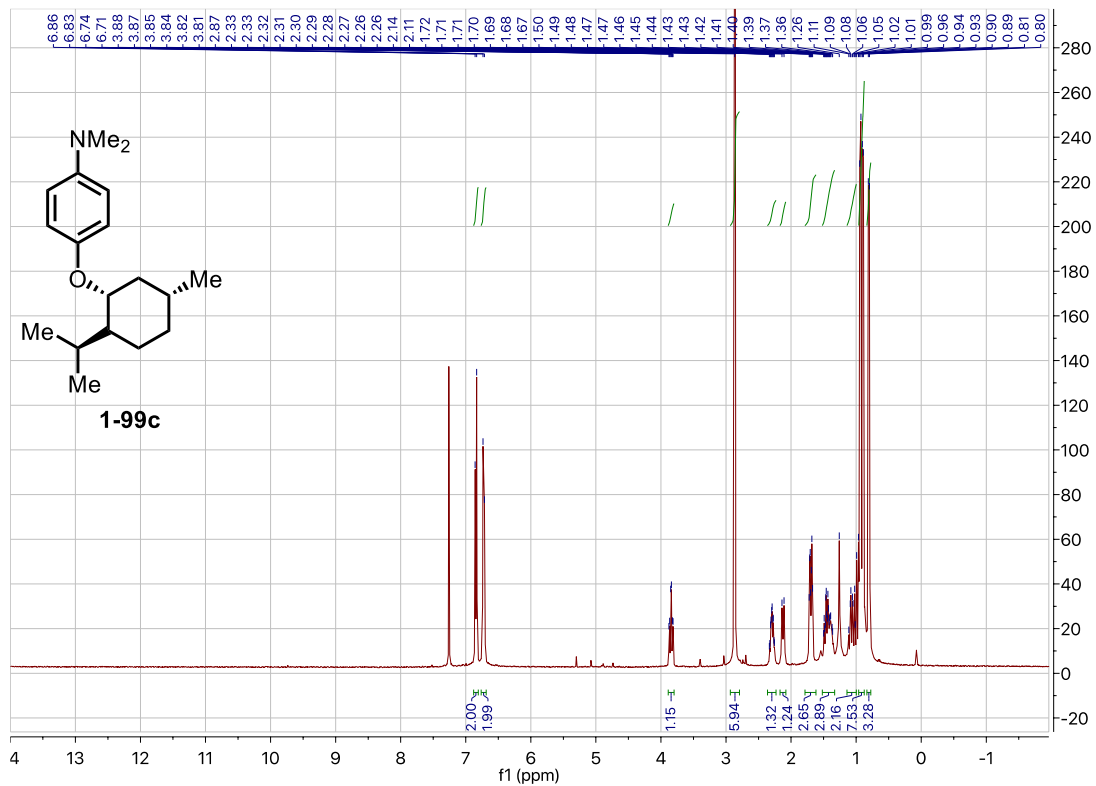


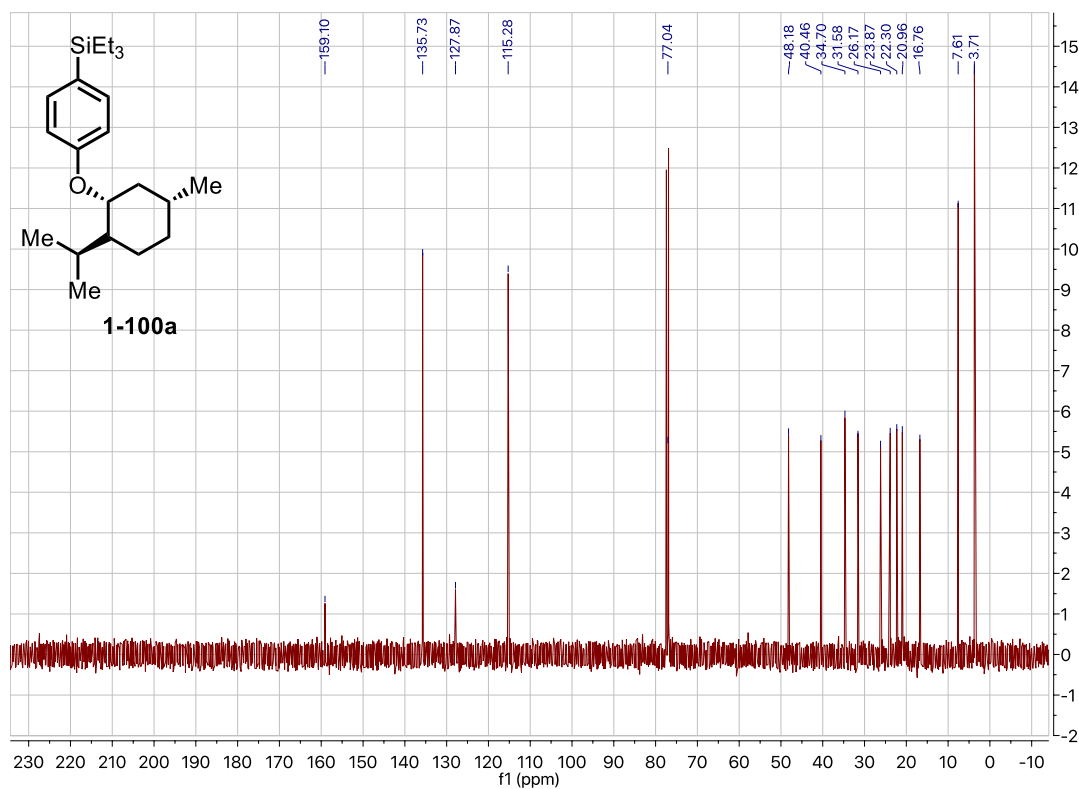
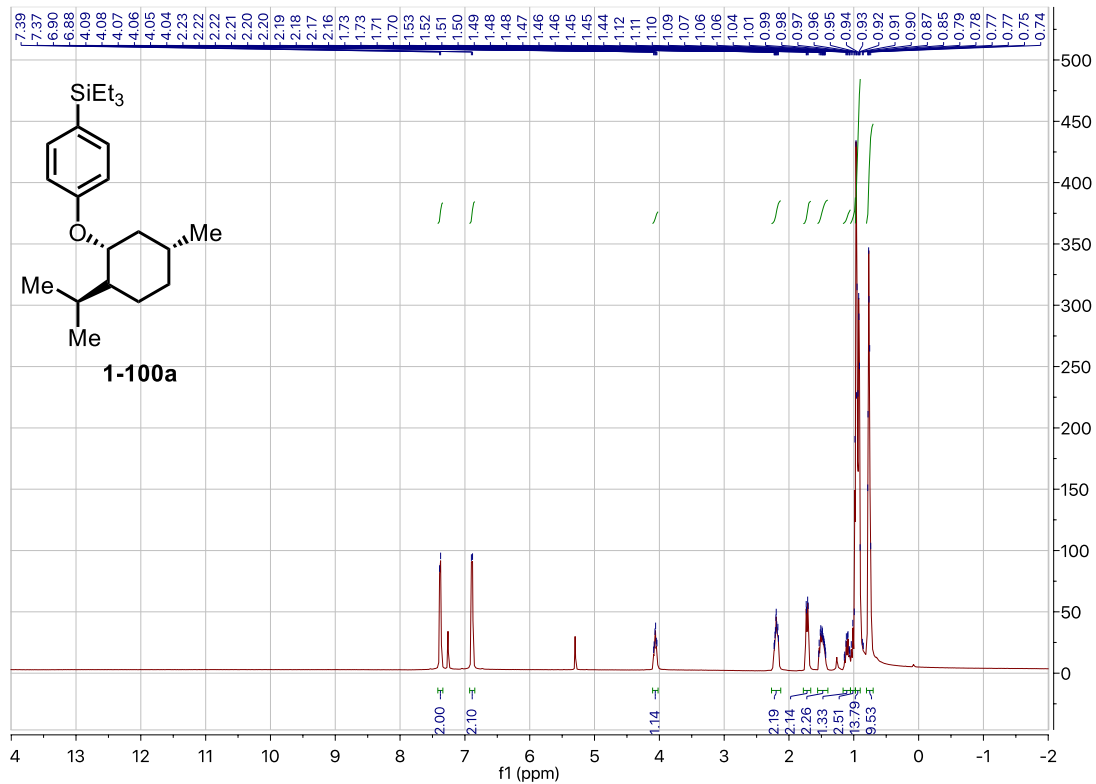


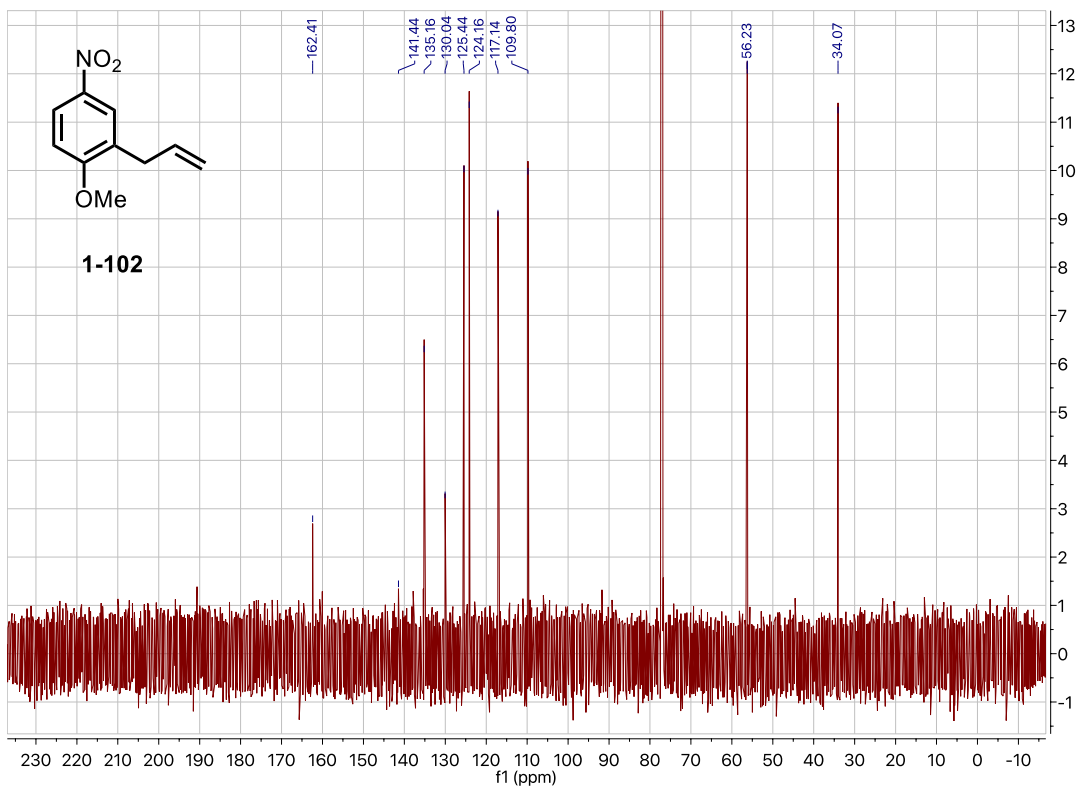
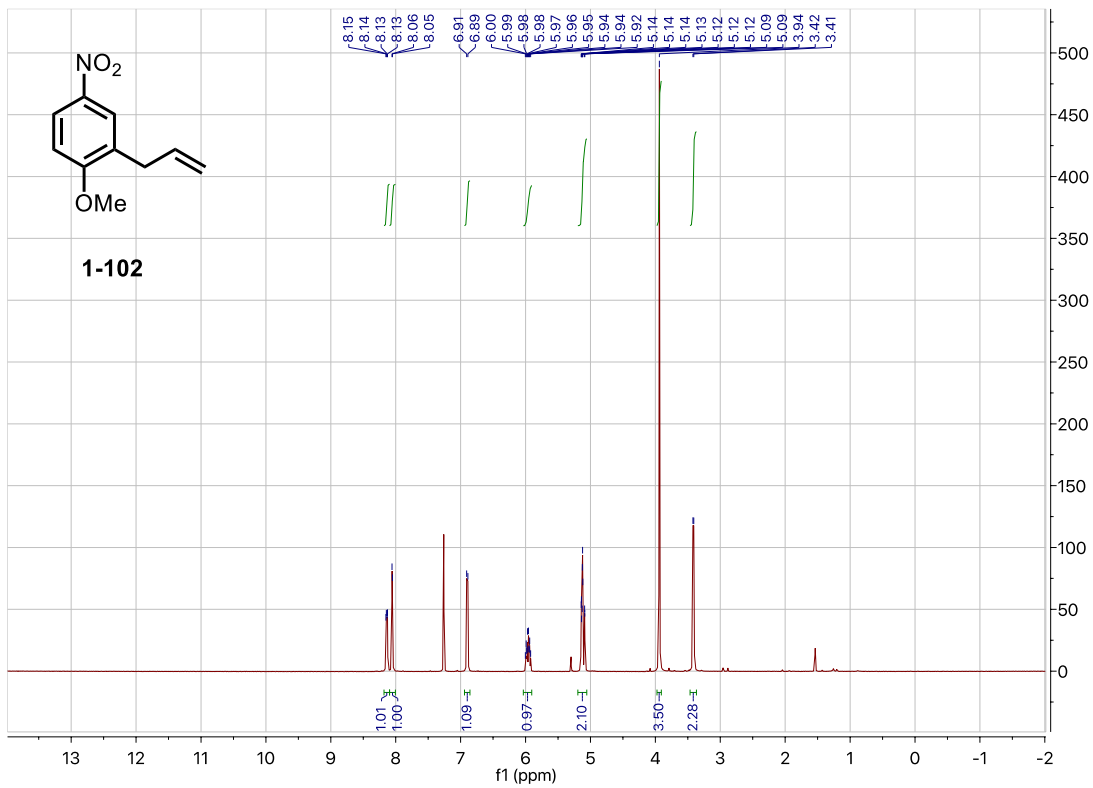


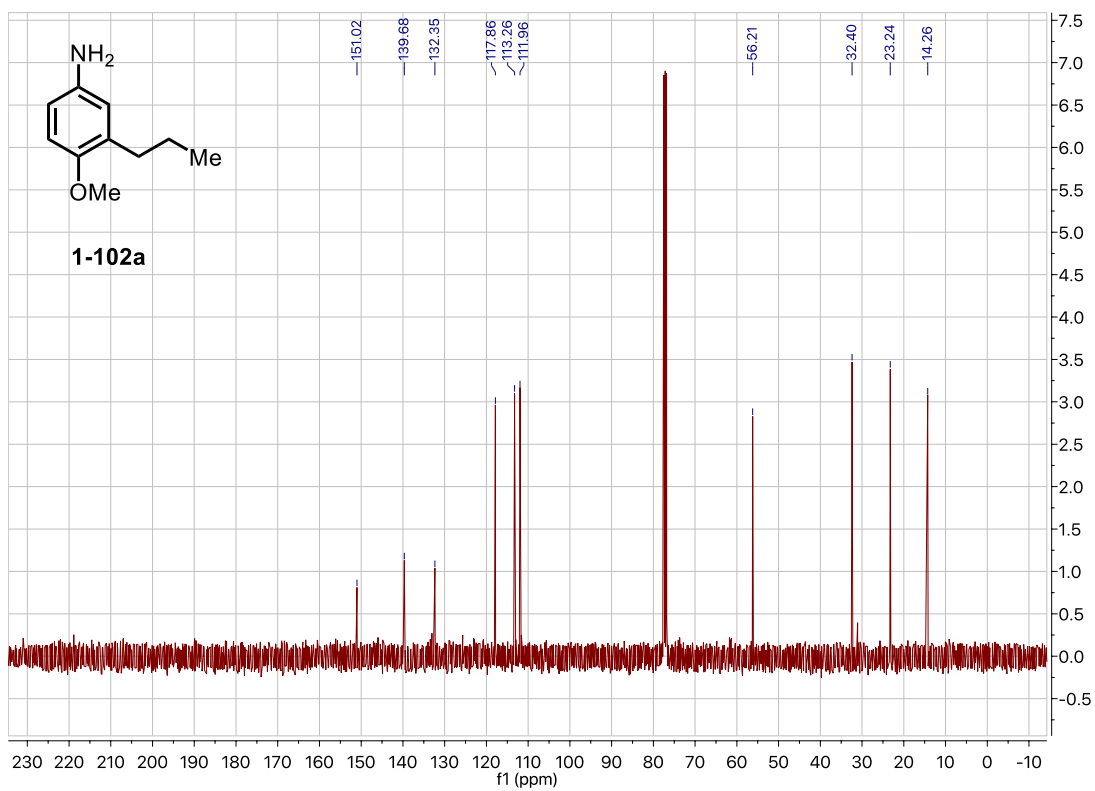
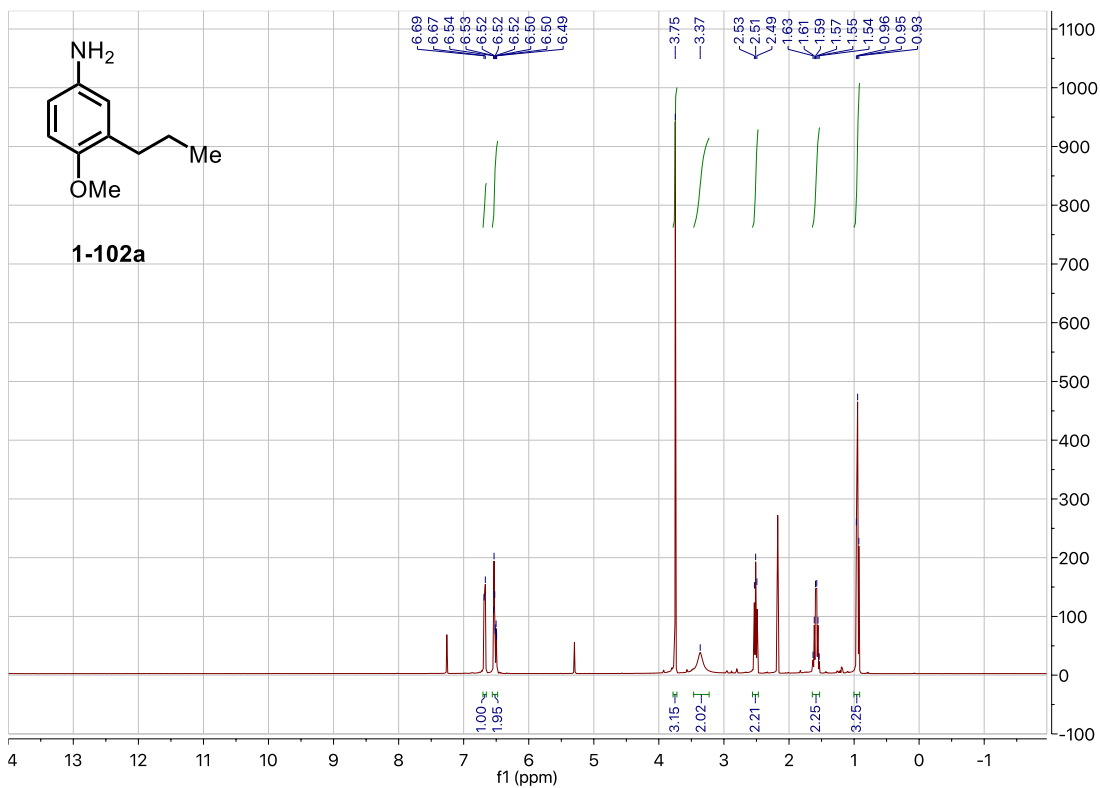


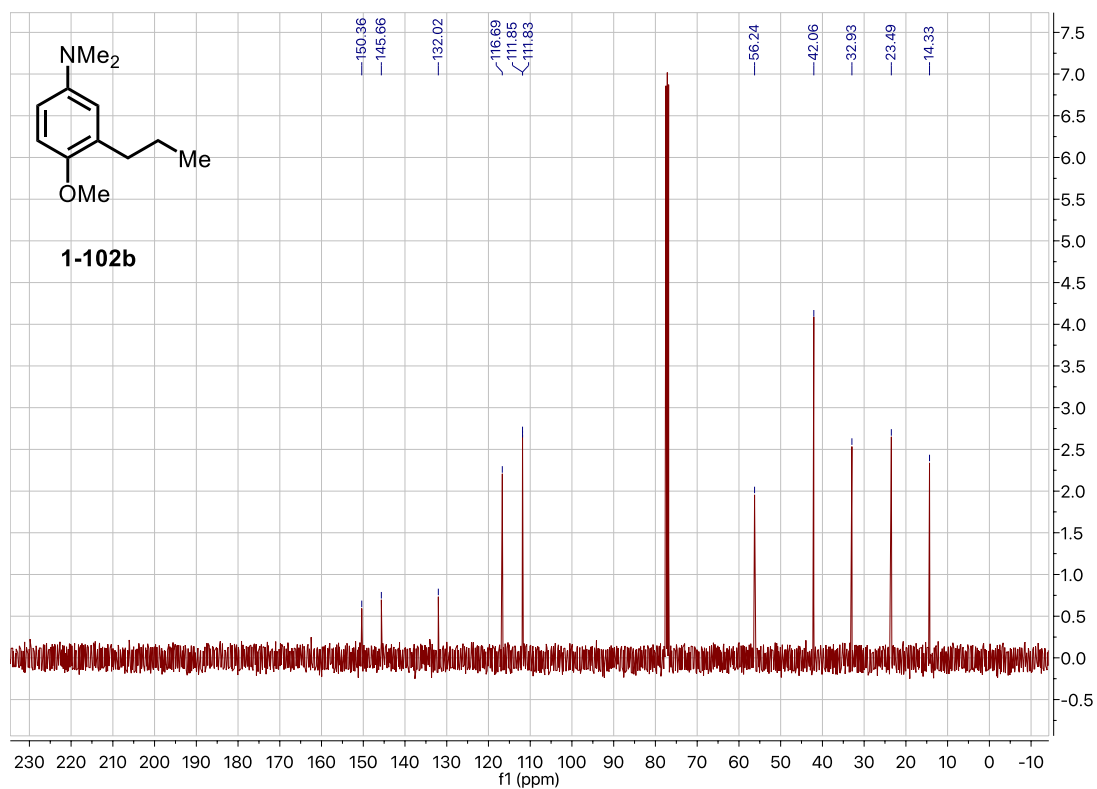
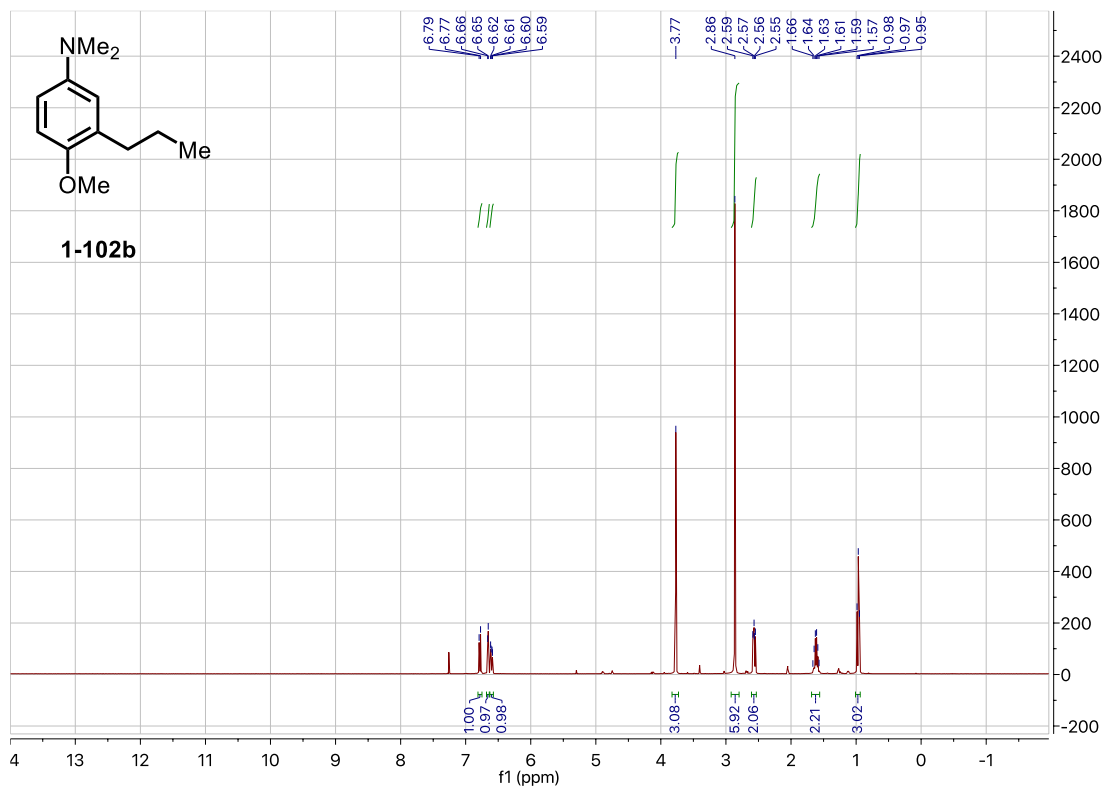


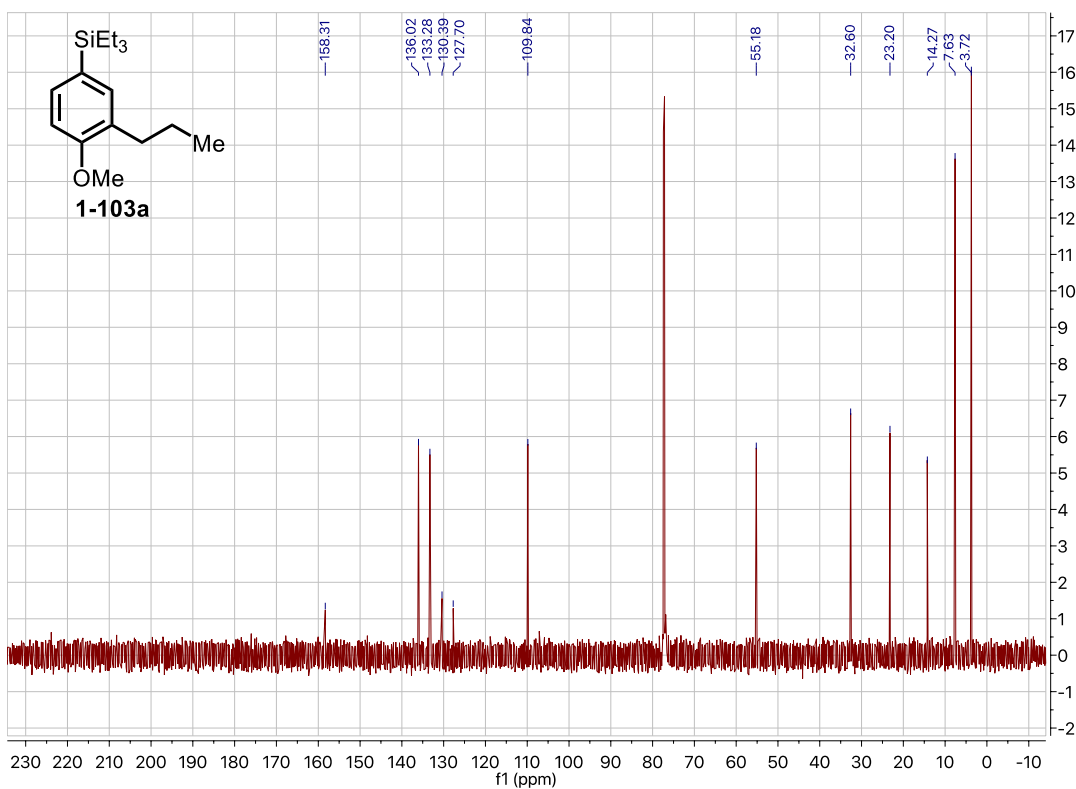
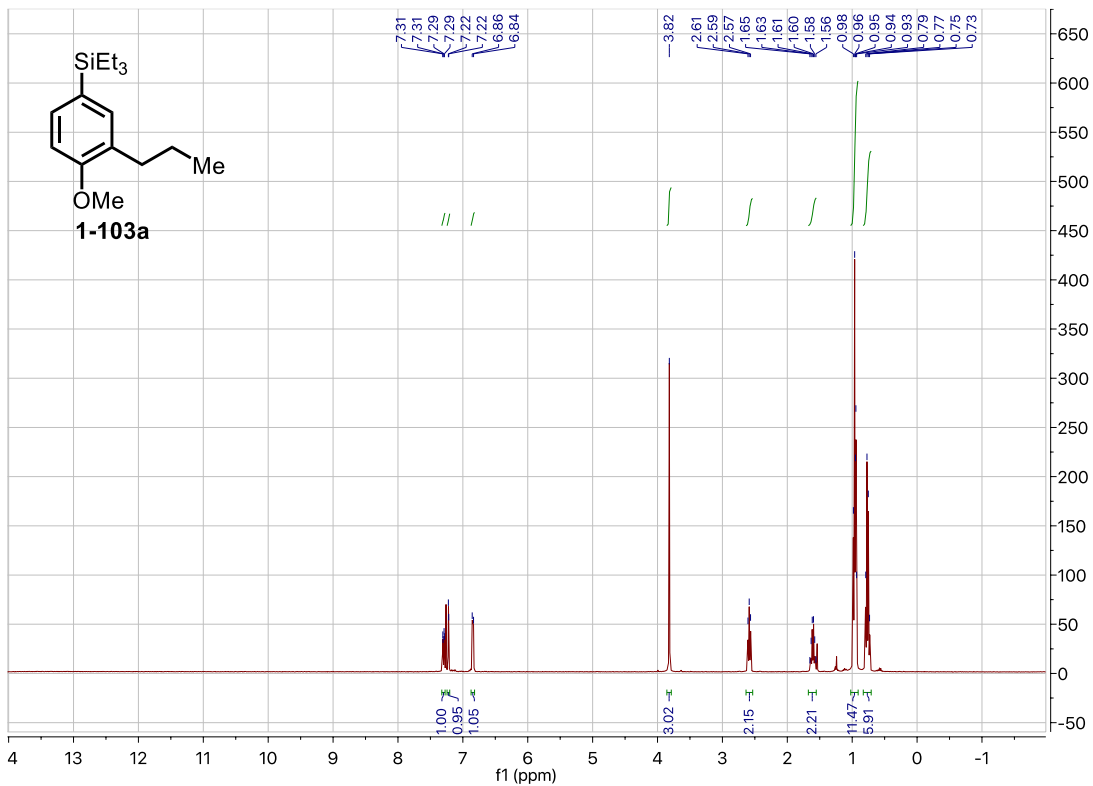


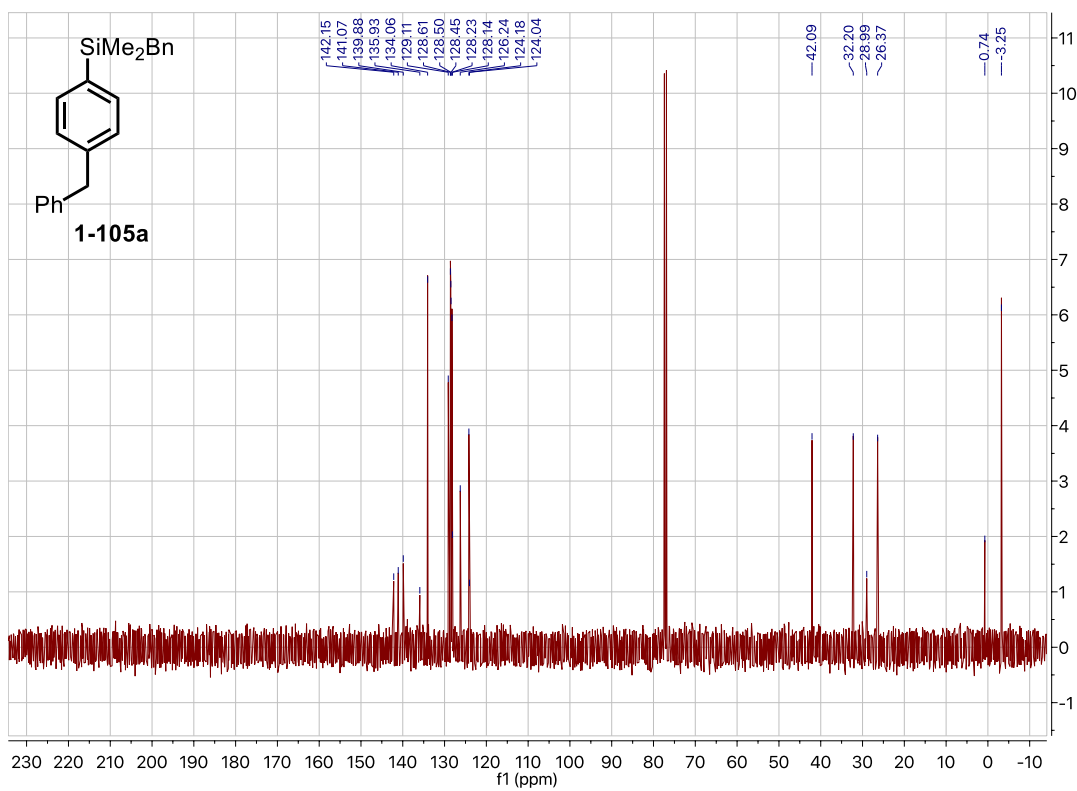
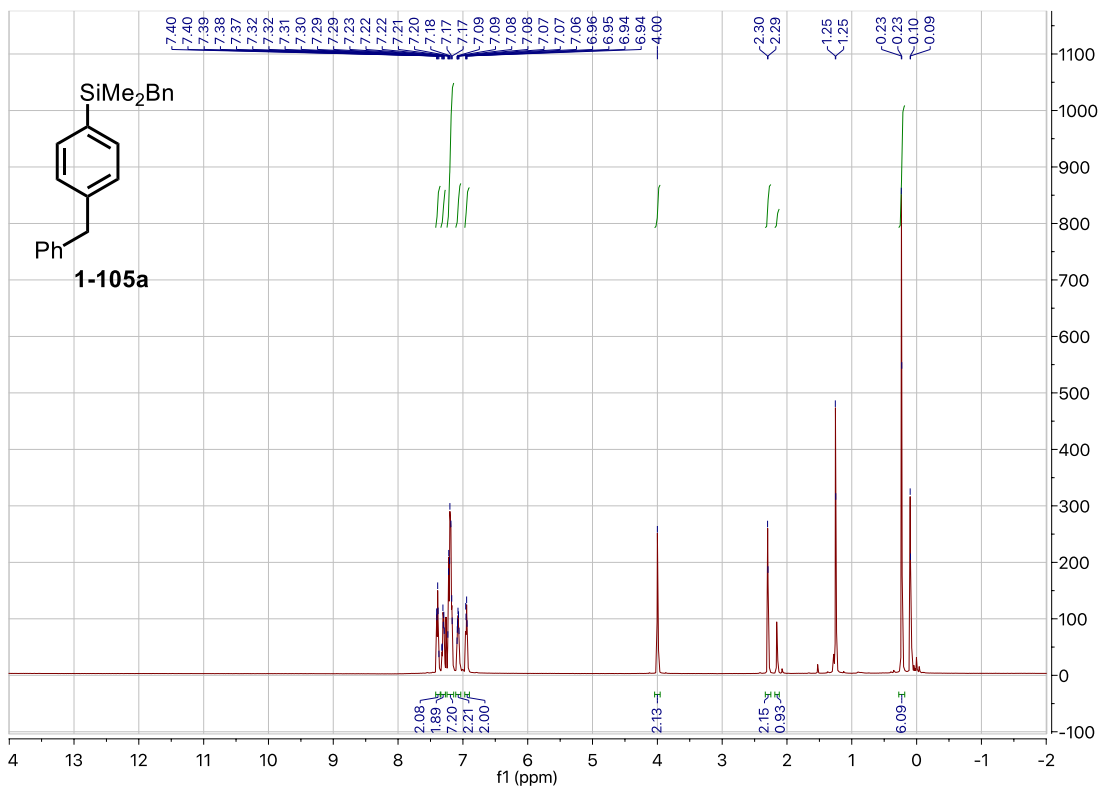


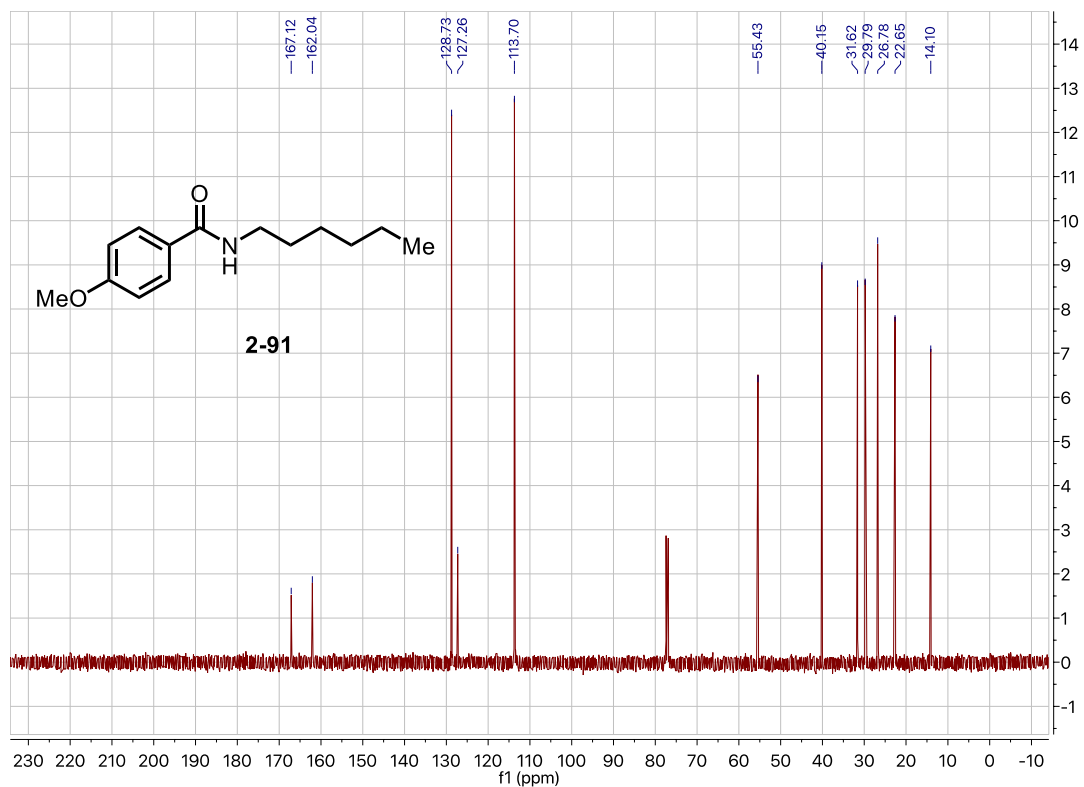
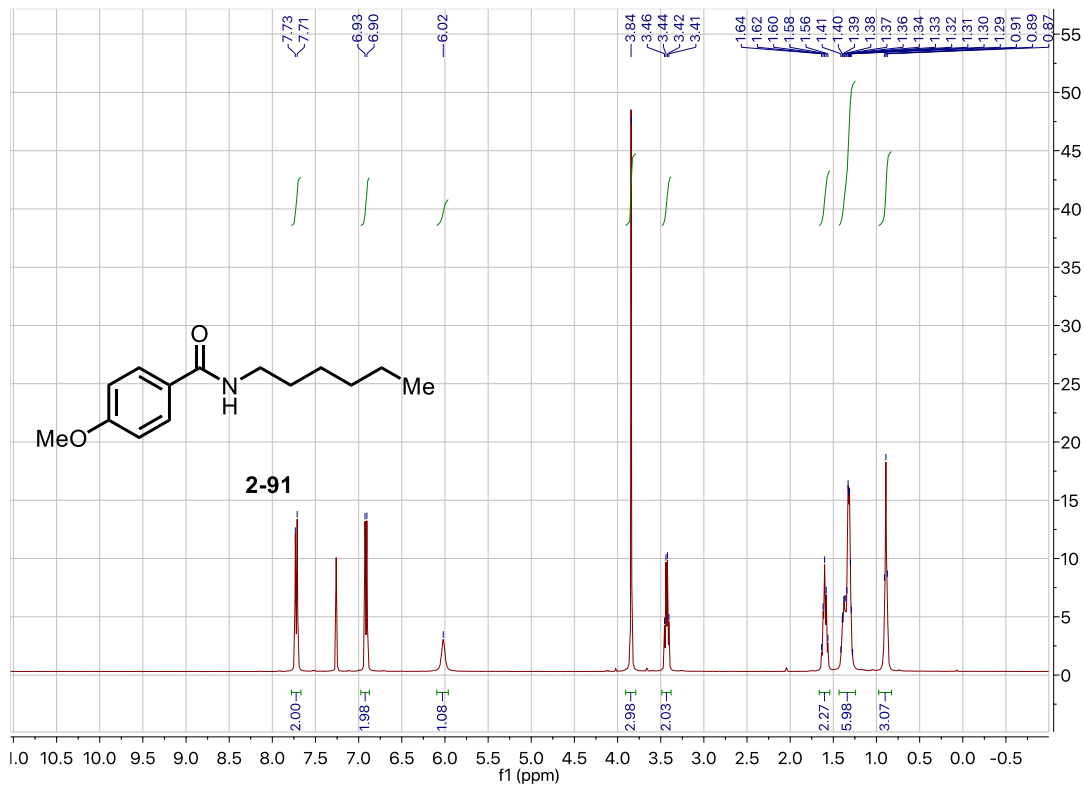


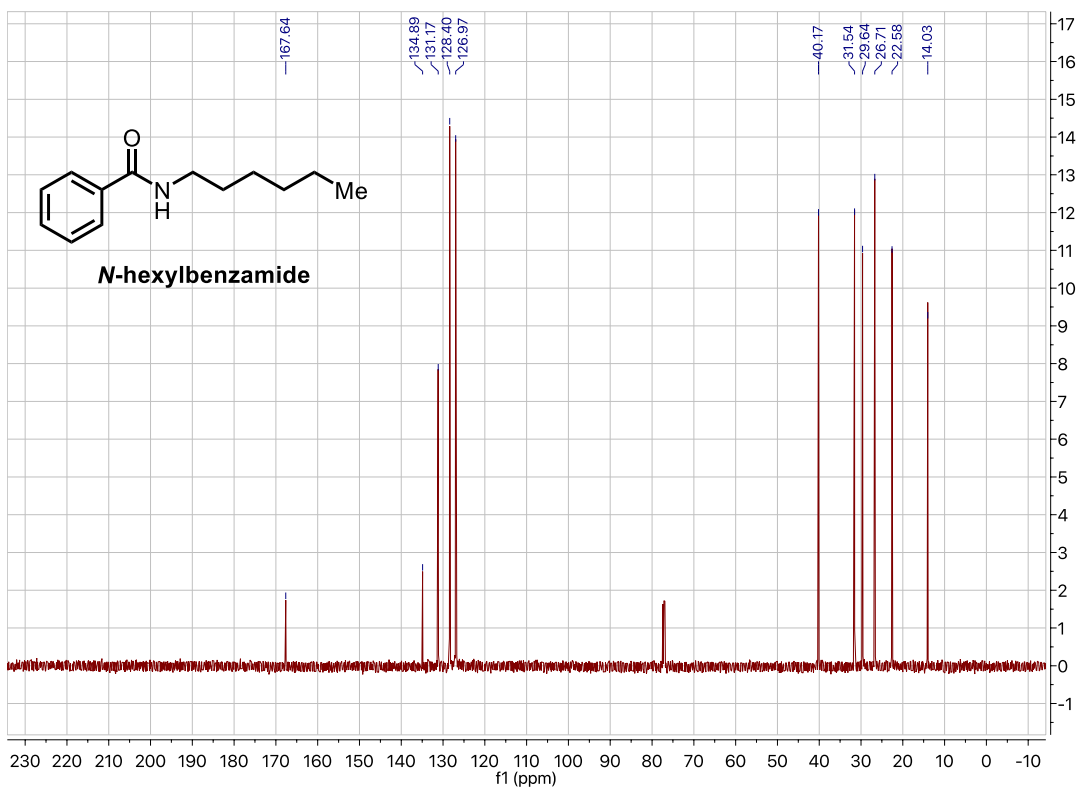
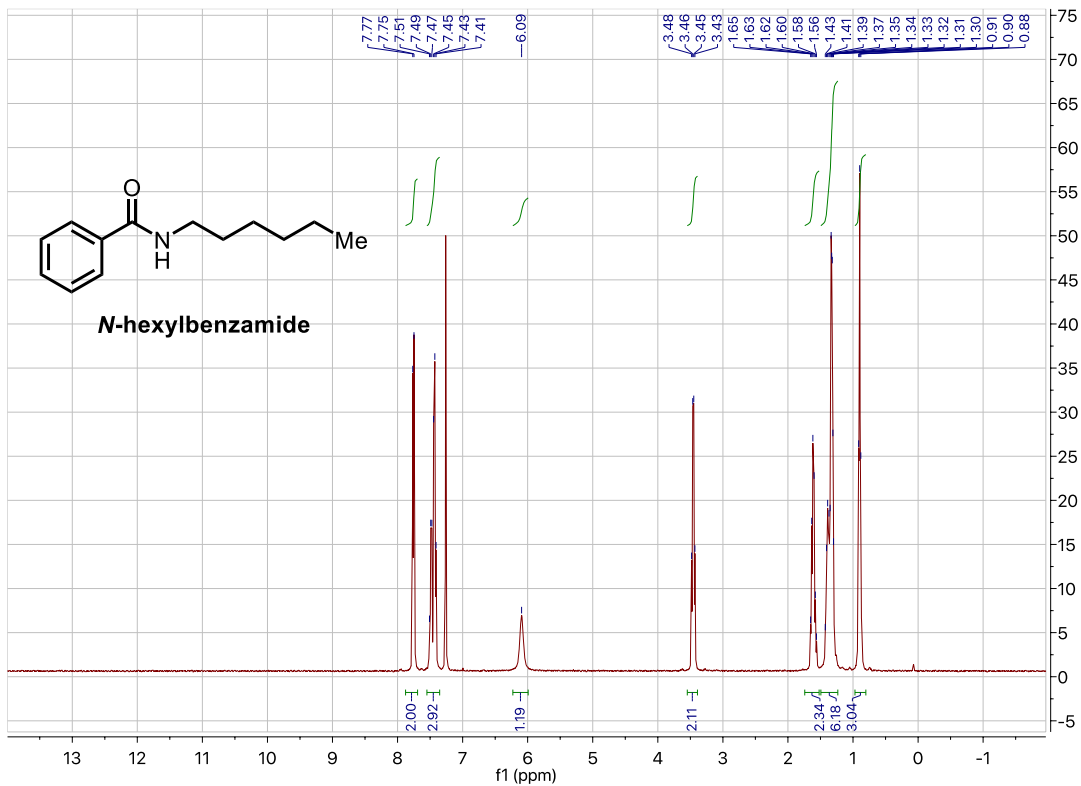


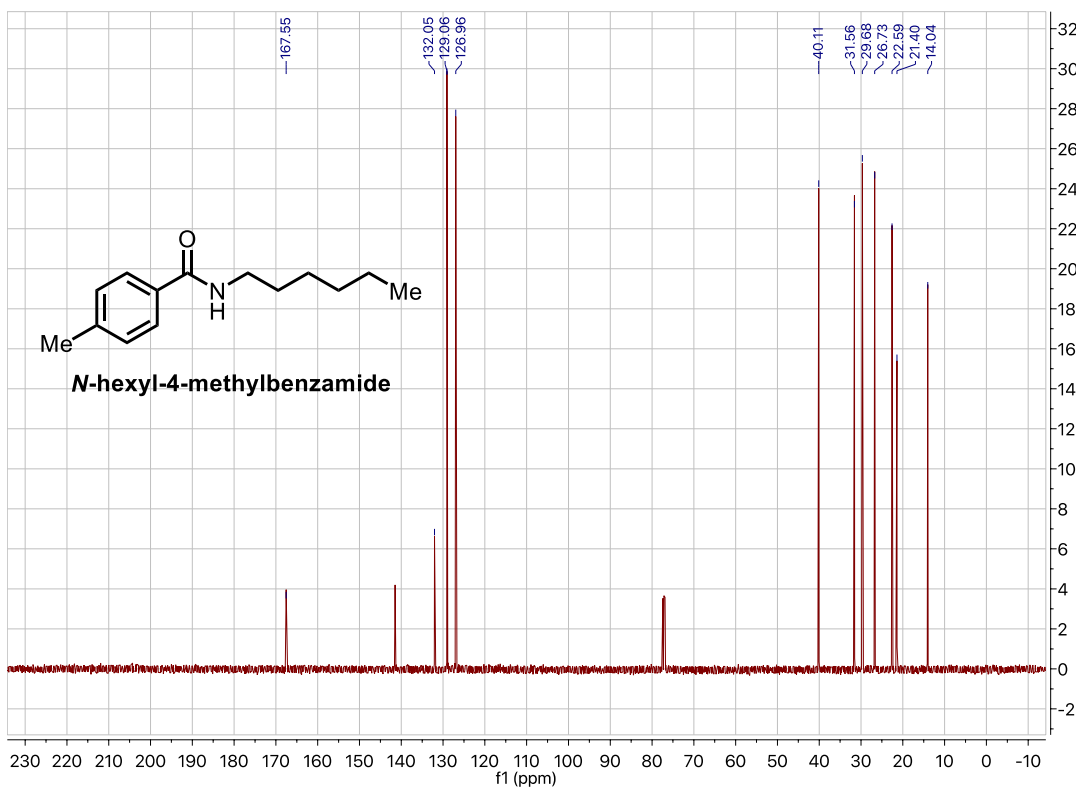
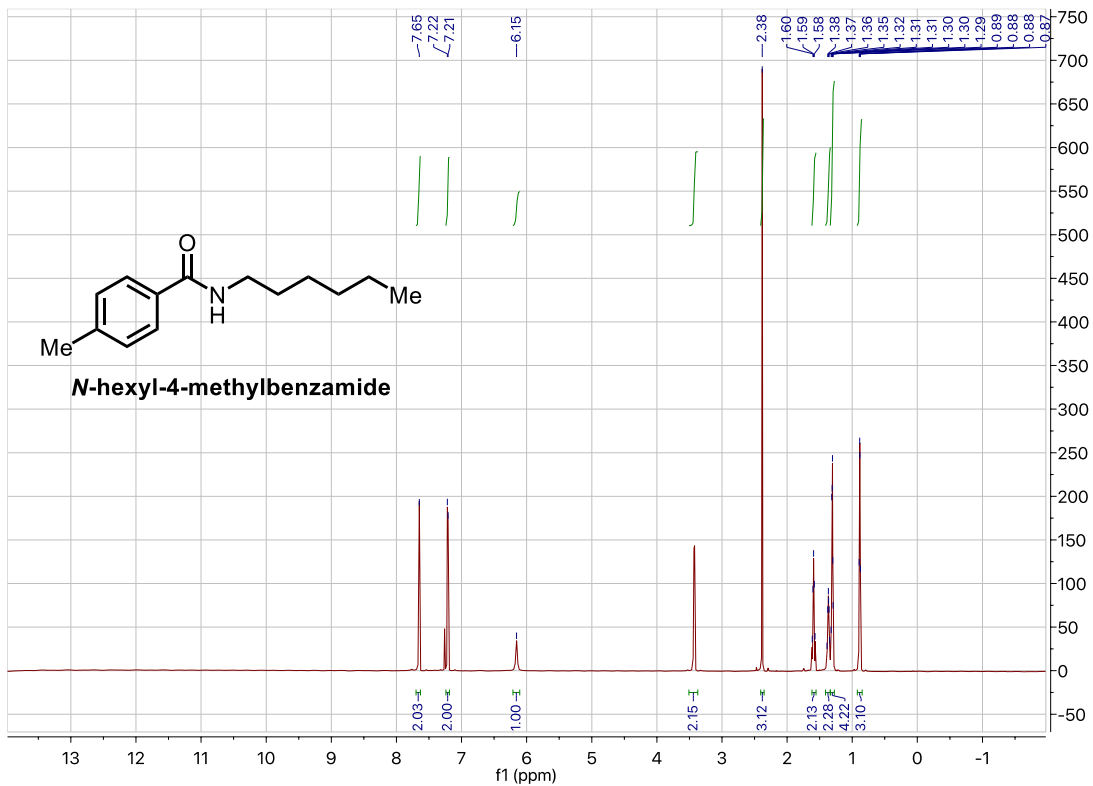


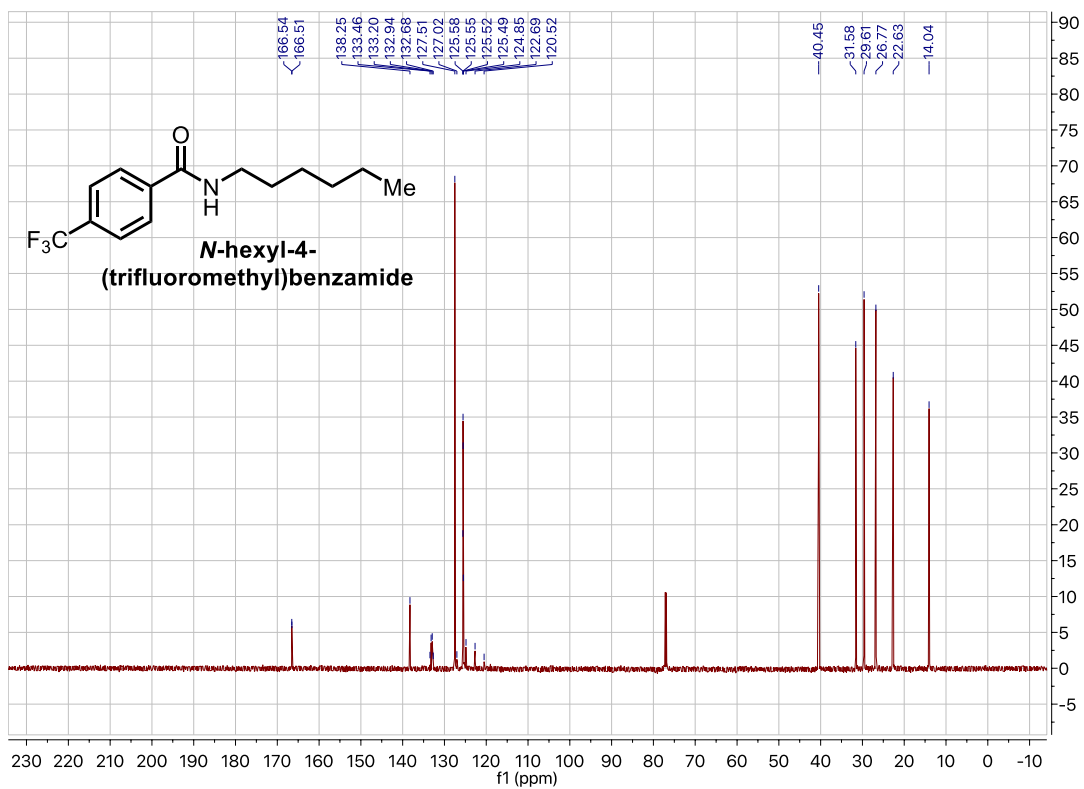
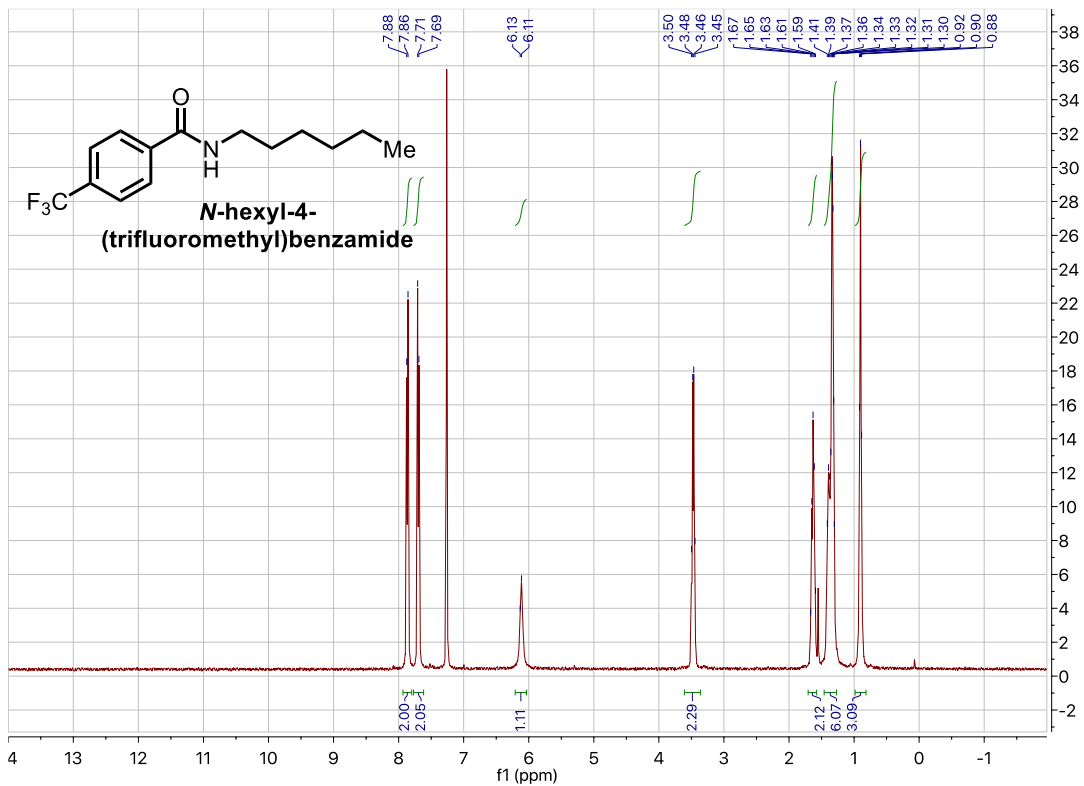


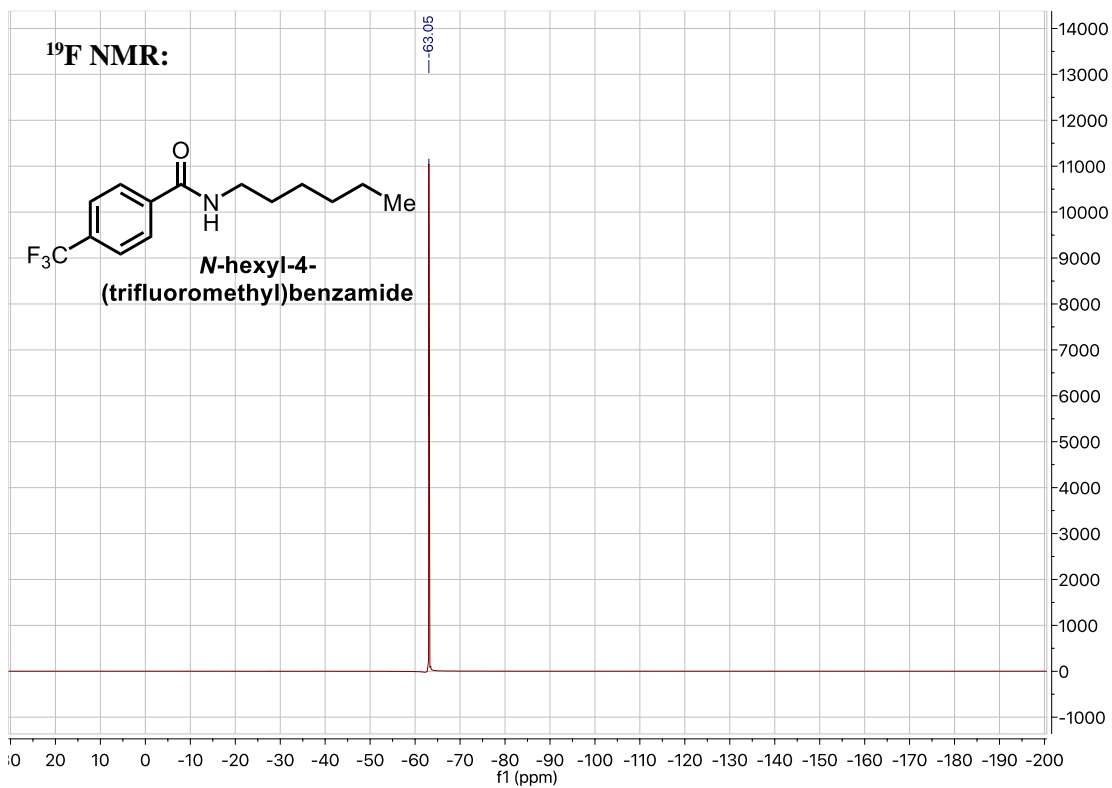


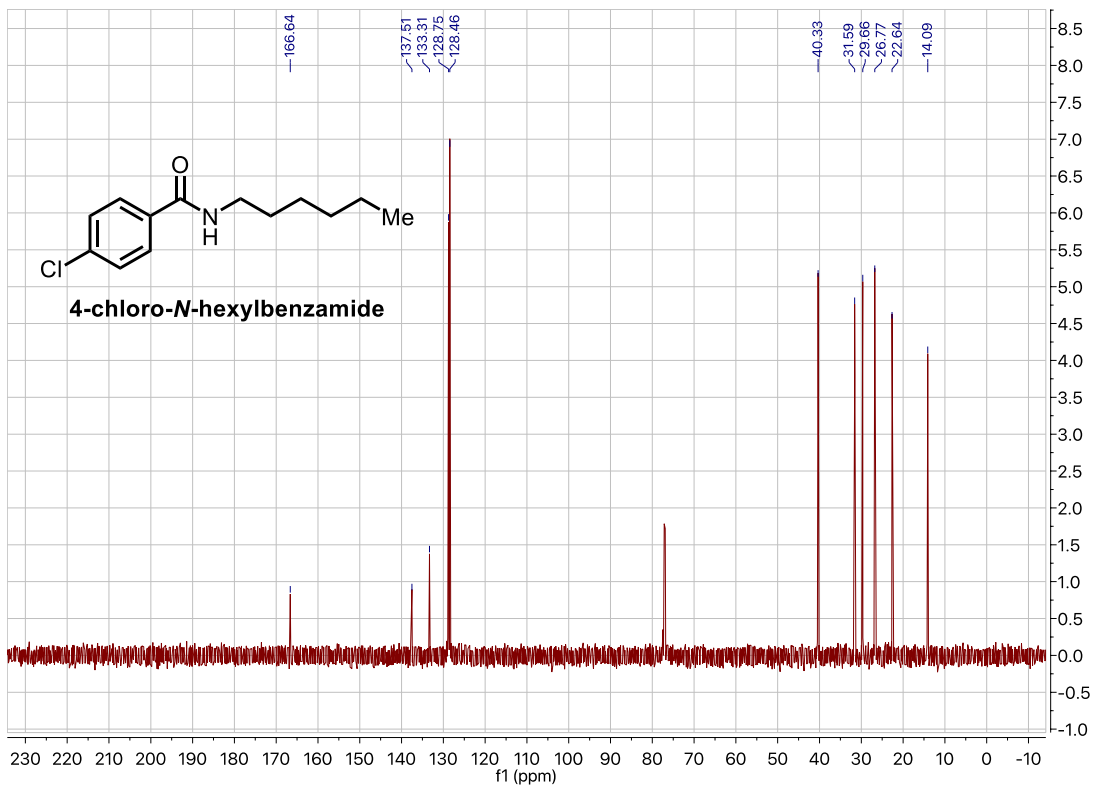
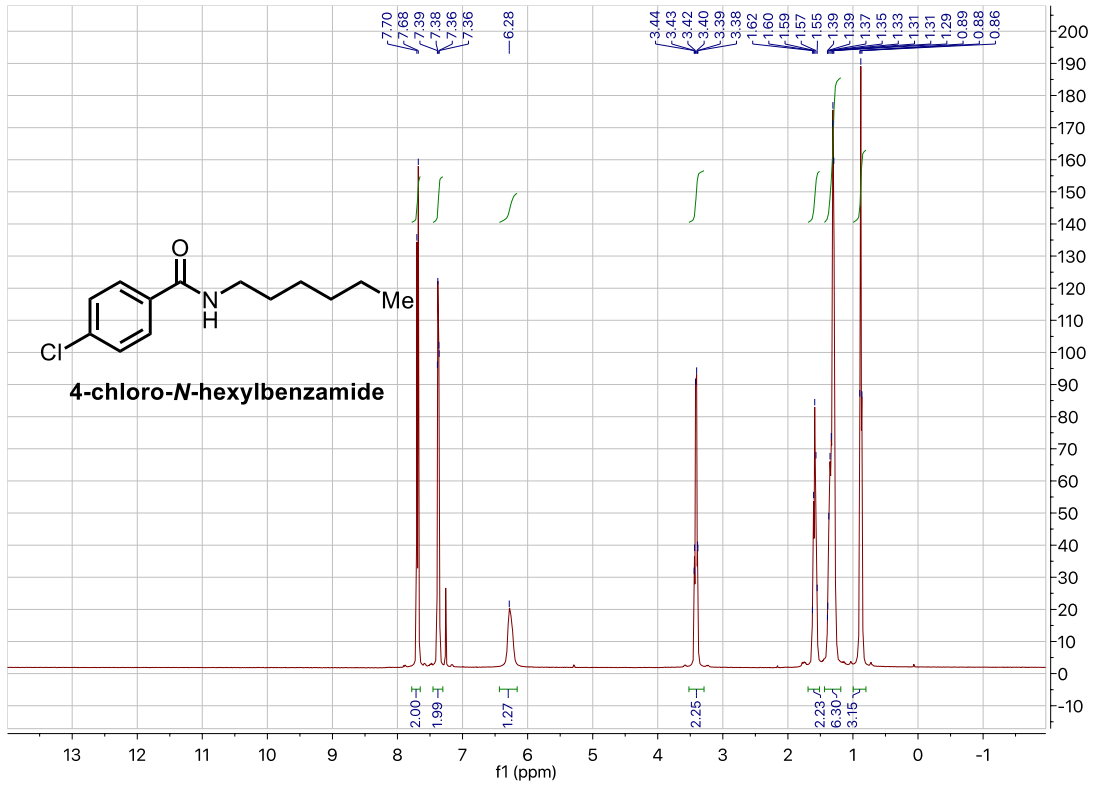


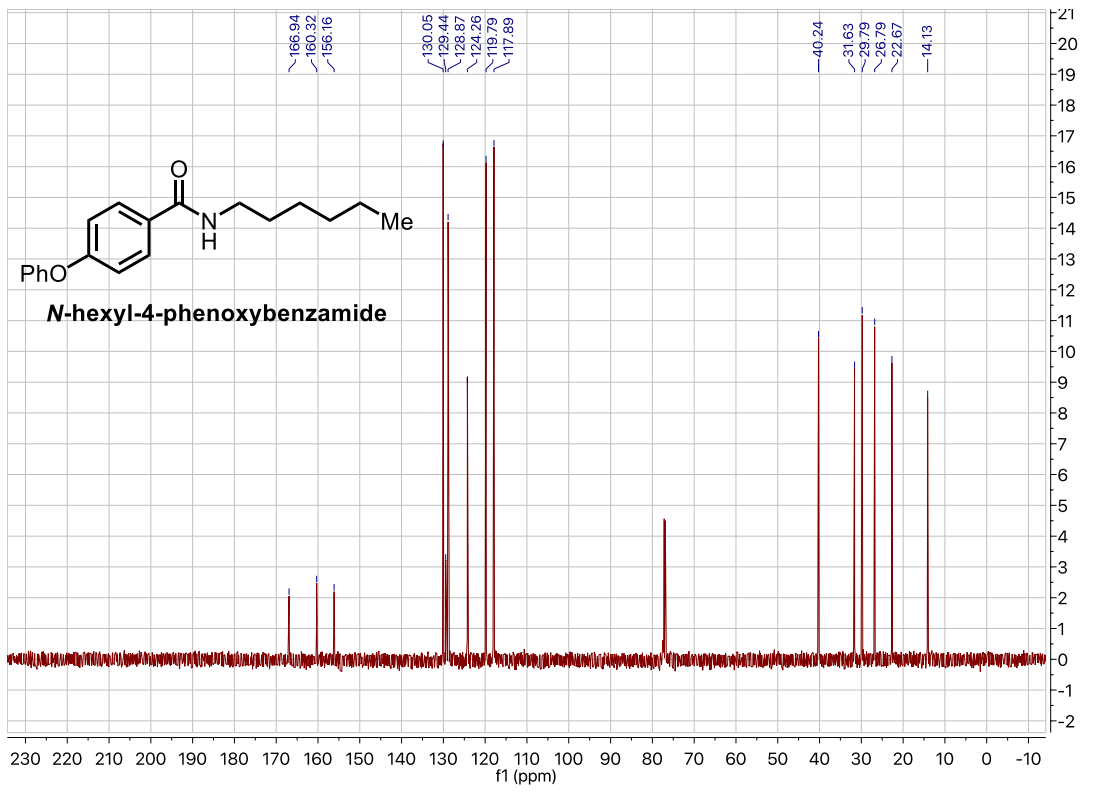
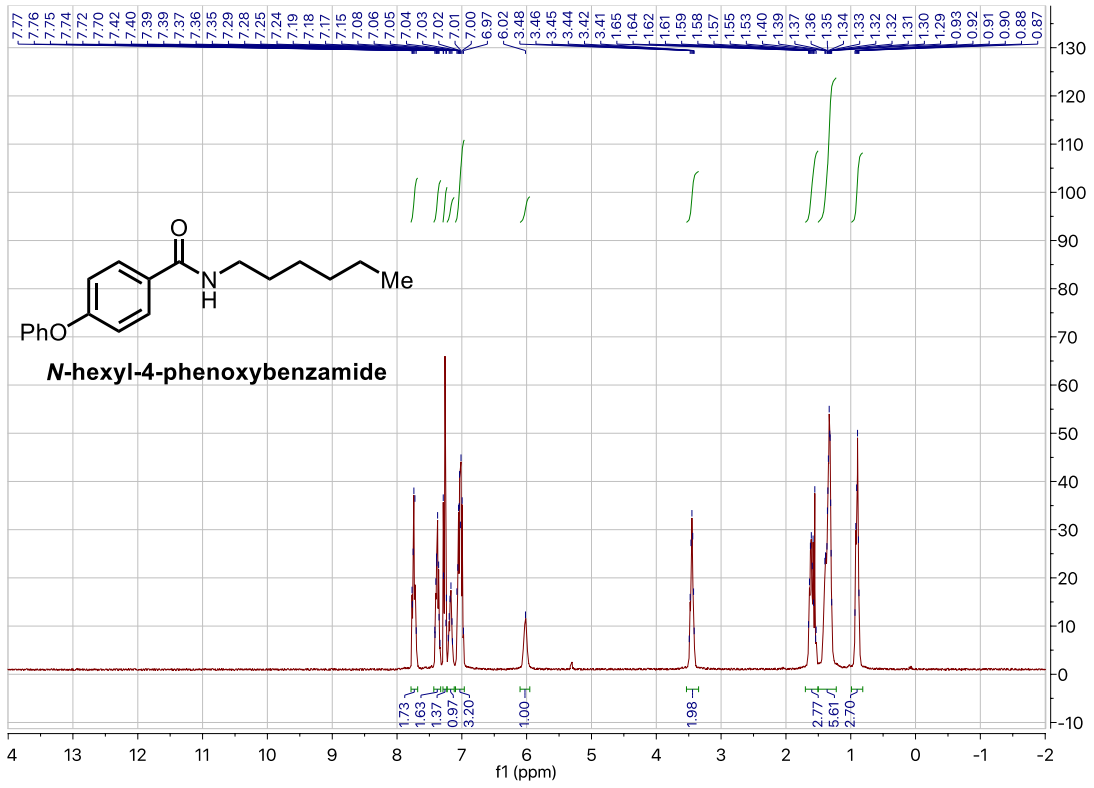


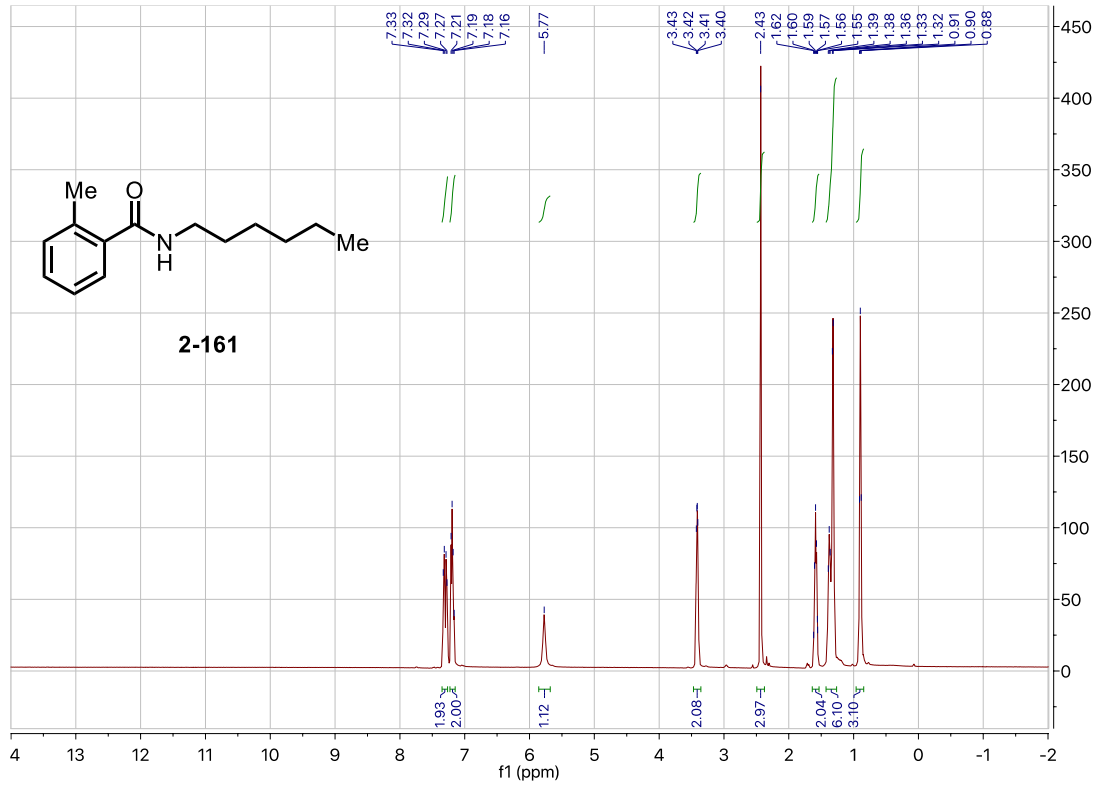


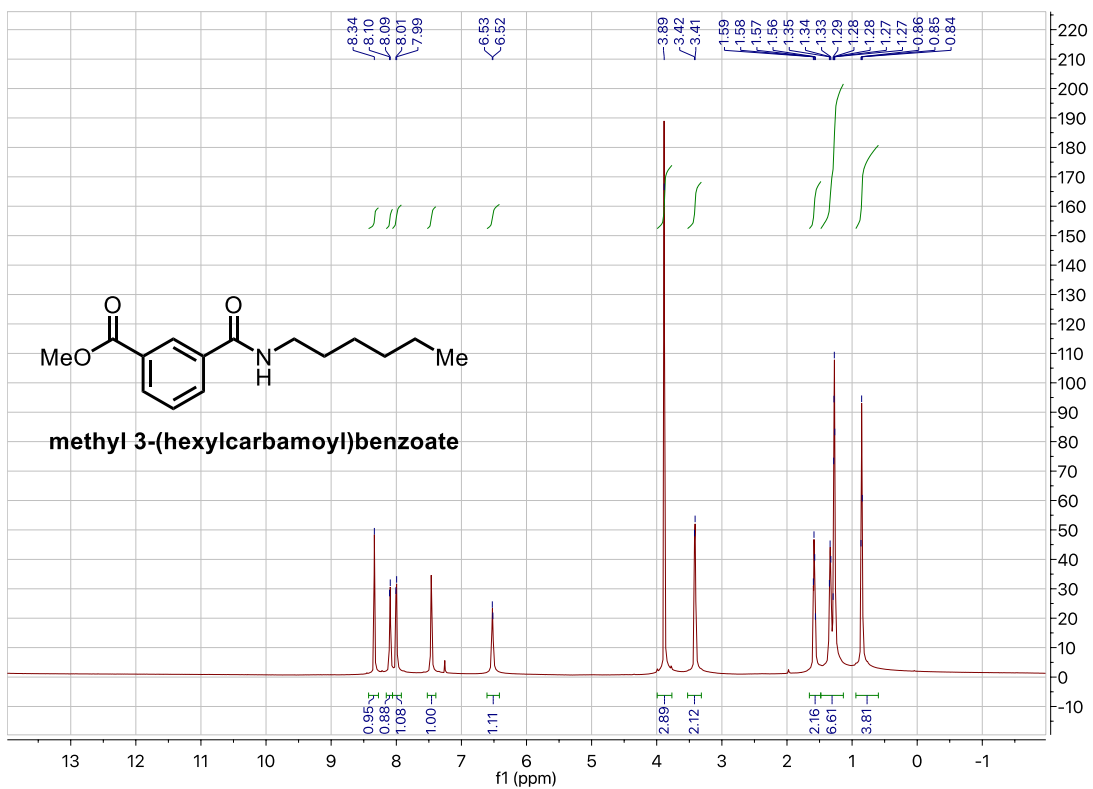
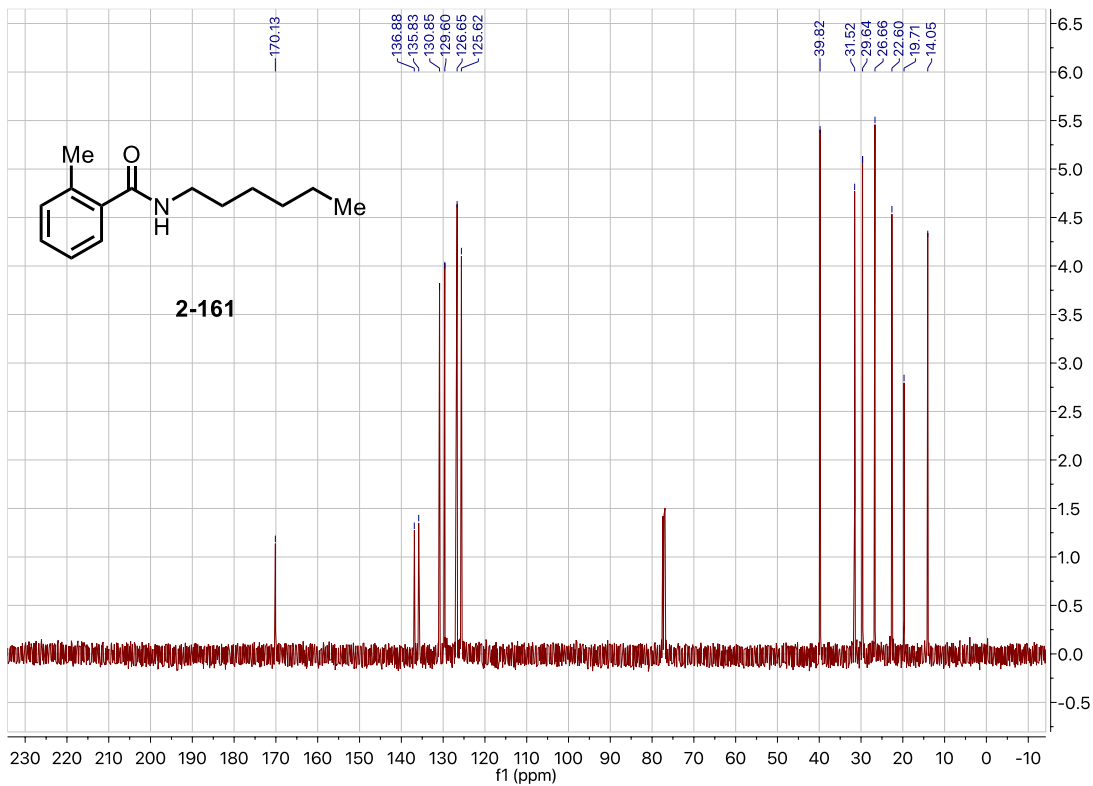


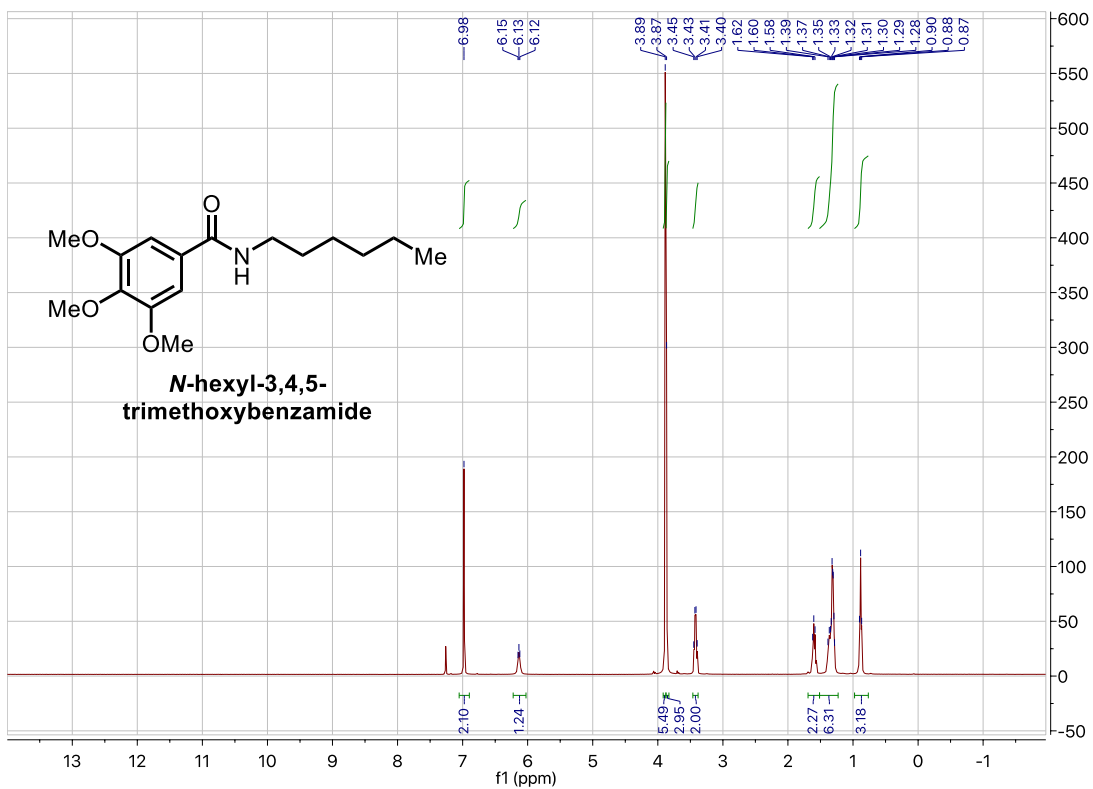
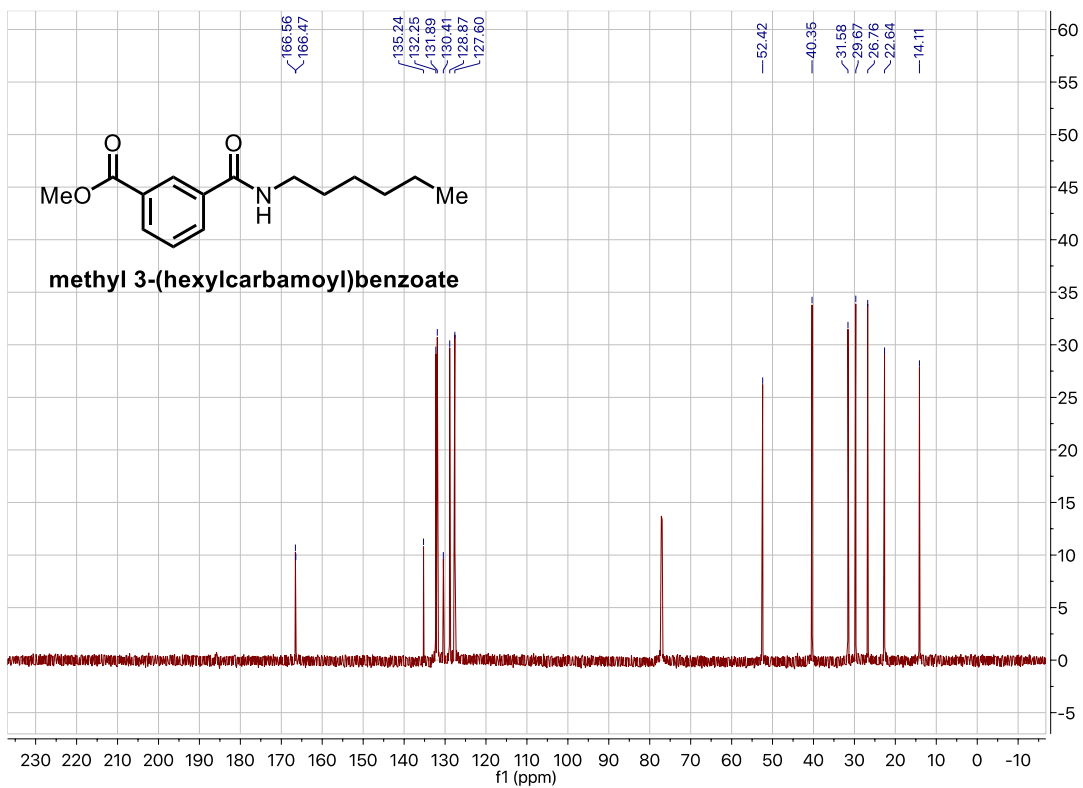


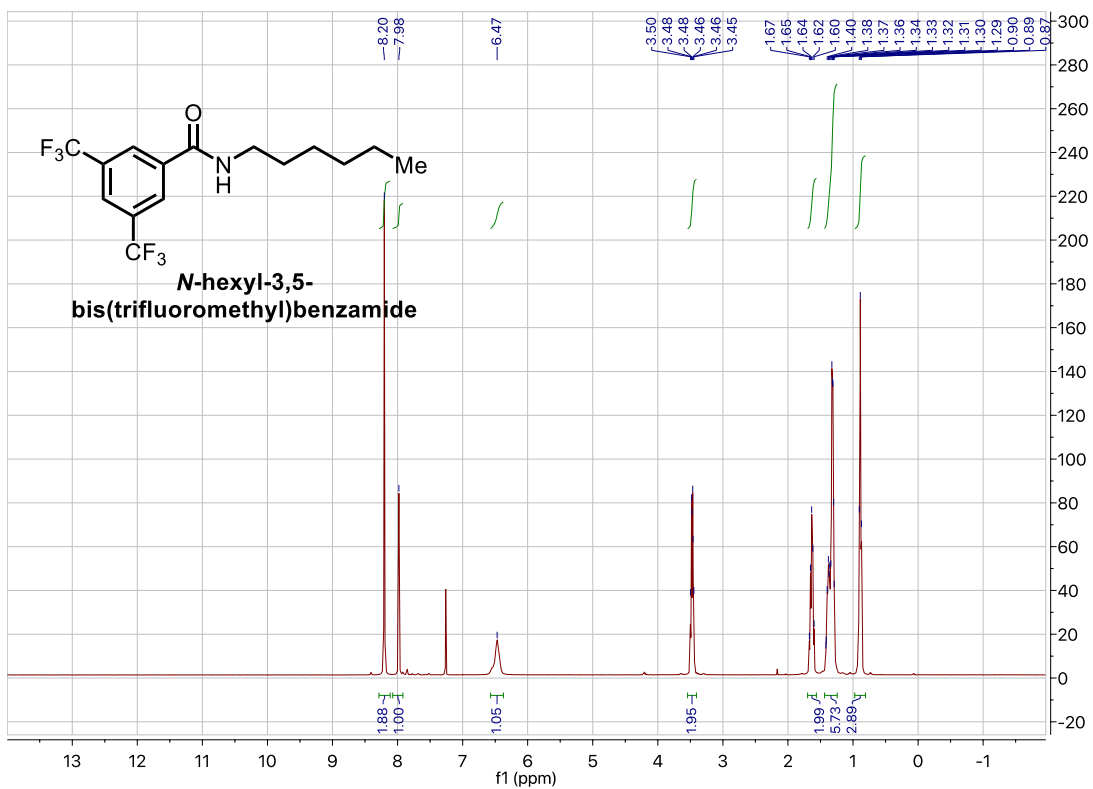
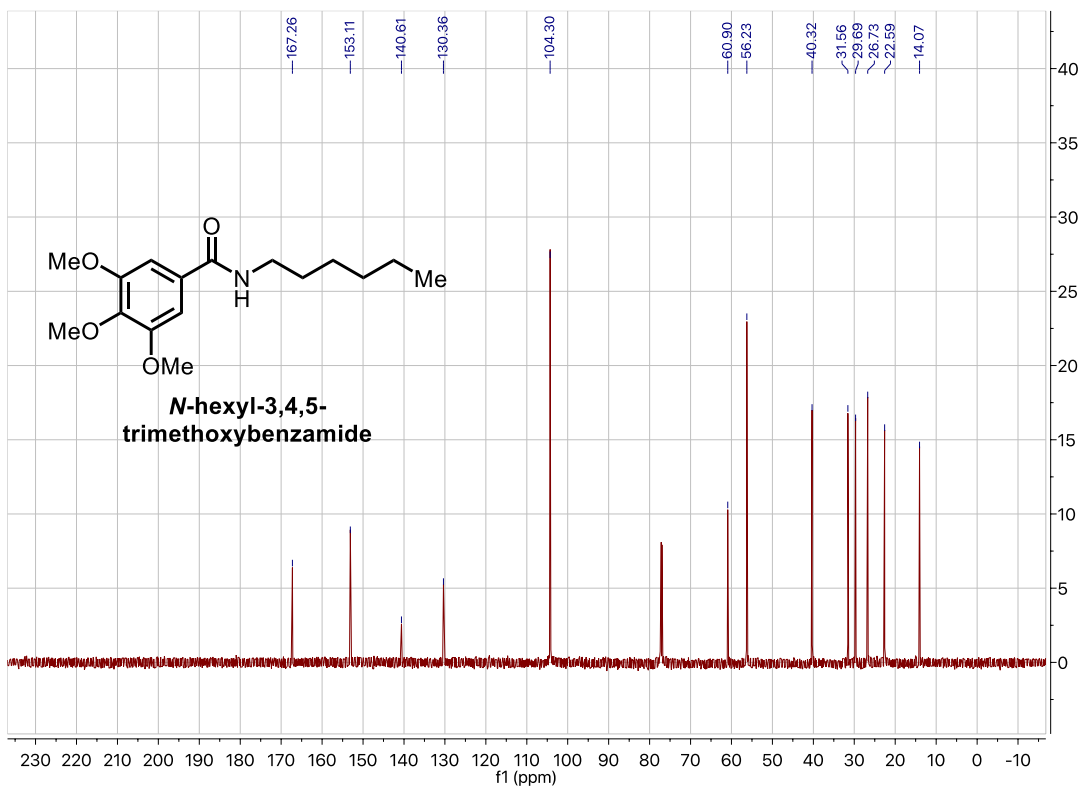


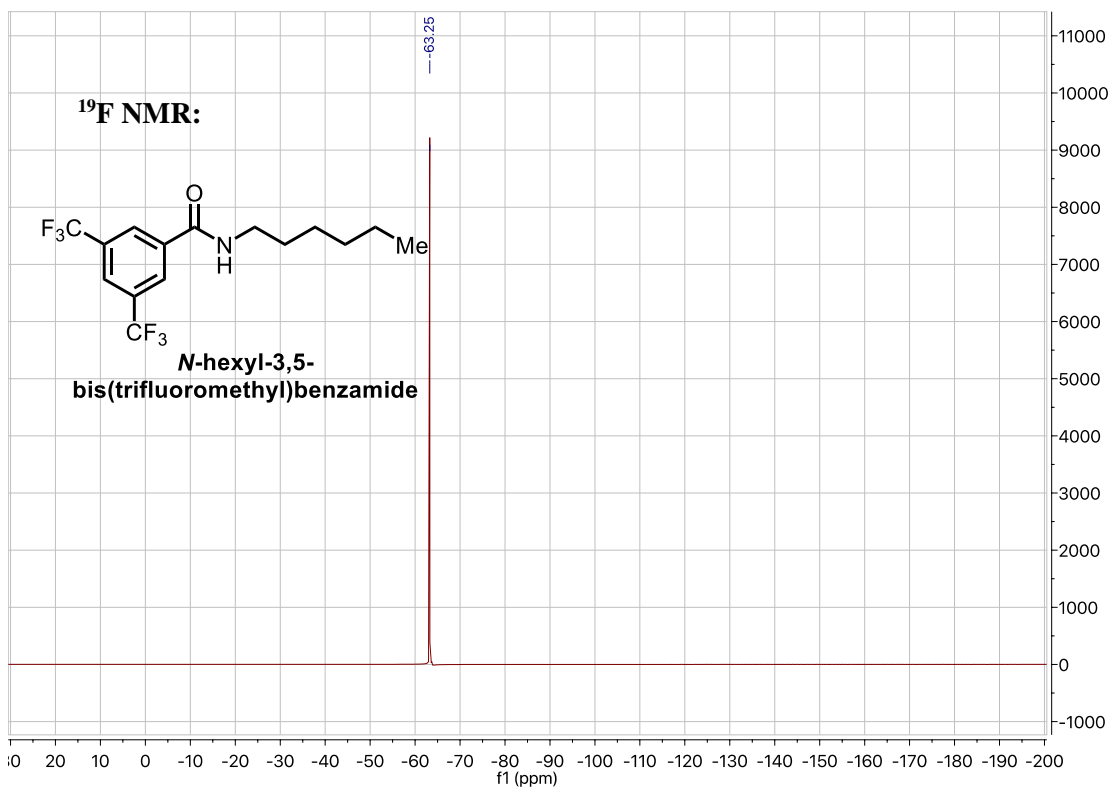
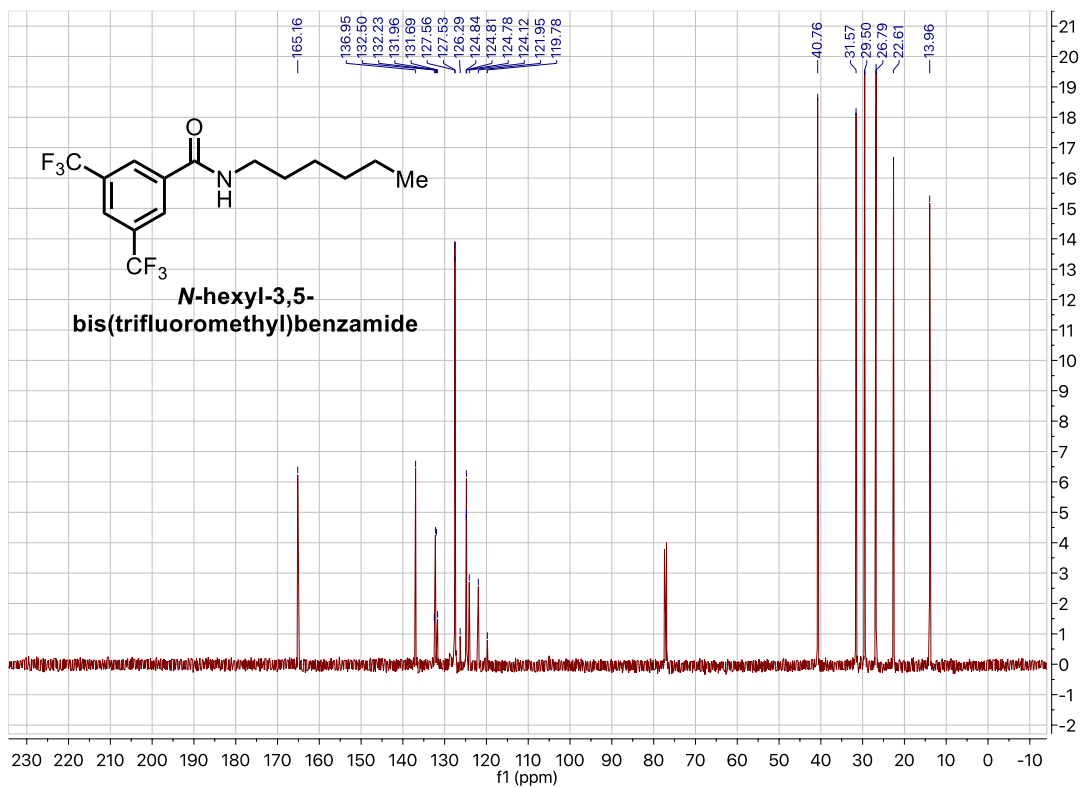


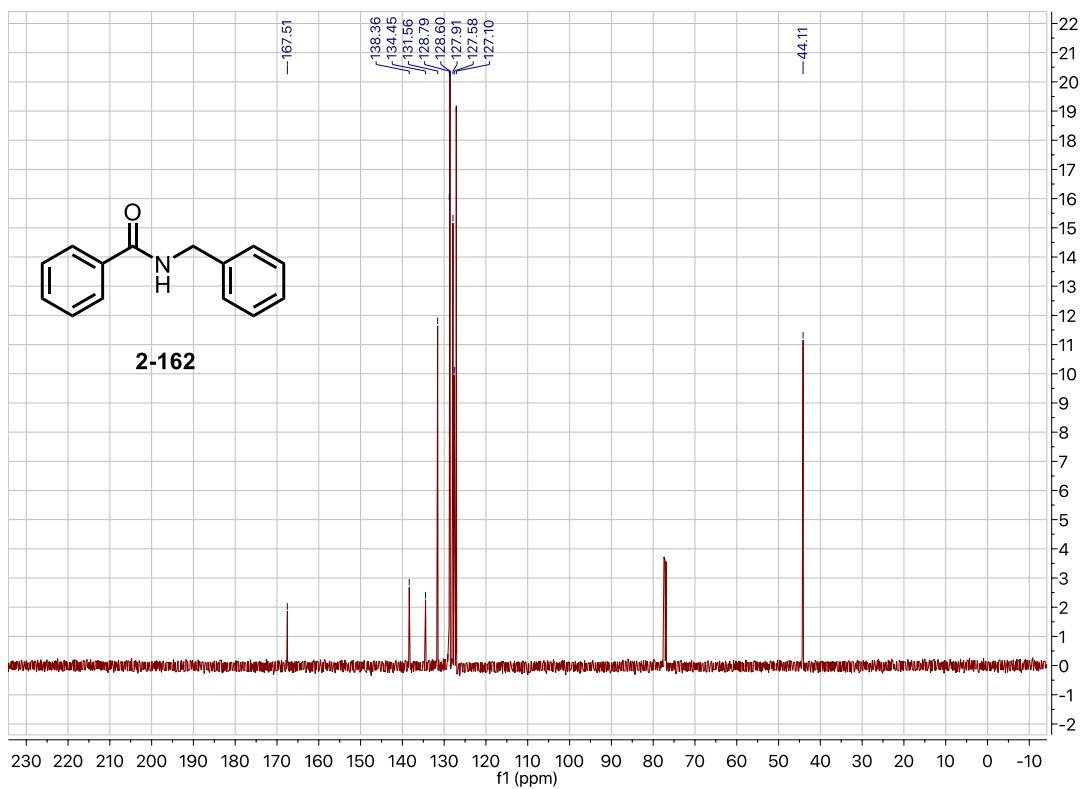
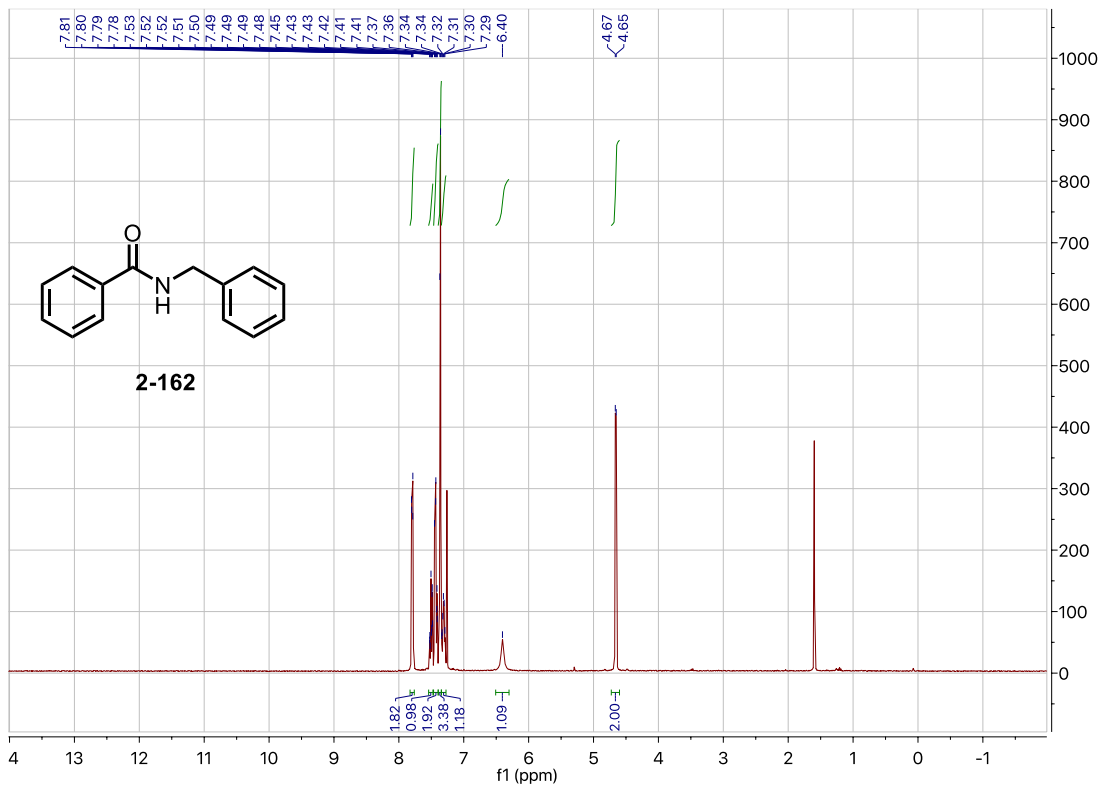


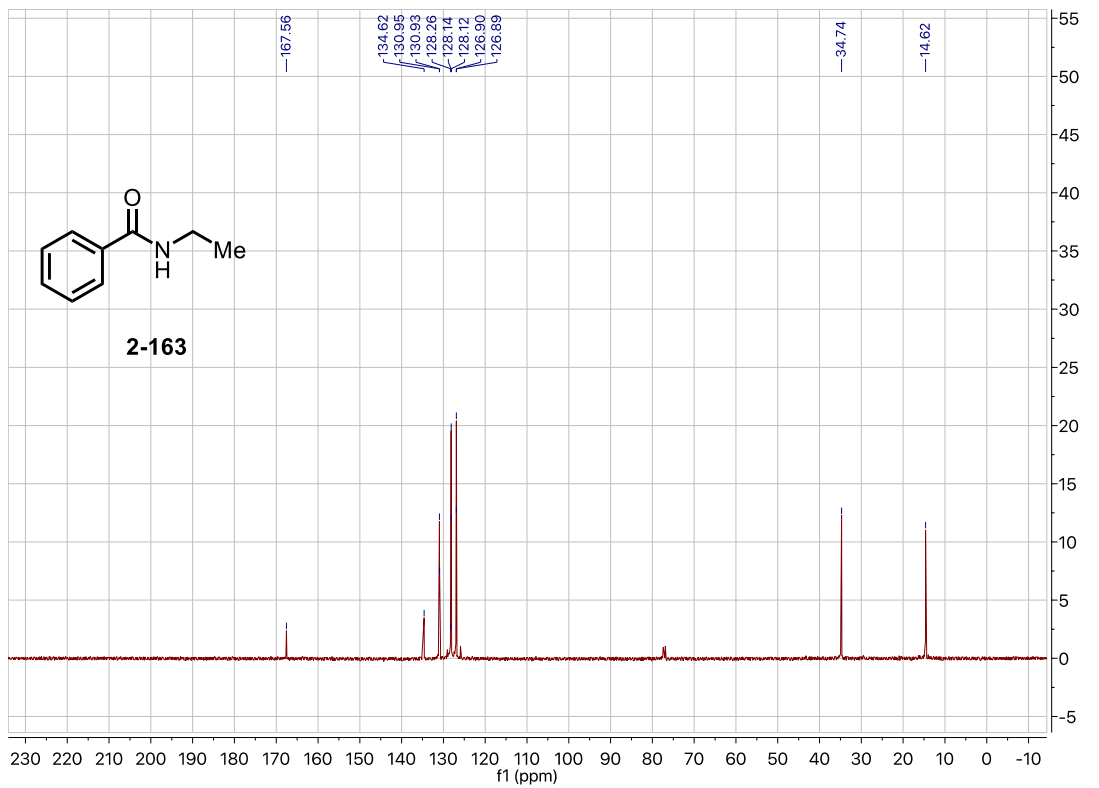
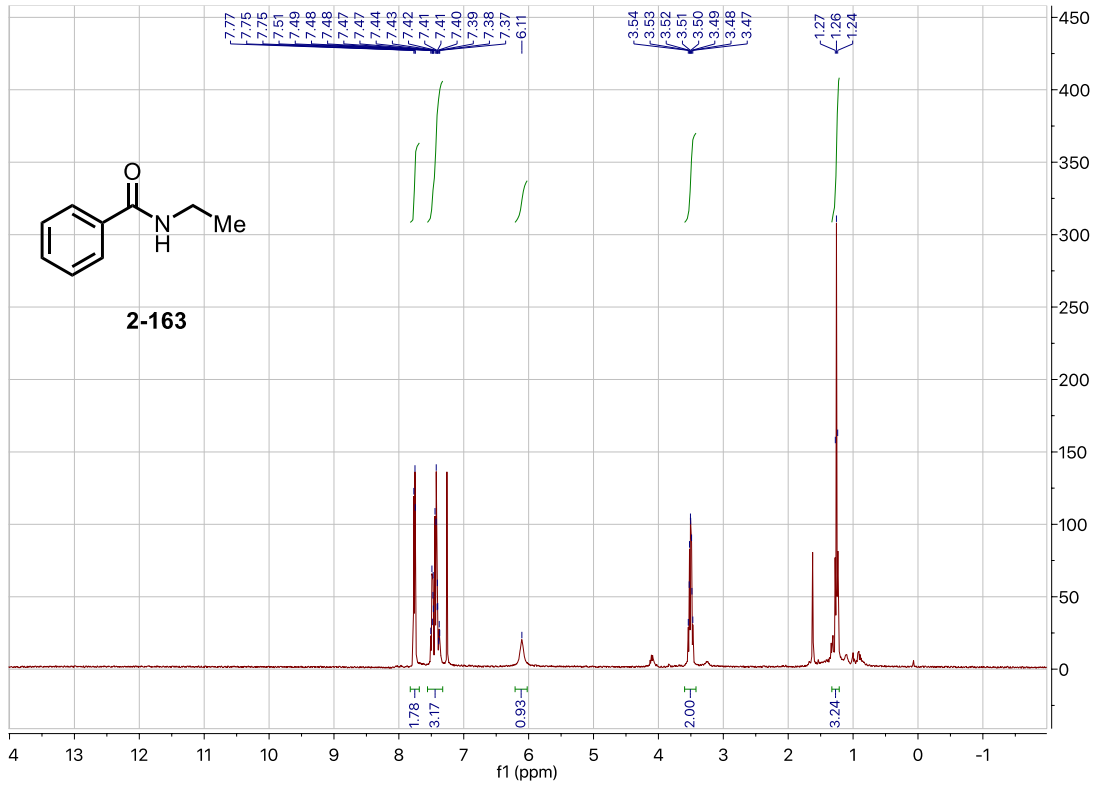


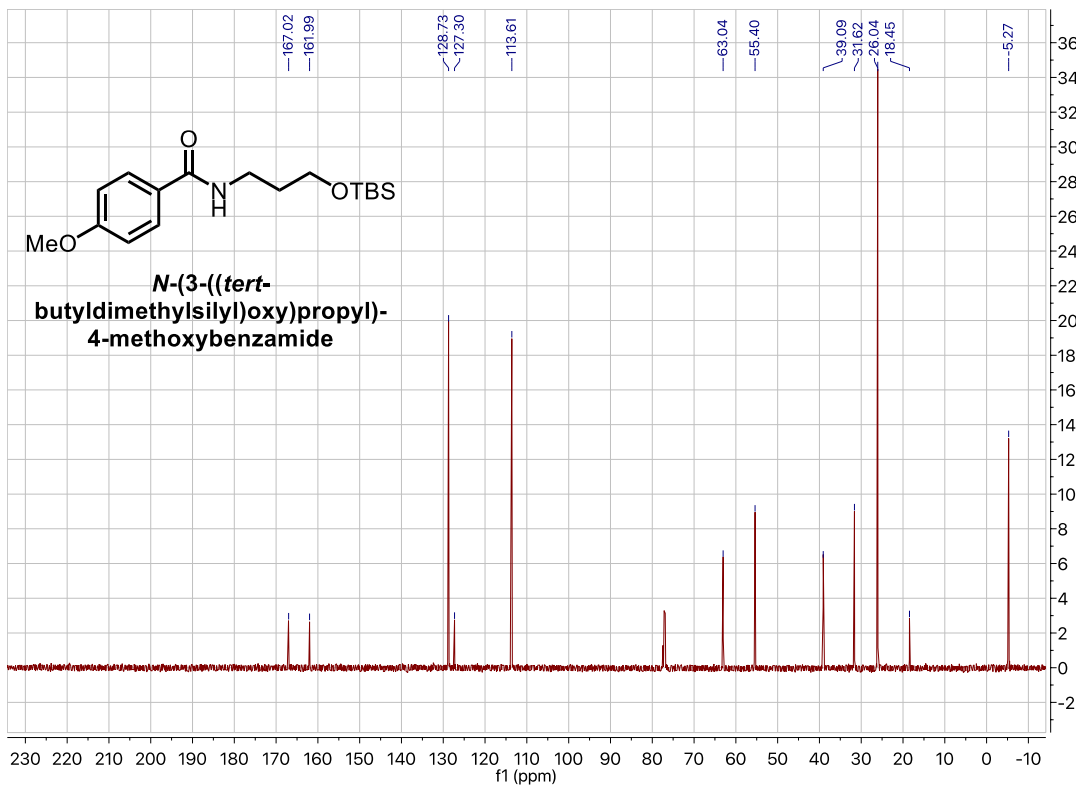
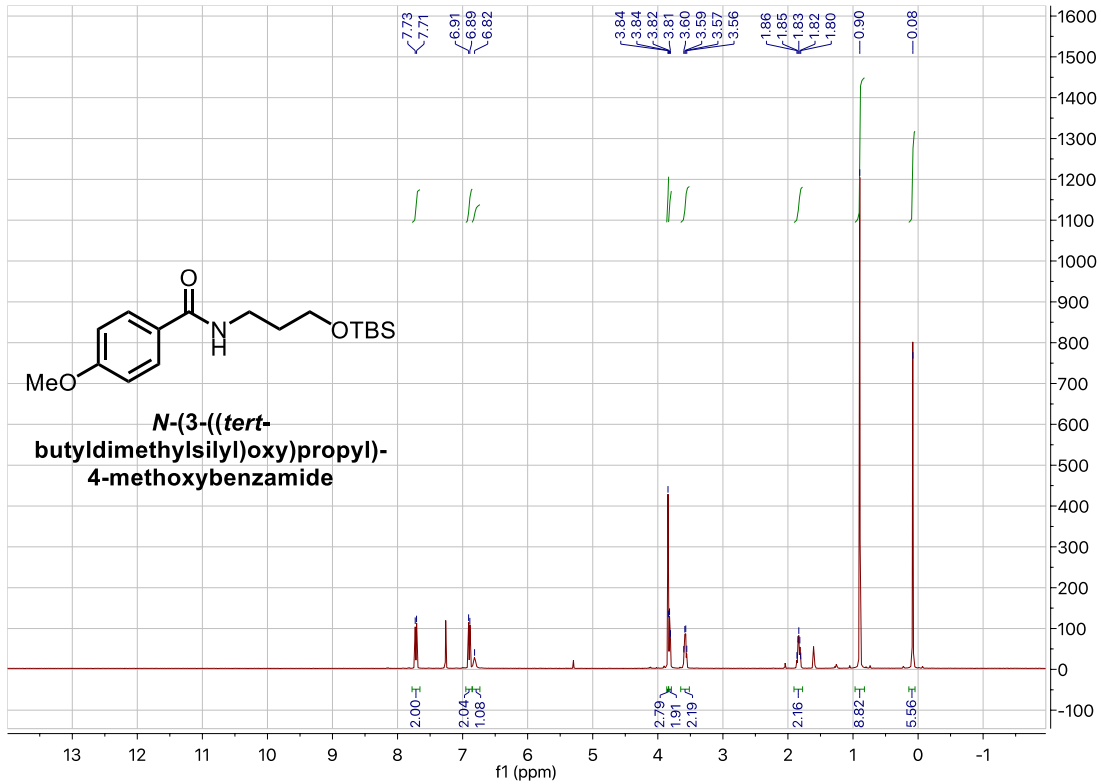


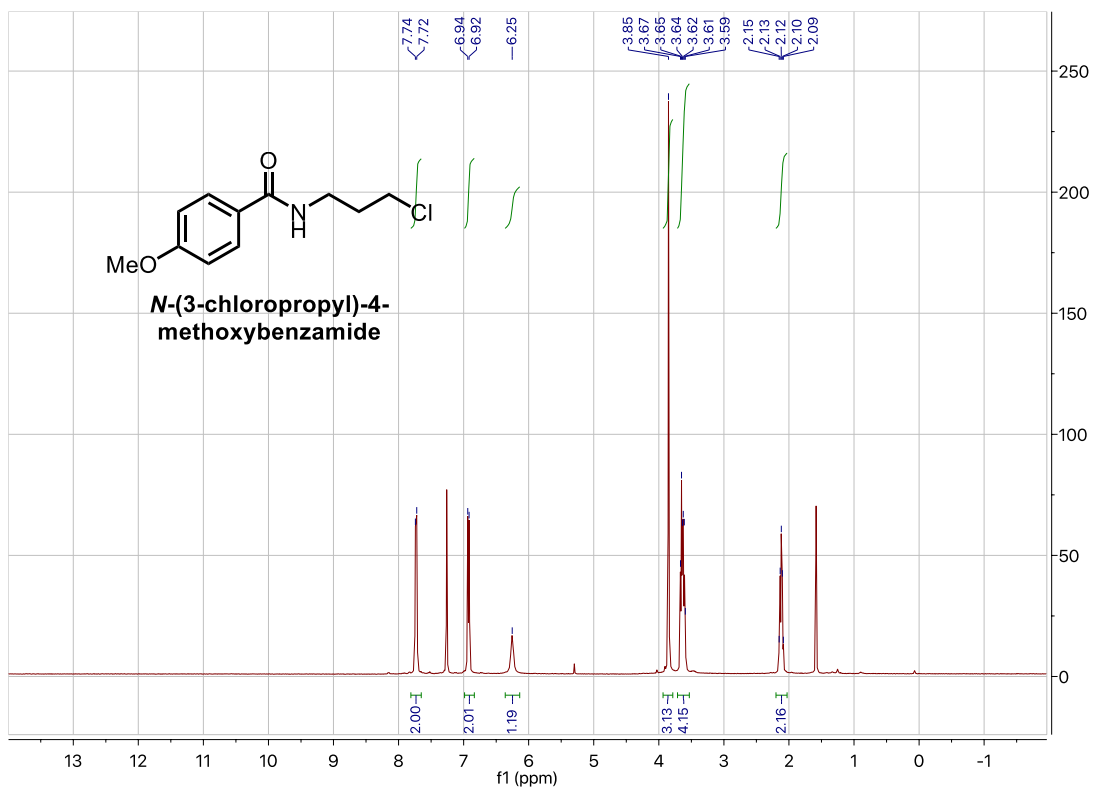


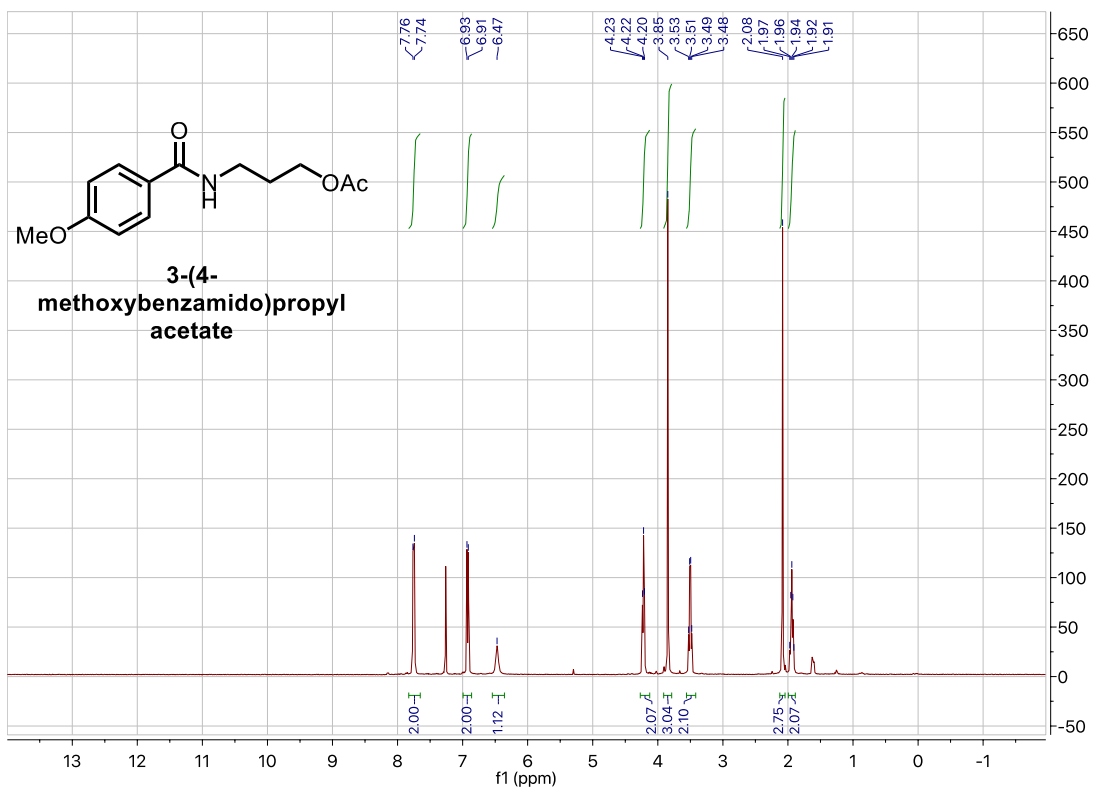
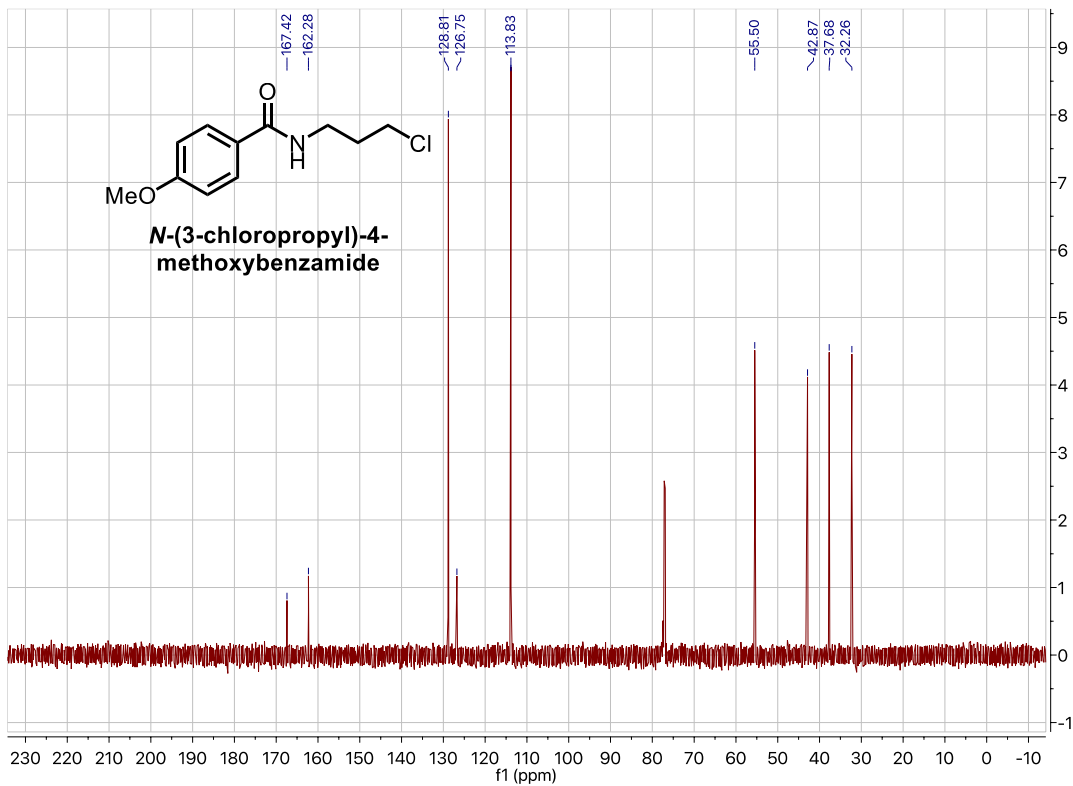


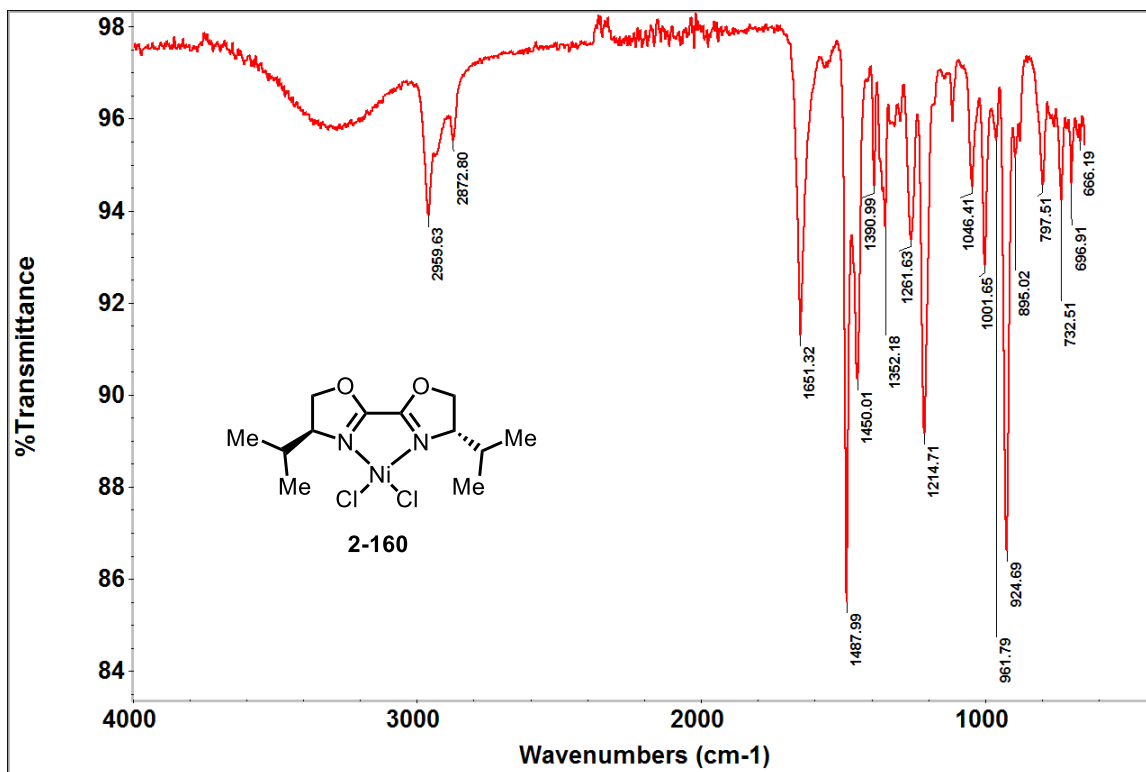




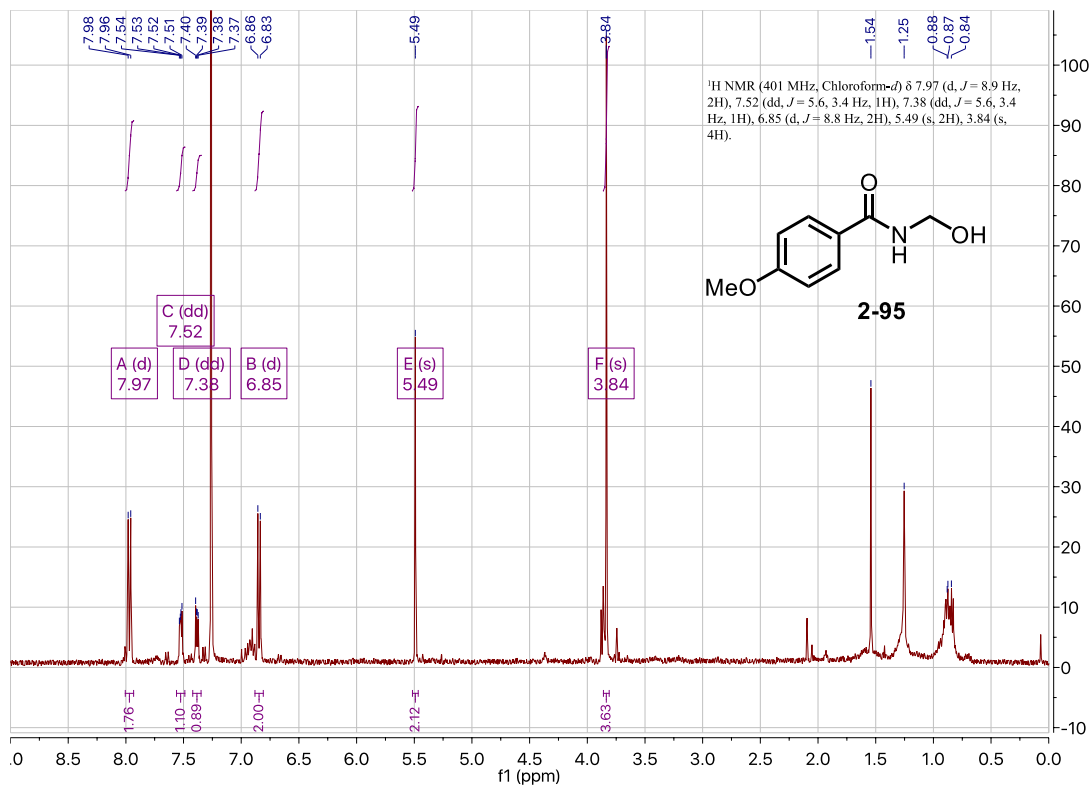


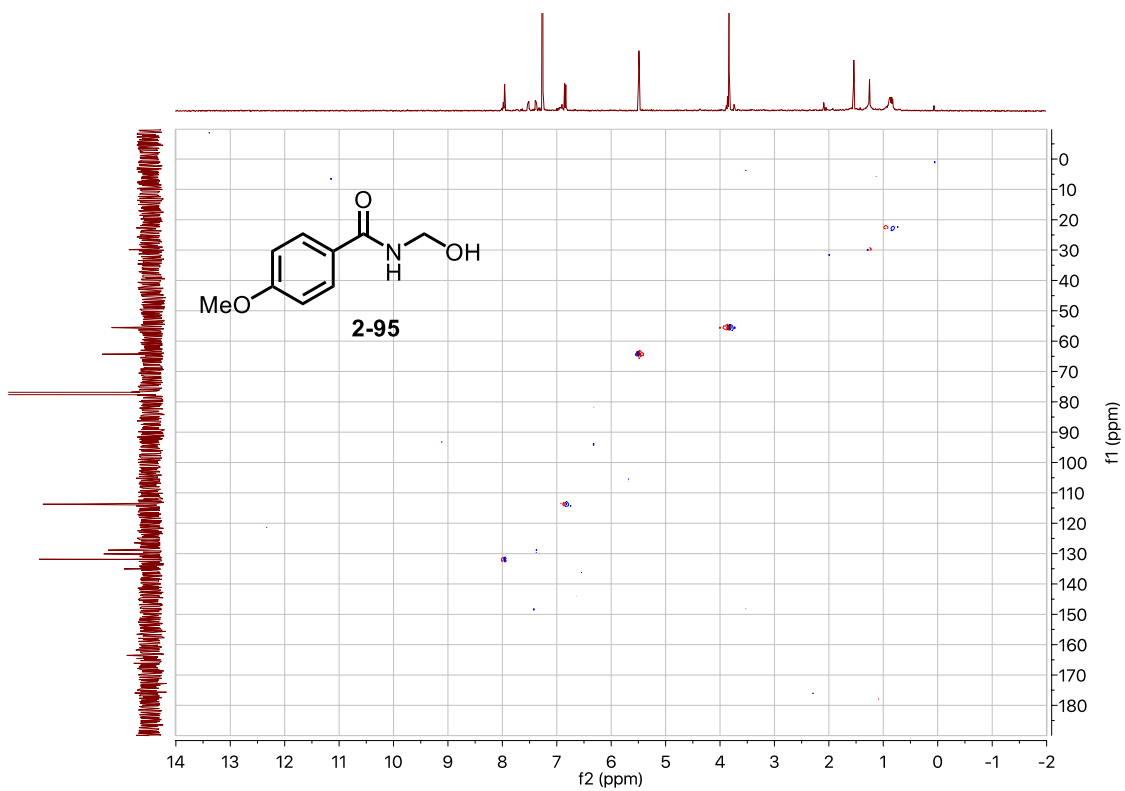
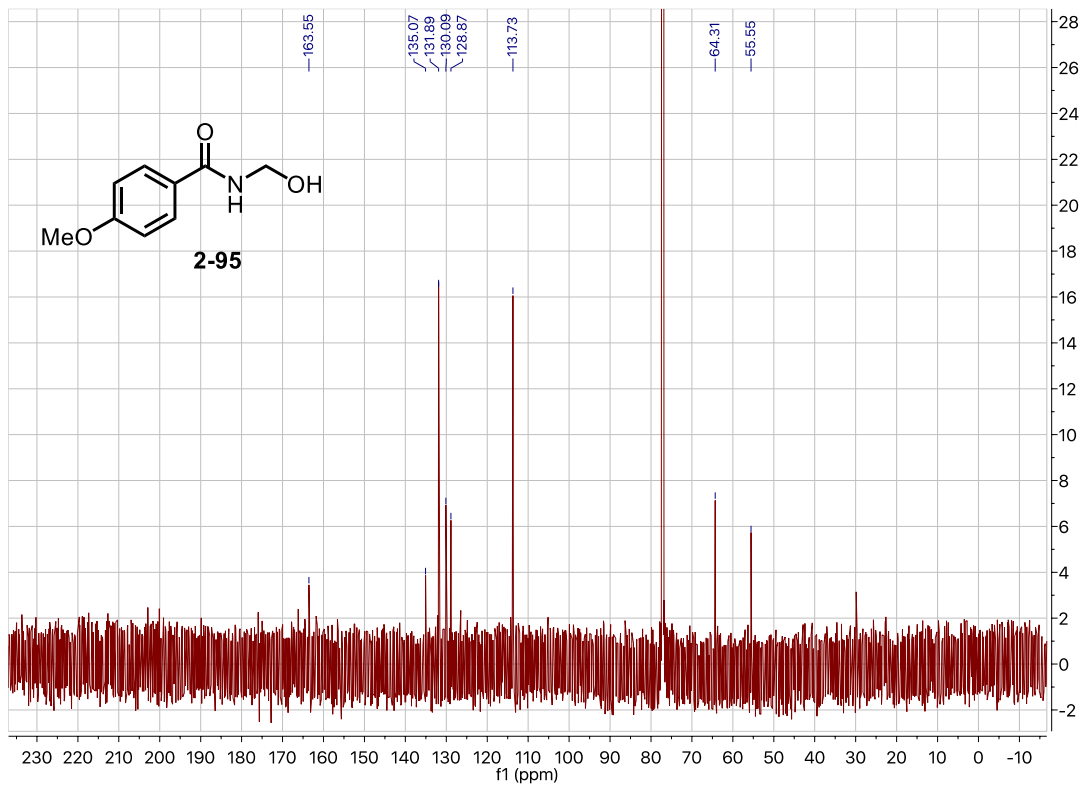


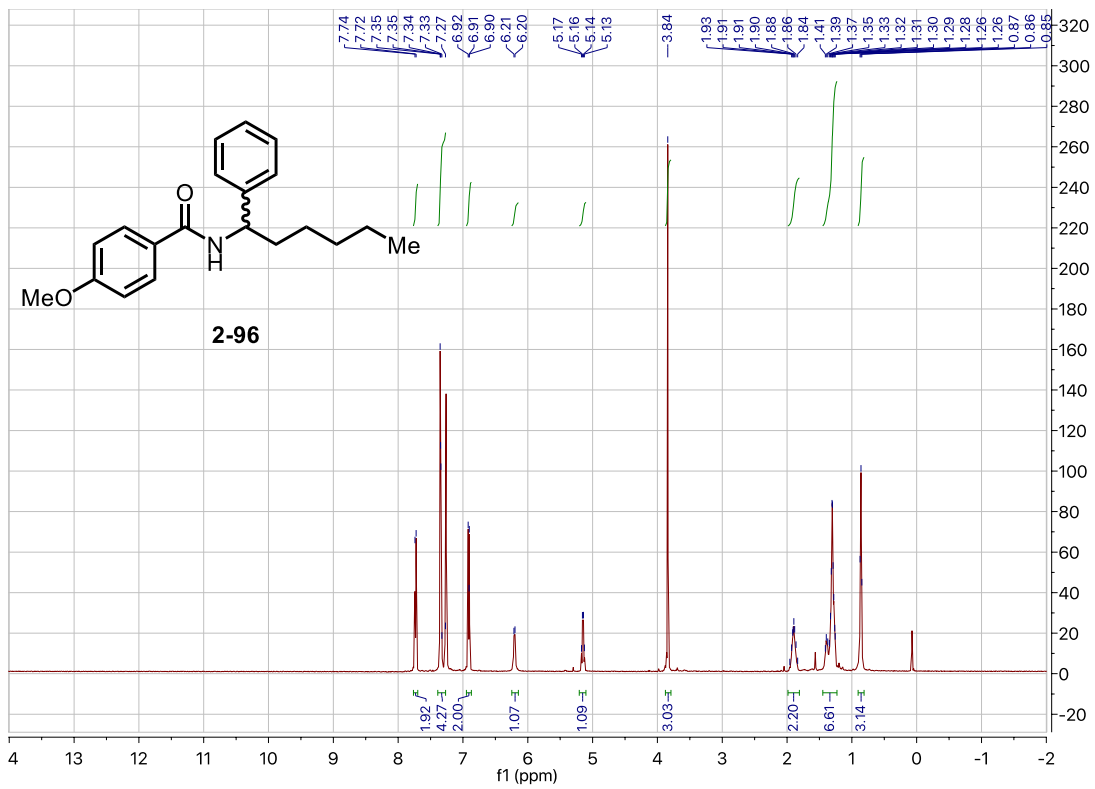
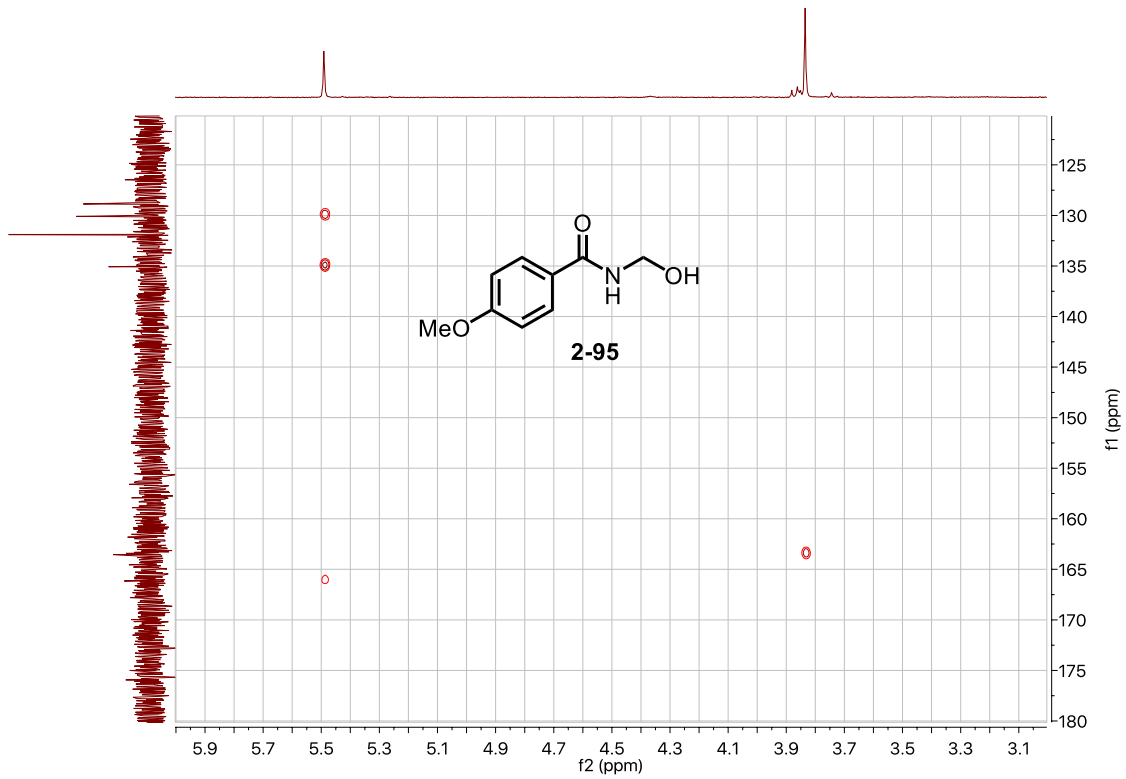


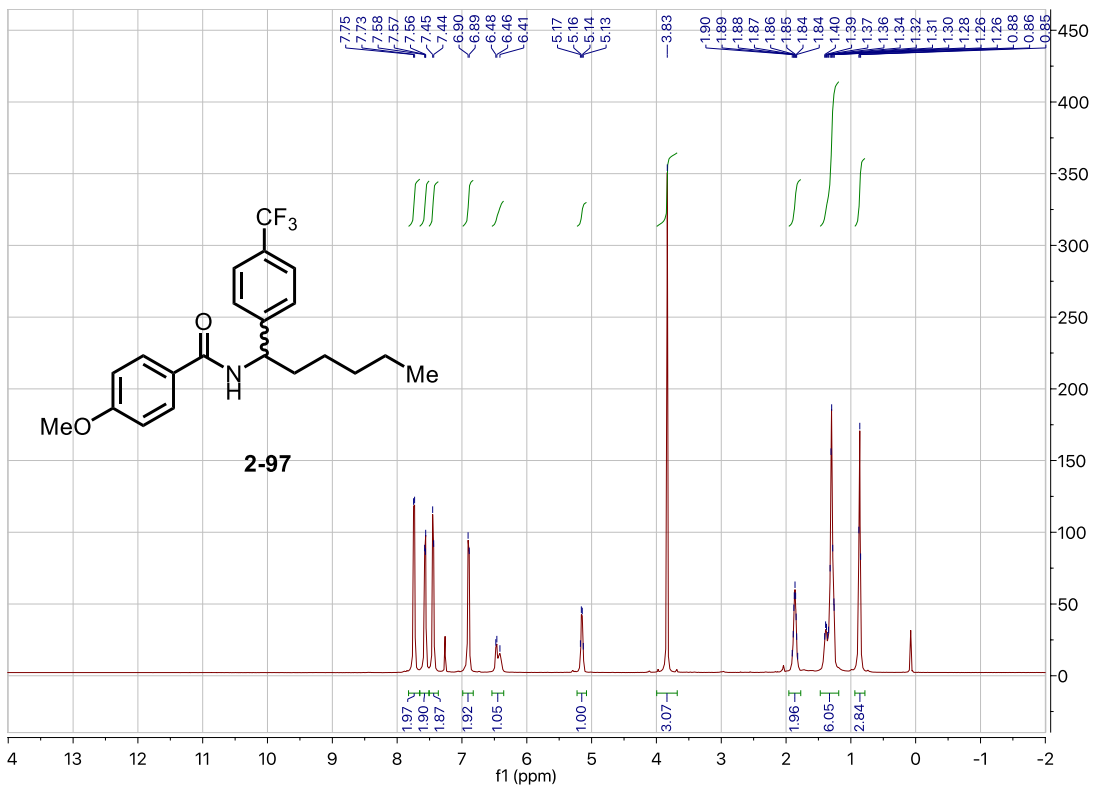
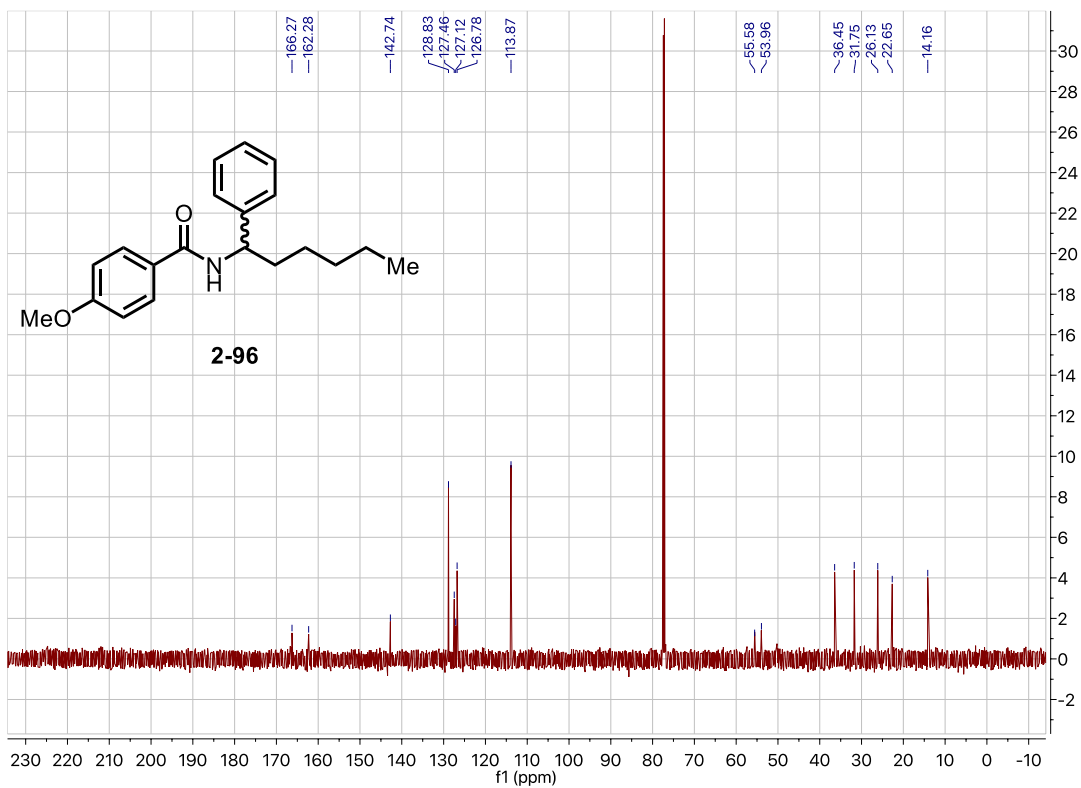


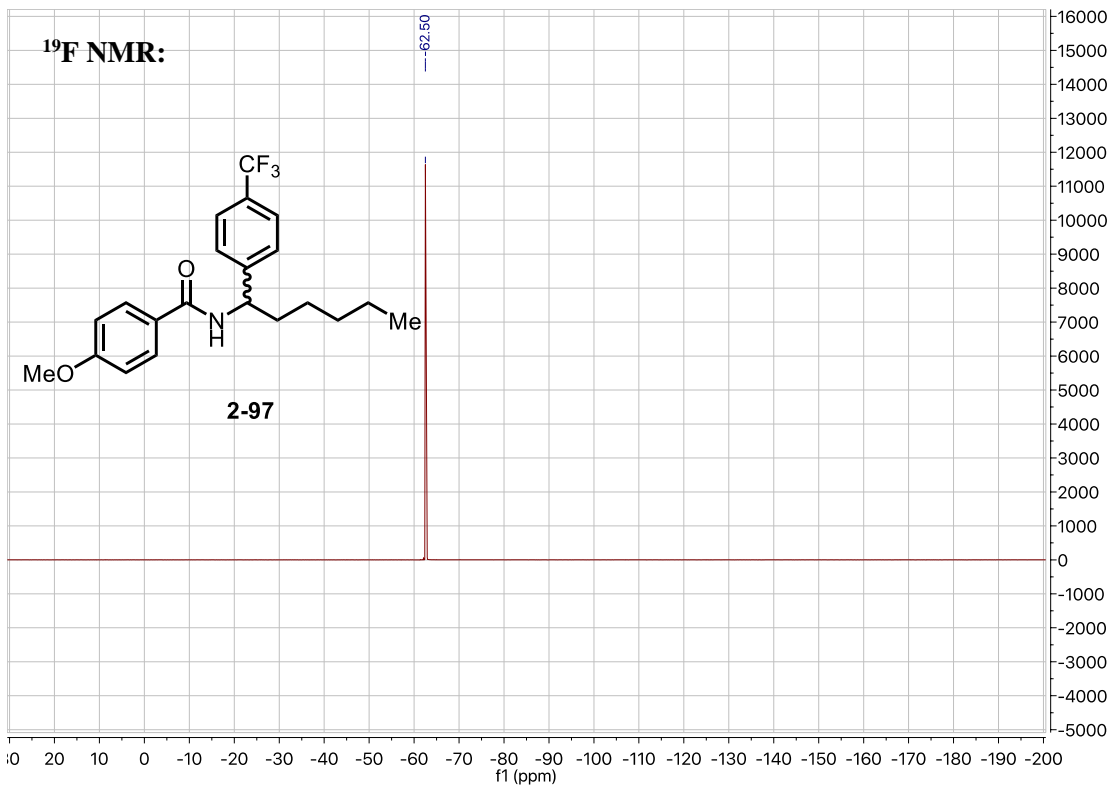
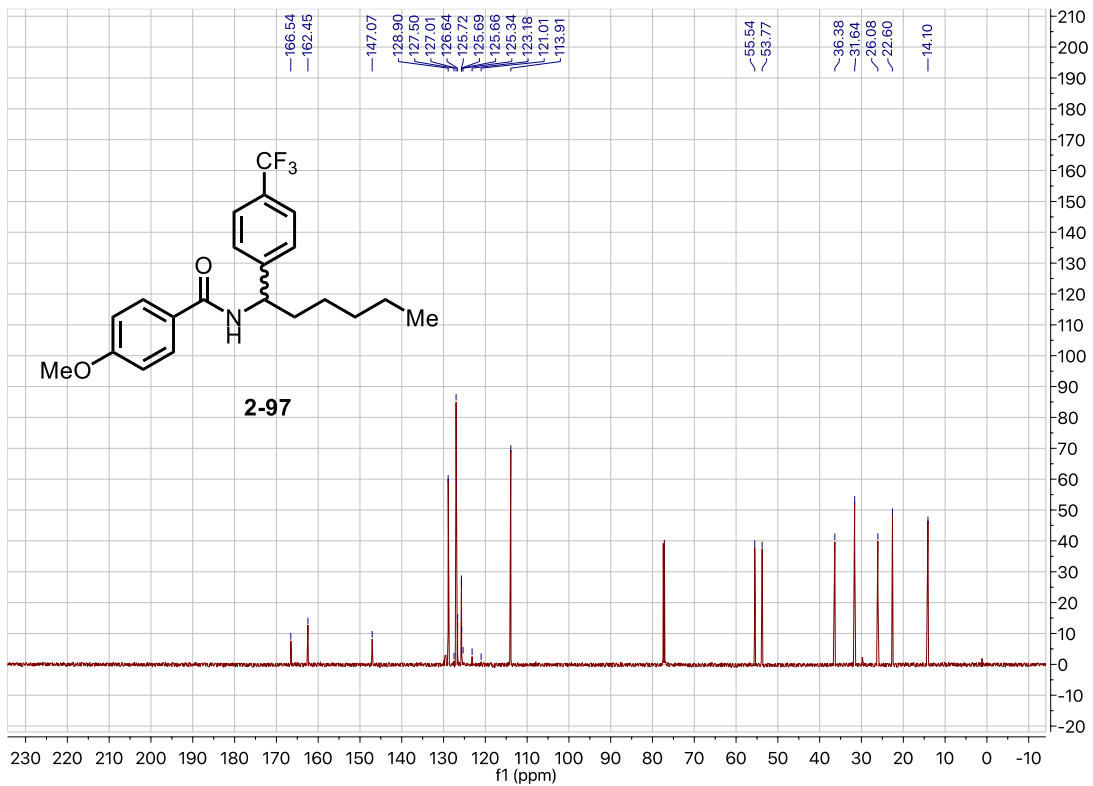
XIII) NMR Spectra of Products:

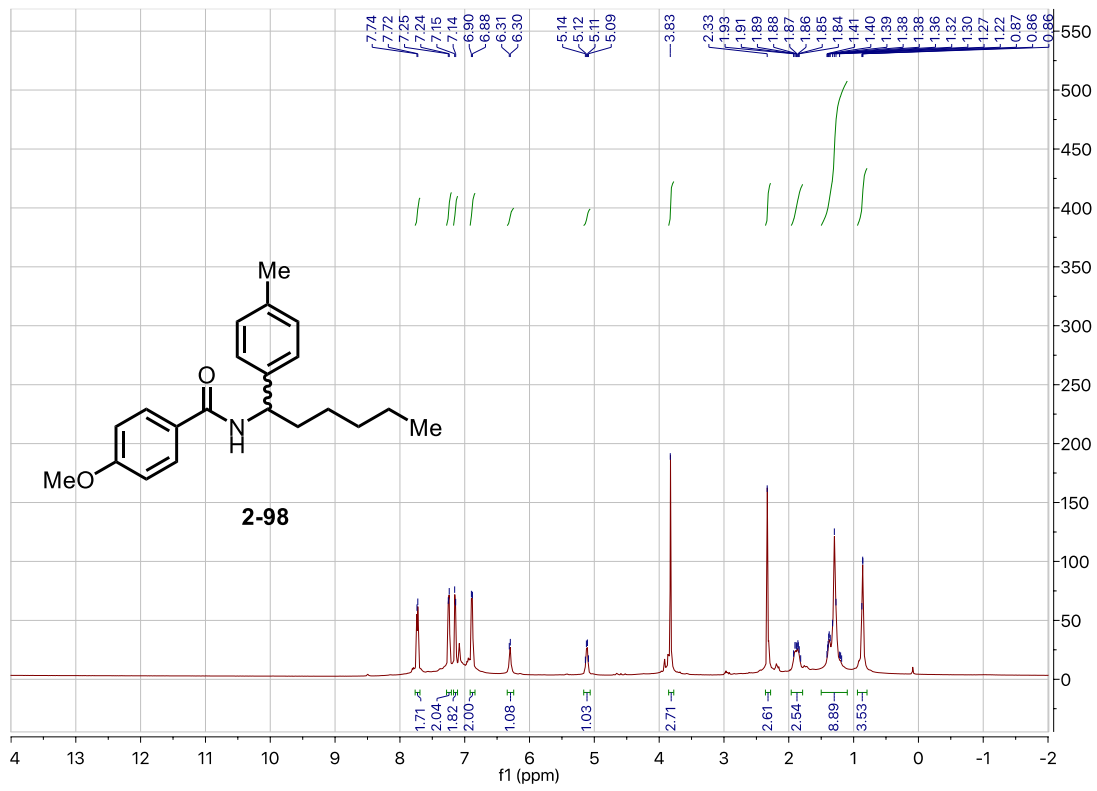


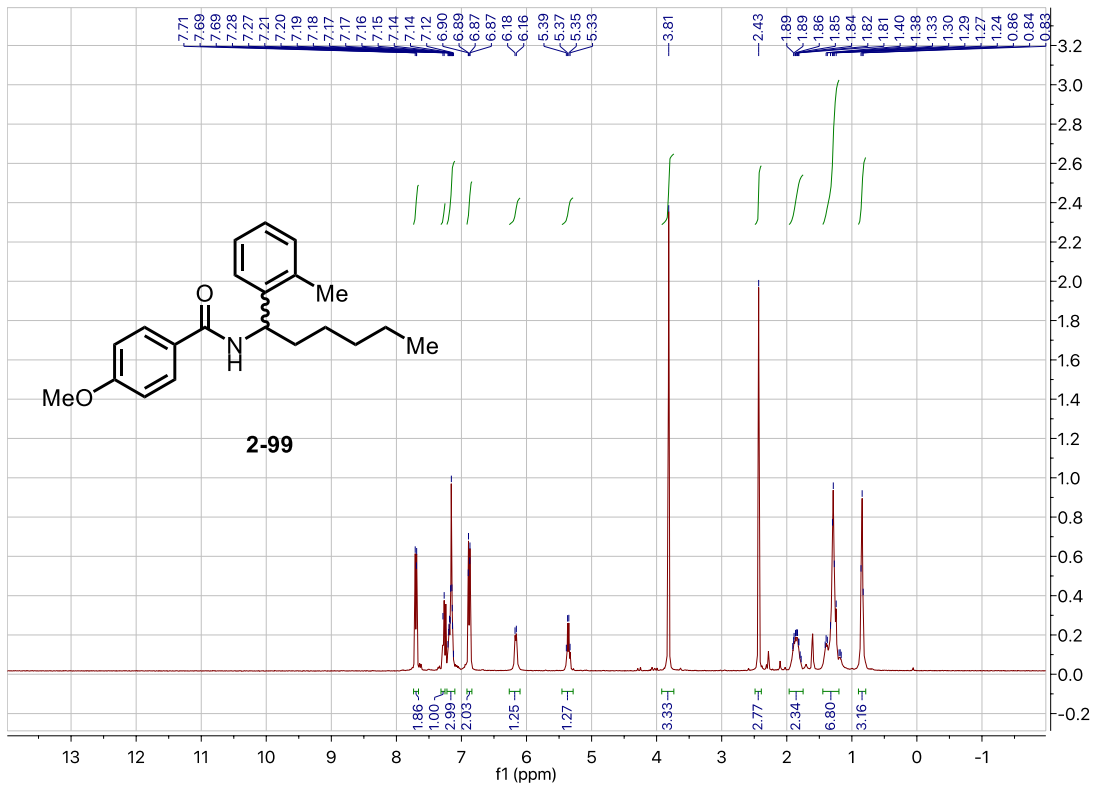
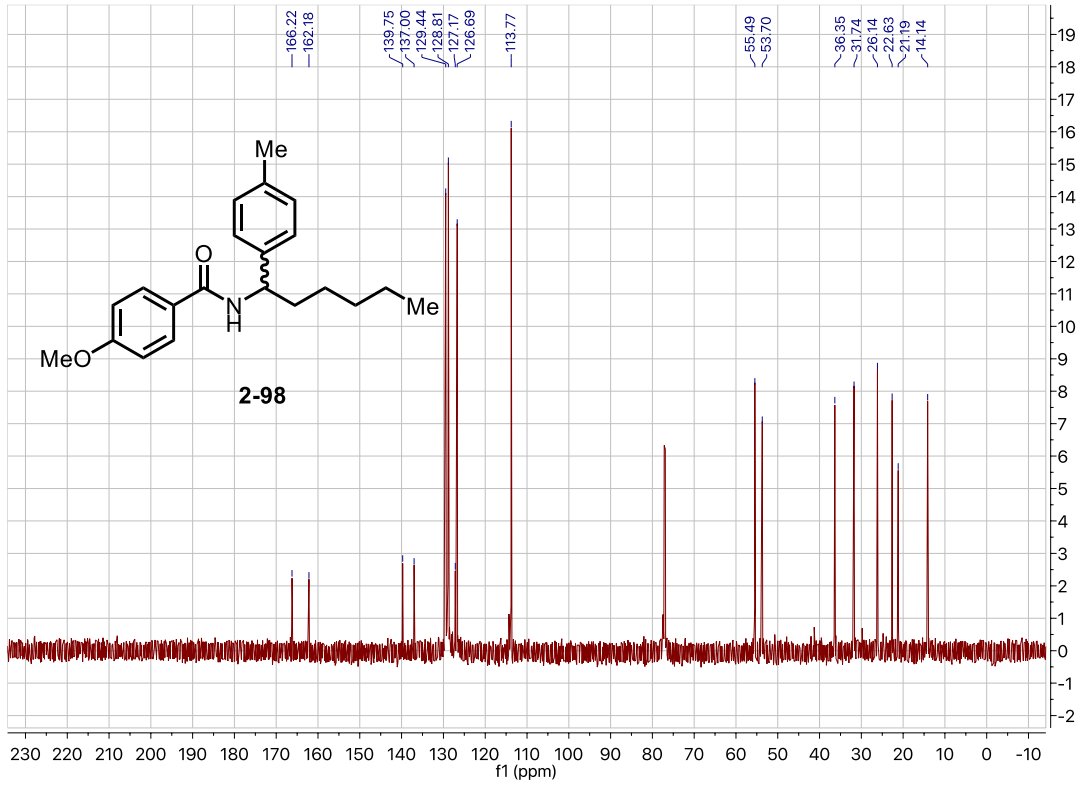


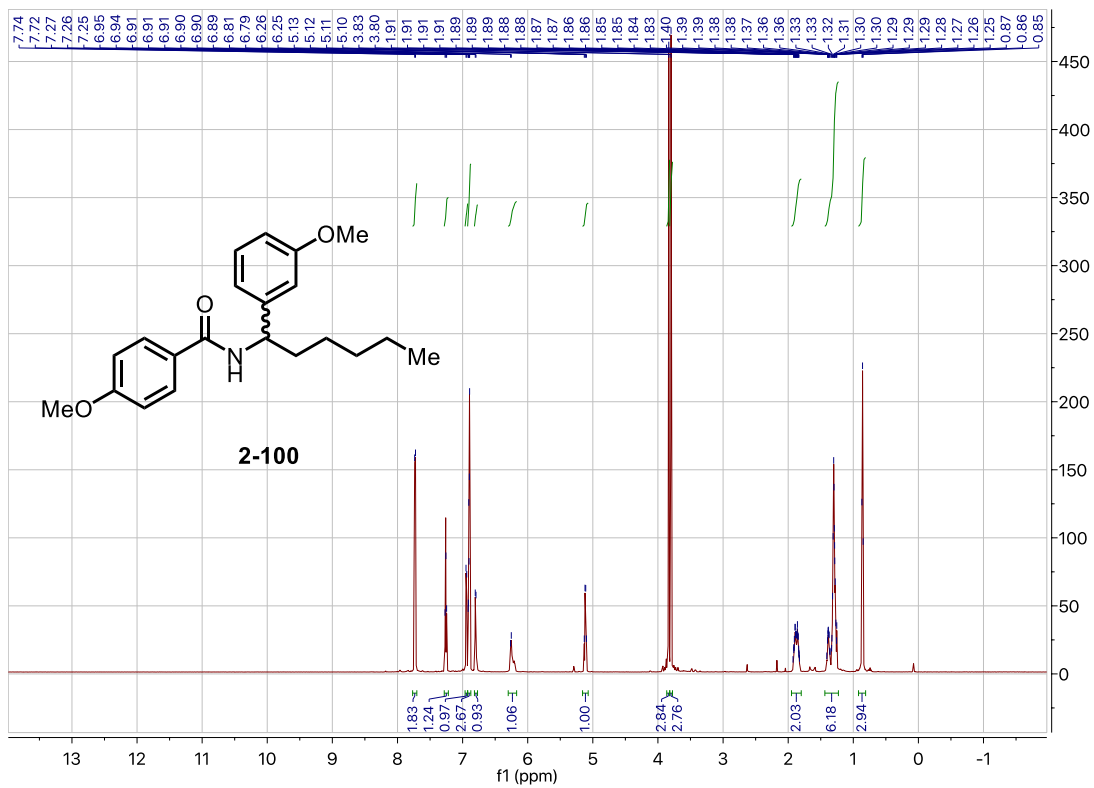
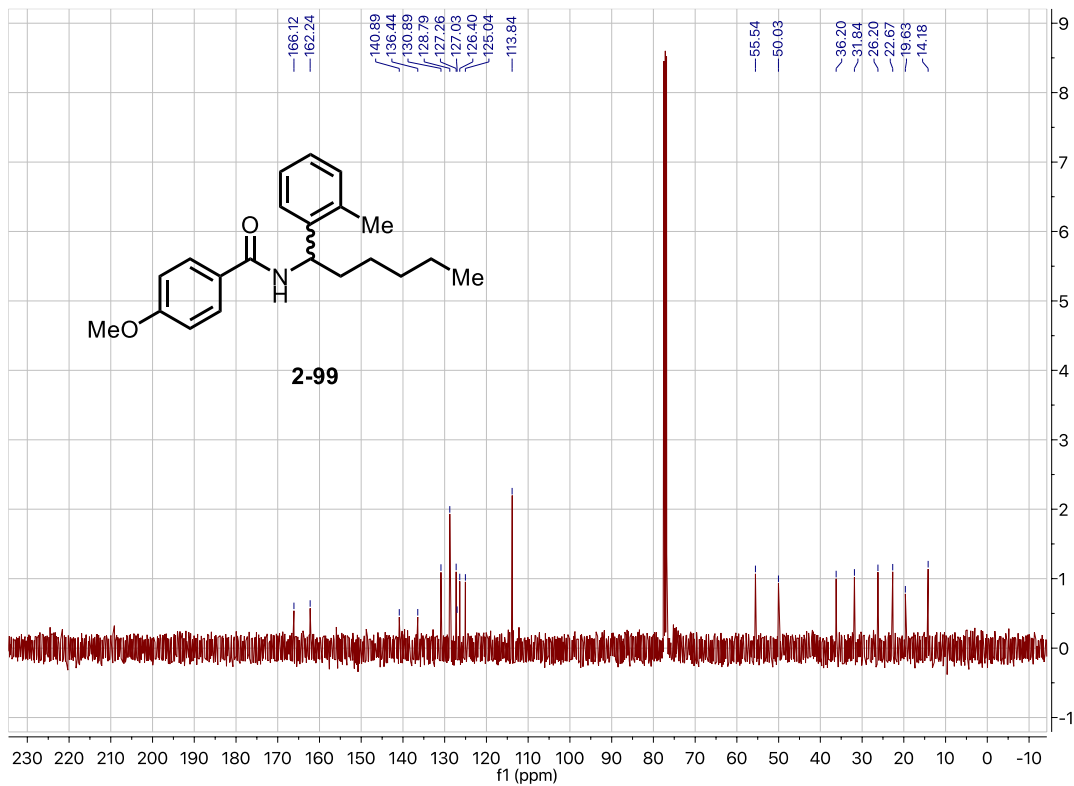


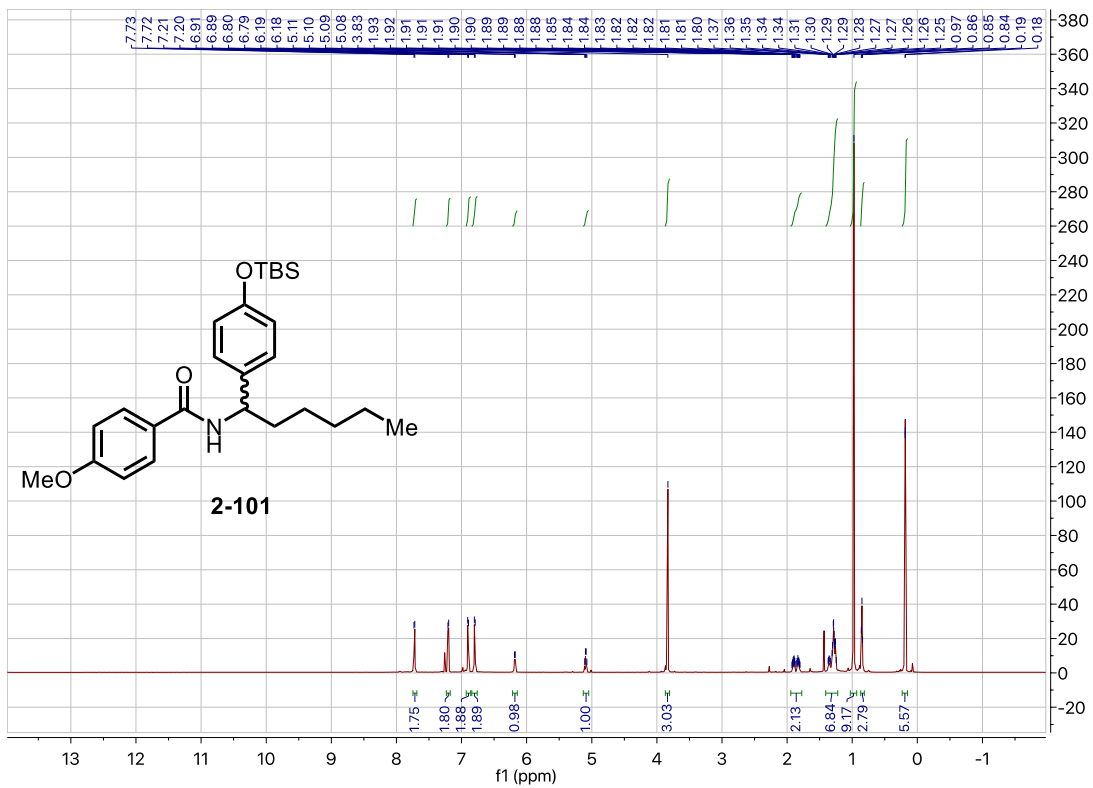
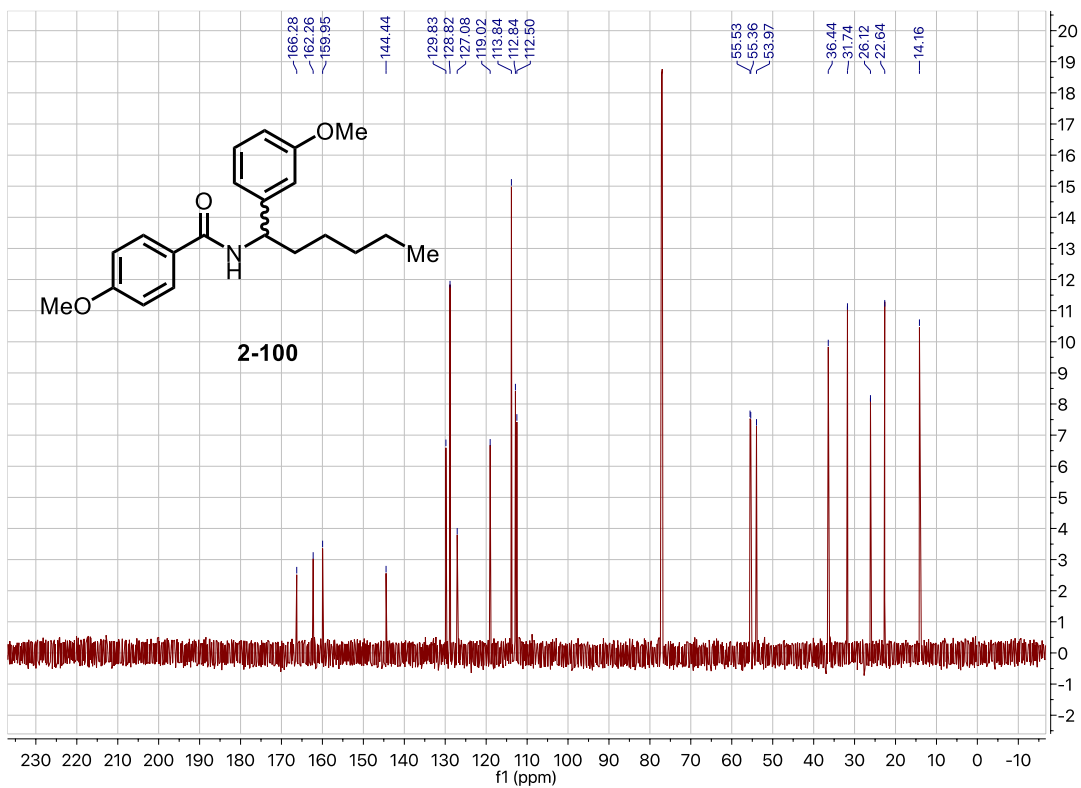


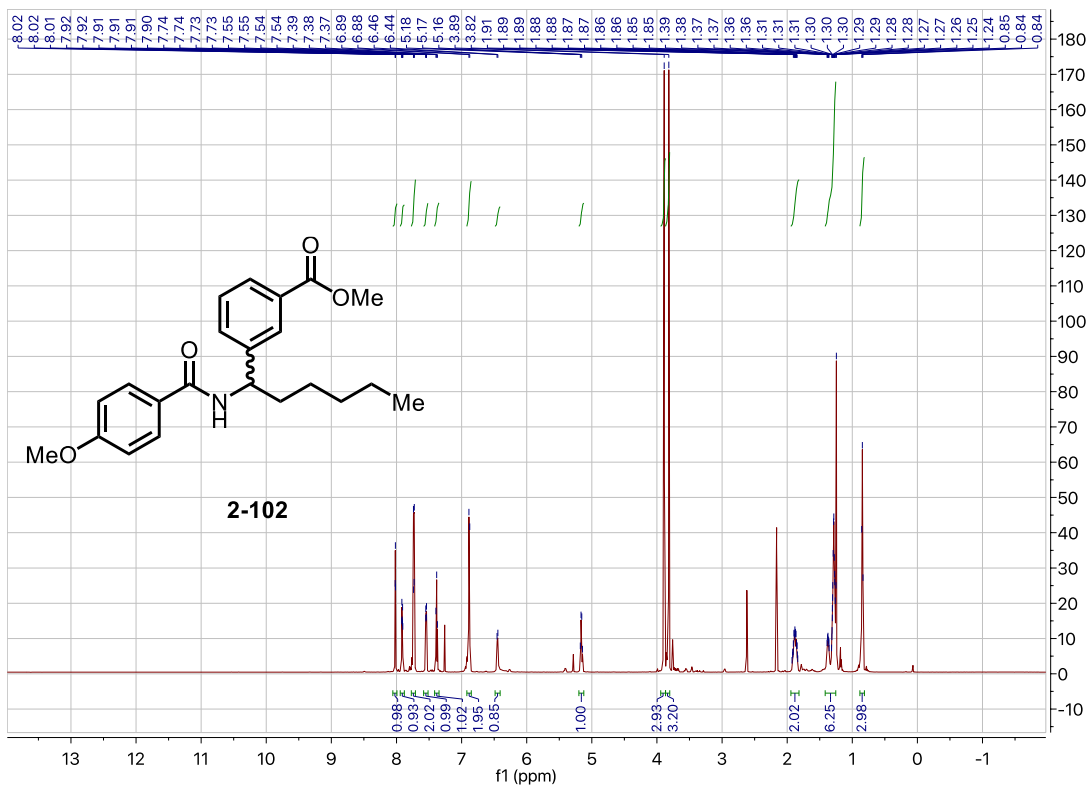
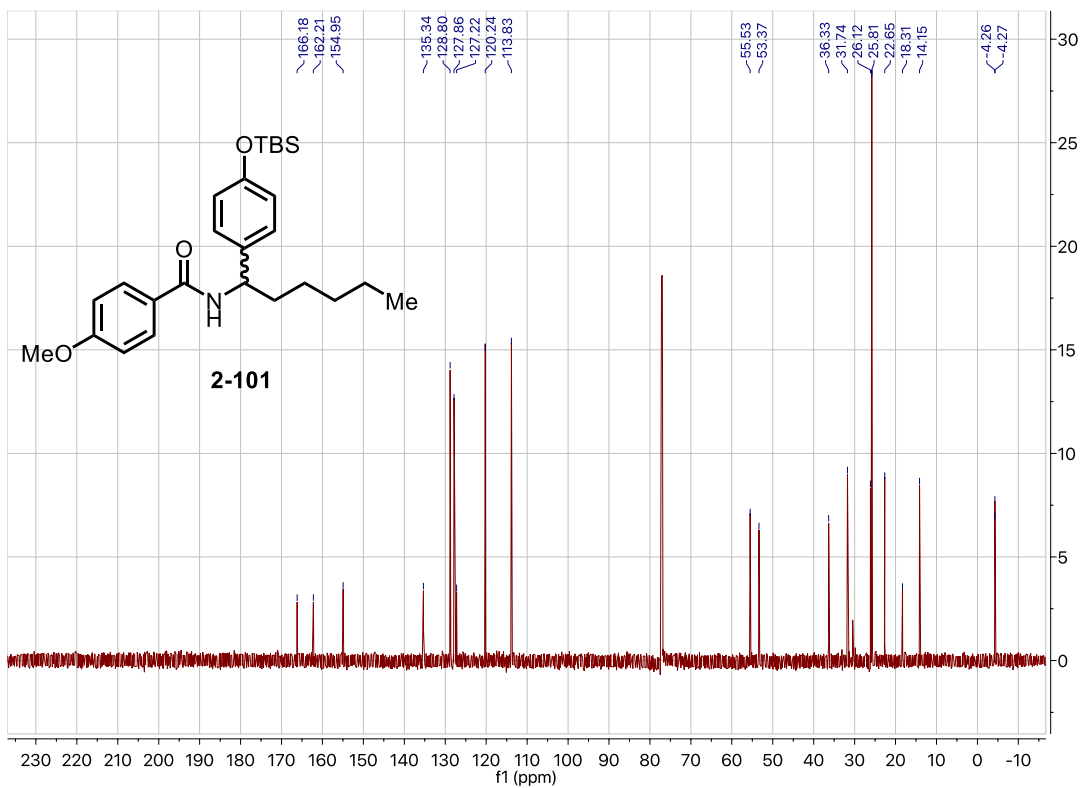


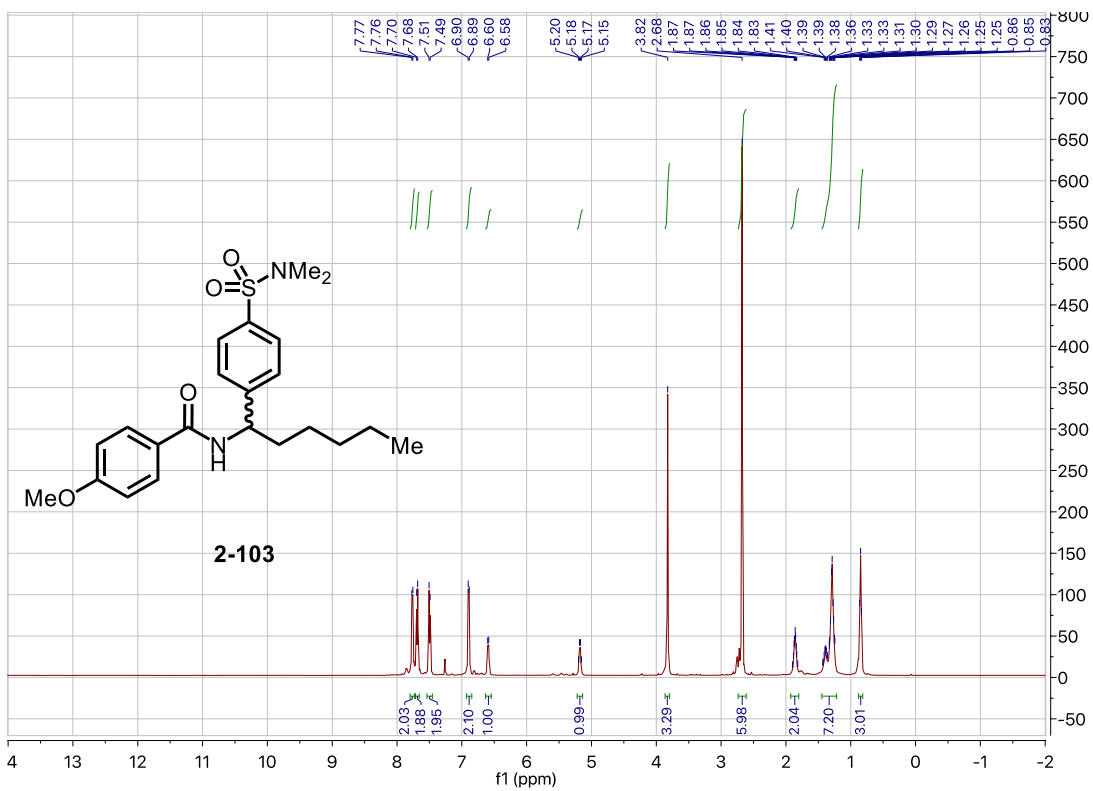
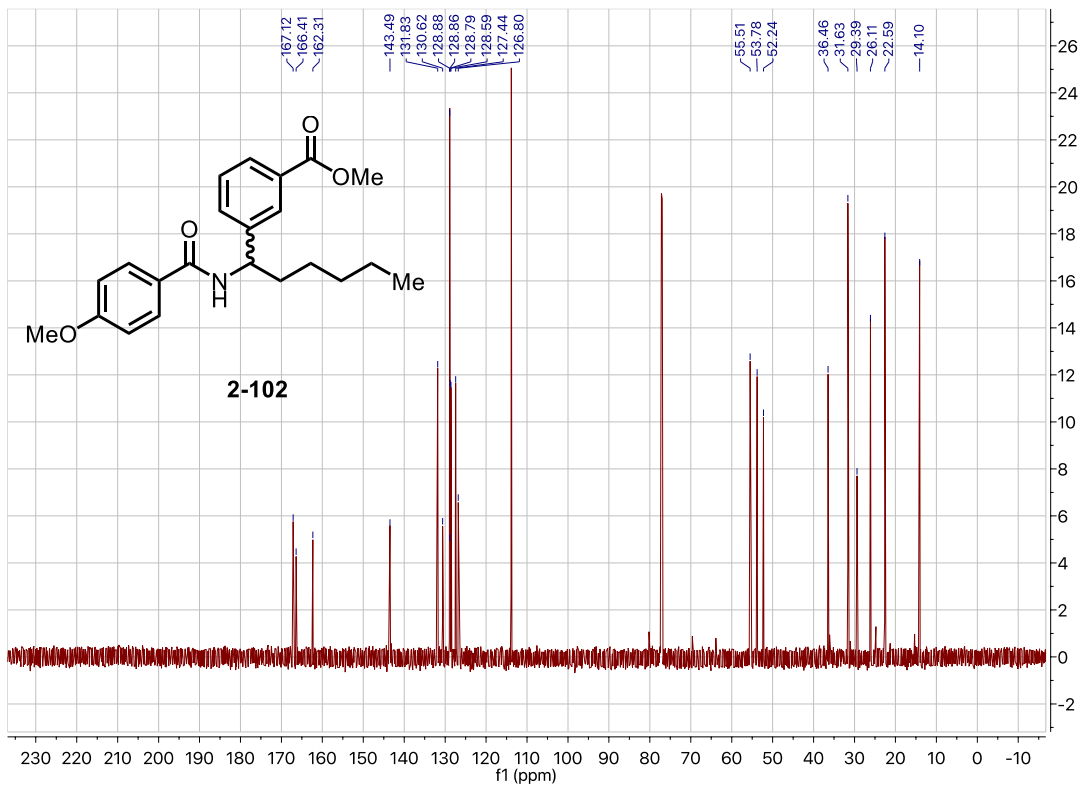


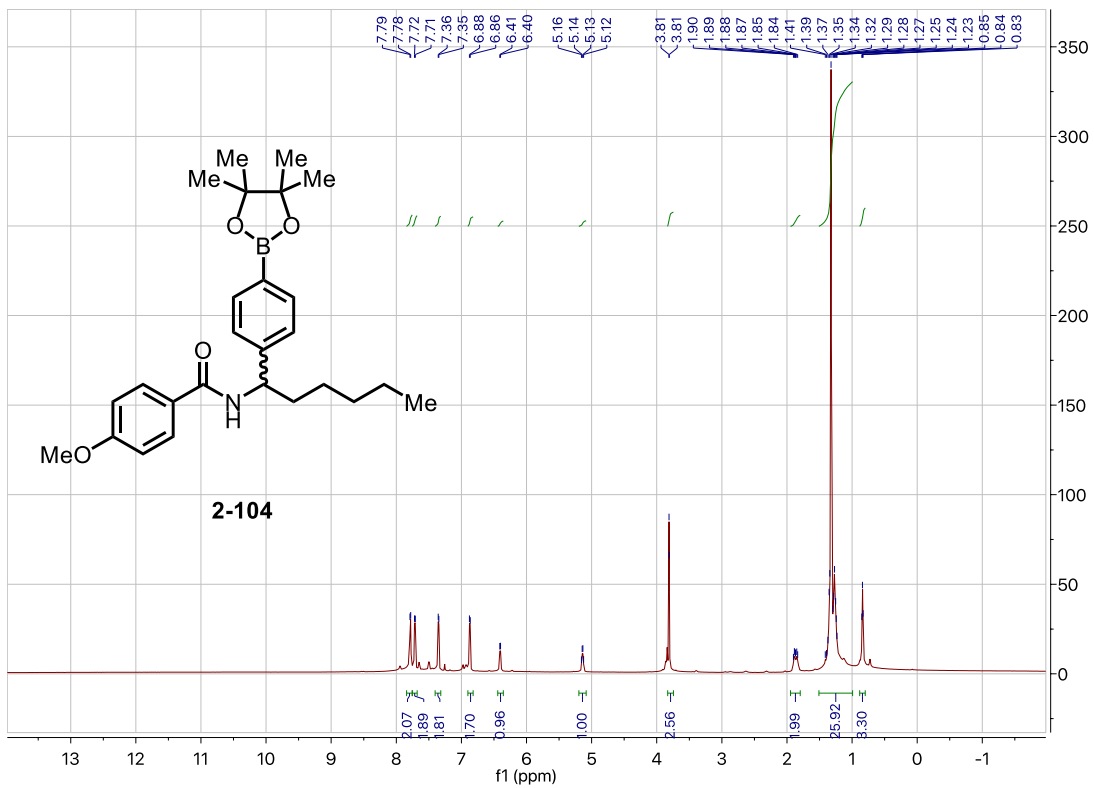
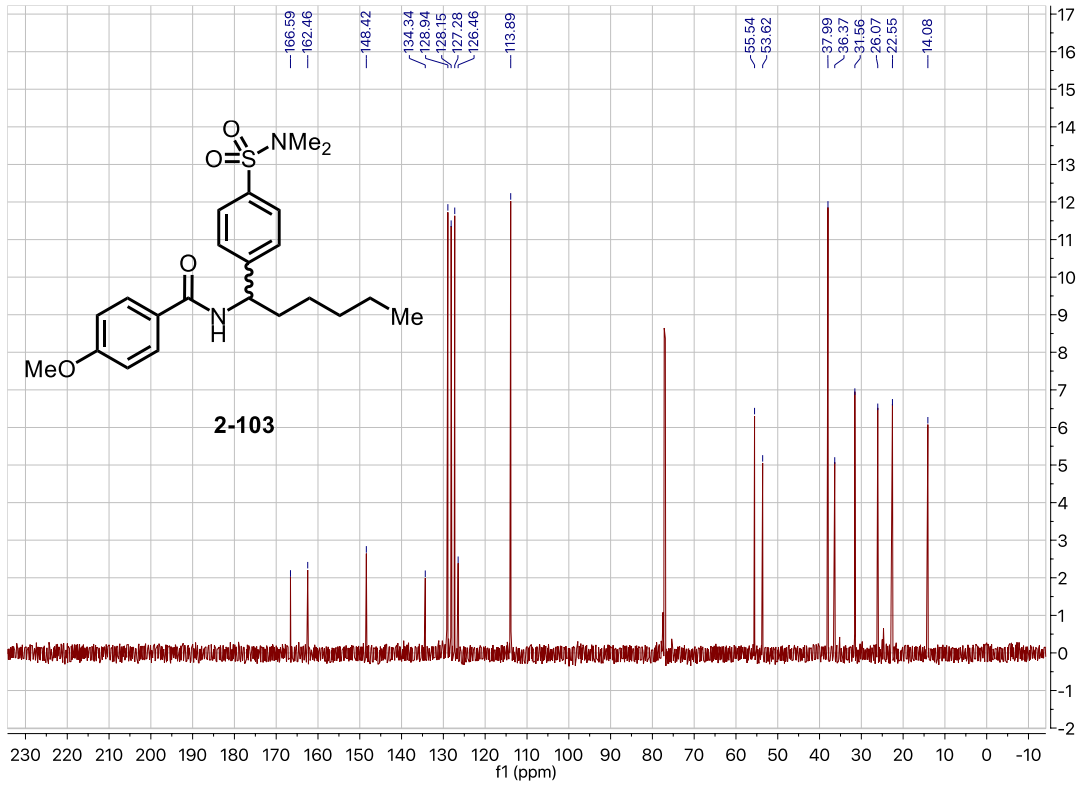


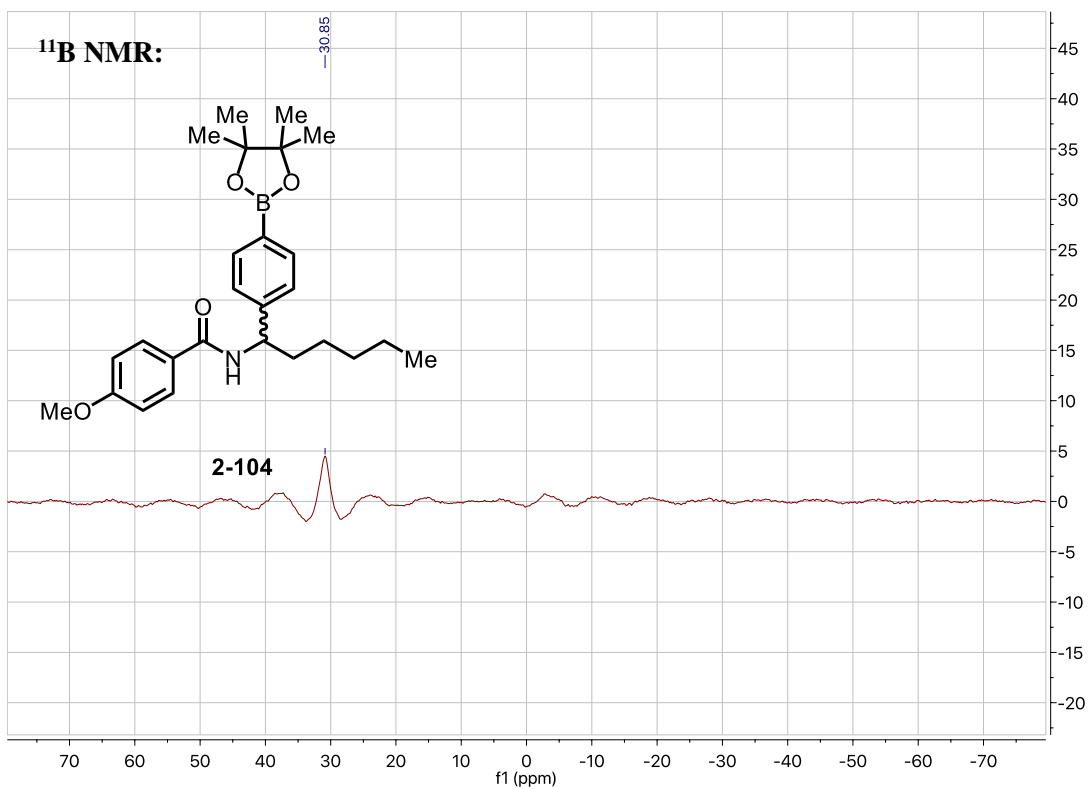
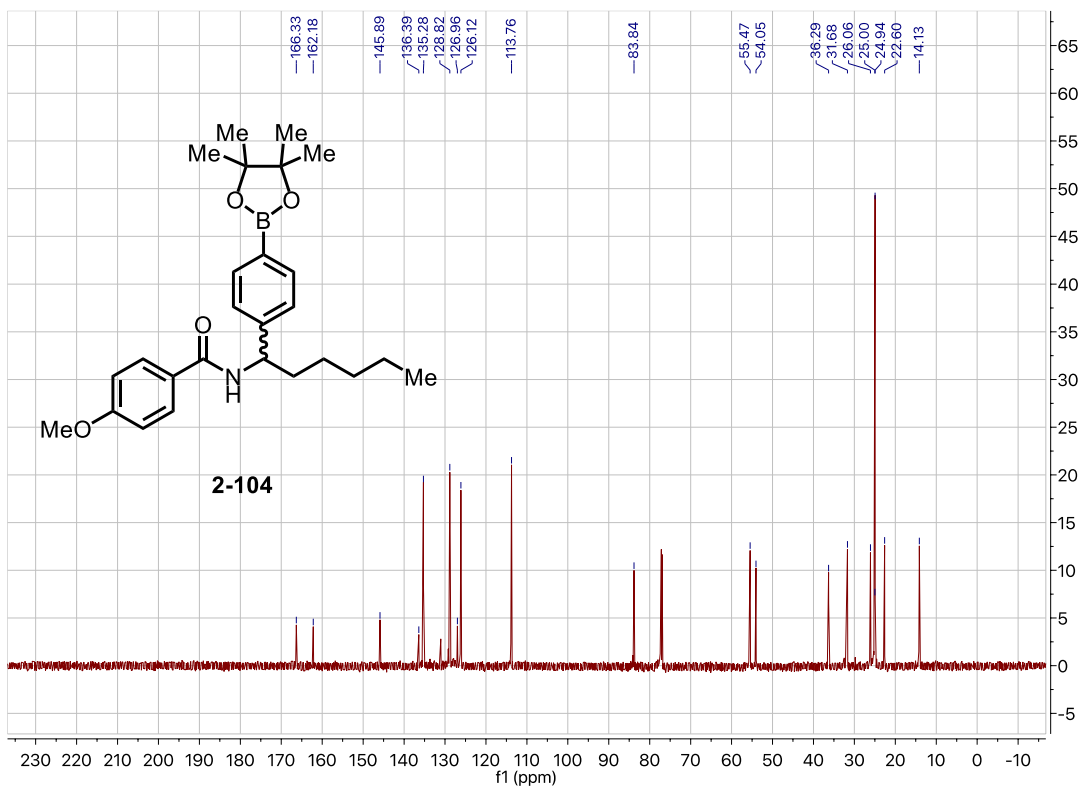


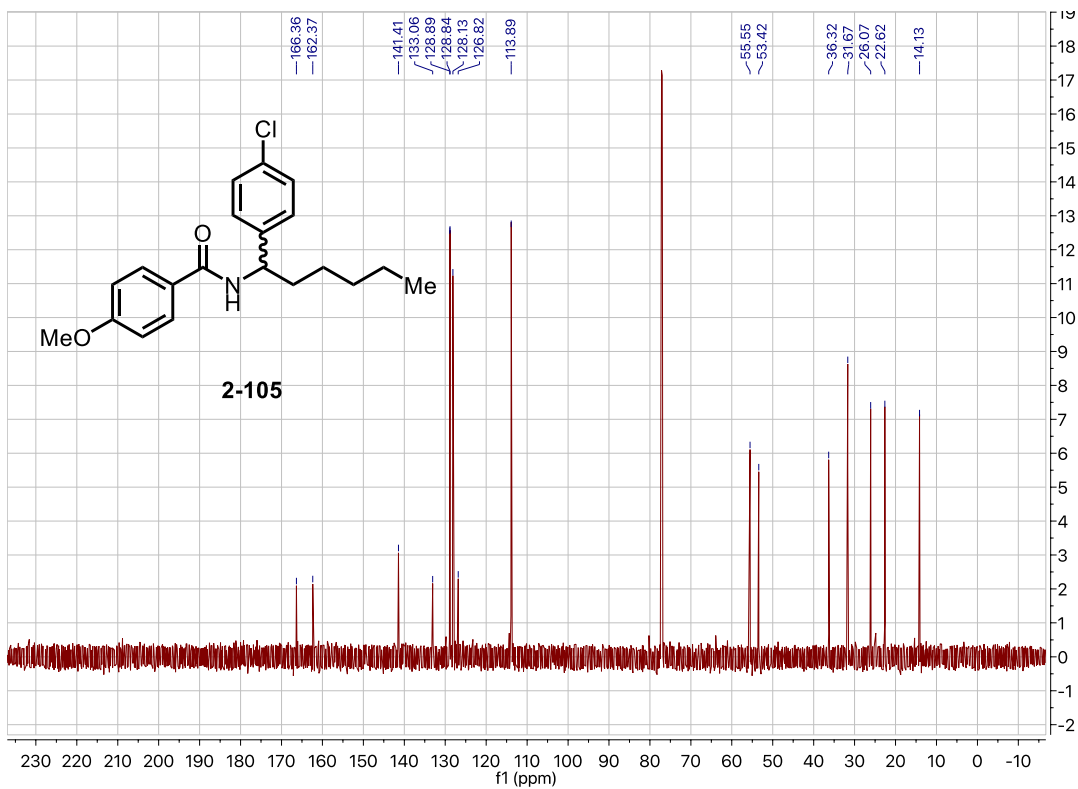
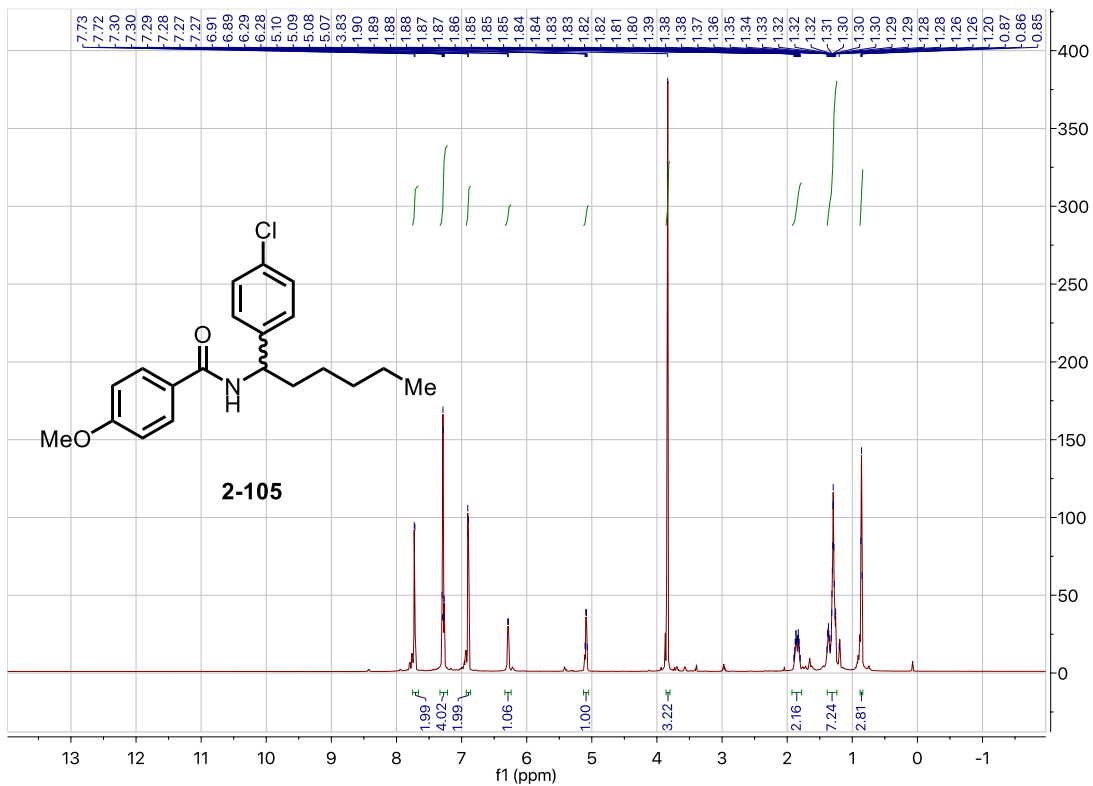


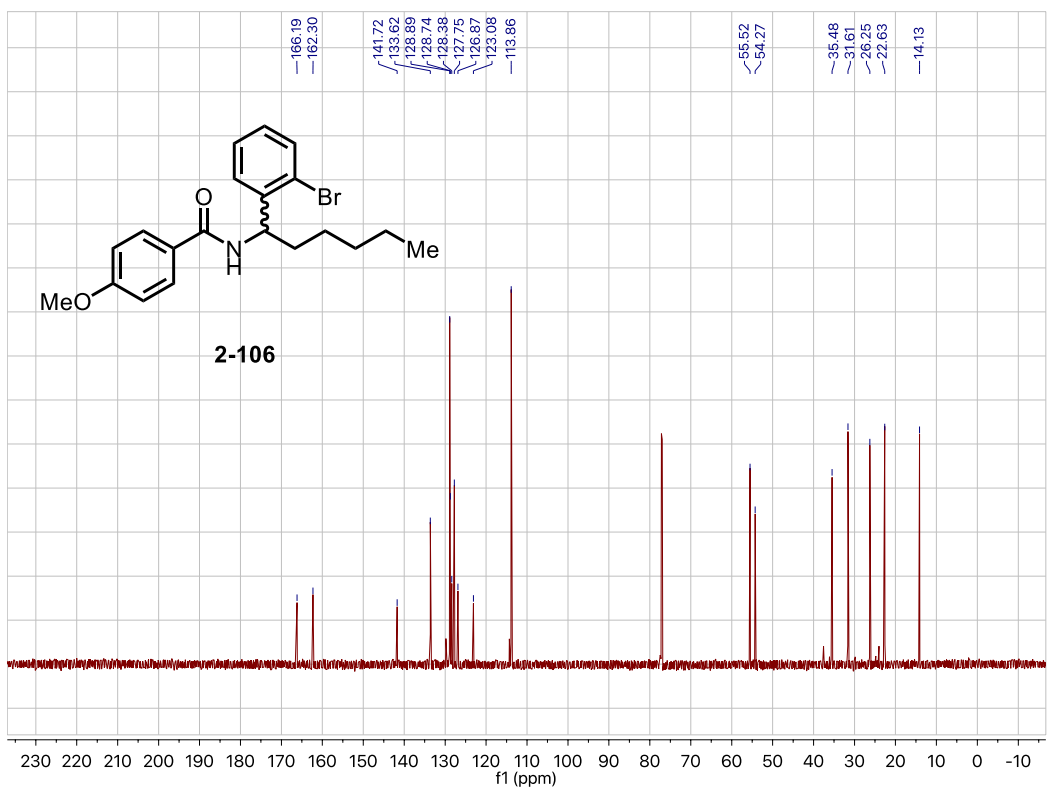
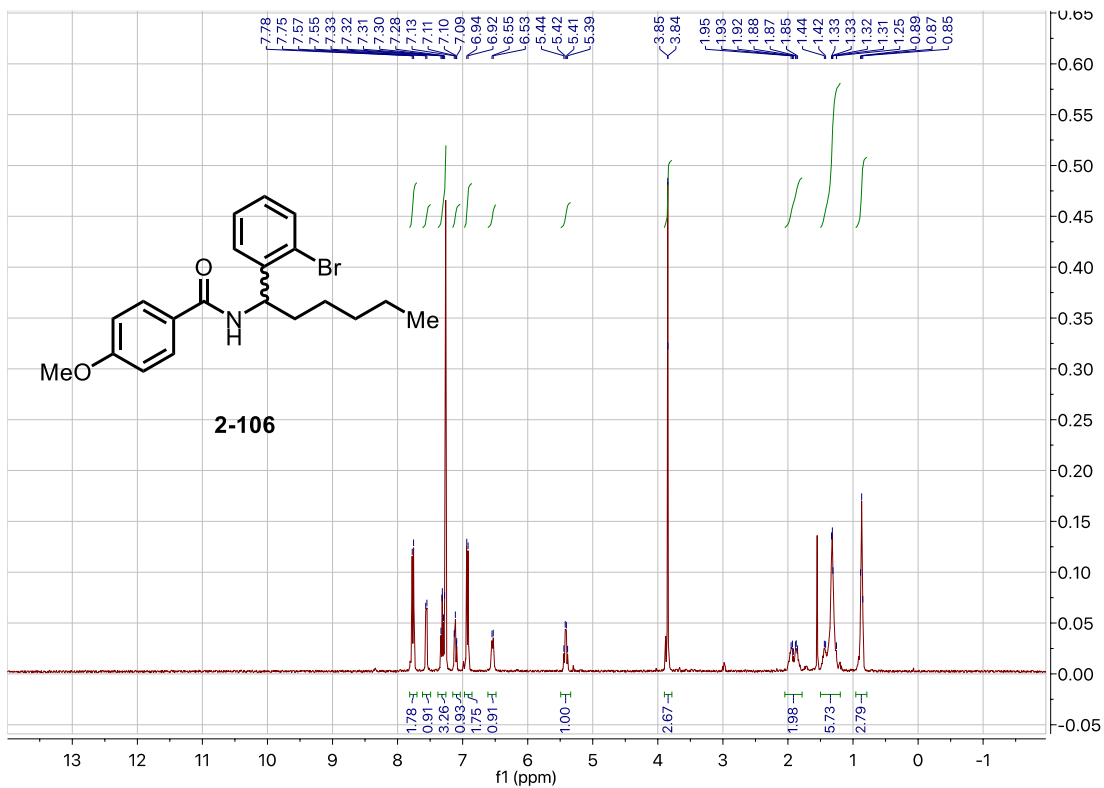


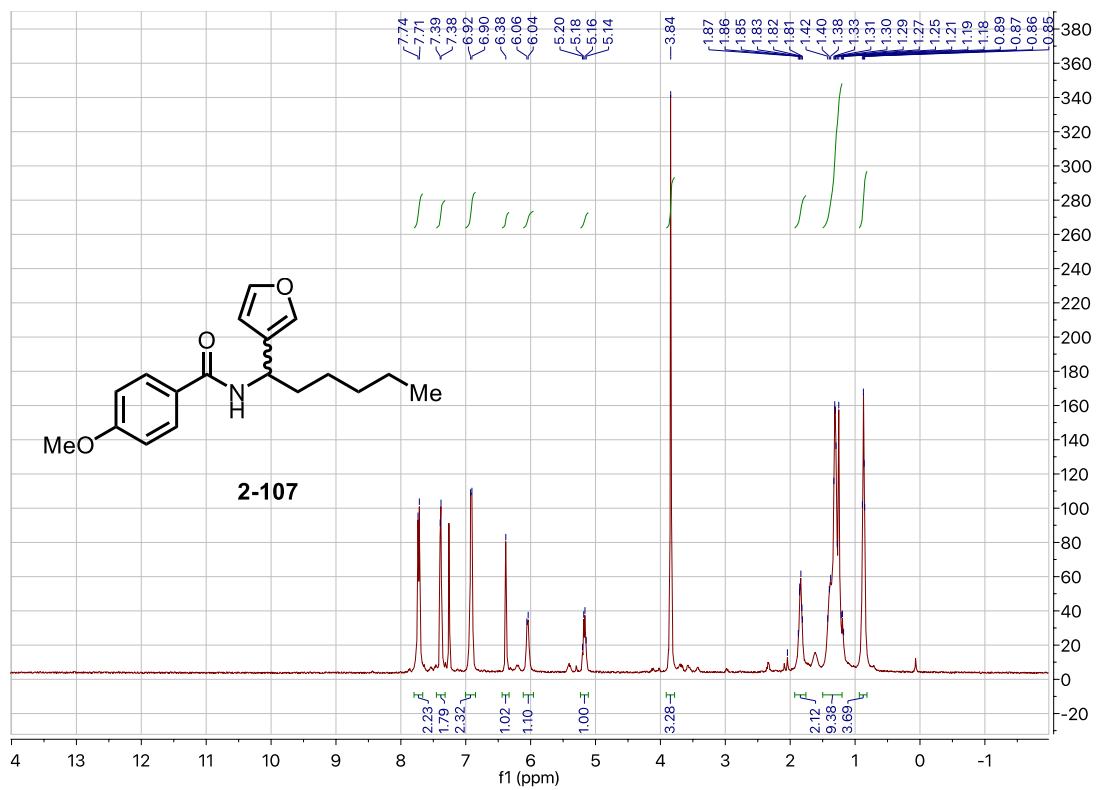


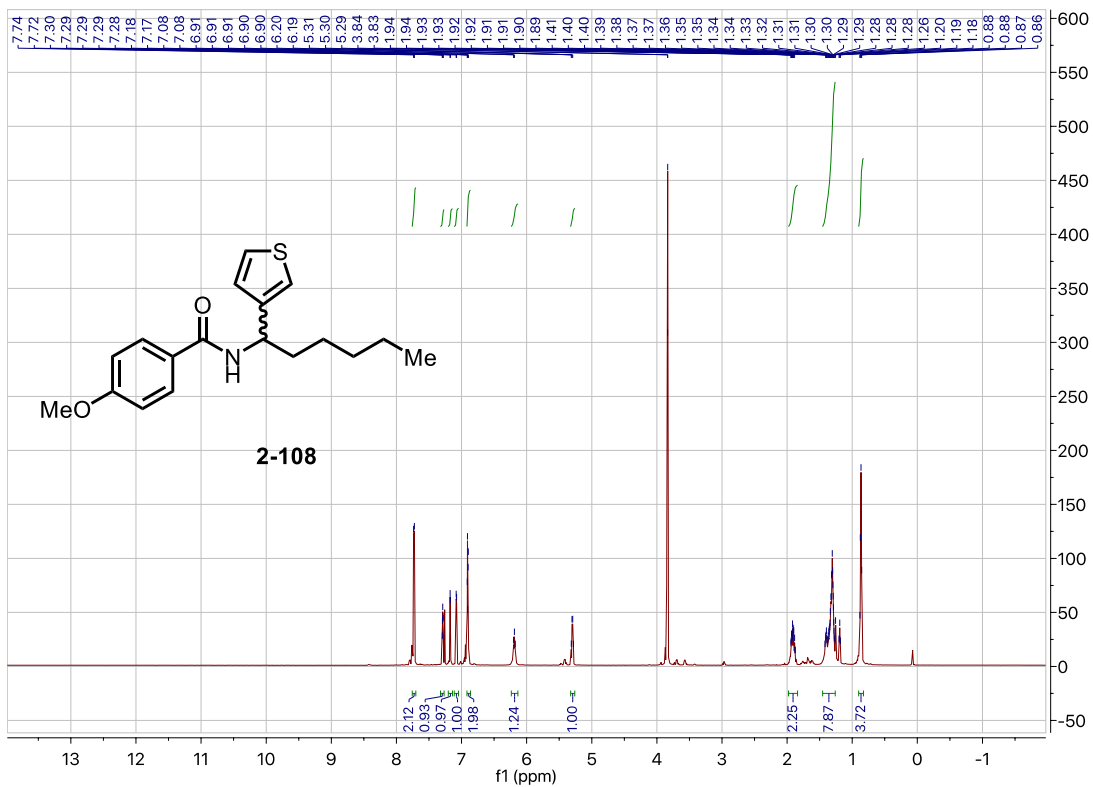
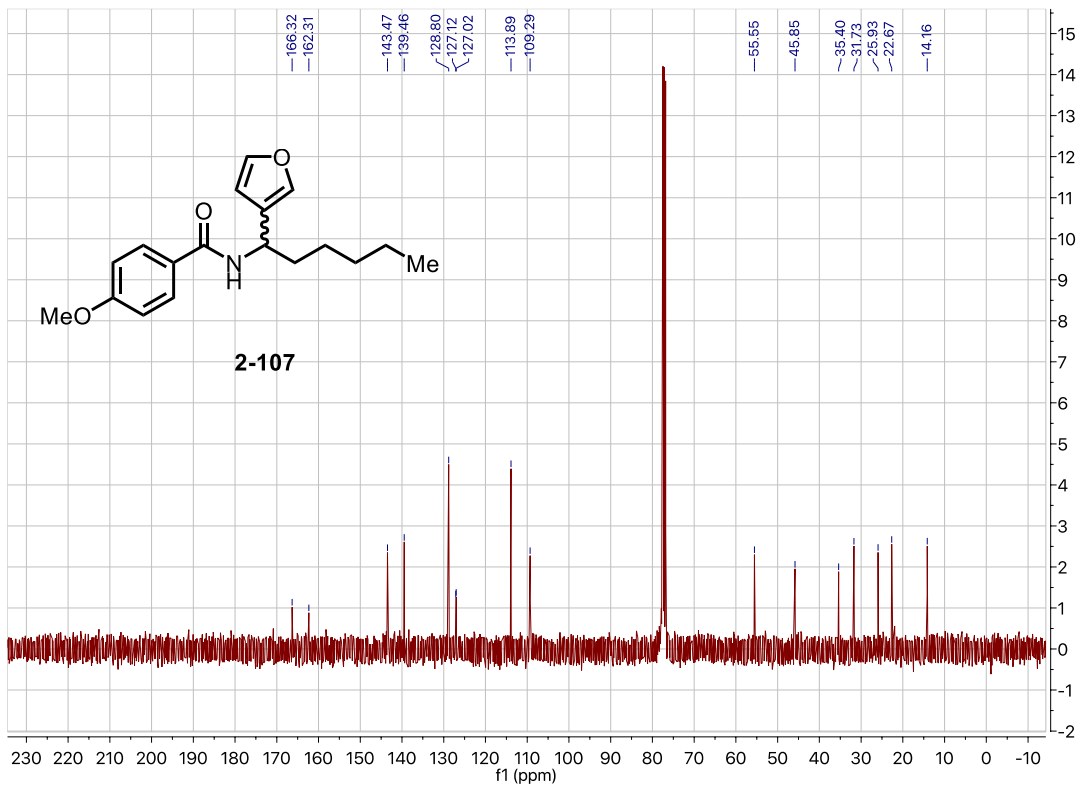


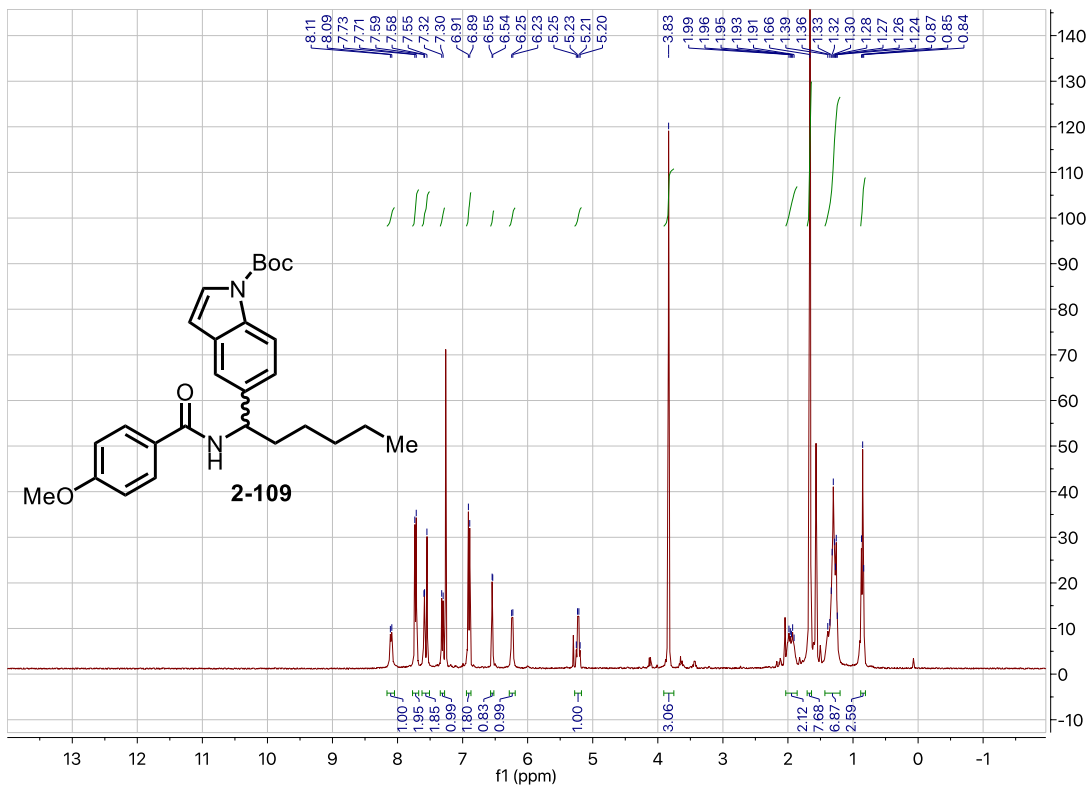
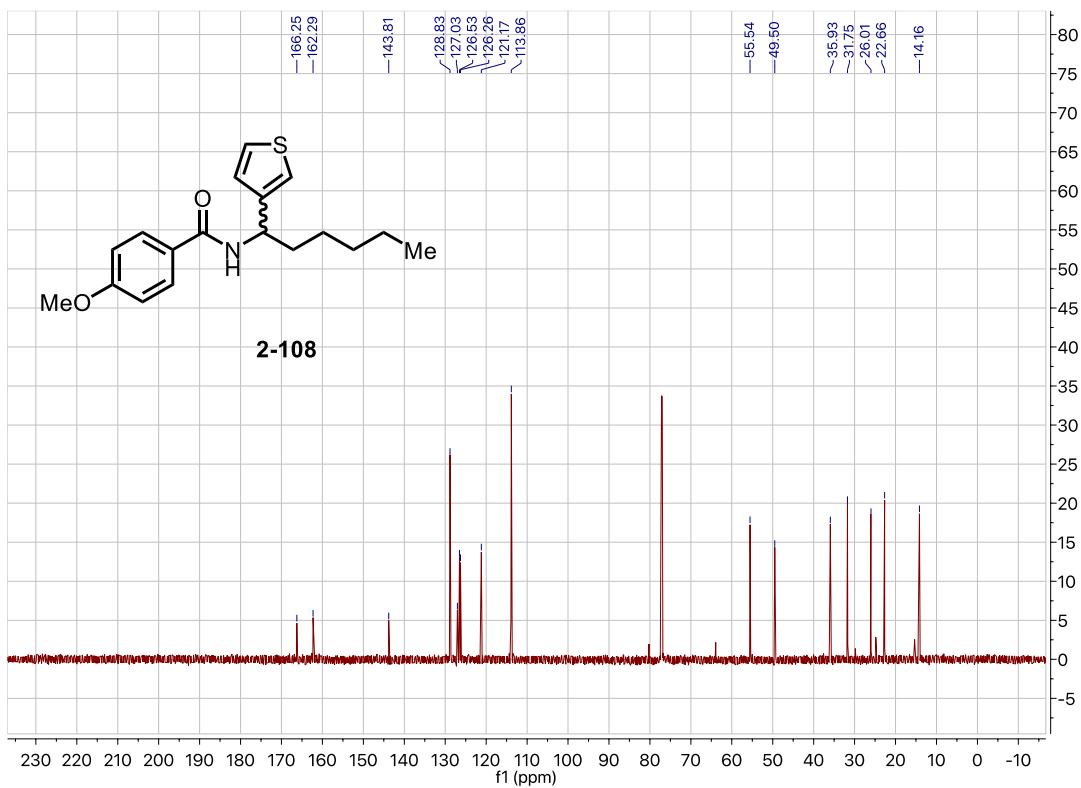


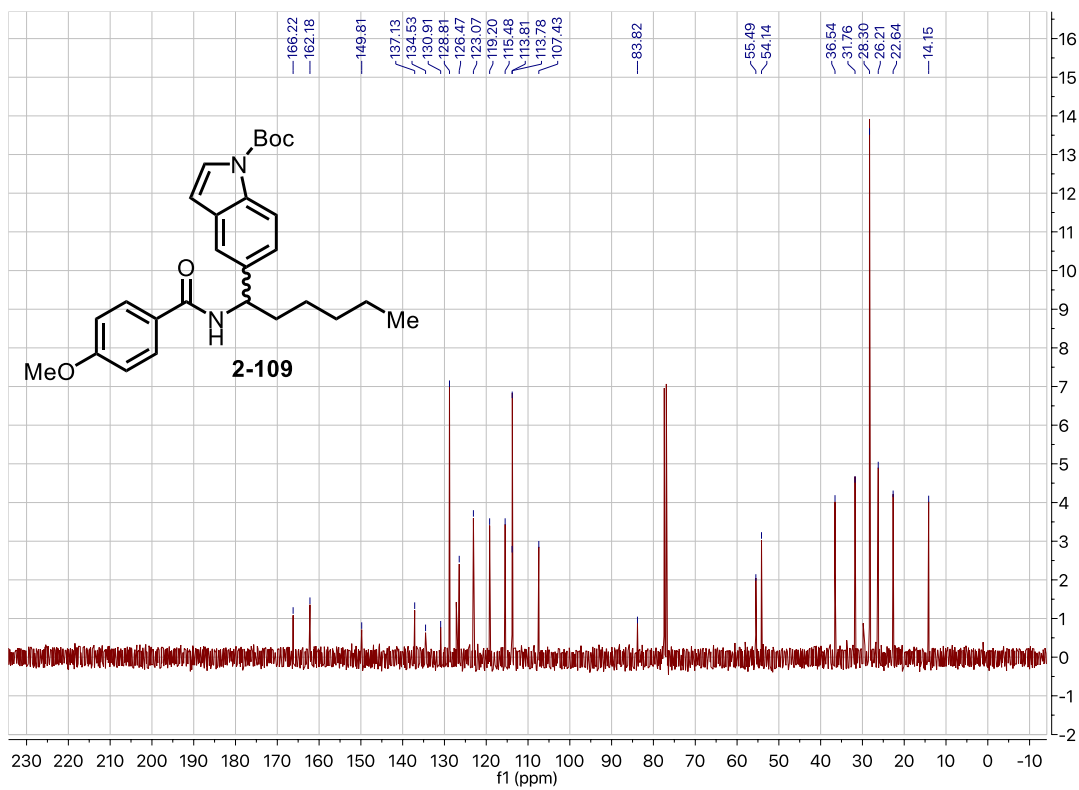


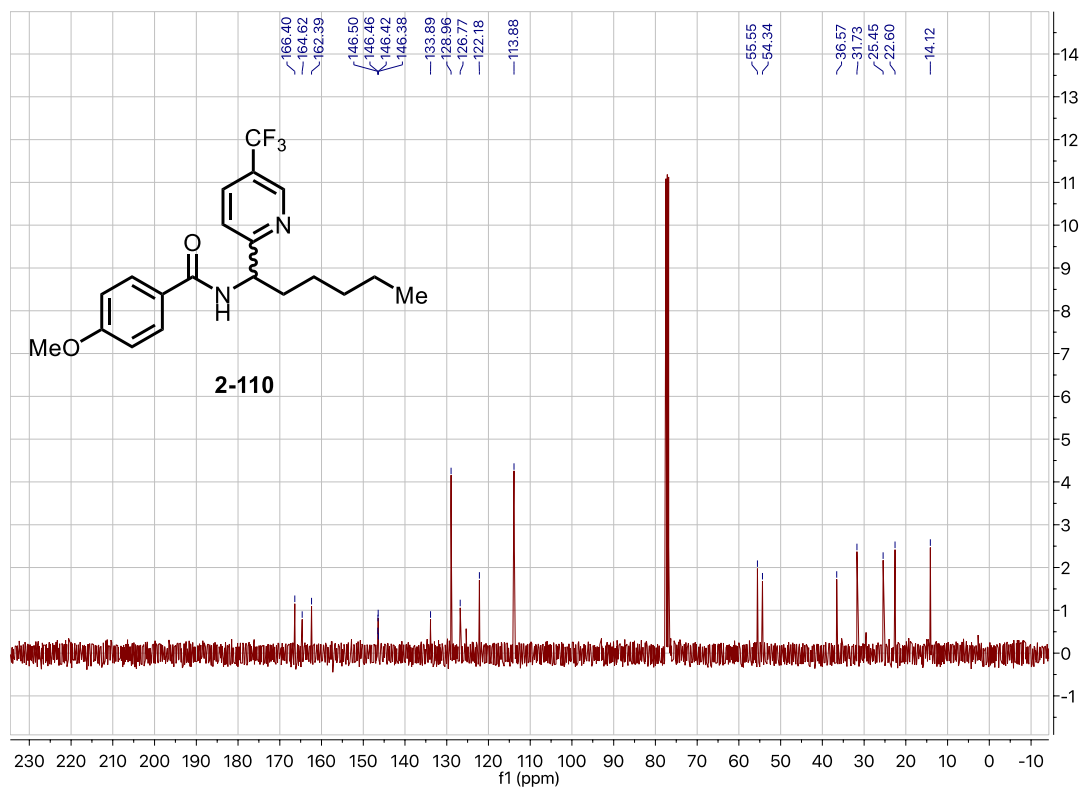
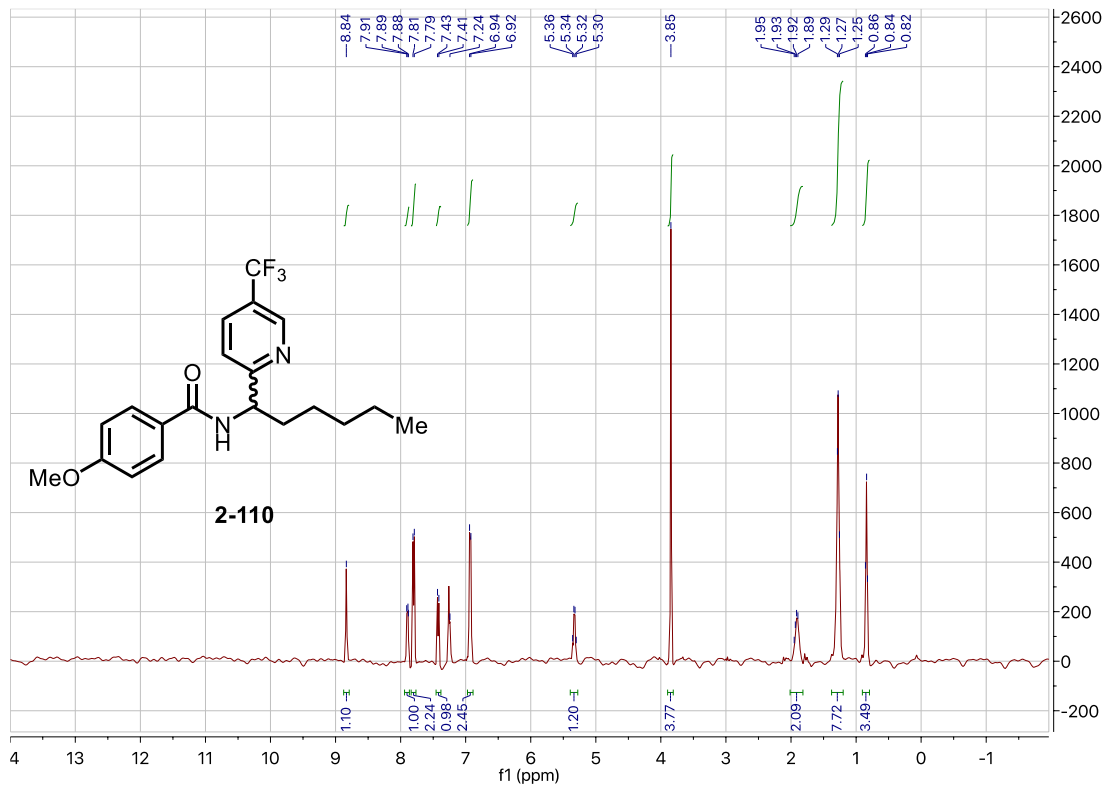


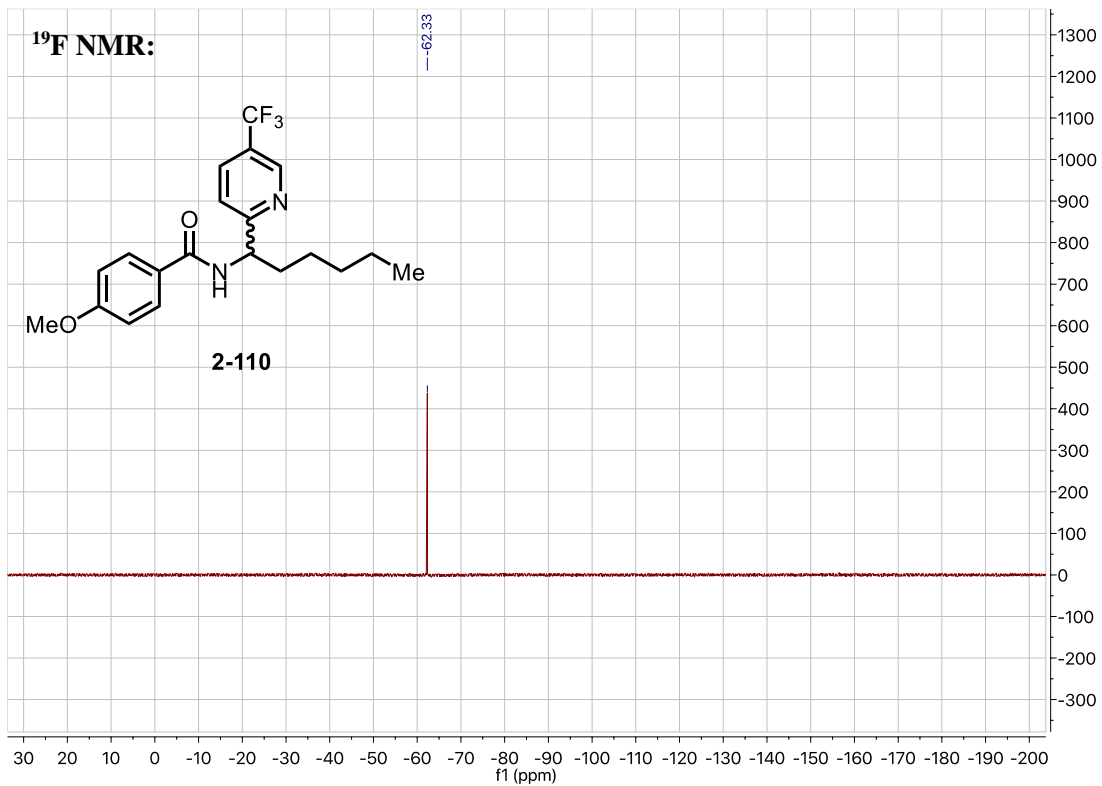


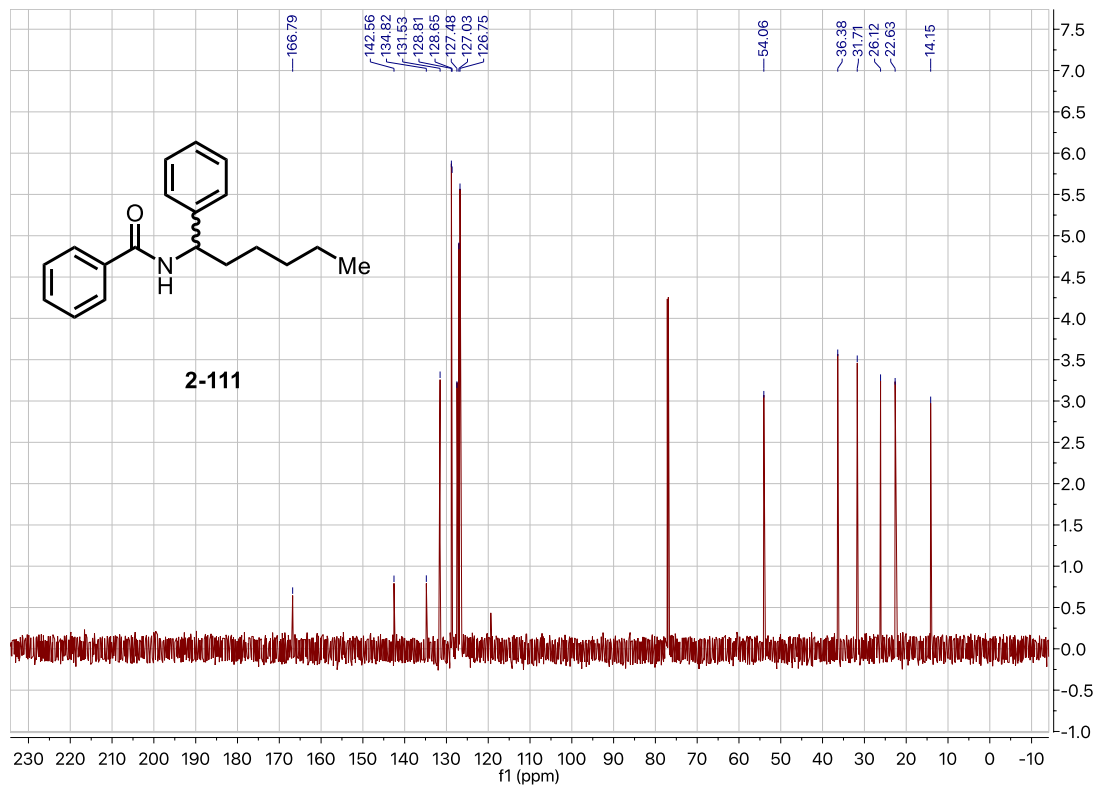
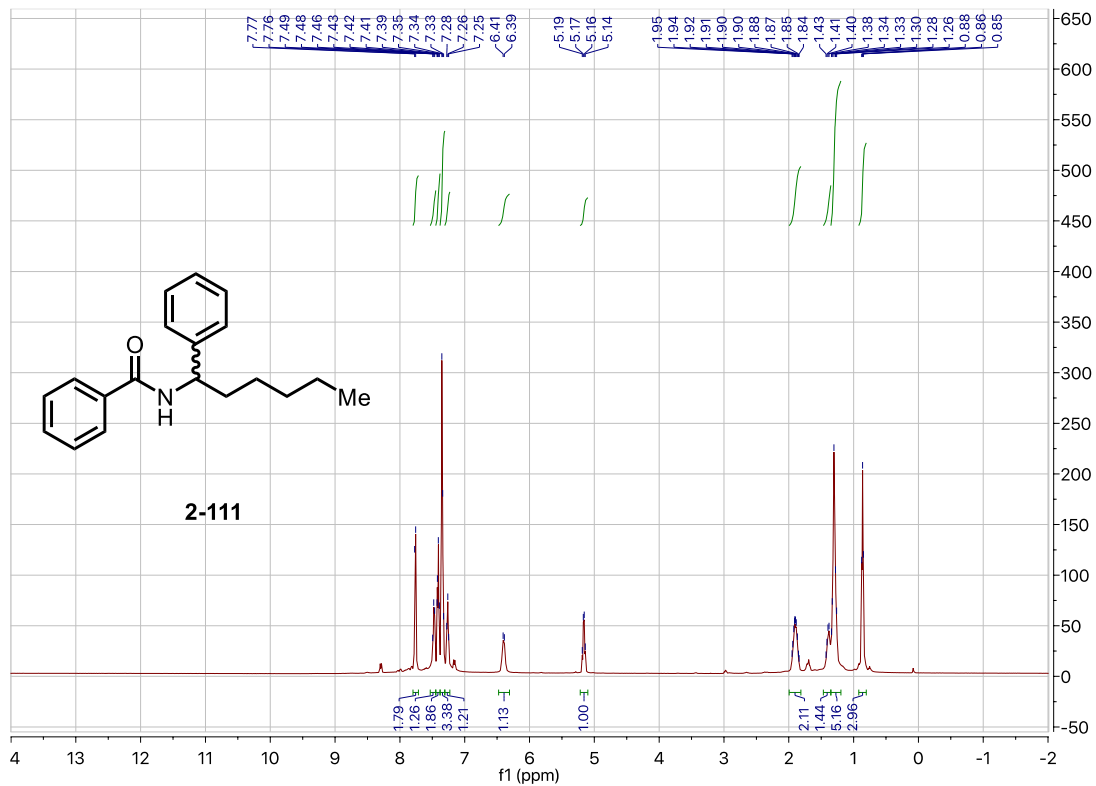


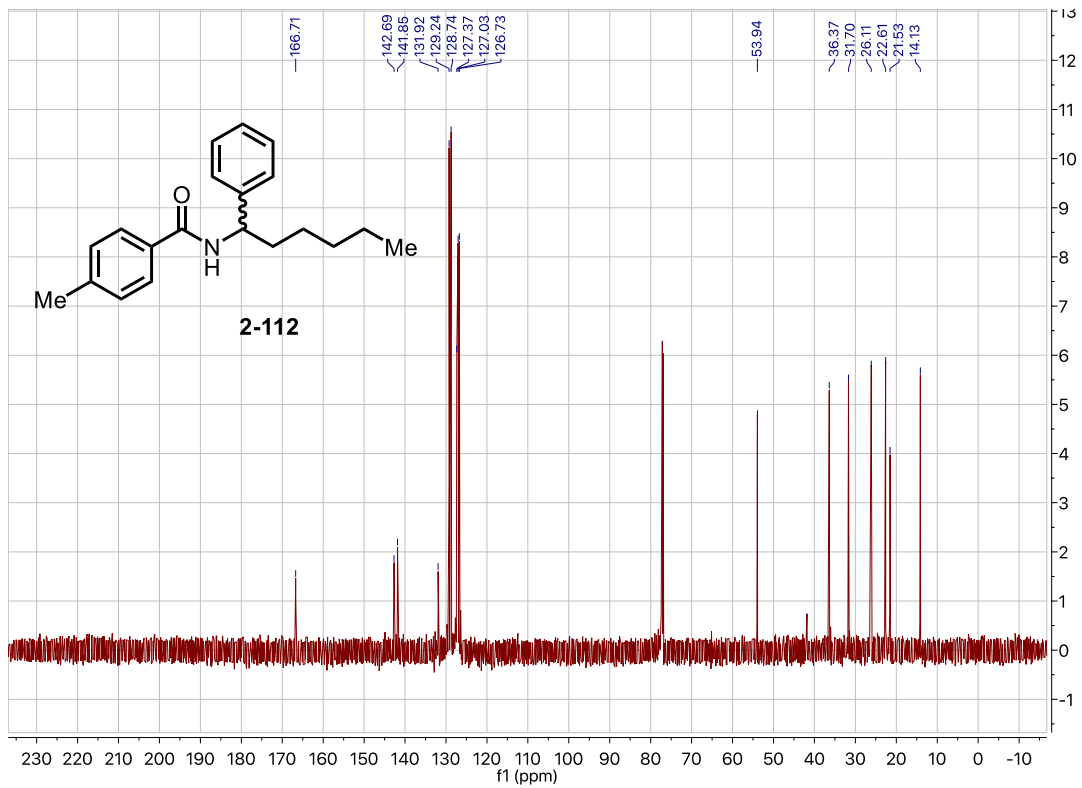
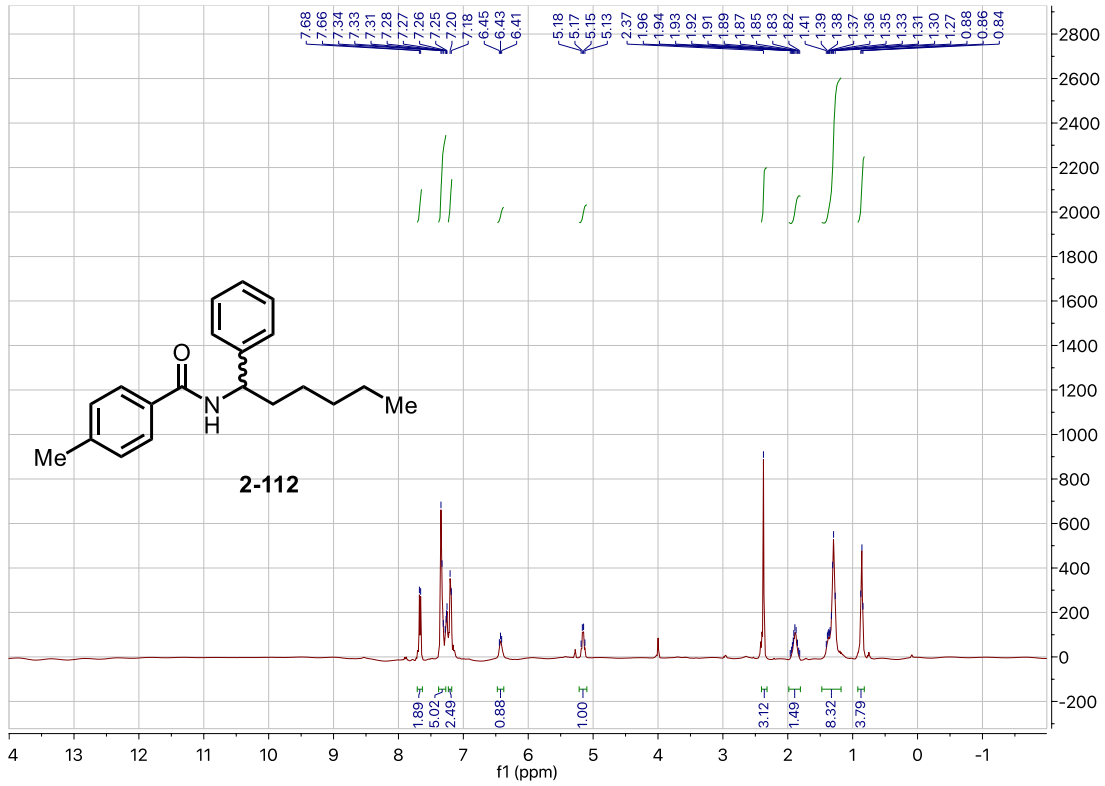


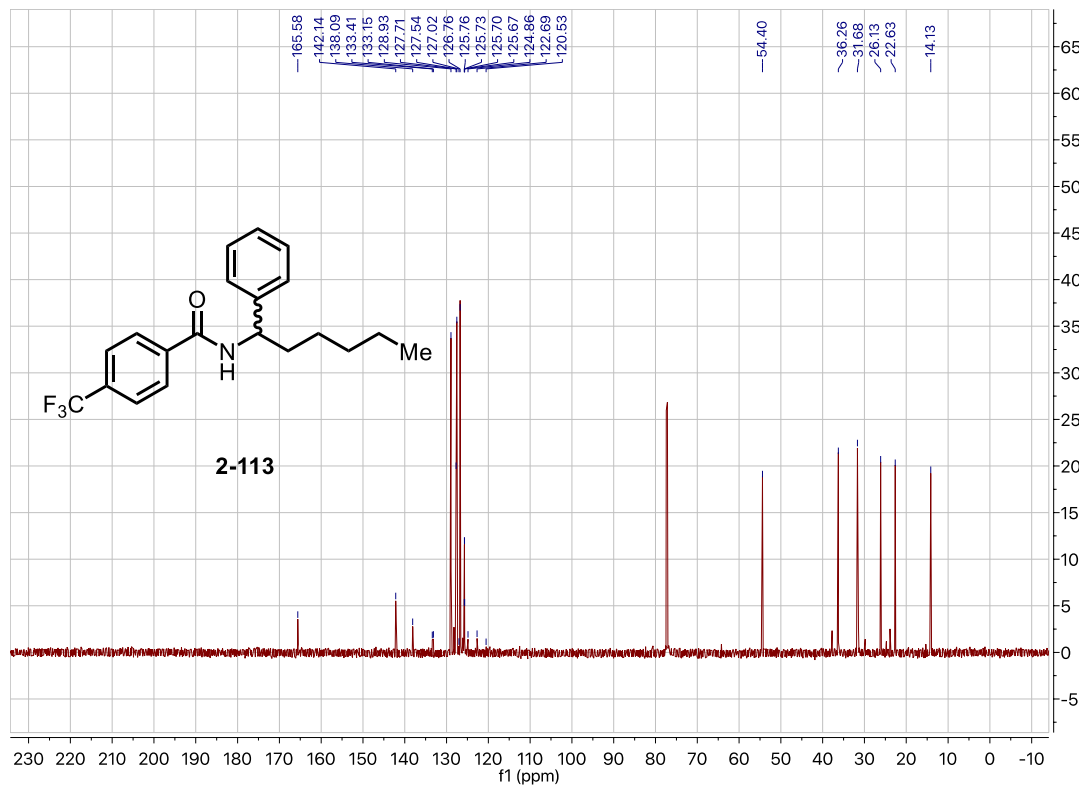
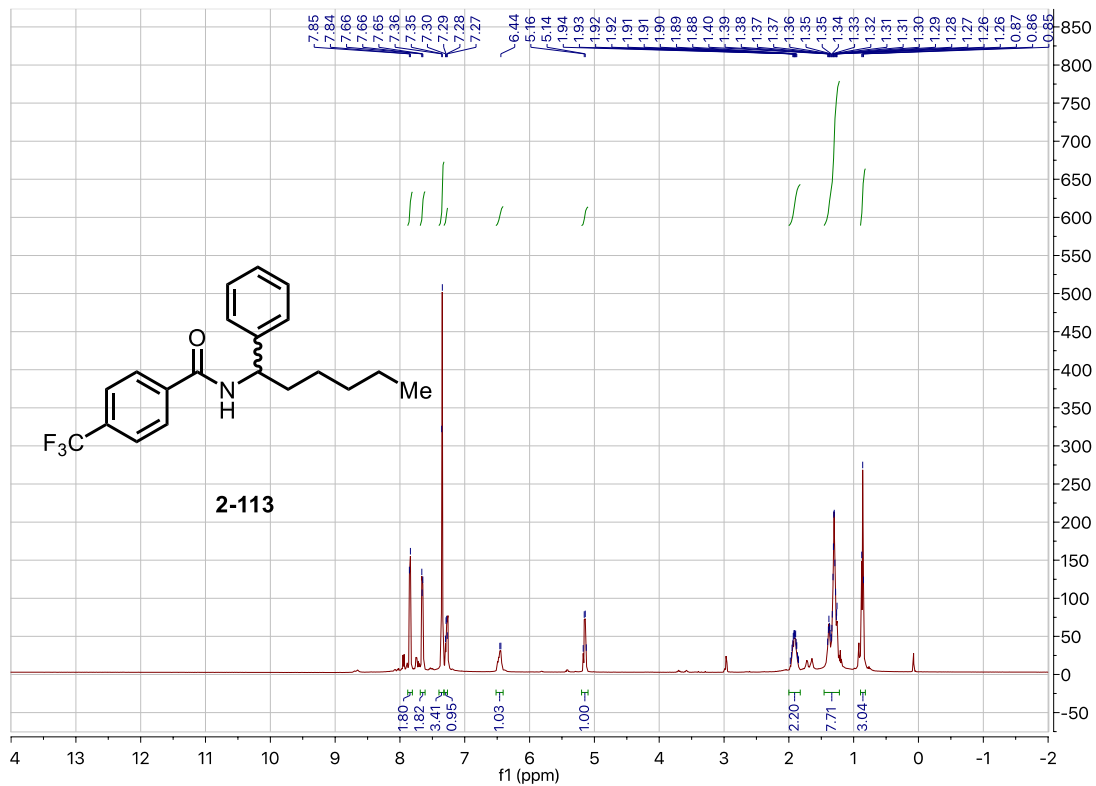


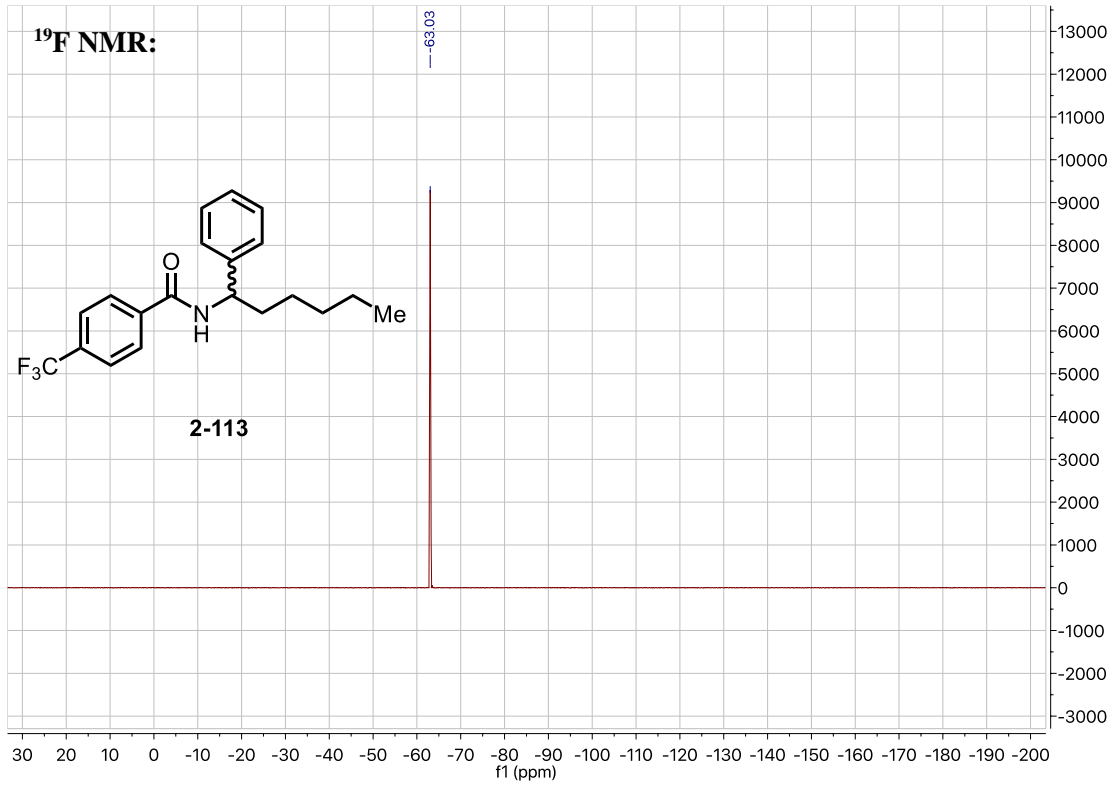


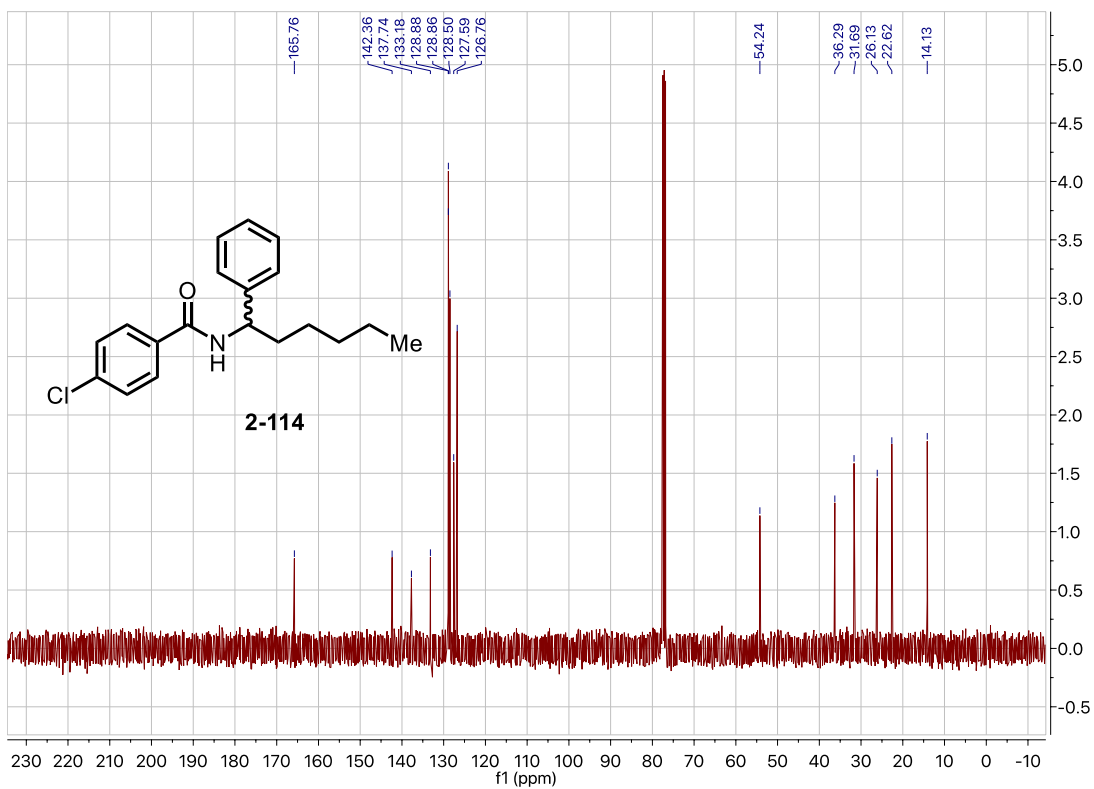
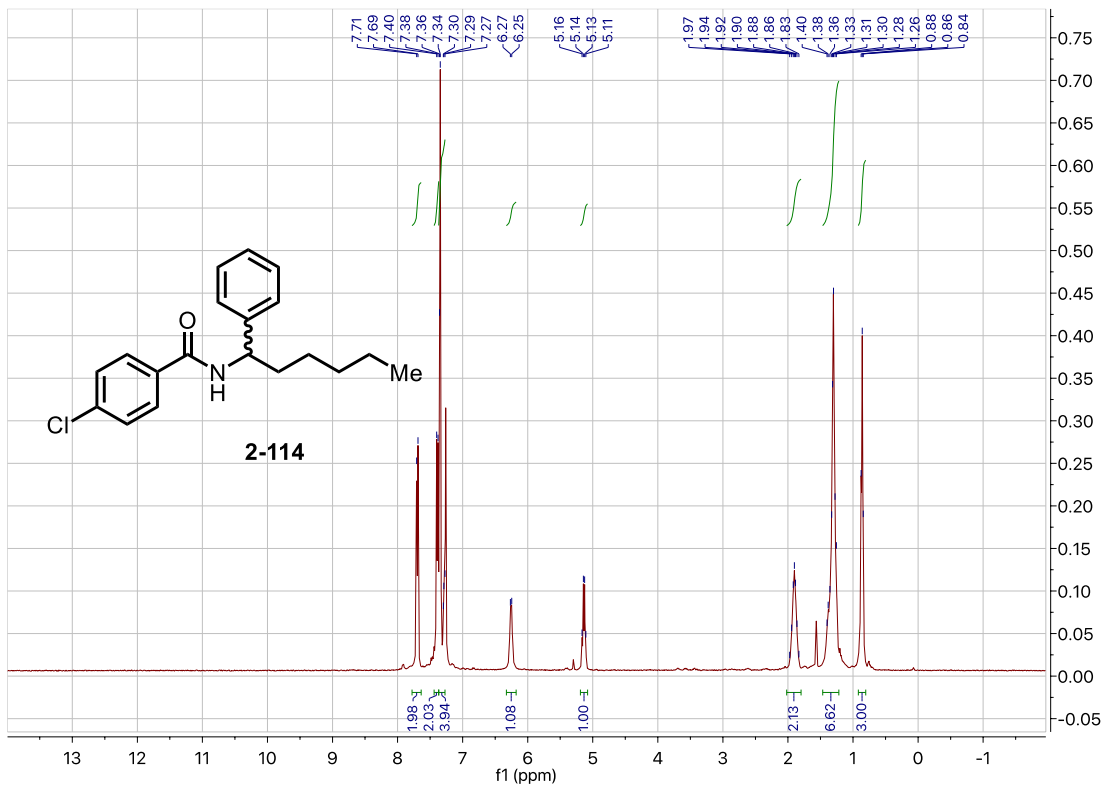


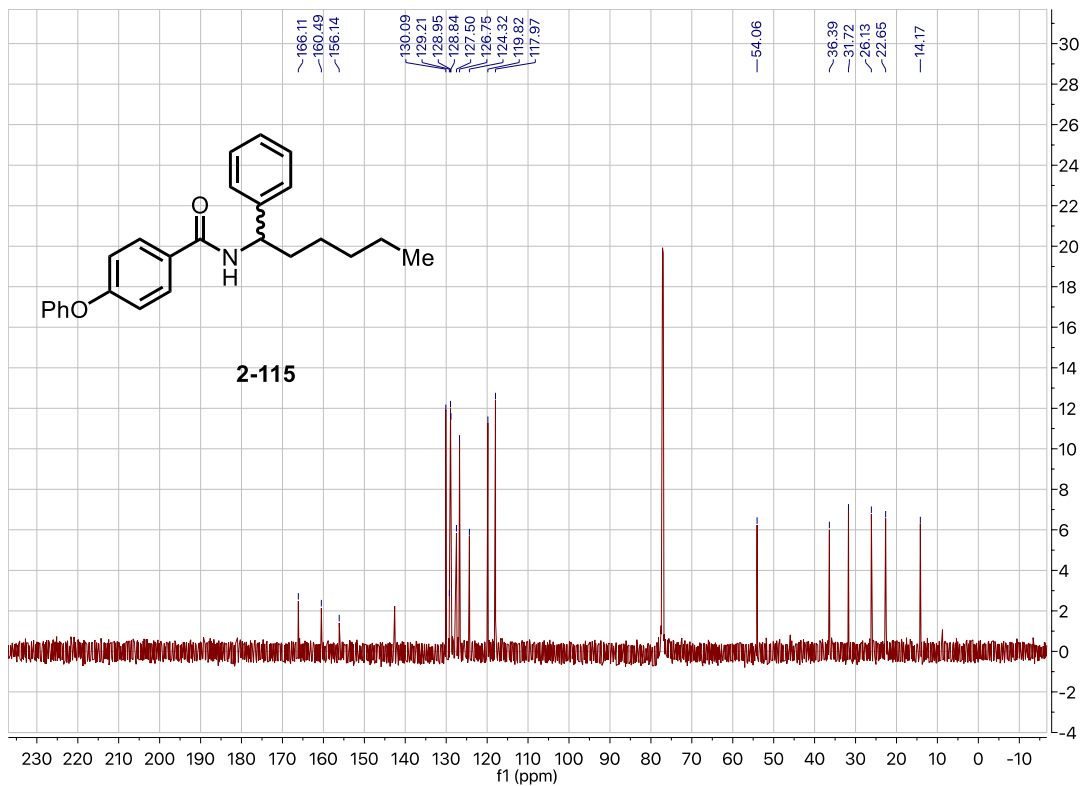
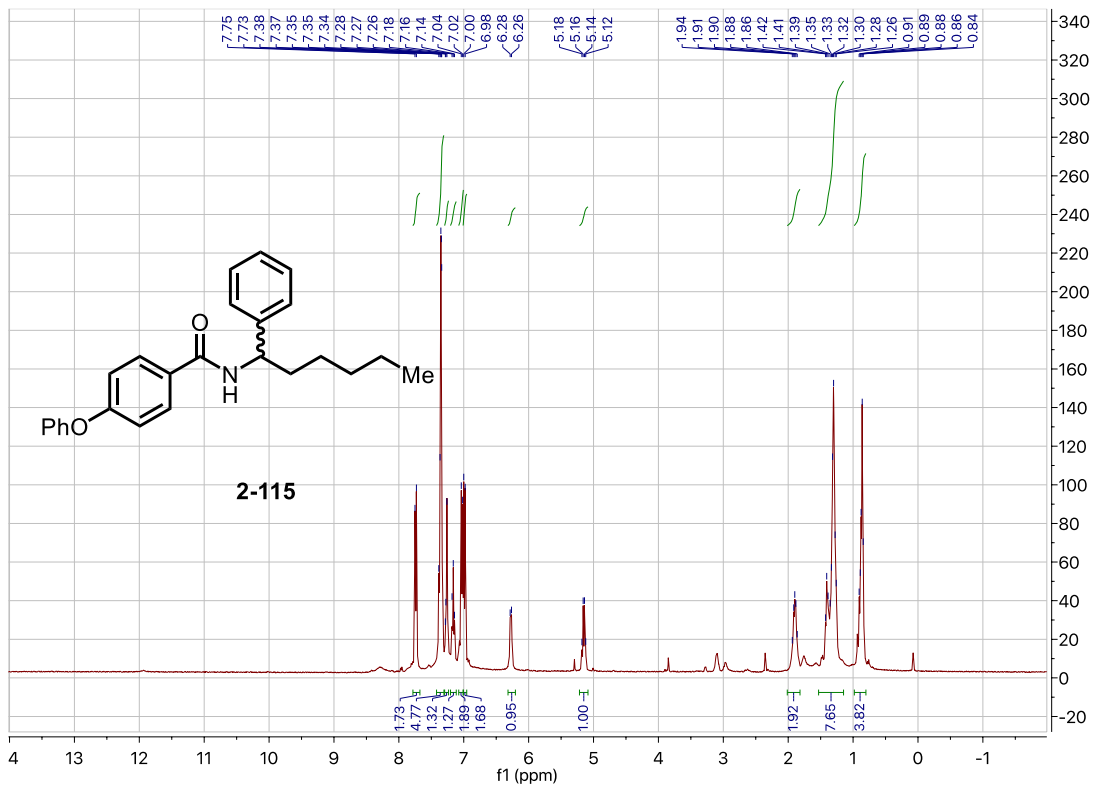


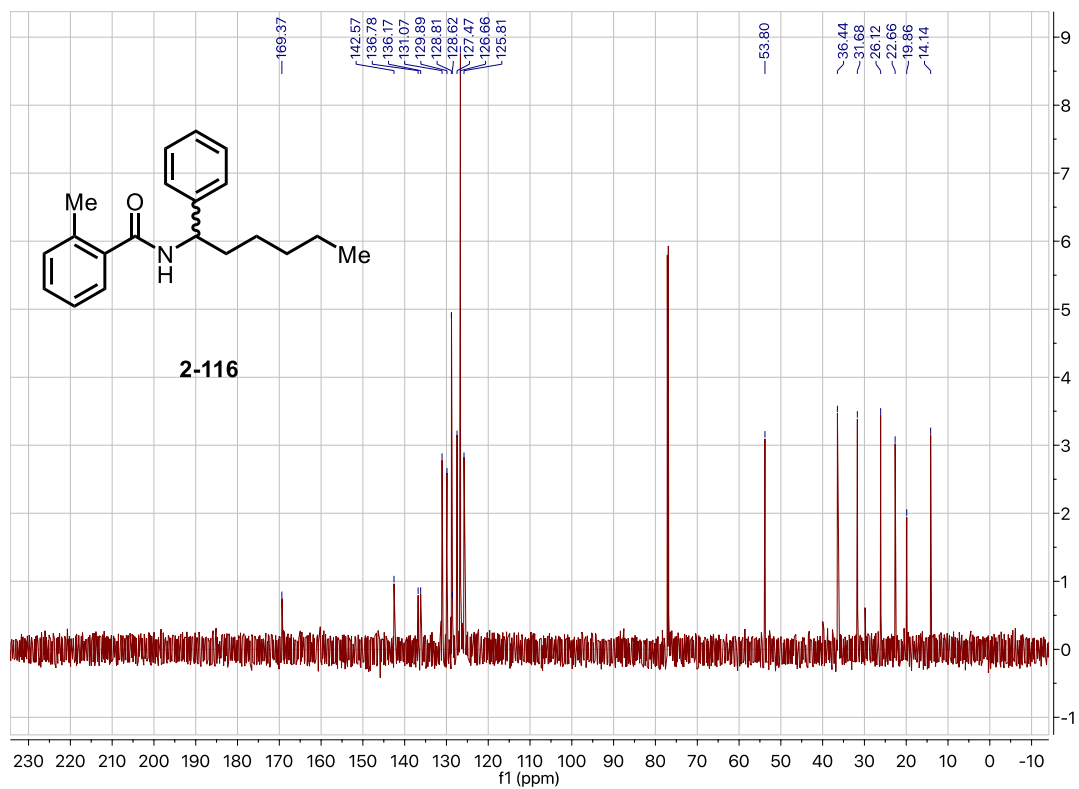
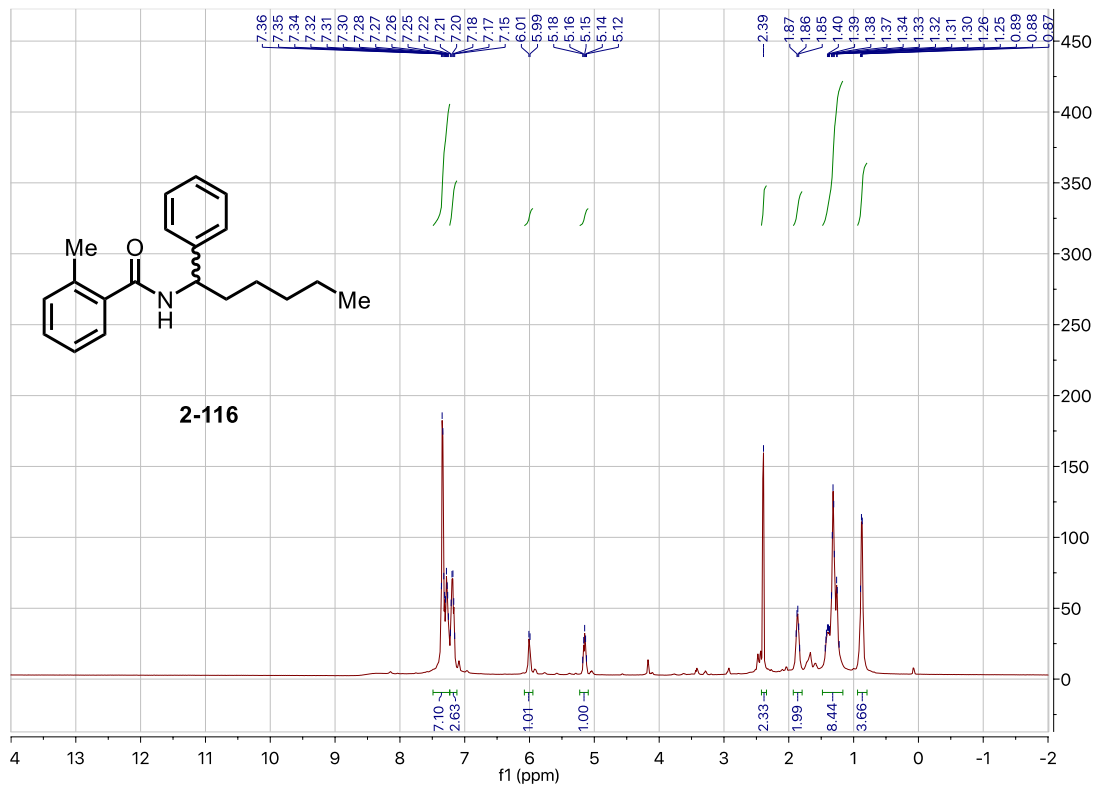


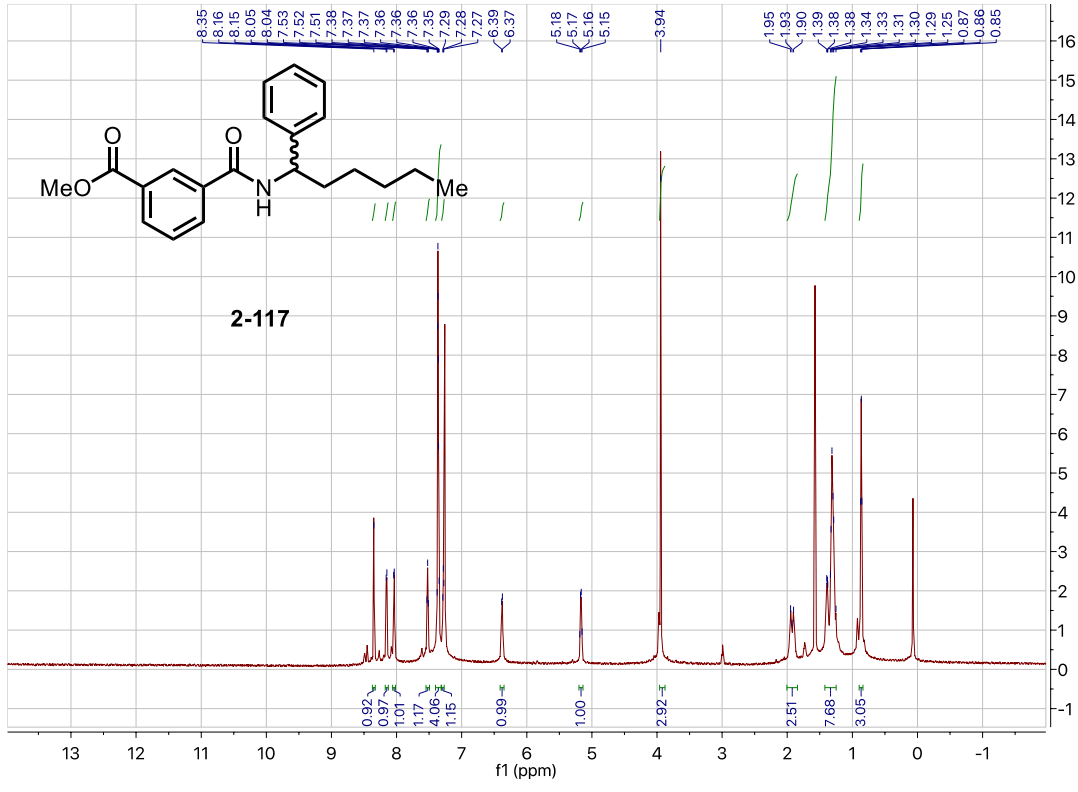


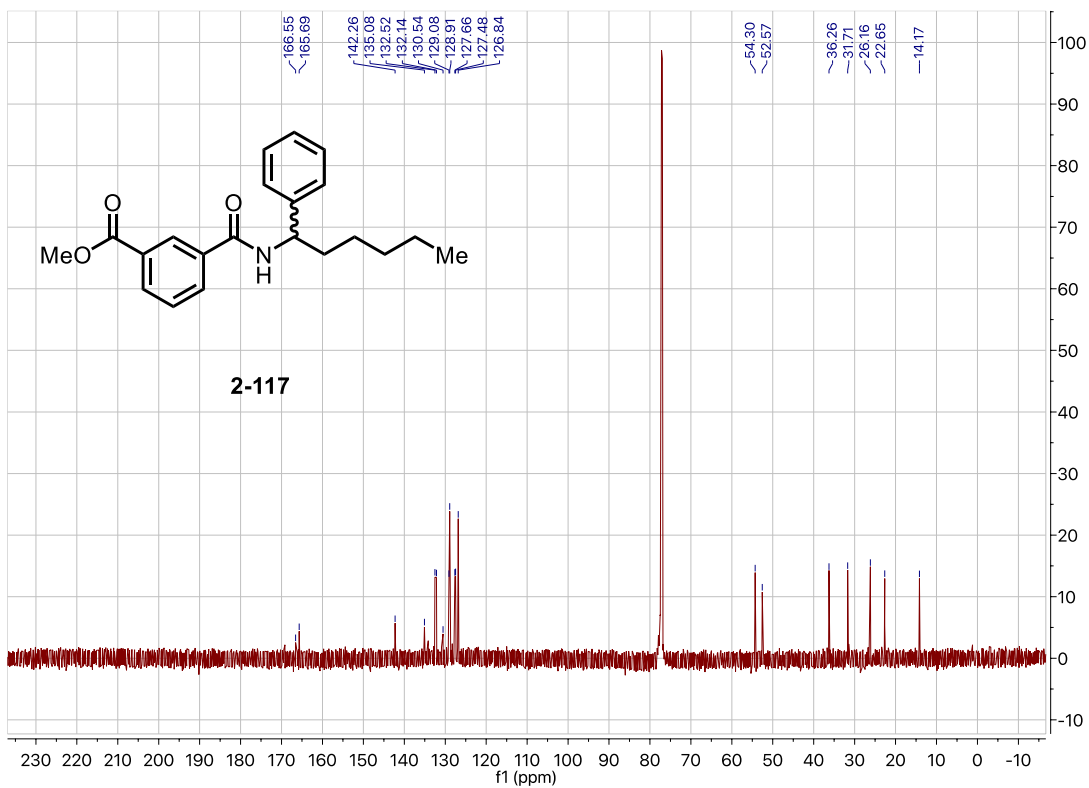


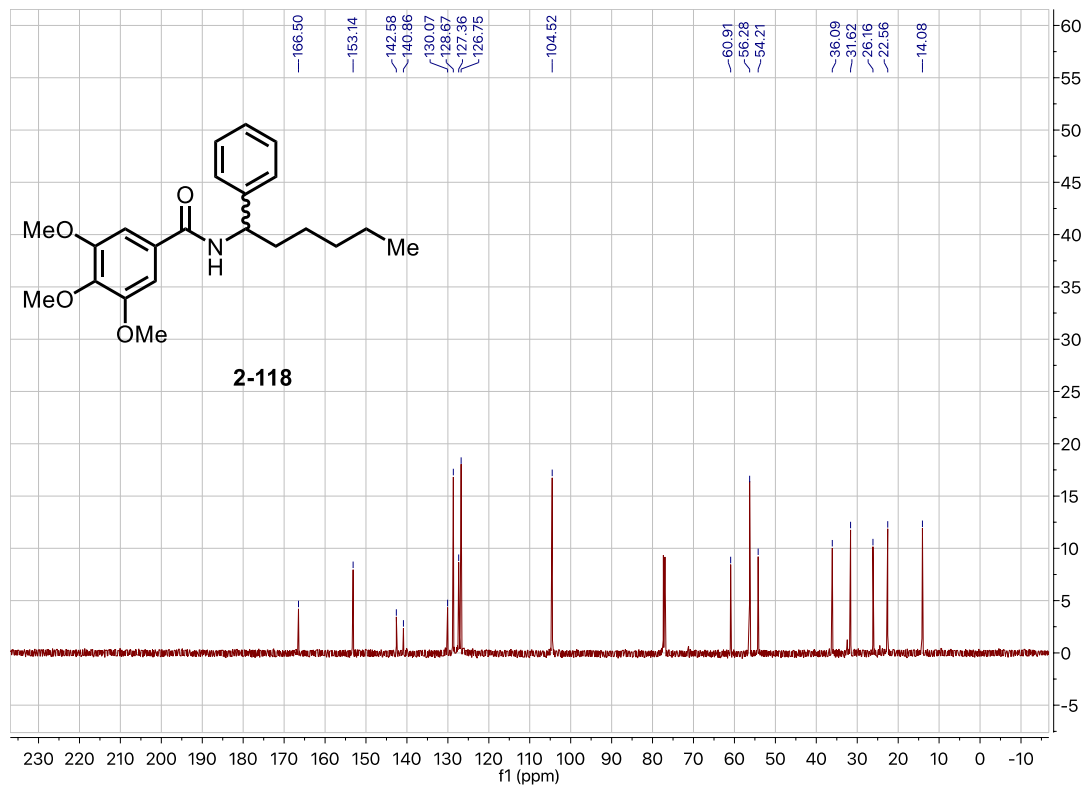
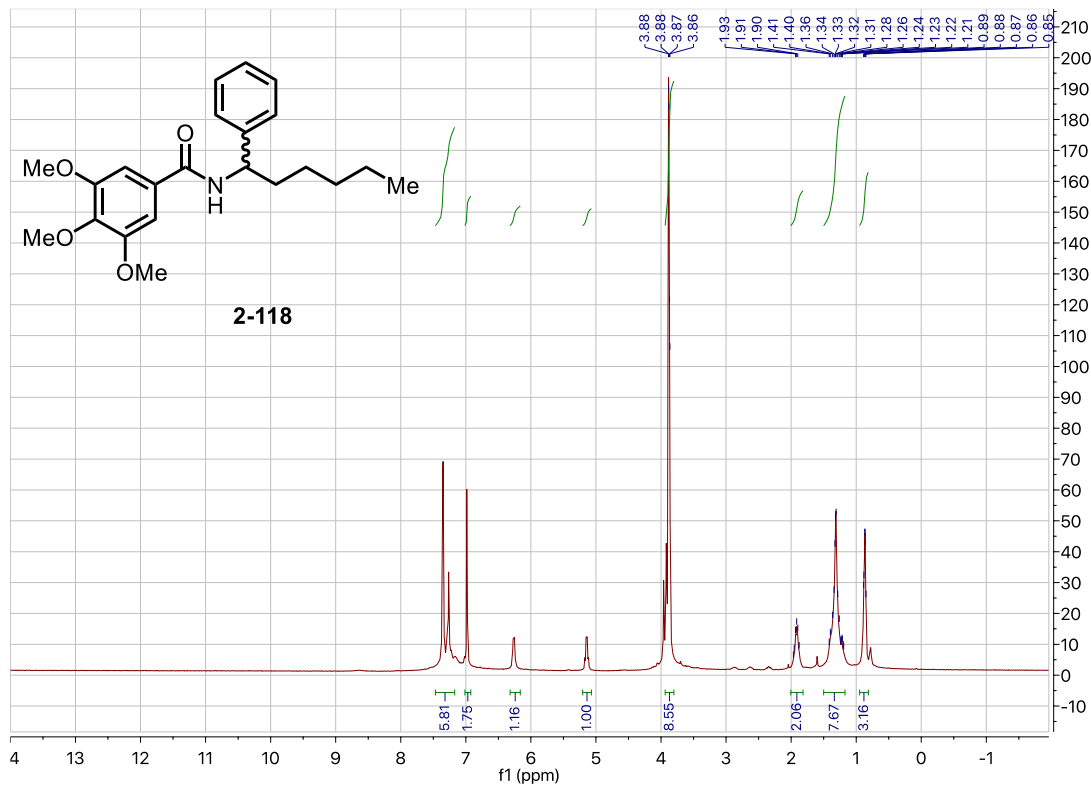


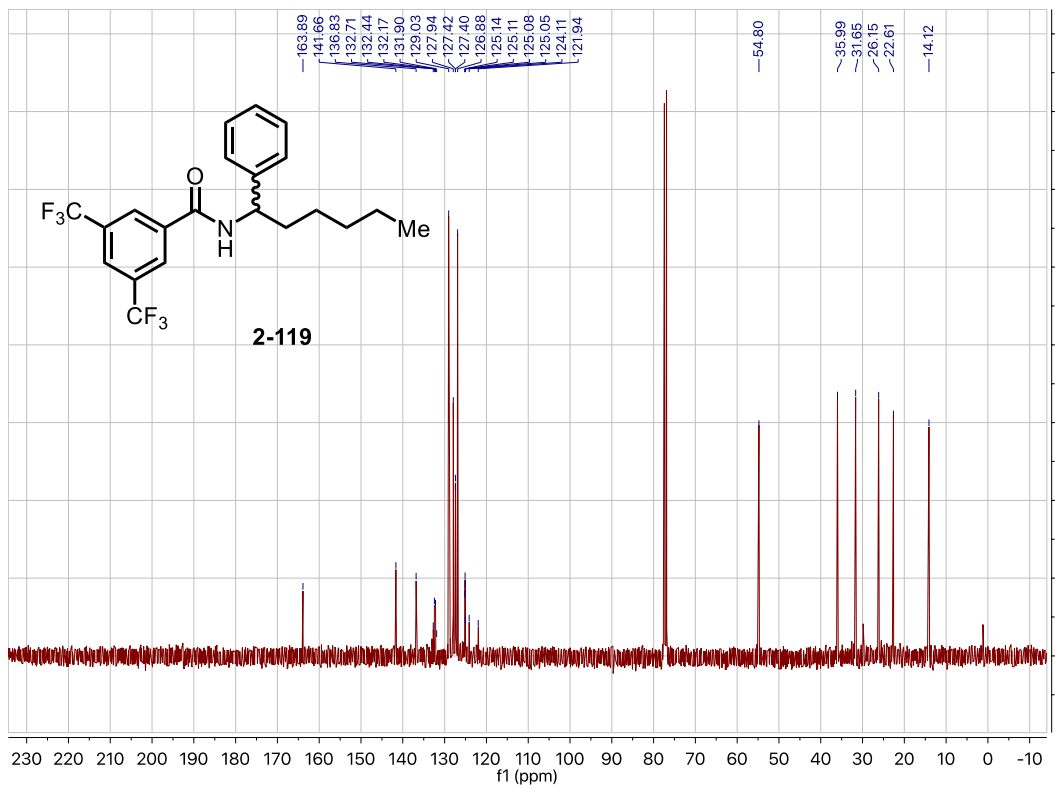
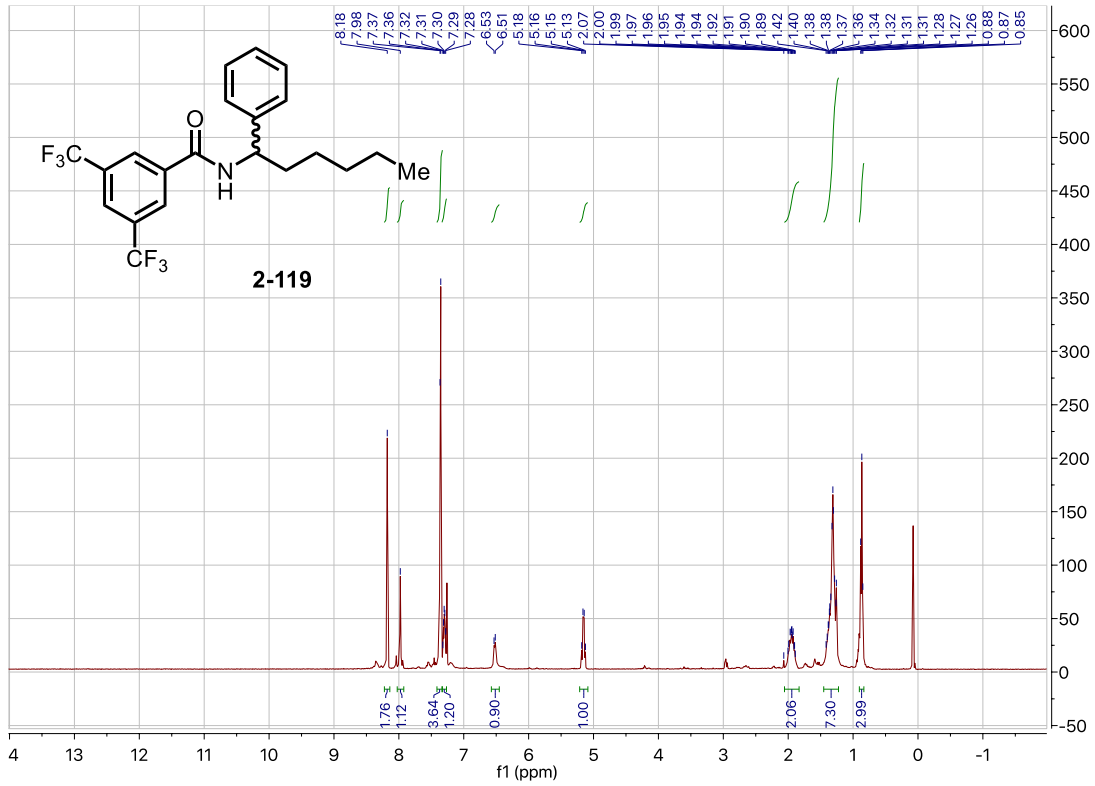


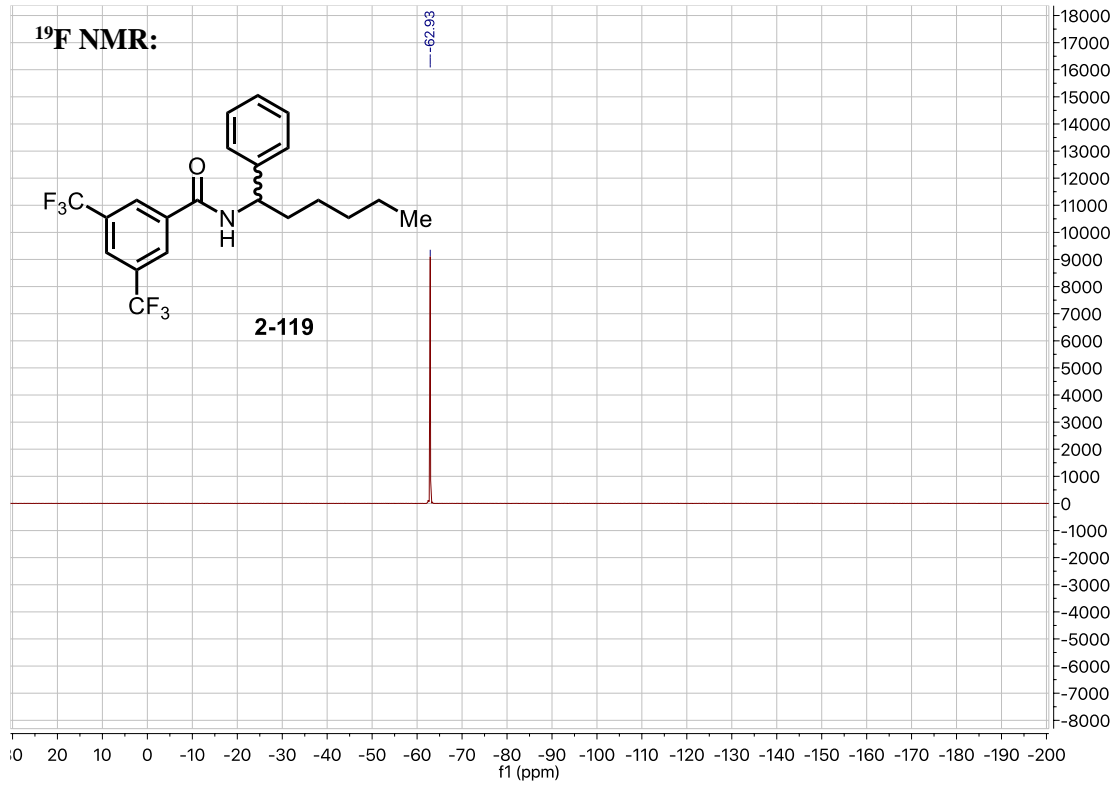


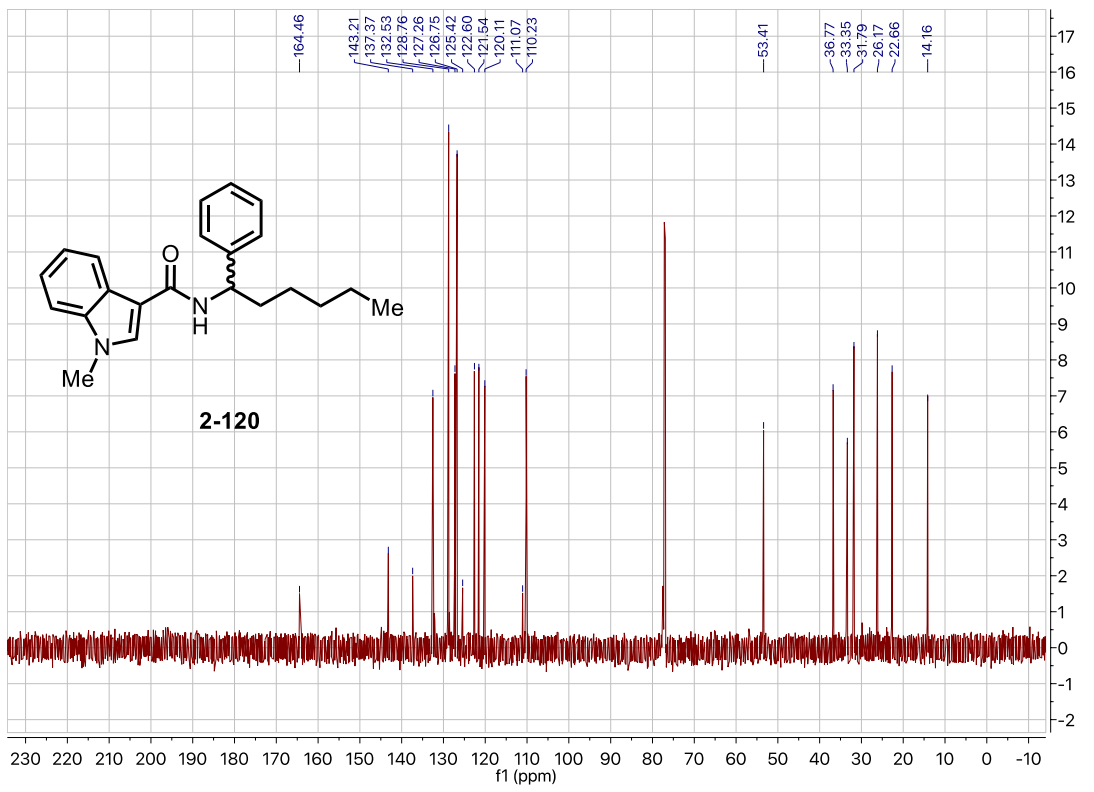
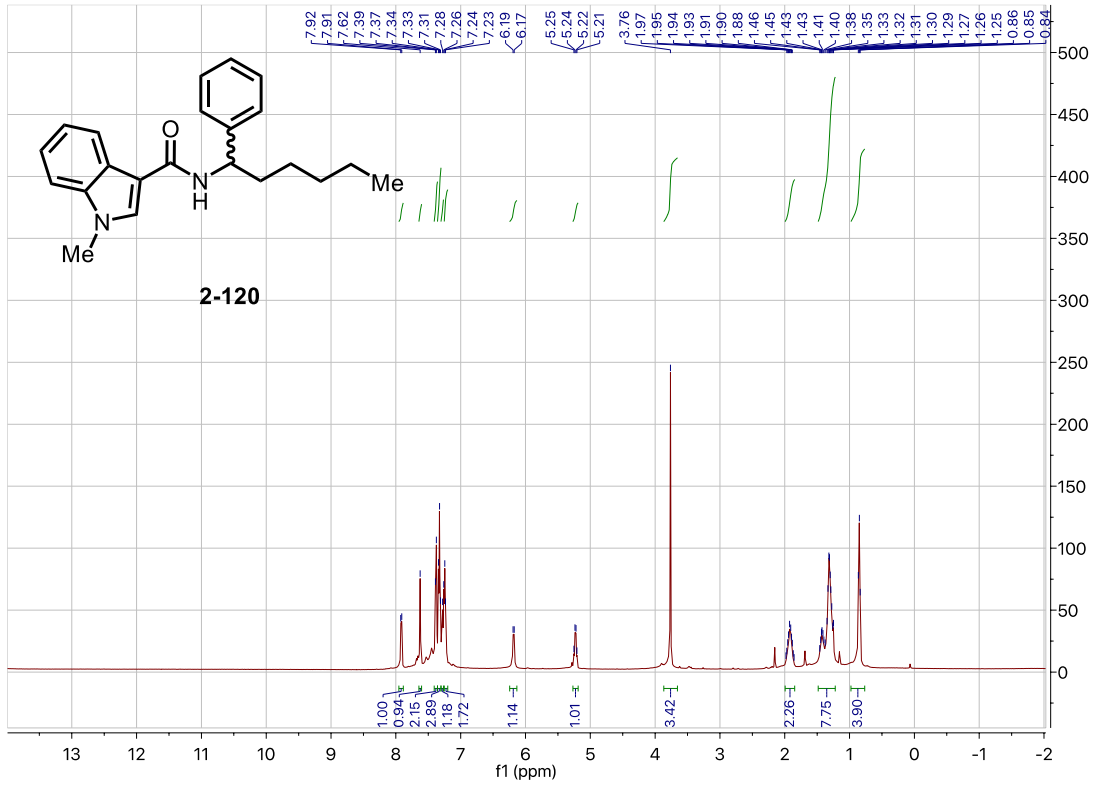


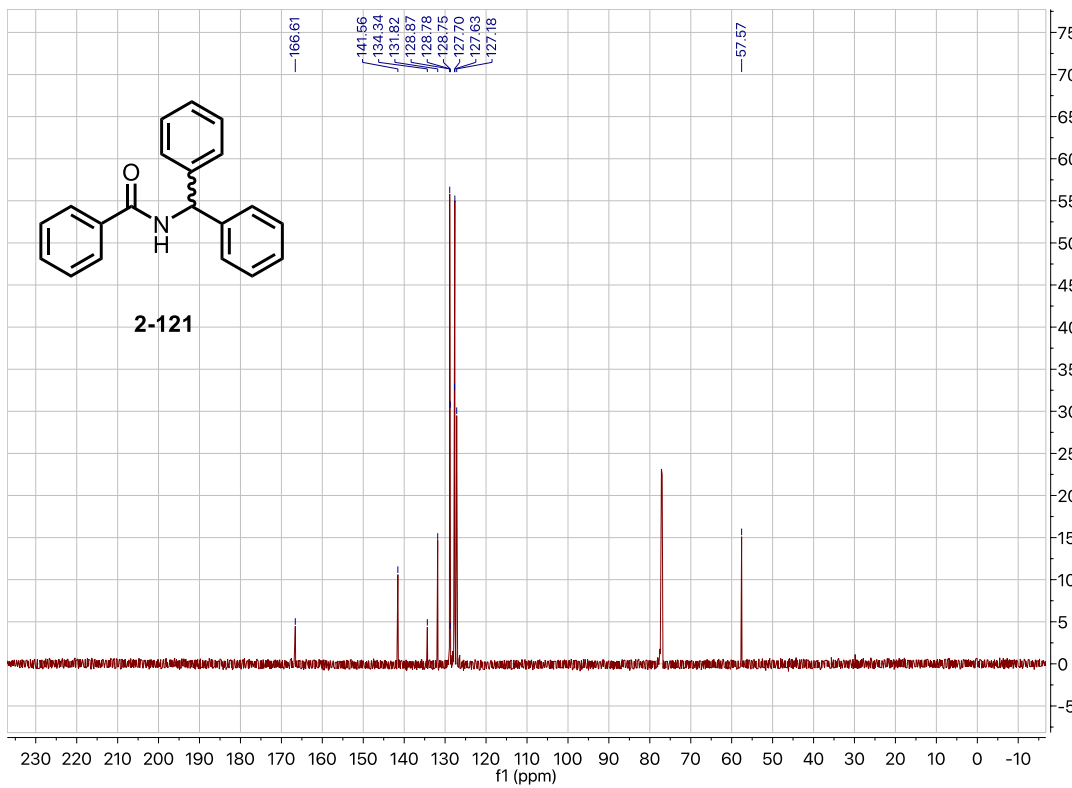
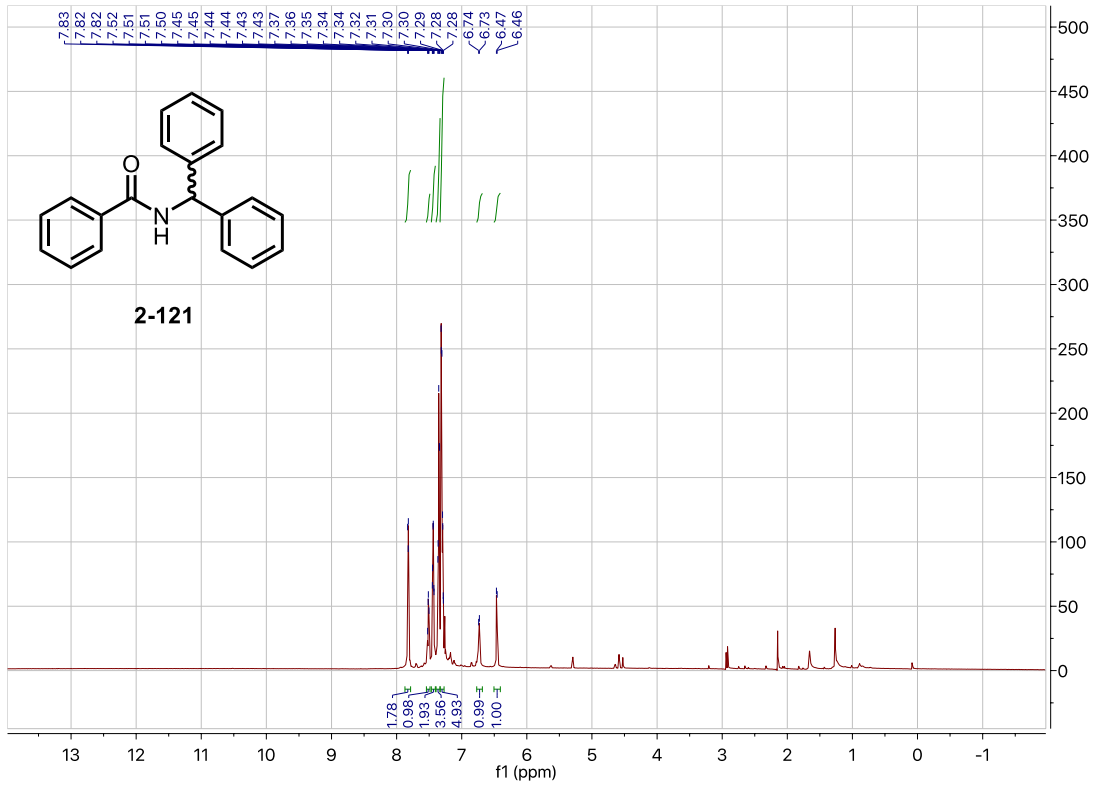


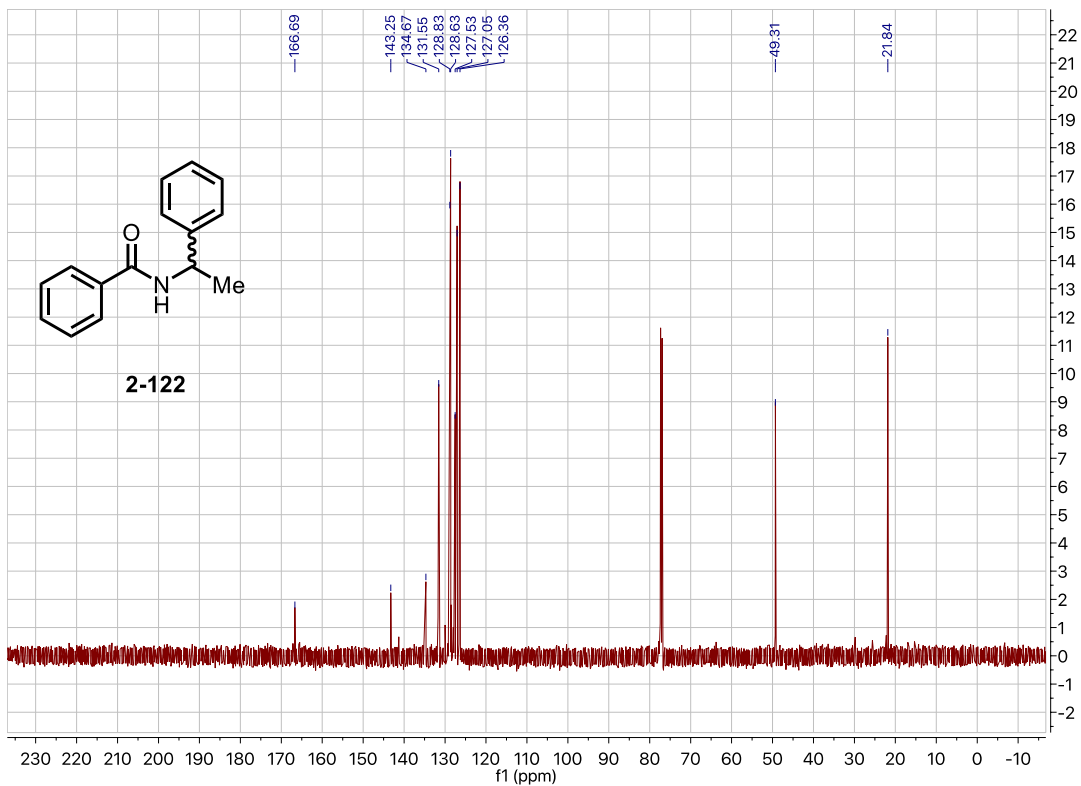
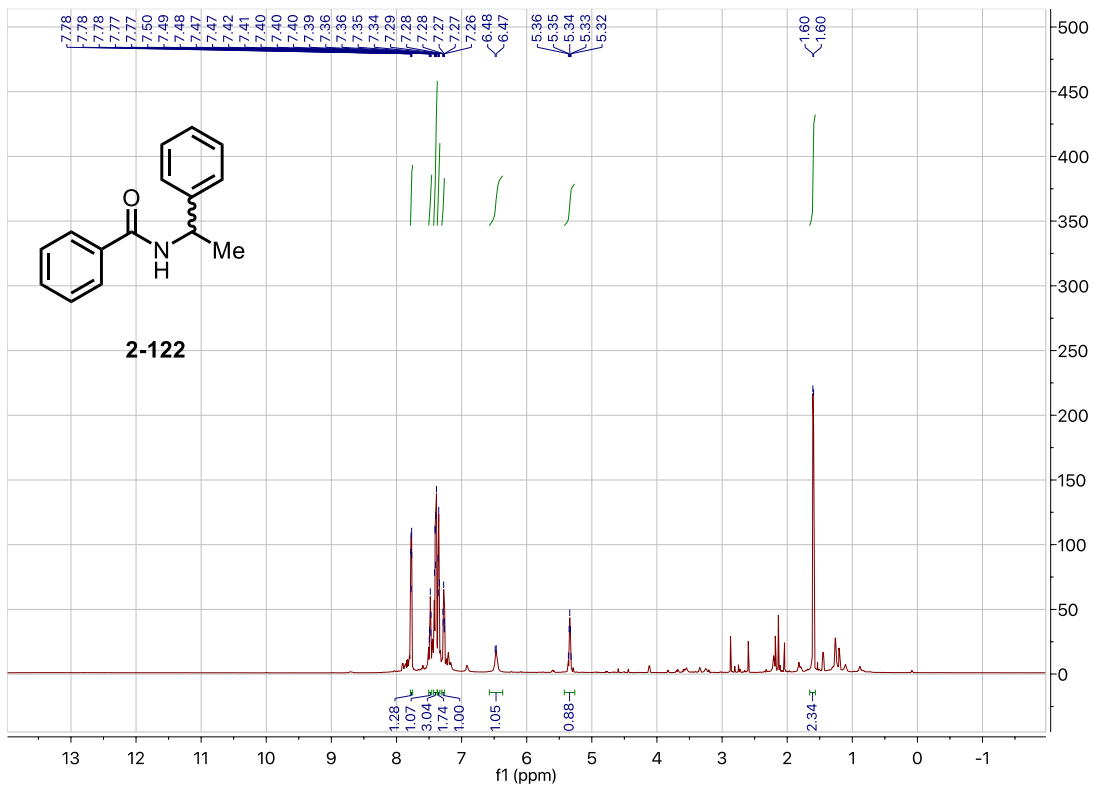


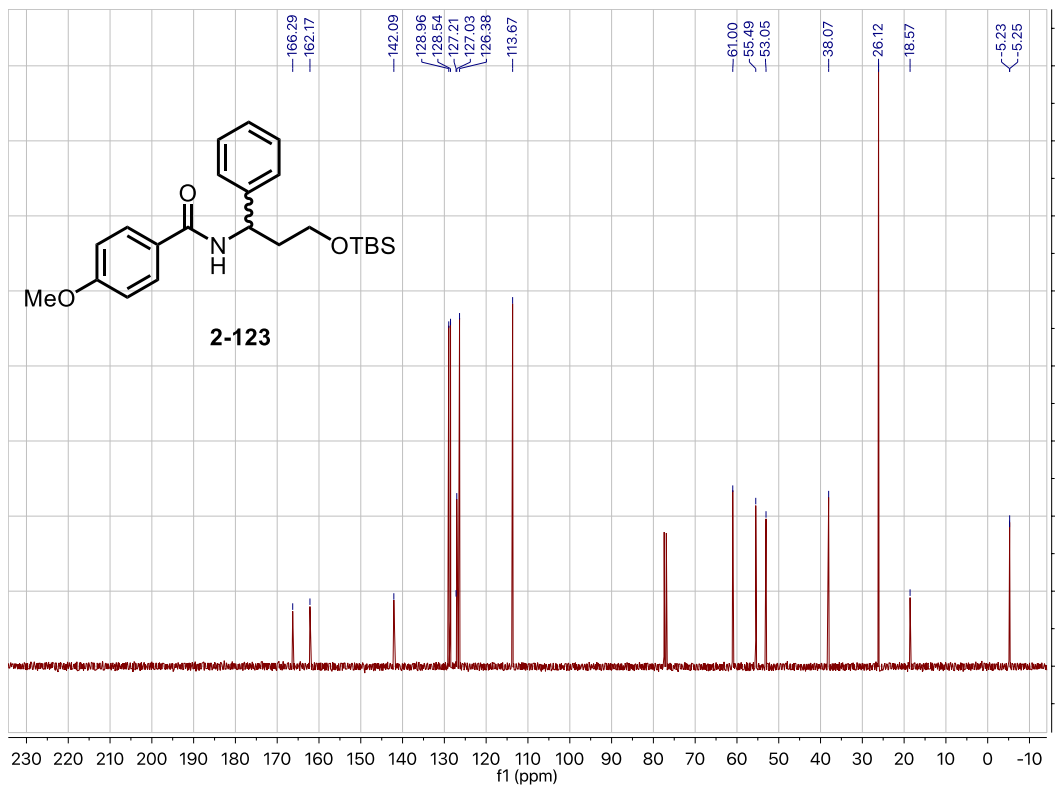
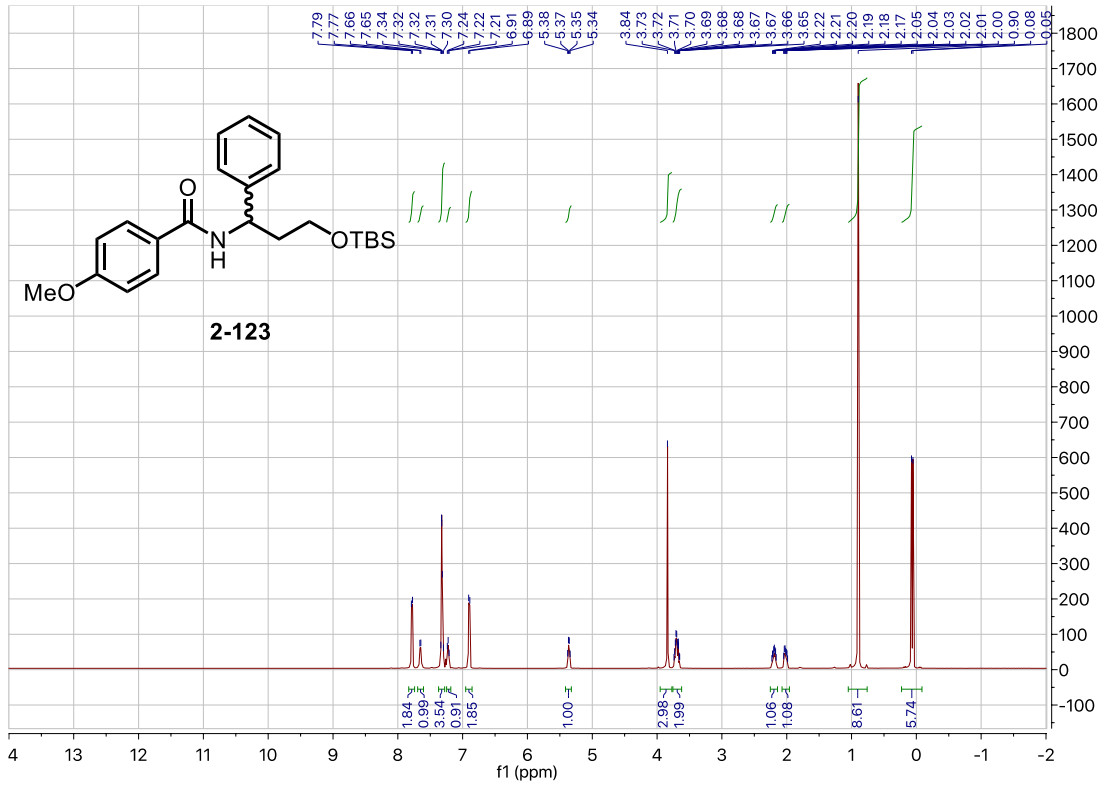


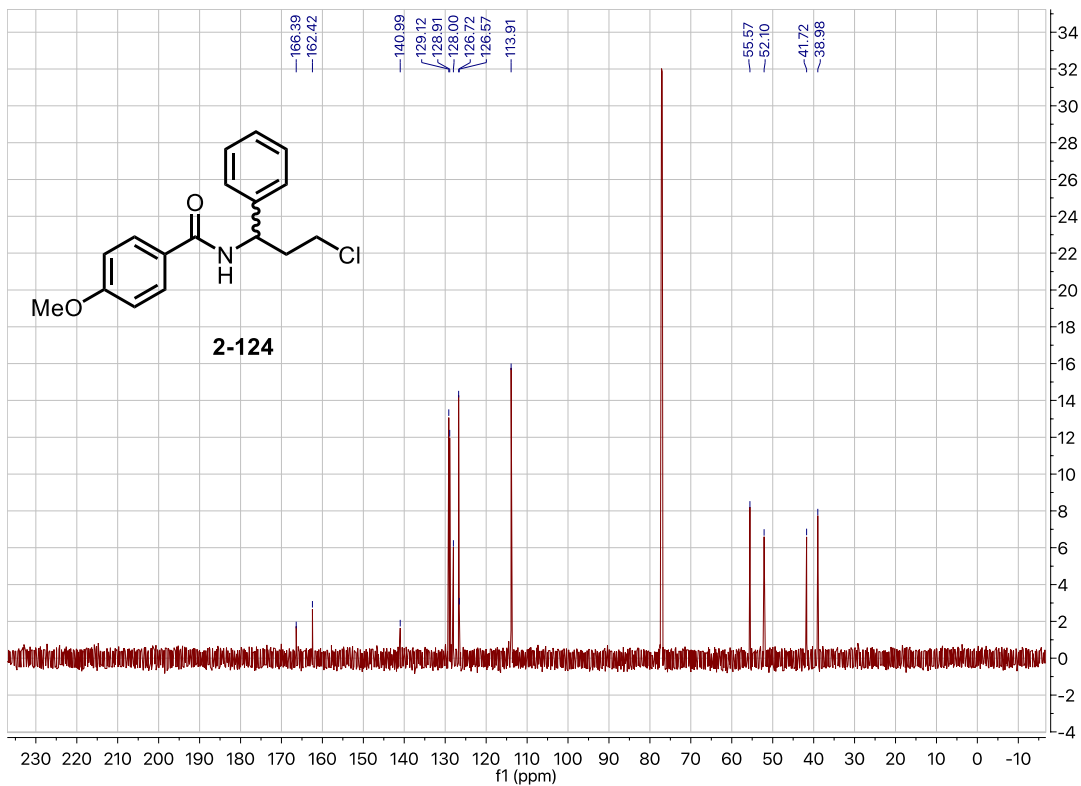
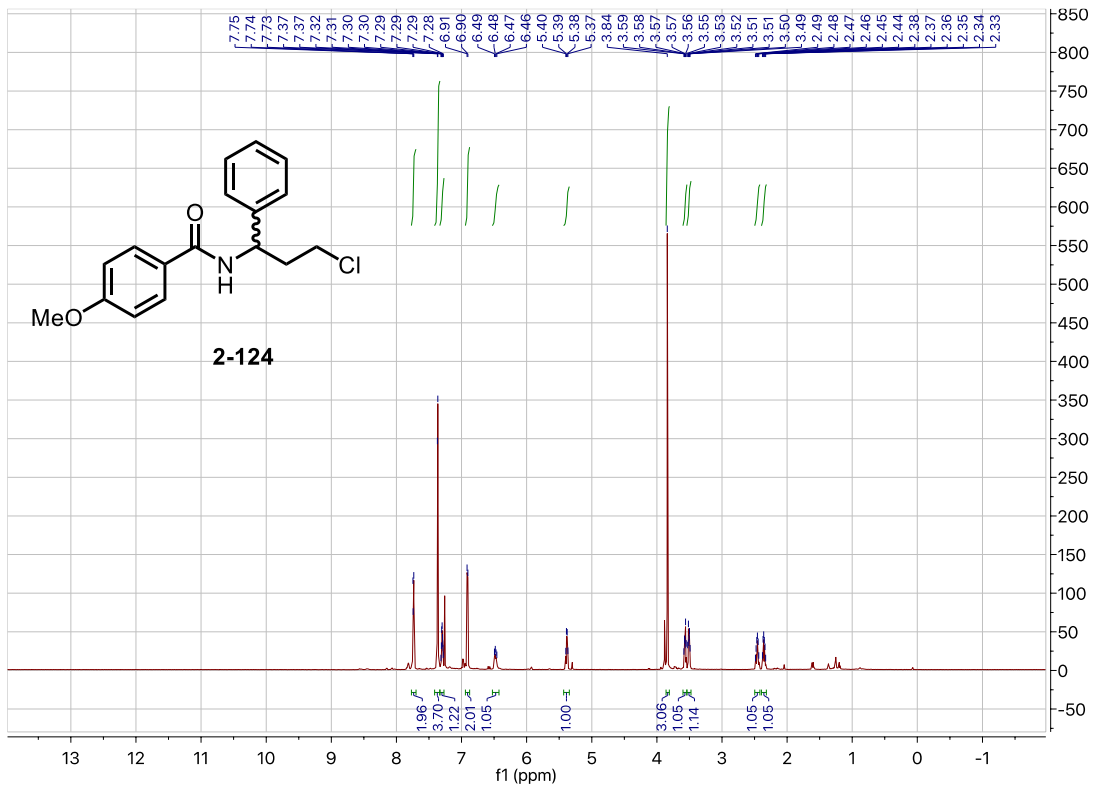


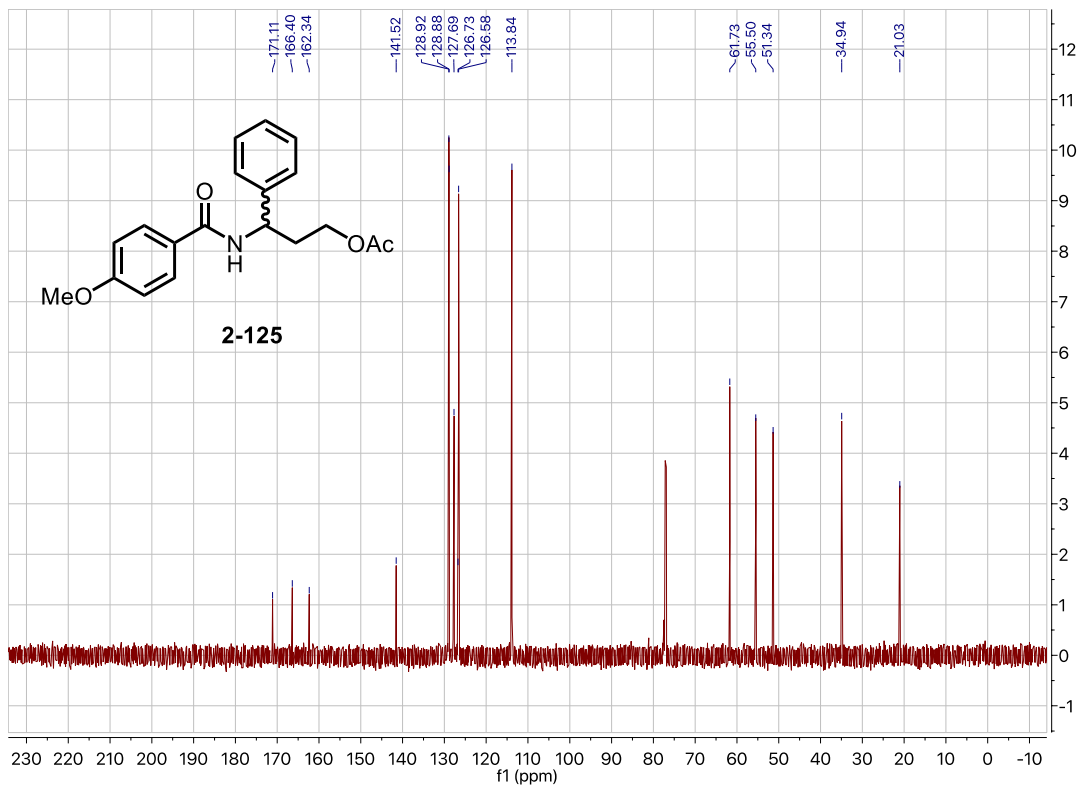
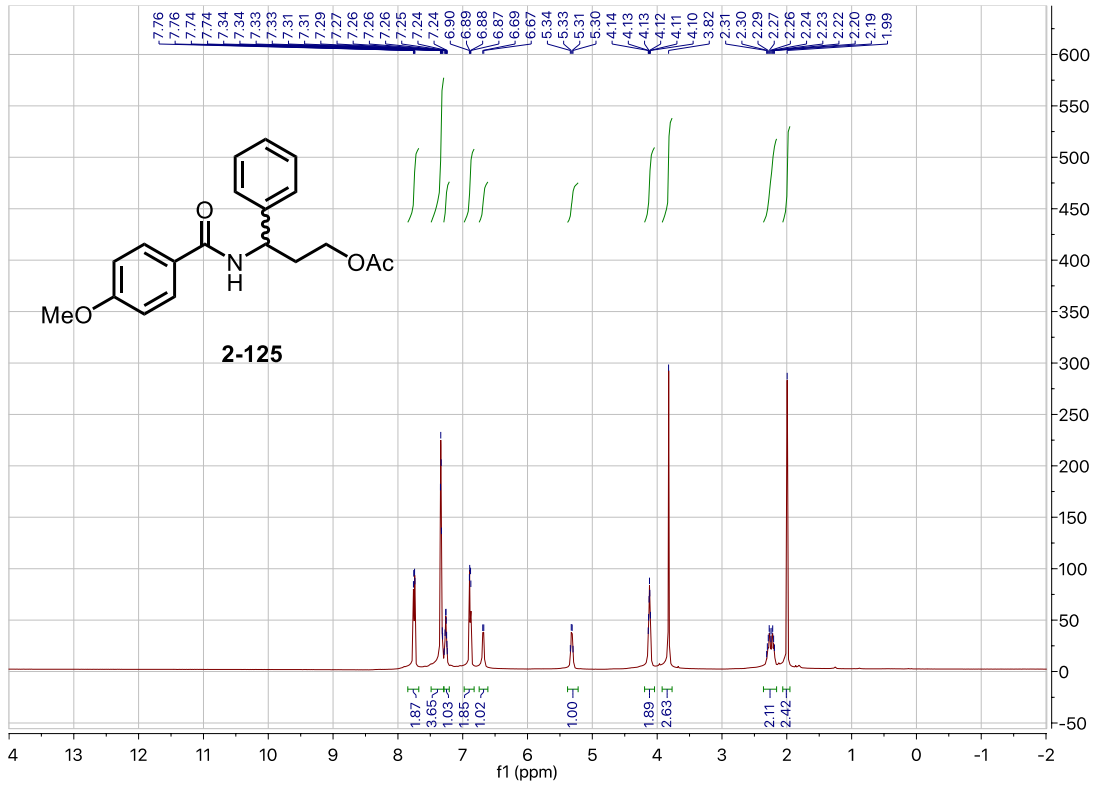


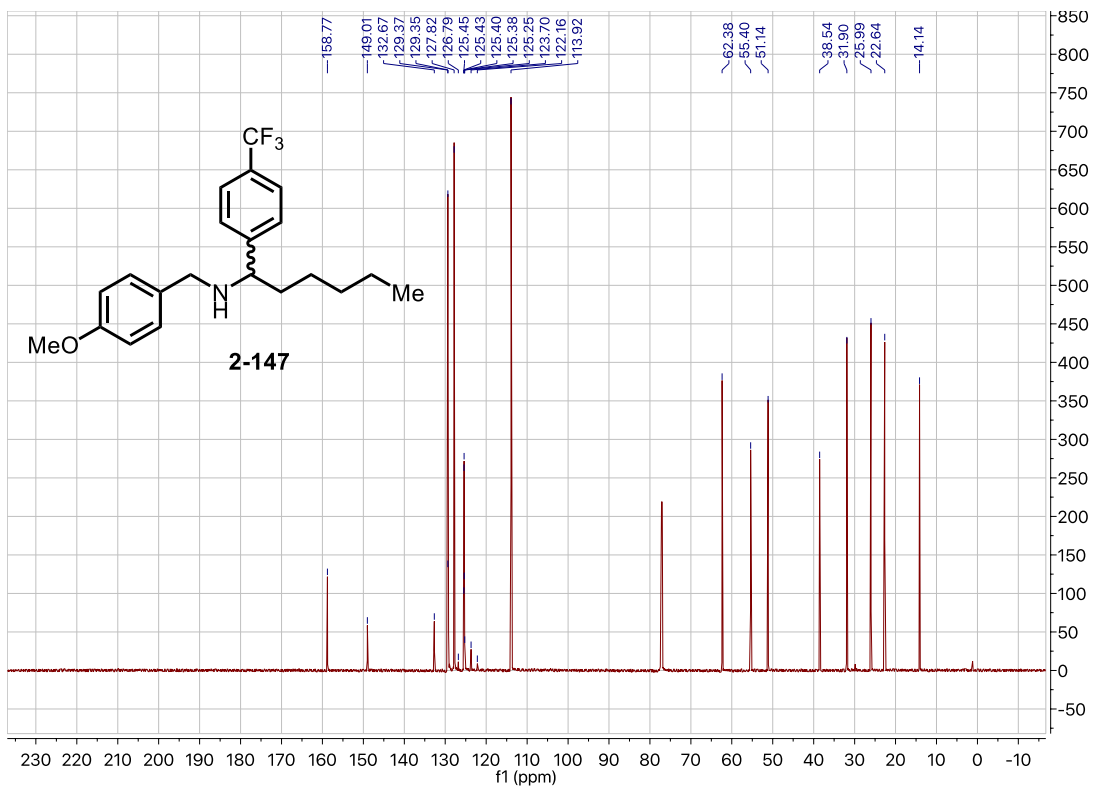
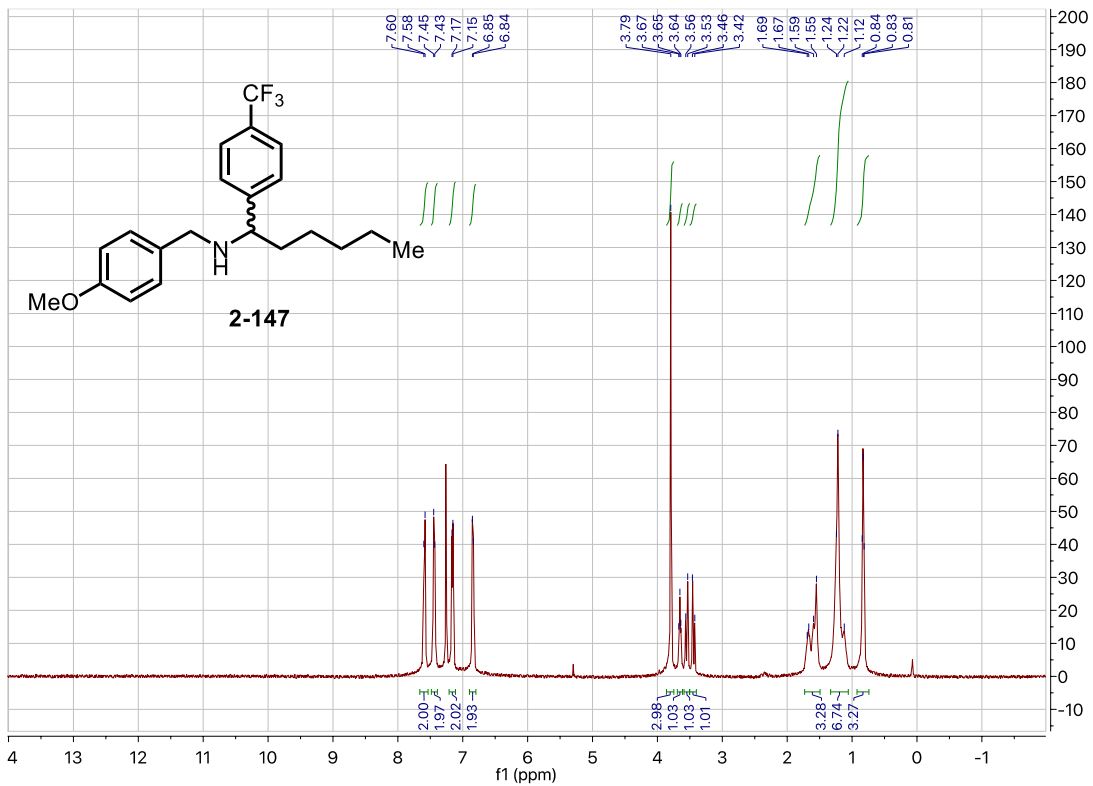


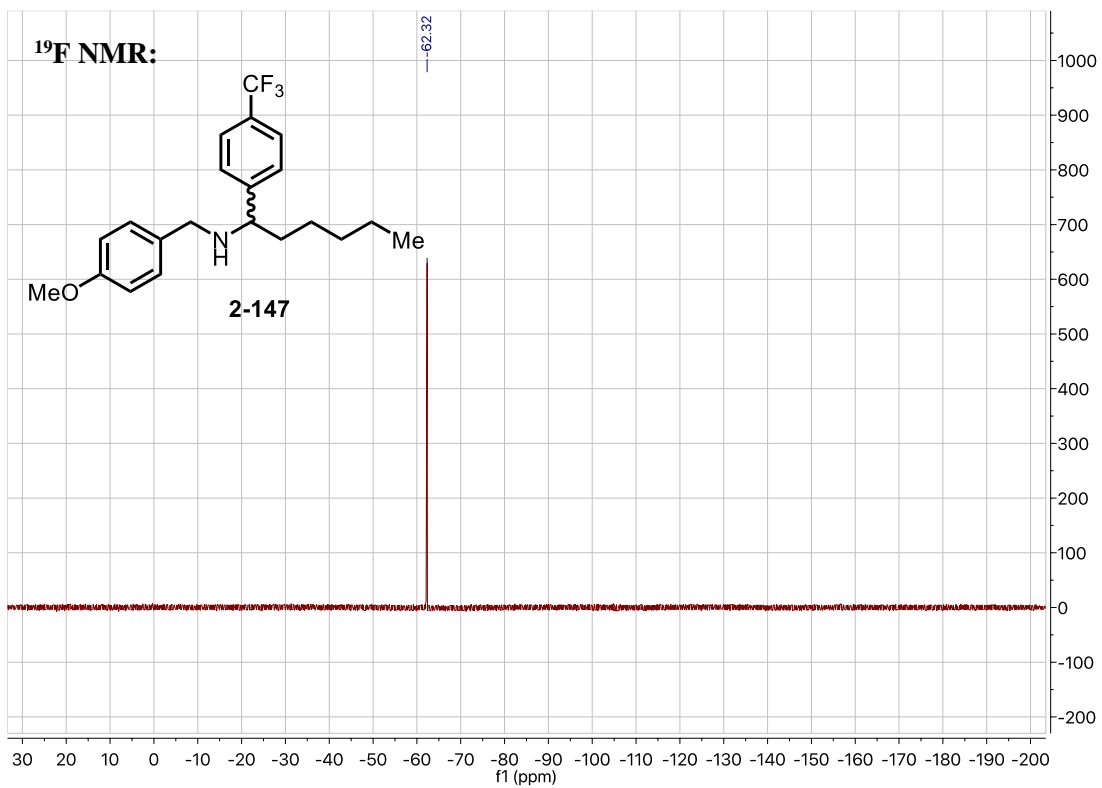


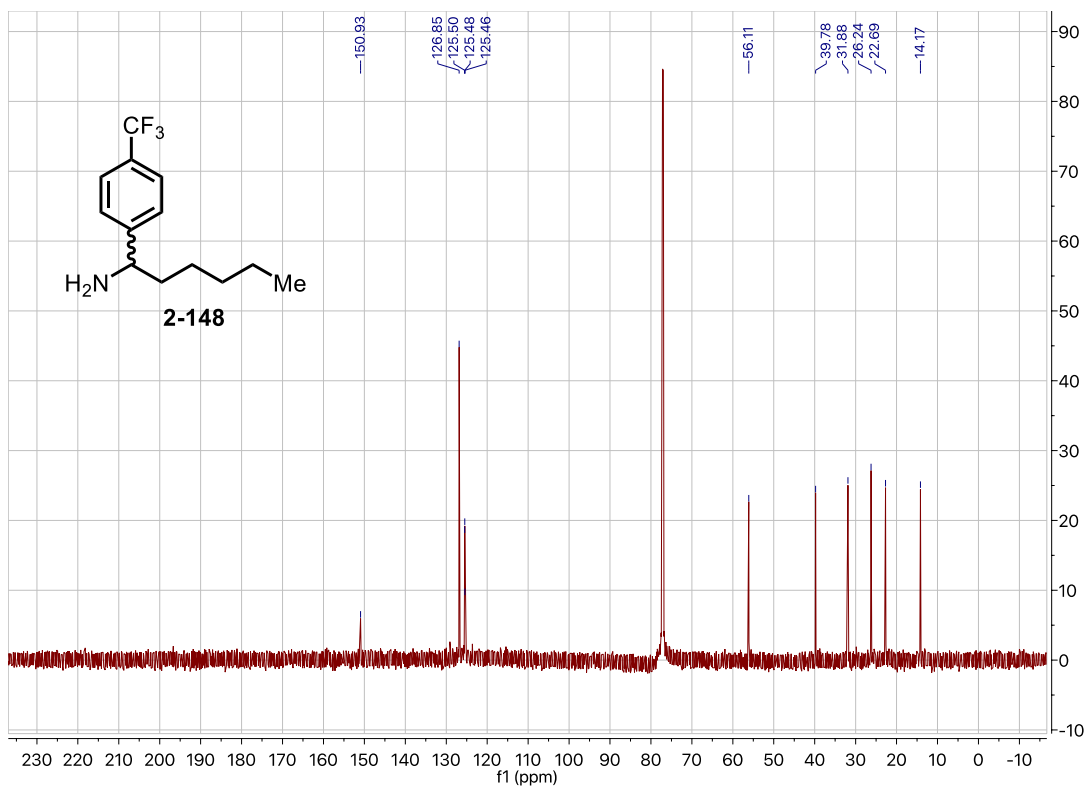
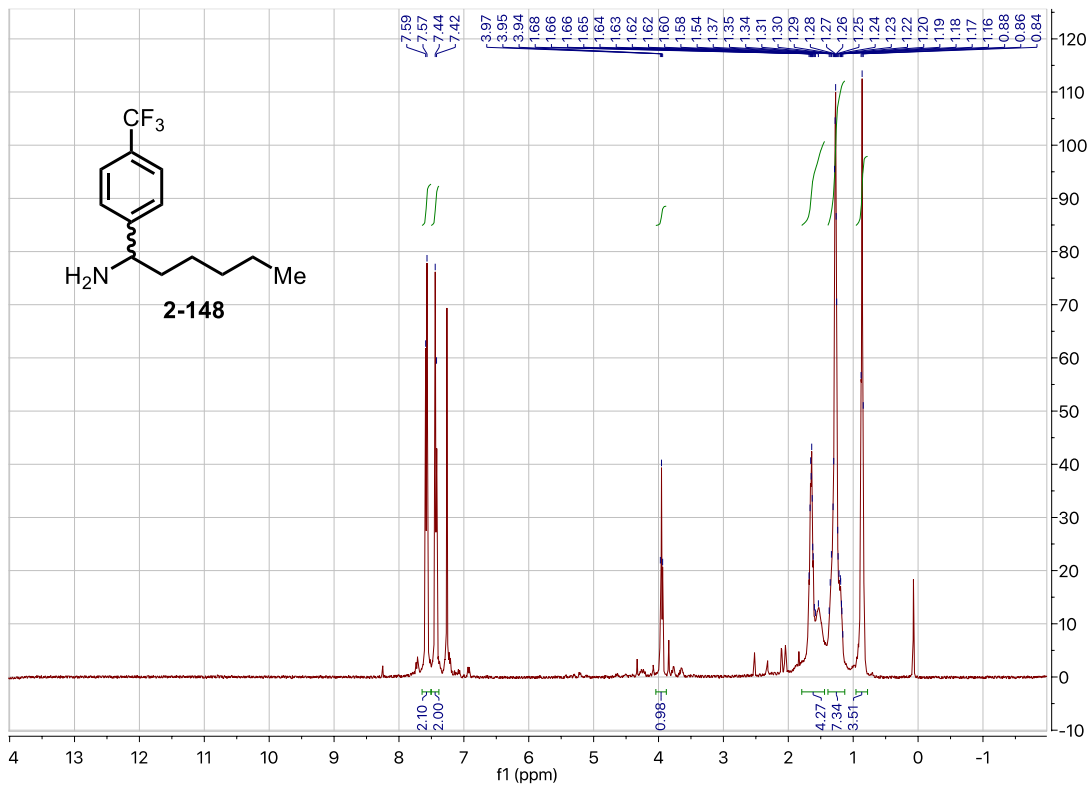


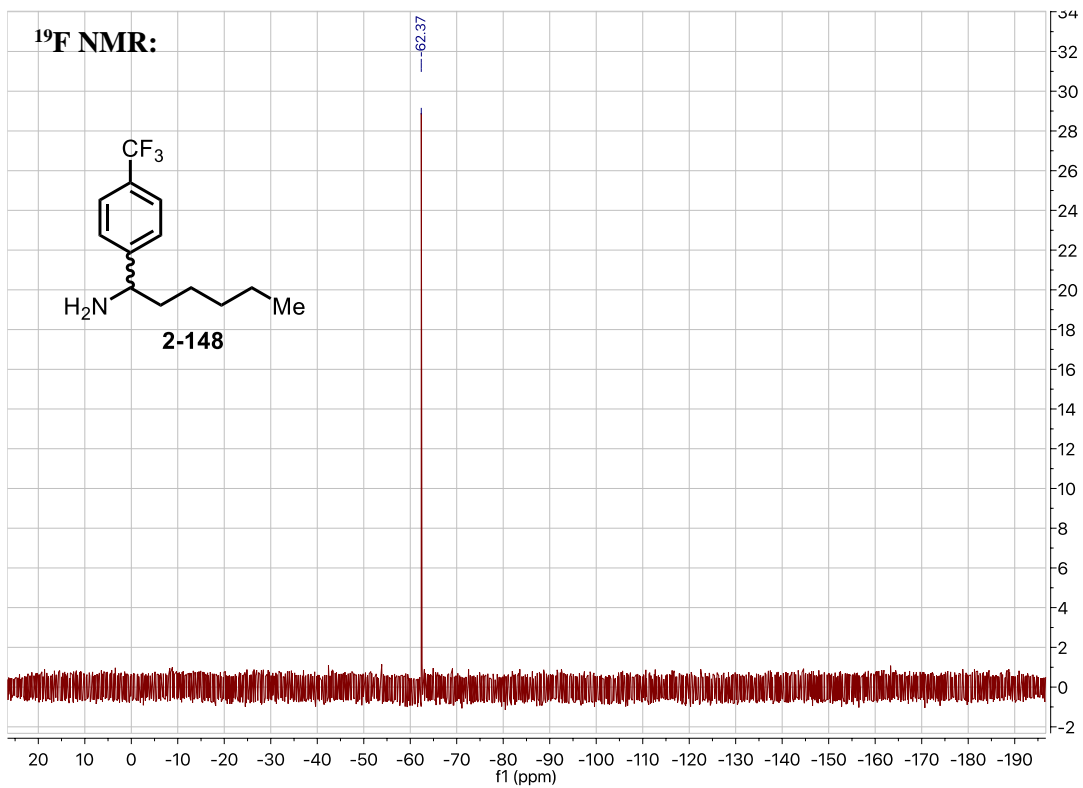


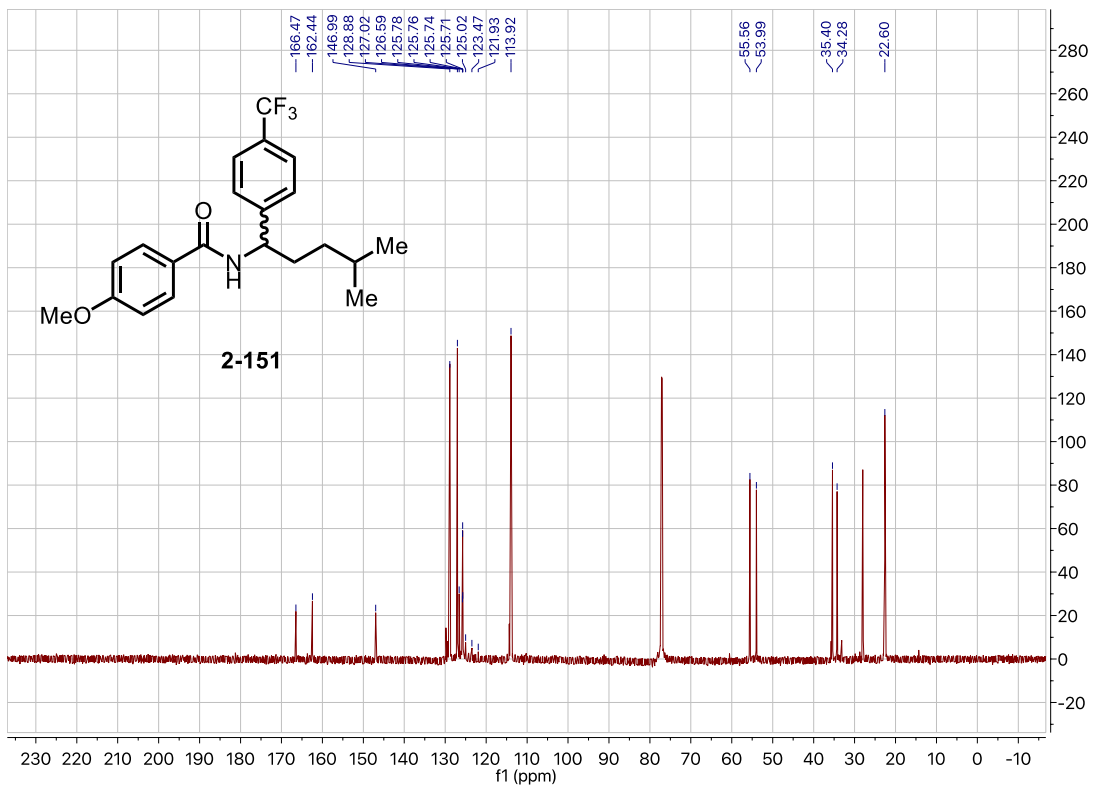
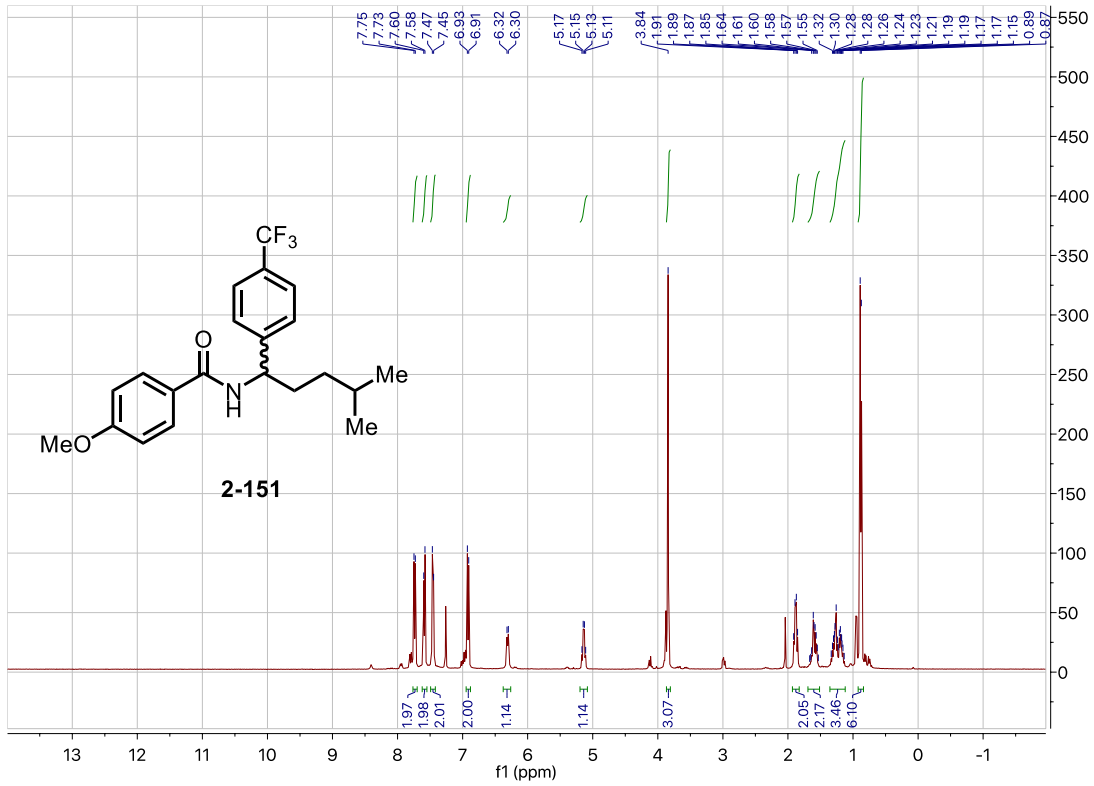


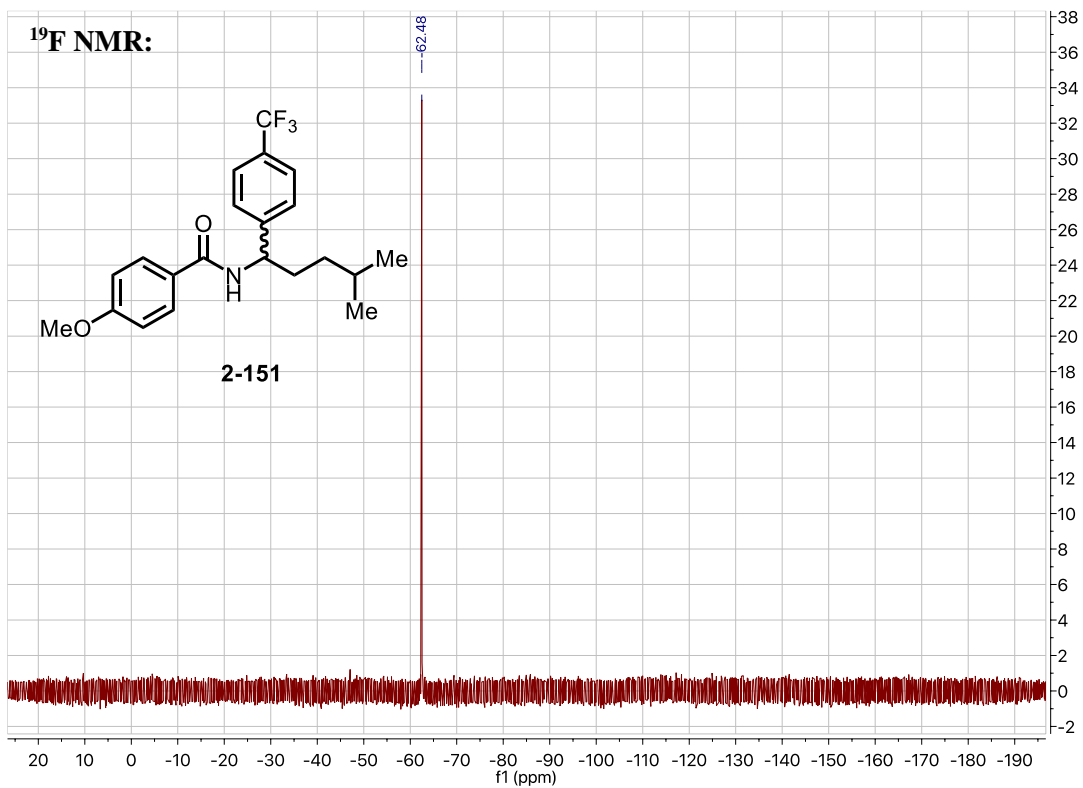


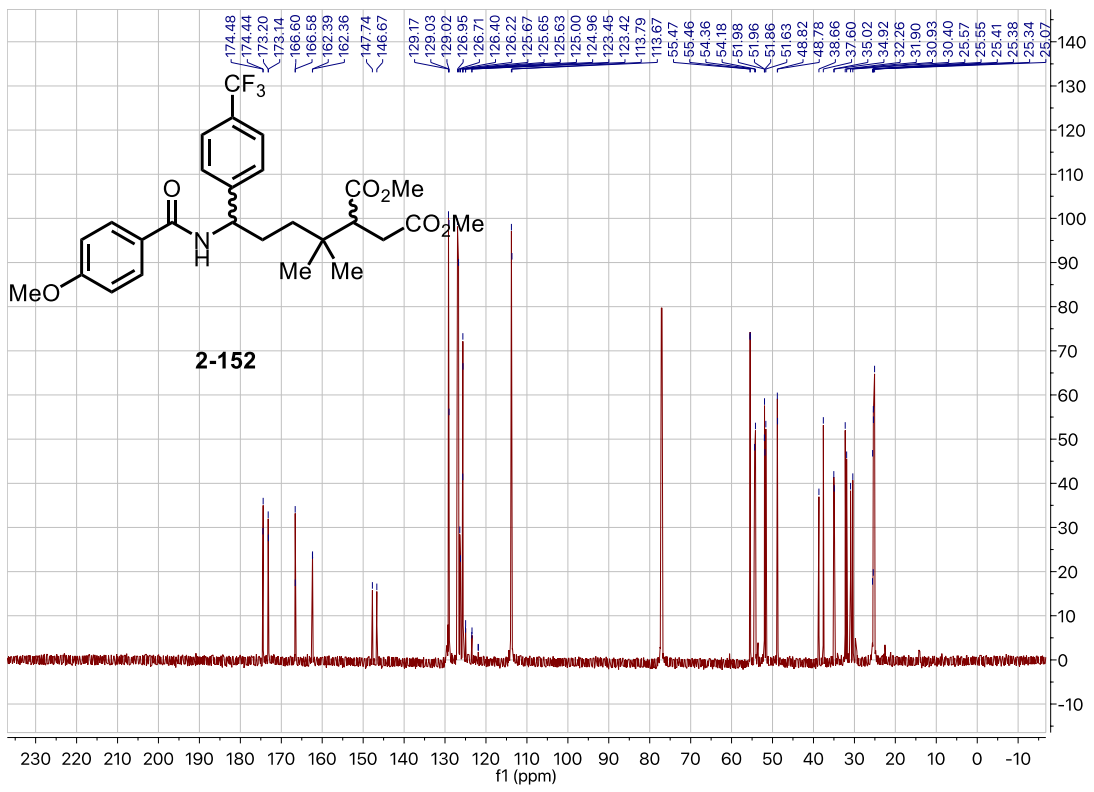
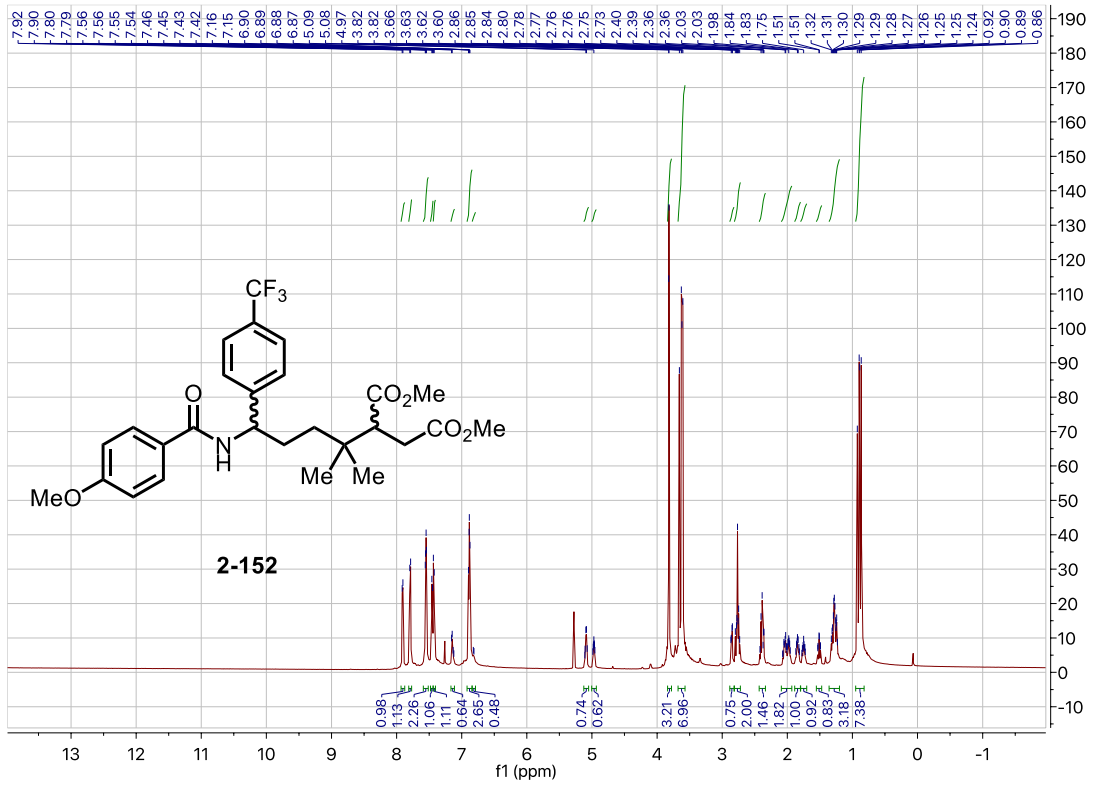


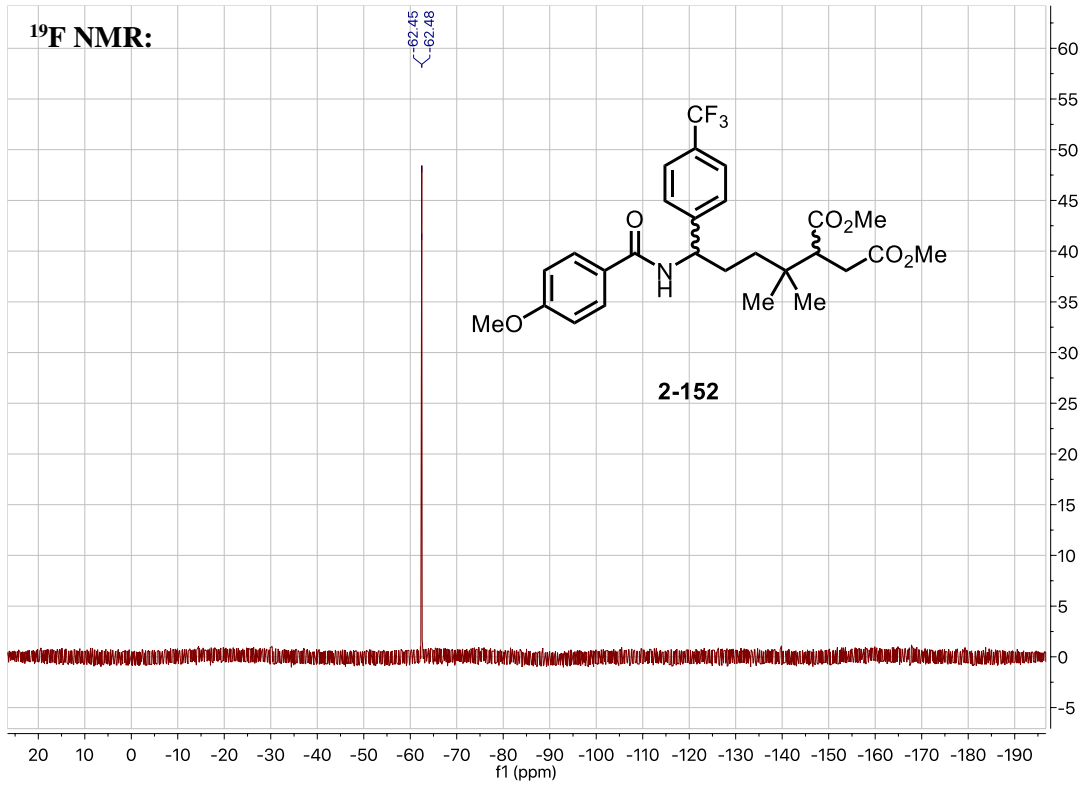




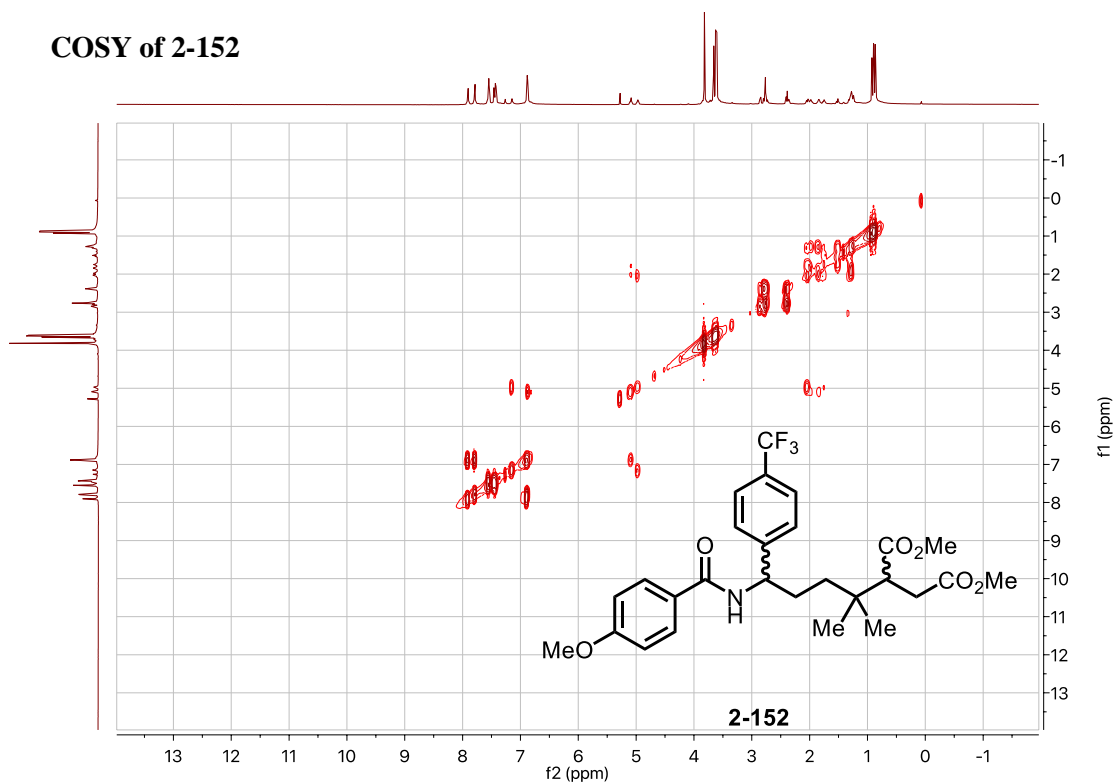




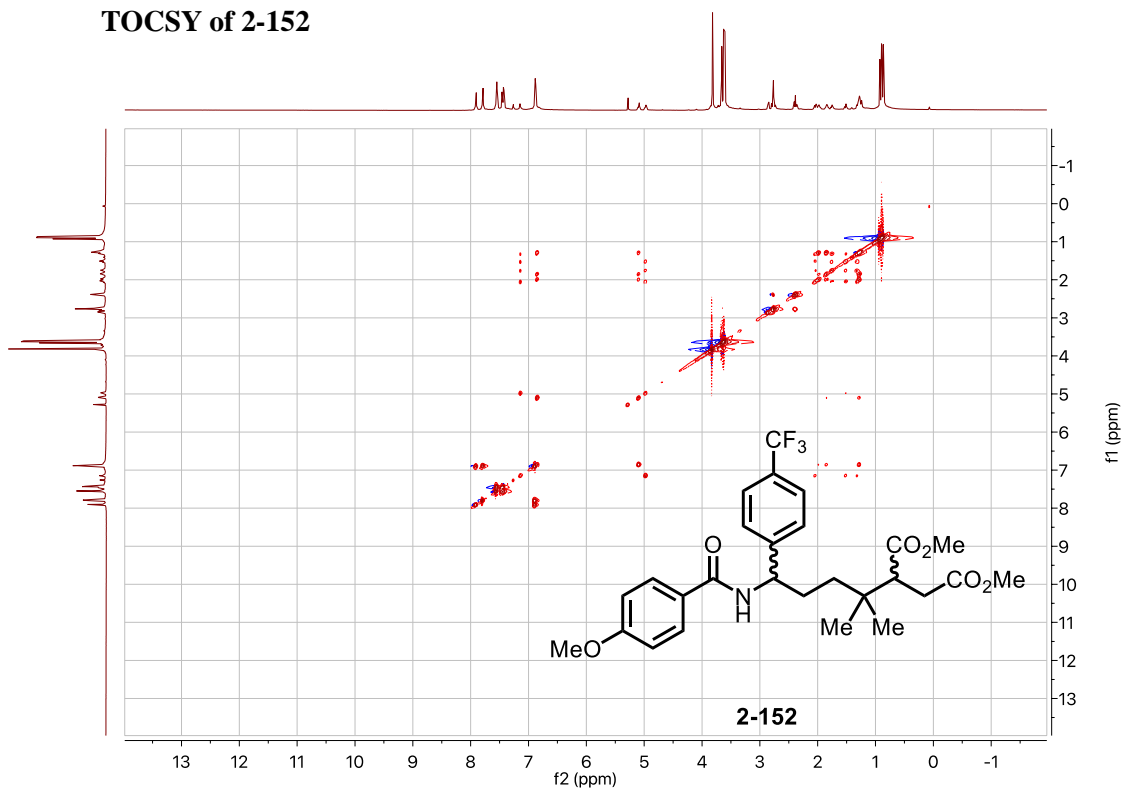


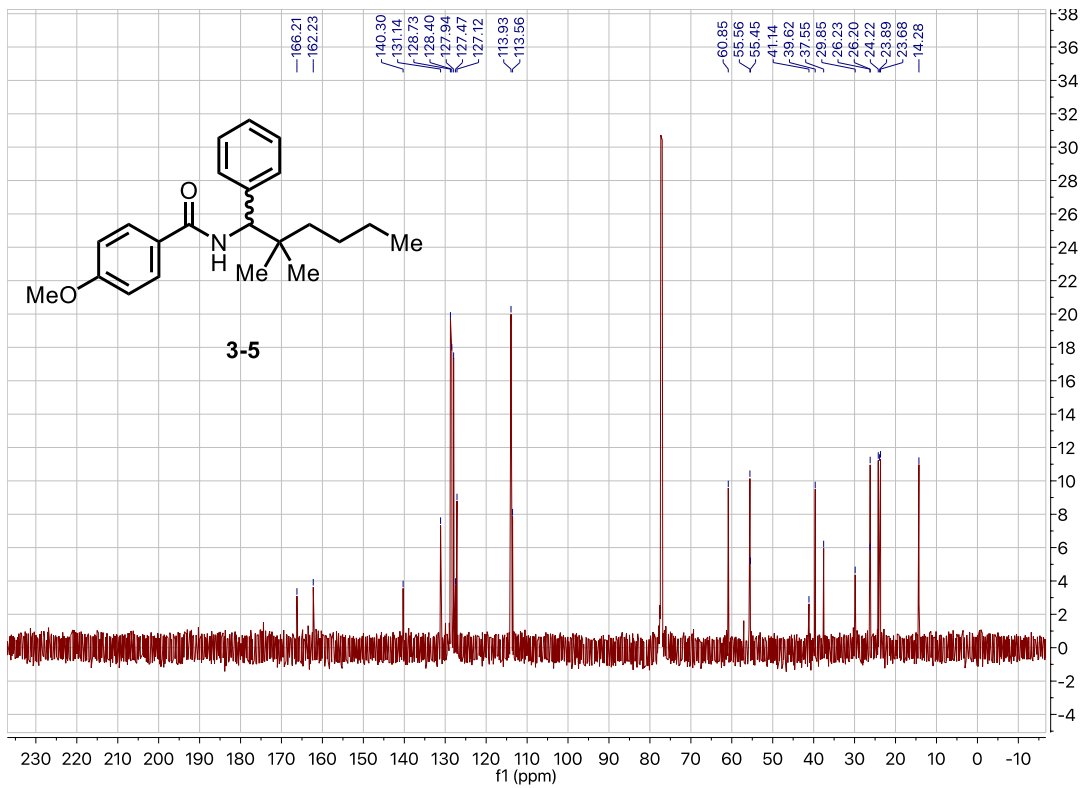
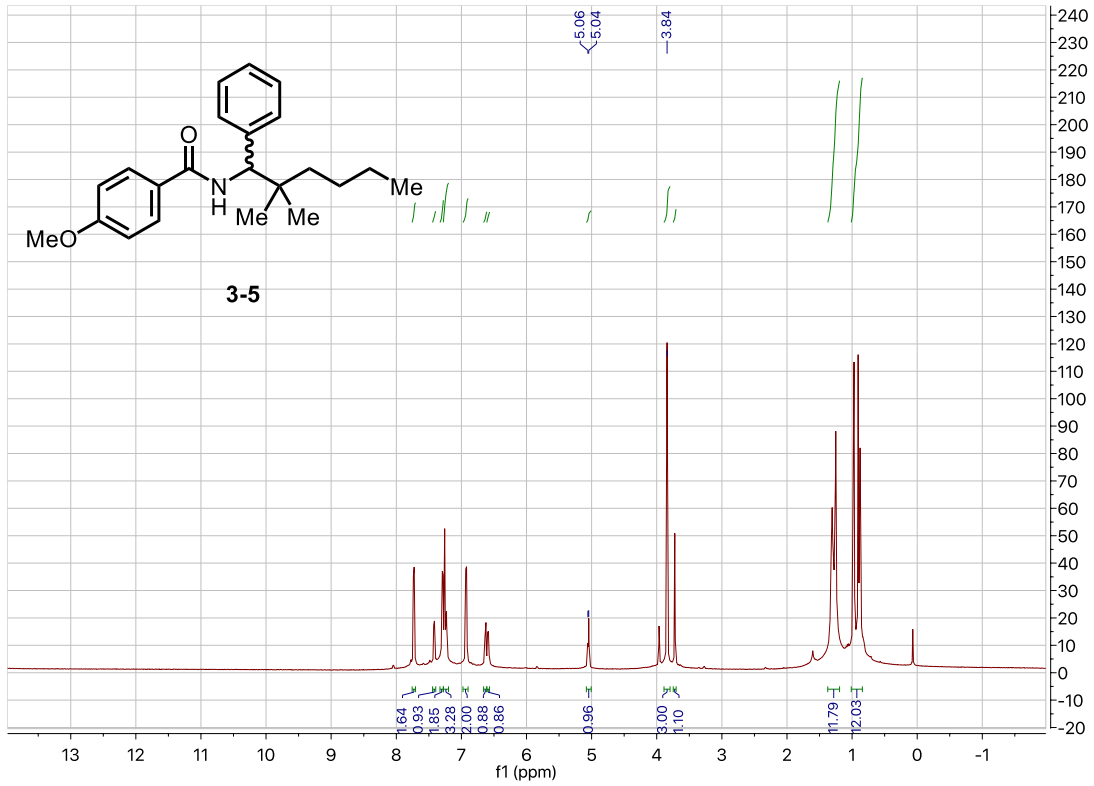


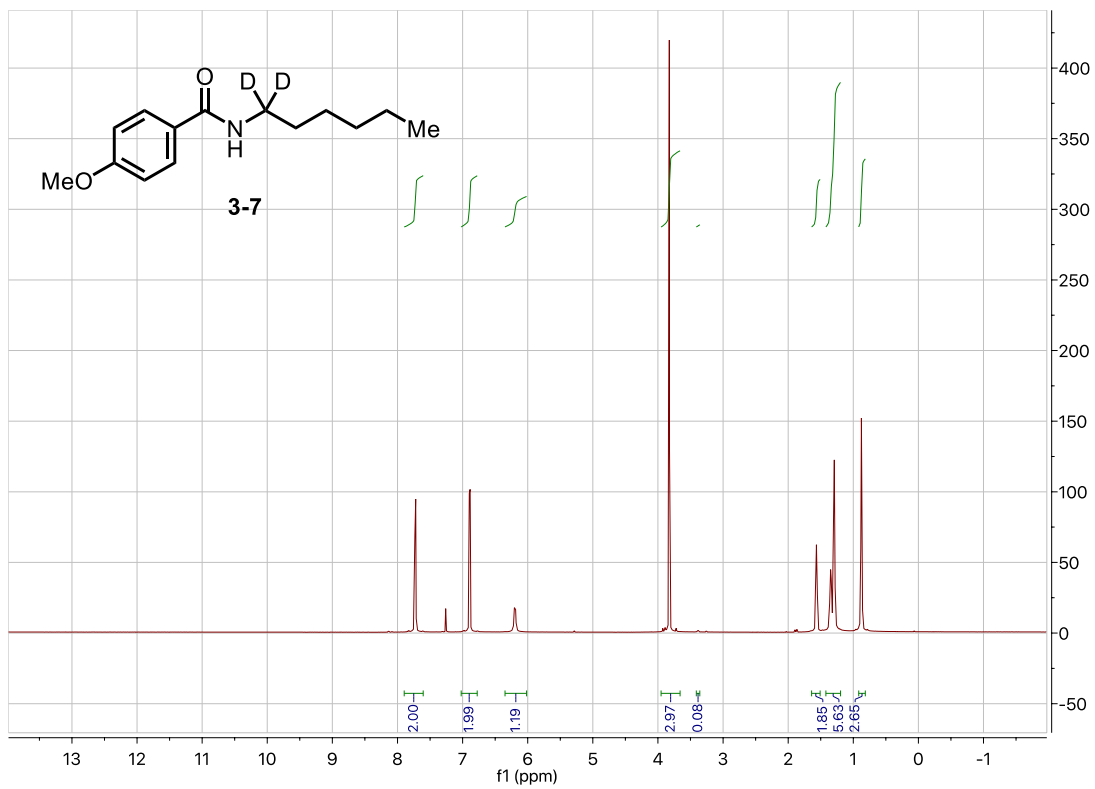
COSY of 2-152

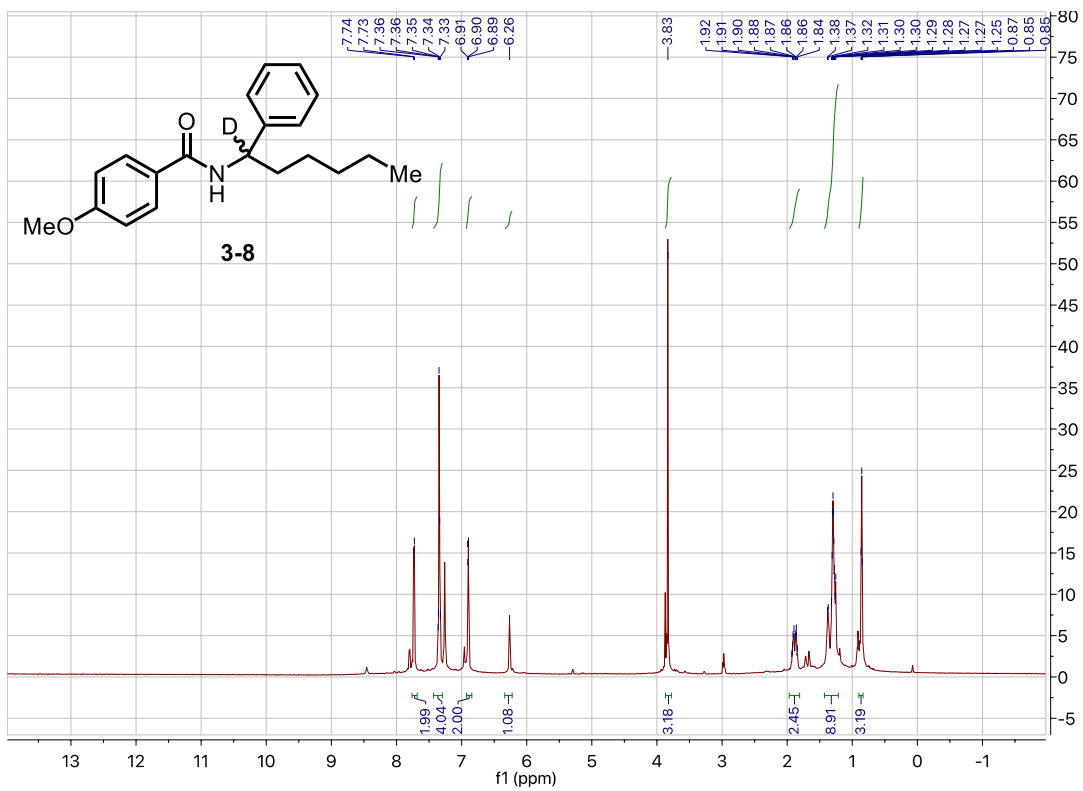
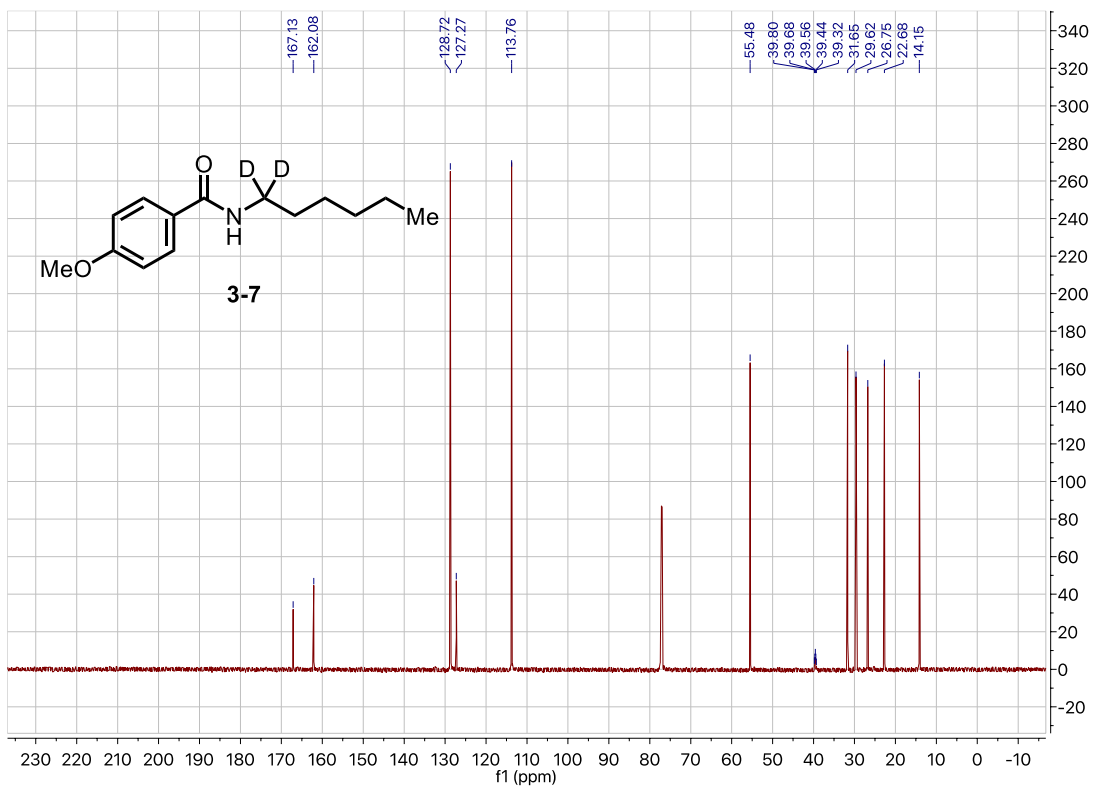


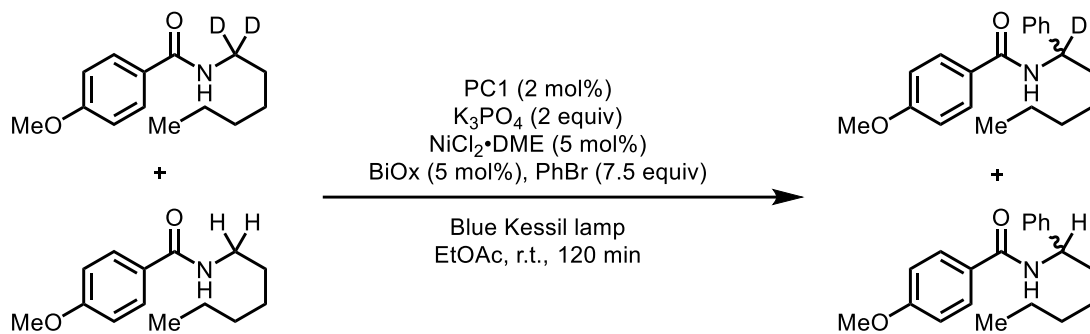
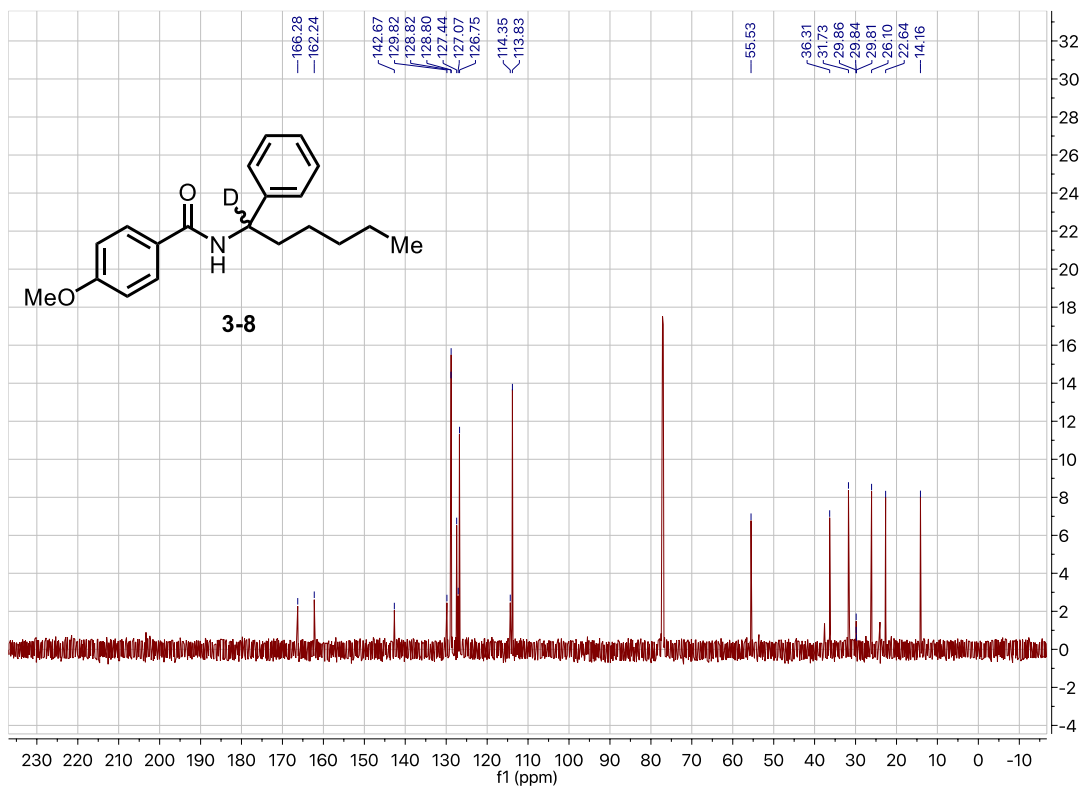
TOCSY of 2-152



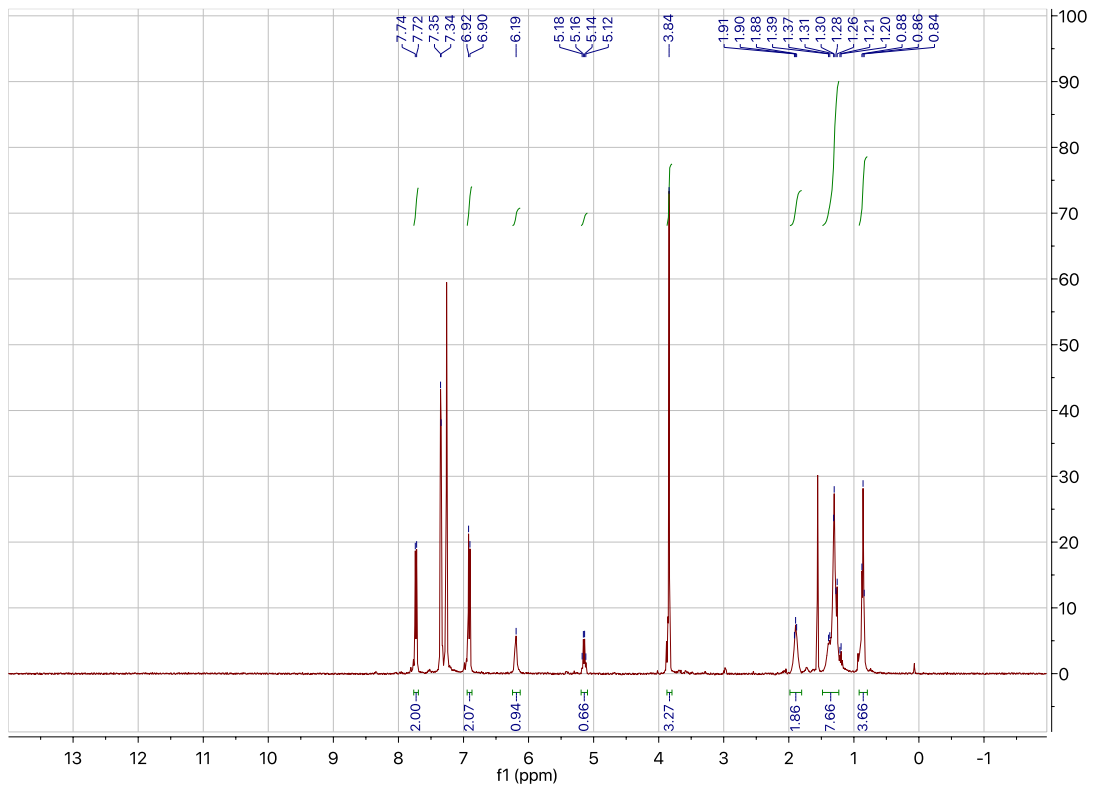




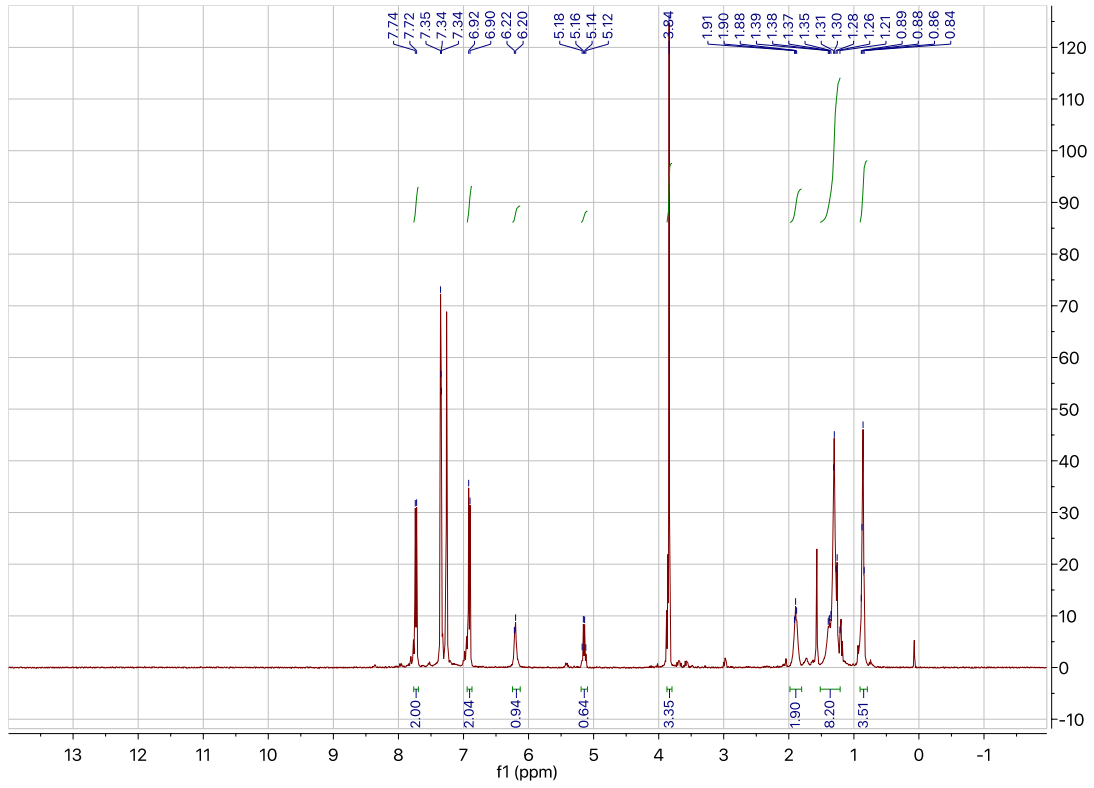


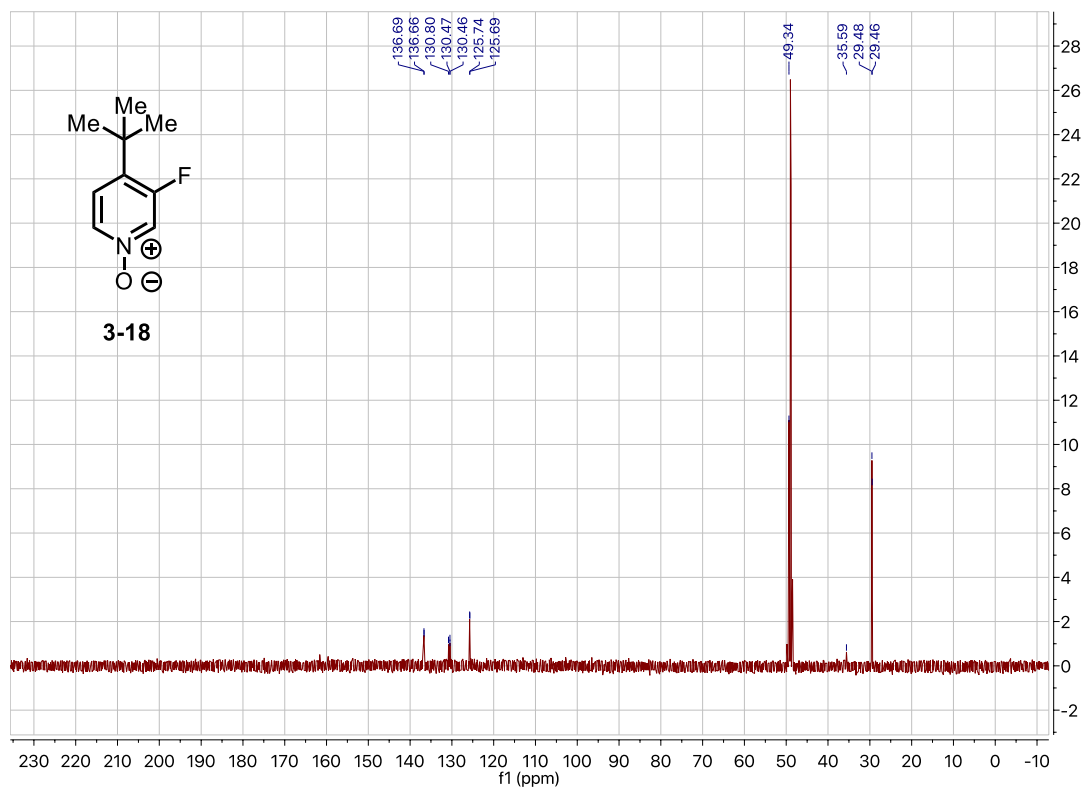
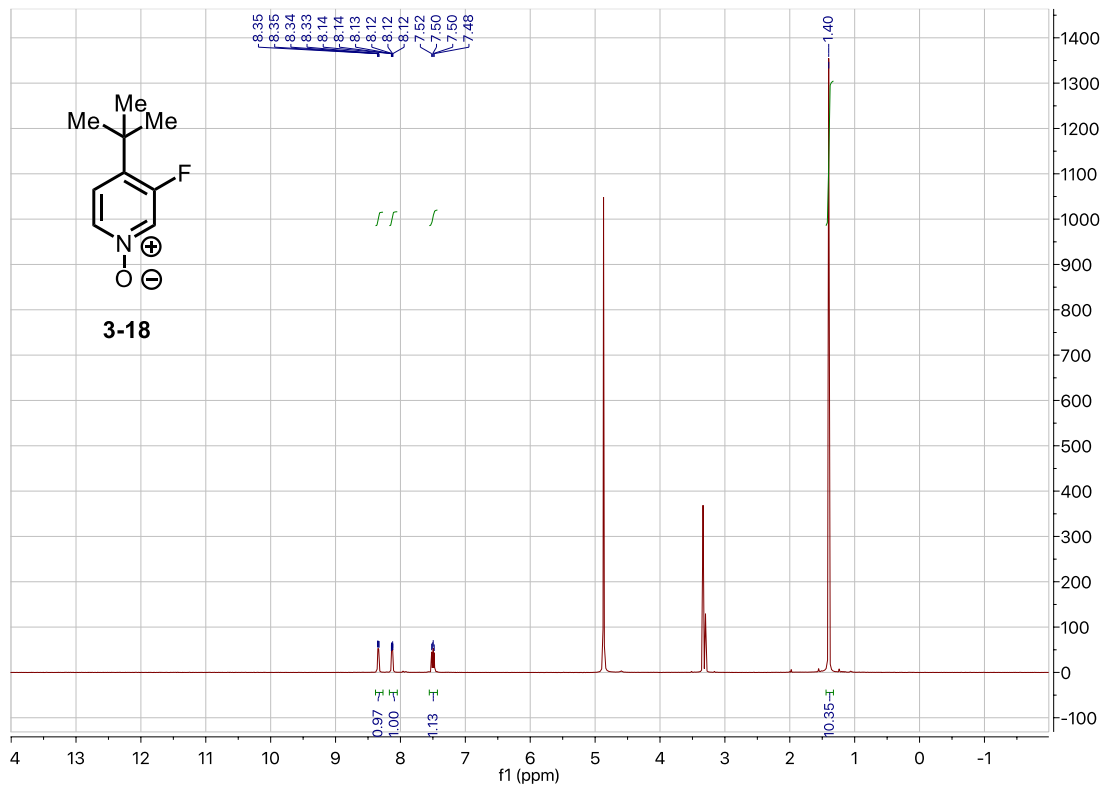


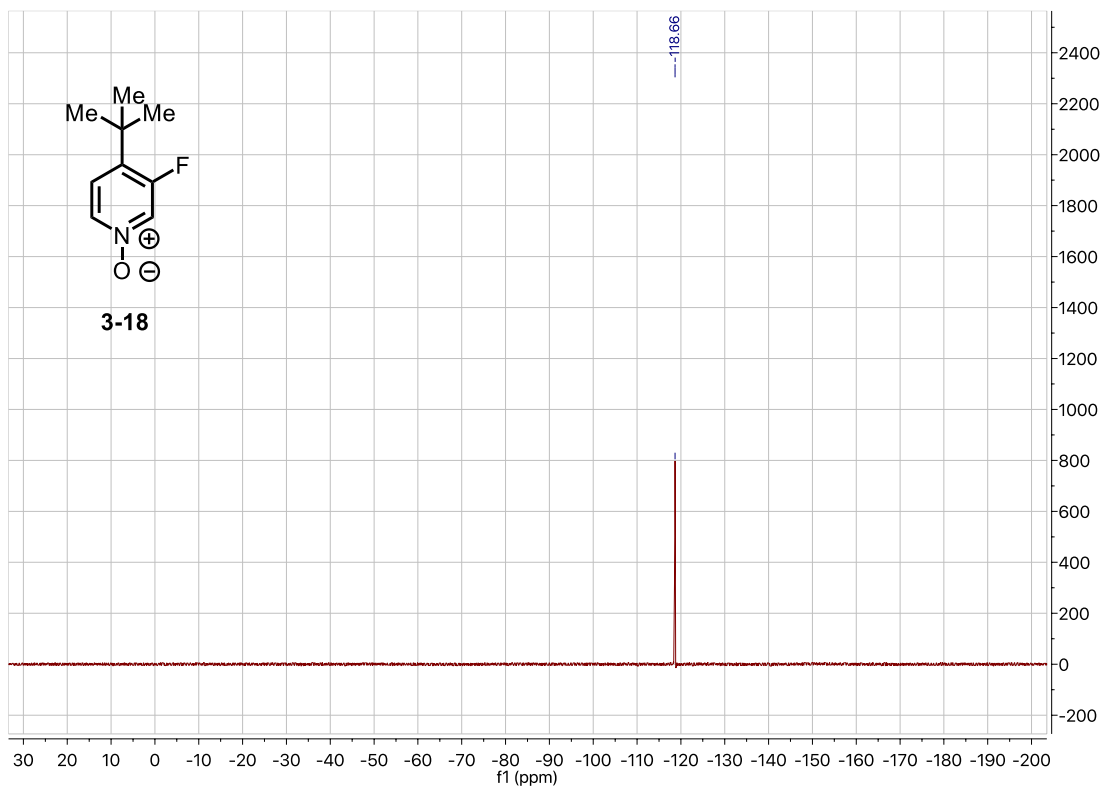
KIE Experiment #1:

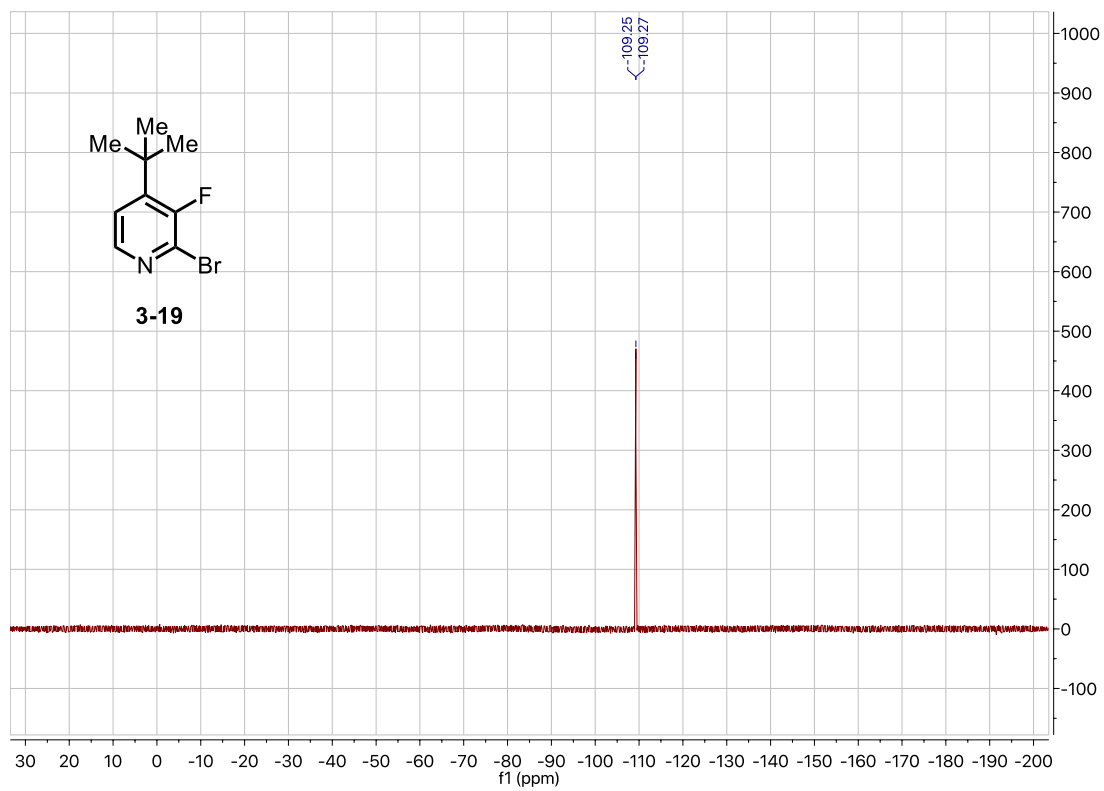
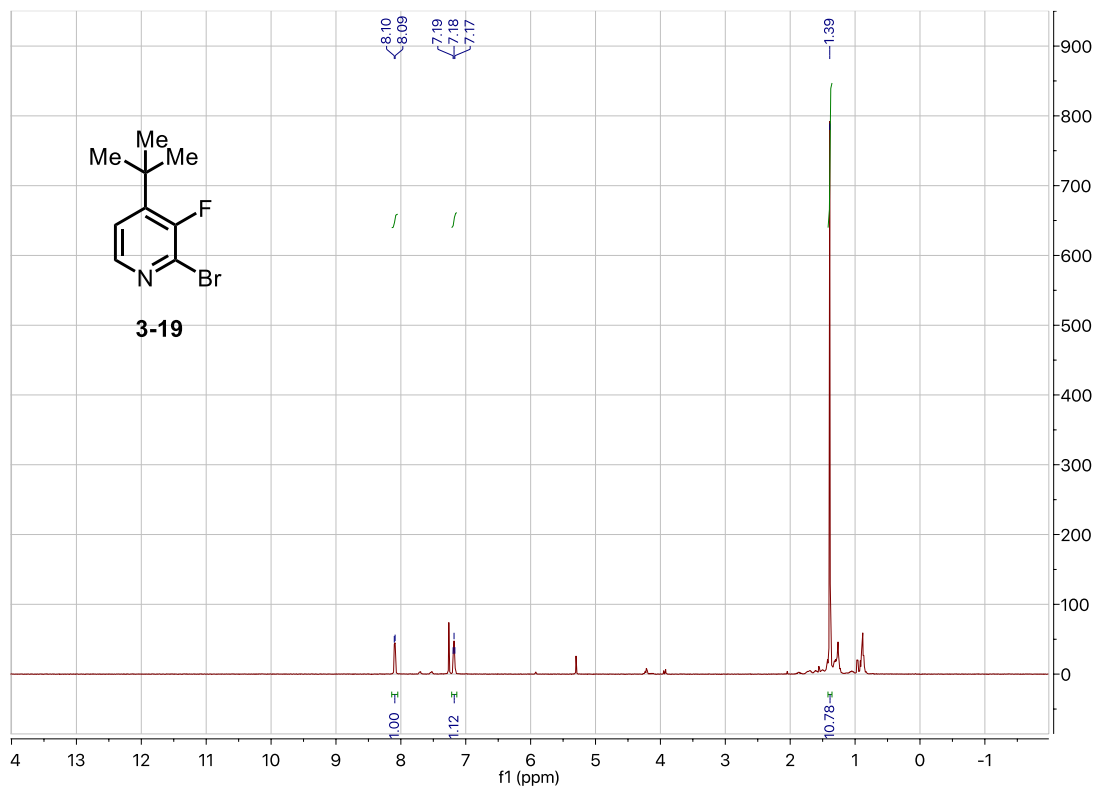


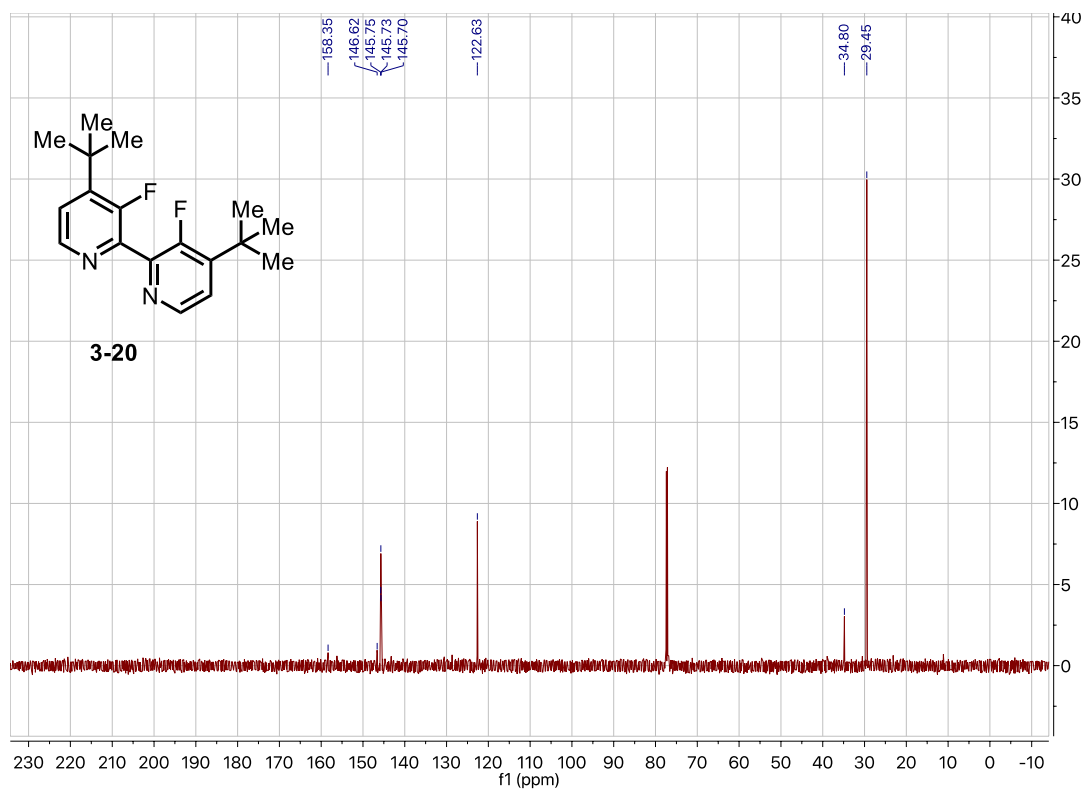
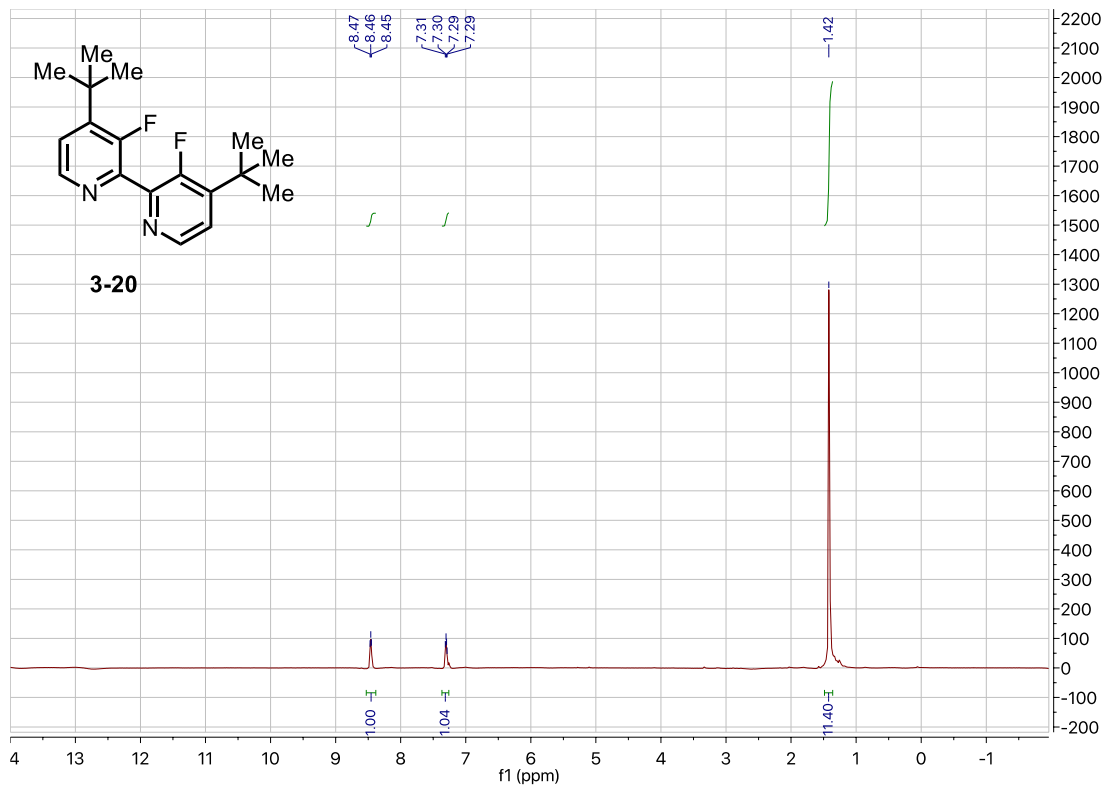
KIE Experiment #2:

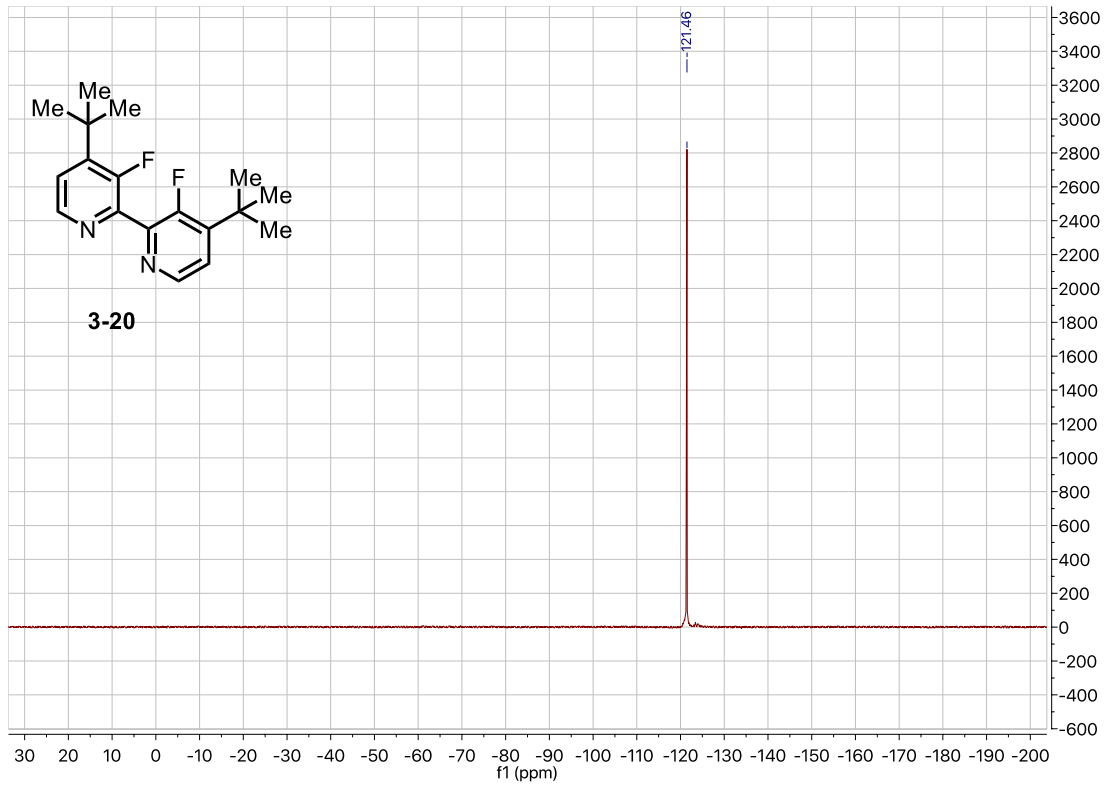


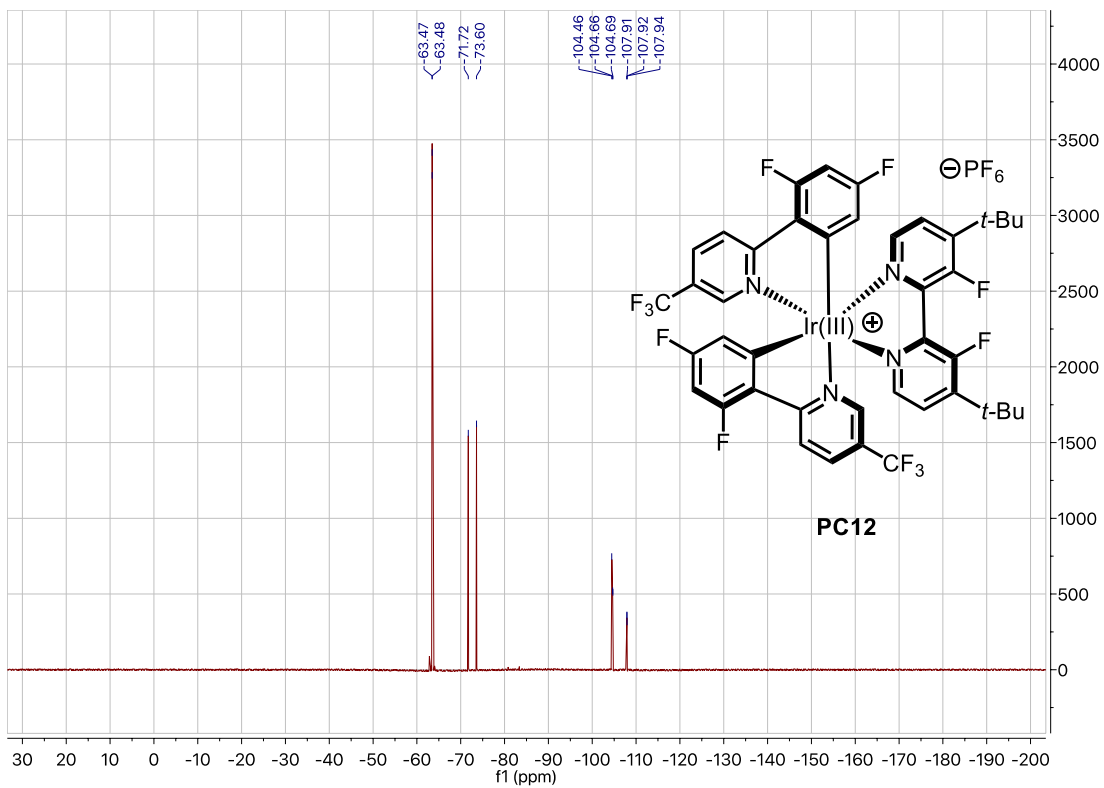
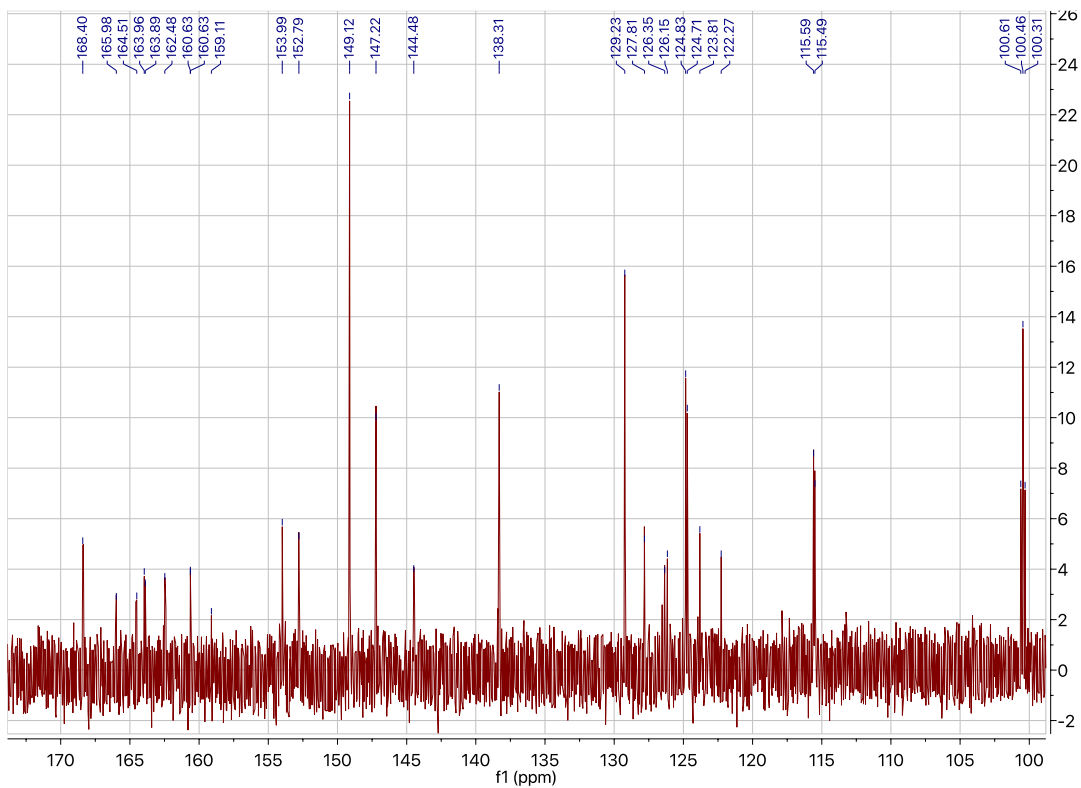


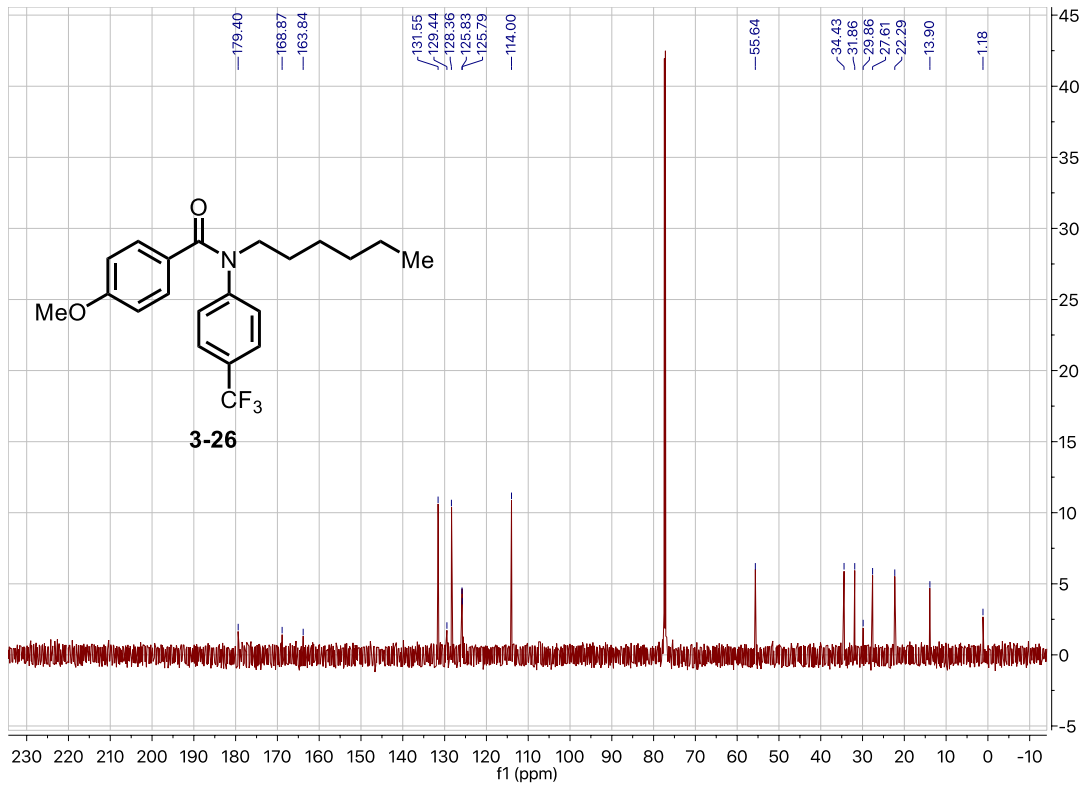
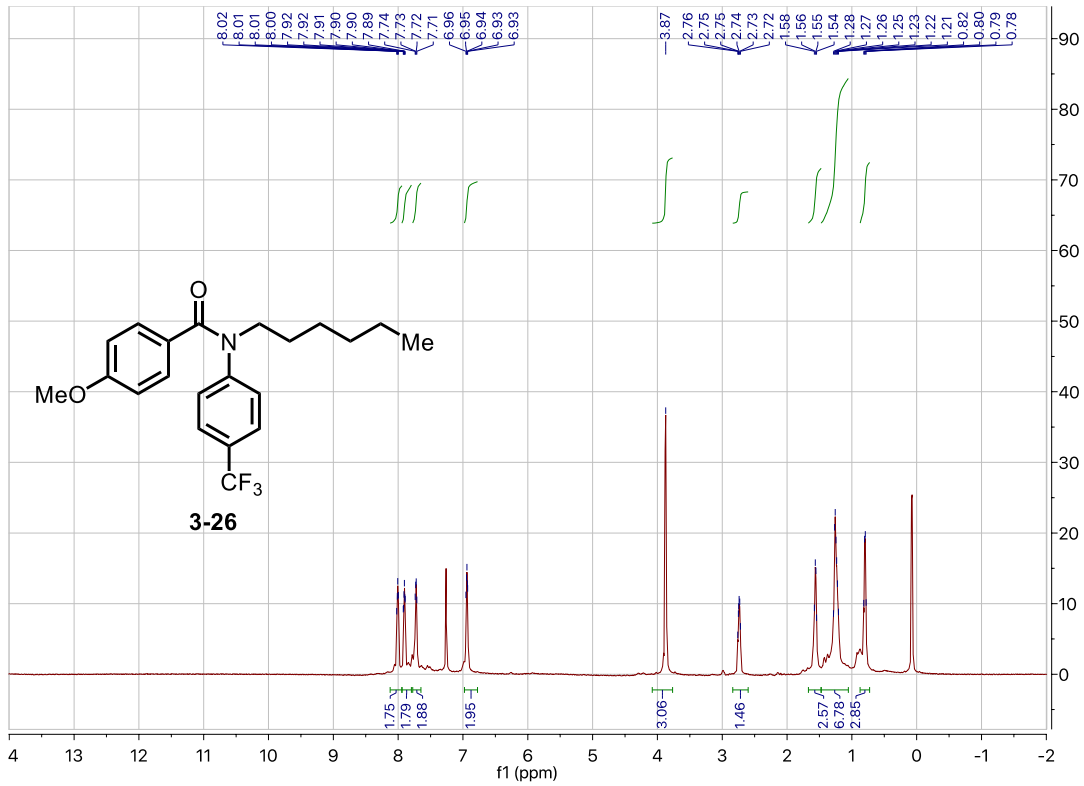


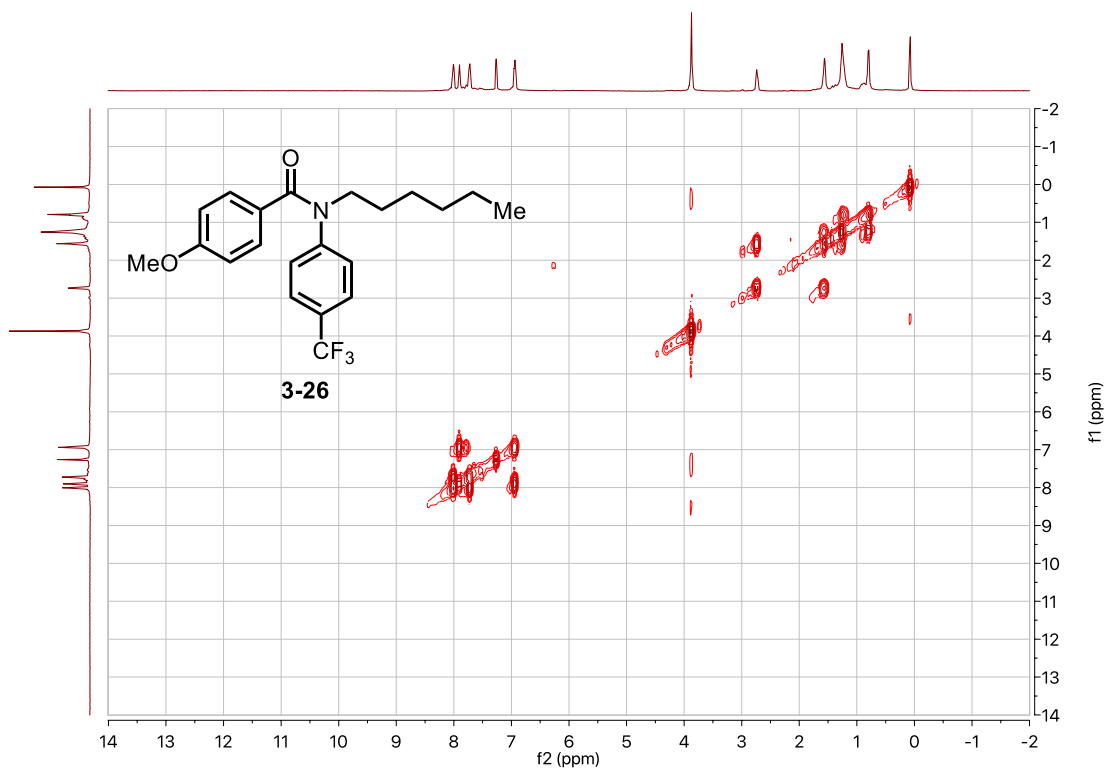
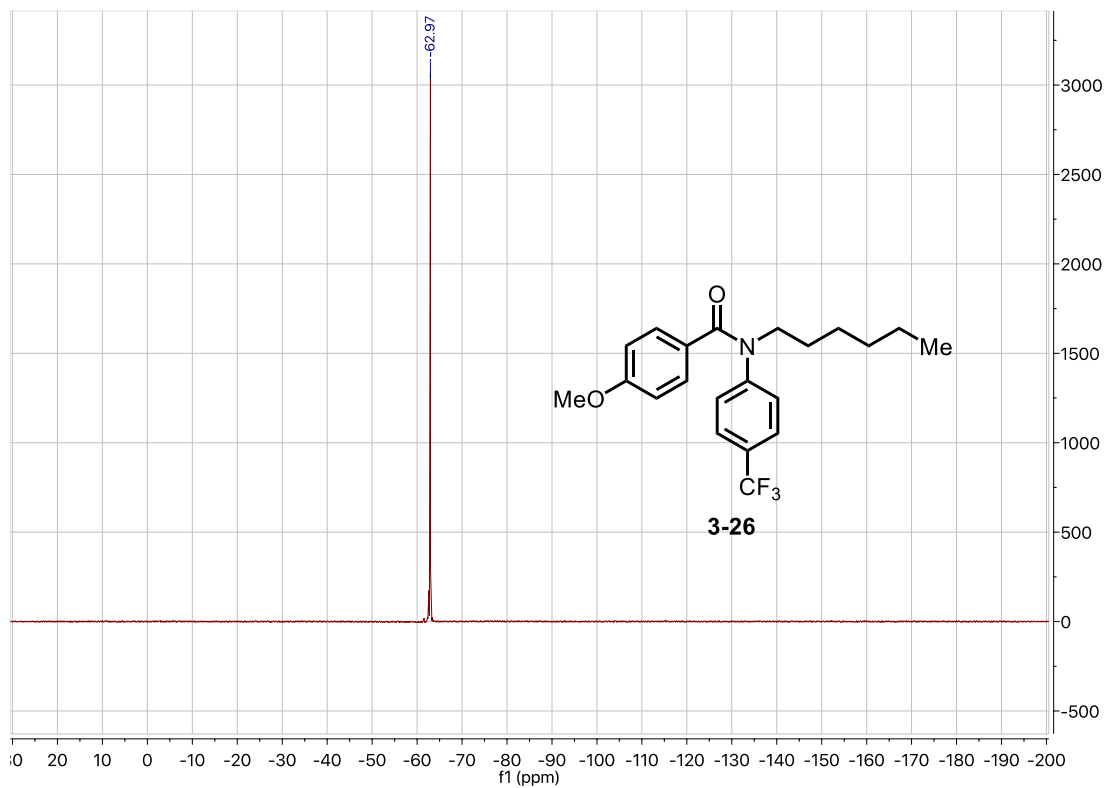


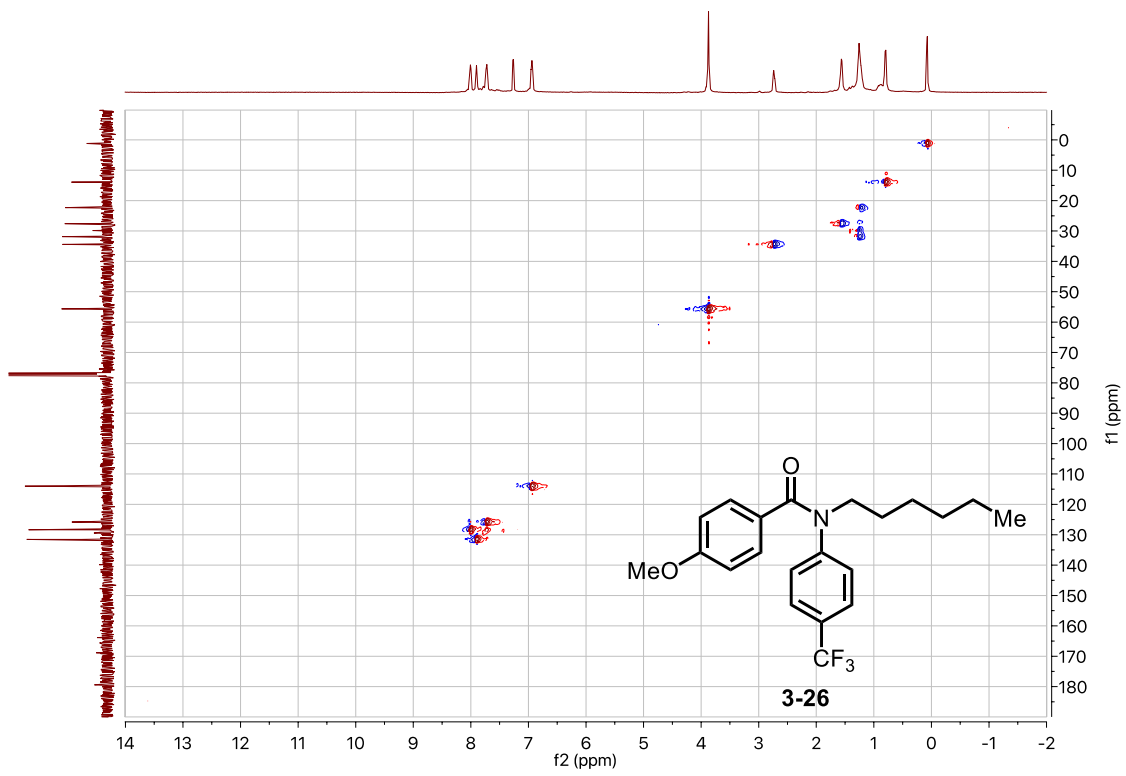












Bibliography

1. Eller, K.; Henkes, E.; Rossbacher, R.; Höke, H., Amines, Aliphatic. In *Ullmann's Encyclopedia of Industrial Chemistry*, 2000.
2. Ouyang, K.; Hao, W.; Zhang, W. X.; Xi, Z., Transition-Metal-Catalyzed Cleavage of C-N Single Bonds. *Chem. Rev.* **2015**, *115* (21), 12045-90.
3. Pound, S. M.; Watson, M. P., Asymmetric synthesis via stereospecific C-N and C-O bond activation of alkyl amine and alcohol derivatives. *Chem. Commun.* **2018**, *54* (87), 12286-12301.
4. Hie, L.; Fine Nathel, N. F.; Shah, T. K.; Baker, E. L.; Hong, X.; Yang, Y. F.; Liu, P.; Houk, K. N.; Garg, N. K., Conversion of amides to esters by the nickel-catalysed activation of amide C-N bonds. *Nature* **2015**, *524* (7563), 79-83.
5. Dander, J. E.; Garg, N. K., Breaking Amides using Nickel Catalysis. *ACS Catal.* **2017**, *7* (2), 1413-1423.
6. Meng, G.; Szostak, M., N-Acyl-Glutarimides: Privileged Scaffolds in Amide N-C Bond Cross-Coupling. *Euro. J. Org. Chem.* **2018**, *2018* (20-21), 2352-2365.
7. Weires, N. A.; Baker, E. L.; Garg, N. K., Nickel-catalysed Suzuki–Miyaura coupling of amides. *Nat. Chem.* **2015**, *8* (1), 75-79.
8. Ji, C. L.; Hong, X., Factors Controlling the Reactivity and Chemoselectivity of Resonance Destabilized Amides in Ni-Catalyzed Decarbonylative and Nondecarbonylative Suzuki–Miyaura Coupling. *J. Am. Chem. Soc.* **2017**, *139* (43), 15522-15529.
9. Lei, P.; Meng, G.; Ling, Y.; An, J.; Nolan, S. P.; Szostak, M., General Method for the Suzuki–Miyaura Cross-Coupling of Primary Amide-Derived Electrophiles Enabled by [Pd(NHC)(cin)Cl] at Room Temperature. *Org. Lett.* **2017**, *19* (24), 6510-6513.
10. Lei, P.; Meng, G.; Ling, Y.; An, J.; Szostak, M., Pd-PEPPSI: Pd-NHC Precatalyst for Suzuki–Miyaura Cross-Coupling Reactions of Amides. *J. Org. Chem.* **2017**, *82* (13), 6638-6646.

11. Meng, G.; Lalancette, R.; Szostak, R.; Szostak, M., N-Methylamino Pyrimidyl Amides (MAPA): Highly Reactive, Electronically-Activated Amides in Catalytic N-C(O) Cleavage. *Org. Lett.* **2017**, *19* (17), 4656-4659.
12. Simmons, B. J.; Weires, N. A.; Dander, J. E.; Garg, N. K., Nickel-Catalyzed Alkylation of Amide Derivatives. *ACS Catal.* **2016**, *6* (5), 3176-3179.
13. Medina, J. M.; Moreno, J.; Racine, S.; Du, S.; Garg, N. K., Mizoroki-Heck Cyclizations of Amide Derivatives for the Introduction of Quaternary Centers. *Angew. Chem. Int. Ed. Engl.* **2017**, *56* (23), 6567-6571.
14. Walker, J. A., Jr.; Vickerman, K. L.; Humke, J. N.; Stanley, L. M., Ni-Catalyzed Alkene Carboacylation via Amide C-N Bond Activation. *J. Am. Chem. Soc.* **2017**, *139* (30), 10228-10231.
15. Weires, N. A.; Caspi, D. D.; Garg, N. K., Kinetic Modeling of the Nickel-Catalyzed Esterification of Amides. *ACS Catal.* **2017**, *7* (7), 4381-4385.
16. Meng, G.; Lei, P.; Szostak, M., A General Method for Two-Step Transamidation of Secondary Amides Using Commercially Available, Air- and Moisture-Stable Palladium/NHC (N-Heterocyclic Carbene) Complexes. *Org. Lett.* **2017**, *19* (8), 2158-2161.
17. Zhou, T.; Li, G.; Nolan, S. P.; Szostak, M., [Pd(NHC)(acac)Cl]: Well-Defined, Air-Stable, and Readily Available Precatalysts for Suzuki and Buchwald-Hartwig Cross-coupling (Transamidation) of Amides and Esters by N-C/O-C Activation. *Org. Lett.* **2019**, *21* (9), 3304-3309.
18. Liu, X.; Yue, H.; Jia, J.; Guo, L.; Rueping, M., Synthesis of Amidines from Amides Using a Nickel-Catalyzed Decarbonylative Amination through CO Extrusion Intramolecular Recombination Fragment Coupling. *Chemistry* **2017**, *23* (49), 11771-11775.
19. Dey, A.; Sasmal, S.; Seth, K.; Lahiri, G. K.; Maiti, D., Nickel-Catalyzed Deamidative Step-Down Reduction of Amides to Aromatic Hydrocarbons. *ACS Catal.* **2016**, *7* (1), 433-437.
20. Meng, G.; Szostak, M., Site-Selective C-H/C-N Activation by Cooperative Catalysis: Primary Amides as Arylating Reagents in Directed C-H Arylation. *ACS Catal.* **2017**, *7* (10), 7251-7256.
21. Ni, S.; Zhang, W.; Mei, H.; Han, J.; Pan, Y., Ni-Catalyzed Reductive Cross-Coupling of Amides with Aryl Iodide Electrophiles via C-N Bond Activation. *Org. Lett.* **2017**, *19* (10), 2536-2539.
22. Shi, S.; Szostak, M., Decarbonylative Cyanation of Amides by Palladium Catalysis. *Org. Lett.* **2017**, *19* (12), 3095-3098.

23. Liu, L.; Zhou, D.; Liu, M.; Zhou, Y.; Chen, T., Palladium-Catalyzed Decarbonylative Alkynylation of Amides. *Org. Lett.* **2018**, *20* (9), 2741-2744.
24. Katritzky, A. R.; Marson, C. M., Pyrylium Mediated Transformations of Primary Amino Groups into Other Functional Groups. New Synthetic Methods (41). *Angew. Chem. Int. Ed. Engl.* **1984**, *23* (6), 420-429.
25. He, F.-S.; Ye, S.; Wu, J., Recent Advances in Pyridinium Salts as Radical Reservoirs in Organic Synthesis. *ACS Catal.* **2019**, *9* (10), 8943-8960.
26. JT, M. C.; V, A. F.; Matsuo, B. T.; JA, C. D.; de Souza, W. C.; Paixao, M. W., Photoinduced deaminative strategies: Katritzky salts as alkyl radical precursors. *Chem. Commun.* **2020**, *56* (4), 503-514.
27. Rossler, S. L.; Jelier, B. J.; Magnier, E.; Dagousset, G.; Carreira, E. M.; Togni, A., Pyridinium Salts as Redox-Active Functional Group Transfer Reagents. *Angew. Chem. Int. Ed. Engl.* **2019**.
28. Basch, C. H.; Liao, J.; Xu, J.; Piane, J. J.; Watson, M. P., Harnessing Alkyl Amines as Electrophiles for Nickel-Catalyzed Cross Couplings via C-N Bond Activation. *J. Am. Chem. Soc.* **2017**, *139* (15), 5313-5316.
29. Guan, W.; Liao, J.; Watson, M. P., Vinylation of Benzylic Amines via C-N Bond Functionalization of Benzylic Pyridinium Salts. *Synth.* **2018**, *50* (16), 3231-3237.
30. Liao, J.; Guan, W.; Boscoe, B. P.; Tucker, J. W.; Tomlin, J. W.; Garnsey, M. R.; Watson, M. P., Transforming Benzylic Amines into Diarylmethanes: Cross-Couplings of Benzylic Pyridinium Salts via C-N Bond Activation. *Org. Lett.* **2018**, *20* (10), 3030-3033.
31. Baker, K. M.; Lucas Baca, D.; Plunkett, S.; Daneker, M. E.; Watson, M. P., Engaging Alkenes and Alkynes in Deaminative Alkyl-Alkyl and Alkyl-Vinyl Cross-Couplings of Alkylpyridinium Salts. *Org. Lett.* **2019**, *21* (23), 9738-9741.
32. Hoerrner, M. E.; Baker, K. M.; Basch, C. H.; Bampo, E. M.; Watson, M. P., Deaminative Arylation of Amino Acid-derived Pyridinium Salts. *Org. Lett.* **2019**, *21* (18), 7356-7360.
33. Plunkett, S.; Basch, C. H.; Santana, S. O.; Watson, M. P., Harnessing Alkylpyridinium Salts as Electrophiles in Deaminative Alkyl-Alkyl Cross-Couplings. *J. Am. Chem. Soc.* **2019**, *141* (6), 2257-2262.
34. Klauck, F. J. R.; James, M. J.; Glorius, F., Deaminative Strategy for the Visible-Light-Mediated Generation of Alkyl Radicals. *Angew. Chem. Int. Ed. Engl.* **2017**, *56* (40), 12336-12339.
35. Wu, J.; He, L.; Noble, A.; Aggarwal, V. K., Photoinduced Deaminative Borylation of Alkylamines. *J. Am. Chem. Soc.* **2018**, *140* (34), 10700-10704.

36. Li, C.-L.; Jiang, X.; Lu, L.-Q.; Xiao, W.-J.; Wu, X.-F., Cobalt(II)-Catalyzed Alkoxyacylation of Aliphatic Amines via C–N Bond Activation. *Org. Lett.* **2019**, *21* (17), 6919-6923.
37. Kim, I.; Im, H.; Lee, H.; Hong, S., N-Heterocyclic carbene-catalyzed deaminative cross-coupling of aldehydes with Katritzky pyridinium salts. *Chem. Sci.* **2020**, *11* (12), 3192-3197.
38. Liao, J.; Basch, C. H.; Hoerrner, M. E.; Talley, M. R.; Boscoe, B. P.; Tucker, J. W.; Garnsey, M. R.; Watson, M. P., Deaminative Reductive Cross-Electrophile Couplings of Alkylpyridinium Salts and Aryl Bromides. *Org. Lett.* **2019**, *21* (8), 2941-2946.
39. Martin-Montero, R.; Yatham, V. R.; Yin, H.; Davies, J.; Martin, R., Ni-catalyzed Reductive Deaminative Arylation at sp³ Carbon Centers. *Org. Lett.* **2019**, *21* (8), 2947-2951.
40. Sun, S. Z.; Romano, C.; Martin, R., Site-Selective Catalytic Deaminative Alkylation of Unactivated Olefins. *J. Am. Chem. Soc.* **2019**, *141* (41), 16197-16201.
41. Wu, J.; Grant, P. S.; Li, X.; Noble, A.; Aggarwal, V. K., Catalyst-Free Deaminative Functionalizations of Primary Amines by Photoinduced Single-Electron Transfer. *Angew. Chem. Int. Ed. Engl.* **2019**, *58* (17), 5697-5701.
42. Yi, J.; Badir, S. O.; Kammer, L. M.; Ribagorda, M.; Molander, G. A., Deaminative Reductive Arylation Enabled by Nickel/Photoredox Dual Catalysis. *Org. Lett.* **2019**, *21* (9), 3346-3351.
43. Moser, D.; Duan, Y.; Wang, F.; Ma, Y.; O'Neill, M. J.; Cornella, J., Selective Functionalization of Aminoheterocycles by a Perylum Salt. *Angew. Chem. Int. Ed. Engl.* **2018**, *57* (34), 11035-11039.
44. Hu, J.; Sun, H.; Cai, W.; Pu, X.; Zhang, Y.; Shi, Z., Nickel-Catalyzed Borylation of Aryl- and Benzyltrimethylammonium Salts via C-N Bond Cleavage. *J. Org. Chem.* **2016**, *81* (1), 14-24.
45. Ruiz-Castillo, P.; Buchwald, S. L., Applications of Palladium-Catalyzed C-N Cross-Coupling Reactions. *Chem. Rev.* **2016**, *116* (19), 12564-12649.
46. Nicholas A. McGrath, M. B., and Jon T. Njardarson, A Graphical Journey of Innovative Organic Architectures That Have Improved Our Lives. *J. Chem. Ed.* **2012**, *87* (12), 1348-1359.
47. Dong, Z.; Wang, J.; Dong, G., Simple Amine-Directed Meta-Selective C-H Arylation via Pd/Norbornene Catalysis. *J. Am. Chem. Soc.* **2015**, *137* (18), 5887-90.

48. Zhang, H.; Hagihara, S.; Itami, K., Making Dimethylamino a Transformable Directing Group by Nickel-Catalyzed C-N Borylation. *Chemistry* **2015**, *21* (47), 16796-800.
49. Yang, S.; Li, B.; Wan, X.; Shi, Z., Ortho Arylation of Acetanilides via Pd(II)-Catalyzed C-H Functionalization. *J. Am. Chem. Soc.* **2007**, *129* (19), 6066-6067.
50. Nishikata, T.; Abela, A. R.; Huang, S.; Lipshutz, B. H., Cationic palladium(II) catalysis: C-H activation/Suzuki-Miyaura couplings at room temperature. *J. Am. Chem. Soc.* **2010**, *132* (14), 4978-9.
51. Crisenza, G. E.; Sokolova, O. O.; Bower, J. F., Branch-Selective Alkene Hydroarylation by Cooperative Destabilization: Iridium-Catalyzed ortho-Alkylation of Acetanilides. *Angew. Chem. Int. Ed. Engl.* **2015**, *54* (49), 14866-70.
52. Leitch, J. A.; McMullin, C. L.; Paterson, A. J.; Mahon, M. F.; Bhonoah, Y.; Frost, C. G., Ruthenium-Catalyzed para-Selective C-H Alkylation of Aniline Derivatives. *Angew. Chem. Int. Ed. Engl.* **2017**, *56* (47), 15131-15135.
53. Larock, R. C.; Yum, E. K., Synthesis of indoles via palladium-catalyzed heteroannulation of internal alkynes. *J. Am. Chem. Soc.* **1991**, *113* (17), 6689-6690.
54. Sandmeyer, T., Ueber die Ersetzung der Amidgruppe durch Chlor in den aromatischen Substanzen. *Berichte der deutschen chemischen Gesellschaft* **1884**, *17* (2), 1633-1635.
55. Mo, F.; Dong, G.; Zhang, Y.; Wang, J., Recent applications of arene diazonium salts in organic synthesis. *Org. Biomol. Chem.* **2013**, *11* (10), 1582-93.
56. Anna Roglans, A. P.-Q., and Marcial Moreno-Manas, Diazonium Salts as Substrates in Palladium-Catalyzed Cross-Coupling Reactions. *Chem. Rev.* **2006**, *106*, 4622-4643.
57. Matsuda, K. K. a. T., Reaction of Diazonium Salts with Transition Metals. I. Arylation of Olefins with Arenediazonium Salts Catalyzed by Zero Valent Palladium. *Chem. Lett.* **1977**, *6*, 159-162.
58. Oger, N.; d'Halluin, M.; Le Grogne, E.; Felpin, F.-X., Using Aryl Diazonium Salts in Palladium-Catalyzed Reactions under Safer Conditions. *Org. Process Res. Dev.* **2014**, *18* (12), 1786-1801.
59. Cong, X.; Fan, F.; Ma, P.; Luo, M.; Chen, H.; Zeng, X., Low-Valent, High-Spin Chromium-Catalyzed Cleavage of Aromatic Carbon-Nitrogen Bonds at Room Temperature: A Combined Experimental and Theoretical Study. *J. Am. Chem. Soc.* **2017**, *139* (42), 15182-15190.
60. Ueno, S.; Chatani, N.; Kakiuchi, F., Ruthenium-Catalyzed Carbon-Carbon Bond Formation via the Cleavage of an Unreactive Aryl Carbon-Nitrogen Bond in

- Aniline Derivatives with Organoboronates. *J. Am. Chem. Soc.* **2007**, *129* (19), 6098-6099.
61. Cao, Z.-C.; Xie, S.-J.; Fang, H.; Shi, Z.-J., Ni-Catalyzed Cross-Coupling of Dimethyl Aryl Amines with Arylboronic Esters under Reductive Conditions. *J. Am. Chem. Soc.* **2018**, *140* (42), 13575-13579.
 62. Tetsuro Koreeda, T. K., and Fumitoshi Kakiuchi, Cleavage of C–N Bonds in Aniline Derivatives on a Ruthenium Center and Its Relevance to Catalytic C–C Bond Formation. *J. Am. Chem. Soc.* **2009**, *131*, 7236-7239.
 63. Cao, Z. C.; Li, X. L.; Luo, Q. Y.; Fang, H.; Shi, Z. J., Direct Borylation of Tertiary Anilines via C-N Bond Activation. *Org. Lett.* **2018**, *20* (7), 1995-1998.
 64. Scholl, B., Jolidon, Synèse, and Hansen, Hans-Jürgen, Photosolvolysis of 2-Allylated Anilines to 2-Indanols. *Helv. Chim. Acta* **1986**, *69* (1), 184-194.
 65. Zhao, Y.; Snieckus, V., Amide-Directed Ru-Catalyzed Hydrodemethoxylation of ortho-Methoxy-Benzamides and -Naphthamides: A D oM Reaction Counterpart. *Org. Lett.* **2018**, *20* (10), 2826-2830.
 66. Ernest Wenkert, A.-L. H., and Christian-Johannes Jenny, Nickel-Induced Conversion of Carbon–Nitrogen into Carbon– Carbon Bonds. One-step Transformations of Aryl, Quaternary Ammonium Salts into Alkylarenes and Biaryls. *J. Chem. Soc. Chem. Commun.* **1988**, *0*, 975-976.
 67. Napolitano, J. P. Dealkylation of n-alkyl aromatic amines. 3,759,997, 2-14-1969, 1973.
 68. Guo, W.-J.; Wang, Z.-X., Iron-catalyzed cross-coupling of aryltrimethylammonium triflates and alkyl Grignard reagents. *Tetrahedron* **2013**, *69* (46), 9580-9585.
 69. Johnathan T Reeves, D. R. F., Zhulin Tan, Jinhua J. Song, Heewon Lee, Nathan K. Yee, and Chris H. Senanayake, Room Temperature Palladium-Catalyzed Cross Coupling of Aryltrimethylammonium Triflates with Aryl Grignard Reagents. *Org. Lett.* **2010**, *12* (19), 4388-4391.
 70. MacMillan, S. B. B. a. D. W. C., The First Suzuki Cross-Couplings of Aryltrimethylammonium Salts. *J. Am. Chem. Soc.* **2003**, *125* (6046-6047).
 71. Xie, L. G.; Wang, Z. X., Nickel-catalyzed cross-coupling of aryltrimethylammonium iodides with organozinc reagents. *Angew. Chem. Int. Ed. Engl.* **2011**, *50* (21), 4901-4.
 72. Zhang, Q.; Zhang, X. Q.; Wang, Z. X., Nickel complexes supported by quinoline-based ligands: synthesis, characterization and catalysis in the cross-coupling of arylzinc reagents and aryl chlorides or aryltrimethylammonium salts. *Dalton Trans.* **2012**, *41* (34), 10453-64.

73. Zhang, X. Q.; Wang, Z. X., Cross-coupling of aryltrimethylammonium iodides with arylzinc reagents catalyzed by amido pincer nickel complexes. *J. Org. Chem.* **2012**, *77* (7), 3658-63.
74. Chen, Q.; Gao, F.; Tang, H.; Yao, M.; Zhao, Q.; Shi, Y.; Dang, Y.; Cao, C., Sonogashira Cross-Coupling of Aryltrimethylammonium Salts. *ACS Catal.* **2019**, *9* (4), 3730-3736.
75. Wang, D. Y.; Kawahata, M.; Yang, Z. K.; Miyamoto, K.; Komagawa, S.; Yamaguchi, K.; Wang, C.; Uchiyama, M., Stille coupling via C-N bond cleavage. *Nat. Commun.* **2016**, *7*, 12937.
76. Basch, C. H.; Cobb, K. M.; Watson, M. P., Nickel-Catalyzed Borylation of Benzylic Ammonium Salts: Stereospecific Synthesis of Enantioenriched Benzylic Boronates. *Org. Lett.* **2016**, *18* (1), 136-9.
77. Alicia B. Chopa, M. T. L., and Gustavo Silbestri, Synthesis of Aryl Stannanes from Arylamines. *Organometallics* **2001**, *20*, 3358-3360.
78. Yang, B.; Wang, Z. X., Ni-Catalyzed C-P Coupling of Aryl, Benzyl, or Allyl Ammonium Salts with P(O)H Compounds. *J. Org. Chem.* **2019**, *84* (3), 1500-1509.
79. Wang, D. Y.; Yang, Z. K.; Wang, C.; Zhang, A.; Uchiyama, M., From Anilines to Aryl Ethers: A Facile, Efficient, and Versatile Synthetic Method Employing Mild Conditions. *Angew. Chem. Int. Ed. Engl.* **2018**, *57* (14), 3641-3645.
80. Zhang, X. Q.; Wang, Z. X., Nickel-catalyzed cross-coupling of aryltrimethylammonium triflates and amines. *Org. Biomol. Chem.* **2014**, *12* (9), 1448-53.
81. Paras, N. A.; Simmons, B.; MacMillan, D. W. C., A process for the rapid removal of dialkylamino-substituents from aromatic rings. Application to the expedient synthesis of (R)-tolterodine. *Tetrahedron* **2009**, *65* (16), 3232-3238.
82. Yi, Y. Q.; Yang, W. C.; Zhai, D. D.; Zhang, X. Y.; Li, S. Q.; Guan, B. T., Nickel-catalyzed C-N bond reduction of aromatic and benzylic quaternary ammonium triflates. *Chem. Commun.* **2016**, *52* (72), 10894-7.
83. Shacklady-McAtee, D. M.; Roberts, K. M.; Basch, C. H.; Song, Y. G.; Watson, M. P., A General, Simple Catalyst for Enantiospecific Cross Couplings of Benzylic Ammonium Triflates and Boronic Acids: No Phosphine Ligand Required. *Tetrahedron* **2014**, *70* (27-28), 4257-4263.
84. Auner, N.; Weis, J., *Organosilicon chemistry VI: from molecules to materials*. Wiley-VCH: 2005.

85. Komiyama, T.; Minami, Y.; Hiyama, T., Aryl(triethyl)silanes for Biaryl and Teraryl Synthesis by Copper(II)-Catalyzed Cross-Coupling Reaction. *Angew. Chem. Int. Ed. Engl.* **2016**, *55* (51), 15787-15791.
86. Simmler, W., *Silicon Compounds, Inorganic*. 2000.
87. Barnes, M. J.; Conroy, R.; Miller, D. J.; Mills, J. S.; Montana, J. G.; Pooni, P. K.; Showell, G. A.; Walsh, L. M.; Warneck, J. B., Trimethylsilylpyrazoles as novel inhibitors of p38 MAP kinase: a new use of silicon bioisosteres in medicinal chemistry. *Bioorg. Med. Chem. Lett.* **2007**, *17* (2), 354-7.
88. Kenji Funaki, T. S., and Shuichi Oi, Pd-Catalyzed β -Selective Direct C–H Bond Arylation of Thiophenes with Aryltrimethylsilanes. *Org. Lett.* **2012**, *14* (24), 6186-6189.
89. Ma, Y.; Wang, B.; Zhang, L.; Hou, Z., Boron-Catalyzed Aromatic C-H Bond Silylation with Hydrosilanes. *J. Am. Chem. Soc.* **2016**, *138* (11), 3663-6.
90. Denmark, S. E.; Regens, C. S., Palladium-Catalyzed Cross-Coupling Reactions of Organosilanols and Their Salts: Practical Alternatives to Boron- and Tin-Based Methods. *Acc. of Chem. Res.* **2008**, *41* (11), 1486-1499.
91. Maji, A.; Guin, S.; Feng, S.; Dahiya, A.; Singh, V. K.; Liu, P.; Maiti, D., Experimental and Computational Exploration of para-Selective Silylation with a Hydrogen-Bonded Template. *Angew. Chem. Int. Ed. Engl.* **2017**, *56* (47), 14903-14907.
92. Modak, A.; Patra, T.; Chowdhury, R.; Raul, S.; Maiti, D., Palladium-Catalyzed Remote meta-Selective C–H Bond Silylation and Germanylation. *Organometallics* **2017**, *36* (13), 2418-2423.
93. Nozawa-Kumada, K.; Osawa, S.; Sasaki, M.; Chataigner, I.; Shigeno, M.; Kondo, Y., Deprotonative Silylation of Aromatic C–H Bonds Mediated by a Combination of Trifluoromethyltrialkylsilane and Fluoride. *J. Org. Chem.* **2017**, *82* (18), 9487-9496.
94. Zarate, C.; Martin, R., A mild Ni/Cu-catalyzed silylation via C-O cleavage. *J. Am. Chem. Soc.* **2014**, *136* (6), 2236-9.
95. Cheng, C.; Hartwig, J. F., Catalytic Silylation of Unactivated C-H Bonds. *Chem. Rev.* **2015**, *115* (17), 8946-75.
96. Lee, T.; Hartwig, J. F., Mechanistic Studies on Rhodium-Catalyzed Enantioselective Silylation of Aryl C-H Bonds. *J. Am. Chem. Soc.* **2017**, *139* (13), 4879-4886.
97. Hartwig, C. C. a. J. F., Rhodium-Catalyzed Intermolecular C-H Silylation of Arenes with High Steric Regiocontrol. *Science* **2014**, *343*, 853-857.

98. Cheng, C.; Hartwig, J. F., Iridium-catalyzed silylation of aryl C-H bonds. *J. Am. Chem. Soc.* **2015**, *137* (2), 592-5.
99. Simmons, E. M.; Hartwig, J. F., Iridium-Catalyzed Arene Ortho-Silylation by Formal Hydroxyl-Directed C-H Activation. *J. Am. Chem. Soc.* **2010**, *132* (48), 17092-17095.
100. Li, Q.; Driess, M.; Hartwig, J. F., Iridium-catalyzed regioselective silylation of aromatic and benzylic C-H bonds directed by a secondary amine. *Angew. Chem. Int. Ed. Engl.* **2014**, *53* (32), 8471-4.
101. Su, B.; Zhou, T. G.; Li, X. W.; Shao, X. R.; Xu, P. L.; Wu, W. L.; Hartwig, J. F.; Shi, Z. J., A Chiral Nitrogen Ligand for Enantioselective, Iridium-Catalyzed Silylation of Aromatic C-H Bonds. *Angew. Chem. Int. Ed. Engl.* **2017**, *56* (4), 1092-1096.
102. Karmel, C.; Chen, Z.; Hartwig, J. F., Iridium-Catalyzed Silylation of C-H Bonds in Unactivated Arenes: A Sterically Encumbered Phenanthroline Ligand Accelerates Catalysis. *J. Am. Chem. Soc.* **2019**, *141* (17), 7063-7072.
103. Fumitoshi, K.; Kimitaka, I.; Mitsutaka, M.; Naoto, C.; Shinji, M., Ruthenium-Catalyzed Dehydrogenative Silylation of Aryloxazolines with Hydrosilanes via C-H Bond Cleavage. *Chem. Lett.* **2001**, *30* (5), 422-423.
104. Murata, M.; Fukuyama, N.; Wada, J.-i.; Watanabe, S.; Masuda, Y., Platinum-catalyzed Aromatic C-H Silylation of Arenes with 1,1,1,3,5,5,5-Heptamethyltrisiloxane. *Chem. Lett.* **2007**, *36* (7), 910-911.
105. Toshiyasu, S.; Yuko, T.; Touru, S.; Masato, T., Catalytic C-H Activation. Silylation of Arenes with Hydrosilane or Disilane by RhCl(CO)(PMe₃)₂ under Irradiation. *Chem. Lett.* **1987**, *16* (12), 2375-2378.
106. Fumitoshi, K.; Kimitaka, I.; Mitsutaka, M.; Tomoo, H.; Naoto, C.; Shinji, M., A New Chelation-Assistance Mode for a Ruthenium-Catalyzed Silylation at the C-H Bond in Aromatic Ring with Hydrosilanes. *Chem. Lett.* **2002**, *31* (3), 396-397.
107. Xu, Z.; Chai, L.; Liu, Z. Q., Free-Radical-Promoted Site-Selective C-H Silylation of Arenes by Using Hydrosilanes. *Org. Lett.* **2017**, *19* (20), 5573-5576.
108. Toutov, A. A.; Liu, W. B.; Betz, K. N.; Fedorov, A.; Stoltz, B. M.; Grubbs, R. H., Silylation of C-H bonds in aromatic heterocycles by an Earth-abundant metal catalyst. *Nature* **2015**, *518* (7537), 80-4.
109. Banerjee, S.; Yang, Y. F.; Jenkins, I. D.; Liang, Y.; Toutov, A. A.; Liu, W. B.; Schuman, D. P.; Grubbs, R. H.; Stoltz, B. M.; Krenske, E. H.; Houk, K. N.; Zare, R. N., Ionic and Neutral Mechanisms for C-H Bond Silylation of Aromatic Heterocycles Catalyzed by Potassium tert-Butoxide. *J. Am. Chem. Soc.* **2017**, *139* (20), 6880-6887.

110. Liu, W. B.; Schuman, D. P.; Yang, Y. F.; Toutov, A. A.; Liang, Y.; Klare, H. F. T.; Nesnas, N.; Oestreich, M.; Blackmond, D. G.; Virgil, S. C.; Banerjee, S.; Zare, R. N.; Grubbs, R. H.; Houk, K. N.; Stoltz, B. M., Potassium tert-Butoxide-Catalyzed Dehydrogenative C-H Silylation of Heteroaromatics: A Combined Experimental and Computational Mechanistic Study. *J. Am. Chem. Soc.* **2017**, *139* (20), 6867-6879.
111. Gu, Y.; Shen, Y.; Zarate, C.; Martin, R., A Mild and Direct Site-Selective sp² C-H Silylation of (Poly)Azines. *J. Am. Chem. Soc.* **2019**, *141* (1), 127-132.
112. Cornella, J.; Gomez-Bengoa, E.; Martin, R., Combined experimental and theoretical study on the reductive cleavage of inert C-O bonds with silanes: ruling out a classical Ni(0)/Ni(II) catalytic couple and evidence for Ni(I) intermediates. *J. Am. Chem. Soc.* **2013**, *135* (5), 1997-2009.
113. Wang, B.; Zhang, Q.; Jiang, J.; Yu, H.; Fu, Y., Mechanistic Study on Nickel-Catalyzed Silylation of Aryl Methyl Ethers. *Chem. –Eur. J.* **2017**, *23* (68), 17249-17256.
114. Zarate, C.; Nakajima, M.; Martin, R., A Mild and Ligand-Free Ni-Catalyzed Silylation via C-OMe Cleavage. *J. Am. Chem. Soc.* **2017**, *139* (3), 1191-1197.
115. Wiensch, E. M.; Todd, D. P.; Montgomery, J., Silyloxyarenes as Versatile Coupling Substrates Enabled by Nickel-Catalyzed C–O Bond Cleavage. *ACS Catal.* **2017**, *7* (9), 5568-5571.
116. Minami, Y.; Komiyama, T.; Furuya, Y.; Hiyama, T., Palladium/Copper Dual Catalysis for Cross - coupling of Aryl(trialkyl)silanes with Aryl Bromides. *Angew. Chem. Int. Ed. Engl.* **2018**.
117. Saper, N. I.; Hartwig, J. F., Mechanistic Investigations of the Hydrogenolysis of Diaryl Ethers Catalyzed by Nickel Complexes of N-Heterocyclic Carbene Ligands. *J. Am. Chem. Soc.* **2017**, *139* (48), 17667-17676.
118. Xu, L.; Chung, L. W.; Wu, Y.-D., Mechanism of Ni-NHC Catalyzed Hydrogenolysis of Aryl Ethers: Roles of the Excess Base. *ACS Catal.* **2016**, *6* (1), 483-493.
119. Wititsuwannakul, T.; Tantirungrotechai, Y.; Surawatanawong, P., Density Functional Study of Nickel N-Heterocyclic Carbene Catalyzed C–O Bond Hydrogenolysis of Methyl Phenyl Ether: The Concerted β -H Transfer Mechanism. *ACS Catal.* **2016**, *6* (3), 1477-1486.
120. Collins, K. D.; Glorius, F., A robustness screen for the rapid assessment of chemical reactions. *Nat. Chem.* **2013**, *5* (7), 597-601.
121. Sergeev, A. G.; Hartwig, J. F., Selective, Nickel-Catalyzed Hydrogenolysis of Aryl Ethers. *Science* **2011**, *332* (6028), 439.

122. Hofmann, A. W., Ueber die Einwirkung des Broms in alkalischer Lösung auf Amide. *Berichte der deutschen chemischen Gesellschaft* **1881**, *14* (2), 2725-2736.
123. Nechab, M.; Mondal, S.; Bertrand, M. P., 1,n-Hydrogen-atom transfer (HAT) reactions in which n not equal 5: an updated inventory. *Chemistry* **2014**, *20* (49), 16034-59.
124. Ma, Z. Y.; Guo, L. N.; You, Y.; Yang, F.; Hu, M.; Duan, X. H., Visible Light Driven Alkylation of C(sp³)-H Bonds Enabled by 1,6-Hydrogen Atom Transfer/Radical Relay Addition. *Org. Lett.* **2019**, *21* (14), 5500-5504.
125. Breslow, R.; Baldwin, S.; Flechtner, T.; Kalicky, P.; Liu, S.; Washburn, W., Remote oxidation of steroids by photolysis of attached benzophenone groups. *J. Am. Chem. Soc.* **1973**, *95* (10), 3251-3262.
126. Short, M. A.; Blackburn, J. M.; Roizen, J. L., Modifying Positional Selectivity in C-H Functionalization Reactions with Nitrogen-Centered Radicals: Generalizable Approaches to 1,6-Hydrogen-Atom Transfer Processes. *Synth. Lett.* **2019**, *31* (02), 102-116.
127. Sathyamoorthi, S.; Banerjee, S.; Du Bois, J.; Burns, N. Z.; Zare, R. N., Site-selective bromination of sp³ C-H bonds. *Chem. Sci.* **2018**, *9* (1), 100-104.
128. Short, M. A.; Shehata, M. F.; Sanders, M. A.; Roizen, J. L., Sulfamides direct radical-mediated chlorination of aliphatic C-H bonds. *Chem. Sci.* **2020**, *11* (1), 217-223.
129. Short, M. A.; Blackburn, J. M.; Roizen, J. L., Sulfamate Esters Guide Selective Radical-Mediated Chlorination of Aliphatic C-H Bonds. *Angew. Chem. Int. Ed. Engl.* **2018**, *57* (1), 296-299.
130. Quinn, R. K.; Konst, Z. A.; Michalak, S. E.; Schmidt, Y.; Szklarski, A. R.; Flores, A. R.; Nam, S.; Horne, D. A.; Vanderwal, C. D.; Alexanian, E. J., Site-Selective Aliphatic C-H Chlorination Using N-Chloroamides Enables a Synthesis of Chlorolissoclimide. *J. Am. Chem. Soc.* **2016**, *138* (2), 696-702.
131. Liu, T.; Myers, M. C.; Yu, J.-Q., Copper-Catalyzed Bromination of C(sp³)-H Bonds Distal to Functional Groups. *Angew. Chem. Int. Ed. Engl.* **2017**, *56* (1), 306-309.
132. Tierney, M. M.; Crespi, S.; Ravelli, D.; Alexanian, E. J., Identifying Amidyl Radicals for Intermolecular C-H Functionalizations. *J. Org. Chem.* **2019**, *84* (20), 12983-12991.
133. Carestia, A. M.; Ravelli, D.; Alexanian, E. J., Reagent-dictated site selectivity in intermolecular aliphatic C-H functionalizations using nitrogen-centered radicals. *Chem. Sci.* **2018**, *9* (24), 5360-5365.

134. Schmidt, V. A.; Quinn, R. K.; Brusoe, A. T.; Alexanian, E. J., Site-selective aliphatic C-H bromination using N-bromoamides and visible light. *J. Am. Chem. Soc.* **2014**, *136* (41), 14389-92.
135. Wang, D.; Mao, J.; Zhu, C., Visible light-promoted ring-opening functionalization of unstrained cycloalkanols via inert C-C bond scission. *Chem. Sci.* **2018**, *9* (26), 5805-5809.
136. Egami, H.; Masuda, S.; Kawato, Y.; Hamashima, Y., Photofluorination of Aliphatic C-H Bonds Promoted by the Phthalimide Group. *Org. Lett.* **2018**, *20* (5), 1367-1370.
137. Zhang, Z.; Stateman, L. M.; Nagib, D. A., δ C-H (hetero)arylation via Cu-catalyzed radical relay. *Chem. Sci.* **2019**, *10* (4), 1207-1211.
138. Li, Z.; Wang, Q.; Zhu, J., Copper-Catalyzed Arylation of Remote C(sp³)-H Bonds in Carboxamides and Sulfonamides. *Angew. Chem. Int. Ed. Engl.* **2018**, *57* (40), 13288-13292.
139. Stateman, L. M.; Wappes, E. A.; Nakafuku, K. M.; Edwards, K. M.; Nagib, D. A., Catalytic beta C-H amination via an imidate radical relay. *Chem. Sci.* **2019**, *10* (9), 2693-2699.
140. Becker, P.; Duhamel, T.; Martinez, C.; Muniz, K., Designing Homogeneous Bromine Redox Catalysis for Selective Aliphatic C-H Bond Functionalization. *Angew. Chem. Int. Ed. Engl.* **2018**, *57* (18), 5166-5170.
141. Chang, D.; Zhao, R.; Wei, C.; Yao, Y.; Liu, Y.; Shi, L., Sulfonamide-Directed Chemo- and Site-Selective Oxidative Halogenation/Amination Using Halogenating Reagents Generated in Situ from Cyclic Diacyl Peroxides. *J. Org. Chem.* **2018**, *83* (6), 3305-3315.
142. Tang, Y.; Qin, Y.; Meng, D.; Li, C.; Wei, J.; Yang, M., Diverse secondary C(sp³)-H bond functionalization via site-selective trifluoroacetoxylation of aliphatic amines. *Chem. Sci.* **2018**, *9* (30), 6374-6378.
143. Liu, T.; Mei, T. S.; Yu, J. Q., gamma,delta,epsilon-C(sp³)-H Functionalization through Directed Radical H-Abstraction. *J. Am. Chem. Soc.* **2015**, *137* (18), 5871-4.
144. Tang, N.; Wu, X.; Zhu, C., Practical, metal-free remote heteroarylation of amides via unactivated C(sp³)-H bond functionalization. *Chem. Sci.* **2019**, *10* (28), 6915-6919.
145. Crespin, L. N. S.; Greb, A.; Blakemore, D. C.; Ley, S. V., Visible-Light-Mediated Annulation of Electron-Rich Alkenes and Nitrogen-Centered Radicals from N-Sulfonylallylamines: Construction of Chloromethylated Pyrrolidine Derivatives. *J. Org. Chem.* **2017**, *82* (24), 13093-13108.

146. Mayer, J. M.; Rhile, I. J., Thermodynamics and kinetics of proton-coupled electron transfer: stepwise vs. concerted pathways. *Biochim. Biophys. Acta.* **2004**, *1655* (1-3), 51-8.
147. Mayer, J. M.; Hrovat, D. A.; Thomas, J. L.; Borden, W. T., Proton-Coupled Electron Transfer versus Hydrogen Atom Transfer in Benzyl/Toluene, Methoxyl/Methanol, and Phenoxy/Phenol Self-Exchange Reactions. *J. Am. Chem. Soc.* **2002**, *124* (37), 11142-11147.
148. Miller, D. C.; Tarantino, K. T.; Knowles, R. R., Proton-Coupled Electron Transfer in Organic Synthesis: Fundamentals, Applications, and Opportunities. *Topics Curr. Chem.* **2016**, *374* (3), 30.
149. Mayer, J. M., Proton-coupled electron transfer: a reaction chemist's view. *Annu. Rev. Phys. Chem.* **2004**, *55*, 363-90.
150. Gentry, E. C.; Knowles, R. R., Synthetic Applications of Proton-Coupled Electron Transfer. *Acc. Chem. Res.* **2016**, *49* (8), 1546-56.
151. Tarantino, K. T.; Miller, D. C.; Callon, T. A.; Knowles, R. R., Bond-weakening catalysis: conjugate aminations enabled by the soft homolysis of strong N-H bonds. *J. Am. Chem. Soc.* **2015**, *137* (20), 6440-3.
152. Choi, G. J.; Knowles, R. R., Catalytic Alkene Carboaminations Enabled by Oxidative Proton-Coupled Electron Transfer. *J. Am. Chem. Soc.* **2015**, *137* (29), 9226-9.
153. Miller, D. C.; Choi, G. J.; Orbe, H. S.; Knowles, R. R., Catalytic Olefin Hydroamidation Enabled by Proton-Coupled Electron Transfer. *J. Am. Chem. Soc.* **2015**, *137* (42), 13492-5.
154. Chu, J. C.; Rovis, T., Amide-directed photoredox-catalysed C-C bond formation at unactivated sp³ C-H bonds. *Nature* **2016**, *539* (7628), 272-275.
155. Choi, G. J.; Zhu, Q.; Miller, D. C.; Gu, C. J.; Knowles, R. R., Catalytic alkylation of remote C-H bonds enabled by proton-coupled electron transfer. *Nature* **2016**, *539* (7628), 268-271.
156. Chen, D. F.; Chu, J. C. K.; Rovis, T., Directed gamma-C(sp³)-H Alkylation of Carboxylic Acid Derivatives through Visible Light Photoredox Catalysis. *J. Am. Chem. Soc.* **2017**, *139* (42), 14897-14900.
157. Xu, B.; Tambar, U. K., Remote Allylation of Unactivated C(sp³)-H Bonds Triggered by Photogenerated Amidyl Radicals. *ACS Catal.* **2019**, *9* (5), 4627-4631.
158. Thullen, S. M.; Treacy, S. M.; Rovis, T., Regioselective Alkylative Cross-Coupling of Remote Unactivated C(sp³)-H Bonds. *J. Am. Chem. Soc.* **2019**, *141* (36), 14062-14067.

159. Shu, W.; Zhang, H.; Huang, Y., gamma-Alkylation of Alcohols Enabled by Visible-Light Induced 1,6-Hydrogen Atom Transfer. *Org. Lett.* **2019**, *21* (15), 6107-6111.
160. Snieckus, V.; Cuevas, J. C.; Sloan, C. P.; Liu, H.; Curran, D. P., Intramolecular .alpha.-amidoyl-to-aryl 1,5-hydrogen atom transfer reactions. Heteroannulation and .alpha.-nitrogen functionalization by radical translocation. *J. Am. Chem. Soc.* **1990**, *112* (2), 896-898.
161. Yan, H.; Lu, L.; Rong, G.; Liu, D.; Zheng, Y.; Chen, J.; Mao, J., Functionalization of amides via copper-catalyzed oxyalkylation of vinylarenes and decarboxylative alkenylation of sp³ C-H. *J. Org. Chem.* **2014**, *79* (15), 7103-11.
162. Yang, X. H.; Wei, W. T.; Li, H. B.; Song, R. J.; Li, J. H., Oxidative coupling of alkenes with amides using peroxides: selective amide C(sp³)-H versus C(sp²)-H functionalization. *Chem. Commun.* **2014**, *50* (85), 12867-9.
163. Tahara, Y. K.; Michino, M.; Ito, M.; Kanyiva, K. S.; Shibata, T., Enantioselective sp³ C-H alkylation of gamma-butyrolactam by a chiral Ir(I) catalyst for the synthesis of 4-substituted gamma-amino acids. *Chem. Commun.* **2015**, *51* (93), 16660-3.
164. Angioni, S.; Ravelli, D.; Emma, D.; Dondi, D.; Fagnoni, M.; Albin, A., Tetrabutylammonium Decatungstate (Chemo)selective Photocatalyzed, Radical C-H Functionalization in Amides. *Adv. Synth. Catal.* **2008**, *350* (14-15), 2209-2214.
165. McManus, J. B.; Onuska, N. P. R.; Nicewicz, D. A., Generation and Alkylation of alpha-Carbamyl Radicals via Organic Photoredox Catalysis. *J. Am. Chem. Soc.* **2018**.
166. Nagatomo, M.; Yoshioka, S.; Inoue, M., Enantioselective Radical Alkynylation of C(sp³)-H Bonds Using Sulfoximine as a Traceless Chiral Auxiliary. *Chem.: Asian J.* **2015**, *10* (1), 120-123.
167. Le, C.; Liang, Y.; Evans, R. W.; Li, X.; MacMillan, D. W. C., Selective sp³ C-H alkylation via polarity-match-based cross-coupling. *Nature* **2017**, *547* (7661), 79-83.
168. Ye, J.; Kalvet, I.; Schoenebeck, F.; Rovis, T., Direct alpha-alkylation of primary aliphatic amines enabled by CO₂ and electrostatics. *Nat. Chem.* **2018**, *10* (10), 1037-1041.
169. Ashley, M. A.; Yamauchi, C.; Chu, J. C. K.; Otsuka, S.; Yorimitsu, H.; Rovis, T., Photoredox-Catalyzed Site-Selective alpha-C(sp³)-H Alkylation of Primary Amine Derivatives. *Angew. Chem. Int. Ed. Engl.* **2019**, *58* (12), 4002-4006.
170. Bosset, C.; Beucher, H.; Bretel, G.; Pasquier, E.; Queguiner, L.; Henry, C.; Vos, A.; Edwards, J. P.; Meerpoel, L.; Berthelot, D., Minisci-Photoredox-Mediated alpha-

- Heteroarylation of N-Protected Secondary Amines: Remarkable Selectivity of Azetidines. *Org. Lett.* **2018**, *20* (19), 6003-6006.
171. Dong, J.; Xia, Q.; Lv, X.; Yan, C.; Song, H.; Liu, Y.; Wang, Q., Photoredox-Mediated Direct Cross-Dehydrogenative Coupling of Heteroarenes and Amines. *Org. Lett.* **2018**, *20* (18), 5661-5665.
172. Jain, P.; Verma, P.; Xia, G.; Yu, J. Q., Enantioselective amine alpha-functionalization via palladium-catalysed C-H arylation of thioamides. *Nat. Chem.* **2017**, *9* (2), 140-144.
173. Heitz, D. R.; Tellis, J. C.; Molander, G. A., Photochemical Nickel-Catalyzed C-H Arylation: Synthetic Scope and Mechanistic Investigations. *J. Am. Chem. Soc.* **2016**, *138* (39), 12715-12718.
174. Perry, I. B.; Brewer, T. F.; Sarver, P. J.; Schultz, D. M.; DiRocco, D. A.; MacMillan, D. W. C., Direct arylation of strong aliphatic C-H bonds. *Nature* **2018**, *560* (7716), 70-75.
175. Shen, Y.; Gu, Y.; Martin, R., sp(3) C-H Arylation and Alkylation Enabled by the Synergy of Triplet Excited Ketones and Nickel Catalysts. *J. Am. Chem. Soc.* **2018**, *140* (38), 12200-12209.
176. Dai, C.; Meschini, F.; Narayanam, J. M.; Stephenson, C. R., Friedel-Crafts amidoalkylation via thermolysis and oxidative photocatalysis. *J. Org. Chem.* **2012**, *77* (9), 4425-31.
177. Verheyen, T.; van Turnhout, L.; Vandavasi, J. K.; Isbrandt, E. S.; De Borggraeve, W. M.; Newman, S. G., Ketone Synthesis by a Nickel-Catalyzed Dehydrogenative Cross-Coupling of Primary Alcohols. *J. Am. Chem. Soc.* **2019**, *141* (17), 6869-6874.
178. Fagnoni, M., Modern Molecular Photochemistry of Organic Molecules. By Nicholas J. Turro, V. Ramamurthy and Juan C. Scaiano. *Angew. Chem. Int. Ed. Engl.* **2010**, *49* (38), 6709-6710.
179. Anslyn, E. V.; Dougherty, D. A.; Dougherty, E. V.; Books, U. S., *Modern Physical Organic Chemistry*. University Science Books: 2006.
180. Roth, H. G.; Romero, N. A.; Nicewicz, D. A., Experimental and Calculated Electrochemical Potentials of Common Organic Molecules for Applications to Single-Electron Redox Chemistry. *Synth. Lett.* **2016**, *27* (05), 714-723.
181. Elgrishi, N.; Rountree, K. J.; McCarthy, B. D.; Rountree, E. S.; Eisenhart, T. T.; Dempsey, J. L., A Practical Beginner's Guide to Cyclic Voltammetry. *J. Chem. Ed.* **2018**, *95* (2), 197-206.

182. Skubi, K. L.; Blum, T. R.; Yoon, T. P., Dual Catalysis Strategies in Photochemical Synthesis. *Chem. Rev.* **2016**, *116* (17), 10035-10074.
183. Dicciani, J. B.; Diao, T., Mechanisms of Nickel-Catalyzed Cross-Coupling Reactions. *Trends Chem.* **2019**, *1* (9), 830-844.
184. Chuentragool, P.; Yadagiri, D.; Morita, T.; Sarkar, S.; Parasram, M.; Wang, Y.; Gevorgyan, V., Aliphatic Radical Relay Heck Reaction at Unactivated C(sp³)-H Sites of Alcohols. *Angew. Chem. Int. Ed. Engl.* **2019**, *58* (6), 1794-1798.
185. Parasram, M.; Chuentragool, P.; Wang, Y.; Shi, Y.; Gevorgyan, V., General, Auxiliary-Enabled Photoinduced Pd-Catalyzed Remote Desaturation of Aliphatic Alcohols. *J. Am. Chem. Soc.* **2017**, *139* (42), 14857-14860.
186. Chuentragool, P.; Parasram, M.; Shi, Y.; Gevorgyan, V., General, Mild, and Selective Method for Desaturation of Aliphatic Amines. *J. Am. Chem. Soc.* **2018**, *140* (7), 2465-2468.
187. Fuse, H.; Kojima, M.; Mitsunuma, H.; Kanai, M., Acceptorless Dehydrogenation of Hydrocarbons by Noble-Metal-Free Hybrid Catalyst System. *Org. Lett.* **2018**, *20* (7), 2042-2045.
188. Waidmann, C. R.; Miller, A. J. M.; Ng, C.-W. A.; Scheuermann, M. L.; Porter, T. R.; Tronic, T. A.; Mayer, J. M., Using combinations of oxidants and bases as PCET reactants: thermochemical and practical considerations. *Energy Environ. Sci.* **2012**, *5* (7), 7771-7780.
189. Tarantino, K. T.; Liu, P.; Knowles, R. R., Catalytic Ketyl-Olefin Cyclizations Enabled by Proton-Coupled Electron Transfer. *J. Am. Chem. Soc.* **2013**, *135* (27), 10022-10025.
190. Yayla, H. G.; Knowles, R. R., Proton-Coupled Electron Transfer in Organic Synthesis: Novel Homolytic Bond Activations and Catalytic Asymmetric Reactions with Free Radicals. *Synth. Lett.* **2014**, *25* (20), 2819-2826.
191. Bordwell, F. G.; Ji, G. Z., Effects of structural changes on acidities and homolytic bond dissociation energies of the hydrogen-nitrogen bonds in amidines, carboxamides, and thiocarboxamides. *J. Am. Chem. Soc.* **1991**, *113* (22), 8398-8401.
192. Bordwell, F. G.; Zhang, S.; Zhang, X.-M.; Liu, W.-Z., Homolytic Bond Dissociation Enthalpies of the Acidic H-A Bonds Caused by Proximate Substituents in Sets of Methyl Ketones, Carboxylic Esters, and Carboxamides Related to Changes in Ground State Energies. *J. Am. Chem. Soc.* **1995**, *117* (27), 7092-7096.
193. Hong, J.; Fauvell, T. J.; Helweh, W.; Zhang, X.; Chen, L. X., Investigation of the photoinduced axial ligation process in the excited state of nickel(II) phthalocyanine. *J. Photochem. Photobiol. A* **2019**, *372*, 270-278.

194. Crites Tears, D. K.; McMillin, D. R., Exciplex quenching of photoexcited platinum(II) terpyridines: influence of the orbital parentage. *Coord. Chem. Rev.* **2001**, *211* (1), 195-205.
195. Armaroli, N., Photoactive mono- and polynuclear Cu()-phenanthrolines. A viable alternative to Ru()-polypyridines? *Chem. Soc. Rev.* **2001**, *30* (2), 113-124.
196. Kim, D.; Kirmaier, C.; Holten, D., Nickel porphyrin photophysics and photochemistry. A picosecond investigation of ligand binding and release in the excited state. *Chem. Phys.* **1983**, *75* (3), 305-322.
197. Markle, T. F.; Darcy, J. W.; Mayer, J. M., A new strategy to efficiently cleave and form C–H bonds using proton-coupled electron transfer. *Science Advances* **2018**, *4* (7), eaat5776.
198. Morton, C. M.; Zhu, Q.; Ripberger, H.; Troian-Gautier, L.; Toa, Z. S. D.; Knowles, R. R.; Alexanian, E. J., C-H Alkylation via Multisite-Proton-Coupled Electron Transfer of an Aliphatic C-H Bond. *J. Am. Chem. Soc.* **2019**, *141* (33), 13253-13260.
199. Darcy, J. W.; Koronkiewicz, B.; Parada, G. A.; Mayer, J. M., A Continuum of Proton-Coupled Electron Transfer Reactivity. *Acc. of Chem. Res.* **2018**, *51* (10), 2391-2399.
200. Warren, J. J.; Menzeleev, A. R.; Kretchmer, J. S.; Miller, T. F.; Gray, H. B.; Mayer, J. M., Long-Range Proton-Coupled Electron-Transfer Reactions of Bis(imidazole) Iron Tetraphenylporphyrins Linked to Benzoates. *J. Phys. Chem. Lett.* **2013**, *4* (3), 519-523.
201. Morris, W. D.; Mayer, J. M., Separating Proton and Electron Transfer Effects in Three-Component Concerted Proton-Coupled Electron Transfer Reactions. *J. Am. Chem. Soc.* **2017**, *139* (30), 10312-10319.
202. Margrey, K. A.; Czaplinski, W. L.; Nicewicz, D. A.; Alexanian, E. J., A General Strategy for Aliphatic C-H Functionalization Enabled by Organic Photoredox Catalysis. *J. Am. Chem. Soc.* **2018**, *140* (12), 4213-4217.
203. Wakaki, T.; Sakai, K.; Enomoto, T.; Kondo, M.; Masaoka, S.; Oisaki, K.; Kanai, M., C(sp³)–H Cyanation Promoted by Visible-Light Photoredox/Phosphate Hybrid Catalysis. *Chemistry* **2018**, *24* (32), 8051-8055.
204. Rosso, J. A.; Caregnato, P.; Mora, V. C.; Gonzalez, M. C.; Mártire, D. O., Reactions of Phosphate Radicals with Monosubstituted Benzenes. A Mechanistic Investigation. *Helv. Chim. Acta* **2003**, *86* (7), 2509-2524.
205. Mártire, D. O.; Gonzalez, M. C., Aqueous Phase Kinetic Studies Involving Intermediates of Environmental Interest: Phosphate Radicals and Their Reactions with Substituted Benzenes. *Prog. React. Kinet. Mech.* **2001**, *26* (2-3), 201-218.

206. Maruthamuthu, P.; Taniguchi, H., An in situ photolysis-electron spin resonance study of some reactions of phosphate radicals. *J. Phys. Chem.* **1977**, *81* (20), 1944-1948.
207. Maruthamuthu, P.; Neta, P., Phosphate radicals. Spectra, acid-base equilibriums, and reactions with inorganic compounds. *J. Phys. Chem.* **1978**, *82* (6), 710-713.
208. Shields, B. J.; Doyle, A. G., Direct C(sp³)-H Cross Coupling Enabled by Catalytic Generation of Chlorine Radicals. *J. Am. Chem. Soc.* **2016**, *138* (39), 12719-12722.
209. Shields, B. J.; Kudisch, B.; Scholes, G. D.; Doyle, A. G., Long-Lived Charge-Transfer States of Nickel(II) Aryl Halide Complexes Facilitate Bimolecular Photoinduced Electron Transfer. *J. Am. Chem. Soc.* **2018**, *140* (8), 3035-3039.
210. Hwang, S. J.; Anderson, B. L.; Powers, D. C.; Maher, A. G.; Hadt, R. G.; Nocera, D. G., Halogen Photoelimination from Monomeric Nickel(III) Complexes Enabled by the Secondary Coordination Sphere. *Organometallics* **2015**, *34* (19), 4766-4774.
211. Esswein, A. J.; Nocera, D. G., Hydrogen Production by Molecular Photocatalysis. *Chem. Rev.* **2007**, *107* (10), 4022-4047.
212. Hwang, S. J.; Powers, D. C.; Maher, A. G.; Anderson, B. L.; Hadt, R. G.; Zheng, S. L.; Chen, Y. S.; Nocera, D. G., Trap-Free Halogen Photoelimination from Mononuclear Ni(III) Complexes. *J. Am. Chem. Soc.* **2015**, *137* (20), 6472-5.
213. Nielsen, M. K.; Shields, B. J.; Liu, J.; Williams, M. J.; Zacuto, M. J.; Doyle, A. G., Mild, Redox-Neutral Formylation of Aryl Chlorides through the Photocatalytic Generation of Chlorine Radicals. *Angew. Chem. Int. Ed. Engl.* **2017**, *56* (25), 7191-7194.
214. Ting, S. I.; Garakyaraghi, S.; Taliaferro, C. M.; Shields, B. J.; Scholes, G. D.; Castellano, F. N.; Doyle, A. G., 3d-d Excited States of Ni(II) Complexes Relevant to Photoredox Catalysis: Spectroscopic Identification and Mechanistic Implications. *J. Am. Chem. Soc.* **2020**, *142* (12), 5800-5810.
215. Rohe, S.; Morris, A. O.; McCallum, T.; Barriault, L., Hydrogen Atom Transfer Reactions via Photoredox Catalyzed Chlorine Atom Generation. *Angew. Chem. Int. Ed. Engl.* **2018**, *57* (48), 15664-15669.
216. Wang, Z.; Ji, X.; Han, T.; Deng, G.-J.; Huang, H., LiBr-Promoted Photoredox Minisci-Type Alkylations of Quinolines with Ethers. *Adv. Synth. Catal.* **2019**, *361* (24), 5643-5647.
217. Isse, A. A.; Lin, C. Y.; Coote, M. L.; Gennaro, A., Estimation of Standard Reduction Potentials of Halogen Atoms and Alkyl Halides. *J. Phys. Chem. B* **2011**, *115* (4), 678-684.

218. Matsui, J. K.; Lang, S. B.; Heitz, D. R.; Molander, G. A., Photoredox-Mediated Routes to Radicals: The Value of Catalytic Radical Generation in Synthetic Methods Development. *ACS Catal.* **2017**, *7* (4), 2563-2575.
219. Bevernaegie, R.; Wehlin, S. A. M.; Piechota, E. J.; Abraham, M.; Philouze, C.; Meyer, G. J.; Elias, B.; Troian-Gautier, L., Improved Visible Light Absorption of Potent Iridium(III) Photo-oxidants for Excited-State Electron Transfer Chemistry. *J. Am. Chem. Soc.* **2020**, *142* (6), 2732-2737.
220. Troian-Gautier, L.; Turlington, M. D.; Wehlin, S. A. M.; Maurer, A. B.; Brady, M. D.; Swords, W. B.; Meyer, G. J., Halide Photoredox Chemistry. *Chem. Rev.* **2019**, *119* (7), 4628-4683.
221. Bacauanu, V.; Cardinal, S.; Yamauchi, M.; Kondo, M.; Fernández, D. F.; Remy, R.; MacMillan, D. W. C., Metallaphotoredox Difluoromethylation of Aryl Bromides. *Angew. Chem. Int. Ed. Engl.* **2018**, *57* (38), 12543-12548.
222. Zhang, P.; Le, C. C.; MacMillan, D. W. C., Silyl Radical Activation of Alkyl Halides in Metallaphotoredox Catalysis: A Unique Pathway for Cross-Electrophile Coupling. *J. Am. Chem. Soc.* **2016**, *138* (26), 8084-8087.
223. Li, G.; Ward, W. M.; Meyer, G. J., Visible Light Driven Nanosecond Bromide Oxidation by a Ru Complex with Subsequent Br-Br Bond Formation. *J. Am. Chem. Soc.* **2015**, *137* (26), 8321-8323.
224. Kawasaki, T.; Ishida, N.; Murakami, M., Dehydrogenative Coupling of Benzylic and Aldehydic C-H Bonds. *J. Am. Chem. Soc.* **2020**, *142* (7), 3366-3370.
225. Pike, S. J.; Hutchinson, J. J.; Hunter, C. A., H-Bond Acceptor Parameters for Anions. *J. Am. Chem. Soc.* **2017**, *139* (19), 6700-6706.
226. O'Brien, C. J.; Droege, D. G.; Jiu, A. Y.; Gandhi, S. S.; Paras, N. A.; Olson, S. H.; Conrad, J., Photoredox Cyanomethylation of Indoles: Catalyst Modification and Mechanism. *J. Org. Chem.* **2018**, *83* (16), 8926-8935.
227. Devery III, J. J.; Douglas, J. J.; Nguyen, J. D.; Cole, K. P.; Flowers II, R. A.; Stephenson, C. R. J., Ligand functionalization as a deactivation pathway in a fac-Ir(ppy)₃-mediated radical addition. *Chem. Sci.* **2015**, *6* (1), 537-541.
228. Meiries, S.; Speck, K.; Cordes, D. B.; Slawin, A. M. Z.; Nolan, S. P., [Pd(IPr*OMe)(acac)Cl]: Tuning the N-Heterocyclic Carbene in Catalytic C-N Bond Formation. *Organometallics* **2013**, *32* (1), 330-339.
229. Bantreil, X.; Nolan, S. P., Synthesis of N-heterocyclic carbene ligands and derived ruthenium olefin metathesis catalysts. *Nat. Protoc.* **2011**, *6* (1), 69-77.

230. Li, L.; Zeng, M.; Herzon, S. B., Broad-Spectrum Catalysts for the Ambient Temperature Anti-Markovnikov Hydration of Alkynes. *Angew. Chem. Int. Ed. Engl.* **2014**, *53* (30), 7892-7895.
231. Querard, P.; Perepichka, I.; Zysman-Colman, E.; Li, C.-J., Copper-catalyzed asymmetric sp³ C–H arylation of tetrahydroisoquinoline mediated by a visible light photoredox catalyst. *Beilstein J. Org. Chem.* **2016**, *12*, 2636-2643.
232. Woods, B. P.; Orlandi, M.; Huang, C.-Y.; Sigman, M. S.; Doyle, A. G., Nickel-Catalyzed Enantioselective Reductive Cross-Coupling of Styrenyl Aziridines. *J. Am. Chem. Soc.* **2017**, *139* (16), 5688-5691.
233. Liu, C.; Han, N.; Song, X.; Qiu, J., A General and Highly Efficient Method for the Construction of Aryl-Substituted N-Heteroarenes. *Euro. J. Org. Chem.* **2010**, *2010* (29), 5548-5551.
234. Camerel, F.; Ulrich, G.; Barberá, J.; Ziessel, R., Ionic Self-Assembly of Ammonium-Based Amphiphiles and Negatively Charged Bodipy and Porphyrin Luminophores. *Chem. –Eur. J.* **2007**, *13* (8), 2189-2200.
235. Li, Z.; Wu, Z.; Fu, W.; Liu, P.; Jiao, B.; Wang, D.; Zhou, G.; Hou, X., Versatile Fluorinated Derivatives of Triphenylamine as Hole-Transporters and Blue-Violet Emitters in Organic Light-Emitting Devices. *J. Phys. Chem. C* **2012**, *116* (38), 20504-20512.
236. Selva, M.; Perosa, A.; Tundo, P.; Brunelli, D., Selective N,N-Dimethylation of Primary Aromatic Amines with Methyl Alkyl Carbonates in the Presence of Phosphonium Salts. *J. Org. Chem.* **2006**, *71* (15), 5770-5773.
237. Huang, L.; Niu, T.; Wu, J.; Zhang, Y., Copper-Catalyzed Oxidative Cross-Coupling of N,N-Dimethylanilines with Heteroarenes under Molecular Oxygen. *J. Org. Chem.* **2011**, *76* (6), 1759-1766.
238. Knauber, T.; Arikan, F.; Röschenthaler, G.-V.; Gooßen, L. J., Copper-Catalyzed Trifluoromethylation of Aryl Iodides with Potassium (Trifluoromethyl)trimethoxyborate. *Chem. –Eur. J.* **2011**, *17* (9), 2689-2697.
239. Hodges, J. A.; Raines, R. T., Energetics of an n → π* Interaction that Impacts Protein Structure. *Org. Lett.* **2006**, *8* (21), 4695-4697.
240. Baciocchi, E.; Bietti, M.; Gerini, M. F.; Lanzalunga, O., Electron-Transfer Mechanism in the N-Demethylation of N,N-Dimethylanilines by the Phthalimide-N-oxyl Radical. *J. Org. Chem.* **2005**, *70* (13), 5144-5149.
241. Wiles, C.; Watts, P.; Haswell, S. J., Clean and selective oxidation of aromatic alcohols using silica-supported Jones' reagent in a pressure-driven flow reactor. *Tetrahedron Lett.* **2006**, *47* (30), 5261-5264.

242. Gerber, R.; Blacque, O.; Frech, C. M., Negishi cross-coupling reaction catalyzed by an aliphatic, phosphine based pincer complex of palladium. biaryl formation via cationic pincer-type PdIV intermediates. *Dalton Trans.* **2011**, 40 (35), 8996-9003.
243. Hill, L. L.; Smith, J. M.; Brown, W. S.; Moore, L. R.; Guevera, P.; Pair, E. S.; Porter, J.; Chou, J.; Wolterman, C. J.; Craciun, R.; Dixon, D. A.; Shaughnessy, K. H., Neopentylphosphines as effective ligands in palladium-catalyzed cross-couplings of aryl bromides and chlorides. *Tetrahedron* **2008**, 64 (29), 6920-6934.
244. Zhang, L.; Zhang, Y.; Deng, Y.; Shi, F., Light-promoted N,N-dimethylation of amine and nitro compound with methanol catalyzed by Pd/TiO₂ at room temperature. *RSC Adv.* **2015**, 5 (19), 14514-14521.
245. Oosterbaan, W. D.; van Gerven, P. C.; van Walree, C. A.; Koeberg, M.; Piet, J. J.; Havenith, R. W.; Zwikker, J. W.; Jenneskens, L. W.; Gleiter, R., Photoinduced Charge Separation in Cyclohexylidene - Based Donor-(σ - Bridge)- Acceptor Compounds- Building Blocks for Materials. *Euro. J. Org. Chem.* **2003**, 2003 (16), 3117-3130.
246. Kim, S.; Oh, C. H.; Ko, J. S.; Ahn, K. H.; Kim, Y. J., Zinc-modified cyanoborohydride as a selective reducing agent. *J. Org. Chem.* **1985**, 50 (11), 1927-1932.
247. Guo, H.; Chen, X.; Zhao, C.; He, W., Suzuki-type cross coupling between aryl halides and silylboranes for the syntheses of aryl silanes. *Chem. Commun.* **2015**, 51 (98), 17410-17412.
248. Guo, L.; Chatupheeraphat, A.; Rueping, M., Decarbonylative Silylation of Esters by Combined Nickel and Copper Catalysis for the Synthesis of Arylsilanes and Heteroarylsilanes. *Angew. Chem. Int. Ed. Engl.* **2016**, 55 (39), 11810-11813.
249. Yamanoi, Y.; Nishihara, H., Direct and Selective Arylation of Tertiary Silanes with Rhodium Catalyst. *J. Org. Chem.* **2008**, 73 (17), 6671-6678.
250. Lee, K.-S.; Katsoulis, D.; Choi, J., Intermolecular C-H Silylation of Arenes and Heteroarenes with HSiEt₃ under Operationally Diverse Conditions: Neat/Stoichiometric and Acceptor/Acceptorless. *ACS Catal.* **2016**, 6 (3), 1493-1496.
251. Olah, G. A.; Gupta, B. G. B.; Narang, S. C.; Malhotra, R., Synthesis methods and reactions. 71. Chlorotrimethylsilane and tert-butyl dimethylsilyl chloride/lithium sulfide, mild and efficient silylating reagents. *J. Org. Chem.* **1979**, 44 (24), 4272-4275.
252. Yoshida, Y.; Otsuka, S.; Nogi, K.; Yorimitsu, H., Palladium-Catalyzed Amination of Aryl Sulfoxides. *Org. Lett.* **2018**, 20 (4), 1134-1137.

253. Chen, W.-B.; Xing, C.-H.; Dong, J.; Hu, Q.-S., Electron-Poor, Fluoro-Containing Arylboronic Acids as Efficient Coupling Partners for Bis(1,5-cyclooctadiene)nickel(0)/Tricyclohexylphosphine-Catalyzed Cross-Coupling Reactions of Aryl Arenesulfonates. *Adv. Synth. Catal.* **2016**, *358* (13), 2072-2076.
254. Gujjar, R.; El Mazouni, F.; White, K. L.; White, J.; Creason, S.; Shackelford, D. M.; Deng, X.; Charman, W. N.; Bathurst, I.; Burrows, J.; Floyd, D. M.; Matthews, D.; Buckner, F. S.; Charman, S. A.; Phillips, M. A.; Rathod, P. K., Lead Optimization of Aryl and Aralkyl Amine-Based Triazolopyrimidine Inhibitors of Plasmodium falciparum Dihydroorotate Dehydrogenase with Antimalarial Activity in Mice. *J. Med. Chem.* **2011**, *54* (11), 3935-3949.
255. Jabbari, A.; Davoodnejad, M.; Alimardani, M.; Assadieskandar, A.; Sadeghian, A.; Safdari, H.; Movaffagh, J.; Sadeghian, H., Synthesis and SAR studies of 3-allyl-4-prenyloxylaniline amides as potent 15-lipoxygenase inhibitors. *Bioorg. Med. Chem.* **2012**, *20* (18), 5518-5526.
256. Schlosser, J.; Johannes, E.; Zindler, M.; Lemmerhirt, J.; Sommer, B.; Schütt, M.; Peifer, C., Novel synthesis of benzofuran- and indol-2-yl-methanamine derivatives. *Tetrahedron Lett.* **2015**, *56* (1), 89-94.
257. Pandey, G.; Jadhav, D.; Tiwari, S. K.; Singh, B., Visible Light Photoredox Catalysis: Investigation of Distal sp³ C-H Functionalization of Tertiary Amines for Alkylation Reaction. *Adv. Synth. Catal.* **2014**, *356* (13), 2813-2818.
258. Zhu, Q.; Graff, D. E.; Knowles, R. R., Intermolecular Anti-Markovnikov Hydroamination of Unactivated Alkenes with Sulfonamides Enabled by Proton-Coupled Electron Transfer. *J. Am. Chem. Soc.* **2018**, *140* (2), 741-747.
259. Hashmi, A. S. K.; Blanco Jaimes, M. C.; Schuster, A. M.; Rominger, F., From Propargylic Amides to Functionalized Oxazoles: Domino Gold Catalysis/Oxidation by Dioxygen. *J. Org. Chem.* **2012**, *77* (15), 6394-6408.
260. Asai, S.; Ban, K.; Monguchi, Y.; Sajiki, H.; Sawama, Y., Selective N-Monoalkylation of Amide Derivatives with Trialkyl Phosphates. *Synth. Lett.* **2018**, *29* (03), 322-325.
261. Sibi, M. P.; Petrovic, G.; Zimmerman, J., Enantioselective Radical Addition/Trapping Reactions with α,β -Disubstituted Unsaturated Imides. Synthesis of anti-Propionate Aldols. *J. Am. Chem. Soc.* **2005**, *127* (8), 2390-2391.
262. Vyklický, L.; Dvořáková, H.; Dvořák, D., Iron Aminocarbene Complexes Containing a Double CC Bond in the N-Substituent: Preparation and Reactivity. *Organometallics* **2001**, *20* (25), 5419-5424.
263. Tang, T. P.; Volkman, S. K.; Ellman, J. A., Asymmetric Synthesis of Protected 1,2-Amino Alcohols Using tert-Butanesulfinyl Aldimines and Ketimines. *J. Org. Chem.* **2001**, *66* (26), 8772-8778.

264. Su, J. Y.; Grünenfelder, D. C.; Takeuchi, K.; Reisman, S. E., Radical Deoxychlorination of Cesium Oxalates for the Synthesis of Alkyl Chlorides. *Org. Lett.* **2018**, *20* (16), 4912-4916.
265. Martínez, C.; Muñiz, K., An Iodine-Catalyzed Hofmann–Löffler Reaction. *Angew. Chem. Int. Ed. Engl.* **2015**, *54* (28), 8287-8291.
266. Haynes, M. T.; Liu, P.; Baxter, R. D.; Nett, A. J.; Houk, K. N.; Montgomery, J., Dimer Involvement and Origin of Crossover in Nickel-Catalyzed Aldehyde–Alkyne Reductive Couplings. *J. Am. Chem. Soc.* **2014**, *136* (50), 17495-17504.
267. Ruffoni, A.; Juliá, F.; Svejstrup, T. D.; McMillan, A. J.; Douglas, J. J.; Leonori, D., Practical and regioselective amination of arenes using alkyl amines. *Nat. Chem.* **2019**, *11* (5), 426-433.